Co-operative failure of *Aire*-mediated clonal deletion and *Cblb*-mediated clonal anergy in the pathogenesis of autoimmunity

Charis Teh En-Yi

Thesis submitted for the degree of
Doctor of Philosophy
of the Australian National University

February 2012

Australian National University

THE JOHN CURTIN SCHOOL OF MEDICAL RESEARCH

Statement of Originality

The research content within this study was performed in the Immunogenomics Laboratory, Department of Immunology, John Curtin School of Medical Research, Australian National University under the supervision of Dr. Anselm Enders and Professor Christopher Goodnow. The data presented is my own original work, with all contributions from others clearly stated in the acknowledgements and methods.

……

Charis Teh

……

Supervisor: Dr. Anselm Enders

……

Supervisor: Professor Christopher Goodnow

Acknowledgements

Anselm Enders

Thank you for being an extraordinary supervisor. Your patient academic guidance and dedication has been inspiring.

Chris Goodnow

Thank you for giving me the opportunity to work on this project and for sharing your tremendous wealth of knowledge. It is such a privilege to work with such a creative and distinguish mentor. I have learnt so much.

Stephen Daley, Chris Parish, Ben Quah, Anna Cowan

Thank you to my supervisory panel for constructive discussion, feedback and ideas throughout my PhD. I have been able to explore more than I could have imagined.

Immunogenomics Laboratory

I feel blessed and humbled to be part of this team. It seemed so easy to come to work everyday when surrounded by such gifted and passionate people. Special thanks to Keisuke Horikawa, Lina Tze, Debbie Howard, Edyta Kucharska, Nadine Barthel and Manu Singh - without your help, advice and expertise this project would have been impossible! Michelle Townsend - without you the lab would probably fall apart!

La Gruta/Doherty Lab at the University of Melbourne

Thank you for so generously welcoming me into your laboratory to learn the multiplex sequencing and retrogenic technology.

Wranglers at ANU Bioscience Services, Animal Division

Holly Burke, Ken Walker, Elizabeth O' Sulivan, Ken Chau, Barbara Burke, Luke Walker, Ryan Dunstan, Derryn Watson, Matt Sutton and Nyasa Fook - Thank you for the tireless effort in taking care of all the mice for this project. I feel so privileged to work alongside wranglers who care so much about the mice and the research.

Resource Teams at the John Curtin School of Medical Research

Thank you Belinda Whittle and the Genotyping Team at the Australian Phenomics Facility for such speedy and accurate genotyping.

Thank you Cathy Gillespie, Harpreet Vohra and Mick Devoy for keeping the FACS machines and microscopes in excellent condition.

Thank you Anne Prins for all the paraffin sectioning and hematoxylin and eosin staining.

Thank you Cameron McCrae and the staff at the Biomolecular Resource Facility for the sequencing.

My family

Dad, mum, Doron, Chara, Charin and Caryl - thank you for being my PhD support team even through I am so far away from home. Also, to Moses Lee, a special thank you for being a patient, loving and supportive husband.

My friends in Canberra

Thank you for being my family-away-from-home and making sure I had an enjoyable PhD journey.

Thank you Jesus for being my pillar of strength.

Table of Contents

List of Abbreviations

α	alpha
Aire	autoimmune regulator
ALPS	autoimmune lymphoproliferative syndrome
APS	autoimmune polyglandular syndrome
β	beta
C	constant
Card11	caspase recruitment domain-containing protein 11
Cblb	casitas B-lineage lymphoma b
CD	celiac disease
cDNA	complimentary deoxyribonucleic acid
CDR	complementarity determining region
CFSE	carboxyfluorescein succinimidyl ester
CrD	Crohn's disease
cTEC	cortical thymic epithelial cell
δ	delta
D	diversity
DN	double negative
DNA	deoxyribonucleic acid
DNT	double negative T
DP	double positive
ε	epsilon
eTAC	extrathymic *Aire*-Expressing Cells
FACS	fluorescent activated cell sorting
FoxP3	forkhead box P3
FSC	forward side scatter
γ	gamma
GFP	grenn fluorescent protein
gld	generalized lymphoproliferative disease
GWAS	genome wide association studies
HEL	hen egg lysozyme
HLA	human leucocyte antigen
HSC	haematopoietic stem cells
IBD	inflammatory bowel disease
IEL	intraepithelial lymphocyte
IL	interleukin
Ins	insulin
IPEX	immunodysregulation polyendocrinopathy enteropathy X-linked syndrome
IRBP	interphotorecpetor retinoid binding protein
iT_{reg}	inducible T regulatory

J	joining
LN	lymph node
MFI	mean fluorescent intensity
MHC	major histocompatibility complex
MS	multiple sclerosis
mTEC	medullary thymic epithelial cells
NFκB	nuclear factor kappa B
nT_{reg}	natural T regulatory
OVA	ovalbumin
PCR	polymerase chain reaction
pMHC	peptide-major histocompatibility complex
PS	psoriasis
RAG	recombination activation genes
Rc3h	ring finger and CCCH-type domains 1
RNA	ribonucleic acid
SLE	systemic lupus erythematosus
SNP	single nucleotide polymorpism
SP	single positive
TCR	T cell receptor
T_{FH}	T follicular helper
Tg	transgenic
TGFβ	transforming growth factor beta
T_H1	T helper type 1
T_H17	T helper type 17
T_H2	T helper type 2
TID	type 1 diabetes
TRAC	T cell receptor alpha constant
TRAJ	T cell receptor alpha joining
TRAV	T cell receptor alpha variable
TRBC	T cell receptor beta constant
TRBD	T cell receptor beta diversity
TRBJ	T cell receptor beta joining
TRBV	T cell receptor beta variable
T_{reg}	T regulatory
UC	ulcerative colitis
V	variable
ζ	zeta

Publications arising from this study

Peer-reviewed journals

Teh, C.E., Daley, S.R., Enders, A., and Goodnow, C.C. (2010). T-cell regulation by casitas B-lineage lymphoma (Cblb) is a critical failsafe against autoimmune disease due to autoimmune regulator (Aire) deficiency. Proceedings of the National Academy of Sciences of the United States of America *107*, 14709-14714.

Hoyne, G.F., Flening, E., Yabas, M., Teh, C., Altin, J.A., Randall, K., Thien, C.B., Langdon, W.Y., and Goodnow, C.C. (2011). Visualizing the role of Cbl-b in control of islet-reactive CD4 T cells and susceptibility to type 1 diabetes. J Immunol *186*, 2024-2032.

Silva, D.G., Daley, S.R., Hogan, J., Lee, S.K., Teh, C.E., Hu, D.Y., Lam, K.P., Goodnow, C.C., and Vinuesa, C.G. (2011). Anti-islet autoantibodies trigger autoimmune diabetes in the presence of an increased frequency of islet-reactive CD4 T cells. Diabetes *60*, 2102-2111.

Conference presentations

Teh, C.E., Daley, S.R., Enders, A., and Goodnow, C.C. (2010). Central tolerance due to *Aire* co-operates with peripheral tolerance defect in *Cblb* but not *Fasl*, *Rc3h1* or *Card11* to precipitate lethal autoimmunity. Midwinter Conference for Immunologist, Asilomar, USA. **Poster Presentation**.

Teh, C.E., Daley, S.R., Enders, A., and Goodnow, C.C. (2010). T cell regulation by *Cblb* but not *Fasl*, *Rc3h1* or *Card11* is a critical failsafe against autoimmune disease

due to *Aire*-deficiency. 40th Annual Scientific Meeting, Australasian Society for Immunology, Young Investigator Award. **Oral Presentation**.

Teh, C.E., Daley, S.R., Enders, A., and Goodnow, C.C. (2010). T cell regulation by *Cblb* but not *Fasl*, *Rc3h1* or *Card11* is a critical failsafe against autoimmune disease due to *Aire*-deficiency. Australasian Society for Immunology, NSW/ACT Branch Meeting. **Oral Presentation.**

Teh, C.E., Daley, S.R., Enders, A., and Goodnow, C.C. (2010). A multistep pathogenesis model for autoimmune diseases. Young Investigator's Forum, Australian Society for Medical Research, ACT Branch. **Oral Presentation.**

Teh, C.E., Daley, S.R., Enders, A., and Goodnow, C.C. (2010). Combinatorial defects in central and peripheral tolerance checkpoints preciptate early onset autoimmune pancreatitis and sialadenitis. Keystone Symposia, Autoimmunity and Tolerance. **Oral and poster presentation.**

Teh, C.E., Daley, S.R., Enders, A., and Goodnow, C.C. (2009). Combinatorial defects in central and peripheral tolerance checkpoints preciptate early onset autoimmune pancreatitis and sialadenitis. 39th Annual Scientific Meeting, Australasian Society for Immunology. **Oral presentation**.

Abstract

Autoimmune Polyendocrinopathy Syndrome type 1 (APS1) results from homozygous *AIRE* mutations that cripple thymic deletion of T cells that recognise a wide array of organ-specific self-antigens. For unknown reasons, APS1 nevertheless exhibits a highly variable onset and pattern of discrete organs affected by autoimmunity. The studies presented in this thesis test the hypothesis that this variable and limited organ involvement reflects the failsafe action of discrete post-thymic mechanisms for imposing self-tolerance in peripheral T cells, so that autoimmunity only manifests when one of these peripheral mechanisms also breaks down.

Aire-deficient mice were crossed with mice carrying specific genetic defects in one of four distinct peripheral tolerance mechanisms: activation-induced cell death ($Fasl^{gld/gld}$), anergy and requirement for CD28 co-stimulation ($Cblb^{-/-}$), inhibition of ICOS and T_{FH} cells ($Rc3h1^{san/san}$), or decreased numbers of $Foxp3^+$ T regulatory cells ($Card11^{unm/unm}$). *Cblb*-deficiency was unique among these four in precipitating rapid clinical autoimmune disease when combined with *Aire*-deficiency, resulting in lethal exocrine pancreatitis and sialoadenitis within weeks after T cells emerged from the thymus. Adoptive transfer experiments established that $CD4^+$ and $CD8^+$ subsets were both necessary to transfer lethal disease, although CD8 cells alone were sufficient to cause extensive pancreatitis. These findings supported a *multistep model* for autoimmune disease pathogenesis and established a simplified experimental model for spontaneous autoimmunity that depends on just two inherited genetic changes on an otherwise uniform genetic background.

The remarkably uniform organ-specificity of autoimmunity in $Aire^{-/-}Cblb^{-/-}$ mice was hypothesised to reflect an underlying property of the T cell repertoire in the mouse. Varying the nascent T cell repertoire by substituting the $H2^k$ MHC haplotype with the $H2^b$ haplotype, or by holding the MHC constant but introducing a TCR transgene that skewed the repertoire towards the pancreatic islet beta cells failed to redirect the

exocrine pancreatic autoimmunity in *Aire*$^{-/-}$*Cblb*$^{-/-}$ mice, albeit these strategies slowed down the intensity and tempo of the disease. This indicated that the organ-specific pattern was not simply governed by the numbers of precursor self-reactive T cells against a particular antigen in the repertoire but must reflect a unique property of the disease-driving T cells that escaped tolerance in *Aire*$^{-/-}$*Cblb*$^{-/-}$ mice.

To illuminate the unique properties of the autoimmune driver cells in *Aire*$^{-/-}$*Cblb*$^{-/-}$ mice, a new approach to isolate pancreas-specific T cell clones was successfully established. This involved enriching for the driver T cells by serial adoptive transfer, followed by RT-PCR amplification and sequencing of mRNAs encoding the paired TCRα and TCRβ chains from single T cells sorted from the pancreas or spleen. A remarkably oligoclonal expansion of CD8 T cells within the pancreas was revealed, comprising several clones within an animal bearing highly related TCRs. The TCR from one of the expanded CD8 T cell clones, 3.5, was expressed in retroviral transgenic (retrogenic) bone marrow chimeras. T cells expressing TCR3.5 were positively selected into the CD8 T cell lineage, showed no evidence of negative selection in *Aire*-wildtype thymi, and accumulated as mature naïve CD8 T cells in the axillary and inguinal lymph nodes. TCR3.5 CD8 T cells were nevertheless activated in the pancreatic lymph node and accumulated in the pancreas, and retrogenic expression of TCR3.5 was sufficient to precipitate extensive exocrine pancreatitis in animals with wild-type *Aire* and *Cblb* genes. These results suggest that *Aire* may not directly regulate the driver CD8 T cells, raising novel possibilities about how the defects in *Aire* and *Cblb* co-operate to precipitate organ-specific autoimmunity.

These findings support the hypothesis that organ-specific autoimmunity manifests only when a defect in thymic deletion is paired with a defect in peripheral T cell tolerance. Even with two inherited defects, other tolerance mechanisms continue to operate so that in the case of *Aire* deficiency combined with *FasL*, *Rc3h1* or *Card11* mutations, no rapidly emergent autoimmune disease was observed. In *Aire* and *Cblb* double deficiencies, only rare self-reactive CD8 T cells with particular TCR specificities escaped the other tolerance mechanisms, causing an extremely rapid but very discrete

pattern of organ-specific autoimmunity directed at the exocrine pancreas and salivary glands. The results illuminate the stringent nature of the mechanisms that protect the body from autoimmune diseases, and provide a framework and experimental approach for interpreting patterns of genetic and phenotypic variability in human autoimmune diseases.

Chapter 1

Literature Review

1.1 Preamble

Four hundred and fifty million years ago, just as microbial pathogens were rapidly evolving to evade the non-specific immune responses, our ancestors responded by co-evolving pathogen-specific immune responses – the *acquired* or *adaptive* arm of immune defence. The two main cellular protagonists of the adaptive immune defence are the B and T lymphocytes. Specificity is achieved through thymus-derived T lymphocytes that express T cell receptors (TCRs), and bone marrow-derived B lymphocytes that express B cell receptors (BCR), each recognizing unique molecules produced by pathogens, referred to as antigens. One of the challenges of the adaptive immune system is to eradicate foreign pathogens while minimally disturbing the host tissue. Hence, the ability to distinguish between *self* and *foreign* proved to be of utmost importance in directing immune effector mechanisms.

In 1901, Paul Ehrlich was the first to propose the concept of immune attack against self (autoimmunity) and tolerance mechanisms that protect the body against it. His "*horror autotoxicus*" theory envisioned that individuals produce immune cells specific for any imaginable antigen and that cells specific for the body's own elements ("*autotoxins*") would be "*dysteleogic*" and not produced (Erhrlich, 1901). Subsequently, Burnet and Fenner postulated that there was a temporal window early in embryonic life where the immune system may tolerise cells that are foreign to the host (Burnet and Fenner, 1948). This paradigm was suggested following Owen's observations of two types of non-identical twin cattle; those that shared a haematopoietic system *in utero* were tolerant of blood cells from each other, while those who had not were not cross-tolerant (Owen, 1945).

Medewar then extended Owen's findings utilising his expertise as a transplant scientist investigating the effects of transferring allogenic blood cells from one mouse to another at different times after birth. Cells transferred within the first few days of life, but not later, rendered the recipient mouse tolerant to the donor antigen throughout life (Billingham et al., 1953). This was the first demonstration of highly specific tolerance to a foreign tissue that was encountered neonatally and triggered Burnet to published his

landmark *clonal selection theory of acquired immunity* with clonal deletion as a caveat to guard against "*horror autotoxicus*" (Burnet, 1959). The idea was that each lymphocyte has a receptor on its surface with specificity towards a particular antigen, and binding to this antigen results in clonal proliferation of only those cells within the T and B cell that have recognized their specific pathogen (Burnet, 1976; Talmage, 1957), a concept later proven experimentally (Nossal and Lederberg, 1958). Self-reactive "*forbidden clones*" are clonally deleted during development. These concepts and key experiments foreshadowed the discovery of autoimmune diseases and tolerance mechanisms.

Today, autoimmune diseases can be broadly classified into two: (i) Systemic autoimmunity directed towards systemic antigens with disease manifestation occurring at a variety of different sites in the body. Examples of this are rheumatoid arthritis (RA) and systemic lupus erythematosus (SLE); (ii) Organ specific autoimmunity directed towards tissue-specific antigens such as type 1 diabetes (T1D), psoriasis (PS), and multiple sclerosis (MS), inflammatory bowel disease (IBD) [which includes Crohn's disease (CrD) and ulcerative colitis (UC)], and celiac disease (CD). Collectively, autoimmune diseases affect 5-8% of the population but their etiology remains poorly understood. While it has been shown that individuals carrying genetic loci that alter tolerance mechanisms may be at higher risk of developing the disease than those not carrying these alleles, current knowledge of the genetic contributions fail to account for the development of autoimmune diseases. The challenge to understand these diseases are further complicated by the heterogenous clinical presentation, variable timing of onset and inconsistent target organs in patients carrying specific autoimmune-predisposing mutations.

To explain the complex genetics and heterogenous nature of autoimmune diseases, the work in this thesis tests a *multistep model* for autoimmune disease progression, whereby combined inherited or somatic deficiencies in two or more tolerance mechanisms must cooperate. This introduction section will review lymphocyte development, tolerance mechanisms controlling self-reactive cells and the spectrum of autoimmune diseases

that arise from genetic defects throughout this process. The focus will be on T cells, although similar concepts could be applied to the B cell counterparts.

1.2 T cell development

A schematic of T cell development in Fig. 1.1 (adapted from (Miller, 2011)) accompanies this section. T cells originate from haematopoietic stem cells (HSC) in the bone marrow (Wu et al., 1991). Hereafter, common lymphoid progenitor cells (CLPs) from the bone marrow migrate to the thymus, a bi-lobe lymphoid organ above the heart, where the cells undergo further maturation processes (Miller, 1959, 1961). The importance of the thymus in T cell development is illustrated by the abolishment of T cells in both mice and humans due to congenital deficiencies in the thymic epithelium when the *whn* gene is mutated (Frank et al., 1999). In the thymus, HSCs develop into common lymphoid progenitors (CLPs) and progressively acquire the characteristic feature of a T cell – the unique T cell receptor (TCR) that determines their specificity. The TCR is a disulphide-bonded heterodimeric glycoprotein composed of a combination of either an α (alpha) and β (beta) chain or a δ (delta) and γ (gamma) chain (Havran and Allison, 1988). The αβ T cells are essential mediators of antigen-specific immunity, while γδ T cells are directed towards early immunity and surveillance of microbial and non-microbial tissue stress (Hayday, 2009; Hein and Mackay, 1991). The remainder of the section will focus on the αβ T cells.

Entering the thymus via the cortico-medullary junction, the CLPs establish themselves in the subcapsular zone in the cortex and begin development into a functional T cell defined by several stages based on the expression of CD4 and CD8 co-receptors – $CD4^-$ $CD8^-$ double negative (DN), $CD4^+CD8^+$ double positive (DP) and $CD4^+CD8^-$ or $CD4^-$ $CD8^+$ single positive (SP) stages (Owens et al., 1987). Two additional markers, CD25 and CD44 further segregate the DN thymocytes into four distinct stages: DN1 ($CD25^-$ $CD44^+$), DN2 ($CD25^+CD44^+$), DN3 ($CD25^+CD44^-$) and DN4 ($CD25^-CD44^-$) (Godfrey et al., 1993; Nikolic-Zugic, 1991; Pearse et al., 1989). The DN1 early thymic precursors originate from multipotent progenitor stem cells (CLPs) from the bone marrow with the capacity of developing into dendritic, natural killer or myeloid cell lineages (Bell and Bhandoola, 2008; Porritt et al., 2004). These cells gradually lose their multipotency to

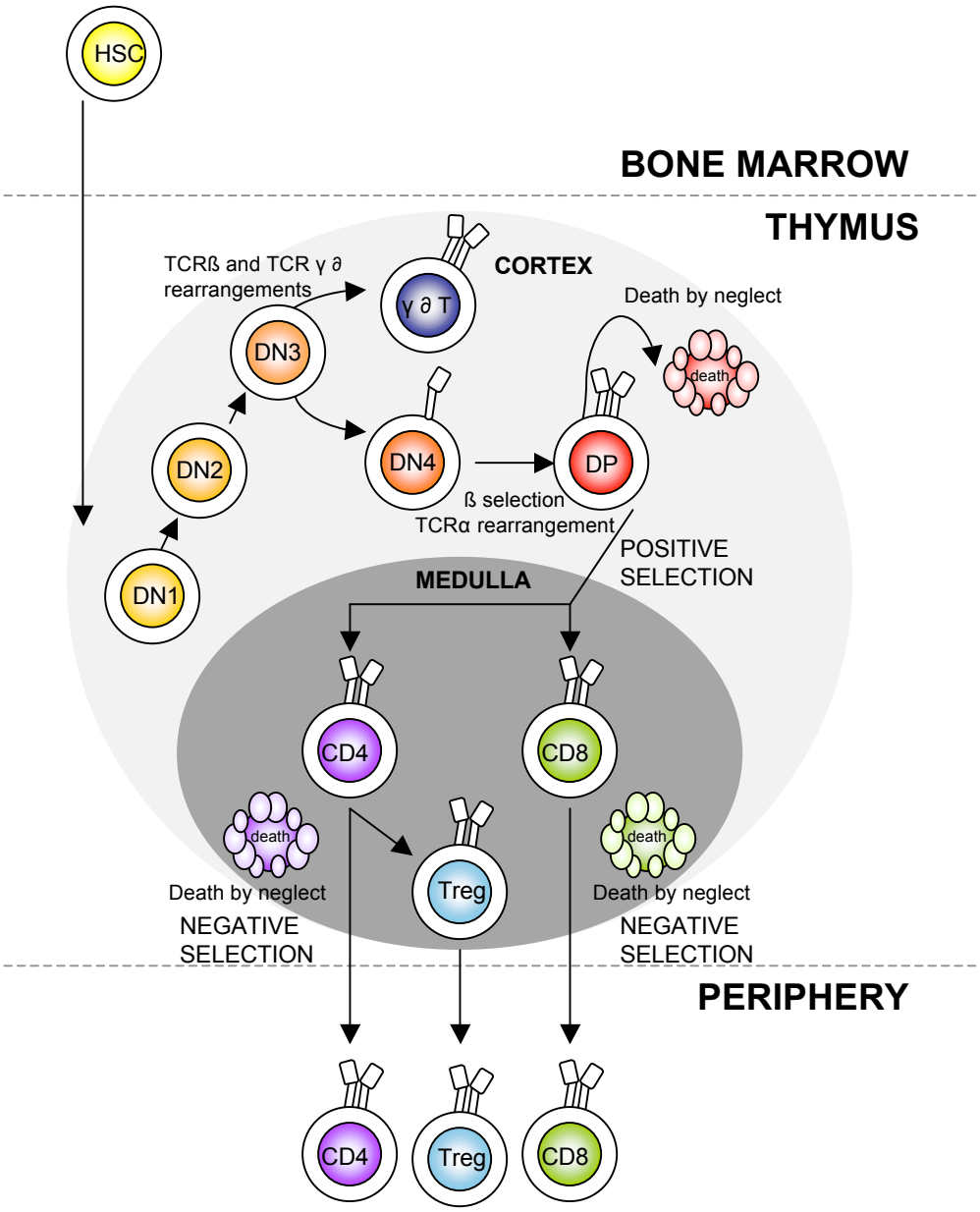

Figure 1.1. Schematic overview of αß T cell development.
Figure illustrating the expression of key developmental markers, anatomical location and major differentiation events (ß selection, negative selection and positive selection) in the thymus. HSC: haematopoietic stem cells; DN: double negative; DP: double positive. Figure adapted from Miller, 2011b.

form distinct T cell precursors that are charaterised by additional expression of the Kit^{hi} surface marker.

At the DN2 stage, the cells begin the construction of a TCR. The uniqueness or variability of the TCR is an important feature of adaptive immunity as the diversity of the TCRs within an individual ultimately determines the ability to recognise and counteract an antigen. Diversity is achieved by the generation of the α and β chains by somatic recombination of non-contiguous variable (V), and joining (J) gene segments, with an additional diversity (D) segment in the β chain, assembled together in a single functional reading frame (Fig. 1.2). Rearrangement of these gene segments generates a functional VDJ_β exon that is transcribed and spliced to join C_β, and the resulting mRNA is translated to yield the β chain. The human β chain genes are located on chromosome 7 (position 7q35) and comprise of 54 *TRBV* elements, 2 *TRBD* elements, 13 *TRBJ* elements and 2 *TRBC* genes (Miles et al., 2011). VDJ recombination can rearrange these 71 genes into 2808 unique β-chain VDJC recombinations. The mouse β chain is encoded on chromosome 6 from 22 *Trbv* elements, 2 *Trbd*, 11 *Trbj* and 2 *Trbc* genes, giving rise to a possible 968 combinations (Miles et al., 2011).

Recombination at the TCR locus requires the collaborative function of several genes. A complex of two proteins encoded by the *recombination activating genes* (*Rag*), *Rag*1 and *Rag*2, recognises the coding sequence that will be joined and introduces double stranded breaks between the V(D)J gene segments, forming DNA hairpins. These double stranded breaks are repaired by non-homologous end joining proteins, such as DNA Ligase IV, DNA-dependent protein kinase, Ku (Ku70:Ku80 heterodimer that associates with DNA-PK) and Artemis. Accordingly, inherited deficiency of any of these proteins in mice and humans blocks this process and precludes lymphocyte development, resulting in severe combined immune deficiency (Li et al., 2005; Mombaerts et al., 1992; Shinkai et al., 1992). The *combinatorial diversity* from recombined genes fragments is further enhanced by the addition of random non-template-dependent (N-nucleotides) or palindromic (P-nucleotides) by terminal deoxynucleotidyl transferase at joints between each gene segment (*junctional diversity*)

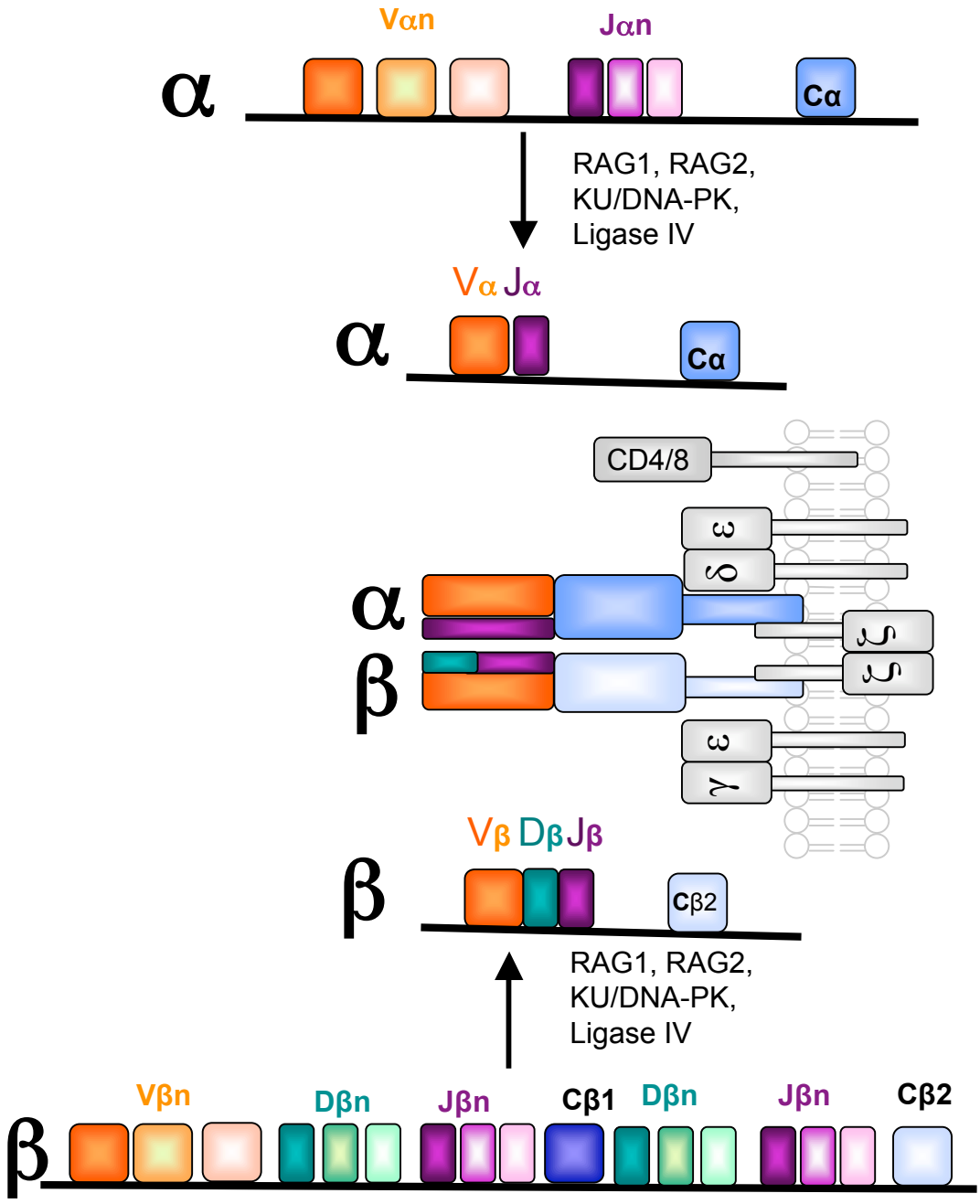

Figure 1.2. TCR α and ß-chain rearrangement and expression.
The TCR α and ß-chain genes are composed of discrete gene segments joined by somatic recombination during T cell development. The TCRα chain is made out of somatic recombination to from the VJα exon that is subsequently joined to Cα (upper). The TCRß chain is made out of somatic recombination to from the VDJß exon that is subsequently joined to Cß (lower). The α and ß-chains pair to form the a functional TCR. The TCR is expressed on the T cell surface together with co-signaling molecules CD3γδεζ and co-receptors CD4 and CD8 .

prior to joining, and by the variable position of the cleavage and joining of the V, D and J elements.

By the start of the DN4 stage, each T cell precursor expresses either a pre-αβTCR (TCRβ chain paired with an invariant preTα) or a γδTCR on the cell surface (Hayes and Love, 2007; von Boehmer, 2005). As the pre-αβTCR does not possess cytoplasmic signalling domains, it collaborates with the invariant CD3 chains, delta (δ), epsilon (ε), gamma (γ) and zeta (ζ) for intracellular assembly, surface expression and signalling (Fig. 1.2). Signals via the pre-αβTCR selects successful functional V(D)J recombination of the *Trb* locus – a process termed β-selection. Having established a functional *Trb* rearrangement, recombination proceeds to the *Tra* locus encoding the alpha chain, and the cell proceeds to the DP stage. Similar to the *TRB* locus, the human *TRA* locus on chromosome 14 (position 14q11.2) houses multiple genes - 47 *TRAV* genes, 57 *TRAJ* genes and a single *TRAC* gene potentially resulting in 2679 unique α-chain VJC gene combinations. The mouse α chain locus on chromosome 14 houses 73 *Trav* genes, 38 *Traj* and 1 *Trac* genes, giving rise to a possible 2774 combinations. Merging all the α- and β-chain gene combination produces an estimate of 7 522 632 and 2 685 232 possible gene combinations in humans and mouse, respectively (Miles et al., 2011). Collectively, coupling *combinatorial* and *junctional diversity*, the theoretical estimate of TCRαβ diversity amounts to 10^{15} genetically unique receptors (Davis and Bjorkman, 1988), albeit humans and mice only contain a maximum of 10^{12} and 10^{8} TCRαβ cells, respectively. Experimentally, diversity in the periphery is estimated to be even lower – 2 $x10^{7}$ for humans (Arstila et al., 1999) and $2x10^{6}$ for mouse repertoires (Casrouge et al., 2000). This constraint is attributed to the vigorous thymic positive and negative selection processes ensuring the TCR on emigrating T cells binds weakly to self peptides bound to self-MHC.

The DP cells acquire the expression of the chemokine CCR4 and CCR7 and migrate to the chemotactic gradient in the thymic medulla (Laan et al., 2009). The cells are retained for several days to complete the transformation from DP to SP cells. While continuous V-Jα recombination occurs in DP cells, the thymocytes test the resulting TCRαβ receptors for binding to self-peptides presented on major histocompatibility

complex molecules (MHC) displayed on thymic cortical epithelium. The MHCs encode *human leukocyte antigens* (*HLA*) genes in human and *H2* genes in mice. At this stage, each TCRαβ comprises a heterodimer bearing six highly variable complementarity determining regions (CDRs)– CDR1, CDR2 and CDR3 for the α-chain and β-chain. Architecturally, the CDR1 and CDR2 loops are germline encoded within the TRAV and TRBV elements and largely fix the TCR to the MHC. On the other hand, the CDR3 loops are hypervariable as they lie across the V(D)J junctions, engaging with the solvent-exposed chains of the MHC-bound peptide (Rudolph et al., 2006).

The strength and specificity of TCR binding to self peptide-MHC (pMHC) complexes (pMHC) dictates the fate of each DP thymocyte. High-affinity binding results in elimination or deletion of the potentially autoreactive cells by a process termed negative selection, primarily at the SP stage but also at the DP stage. Conversely, low affinity binding rescues the cells from programmed cell death and results in further differentiation, allowing the cells to acquire functional competence and lineage differentiation to either CD4 or CD8 single positive (SP) cells. This process is called positive selection. Cells with TCRs that bind weakly to self-peptides presented by MHC Class I (MHC I) are positively selected into the cytotoxic CD8SP lineage, while cells that recognise peptides bound to MHC Class II (MHC II) become helper CD4SP cells (Cosgrove et al., 1991; Zijlstra et al., 1990). It is also possible for TCRs with affinities for self-pMHC at the high end of the positive selection range to induce the FoxP3 transcription factor, causing the cells to differentiate into CD4SP natural T regulatory (nTreg) cells (Josefowicz and Rudensky, 2009). Rearrangement of the *Tra* loci does not stop until successful positive selection occurs, giving the thymocyte multiple chances to undergo recombination events progressing from the 5' to 3' of the Jα loci before the allele is exhausted. As continuous TCRα rearrangement is only halted when the TCR binds to an intrathymic ligand (Borgulya et al., 1992), all mature αβ T cells contain two rearranged TCRα alleles and 30% of such cells have two productive TCRα rearrangement (Casanova et al., 1991). Out of the 30%, only 10% of T cells are estimated to express dual-TCRα on the cell surface as there are unequal preferences for certain TCRα to pair with TCRβ (Heath et al., 1995; Padovan et al., 1993; Saito et al., 1989).

Ninety percent of cells at the DP stage interact poorly with pMHC and are condemned to die by neglect. The transcription factors involved in CD4 or CD8 lineage commitment are thymus selection–associated high-mobility group box factor (Tox), c-Myb and GATA-binding protein 3 (GATA3) which induce T-helper inducing POZ-Kruppel factor (ThPOK or Zbtb7) that is required for CD4 lineage commitment (Aliahmad and Kaye, 2008; Collins et al., 2009; Pai et al., 2003; Wang and Bosselut, 2009). ThPOK and Runx3 (the CD8 lineage commitment transcription factor) form a negative regulatory loop, in which they mutually prevent the expression of each other, resulting in lineage commitment (Collins et al., 2009).

For the committed CD4SP and CD8SP cells to egress the thymus, the cells need to lose the CD69 thymic retention signal and gain expression of the sphingosine-1-phosphate receptor 1 (SIP_1) receptor for blood-borne chemotactic sphingolipids that promotes thymic egress, and gain expression of the lymph node homing receptor, L-selectin or CD62L (Weinreich et al., 2009). CD4 lineage cells can continue to mature in the periphery, assuming either T helper 1 (T_H1), T helper 2 (T_H2) (Mosmann et al., 1986), T helper 17 (T_H17) (Stockinger and Veldhoen, 2007), follicular T helper (T_{FH}) (Vinuesa et al., 2005b) and T regulatory (T_{reg}) (Wing and Sakaguchi, 2010) identity distinguished based on the transcription profiles, cytokines secreted and effector pathways induced as seen in Table 1.1. The CD8 cells directly kill host cells infected with viruses, intracellular bacteria and protozoa by secreting degradative enzymes or inflammatory cytokines and cell-to-cell contact-dependent signalling. The end result of this developmental process is a T cell repertoire with enormous diversity in TCRs capable to responding to any given antigen – *functional diversity*.

Table 1.1. The CD4 subsets of the immune system

Subset	Master transcription factor	Cytokines	Effector pathways	Physiological roles
T_H1	T-bet	IFNγ, IL-2, TNFβ	Inflammation, machophage activation, opsonising IgG2a and IgG3 antibodies	Destruction of intracellular pathogens

T_H2	GATA3	IL-4, IL-5, IL-13	Eosinophil activation, neutralising IgE and IgG1 antibodies	Destruction of extracellular pathogens
T_H17	RORγt	IL-17, IL-23	Inflammation, neutrophil activation	Destruction of extracellular bacteria and fungi
T_{FH}	Bcl-6	IL-21	Germinal centre reactions, high affinity long-lived antibodies	Providing help for germinal centre B cells to produce high affinity antibodies
T_{reg}	FoxP3	IL-2, IL-10, TGFβ	Suppression of self-reactive T cells in the priphery	Maintenance of peripheral T cell tolerance

1.3 T cell tolerance

The random process of somatic recombination that generates the *functional diversity* in the T lymphocyte repertoire brings with it a fundamental dilemma – the generation of self-reactive T lymphocytes. This dilemma is exacerbated by the fact that positive selection is designed to ensure all TCRs are at least weakly self-reactive, presumably to provide maximal sensitivity to one or a few foreign peptides at the outset of an infection (Ebert et al., 2010). Cells whose TCR binds too strongly to self-pMHC nevertheless have the potential to result in a T cell-mediated immune response against crucial self-targets, causing an autoimmune disease. Elimination and deletion of these self-reactive T cells would have been evolutionarily necessary. A number of strategies have evolved to weed out high risk self-reactive T lymphocytes while still preserving the repertoire diversity of weakly self-reactive T cells. These strategies can be divided into mechanisms which occur during development in the thymus (central tolerance) and mechanism controlling the reactive cells that evade deletion in the thymus and escape to the periphery (peripheral tolerance).

1.3.1 Central tolerance

1.3.1.1 Clonal deletion

Burnet was the first to envision that lymphocytes expressing self-antigen specific receptors would be deleted during their development (Burnet, 1959). Later, when self-

MHC restriction of T cells was discovered by Zinkernagel and Doherty and shown to be acquired during their development in the thymus (Zinkernagel and Doherty, 1974a, b), it was predicted that the fate of thymocytes might depend on TCR signalling intensity, whereby strong signals correlated with high affinity and self-reactivity, while weak signals do not. This was experimentally confirmed by analysing the fate of thymocyte responses to stimulation by mouse superantigens or conventional pMHC complexes in transgenic mouse models. Mouse superantigens are proteins encoded by endogenous retroviruses that are inherited in the germline in many mouse strains. The superantigen proteins encoded by the mouse mammary tumour proviral genes *Mtv-8* and *Mtv-9* bind to the MHC Class II molecule I-E^k and bind with high affinity to TCRs that use the Vβ5, Vβ11 and Vβ17a segments (Woodland et al., 1990; Woodland et al., 1991a; Woodland et al., 1991b). Using a monoclonal antibody against Vβ17a TCRs, Kappler and colleagues demonstrated that Vβ17a usage was absent in the peripheral T lymphocyte population of I-E^k expressing mice, but present at the expected frequency amongst immature thymocytes (Kappler et al., 1987). This was the earliest evidence confirming that superantigen-specific T cells are deleted from the T cell repertoire. This observation was extended by studies in transgenic mouse models that express TCRαβ receptors with defined specificity for particular self-antigens (Berg et al., 1989; Kisielow et al., 1988; Pircher et al., 1989; Sha et al., 1988). For example, thymocytes that expressed a transgene-encoded TCRαβ with high affinity for MHC Class I D^b molecules presenting a peptide derived from the product of the *Smcy* gene, which lies on the Y-chromosome and comprises the male-specific HY antigen, were deleted in male mice but positive selected in females that expressed D^b but lacked the *Smcy* – derived peptide (Teh et al., 1988).

Key genes involved in the process of clonal deletion as shown in Fig. 1.3 (adapted from (Goodnow et al., 2005)). For both positive and negative selection to occur, self-peptides need to be presented in the context of the appropriate MHC to the developing thymocytes at the DP stage in the thymic cortex and the SP stage in the thymic medulla. In the cortex, self-peptides are displayed on the cortical thymic epithelial cells (cTEC), and TCRs that bind with weak affinity are triggered to cease α-chain rearrangement and increase homing receptors to progress towards the thymic medulla. The cell continues to interrogate its TCR on the surface by testing its affinity towards self-peptides

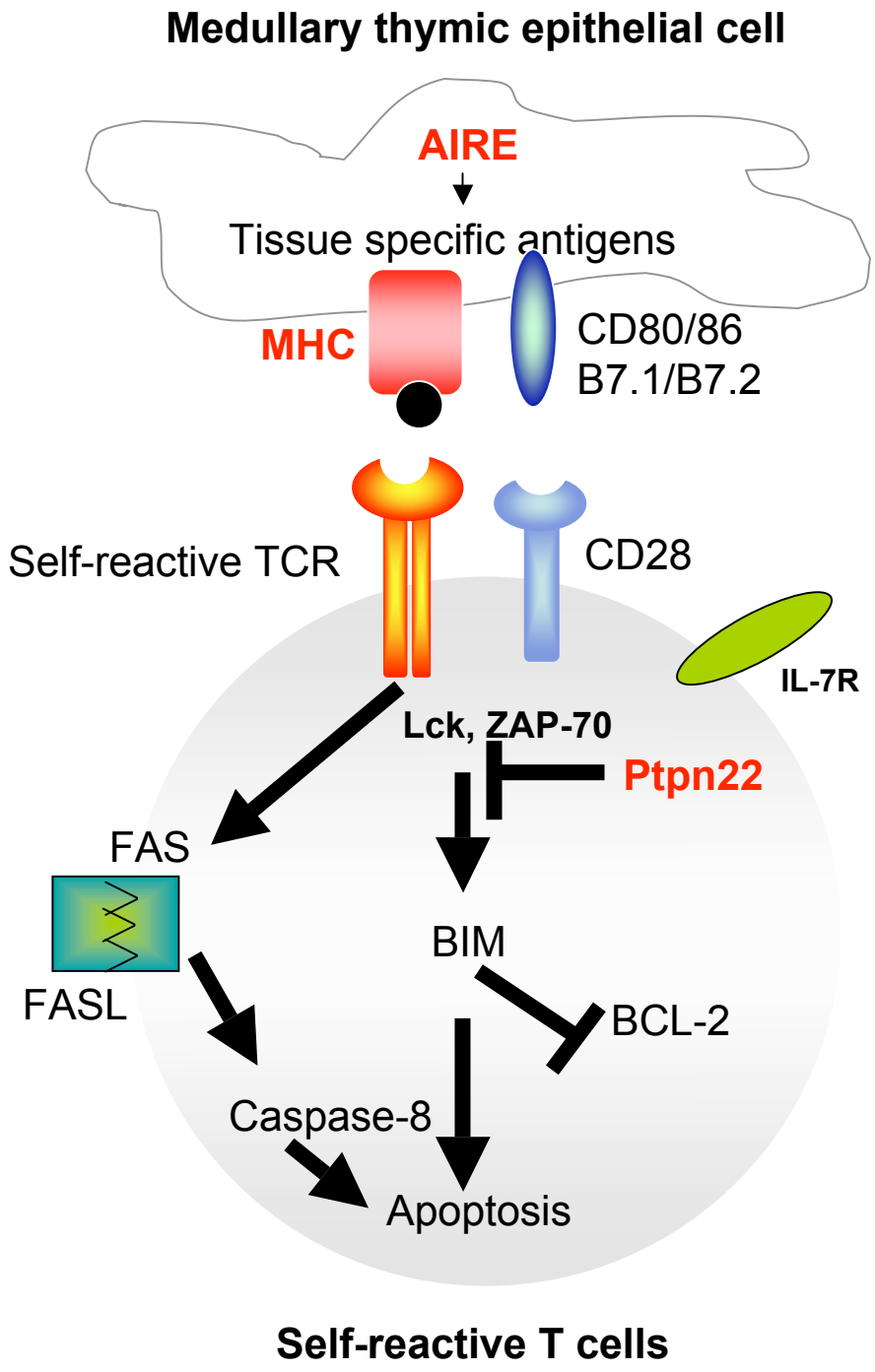

Figure 1.3. Key elements in the pathways for clonal deletion of self-reactive developing T cells

Elements italicised in red correspond to genes associated with human autoimmune diseases. Figure adapted from Goodnow, 2005.

presented in the context of MHC. Self-peptides are presented in the medulla by immature dendritic cells of haematopoietic origin (Steinman et al., 2003) and by medullary thymic epithelial cell (mTEC) that express a plethora of organ-specific transcripts essential for negative selection (Derbinski et al., 2008; Hanahan, 1998).

In a remarkable intersection of discoveries, the transcription factor *Autoimmune regulator* (*Aire*) was discovered to be mutated in people with the multi-organ autoimmune disorder autoimmune polyendocrinopathy syndrome type 1 (APS1) (Aaltonen et al., 1997; Consortium, 1997; Nagamine et al., 1997) and was found to direct the expression in mTECS of many of the mRNAs from otherwise organ-specific genes (Anderson et al., 2002; Derbinski et al., 2005). Consistently, mice that lack *Aire* fail to negatively select organ-specific T cells. This has been formally demonstrated in several TCR transgenic mouse models that have T cells recognising neo-self antigens. Using a transgenic model where hen-egg-lysozyme (HEL) is expressed under the control of the tissue-specific promoters, Liston and colleagues demonstrated that HEL-specific TCR^{3A9} CD4 cells fail to be deleted in *Aire*-deficient mice resulting in severe diabetes when the HEL antigen is coupled to the insulin promoter or thyroiditis when HEL is coupled to the thyroglobulin promoter (Liston et al., 2004a; Liston et al., 2003). Similarly, ovalbumin (OVA)-specific OTII CD4 cells escape deletion and cause infant-onset diabetes when the OVA gene is expressed by the insulin promoter in $Aire^{-/-}$ mice (Anderson et al., 2005) or *Aire* mice harbouring the G228W mutation (Su et al., 2008). Notably, the failure of thymic deletion was specific for organ-specific T cells as *Aire* showed no effect on thymic deletion when the antigen expression was driven by a systemic $H2^{k}$-promoter (Liston et al., 2004a) or when the antigen was made available via a virus-mediated infection (Kedzierska et al., 2010).

Besides the expression of the characteristic transcription regulator *Aire* and expression of tissue-specific antigens, the mTEC cells express T cell co-stimulatory molecules, such as CD80 (B7.1) and CD86 (B7.2), the ligand for the CD28 co-receptor that is present on T cells. CD28 costimulation was shown to enhance death of immature DP thymocytes in tissue culture (Punt et al., 1994). A role for this co-stimulatory signal in the process of negative selection was implied by mouse experiments where the CD80/CD86 molecules were missing or blocked on the mTECs. In such mice, self-

reactive TCRs were not deleted causing graft-versus-host-disease-like inflammation in the periphery (Gao et al., 2002; Laufer et al., 1996).

It is paradoxical that a single TCR can mediate two opposing fates of the thymocyte – positive selection and negative selection. It is clear that signalling events via the TCR are required for both processes but the machinery required for positive and negative selection may differ in several aspects to mediate these opposing outcomes. At the immunological synapse, p56 (Lck) and CD3ζ are recruited to the peripheral edge rather than the centre of the cell (Richie et al., 2002). The tyrosine kinase ζ-chain associated protein kinase of 70 kDa (ZAP70) is required for deletion, and SKG mice harbouring a spontaneous point mutation in the SH2 domain of ZAP70 have diminished negative selection in the HY-TCR transgenic model (Sakaguchi et al., 2003). The translation of the signal from the TCR also requires the growth factor receptor bound protein 2 (GRB2) (Gong et al., 2001) and the misshapen Nck interacting kinase related kinase (MINK) (McCarty et al., 2005). Strong but transient activation of the extracellular signal regulated kinase (ERK) via ras-guanyl nucleotide exchange factors, Sos and RasGRP1, is required for negative selection while low levels of sustained activation is required for positive selection (Mariathasan et al., 2001; Priatel et al., 2002). Further signals are relayed by the c-Jun NH_2-terminal kinase (JNK) (Rincon et al., 1998). The protein tyrosine phosphatase, non-receptor type 22 (PTPN22) is thought to regulate the strength of TCR signals and gain of function alleles weaken TCR signalling, potentially imparing the deletion of autoreactive T cells (Chuang et al., 2009).

At the distal end of the signalling pathway, the signals culminate in the activation of thymocyte death by two possible pathways: activating the Fas-dependent death receptor pathway or the Bim-dependent Bcl2-inhibited mitochondrial death pathway. The death receptor pathway is activated when members of the tumour necrosis factor receptor family that possess a death domain (such as Fas or CD95 or APO-1) bind to its corresponding ligand (such as Fas-ligand), triggering the formation of a death inducing signalling complex, promoting the activation of caspase-8. A series of studies performed by Kishimoto and Sprent demonstrated that *in vitro* stimulation of early SP thymocytes results in a Fas-independent apoptotic response at low antigen concentrations but a Fas-dependent response at high concentrations (Kishimoto and

Sprent, 1999a, b; Kishimoto et al., 1998). Similar studies have demonstrated this Fas-mediated deletion *in vivo* in transgenic DO11.10 mice (Kishimoto and Sprent, 1999a, b; Kishimoto et al., 1998). However, a partial loss of function mutation in Fas did not affect deletion in the HY-TCR transgenic model (Sidman et al., 1992) and absence of the caspase-8 apoptosis inducer did not affect negative selection (Salmena et al., 2003), opposing the view that the Fas-pathway is involved in thymic deletion.

The alternative apoptotic pathway is the Bim/Bcl-2 pathway. In this pathway, Bim antagonises pro-survival proteins including Bcl-2, Bcl_{XL} and Mcl-1, thereby releasing the pro-apoptotic proteins Bax and Bak to trigger release of cytochrome c from mitochondria, and culminating in the activation of caspase-9 required for deletion (Rathmell and Thompson, 2002). Bcl-2 overexpression and elimination of Bax/Bak has been demonstrated to inhibit the developmental death of autoreactive thymocytes specific for both superantigens (Rathmell et al., 2002; Strasser et al., 1991) and conventional antigens (TCR-HY transgenic system) (Strasser et al., 1994). Several studies have demonstrated that anti-CD3 mediated thymic apoptosis is exclusively Bim-dependent and independent of Fas. (Bouillet et al., 1999; Bouillet et al., 2002; Villunger et al., 2003). Most convincingly, Bim acts in a dose-dependent fashion, in that Bim heterozygous thymocytes have an intermediate effect on deletion (Bouillet et al., 2002), suggesting that Bim induction represents the point in the pathway where signal strength is translated into opposing decision of survival or apoptosis.

Deletion also involves induction of the Nur77, an orphan steroid receptor involved in the apoptotic pathway. Overexpression of a dominant negative Nur77 precludes apoptosis and thymic deletion *in vivo*, and loss of Nur77 prevents apoptosis (Cheng et al., 1997; Woronicz et al., 1994; Xue et al., 1997). The defective induction of Bim and Nur77 in the NOD mouse strain account for four of the diabetic susceptibility chromosomal loci (D1mit181, D2mit490, D7mit101, and D15mit229) in this strain (Liston et al., 2004b). The resistance of NOD thymocytes to deletion, thus, appears to be important autoimmune susceptibility contributor to a range of autoimmune manifestations in this strain (Kishimoto and Sprent, 2001; Lesage et al., 2002).

1.3.1.2 Limiting pro-survival signals

Another possible mechanism that could regulate self-reactive T cells is regulating the survival signals the T cells are exposed to, such as the pro-survival cytokine interleukin-7 (IL-7) (Barthlott et al., 2003; Marrack and Kappler, 2004). Under physiological conditions, IL-7 levels are low causing the cells to be in the interphase stage of cell division. However, when strong self-reactive TCR signals are triggered, the cells are forced to undergo transient proliferation that culminate in Bim-induced cell death (Strasser and Bouillet, 2003). In conditions where low numbers of lymphocytes are present, concentrations of pro-survival cytokine IL-7 increase, stimulating naïve T cells, including potentially self-reactive cells, into proliferation to fill up the empty niche. Hence, coupling the imbalance of the IL-7 survival cytokine with conditions of low T cell numbers (lymphopenia) may paradoxically induce an autoimmune disease. X-linked thrombocytopenia is a confounding blend of lymphopenia and autoimmunity caused by a mutations if the *WASp* gene (Villa et al., 1995). Another similar affliction is Omenn syndrome, a combination of limited T and B cell production and graft-versus-host-disease-like autoimmunity (Villa et al., 1998). Owing to partial loss-of-function variants in *Rag1*, *Rag2* and *Artemis* genes (Ege et al., 2005; Gennery et al., 2005), V(D)J recombination is impaired and T lymphocyte repertoire becomes highly restricted in TCR diversity (Santagata et al., 2000).

1.3.1.3 Inhibitory receptors

While negative selection could purge T cells with high affinity towards the autoreactive cells, fine-tuning the TCR signalling could control low affinity autoreactive cells. One essential component in this process is the inhibitory receptor CD5 (Pena-Rossi et al., 1999). CD5 contains a tyrosine-based inhibitory motif on its cytoplasmic tail that directly interacts with TCR signalling molecules such as SHP1, negatively regulating TCR activation (Perez-Villar et al., 1999). Self-reactive thymocytes increase the expression of CD5, tuning down the TCR signals (Wong et al., 2001). The regulation of signalling by CD5 receptor begins in the thymus and continues in the periphery (Smith et al., 2001).

1.3.2 Peripheral tolerance

As an alternative to Burnet's clonal deletion theory, other studies have articulated tolerance mechanisms that might act on mature lymphocytes, controlling self-reactive lymphocytes that escape negative selection. These can be broadly divided into: (i) *recessive* forms of tolerance – *cis*-acting tolerance that is intrinsic to the autoreactive cell or (ii) *dominant* tolerance – *trans*-acting tolerance processes that act extrinsically to control many different autoreactive cells.

1.3.2.1 Recessive cell intrinsic tolerance

One mechanism that regulates peripheral tolerance is the requirement for two signals to activate lymphocytes – TCR binding to peptide/MHC (signal 1) and CD28 binding to CD80 or CD86 (signal 2) (Fig. 1.4) (Bretscher and Cohn, 1970; Lafferty and Cunningham, 1975). Depending on the amount of peptide/MHC, self-reactive T cells are either not activated and remain ignorant or are induced to a state of anergy or non-responsiveness when antigen recognition occurs in the presence of signal 1 alone, without the co-stimulatory signal 2 (Kundig et al., 1996; Nossal, 1983; Schwartz, 1990, 2003). Such a mechanism may have evolved because antigen presenting cells (APCs) routinely present both foreign and self-peptides, meaning that antigen recognition alone is not sufficient to discriminate between self and non-self. Provision of the co-stimulatory signal occurs upon the reception by APCs of danger signals from pathogens that are sensed through innate immune receptors such as the Toll like receptors, which induces the expression of CD80/CD86 on APCs. The inhibitory receptor cytotoxic T-lymphocyte antigen 4 (CTLA-4) inhibits T cell activation by competing with CD28 for binding to the CD80/CD86 molecules, removing CD80 and CD86 from antigen presenting cells (Qureshi et al., 2011), and also by transmitting inhibitory signals to T cells that express CTLA-4 (Ravetch and Lanier, 2000; Sharpe and Freeman, 2002; Walker and Abbas, 2002). The importance of this inhibitory process is underscored by CTLA-4 deficient mice that display massive accumulation of self-reactive T cells in the peripheral lymphoid and non-lymphoid tissues (Tivol et al., 1995; Waterhouse et al., 1995).

When T cells are stimulated in the absence of co-stimulatory signal 2, this still allows

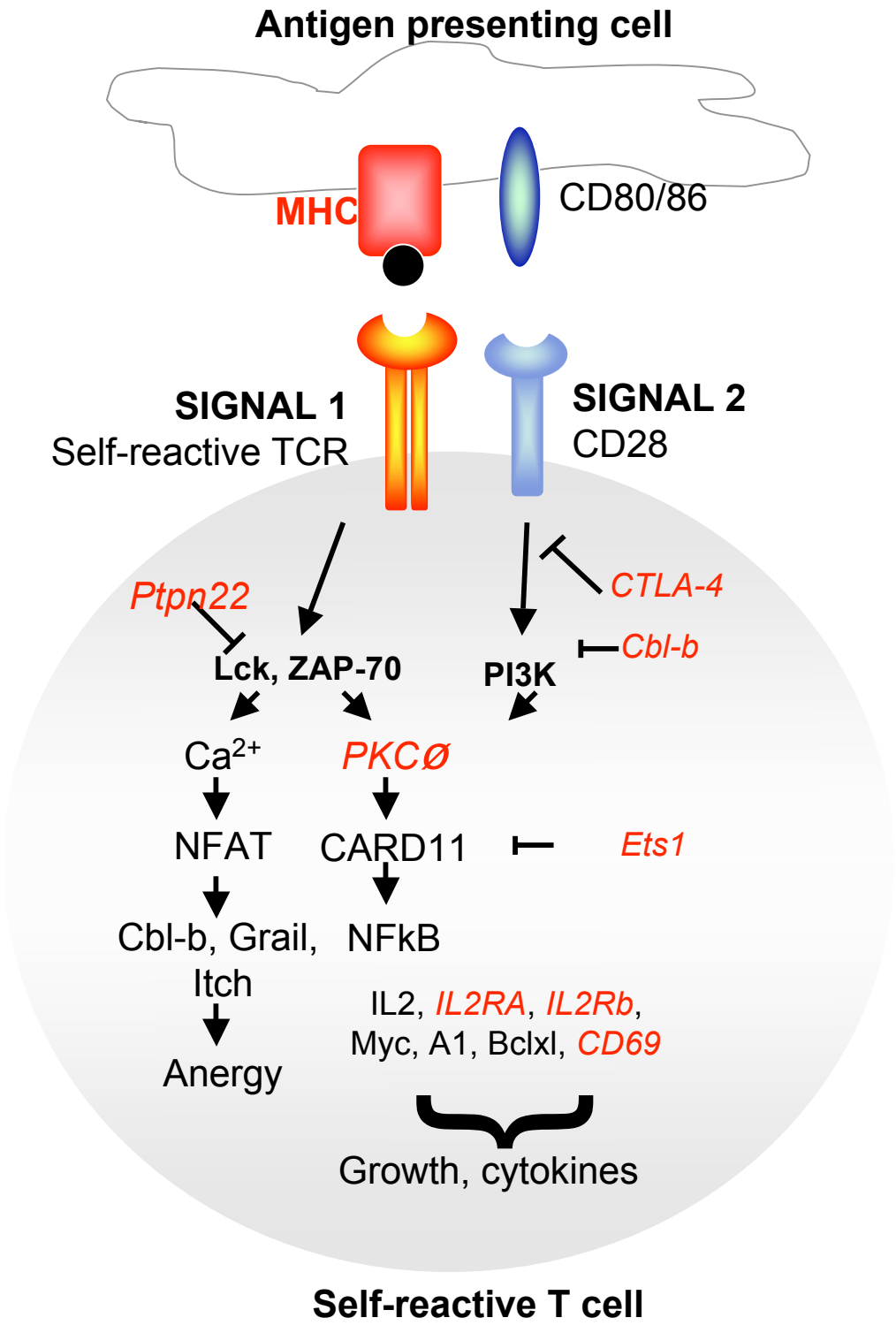

Figure 1.4. Key elements in the pathways for clonal anergy of peripheral T cells.

Elements italicised in red correspond to genes associated with human autoimmune diseases.

activation of the calcium-dependent nuclear factor of activated T-cells (NFAT) pathway unaccompanied by full activation of the AP-1 and NFkB pathways (Macian et al., 2002), inducing the expression of anergy associated genes including ubiquitin ligases such as *casitas B-lineage lymphoma b* (*Cblb*), *gene related to anergy in lymphocytes* (*Grail*), HECT-E3 ligase *Itch* and *Peli1* (Paolino and Penninger, 2009). These ubiquitin ligases bind target substrates, tagging them for protosomal degradation, alter intracellular trafficking of TCRs, trigger endocytosis or allosterically interfere with signaling (Anandasabapathy et al., 2003; Chang et al., 2011; Heissmeyer and Rao, 2004; Jeon et al., 2004; Liu, 2004). These processes render the T cells to a state of anergy or unresponsiveness.

The ubiquitin ligase Cbl-b targets downstream molecules of the TCR signaling pathway, notably ubiquitination of the p85 catalytic subunit of PI3K that alters its intracellular localization and prevents its interaction with CD28 and CD3ζ at the plasma membrane (Fang and Liu, 2001). Cbl-b thus inhibits Akt and PKCθ-mediated NFκB activation, and additionally, prevents Vav1-mediated cytoskeleton rearrangements required for receptor clustering and synapse formation (Krawczyk et al., 2000). In anergic T cells, Cbl-b upregulation occurs together with phospholipase c gamma (PLCγ) and protein kinase c theta (PKCθ) ubiquitylation indicating these two molecules to be crucial targets for Cbl-b anergic functions (Heissmeyer et al., 2004; Jeon et al., 2004). Mice deficient in *Cblb* develop mild autoimmunity and have a decreased threshold for T cell activation (Bachmaier et al., 2000; Chiang et al., 2000). Coupling *Cblb*-deficiency with a particular MHC haplotype causes diabetes in the Komeda diabetes prone (KDP) rat strain (Yokoi et al., 2002). When T cell deficient *c-cbl* (the homologue of *Cblb* expressed in the thymus) mice are crossed with $Cblb^{-/-}$ mice, double-deficient mice showed drastic weight lost by 12 (females) and 16 (males) weeks, accompanied by multi-organ specific autoimmunity in the heart, skin and liver (Naramura et al., 2002). In humans, genome wide association studies (GWAS) have associated a polymorphism in *CBLB* with multiple sclerosis in Sardinian (Sanna et al., 2010) and Italian populations (Corrado et al., 2010), although clarification the mechanism by which the specific CBL-B polymorphism affects autoimmunity in these disease would require further functional characterisation.

Self-reactive T cell proliferation could also be cut short by ensuring T cell death or apoptosis. Similar to the T cell death in the thymus, death could occur as a result of *Fas*-dependent pathway or *Bim*-dependent pathway. In general, the *Fas*-dependent pathway is crucial in aborting peripheral T cells that are have undergone chronic stimulation by antigens such as injection of cytochrome c into transgenic mice with an MHCII TCR (systemic self antigens) (Singer and Abbas, 1994) or in an influenza infection in a transgenic mice with an MHCII restricted hemagglutinin-specific TCR (chronic infection) (Sytwu et al., 1996). By contrast, the *Bim*-dependent pathway predominantly eliminates T cells that undergo transient or intermittent exposure to antigens, which frequently occurs in response to organs-specific antigens. For example, when HY-specific T cells recognising peripheral antigen encoded by the *Smcy* gene on the Y chromosome are introduced into male mice, the cells undergo a sequence of activation, proliferation, anergy and death in a *Bcl2* (*Bim* pathway)-dependent but *Fas*-independent manner (Teh et al., 1996). This same *Bcl2* (*Bim* pathway)-dependent deletion of self-reactive cells is also observed for OT-1 ovalbumin-specific CD8 cells that recognise the ovalbumin neo-self antigen in the pancreas (Kurts et al., 1996; Kurts et al., 1997b).

The importance of the *Fas*-dependent death receptor pathway is exemplified by studies of mouse models and humans deficient in molecules within the pathway. Two key mouse models that have been extensively studied are strains inheriting loss of function mutations, $Fas^{lpr/lpr}$ and $Fasl^{gld/gld}$ (Cohen and Eisenberg, 1991). Binding of Fas-ligand to its cognate receptor, Fas, activates a cascade of events that cumulates in cell death via apoptosis. In both the $Fasl^{gld/gld}$ and $Fas^{lpr/lpr}$ strains, homozygous disruption of this pathway results in extensive lymphoproliferation and high titres of autoantibodies (Krueger et al., 2003). A characteristic feature of the mice is the accumulation of unusual $CD3^+$ $CD4^-$ $CD8^-$ $TCR\beta^+$ $CD45R(B220)^+$ (double negative T, DNT) cells in the periphery (Takahashi et al., 1994; Watanabe-Fukunaga et al., 1992). These cells are thought to be cells that have been stimulated to undergo apoptosis but are unable to complete the process in the absence of CD95 or CD95-ligand (Steinberg, 1994). In skin allograft transgenic mice, wild-type (Priatel et al., 2001; Zhang et al., 2000) or $Fas^{lpr/lpr}$ (Ford et al., 2002) DNT cells have been shown to down-regulate the immune response by killing allogenic $CD8^+$ cells that expressed functional Fas but not $CD8^+$ cells that

express non-functional Fas. The inability to kill the activated T cells is suggested to contribute to the development of autoimmunity in the *Fasl*$^{gld/gld}$ and *Fas*$^{lpr/lpr}$ mice. Mutations in *Fas* and *Fas-ligand* in humans result in a similar syndrome called autoimmune lymphoproliferative syndrome (ALPS) or Canale-Smith syndrome that includes systemic autoimmunity and accumulation of $CD3^+$ $CD4^-$ $CD8^-$ T cells (Fischer et al., 2000; Fisher et al., 1995).

Another E3 ubiquitin ligase that regulates peripheral tolerance is Roquin (Rc3h1). It regulates a subset of T cells, the T_{FH} cells. T_{FH} cells home to the germinal centre and function to provide help to germinal centre B cells. T_{FH} cells are characterized by the expression of the transcription factor Bcl-6 (Johnston et al., 2009; Nurieva et al., 2009; Yu et al., 2009), and the co-stimulatory molecules inducible co-stimulator receptor (ICOS) and CD134 (Walker et al., 2000). Although complete loss of *Roquin* results in embryonic lethality (Bertossi et al., 2011), the importance of this ubiquitin ligase in preventing autoimmunity is demonstrated by its identification and characterization in the *sanroque* mouse model. *Roquin*$^{san/san}$ mice carry a single point mutation in the *Roquin* gene. Roquin acts as a repressor to the inducible co-stimulator receptor, ICOS. The *Roquin*$^{san/san}$ mice exhibit hyperactivation of follicular T cells that are specialized in delivering signals to germinal centre B cells, produce high levels of autoantibody and display high incidences of nephritis, phenotypes similar to the human systemic lupus erythematosus (Linterman et al., 2009; Vinuesa et al., 2005a). *Roquin*$^{san/san}$ mice also have accelerated autoimmune diabetes in a transgenic mouse model due in part to excessive anti-islet autoantibody production (Silva et al., 2011).

1.3.2.2 Dominant cell extrinsic tolerance

The notion of dominant tolerance first arose from observations that neonatally thymectomised mice developed organ-specific autoimmunity that was preventable by adoptive transfer of splenocytes from adult mice (McIntire et al., 1964; Nishizuka and Sakakura, 1969). The initial description of "*suppressor cells*" that could prevent autoimmunity received surges of interest over the next decade and only gained popularity after Shimon Sakaguchi's characterization of the T "*regulatory cells*" (Treg) defined by the surface markers $CD4^+$ and $CD25^+$ (the interleukin-2 receptor alpha chain) (Sakaguchi et al., 1995). The population suppresses T cell proliferation *in vitro* and

prevents autoimmunity *in vivo* (Sakaguchi et al., 1995). The Treg population was further defined and characterised upon the discovery of the master transcription factor for the population, the X-linked forkhead box P3 (FoxP3) that causes severe autoimmunity when mutated in *scurfy* mice (Fontenot et al., 2003; Hori et al., 2003; Khattri et al., 2003). Similar to the mouse counterparts, children with defects in the *Foxp3* gene develop Immunodeficiency, Polyendocrinopathy, and Enteropathy, X-Linked Syndrome (IPEX) (Bennett et al., 2001; Brunkow et al., 2001; Wildin et al., 2001) characterized by watery diarrhea, eczematous dermatitis, and endocrinopathy, typically beginning in the first year of life (Gambineri et al., 2003; Nieves et al., 2004; Wildin et al., 2002).

The Foxp3-expressing cells can originate as natural Treg (nTreg) cells generated in the thymus (Buckner and Ziegler, 2008). Alternatively, naïve CD4 cells can be converted into $FoxP3^+$ inducible Treg (iTreg) cells *in vitro* upon stimulation with transforming growth factor beta (TGFβ) for human and mouse cells or retinoic acid for mouse cells, although it is unclear if these cells could mediated suppressive ability *in vivo* (Coombes et al., 2007; Lathrop et al., 2011; Tran et al., 2007; Walker et al., 2005). $FoxP3^+$ cells mediate suppression either via cell-contact dependent suppression or cytokine dependent suppression to modulate the cytokine microenvironment, metabolically disrupt the target cell, changing the dendritic cell activating capacity, and cytolysis (Sakaguchi et al., 2010; Shevach, 2009; Vignali et al., 2008).

All tolerance mechanism, both *dominant* and *recessive,* can be envisaged to work together to prevent robust autoimmunity, but very little is known about how defects in one tolerance mechanism may or may not be compensated by activity of another. Since multiple genes govern each tolerance mechanism, it seemed logical that mutations in key tolerance genes would lead to autoimmunity. The genetic basis of autoimmunity is described in the following section.

1.4 Genetic basis of autoimmune disease

To examine the genetic contribution to disease susceptibility, genetic epidemiologists have used several measures – examining the concordance of a disease in monozygotic twins compared to that of dizygotic twins, the extent of familial clustering, and examining the increased risk of the disease for a family member of a patient compared to that of the general population.

By these measures, there is a strong inherited predisposition to most autoimmune diseases, with 30-70% concordance in identical twins (Hyttinen et al., 2003), due in most cases to cumulative effects of variants in MHCs and other mostly unknown genes (Barrett et al., 2009; Todd and Wicker, 2001; Wandstrat and Wakeland, 2001). It is not known if these complex genetic factors disrupt a single tolerance mechanism, compromise several cooperating mechanisms, or act at other levels such as inflammatory responses to microbes. Many different cellular mechanisms of actively acquired self-tolerance described in section 1.3, including clonal deletion, clonal anergy and regulatory T cell differentiation are known, but it is not known if these mechanisms act in series as failsafes for one another such that autoimmune disease would require multiple mechanisms to fail (Goodnow, 2007) or if they act independently to protect different tissues from autoimmunity. To put it simply, it is currently unknown whether the compounding of inherited defects in discrete tolerance mechanisms will precipitate autoimmune phenotypes that are simply the sum of each individual defect or will exhibit highly cooperative behaviour to produce emergent autoimmune phenotypes. Understanding how the individual mechanisms fit together for robust tolerance is critical for interpreting patterns of genetic and phenotypic variability in human autoimmune disease.

1.4.1 Monogenic autoimmune disease: Autoimmune polyglandular syndrome 1 as an example

Major advances in understanding the pathogenesis of autoimmune disease have been made by studying monogenic autoimmune diseases. In these experiments of nature, single inborn errors resulting in rare autoimmune diseases are inherited in a simple

Mendelian fashion. Examples of these disease, and corresponding mouse models that have been discussed in section 1.3 are illustrated in Table 1.2. Studies in mice have revealed a great deal aiding the understanding of autoimmune disease pathogenesis. The remainder of the section will focus on *Aire*-mediated autoimmunity, highlighting key principles of autoimmune disease pathogenesis and puzzling disease-traits.

Table 1.2. Single gene defects associated with autoimmune diseases. Table adapted from (Rioux and Abbas, 2005).

Gene	Human disease	Mouse model	Mechanism of autoimmunity
Autoimmune regultor (*Aire*)	Autoimmune polyendocrine syndrome type I (OMIM: 240300) (2007; Nagamine et al., 1997)	Knockout (Anderson et al., 2002; Ramsey et al., 2002b)	Decreased expression of self-antigens in the thymus, resulting in decreased negative selection.
Fas/Fasl	Autoimmune lymphoproliferative syndrome, Canale-Smith syndrome (OMIM: 601859) (Fischer et al., 2000; Fisher et al., 1995)	Lpr/lpr, gld/gld (Cohen and Eisenberg, 1991)	Failure of apoptotic death of self-reactive T and B cells.
FoxP3	Immunedysregulation, polyendocrinopathy and enteropathy, X-linked (OMIM: 304790) (Bennett et al., 2001)	Knockout (Fontenot et al., 2003; Hori et al., 2003; Khattri et al., 2003)	Decrease generation of CD4+CD25_ regulatory T cells

Mutations in the *AIRE* gene have been identified as the cause of autoimmune polyglandular syndrome type 1 (APS1) or polyendocrinopathy-candidiasis-ectodermal dystrophy (APECED). Clinically, three abnormal features are most frequently observed in this syndrome: (i) chronic mucocutaneous *Candida albicans* infections that are now known to be due to autoimmune neutralization of IL-17 (Kisand et al., 2010; Puel et al., 2010) ;(ii) chronic hypoparathyroidism; (iii) autoimmune adrenal insufficiency (Betterle et al., 1998), a clinical triad that was first reported in 1946 (Leonard, 1946) and defined in further detail by Peerhentupa (Perheentupa, 2006). A patient must present with at

least two components of the clinical triad to be diagnosed with APECED. Beyond these features, affected individuals frequently exhibit secondary symptoms including autoimmune endocrinopathies (hypergonadotropic hypogonadism, insulin-dependent diabetes mellitus, autoimmune thyroid diseases, and pituitary defects), autoimmune or immune-mediated gastrointestinal diseases (chronic atrophic gastritis, pernicious anemia, exocrine pancreatic insufficiency and malabsorption), chronic active hepatitis, autoimmune skin diseases (vitiligo and alopecia), ectodermal dystrophy, keratoconjunctivitis, immunologic defects (cellular and humoral), asplenia, and cholelithiasis (Betterle et al., 1998). The disease is very heterogeneous as the secondary clinical features vary from patient to patient and even between two siblings that inherit AIRE deficiency in the same genetic lesion (Ishii et al., 2000). This heterogeneity in clinical picture is also a common feature in many other autoimmune diseases.

Besides the highly variable features of AIRE-deficiency, another feature of the disease is the presence of a latent phase during the development of the disease. Typically, the APS1 disease unfolds in a stepwise manner within the first 20 years of life, while secondary features appear until the fifth decade of life (Table 1.3). The first symptom, typically mucocutaneous candidiasis appears in childhood before the age of five, followed by chronic hypoparathyroidism within the first decade of life, and later by autoimmune adrenal insufficiency or Addison disease. In addition to these characteristics, the patients typically present with tissue-specific autoantibodies correlated with the manifestation of the secondary features (Table 1.3).

Table 1.3. Table shows the clinical features in APS1 patients, average age of onset and putative organ-specific autoantibody associated with particular symptoms. * indicates primary clinical characteristics. # indicates features shared with the mouse models. Table adapted from (Husebye et al., 2009; Kisand et al., 2011; Marx et al., 2010; Perheentupa, 2006; Peterson and Peltonen, 2005).

Manifestation	**Mean onset age in years±SD**	**Prevalence**	Related autoantibodies (% prevalence)

		At 10 years of age (%)	At 30 years of age (%)	
Chronic mucocutaneous candidiasis*	6±6	70	98	IL-22 (91%), IL-17F (75%)
Chronic hypoparathyroidism*	8±7	66	85	NACHT leucine-rich-repeat protein 5 (49%)
Autoimmune adrenal insufficiency*	12±8	40	78	steroid 21 hydroxylase (66%), steroid 17-α-hydroxylase (44%), side-chain cleavage enzyme (52%)
Ovarian failure#	15±7	–	36	
Diabetes mellitus	27±15	1	27	glutamic acid decarboxylase (37%), protein tyrosine phosphatase like protein(7%)
Exocrine pancreatic failure	19±13	7	14	
Testicular failure#	28±10	–	25	TSGA10 (8%)
Hypothyroidism	27±10	1	24	thyroglobulin (36%), thyroid peroxidase (36%)
Gastritis/pernicious anemia#	22±12	1	20	tryptophan hydroxylase (45%), histidine decarboxylase (37%)
Asplenia	Early to late	10	20	
Autoimmune hepatitis	7±4	14	18	cytochrome P450 1A2 (8%),
Chronic diarrhea	12±5	10	18	
Ectodermal manifestations^				
Alopecia	12±7	15	38	tyrosine hydroxylase (40%)
Vitiligo	15±11	11	30	SRY (sex determining region Y)-box 9/10 (22%), aromatic L-amino acid decarboxylase (51%)
Keratopathy	6±4	18	24	
Dental enamel dysplasia	Adult teeth only		75	
Nail dystrophy			50	
Myasthenia gravis				acetylcholine receptor (<5%)

In a *tour de force* of functional genomics, Aaltonen and colleagues performed linkage studies on a cohort of Finnish patients, mapping the disease-locus to a region on chromosome 21q22.3 (Aaltonen et al., 1997). Two independent groups narrowed down the region to a single locus on human chromosome 21 using positional cloning strategies. The 545 amino acid gene encoded in this locus was termed the *AutoImmune REgulator* (*AIRE*) gene. Nagamine and colleagues isolated two common mutations (R257X and K83E) in the *AIRE* gene in the Swiss and Finnish cohort of APS1 patients (Nagamine et al., 1997), while the Finnish-German APECED Consortium identified an additional 4 mutations (Consortium, 1997). Currently, more than 60 different missense mutations have been localized in the *AIRE* gene in APECED patients (Ruan and She, 2004). Interestingly, no single mutation has been shown to correlate with the manifestation of particular secondary phenotypes of the disease, with a few exceptions (Cetani et al., 2001; Su et al., 2008). Halonen and colleagues studied the correlation between HLA Class II and AIRE in APECED patients and found that adrenal insufficiency was associated with HLA-DRB1*03, alopecia with HLA-DRB1*04/DQB1*0302, whereas type 1 diabetes correlated negatively with HLA-DRB1*15/DQB1*0602 (Halonen et al., 2002).

Knocking out the mouse homologue of the human *Aire* gene has created mouse models of the APECED disease. Three independent *Aire*-deficient mouse strains have been described in the literature (Anderson et al., 2002; Kuroda et al., 2005; Ramsey et al., 2002a). Although it is still debatable if *Aire*-deficient mice provide an accurate mouse model for the human disease (Hubert et al., 2009; Kekalainen et al., 2007a), they share two, albeit milder, organ-specific autoimmunity traits with their human counterparts: the presence of inflammatory lymphocytic infiltrates and serum autoantibodies. Studies in mice show that the AIRE protein is present in the medullary thymic epithelial cells (mTECs) (Blechschmidt et al., 1999; Heino et al., 1999). It acts as a transcriptional regulator (Abramson et al., 2010) that relieves pausing of RNA polymerase shortly after transcript start sites (Giraud et al., 2012), allowing promiscuous expression of tissue-specific mRNAs in thymic medullary epithelial cells (Anderson et al., 2002; Derbinski et al., 2001; Jolicoeur et al., 1994). Expression of the corresponding organ-specific proteins enables these antigens to be presented to maturing T cells to stimulate deletion of self-reactive T cells in the thymic medulla (Anderson et al., 2002; Liston et al.,

2004a; Liston et al., 2003). Besides this *transcription model*, alternative models for the main mechanistic action of *Aire* in maintaining thymic tolerance have been suggested: (i) affecting mTEC organization, processing, maturating and emigration which is required for tissue-specific antigen expression (*maturation model*) (Matsumoto, 2011); (ii) priming T cells that develop in the thymus (*autoimmunization model*) (Kisand et al., 2010). Evidence for the maturation model came from analysis of the effects of *Aire*-deficiency in ovalbumin-specific TCR transgenic mice that also expressed an ovalbumin transgene controlled by the rat insulin promoter (Anderson et al., 2005). Ovalbumin-specific CD4 or CD8 T cells were not deleted efficiently, but surprisingly this was despite apparently normal mRNA from the RIP-mOVA transgene in thymic mTECs. Microarray profiling of the *Aire*-deficient mTECs revealed diminished expression of numerous genes involved in antigen processing, leading to the conclusion that failed thymic deletion in this case arose for inefficient presentation of the mTEC-expressed antigens.

Aire expression is also observed at lower levels in secondary lymphoid organs (extra-thymic *Aire*-expressing cells) that regulates the expression of a subset of peripheral tissue-specific genes, and acts to control self-reactive peripheral T cells (Gardner et al., 2008; Lee et al., 2007; Nichols et al., 2007), although it still remains unclear if *Aire* expression in secondary lymphoid tissues plays a physiological role in preventing autoimmune diseases since thymic transplants clearly indicated that it was required solely within the thymus (Anderson et al., 2002; DeVoss and Anderson, 2007). Consistent with the *HLA*-effect in human disease, varying the mouse strain background or specifically changing the *H2* haplotype changes the spectrum of organs targeted by autoimmunity (Jiang et al., 2005; Niki et al., 2006).

Studies of the simple monogenic *Aire*-deficient disease have improved our understanding of human autoimmune disease. Importantly, it has also highlighted two features common to autoimmune disease that present as a challenge in understanding and preventing these diseases – the variability in clinical manifestation and specific targets of autoimmunity, and the presence of a latent phase prior to development of autoimmunity. Most common autoimmune disease appears still much more complex, resulting from a combination of myriad inherited variants that have proved exceedingly

challenging to pinpoint, overlaid by stochastic or environmental factors such as diet, environmental toxins, and infections.

1.4.2 Polygenic autoimmune diseases

At the other extreme from familial syndromes like APS1 that result from complete disruption of single genes is the evidence that genetic susceptibility to common autoimmune diseases reflect interaction of multiple gene variants. This could either be a combination of multiple common allelic variants of low penetrance or of rare allelic variants with higher penetrance (Schork et al., 2009). The common variant hypothesis has been examined by genome wide association studies (GWAS), generally performed by consortiums of investigators on collections of patients and controls by tracking tag single nucleotide polymorphisms (SNPs) for small ancestral haplotypes distributed throughout the genome, to highlight haplotypes that are slightly more or less frequent in people with a particular autoimmune disease (reviewed in (Rai and Wakeland, 2011)).

The strongest genetic effect has been from specific *HLA* haplotypes and genes (Table 1.4), although the basis for autoimmune *HLA* associations are still poorly understood. There are several possibilities: (i) autoimmune-susceptible HLA haplotypes may present driver autoantigens from particular organs less efficiently for negative selection, Treg formation or peripheral tolerance; (ii) they may be better at presenting driver autoantigens to provoke autoimmunity; or (iii) they may have more indirect effects on positive selection against unrelated self-peptides in the thymus, resulting in higher frequencies of cells in the repertoire with damaging cross-reactive TCR specificities against other self antigens.

Table 1.4. *HLA* alleles associated with particular autoimmune disease identified in genome wide association studies. Table adapted from (Rai and Wakeland, 2011) and the GWAS catalogue (http://www.genome.gov/26525384).

HLA genes	Strongest SNP risk allele	Disease	Reference
B	rs2523393-A	Multiple sclerosis	(De Jager et al., 2009)

C	rs10484554-T	Psoriasis	(Liu et al., 2008)
C, CCHCR1	rs9263739-T	Ulcerative colitis	(Asano et al., 2009)
C, MSH5	rs3131379-A	Systemic lupus erythemathosus	(Han et al., 2009)
DQA	rs477515 (IBD), rs2187668-A (CD)	Inflammatory bowel disease, Celiac disease disease	(Kugathasan et al., 2008 ; van Heel et al., 2007)
DRA	rs9268923-C (UC), rs3135388-A (MS), rs3135338-A (MS)	Ulcerative colitis, multiple sclerosis	(Asano et al., 2009; Franke et al., 2008; Franke et al., 2010; Hafler et al., 2007)
DRB	rs660895 (RA), rs2647044-A (T1D), rs9271366-G (MS)	Rheumatoid arthritis, type I diabetes, multiple sclerosis	(Comabella et al., 2008; Sanna et al., 2010; Yang et al., 2006)

Besides HLA, many other loci have been associated with autoimmune diseases. For example, for type I diabetes alone more than 40 loci contribute to increased susceptibility (Barrett et al., 2009) and many also predispose to other autoimmune diseases such as psoriasis (PS), and multiple sclerosis (MS), inflammatory bowel disease (IBD) [includes Crohn's disease (CrD) and ulcerative colitis (UC)], and celiac disease (CD), systemic lupus erythematosus (SLE). It is intriguing that many of the tag SNPs so far associated with human autoimmune disease are near genes that function in thymic deletion or peripheral T cell anergy versus co-stimulation (Fig. 1.3, Fig. 1.4 and Table 1.5).

Limitations in the GWAS method include the low statistical power caused by multiple testing, imperfect correlation between inheritance of tag SNPs and causative gene variants, heterogenous genetic backgrounds, population stratification, inability to test for rare alleles with large effects, uncontrolled environmental variables and constraints on experimental validation. However, the greatest challenge is that despite the large number of loci with statistical evidence of association with autoimmune disease susceptibility, these genotypes only account for a small fraction of the total genetic

heritability (Manolio et al., 2009). So, what could account for this *missing heritability*? It can be suggested that the complex set of loci that contribute to autoimmune susceptibility work together to compromise multiple tolerance checkpoints resulting in severe autoimmune diseases. This epistatic interaction has been generally ignored in GWAS studies as statistical methods for identifying additive and epistatic (synergistic or interfering) interactions between individual alleles typically require even larger population sizes and even then still fail to include the large number of family-specific alleles. Another possibility is that the *missing heritability* comprises variants that are rare in the population as a whole, and hence are not "tagged" by the common SNPs used in GWAS studies.

Table 1.5. Autoimmune susceptibility loci involved in thymic deletion and T cell anergy. Type 1 diabetes (T1D), psoriasis (PS), and multiple sclerosis (MS), inflammatory bowel disease (IBD) includes Crohn's disease (CrD) and ulcerative colitis (UC)], and celiac disease (CD), systemic lupus erythematosus (SLE). Table adapted from (Rai and Wakeland, 2011) and the GWAS catalogue (http://www.genome.gov/26525384).

Thymic deletion – associated genes	Human disease	Reference
Ptpn2	T1D, CrD, CD, UC, RA	(Barrett et al., 2009; Dubois et al., 2010; Todd et al., 2007)
Ptpn22	RA, T1D, SLE, CrD	(Barrett et al., 2009; 2007; Todd et al., 2007)
RasGFP	SLE	(Han et al., 2009)
T cell anergy – associated genes	Human disease	Reference
TLR7/TLR8	CD, SLE	(Dubois et al., 2010; Shen et al., 2010))
CTLA4/ICOS/CD28	CD, T1D, IBD, RA, MS, SLE	(Dubois et al., 2010)
CBLB	MS	(Sanna et al., 2010)
PKCθ	T1D, RA, CD	(Cooper et al., 2008)
ETS1	SLE, CD	(Dubois et al., 2010; Han et al., 2009; Yang et al., 2010)}
SH2B3	TID, CD	(2007)
CD40	RA, MS, CrD	(Stahl et al., 2010)
CD69	T1D	(Barrett et al., 2009)

IL2RA	RA, MS, T1D	(Hafler et al., 2007; Stahl et al., 2010)

1.5 Hypothesis of the study

1.5.1 Hypothesis

As reviewed in previous sections, multiple tolerance checkpoints prevent self-reactive lymphocytes from attacking self. While complete disruption in individual genes such as *Aire*, *FoxP3*, or *Fas* are able to cause rare monogenic autoimmune disease, more common autoimmune diseases are associated with multiple subtle allelic variants in different genes or loci. Many loci associated with human autoimmune diseases are close to genes that function in thymic deletion or peripheral T cell anergy (Fig. 1.3 and 1.4) suggesting that multiple defects in immune tolerance pathways cause autoimmune diseases. Little is known, however about the consequence of combined defects in thymic and peripheral tolerance pathways.

Understanding how multiple genetic variations in individual tolerance mechanisms cooperate to determine the onset and clinical course of autoimmune disease has been challenging in part because so many genetic variants need to come together and many cause subtle quantitative changes in function. Even when combined there is a substantial and variable latent period representing the need for unknown stochastic or environmental events. Additive or cooperative effects of susceptibility genes in man or mouse may reflect *death by a thousand cuts* in a single pathway, as demonstrated for the dysregulated B cell response to autoantigen when multiple heterozygous mutations in the Lyn-CD22-SHP1 pathway are combined (Cornall et al., 1998) and for the failure of thymic deletion in NOD mice (Choisy-Rossi et al., 2004; Liston et al., 2004b; Venanzi et al., 2004). Alternatively, cooperative predisposition to autoimmune disease may result from failure of separate pathways that function as failsafes for one another - *death by single cuts in complimentary failsafe mechanisms*.

This dissertation explores the latter possibility, a *multi-step model* for the pathogenesis of autoimmune diseases. Since each tolerance pathway is governed by a unique set of genes

In this model, it is predicted that deficiencies in two (or more) genes that cripple different tolerance mechanisms would co-operate to accelerate autoimmune disease, hasten the tempo of the disease and unveil features not seen in individual defects. This requirement for co-operation in more than one tolerance defect in the development of fulminant autoimmune disease is an attractive explanation for why autoimmune manifestations are heterogeneous in nature and present with a latent period. This is likely scenario as the frequency of germline mutations, multiplied over the large number of failsafe or tolerance genes would result in virtually all individuals harbouring deleterious alleles in a heterozygous state in at least one of the genes involved in tolerance. An autoimmune-prone homozygous phenotype could easily emerge in the scenario of a disadvantageous breeding (inherited) or if a somatic mutation were to occur. The latent period in autoimmune disease pathogenesis may allow accumulation of successive mutations in different tolerance pathways leading to fulminant autoimmunity (Goodnow, 2007). In his 1972 monograph, Burnet himself alluded to the idea that the latent onset of autoimmune diseases may reflect "*a conditioned malignancy*" when "*forbidden clones*" failed to be eliminated or inactivated as a result of germline and somatic mutations that disrupt tolerance mechanisms (Burnett, 1972).

1.5.2 Direction of the study

To explore the *multi-step model* for the pathogenesis of autoimmune diseases, a reductionist strategy was employed. As each tolerance pathway is governed by a set of genes, and mouse models that are deficient in key genes involved in particular tolerance mechanisms have been extensively studied, the study began by testing the consequences of pairing defective thymic deletion due to Aire deficiency with four different molecularly defined defects that disrupt specific peripheral tolerance mechanisms. Specifically, the *Aire*-deficient mice – which have a profound defect in thymic deletion to organ specific antigens - were crossed with mice carrying genetic defects in one of four distinct peripheral tolerance mechanisms that have been summarized above:

decreased numbers of Foxp3^{+} T regulatory cells (*Card11*$^{unm/unm}$), apoptosis (*Fasl*$^{gld/gld}$), anergy (*Cbl-b*$^{-/-}$), or deregulated activation of T follicular helper cells (*Rc3h1*$^{san/san}$).

This strategy simplifies the co-operating genetic and cellular events resulting in spontaneous autoimmune disease to pinpoint which tolerance pathways cooperate and establish a mechanistic basis for cooperative pathogenesis of autoimmunity. A prediction of the model was that combination of *Aire* deficiency with a defined molecular lesion in peripheral tolerance would dramatically accelerate autoimmunity and lead to emergent autoimmune disease not seen with either individual defect. By contrast, no acceleration of autoimmunity and an additive combination of the individual autoimmune phenotypes would result from compounding *Aire* deficiency with a defect in peripheral tolerance that does not serve as a failsafe. Should cooperation be found between *Aire* deficiency and a specific peripheral tolerance defect, a virtue of this reductionist approach would in principle be at the level of analysing the cellular basis for genetic co-operation. Comparing the fate of self-reactive T cells in resistant or susceptible backgrounds would be simplified by the need for only two Mendelian defects, as compared to the myriad genetic loci with difficult to pinpoint defects that are needed for autoimmune susceptibility or resistance in NOD mice.

Chapter 2

Mice, materials and methods

2.1 Mice

All mice described were housed and maintained under specific pathogen-free conditions in the Animal Service Department, Australian National University. All mice used in the hematopoietic chimera experiments were housed in the Containment Suites, John Curtin School of Medical Research, Australian National University. All animal procedures were approved by the Australian National University Animal Ethics and Experimentation Committee.

2.1.1 Basic strains

Table 2.1 Basic mouse strains used in this study.

Basic Strains	Description
C57BL/6	Inbred C57BL/6 strain of haplotype $H2^b$. Imported from Stanford University.
C57BL/6.SJL-*Ptprca*/BoAiTac (abbreviated as C57BL/6 Ly5^a)	C57BL/6 strain congenic for the SJL CD45 allele, CD45.1/Ly5^a, in place of CD45.2/Ly5^b. Originally imported from Jackson Laboratories (Bar Harbor, ME).
B10.BR-$H2^k$/SgSnJ (B10.BR)	C57BL/10 substrain congenic for the C57BR H2 locus, $H2^k$. Abbreviated as B10.BR. Imported from Jackson Laboratories (Bar Harbor, ME).

2.1.2 Knock-out strains

Table 2.2 Knock-out mouse strains used in this study.

Knock-out strains	Description
Aire^{tm1Pltn}	The *Aire*-deficient mouse strain, a kind gift from Prof. Leena Peltonen, bears the truncating R257X nonsense mutation through an insertion of a neomycin resistance cassette, eliminating exon 6 at amino acid position 218, similar to the major human Finnish APS1 mutation (Ramsey et al., 2002b)

Rag1^{tm1Mom}	A 1356 bp genomic fragment of *Rag1* gene was replaced by the insertion of a neomycin resistance cassette. Originally produced with AB1 ES cells (129S7/SvEvBrd-Hprt+ background) and crossed to B6 (Mombaerts et al., 1992). Imported from the Animal Resources Centre, Government of Western Australia and backcrossed to C57/BL6 for > 15 generations.
Cblb^{tm1Pngr}	The *Cblb*^{tm1Pngr} (abbreviated as *Cblb*$^{-/-}$) knockout mouse strain was obtained from Prof. Wallace Langdon. The mouse was generated by introducing a neomycin cassette replacing the region encoding a portion of the tyrosine kinase-binding and RING finger domains, corresponding to amino acids 300 through 340 of the encoded protein (Bachmaier et al., 2000). The mutation has been and backcrossed to C57/BL6 for > 10 generations.
Fasl$^{gld/gld}$	The *Fasl*^{gld} mouse strain was obtained from the Jackson Laboratories. The mouse strain harbours a spontaneous thymine to cytosine point mutation near the 3' end of the coding sequence which results in a replacement of a highly conserved phenylalanine with a leucine at position 273 in the extracellular region of the encoded protein (Takahashi et al., 1994).
Card11$^{unm/unm}$	The *Card11*$^{unm/unm}$ C57/BL6 mouse strain was generated in the Immunogenomics Laboratory from *N*-ethyl-*N*-nitrosuria mutagenesis screen of third generation offspring in a pedigree which displayed high level of surface IgM antigen receptors on circulating IgD^{+} B cells. The mice have a point mutation changing a thymine to adenine nucleotide, which results in a non-polar leucine to a polar glutamine codon substitution in the coiled-coiled domain of Card11 (also called Carma-1)(Jun et al., 2003).
Rc3h1$^{san/san}$	The C57BL/6.*Rc3h1*$^{san/san}$ mouse strain was also generated in the Immunogenomics Laboratory from an *N*-ethyl-*N*-nitrosuria mutagenesis screen of third generation offspring in a pedigree that displayed high amounts of anti-nuclear antibodies and lymphadenopathy. The mice carry a thymine to guanine substitution in the Rc3h1 ubiquitin ligase resulting in a non-conservative methionine to arginine codon change.

The breeding of Aire-deficient mice to heterozygous *Card11*$^{unm/unm}$, *Cblb*$^{-/-}$, *Fasl*$^{gld/gld}$ and *Rc3h1*$^{san/san}$ mouse models, and preliminary intercrosses of the first three filial

generations were performed by Dr. Anselm Enders. This thesis includes data from the fourth to ninth filial generation of mouse breeding in each strain.

2.1.3 Transgenic strains

Table 2.3 Transgenic mouse strains used in this study.

Transgenic strains	Description
TCR^{3A9}	TCR α and β transgenic produced in C57BL/6J mice were backcrossed >7 generations to B10.BR (Ho et al., 1994).
InsHEL	The ILK-3 transgene consists of a membrane-bound (class I transmembrane region) hen egg lysozyme (HEL) antigen driven by the rat insulin promoter. Produced in C57BL/6J mice (Akkaraju et al., 1997b) and backcrossed >7 generations to B10.BR.
ThyrHEL	The TLK-2 transgene consists of membrane-bound HEL driven by a fragment of the rat thyroglobulin promoter. Produced in C57BL/6J mice(Akkaraju et al., 1997b) and backcrossed >7 generations to B10.BR (Akkaraju et al., 1997a; Akkaraju et al., 1997b).

2.2 Materials

2.2.1 Antibodies

Table 2.4 Antibodies used for flow cytometry. The clone designations, fluorochrome conjugations (if applicable) and vendors are listed for each antibody. Each antibody was titrated and used at the minimal concentration required for saturation.

Antibodies	Clone	Conjugation	Vendor
7-Amino-actinomycin D	None	None	BD Pharmingen™
Anti-human Ki-67	B56	A647	BD Pharmingen™
Anti-mouse Bim	3C5	A647	Gift from Andreas Strasser, Walter and Eliza Hall Institute
Anti-mouse CD122	Mik-β3	Biotin	BD Pharmingen™
Anti-mouse CD134	OX40	Biotin	BD Pharmingen™
Anti-mouse CD152 (CTLA4)	UC10-4F10-11	PE	BD Pharmingen™
Anti-mouse CD16/32	2.4G2		BD Pharmingen™
Anti-mouse CD24	M1/69	Alexa Fluor® 405	BD Pharmingen™
Anti-mouse CD25 (IL-2 Receptor a chain, p55)	PC61	Alexa Fluor® 700, APC, APC Cy7, PE, PerCP	BD Pharmingen™
Anti-mouse CD3	17A2	Alexa Fluor® 700	eBioscience
Anti-mouse CD4	RM4-5	PE Cy7	BD Pharmingen™
Anti-mouse CD4	GK1.5	None	BioXCell
Anti-mouse CD44	IM7	Biotin, Pacific Blue, PE	BD Pharmingen™
Anti-mouse CD45.1 (Ly-5.1, Ly5a)	A20	Alexa Fluor® 700, FITC	BD Pharmingen™
Anti-mouse CD45.2 (Ly-5.2, Ly5b)	104	Alexa Fluor® 405, Alexa Fluor® 700, PerCP, PE Cy7	BD Pharmingen™
Anti-mouse CD45R (B220)	RA3-6B2	Alexa Fluor® 405, APC Cy7, PerCP Cy5.5	BD Pharmingen™

Anti-mouse CD5 (Ly-1)	53-7.3	PE, PerCP	BD Pharmingen™
Anti-mouse CD62L (L-selectin, LECAM-1, Ly-22)	MEL-14	FITC, PerCP	BD Pharmingen™
Anti-mouse CD69 (Very Early Activation Antigen)	H1.2F3	PE Cy7	BD Pharmingen™
Anti-mouse CD8	53-6.7	APC Cy7, Biotin, PE Cy7, PerCP	BD Pharmingen™
Anti-mouse Foxp3	MF23	Alexa Fluor® 700, e450, FITC	BD Pharmingen™
Anti-mouse GITR	DTA-1	Alexa Fluor® 700, PE Cy7	BD Pharmingen™
Anti-mouse ICOS	7E.17G9	PE	BD Pharmingen™
Anti-mouse IgG1	G235-2356	PE, APC	BD Pharmingen™
Anti-mouse NK1.1 (NKR-P1B and NKR-P1C)	PK136	APC	BD Pharmingen™
Anti-mouse TCR	H57-597	FITC	BD Pharmingen™
Anti-TCR^{3A9} clonotype	1G12	None	Homemade
Ant-mouse CD8	53-6.72	None	BioXCell
Mouse IgG2b Isotype control	MPC-11	None	BioXCell
Rat-anti mouse CD44	IM7.8.1	Alexa Fluor® 405	Caltag™ Laboratories
Streptavidin		Qdot® 605	Invitrogen™

Note: Antibody conjugation to A647 was done using the Protein Labelling Kit (Molecular Probes, A20173).

2.2.2 Bioinfomatic tools

Table 2.5 Bioinformatic tools used in this study.

Bioinformatics tools	Website	Description
ENSEMBL Genome Browser	http://www.ensembl.org/index.html	Produces and maintains automatic annotation on selected eukaryotic genomes.
ExPASy Proteomics Server	http://au.expasy.org/tools/dna.html	Allows the translation of a nucleotide (DNA/RNA) sequence to a protein sequence in three reading frames.
FinchTV	http://www.geospiza.com/Products/finchtv.shtml	Viewing and editing nucleotide sequence traces.

ImMunoGeneTics	http://www.imgt.org/	Reference for TRAV, TRAJ, TRBV, TRBJ nucleotide sequences and translations.
Mouse Genome Informatics	http://www.informatics.jax.org/	Provides integrated access to data on the genetics, genomics and biology of laboratory mice.
Musterer	http://musterer.apf.edu.au/	Database of mouse strains used in the project.
Primer3	http://frodo.wi.mit.edu/cgi-bin/primer3/primer3_www.cgi	PCR primer design program.

2.2.3 Buffers, solution and media

2.2.3.1 Common buffers, solutions and media

Table 2.6 Common buffers, solution and media and the respective vendors.

Buffer	Vendors
DMEM	Ordered from GibcoBRL
Phosphate buffer saline	Obtained from the John Curtin School of Medical Research Media Facility
RPMI	Ordered from GibcoBRL

2.2.3.2 Buffers, solution and media for cell biology assays and techniques

Table 2.7 Buffers used for cell biology techniques and the respective compositions.

Buffer	Composition
cDMEM	DMEM (GibcoBRL), 10 % (v/v) HI-FCS (Sigma), 2mM L-glutamine (GibcoBRL), 1mM MEM sodium pyruvate (GibcoBRL), 100µM MEM non essential amino acids (GibcoBRL), 5mM HEPES buffer solution (GibcoBRL), 55µM 2-mercaptoethanol (GibcoBRL), 100u/ml penicillin, 100µg/ml streptomycin (GibcoBRL)

Cell culture medium	RPMI (GibcoBRL), 10 % (v/v) HI-FCS (Sigma), 10 mM HEPES, pH7.4 (GibcoBRL), 0.1 mM non-essential amino-acid solution (GibcoBRL), 1 mM sodium pyruvate (Sigma), 50 uM beta-mercaptoethanol (GibcoBRL), 10 mL L-glutamate and penicillin/streptomycin (GibcoBRL)
Cell culture freezing media	90 % (v/v) HI-FCS (Sigma), 10% DMSO, 2mM L-glutamine (GibcoBRL), 1mM MEM sodium pyruvate (GibcoBRL), 100µM MEM non essential amino acids (GibcoBRL), 5mM HEPES buffer solution (GibcoBRL), 55µM 2-mercaptoethanol (GibcoBRL), 100u/ml penicillin, 100µg/ml streptomycin (GibcoBRL)
D_{20}	cDMEM except 20 % (v/v) HI-FCS (Sigma) instead of 10 % (v/v) HI-FCS (Sigma)
ELISA Blocking Buffer	1% bovine serum albumin in phosphate buffer saline
ELISA Coating Buffer	0.05 M carbonate, 1.59 g sodium carbonate anhydrous and 2.93 g sodium hydrogen carbonaye in 1 L deionized water adjusted to pH 9.6 with hydrochloric acid solution
ELISA Developer Buffer	0.1 M glycine, 0.1 mM zinc chloride, 1.0 M magnesium chloride in deionized water adjusted to pH 10.4 with sodium hydroxide solution
ELISA Dilution buffer	1% bovine serum albumin and 0.05% Tween 20 (Sigma, St. Louis, Illinois) in phosphate buffer saline
ELISA Wash Buffer	0.05% Tween 20 (Sigma, St. Louis, Illinois) in phosphate buffer saline
FACS Buffer	5% fetal calf serum and 0.1% sodium azide in phosphate buffer saline
Low serum culture media	RPMI (GibcoBRL), 2 % (v/v) HI-FCS (Sigma), 10 mM HEPES, pH7.4 (Sigma), 0.1 mM non-essential amino-acid solution (GibcoBRL), 1 mM sodium pyruvate (Sigma), 50 uM beta-mercaptoethanol (GibcoBRL), 10 mL L-glutamate and penicillin/streptomycin (GibcoBRL)
Magnetic cell separation buffer	0.5% bovine serum albumin and 2 mM EDTA in phosphate buffer saline
OptiMEM	Ordered from GibcoBRL
Red blood cell lysis buffer (10×)	8.99 g ammonium chloride,1 g potassium bicarbonate, 37 mg sodium EDTA in 100 mL deionized water, adjusted to pH 7.3 with hydrochloric acid solution
Turks solution	1% (v/v) acetic acid and gention violet in deionised water

2.2.3.3 Buffers solutions and media for molecular biology assays and techniques

Table 2.8. Buffers used for molecular biology techniques and the respective compositions.

Buffer	Composition
Agarose gel loading buffer (6×)	Bromophenol blue and 30% glycerol in deionized water
CSA Sequencing Buffer (5×)	400 mM Tris-hydrochloric acid adjusted to pH 9 and 10 mM magnesium chloride
Sodium borate buffer	5 mM sodium tetraborate

2.2.4 Cell lines

2.2.4.1 293T cells

The 293T cells (D. Baltimore, California Institute of Technology) (a kind gift from Dr. Nicole La Gruta, University of Melbourne) were used as a readily transfected cell line to test for gene expression from retroviral vectors and for the generation of stable retroviral producer cell lines. Cells were maintained in NUNC T_{75} flasks (Thermo Scientific) in complete-DMEM (cDMEM) medium at 37°C until the monolayers were confluent. For passage, the monolayers were washed with 10 mL PBS and treated with 1.5 mL trypsin-EDTA at 37°C for 4-5 minutes. cDMEM was added to inactivate the trypsin-EDTA and the cells were seeded onto fresh tissue culture flask.

2.2.4.2 GP+E86 cells

The GP+E86 (American Tissue Culture Type Collection: CRL-9642) (a kind gift from Dr. Nicole La Gruta, University of Melbourne), a 3T3-based retroviral packaging cell line stably transfected with two plasmids encoding *gag*, *pol* and *env* genes from Moloney Leukaemia virus (Markowitz et al., 1988). The cells were used to establish stable ecotropic retrovirus producer cell lines. Culture and passage conditions were the same as 293T cells.

2.2.4.3 3T3 cells

The 3T3 cells (American Tissue Culture Type Collection: CRL-1658) (a kind gift from Dr. Nicole La Gruta, University of Melbourne) are a fibroblast cell line used for determining the titres of retroviral producer cell lines.

2.2.5 Chemicals

All chemicals were of analytical grade or the highest grade available, and were purchased from Sigma-Aldrich unless otherwise stated.

2.2.6 Kits

Table 2.9 Kits and the respective vendors used in this study.

Kits	Vendor
AccuPrime™ *Taq* DNA Polymerase High Fidelity	Invitrogen
CD4 (L3T4) MicroBeads	Miltenyi Biotec
CD4+ CD25+ Regulatory T Cell Isolation Kit	Miltenyi Biotec
CD8 (Ly-2) MicroBeads	Miltenyi Biotec
CellTrace™ CFSE Cell Proliferation Kit	Invitrogen
CellTrace™ Violet Cell Proliferation Kit	Invitrogen
DyeEx 96 Kit	Qiagen
ExoSAP-IT	USB Corporation
Flow Cytometry Fixation and Permeablisation	eBioscience
Fugene 6 reagent	Roche Diagnostics
iScript cDNA Synthesis Kit	Bio-Rad

2.2.7 Molecular weight markers

Table 2.10 Molecular weight markers used in this study.

Molecular Weight Markers	Vendor
1Kb Plus DNA Ladder	Invitrogen

2.2.8 Primers

Table 2.11. **Primers used in single cell multiplex PCRs.** Primer sequences were obtained from (Dash et al., 2011) and synthesized by Invitrogen. Each desiccated primer was reconstituted to 100 pmol/µL in water. 5 pmol/µL working dilutions of *Trav* external, *Trav* internal, *Trbv* external and *Trbv* internal forward primers were prepared by combining equal volumes of the appropriate primers and stored at -20°C.

Primers	Sequence	
Trav1 external forward	5' GGTTATCCTGGTACCAGCA	3'
Trav2 external forward	5' CATCTACTGGTACCGACAGG	3'
Trav3.5D4.10 external forward	5' CCTGAGTGTICVRGAGGGA	3'
Trav4 external forward	5' TCTGSTCTGAGATGCAATTTT	3'
Trav5-1.7D-2 external forward	5' CCTSATTGTICMRGAGGGAG	3'
Trav5(D)-4 external forward	5' CTTCCTTCCATCCTGAGAG	3'
Trav6.12-2 external forward	5' TMMCCDDIICTKTTCTGGTATGT	3'
Trav6.5_6.6(D) external forward	5' GAYTCVGTGACTCARACAGAAGG	3'
Trav7.10Da13 external forward	5' SRDCAGIAAGTRCAGCAGAG	3'
Trav8 external forward	5' GAGCRTCCASGAGGGTG	3'
Trav9.17 external forward	5' GAGMCTCBSTGSAGCTSAGATGCA	3'
Trav11 external forward	5' AAGACCCAAGTGGAGCAG	3'
Trav12 external forward	5' TGACCCAGACAGAAGGC	3'
Trav14.19 external forward	5' CAGCAGCAGGTKARACAAAG	3'
Trav15 external forward	5' CASCTTYTTAGTGGAGAGATGG	3'
Trav16 external forward	5' GTACAAGCAAACAGCAAGTG	3'
Trav18 external forward	5' AACGGCTGGAGCAGAG	3'
Trav21 external forward	5' GTGCACTTGCCTTGTAGC	3'
Trac external reverse	5' GGCATCACAGGGAACG	3'
Trav1 internal forward	5' CTCCACATTCCTGAGCC	3'
Trav2 internal forward	5' ACTCTGAGCCTGCCCT	3'
Trav3.5D4.10 internal forward	5' AACGAITCTCICTGMACMTCACAG	3'
Trav4- internal forward	5' GGITIMAGGAACAAAGGAGAAT	3'
Trav5-1.7D-2 internal forward	5' TGGTAIARRCARSASICTGGGAA	3'
Trav5(D)-4 internal forward	5' AGAATCCTAAGCTCATCATTGAC	3'
Trav6.12-2 internal forward	5' TCCAIITRCAGAARDCCTCAG	3'
Trav6.5_6.6(D) internal forward	5' GTKCRRTATCCYGGAGAAGGTC	3'
Trav7.10Da internal forward	5' CATGRCITCIITCAACTGCAC	3'
Trav8 internal forward	5' AGAGCCACCCTTGACAC	3'
Trav9.17 internal forward	5' GGCTTIGAGGCIGAGTT	3'
Trav11 internal forward	5' AACAGGACACAGGCAAAG	3'
Trav12 internal forward	5' GGTTCCACGCCACTC	3'
Trav13 internal forward	5' CCTTGGTTCTGCAGGAG	3'
Trav14 internal forward	5' CTCTGACAGTCTGGGAAGG	3'

Trav15 internal forward	5'	AYTCTGTAGTCTTCCAGAAATCAC	3'
Trav16 internal forward	5'	ATTATTCTCTGAACTTTCAGAAGC	3'
Trav18 internal forward	5'	CAAGATTTCACCGCACG	3'
Trav19 internal forward	5'	GCTGACTGTTCAAGAGGGA	3'
Trav21 internal forward	5'	AATAGTATGGCTTTCCTGGC	3'
Trac internal reverse	5'	GCACATTGATTTGGGAGTC	3'
Trbv1 external forward	5'	TACCACGTGGTCAAGCTG	3'
Trbv16 external forward	5'	CCTAGGCACAAGGTGACAG	3'
Trbv12 external forward	5'	GGGGTTGTCCAGTCTCC	3'
Trbv5 external forward	5'	GGTATAAACAGAGCGCTGAG	3'
Trbv29 external forward	5'	GCTGGAATGTGGACAGG	3'
Trbv20 external forward	5'	GGATGGAGTGTCAAGCTG	3'
Trbv13 external forward	5'	GCTGCAGTCACCCAAAG	3'
Trbv14 external forward	5'	GCAGTCCTACAGGAAGGG	3'
Trbv15 external forward	5'	GAGTTACCCAGACACCCAG	3'
Trbv17 external forward	5'	GAAGCCAAACCAAGCAC	3'
Trbv19 external forward	5'	GATTGGTCAGGAAGGGC	3'
Trbv2 external forward	5'	CAGTATCTAGGCCACAATGC	3'
Trbv23 external forward	5'	CTGCAGTTACACAGAAGCC	3'
Trbv24 external forward	5'	CAGACTCCACGATACCTGG	3'
Trbv26 external forward	5'	GGTGAAAGGGCAAGGAC	3'
Trbv3 external forward	5'	CCCAAAGTCTTACAGATCCC	3'
Trbv30 external forward	5'	CCTCCTCTACCAAAAGCC	3'
Trbv31 external forward	5'	CTAACCTCTACTGGTACTGGCAG	3'
Trbv4 external forward	5'	GACGGCTGTTTTCCAGAC	3'
Cβa (*Trbc*) external reverse	5'	CCAGAAGGTAGCAGAGACCC	3'
Trbv1 internal forward	5'	GTATCCCTGGATGAGCTG	3'
Trbv16 internal forward	5'	GAAGCAACTCTGTGGTGTG	3'
Trbv12 internal forward	5'	CCAGCAGATTCTCAGTCC	3'
Trbv5 internal forward	5'	GCCAGAGCTCATGTTTCTC	3'
Trbv29 internal forward	5'	GTACTGGTATCGACAAGACCC	3'
Trbv20 internal forward	5'	GCTTGGTATCGTCAATCG	3'
Trbv13 internal forward	5'	GTACTGGTATCGGCAGGAC	3'
Trbv14 internal forward	5'	GGTATCAGCAGCCCAGAG	3'
Trbv15 internal forward	5'	GTGTGAGCCAGTTTCAGG	3'
Trbv17 internal forward	5'	GAACAGGGAAGCTGACAC	3'
Trbv19 internal forward	5'	GGTACCGACAGGATTCAG	3'
Trbv2 internal forward	5'	GGACAATCAGACTGCCTC	3'
Trbv23 internal forward	5'	GCCAGGAAGCAGAGATG	3'
Trbv24 internal forward	5'	GCACACTGCCTTTTACTGG	3'
Trbv26 internal forward	5'	GAGGTGTATCCCTGAAAAGG	3'
Trbv3 internal forward	5'	GATATGGGGCAGATGGTG	3'
Trbv30 internal forward	5'	GGACATCTGTCAAAGTGGC	3'
Trbv31 internal forward	5'	CTGTTGGCCAGGTAGAGTC	3'
Trbv4 internal forward	5'	CAGGTGGGAAATGAAGTG	3'
Trbc internal reverse	5'	CCTCCTTGCCATTCACCCAC	3'

Table 2.12 Primers for verification of pMIGII retrogenic vector and TCR insert sequences. Primer sequences were obtained from the La Gruta/Doherty Laboratory, University of Melbourne and synthesized by Geneworks. Each desiccated primer was reconstituted to 100 μM in Buffer TE and 10 μM working stocks are stored at -20°C.

Primers	Sequence
MSCV forward	5' ACACCCTAAGCCTCCGCCTCC 3'
Cα5 internal	5' GAACCTGCTGTGTAC 3'
IRES reverse	5' AACGCACACCGGCCTTATTCC 3'

2.2.9 T cell stimuli

Table 2.13 T cell stimuli used in this study. The initial concentrations, final concentrations in tissue culture and vendor are listed for each agonist.

Agonist	Initial concentration	Used concentration	Vendor
Anti-CD3	0.5 mg/mL	10 μg/mL	BD Pharmingen
Anti-CD28	0.5 mg/mL	5 μg/mL	BD Pharmingen
HEL peptide	1 mg/mL	10 μg/mL	JCSMR Biomolecular Resource Facility

2.3 Methods

2.3.1 Cell biology assays and techniques

2.3.1.1 Preparation of peripheral blood samples

Blood was collected from the retro-orbital sinus of mice using a glass capillary and placed into 1 mL cluster tubes containing 20 µL of 1000 U/mL heparin solution. The red blood cells were lysed by addition of 160 µL red blood cell (RBC) lysis buffer to 40 µL of blood, followed by 10 minute incubation at room temperature and centrifugation for 4 minutes at a rate of 1340 r.p.m. at 18ºC. The supernatant was discarded and the pellet was resuspended in 180 µL RBC lysis buffer, followed by incubation and centrifugation as described above. The pellet was subsequently washed with 180 µL FACS buffer, resuspended in 180 µL FACS buffer and kept on ice until use.

2.3.1.2 Preparation of lymphocytes from organs

Mice were sacrificed by cervical dislocation or carbon dioxide inhalation. Solid organs (spleens, lymph nodes and thymus) were collected and placed into 5 mL of ice-cold RPMI1640 + 5% fetal calf serum (FCS). Bone marrow cells were flushed from tibias and femurs, which were aseptically cut at both ends with ice-cold RPMI1640 + 5% FCS using a 3 mL syringe. For the isolation of pancreas infiltrating lymphocytes, the pancreas (free of pancreatic lymph nodes) was finely cut and incubated at 37°C for 15 minutes in 4 mL RPMI supplemented with 10 mg Collagenase P (Roche Diagnostics) and 10 µg DNase1 (Roche Diagnostics). The mixture was centrifuged at 1200 r.p.m. for 5 minutes at 8°C and resuspended in 10mL of Ficoll-Paque Plus solution. Gently, 10 mL RPMI 1640 was layered on top of the Ficoll-Paque Plus solution without disrupting the bottom layer. After centrifugation at 2300 r.p.m. for 15 minutes at 20°C using slow acceleration and deceleration (no breaks), the lymphocytes in the interphase of the two layers were harvested. Single cell suspensions of splenocytes, pancreatic infiltrated lymphocytes, thymocytes, bone marrow and lymph node cells were prepared by teasing the tissues apart through a 70 µm nylon mesh filter (BD Biosciences, NJ, USA) with a 1 mL syringe plunger.

All cells mentioned above were pelleted by centrifugation for 4 minutes, 1340 r.p.m. at 4ºC. RBCs were lysed in 5 mL of RBC lysis buffer for 10 minutes. The RBC lysis buffer reaction was quenched by addition of 10 mL ice-cold PBS and the cell suspensions were pelleted by centrifugation for 10 minutes, 1340 r.p.m. at 4ºC. RBC lysis was not performed for thymocytes. Cells were resuspended in 5 mL of RPMI1640 + 5% FCS and kept on ice until use.

2.3.1.3 Flow cytometry analysis of cell surface markers

The expression of cell surface markers was analyzed by flow cytometry using fluorochrome-conjugated antibodies, according to the following procedure. Lymphocytes were prepared as described above, resuspended in FACS buffer and aliquoted into 96-well round-bottom plates (Nunc, Roskilde, Denmark) at 5×10^5 to 1×10^6 cells per well. The cells were incubated with 20 µL F_c blocking antibody (CD16/CD32, 1 in 150 dilution of the 0.5 mg/mL stock) for 20 minutes at 4ºC to block non-specific antibody binding through F_c-receptor interactions. In cases where biotin-conjugated primary antibodies were used, the appropriate antibody was added to the F_c blocking antibody mixture (both diluted to its optimal concentration in FACS buffer). The cells were washed by addition of 160 µL FACS buffer and centrifugation for 4 minutes, 1340 r.p.m. at 4ºC.

A cocktail of premixed fluorochrome-labelled antibodies (each diluted to its optimal concentration in FACS Buffer) was added at 30 µL per well, followed by an incubation for 30 minutes at 4ºC in the dark. In cases where biotin-conjugated primary antibodies were used, the appropriate strepavidin-conjugated secondary reagents were added to the premix (diluted to its optimal concentration in FACS buffer). Intracellular staining was performed according to the manufacturers instructions (FoxP3 Staining Buffer Kit, eBioscience). Following incubation, cells were washed and resuspended in 120 µL FACS buffer and stored at 4ºC in the dark, not more than 2 hours, before analysis on the FACS Calibur (Becton, Dickinson and Co, NJ, USA) or LSRII Flow Cytometer (BD Biosciences, CA, USA).

For single cell sorting, cells were stained as described above replacing the FACS buffer with 0.1% FSC in PBS supplemented with magnesium and calcium (GibcoBRL). Samples were filtered through a 70 μm filter into 5 mL polypropylene Falcon tubes. Cells were sorted directly onto Eppendorf 96-well PCT plates (Twin.tec skirted PCR plates). For each plate, 80 cells were sorted (e.g. A1-A10, B1-B10). The last row (row 12) is a "no sort" control. The plates were capped immediately (Cap Strips, Eppendorf), centrifuged for 1200 r.p.m. for 3 minutes and stored at -80°C until processed further to cDNA. Sorting was performed on the Aria II Flow Cytometer (BD Biosciences, CA, USA).

Lymphocytes were identified based on their forward scatter (FSC) and side scatter (SSC) properties. Cells separately stained with each of the fluorochrome-labelled antibodies were used as controls to compensate for the overlap between emission spectra of the various fluorochromes. Flow cytometric data was analysed using FlowJo software (Treestar, San Carlos, California, USA).

2.3.1.4 Embedding and cryosectioning of organ samples

Eye, salivary gland, thyroid, heart, lung, liver, kidney, pancreas, testes/ovary samples from *Rag*1-deficient mice were excised into 5 mm segments and embedded in Tissue-Tek® Optimal Cutting Temperature compound (Sakura). The embedded sections were kept at -80ºC until use. Prior to cryosectioning, the embedded samples were frozen onto an aluminium block by cooling on dry ice. Cryosections of 8 microns-thick were made with a cryomicrotome (Bright Instruments, England) adjusted to -20°C and mounted on silane-coated slides. The sections on the slide were immediately air-dried for 1.5 hours, fixed with cold acetone for 10 minutes, air-dried for another 1.5 hours and stored in a sealed container, which was placed in a sealed bag with silica gel and stored at -20ºC until use.

2.3.1.5 Hematoxylin and eosin staining

Tissue sections were fixed in 10% neutral buffered formalin, paraffin embedded, cut, mounted and stained with hematoxylin and eosin staining at the Microscopy Facility, John Curtin School of Medical Research. All sections were inspected for infiltrates

using an Olympus microscope, and images were captured with the DP70-BSW (Olympus) software.

2.3.1.6 Immunofluorescent staining

Frozen sections of the spleen were air-dried for 0.5 hours. The non-specific absorption sites were blocked by incubation with 50 µL Blocking Serum for 30 minutes at 37ºC in a moist chamber. Blocking serum was removed and 50 µL of appropriate 1 in 30 diluted mouse serum (primary antibody) was added to each section, followed by 30 minutes incubation at 37ºC in a moist chamber. Slides were washed three times with PBS, 5 minutes per wash at room temperature. Primary antibody was removed and slides were washed three times with PBS, 5 minutes per wash at room temperature. Subsequently, 50 µL of Alexa 488 goat anti-mouse IgG (Invitrogen) secondary antibody was added to each section, followed by 30 minute incubation at 37ºC in a moist chamber in the dark. Secondary antibody was removed and slides were washed three times with PBS, 5 minutes per wash at room temperature. Nuclear staining was done by a 5 minute staining with 0.1 µg/ mL DAPI (Invitrogen). Slides were mounted in Fluorescent Mounting Medium (DakoCytomation) before affixing a coverslip. Sections were viewed under an Olympus IX71 Microscope (Olympus). For each organ viewed, an appropriate exposure time that gave bright staining with the positive control and no staining with the negative control was determined and used for capturing images for all samples tested against a particular organ allowing for accurate comparison of the different images.

2.3.1.7 Generation of bone marrow chimeras

To harvest bone marrow, cells were flushed from tibias and femurs, which were aseptically cut at both ends, with ice-cold RPMI 1640 using a 3 mL syringe. Single cell suspensions were prepared by teasing the tissues apart through a 70 µm nylon mesh filter (BD Biosciences, NJ, USA) with a 1 mL syringe plunger. Cells were then pelleted by centrifugation for 10 minutes, 1340 r.p.m. at 4ºC. Cells were resuspended in 1 mL of RPMI 1640 and kept on ice until use. The cells were counted and adjusted to 1×10^7 cells/mL in RPMI 1640. Samples were then mixed to the required ratios and injected intravenously at 200 µL (2×10^6 cells) per mouse into the tail veins of irradiated

recipients. Recipients were irradiated (X-RAD 320, CMS Alphatech, Sydney, Australia) with two doses of 450 cGy separated by 4 hours or a single dose of 500 cGy for *Rag*1-deficient lymphopenic recipients. After bone marrow irradiation, the recipient mice were given 25 μg/mL Neomycin sulphate and 13 μg/mL Polymyxin B sulphate in their drinking water for 6 weeks. Before subsequent analysis, hematopoietic cells were allowed to reconstitute in the chimeras for six weeks or earlier if mice needed to be sacrificed after losing 20% of the mice body weight.

2.3.1.8 Retroviral-mediated bone marrow transduction

The retroviral-mediated bone marrow transduction was performed according to a published protocol (Holst et al., 2006a). Briefly, bone marrow donor mice received 0.15 mg 5-fluorouuracil per gram weight of the mice intraperitoneally 48 hour prior to bone marrow harvest. Following harvest, bone marrow cells were cultured for 48 hours at 37°C, 10% CO_2 in 150 mm tissue culture dishes at 4×10^6 cells/mL in D_{20} media supplemented with 50 ng/mL hIL-6, 20 ng/mL mIL-3 and 50 ng/mL mSCF (all from all Biosource International, Camarillo, CA, USA).

Meanwhile, the GP+E86 retroviral producer cells were irradiated with 1200 rads and seeded onto 150 mm tissue culture dishes (8×10^6 cells in 19 mL D_{20} per plate). The cells were incubated for 24 hours at 37°C, 10% CO_2. After incubation, the bone marrow cells were treated with RBC lysis buffer for 5 minutes to lyse erythrocytes prior to addition to GP+E86 producer cell plates. Bone marrow cells were retrovirally transduced by co-culture with GP+E86 cells for 48 hours in the presence of 50 ng/mL hIL-6, 20 ng/mL mIL-3, 50 ng/mL mSCF and 6 μg/mL hexadimethrine bromide.

To generate retrogenic mice, the *Rag1*-deficient recipient mice were sub-lethally irradiated with 500 rads and reconstituted with 200 μL 1.5×10^6 bone marrow cells injected intravenously with 20 U/mL heparin. Irradiated mice were administered antibiotics in their drinking water (25 μg/mL Neomycin sulphate and 13 μg/mL Polymyxin B sulphate (both Sigma-Alrich)) and allowed to recover for 2 weeks before analysis of peripheral blood neutrophils, monocytes and lymphocytes to assess GFP expression.

2.3.1.9 Adoptive transfer assays

Single cell spleen suspensions were prepared in RPMI 1640 medium (Gibco) supplemented with 5% fetal calf serum. Where $CD4^+$ or $CD8^+$ purification was necessary, cells were purified using anti-CD4 MACS beads (Miltenyi Biotec, clone L3T4) or anti-CD8 MACS beads (Miltenyi Biotec, clone 53-6.7) and separated using an autoMACS™ Separator (Miltenyi Biotec) according to manufacturer's instructions. The purity was >92% for both CD4 and CD8. Whole splenocytes, CD4 enriched, CD4 depleted, CD8 enriched and CD8 depleted were transferred intravenously into B10.BR.*Rag-1*$^{-/-}$ recipients. On days 0, 1, 7 and 14 days post-transfer, recipients of CD8-depleted cells or CD4-depleted cells were treated with 0.3 mg of anti-CD8 (Bio X Cell, clone 2.43) or anti-CD4 (Bio X Cell, clone GK1.5) respectively, to deplete any residual $CD4^+$ or $CD8^+$ cells.

2.3.1.10 Enzyme-linked immunosorbent assay

High protein-binding 96-well flat-bottom plates (Nunc, Roskilde, Denmark) were coated with 100 µL/well of 5 µg/ mL appropriate coating antigen (diluted in coating buffer) and incubated overnight at 4ºC. The unbound antigen was removed and plates were washed three times with Wash Buffer. The remaining absorption sites were blocked by a 1.5 hour incubation at 37ºC after addition of Blocking Buffer. The Blocking Buffer was removed and plates were washed three times with Wash Buffer. Appropriate serum dilutions were prepared with Dilution Buffer and added to the first row of the plate except the first column (200 µL per well). Control serum (defined in each experiment in the section 3) was added to the first column on the first row of the plate. The remainders of the plate wells were filled with 100 µL dilution buffer. The samples were then serially diluted eight times by successive transfer of 100 µL along the columns of the plates, with mixing, giving a 2 fold dilution every row from top to bottom of plate. Plates were washed three times with wash buffer after a 1 hour incubation at 37ºC. Detection antibody for the different antibody isotypes were added to each well (100 µL per well), followed by a one hour incubation at 37ºC. Plates were washed three times with wash buffer. In cases where goat anti mouse $IgG2a^b$-biotin was used, 1 µg/ mL strepavidin-alkaline phosphate was added (100 µL per well), followed by a 20 minute incubation at 37ºC. Phosphate substrate (Sigma, St. Louis, Illnois, USA) (1 tablet per 5 mL developer buffer) was added at 100 µL/well and plates were

incubated at 37ºC to induce colour development. Optical densities at 405 nm and 650 nm were determined for each well using ThermoMax microplate reader (Molecular Devices, Sunnyvale, California) and SoftMAX Pro software (SD, California, USA). Each ELISA plate was analysed separately. For each plate, sigmoidal dose-response (variable slopes) nonlinear regression was performed on the dose response curves of the samples. Values for the top and bottom were constrained to be the plate maximum and minimum readings. The hill-slope was calculated for the samples with the maximum and minimum readings. This constant hill-slope was applied to all samples on the plate. The logEC50 value (point of inflection which is proportional to the antibody concentration) was determined. The difference between the logEC50 values of each sample compared to the control on each plate was calculated by subtraction. The control was given an arbitary unit of 100 and the samples were plotted on graphs relative to the control. Graphpad Prism 4 (GraphPad Software, San Diego, USA) was used for statistical analysis, and the differences were taken to be significant when $P<0.05$.

2.3.2 Molecular biology assays and techniques

2.3.2.1 Processing tissue samples for genomic DNA

Ear or tails samples were harvested from mice for preparation of genomic DNA for initial genotyping after weaning or for confirmation after experimentations. Ear samples were prepared by the ANU Bioscience Services, by addition of Ear Punch Digestion Buffer mix (50 mM Tris HCl (pH 8.0), 2 mM NaCl, 10mM EDTA, 1% SDS, 2 mg/ mL Proteinase K), digestion at 55°C for 40 minutes and denaturation of Proteinase K at 99°C for 10 minutes. Tail samples were processed using the Qiagen DNeasy 96 tissue kit based on manufacturers instructions.

2.3.2.2 Genotyping by polymerase chain reaction

Genomic DNA was used for genotyping. AccuPrime *Taq* DNA Polymerase High Fidelity was used in reactions according to manufacturer's instructions. The reactions were performed in 0.2 mL thin walled 96-well plates (Quality Scientific Plastics, ON, Canada) using a PTC-225 Peltier Thermal cycler. The 50 µL PCR reactions contained 1 U of polymerase, 20 ng tempate DNA, 10 µM forward and reverse primers and 10×

AccuPrime PCR Buffer I. Variations of the method, PCR cycling conditions and primers are seen in Table 2.14. Reactions were resolved by running samples on a 2% agarose gel.

Table 2.14 Genotyping conditions. All primers are listed from 5' to 3'.

PCR	Primers	Conditions	Cycle	Resolution
Aire	5.0 µM: TCCTGGAACTCACTCACTCTG 5.0 µM: GCCCACTTTCTGCTCATCTC 8.0 µM: AAGGTGAGATGACAGGAGATC	Qiagen Multiplex PCR kit	95°C 15 min followed by 35 cycles of (95°C 20 sec, 56°C 30 sec, 72°C 90 sec), 72°C 2 min	Top band WT, Bottom band MUT
Cblb	2.0µM Cblb WT: CAGACAGTGCCTGCATGA 2.0µM Cblb Rev: GGAAAAATATTAGTTACAACTGG 2.0µM Cblb Mut: TTCCTCCCACTCATGATCTATAG	Qiagen Multiplex PCR kit	95°C 15 min followed by 35 cycles of (94°C 30 sec, 61°C 30 sec, 72°C 50 sec), 72°C 2 min	600bp WT, 550bp MUT
Gld	3.0µM GldA: TCTCAACTCTCTCTGATCAATTTTGAGGAA 5.0µM GldC: ATTCCTGGTGCCCATGATAA	Qiagen Multiplex PCR kit, *Stu*I overnight digestion (Sedger et al., 2010)	95°C 1 min followed by 35 cycles of (95°C 15 sec, 62°C 15 sec, 72°C 10 sec), 72°C 2 min	Bottom band WT, Top band MUT
H2	2.0µM Eα5: AGTCTTCCCAGCCTTCACACTCAGAGGTAC 2.0µM Eα3: CATAGCCCCAAATGTCTGACCTCTGGAGAG 2.0µM K5: CATGGGCATAGAAAGGGCACTCTTTGAACT	Standard	94°C 2 min followed by 35 cycles of 94°C 30 sec, 60°C 30 sec, 72°C 45 sec.	250bp $H2^k$, 150bp $H2^b$
HEL,TCR^{3A9}	5.0µMIg F2: CTGGAGCCCTAGCCAAGGAT 5.0µMIg R1: ACCACAGACCAGCAGGCAGA 0.5µM TCR F1: GCAGTCACCCAAAGCCCAAG 0.5µM TCR R1: CCCCAGCTCACCTAACACTG 4.0µMHEL 4F: ATCCTAAGCGCCCTGGTTTT 4.0µM HEL 4R: TGACCTTCCCACATCAGCAC	Standard	94°C 2 min followed by 35 cycles of (94°C 15 sec, 62°C 30 sec, 72°C 45 sec), 72°C 2 min	371bp TCR^{3A9}, 184bp HEL, 264bp endogenours Ig
Ly5a/b	0.5µM Ly5a/b-1: GAAGGTCGGAGTCAACGGATTTCTTGGCCTGAGCCTGC	Amplifluor® SNPs HT Genotyping	94°C 4 min followed by 35 cycles of	NA

	0.5µM Ly5a/b-2: GAAGGTGACCAAGTTCATGCTTCTCTTGGCCTGAGCCTGT 7.5µM Ly5a/b-R: GCATAAAACATATCCATGGGGTTTAGA 0.5µM SNP FAM Primer (amplifluor kit) 0.5µM SNP JOE Primer (amplifluor kit)	System	(94°C 10 sec, 60°C 20 sec, 72°C 40 sec), 72°C 3 min	
Neo	3µM NeoF: TGAATGAACTGCAGGACGAGG 3µM NeoR: AAGGTGAGATGACAGGAGATC	Standard	94°C 2 min followed by 35 cycles of (94°C 20 sec, 62°C 30 sec, 72°C 45 sec)	Band Neo+
Rag	0.5µM Rag1-1: GAA AGGTCGGAGTCAACGGATTAGC ACCAAACCAGGAACCTGT 0.5µM Rag1-2: GAAGGTGACCAAGTTCATGCTG CACCAAACCAGGGAACCTGC 7.5µM Rag1-R: GCACACTGACAATGAGGCAT 0.5µM SNP FAM Primer (amplifluor kit) 0.5µM SNP JOE Primer (amplifluor kit)	Amplifluor® SNPs HT Genotyping System	94°C 4 min followed by 35 cycles of (94°C 10 sec, 60°C 20 sec, 72°C 40 sec), 72°C 3 min	NA
San roque	0.5µM Sanroque-1: GAAGGTGACCAAGTTCATGCTTTCAGAGCTTCCTCCTGCC 0.5µM Sanroque-2: GAAGGTCGGAGTCAACGGATTCTTCAGAGCTTCCTCTGCA 7.5µM Sanroque-R: GTGTTTAGTTCATCTTTGTTCACCAT 0.5µM SNP FAM Primer (amplifluor kit) 0.5µM SNP JOE Primer (amplifluor kit)	Amplifluor® SNPs HT Genotyping System	94°C 4 min followed by 35 cycles of (94°C 10 sec, 60°C 20 sec, 72°C 40 sec), 72°C 3 min	NA
Unmodulated	0.5µM Unmod-1: GAA AAGGGTCGGAGTCAACCGGATTCTCCTTCCGGGTCATGTTCCT 0.5µM Unmod-2: GAAGGTGACCAAGTTCATGCTTCTCCTTCCGGTCATGTTCCA 7.5µM Unmod-R: CAGACAAGGCCATCTTGGACAT 0.5µM SNP FAM Primer (amplifluor kit) 0.5µM SNP JOE Primer (amplifluor kit)	Amplifluor® SNPs HT Genotyping System	94°C 4 min followed by 35 cycles of (94°C 10 sec, 60°C 20 sec, 72°C 40 sec), 72°C 3 min	NA

2.3.2.3 Agarose gel electrophoresis

2.0 % (w/v) agarose gels were made by dissolving agarose (Amresco, Solon, OH, USA) in 5 mM sodium borate buffer, which was poured into a casting tray and allowed to solidify at room temperature. Electrophoresis was performed in 5 mM sodium borate buffer. Molecular weight markers and DNA samples were mixed with 6× loading dye (5:1 DNA sample: dye ratio), loaded on the solidified gel and electrophoresed at 200-250 volts until the dye-front reached 1 cm from the end of the gel. The gels were stained with GelRed^{TM} (Life Technologies) and visualized under ultraviolet light using the Gene Genios Bioimaging system (SynGene, Frediick, MD, USA). Gel images were taken using the GeneSnap software (SynGene, Cambridge, UK).

2.3.2.4 cDNA synthesis from single cell

cDNA synthesis was performed on single cells in the plates that they had been sorted into using the iScript (Biorad) cDNA synthesis kit according to the manufacturer's instructions. A 2.5 µL mix comprising of 0.5 µL 5× iScript reaction mix, 0.125 µL iScript reverse transcriptase, 0.275 µL 1% Triton X-100 and 1.6 µL nuclease-free water was added to each well. The reaction was incubated for 25°C for 5 minutes, 42°C for 30 minutes, 85°C for 5 minutes. The reaction was centrifuged at 2400 r.p.m. for 1 minute before proceeding to the next step or stored at -20°C before used.

2.3.2.5 Single cell multiplex PCR

After cDNA synthesis, TCR cDNAs were amplified by multiplex PCR according to an established protocol (Dash et al., 2011). Two rounds of nested PCR were done using a Qiagen *Taq* polymerase PCR kit to amplify the TCRα and TCRβ transcripts from each cell in a 25 µL reaction containing 2.5 µL cDNA. The first round of PCR contained 10× PCR buffer, 0.7 µL 50mM $MgCl_2$, 0.5 µL 10mM dNTP mix, 0.5 µL mix of 23 *Trav* external primers (5pmol/µL ea.), 0.5 µL single *Trac* external primer (5 pmol/µL), 0.5 µL mix of 19 *Trbv* external primers (5 pmol/µL ea.), 0.5 µL single *Cβa* external reverse primer (5 pmol/µl) and 0.75U *Taq* DNA Polymerase. Two parallel second rounds of PCR were performed using 2.5 µL of product from the initial PCR reaction: TCRα was amplified by adding 5 pmol/µL mix of 23 *Trav* internal primers and 0.5 µL single *Trac* internal reverse primer (5 pmol/µL); TCRβ was amplified separately by adding 5 pmol/µL mix of 19 *Trbv* internal primers and 0.5 µL single *Trbc* internal reverse primer

(5 pmol/μL). The PCR conditions were 95°C for 5 minutes, followed by 35 cycles of 95°C for 30 seconds, 55°C for 30 seconds, 72°C for 1 minute with a final extension of 72°C for 5 minutes. The PCR products were visualised on a 2% agarose gel, and unincorporated primers and dNTPs were eliminated using by the addition of 1 μL ExoSAP-IT (Affymetrix) to 5 μL PCR product by incubation at 37°C for 15 minutes and 80°C for 15 minutes.

2.3.2.6 DNA sequencing reaction

DNA sequencing reactions were performed in 0.2 mL thin walled 96-well plates (Quality Scientific Plastics, ON, Canada) using a PTC-225 Peltier Thermal cycler. The 20 μL sequencing reactions consist of 1 μL Big Dye 3.1 mix (Amersham, NJ, USA), 6 μL template DNA, 5 pmol appropriate *Trac* internal reverse or *Trbc* internal reverse primers, 1 μL of DMSO and 5 μL 5× CSA Buffer. The PCR conditions were 95°C for 5 minutes, followed by 30 cycles of 96°C for 10 seconds, 55°C for 5 seconds, 60°C for 4 minutes. Terminators were removed using the Qiagen DyeEx 96 Kit. The plates were dried at 95°C for 30 minutes. The samples were sequenced by the Biomolecular Resource Facility (JCSMR, ACT, Australia) on an ABI 3730 capillary sequencer, and analyzed using Finch TV and ExPASy bioinformatic tools.

2.3.2.7 Verification of TCR expression from pMIGII.TCR vectors

293T cells were plated at $2x10^6$ cells in 10 mL cDMEM on 100 mm cell culture dishes (NUNC, Thermo Scientific) and incubated at 37°C, 10% CO_2 overnight. The cells were transfected with 4μg pMIGII.TCR and 4μg pMIGII.CD3δγεξ vector (Szymczak et al., 2004) using the FuGENE 6 transfection reagent (Roche Diagnostics) according to the manufacturer's instructions. Following a 24 hour incubation at 37°C, 10% CO_2, the media on the cells were replaced with 10 mL cDMEM and the cells were incubated for a further 24 hours. Cells were examined under a confocal microscope fitted with a UV filter for detection of GFP to confirm reporter expression by 293T cells. Flow cytometric analysis using anti-TCRβ antibody was performed to determine cell surface expression of TCR.

2.3.2.8 Generation of a stable retroviral producer cell line

293T cells were plated in 100 mm cell cuture dishes at 1×10^6 cells in 10 mL cDMEM and incubated for 24 hours at 37°C, 10% CO_2. Cells were transfected with 4 μg pMIGII.TCR, 4 μg pEQ-Pam3(-E) packaging and 2 μg pVSVg envelope vectors (Holst et al., 2006a) using the FuGENE 6 transfection reagent according to the manufacturer's instructions. Following a 24 hour incubation at 37°C, 10% CO_2, the media from 293T cells were replaced with 10 mL cDMEM. Retrovirus-containing supernatants from the 293T cells were harvested every 12 hours over a 72 hour period. At each harvest, the supernatant was passed through a 0.45 μm filter and used for repeated transduction of GP+E86 cells (plated at 1×10^5 cells in 100mm cell cuture dishes) in the presence of 6 μg/mL hexadimethrine bromide (polybrene). GP+E86 cells were analysed by flow cytometry to assess the GFP expression. Retroviral titres in supernatants from stably transduced GP+E86 producer cell lines were determined by plating 2×10^6 producer cells in 2 mL cDMEM in a 6 well plate and incubating at 37°C, 10% CO_2 for 24 hours. The supernatant was harvested, applied to a 0.45 μm filter and added dropwise to 3T3 cell (plated at 1×10^4 cells in 1 mL cDMEM in a 24 well plate) at concentrations of 1:10, 1:33 and 1:100 in the presence of 6 μg/mL hexadimethrine bromide (polybrene). The cells were incubated for 72 hours prior to analysis of GFP expression by flow cytometry. GP+E86 retroviral producer cells were stored frozen in at -80°C in freezing media.

2.4 *In vivo* studies

2.4.1 Weight studies

Mice were weighed weekly at mid-day by placing the mice in a small box on an electronic weighing scale.

2.4.2 Diabetes incidence studies

Mice were monitored for diabetes by testing urine glucose levels using Bayer Diastix Reagent Strips for Urinalysis to test urine glucose at weekly intervals or tri-weekly intervals (for CFA-HEL adoptive transfer study). Mice with two successive positive

readings of 500 mg/dL (++) were called diabetic. Non-diabetic mice were sacrificed at 20 weeks of age.

2.5 Statistical analysis

Unless otherwise stated, the different groups were compared using the One-Way analysis of variance (ANOVA), followed by pair-wise comparison with a Bonferroni Post Test. This test was used when the data was assumed to follow a normal distribution. When the overall differences were significant, the Bonferroni post-test made pair-wise comparisons between all possible combinations of pairs and corrected for multiple testing amongst the permutations. When data was not expected to be normally distributed, as in histological disease scoring, the Krustal-Wallis test was used to comparethe different groups, followed by pairwise comparisons using the Dunn's Multiple Comparison Test. P-values were taken to be statistically significant when less than 0.05. In instances of mortality or diabetes incidences, the survival log-rank Mantel Cox test was used. All statistical analysis was performed using GraphPad Prism 4 (GraphPad Software, San Diego, USA).

Chapter 3

Genetic deficiency in AIRE co-operates with genetic deficiency in CBLB

Acknowledgements of assistance in the work described in this chapter: Material in this chapter appeared in the Proceedings of the National Academy of Science (Teh et al., 2010). The initial breeding of Aire-deficient mice to Card11$^{unm/wt}$, Fasl$^{gld/gld}$, Rc3h1$^{san/wt}$ or Cblb$^{+/-}$ mice, and preliminary intercrosses of the first three filial generations were performed by Dr. Anselm Enders. The mice were genotyped by the Australian Phenomics Facility, except that most of the Aire genotyping was performed by me. For section 3.4, the weekly weight measurements were done by Ms. Elizabeth Sullivan (Animal Staff, Australian Phenomics Facility). For sections 3.5, the hematoxylin and eosin section cutting and staining was done by Ms. Anne Prins (Flow Cytometry and Microscopy, John Curtin School of Medical Research). Cryosectioning was performed by Ms. Michelle Townsend (IGL Lab Manager). Technical assistance from Mehmet Yabas, Mandeep Singh and Hannes Bergmann were provided for the bone marrow chimera takedown and organ processing in Section 3.6.1 and 3.6.2. Technical help for intraperitoneal injections for section 3.8 was obtained from Dr. Anselm Enders. In section 3.9, Experiment 1 was conducted by me and technical assistance for Experiment 2 was obtained from Debbie Howard (IGL Lab Technician). Unless stated, all other experiments were conducted by me.

3.1 Preamble

To explore the *multi-step model* for the pathogenesis of autoimmune disease, *Aire*-deficient mice (Ramsey et al., 2002b) were intercrossed on a uniform genetic background that is not prone to autoimmunity (B10.BR/SgSnJ; $H2^k$) with mice carrying molecularly defined genetic defects disrupting one of four distinct peripheral T cell tolerance mechanisms: decreased numbers of Foxp3$^+$ T regulatory cells ($Card11^{un/un}$), apoptosis ($Fasl^{gld/gld}$), anergy ($Cbl\text{-}b^{-/-}$), or deregulated activation of T follicular helper cells ($Rc3h1^{san/san}$).

It is predicted that the combination of *Aire*-deficiency with a defined molecular lesion in peripheral tolerance, that acts as a critical failsafe for the *Aire*-pathway, would dramatically accelerate autoimmunity and lead to emergent autoimmune disease not seen with either individual defect. By contrast, no acceleration of autoimmunity and an additive combination of the individual autoimmune phenotypes would result from compounding *Aire* deficiency with a mechanism that does not serve as a failsafe. This chapter describes the preliminary results of the crosses, focusing on one double-deficient combination that displayed severely accelerated lethal organ-specific autoimmunity.

3.2 Mouse strains used in this chapter

3.2.1 The *Aire*-deficient mouse strain

The *Aire*-deficient mouse strain, a kind gift from Prof. Leena Peltonen, bears the truncating nonsense mutation through an insertion of a neomycin resistance cassette at the beginning of exon 6, similar to the major human Finnish APS1 mutation (Ramsey et al., 2002b). RT-PCR and immunostaining using an *Aire*-specific antibody confirmed the absence of *Aire* transcripts and polypeptides, respectively, validating that the mutation was a null mutation (Ramsey et al., 2002b). The $Aire^{-/-}$ mouse was generated on the 129/Sv embryonic stem cell background, and subsequently crossed to the C57BL/6 strain. The mice were imported as (129/Sv x C57BL6)F_2 $Aire^{+/-}$ mice and backcrossed to the B10.BR/SgSnJ; $H2^k$ (B10.BR) background for three generations in our facility.

The final back cross was to the TCR^{3A9} transgenic, insHEL transgenic and *Rag1*-deficient mouse strain[1]. The mouse colony was maintained by intercrossing heterozygous mice for 6 generations. Thus, the original *Aire*-deficient mouse that was used to establish the double deficient crosses had a mixed B10.BR.C57BL/6.N_3F_6 background, homozygous for *Aire*- and *Rag1*-deficiency, and hemizygous for either the TCR^{3A9} on chromosome 5 or insHEL on chromosome 12.

3.2.2 The *Card11*$^{unm/unm}$ mouse strain

The *Card11*$^{unm/unm}$ C57/BL6 mouse strain was generated in the Immunogenomics Laboratory from *N*-ethyl-*N*-nitrosuria mutagenesis screen of third generation offspring in a pedigree that displayed high levels of surface IgM antigen receptors on circulating IgD^+ B cells. The mice had a point mutation changing a thymine to adenine nucleotide, which resulted in a non-polar leucine to a polar glutamine codon substitution in the coiled-coiled domain of Card11 (also called Carma-1) (Jun et al., 2003). Western blotting with an antiserum directed towards Card11 revealed normal levels of expression in B cells, although this has not been tested in T cells. The mutation decreased TCR-CD28 signalling and decreased $FoxP3^+$ regulatory T cells to one sixth of the normal frequency but allowed T cell activation and resulted in T_h2-biased inflammatory disease (Altin et al., 2011). This contrasted with the null mutation in *Card11* that results in a complete absence of $FoxP3^+$ regulatory T cells, abolished T cell activation and caused profound immunodeficiency (Hara et al., 2003; Molinero et al., 2009). The original mice used to establish the double deficient cross was a heterozygous *Card11*$^{unm/wt}$ mouse, hemizygous for TCR^{3A9} on a mixed B10.BR.C57BL/6.N_2F_3 genetic background, having been backcrossed to B10.BR background and intercrossed

---

[1] The TCR^{3A9} and insHEL transgene were included for further study of the central and peripheral tolerance mechanisms. The *Rag1*-deficient strain was used as it was readily available in our laboratory. Subsequent breeding for two filial generations fixed the *Rag1* allele to be homozygous wild-type.

for three generations. The mouse was crossed to an *Aire*$^{-/-}$ mouse that was hemizygous for insHEL (section 3.2.1). The offspring of this breeder pair was intercrossed to generate filial generations for analysis.

3.2.3 The *Fasl*$^{gld/gld}$ mouse strain

The *Fasl*^{gld} mouse strain was obtained from the Jackson Laboratories. The mouse strain harboured a spontaneous thymine to cytosine point mutation near the 3' end of the coding sequence which resulted in a replacement of a highly conserved phenylalanine with a leucine at position 273 in the extracellular region of the encoded protein (Takahashi et al., 1994). The point mutation in the ligand disrupted activation-induced cell death of chronically stimulated mature T cells and caused a slow onset, subclinical autoimmune syndrome characterised by extensive T cell lymphoproliferation and antinuclear autoantibodies in B6 or B10.BR mice (Cohen and Eisenberg, 1991). A B10.BR.*Aire*$^{-/-}$ hemizygous for insHEL (section 3.2.1) was bred with a B10.BR.*Fasl*$^{gld/gld}$ mouse that had been maintained in the laboratory and intercrossed for 14 generations. The offspring of this breeder pair was intercrossed to generate filial generations for analysis.

3.2.4 The *Rc3h1*$^{san/san}$ mouse stain

The C57BL/6.*Rc3h1*$^{san/san}$ mouse strain was generated in the Immunogenomics Laboratory from an *N*-ethyl-*N*-nitrosuria mutagenesis screen of third generation offspring in a pedigree that displayed anti-nuclear antibodies and lymphadenopathy. The mice carried a thymine to guanine substitution in the Rc3h1 ubiquitin ligase resulting in a non-conservative methionine to arginine codon change. This missense mutation caused accumulation of activated T cells and lupus-like autoimmunity in B10.BR mice due to elevated expression of the co-stimulatory ICOS receptor and excessive formation of T follicular helper cells (Linterman et al., 2009; Vinuesa et al., 2005a). To establish a double deficient mouse model, a heterozygous *Rc3h1*$^{san/wt}$ mouse, hemizygous for insHEL was crossed to an *Aire*-deficient mouse (section 3.2.1) that was TCR^{3A9}. The *Rc3h1*$^{san/wt}$ had a mixed CBA.(B10.BR-C57BL/6).N_2F_4. The original strain produced on the C57/BL6 background was backcrossed to CBA, *H2*^{k} for two

generations, and further crossed to CBA.B10.BR. Thus, the complete genomic composition of the mouse was 75% CBA, 12.5% B10.BR and 12.5% B6. The mouse was also hemizygous for TCR^{3A9} and insHEL. The offspring of this breeder pair was intercrossed to generate filial generations for further analysis.

3.2.5 The *Cblb* knockout mouse strain

The *Cblb*^{tm1Pngr} knockout mouse strain (abbreviated as *Cblb*$^{-/-}$ in this thesis) was obtained from Prof. Wallace Langdon. The mouse was generated by introducing a neomycin cassette replacing the region encoding a portion of the tyrosine kinase-binding and RING finger domains, corresponding to amino acids 300 through 340 of the encoded protein. The targeted allele appears to be a null mutation as western blot analysis shows an absence of protein expression in lymph nodes and splenocytes from homozygous mice (Bachmaier et al., 2000). The mutation disrupts mature T cell anergy and releases T cell proliferation from the requirement for CD28 co-stimulation (Bachmaier et al., 2000; Chiang et al., 2000; Fang and Liu, 2001; Gronski et al., 2004; Heissmeyer et al., 2004; Jeon et al., 2004; Naramura et al., 2002; Qiao et al., 2008; Thien and Langdon, 2005) but is insufficient to cause any detectable accumulation of activated T cells, autoimmunity or autoantibodies on the B10.BR background.The *Cblb*$^{-/-}$ mice, originally produced on the 129/B6 background were backcrossed to C57BL/6 for ten generations, backcrossed two generations to B10.BR, and subsequently intercrossed for six generations (B10.BR.C57BL/6.N_2F_6). To generate double deficient mice, a heterozygous *Cblb*$^{-/+}$ mouse, that was hemizygous for insHEL was crossed to a homozygous *Aire*$^{-/-}$ mouse from section 3.2.1. Breeding to subsequent fillial generations was performed by intercrossing mice of the appropriate genotype with each other.

3.3 *Aire*$^{-/-}$*Cblb*$^{-/-}$ double deficient mice have a gravely shortened lifespan

In each of the Aire × peripheral tolerance defect crosses, offspring were monitored for signs of strong co-operative interaction to precipitate early autoimmunity in absence of a latent phase. Three of the four combinations, *Aire*$^{-/-}$*Card11*$^{unm/unm}$, *Aire*$^{-/-}$*Fasl*$^{gld/gld}$ and *Aire*$^{-/-}$*Rc3h1*$^{san/san}$ displayed normal survival rates, remained overtly healthy up to 140 days (Fig. 3.1*A*, *B* and *C*), and showed no clinical signs of accelerated autoimmune

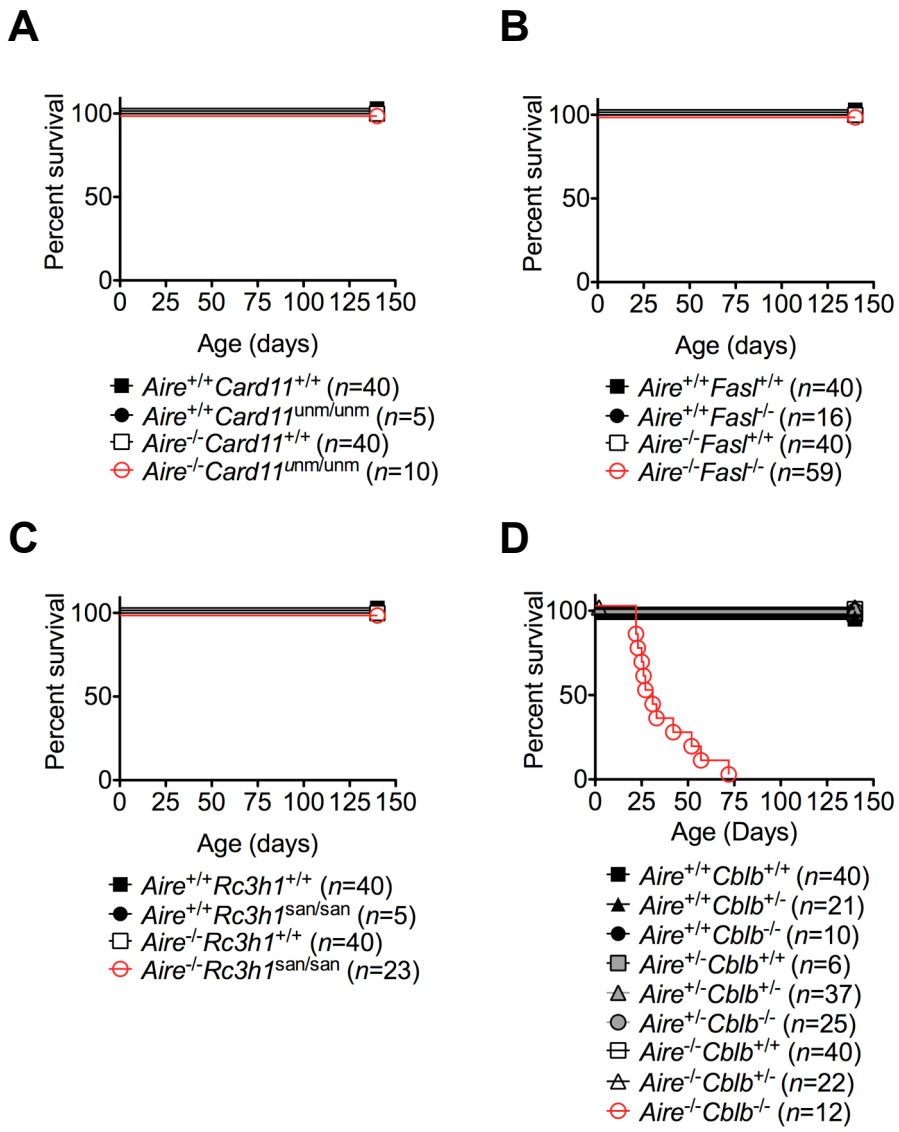

Figure 3.1 Effects of combined genetic defects in central and peripheral tolerance mechanisms.
Survival measured from birth to 140 days for mice with single and double mutations in: (A) *Aire* and *Card11*; (B) *Aire* and *Fasl*; (C) *Aire* and *Rc3h1* (D) *Aire* and *Cblb.* Statistical analysis comparing the *Aire*$^{-/-}$*Cblb*$^{-/-}$ group with all other genotype combinations using a log-rank Mantel-Cox test showed a P value of <0.001.

disease compared to control mice with each individual mutation. By contrast, *Aire*$^{-/-}$ *Cblb*$^{-/-}$ mice either died or needed to be euthanased due to emaciation with median survival of 25 days (Fig. 3.1*D*). Mice with single deficiencies in either *Aire* or *Cblb* remained healthy for at least 140 days.

These preliminary observations allude to the possibility of a *multi-step model* in pathogenesis of autoimmune diseases but only when coupling deficiencies in certain tolerance genes - *Aire*-deficient negative selection mice and *Cblb* mediated T cell anergy**.** Understanding the mechanistic basis of this combination will be the focus of the remaining chapters of the thesis.

3.4 *Aire*$^{-/-}$*Cblb*$^{-/-}$ double deficient mice were produced at normal Mendelian ratios but displayed severe weight loss

Due to the mixed genomic background in the *Aire*$^{-/-}$*Cblb*$^{-/-}$ double deficient cross, control littermate pups were required, necessitating the breeding of all nine possible genotypic combinations. The F_4 to F_9 breeders were able to yield litter sizes of 5.5±3 (average±standard deviation) pups. Each of the 45 litters were analysed for expected Mendelian ratios of the nine possible genotypes based on the genotypes of the parent breeders. This was different in each breeder pair depending on the availability of the mice that were used for breeding. The raw data for the analysis of the breeder pairs are shown in Appendix 3.1. The sum of the observed genotypes and the expected genotypes are shown in Table 3.1. A chi-squared analysis demonstrated that there were no significant statistical differences between the ratio of the mice observed and the expected Mendelian ratios as seen in Table 3.1, except for the *Aire*$^{+/-}$*Cblb*$^{-/-}$ group (25 mice obtained, 30 mice expected) that had a weakly statistical significant P value of 0.0384. In particular, *Aire*$^{-/-}$*Cblb*$^{-/-}$ mice were born at Mendelian frequencies.

At birth, the *Aire*$^{-/-}$*Cblb*$^{-/-}$ mice appeared indistinguishable from littermate counterparts, in size and activity. The weights of the mice were monitored by measurements at weekly intervals for a period of 140 days (Fig. 3.2*A*). Both male and female *Aire*$^{-/-}$*Cblb*$^{-/-}$ mice failed to gain any further weight after 2 weeks of age (Fig. 3.2*B*). Littermates that were deficient in only one gene appeared overtly healthy and did not exhibit any

Table 3.1 Table shows the sum of the obtained and expected Mendelian ratios for 257 mice from 45 litters of the F_4 to F_9 intercrosses of all possible genotype combinations of *Aire*- and *Cblb*- sufficient and deficient mice.

Number of breeder pairs analysed: 8
Number of litter analysed: 45
Number of females: 132
Number of males: 145

Obtained	*Aire*$^{+/+}$	*Aire*$^{+/-}$	*Aire*$^{-/-}$
Cblb$^{+/+}$	10	29	25
Cblb$^{+/-}$	24	53	53
Cblb$^{-/-}$	20	25	18

Expected	*Aire*$^{+/+}$	*Aire*$^{+/-}$	*Aire*$^{-/-}$
Cblb$^{+/+}$	10	24	25
Cblb$^{+/-}$	26	52	48
Cblb$^{-/-}$	16	30	25

Chi-squared test P values	*Aire*$^{+/+}$	*Aire*$^{+/-}$	*Aire*$^{-/-}$
Cblb$^{+/+}$	0.970	0.849	0.757
Cblb$^{+/-}$	0.774	0.996	0.505
Cblb$^{-/-}$	0.530	0.038	0.929

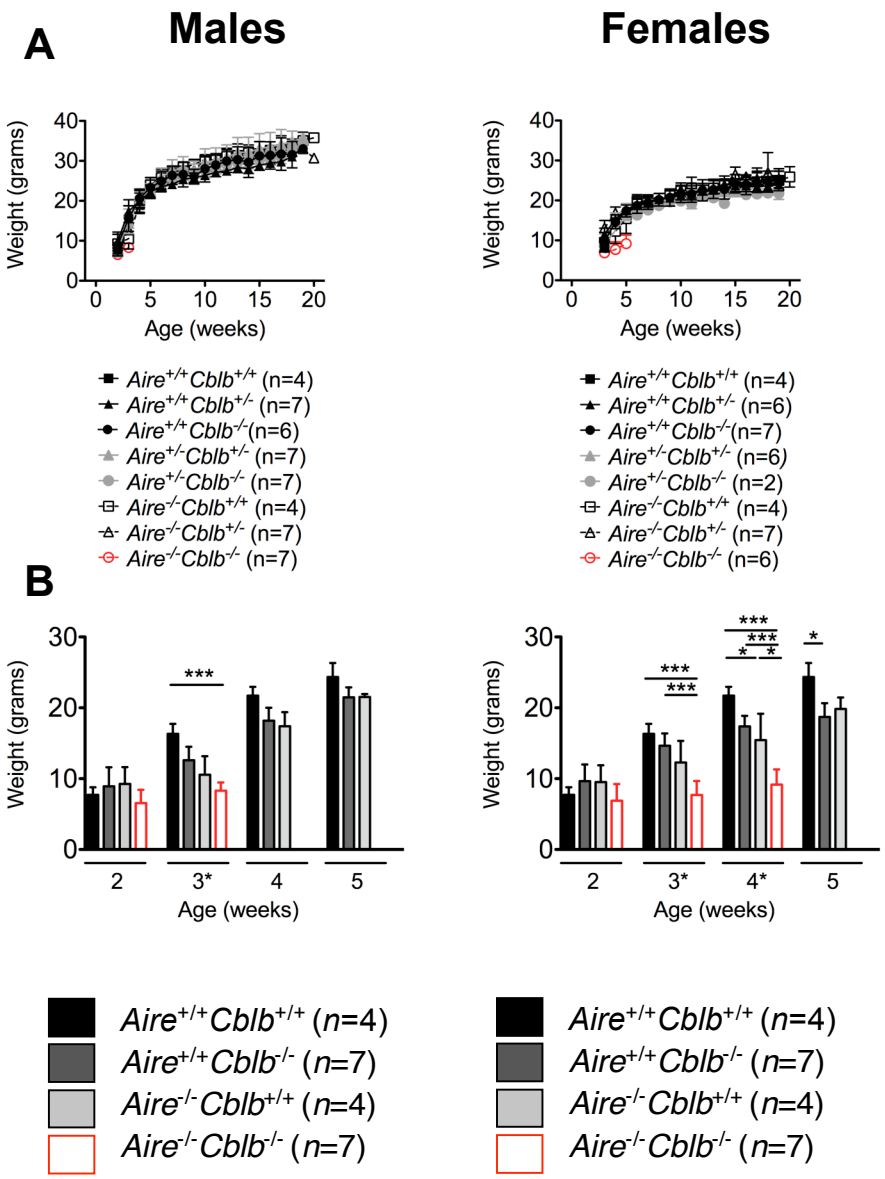

Figure 3.2 *Aire*$^{-/-}$*Cblb*$^{-/-}$ mice fail to gain weight after 2 weeks of age.

A. Body weight of male (left) and female (right) mice of different *Aire* and *Cblb* genotype combinations for 20 weeks.

B. Body weight at 2, 3, 4 and 5 weeks after birth of male (left) and female (right) mice of the indicated genotypes: *Aire*$^{+/+}$*Cblb*$^{+/+}$ (*n* = 4 males, 4 females); *Aire*$^{+/+}$*Cblb*$^{-/-}$ (*n* = 7 males, 7 females) and *Aire*$^{-/-}$*Cblb*$^{+/+}$ (*n* = 4 males, 4 females) or *Aire*$^{-/-}$*Cblb*$^{-/-}$ (*n* = 7 males, 7 females).

significant weight difference by 5 weeks of age, although there was a trend for *Aire*$^{-/-}$ and to a lesser extent *Cblb*$^{-/-}$ mice to be smaller than completely wild-type mice at 3 and 4 weeks of age (Fig. 3.2*B*).

The *Aire*$^{-/-}$*Cblb*$^{-/-}$ mice appeared runted in size, emaciated and possessed rough fur coats compared to control littermates (Fig. 3.3*A*). The mice displayed a decrease in activity and either die suddenly or were euthanised when moribund after losing more than 20% of their body weight, usually immediately after weaning. Gross pathology at necropsy revealed evidence of cachectic wasting including little or no body fat, an involuted thymus, peripheral lymphoid hypoplasia, and a thin, translucent pancreas in all *Aire*$^{-/-}$ *Cblb*$^{-/-}$ animals (Fig. 3.3*B*) but no other abnormalities were detected.

3.5 *Aire*$^{-/-}$*Cblb*$^{-/-}$ double deficient mice had autoimmunity directed towards exocrine pancreas and salivary gland

3.5.1 Histological analysis

To determine the cause of the infant-onset morbidity and mortality, a broad histopathological survey of organs in *Aire*$^{-/-}$*Cblb*$^{-/-}$ mice was conducted. Single deficient *Aire*$^{-/-}$ mice on various backgrounds have previously been shown to display lymphocytic infiltration in the salivary glands, pancreas, eye, thyroid, lung, heart, liver, kidney and testis or ovary (Anderson et al., 2002; Jiang et al., 2005; Niki et al., 2006). However, most of the B10.BR.*Aire*$^{-/-}$ mice analysed here only exhibited mild to moderate gastritis and little or no inflammation of other organs except mild sialoadenitis in approximately 50% of the animals, mild pancreatitis and lung infiltration in approximately 30% and mild hepatitis in 20% of the animals (Figs. 3.4 and 3.5). Hematoxylin and eosin staining of fixed organ sections from 3-6 week old *Aire*$^{-/-}$*Cblb*$^{-/-}$ mice (at time of death or sacrifice) and 20 week old control counterparts were made and the degree of lymphocytic infiltration was scored blinded to genotype on a scale of 1 to 5. A representative hematoxylin and eosin section of each organ from *Aire*$^{+/+}$*Cblb*$^{+/+}$, *Aire*$^{+/+}$*Cblb*$^{-/-}$, *Aire*$^{-/-}$*Cblb*$^{+/+}$ and *Aire*$^{-/-}$*Cblb*$^{-/-}$ is shown in Fig. 3.4 and the corresponding disease scores are shown in Fig 3.5. The scoring was conducted according to the scale in Appendix 3.2: score of (0) indicated no infiltration detected; (1) indicates <12.5%

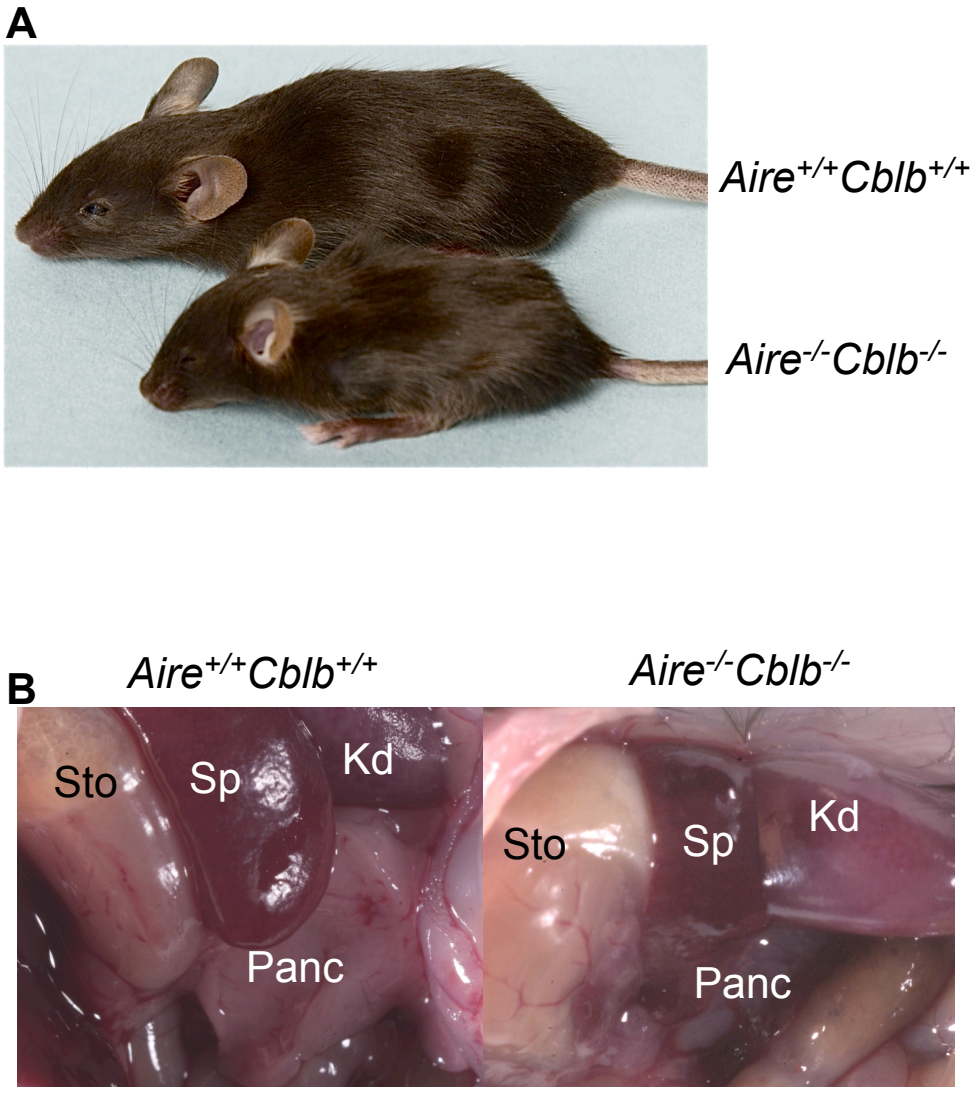

Figure 3.3 Runted appearance and pancreatic atrophy of *Aire*$^{-/-}$ *Cblb*$^{-/-}$ mice.

A. A representative 24 day old female *Aire*$^{-/-}$*Cblb*$^{-/-}$ mouse (bottom) compared to a littermate control (top).

B. An image of the pancreatic atrophy in *Aire*$^{-/-}$*Cblb*$^{-/-}$ mouse (right) compared to a littermate control (left). Sto, stomach; Sp, spleen; Kd, kidney; Panc, pancreas.

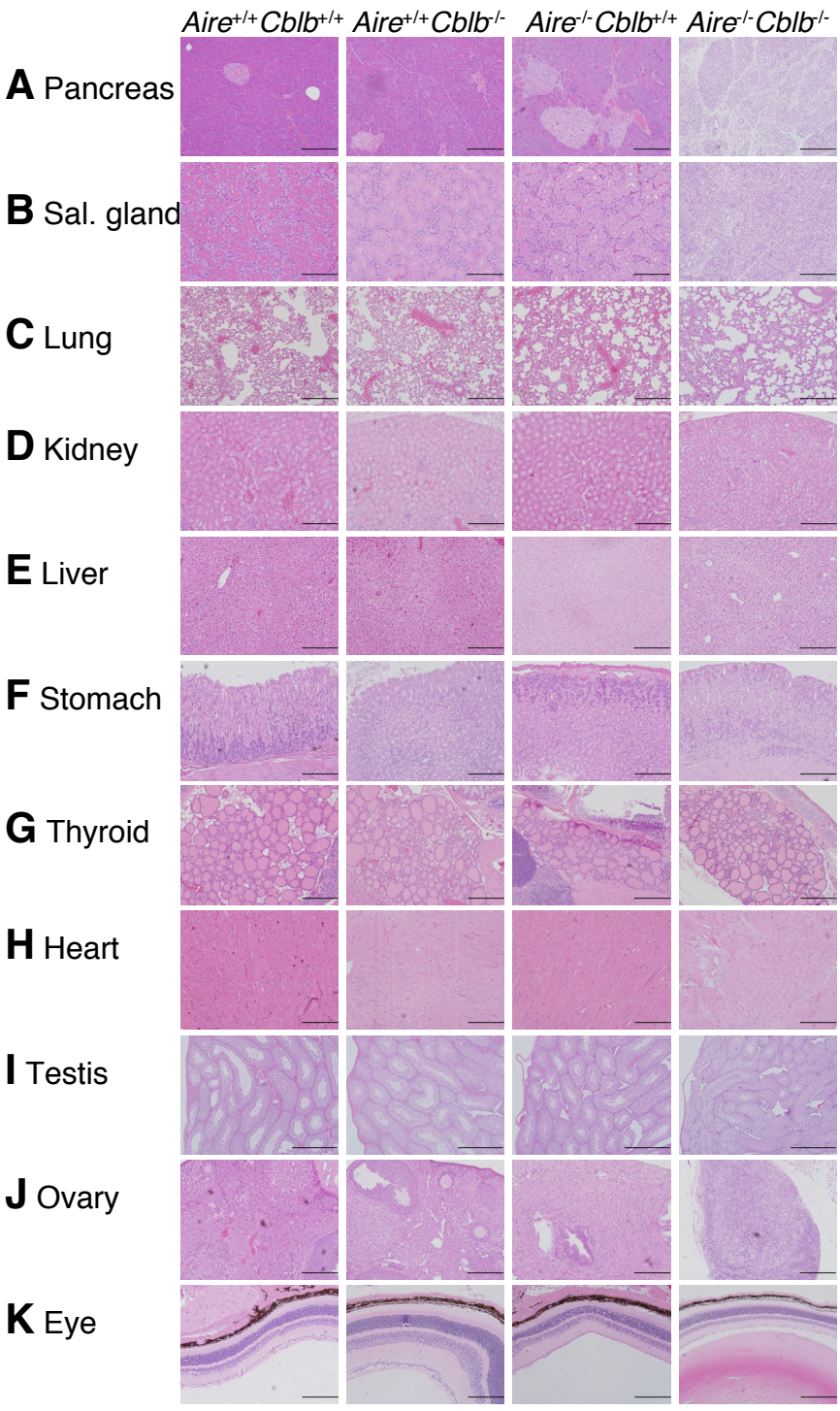

Figure 3.4 Representative hematoxylin and eosin-stained sections from *Aire*$^{+/+}$*Cblb*$^{+/+}$, *Aire*$^{+/+}$*Cblb*$^{-/-}$, *Aire*$^{-/-}$*Cblb*$^{+/+}$ and *Aire*$^{-/-}$*Cblb*$^{-/-}$ mice. Hematoxylin and eosin stained organ sections taken from mouse pancreas (A), salivary gland (B), lung (C), kidney (D), liver (E), stomach (F), thyroid (G), heart (H), testis (I), ovary (J) and eye (K). Organ sections were taken from 20 weeks old mice except for the *Aire*$^{-/-}$*Cblb*$^{-/-}$ group, which were 3-6 weeks old. Original magnification: x200 magnification (bars:200 μm) for all organs except testis (x100 magnification, bars:500 μm).

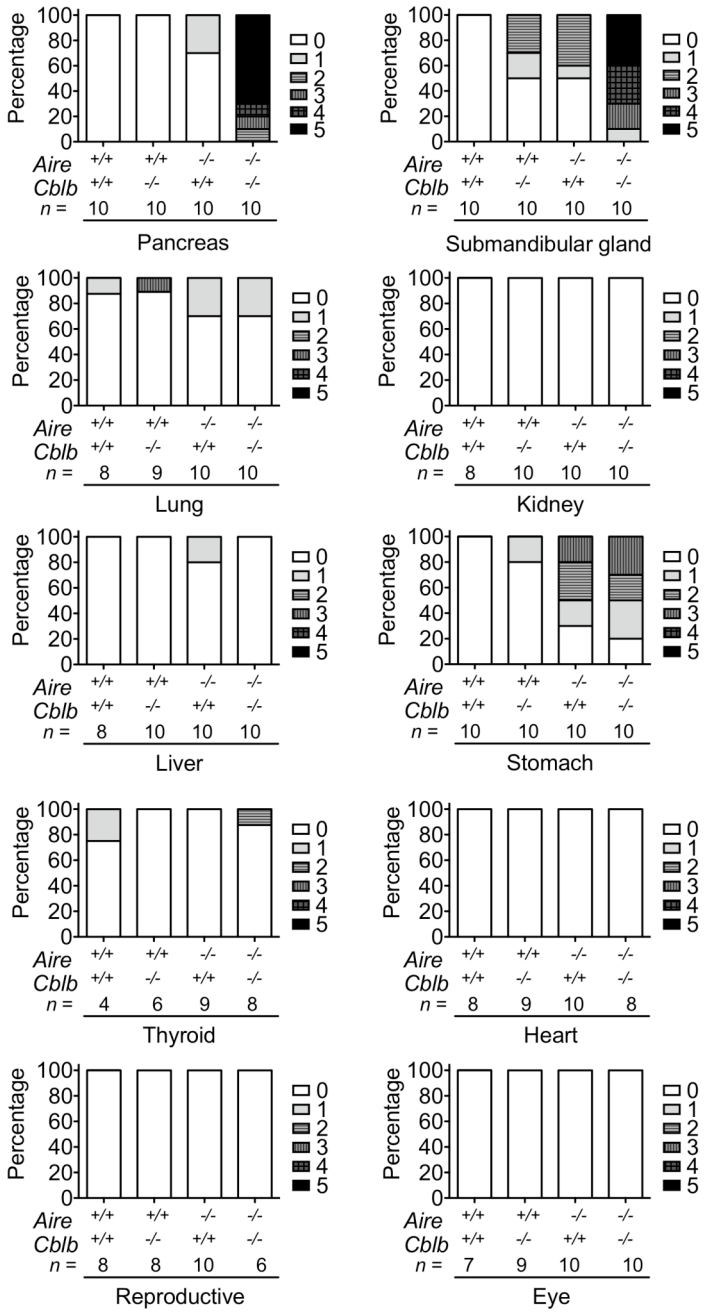

Figure 3.5 Lymphocytic pancreatitis, sialoadenitis and gastritis in *Aire*$^{-/-}$*Cblb*$^{-/-}$ mice.

Percentage of mice of the indicated genotypes with different grades of infiltration in haematoxylin and eosin stained sections from pancreas, submandibular salivary gland, lung, kidney, liver, stomach, thyroid, heart, reproductive organs (testis or ovary) and eye. All mice were 20 weeks of age except *Aire*$^{-/-}$*Cblb*$^{-/-}$ mice that were 3-6 weeks old. Pathology was scored blinded to mouse identifier and genotype, according to the scale shown in Appendix 3.2.

infiltration detected; (2) indicates between 12.5% and 25% infiltration; (3) indicates 25% to 50% infiltration; (4) 50% to 90% infiltration and (5) indicates complete destruction of normal tissue.

For the pancreas, submandibular salivary glands and stomach, a detailed analysis of the organs from all nine possible genotypic combinations of *Aire* and *Cblb* was performed. Of the nine possible genotypic combinations of *Aire* and *Cblb*, all combinations displayed a median disease pancreatitis score of <0.5 except *Aire*$^{-/-}$*Cblb*$^{-/-}$ (median score of 5) and *Aire*$^{-/-}$*Cblb*$^{+/-}$ mice (median score of 1) (Fig. 3.6*A*). Pancreatitis was characterized by a diffused lymphocytic infiltration of the exocrine acinar tissue. This was accompanied by extensive or complete loss of acinar cells, leaving fibrous and adipose tissue interspersed with ducts lined by simple cuboidal epithelium (Fig. 3.6*B*). No evidence of pancreatic islet infiltration was observed and islets remained intact despite the loss of acinar cells. Consistent with these findings, the mice showed no evidence of hyperglycaemia or diabetes.

Similarly, diffuse lymphocytic infiltration was observed in the submandibular salivary glands of *Aire*$^{-/-}$*Cblb*$^{-/-}$ double mutant (median score of 5), mild lymphocytic infiltration in the *Aire*$^{-/-}$*Cblb*$^{+/-}$ (median score of 1) and the single *Aire*$^{-/-}$ and *Cblb*$^{-/-}$ groups (both with a median score of 0.5) (Figs. 3.7*A*), while all other combinations yielded a disease score of <0.5. The male and female submandibular salivary gland exhibits sexual dimorphism, whereby, female glands appear to have smaller serous secreting cells. However, consistent with the results seen for the pancreas, both male and female glands from *Aire*$^{-/-}$*Cblb*$^{-/-}$ mice had infiltrations that were accompanied by partial or complete loss of serous secreting and mucous secreting acinar cells, leaving collapsed structures of the ring shaped serous-secreting acinar cells (Figs. 3.7*B*). The sublingual and parotid salivary glands remained free of ≥ grade 3 lymphocytic infiltrations.

The stomach displayed moderate lymphocyte infiltration in *Aire*$^{-/-}$*Cblb*$^{-/-}$ and *Aire*$^{-/-}$ *Cblb*$^{+/-}$, with a median disease score of 1, although this did not appear to be more severe than in B10.BR littermate mice harbouring single gene deficiency in *Aire* (median score of 1.5) (Fig. 3.8*A*). This indicated that on the B10.BR background, *Aire*$^{-/-}$ mice were

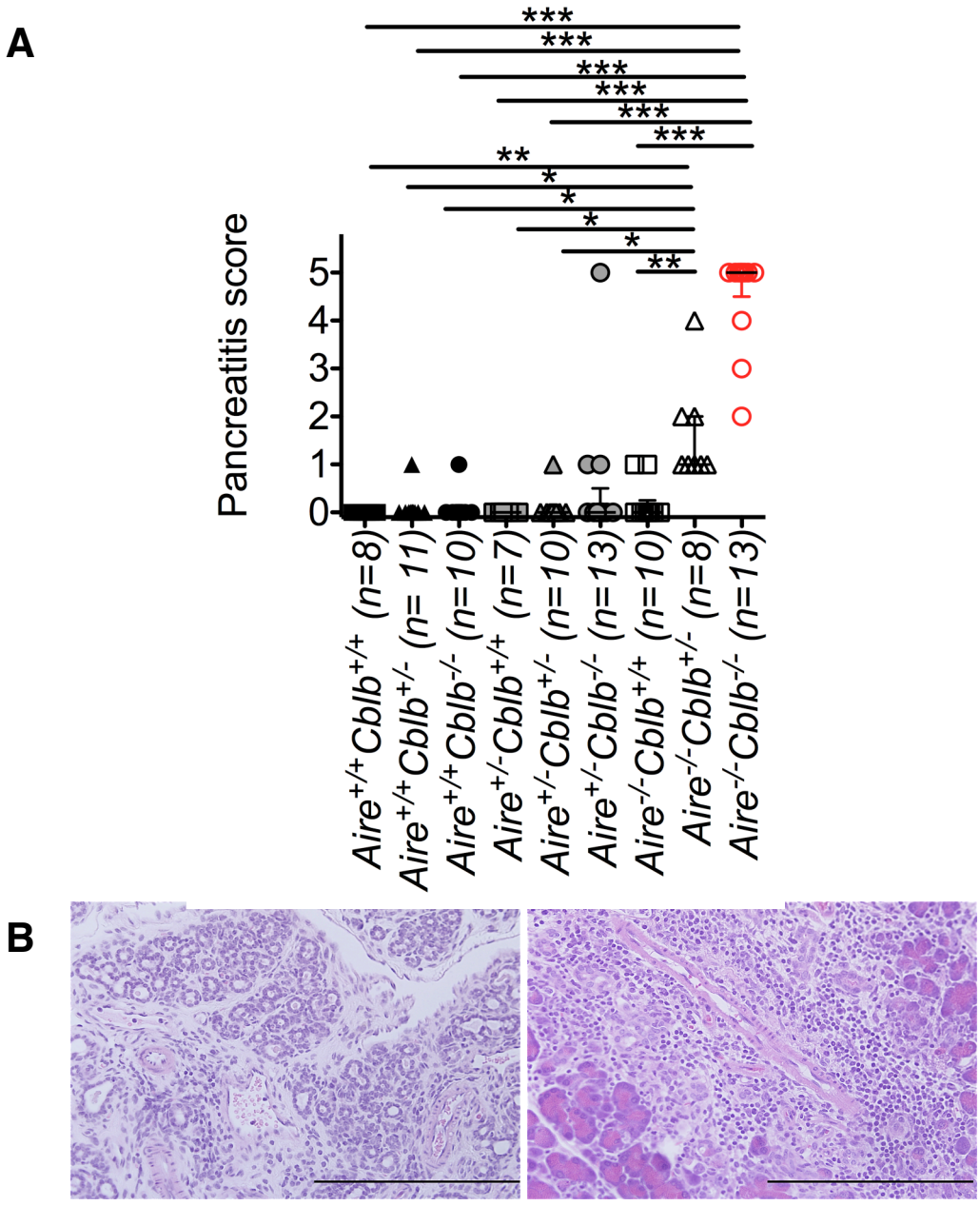

Figure 3.6 Lymphocytic infiltration targeted towards exocrine acinar tissue in pancreas of *Aire*$^{-/-}$*Cblb*$^{-/-}$ mice.

A. Histological scores for the pancreas in 3-6 week old *Aire*$^{-/-}$ *Cblb*$^{-/-}$ mice (taken at time of death or euthanasia) and 20 week old control counterparts (endpoint of study) of the indicated genotypes. Bars represent medians and interquartile ranges. Data were analysed by a Kruskal-Wallis and Dunn's Multiple Comparison test to compare the medians of each group.

B. Higher power images of pancreas from *Aire*$^{-/-}$*Cblb*$^{-/-}$ mice. Left, grade 5 pancreatitis; right, grade 3 pancreatitis. Bars: 200 μm.

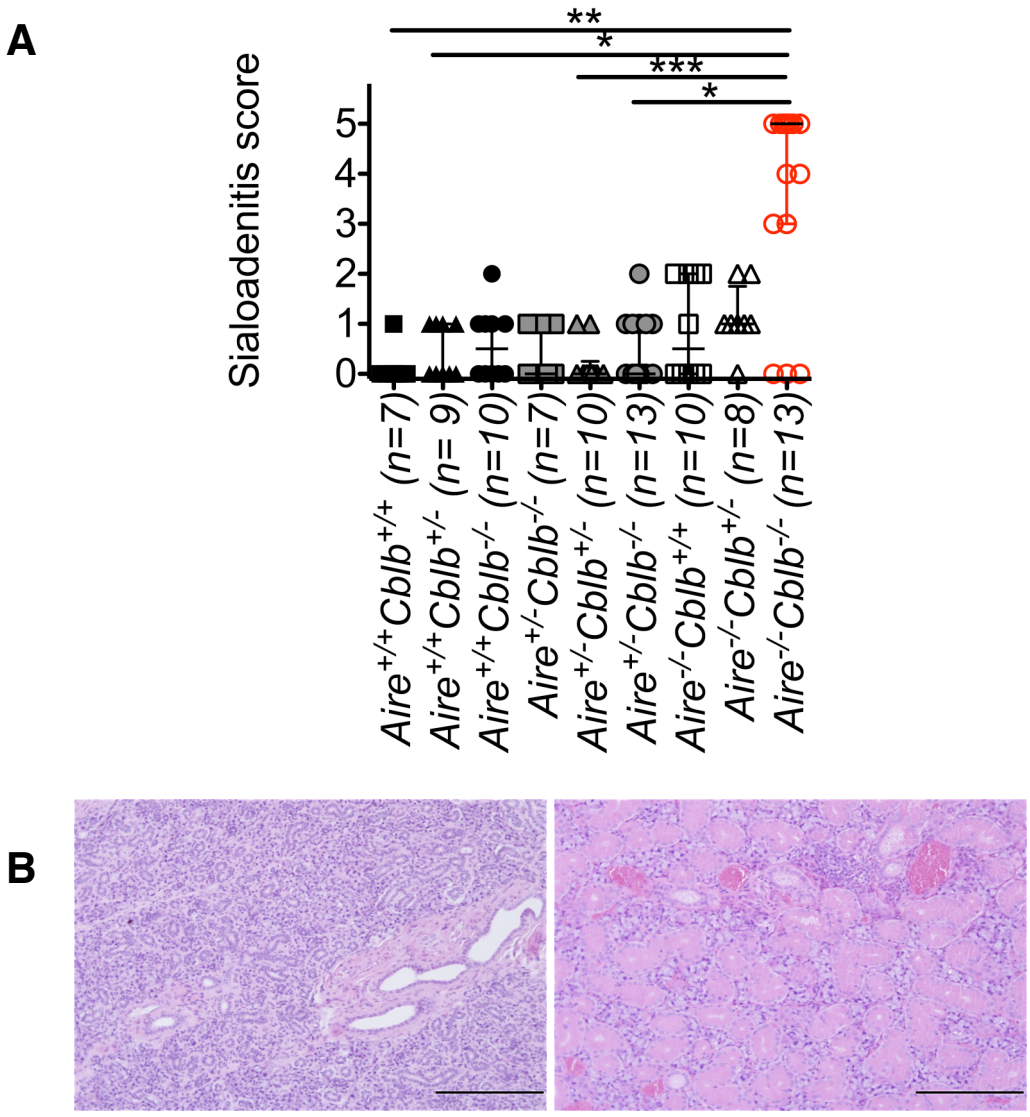

Figure 3.7 Lymphocytic infiltration targeted towards acinar tissue in the submandibular salivary glands of *Aire*$^{-/-}$ *Cblb*$^{-/-}$ mice.

A. Histological scores for the salivary gland from 3-6 week old *Aire*$^{-/-}$*Cblb*$^{-/-}$ mice (taken at time of death or euthanasia) and 20 week old control counterparts (endpoint of study) of the indicated genotypes. Bars represent medians and interquartile ranges. Data were analysed by a Kruskal-Wallis and Dunn's Multiple Comparison test to compare the medians of each group.

B. Submandibular salivary gland from *Aire*$^{-/-}$*Cblb*$^{-/-}$ mice. Left, grade 5 sialoadenitis; right, grade 1 sialoadenitis. Bars: 200 μm.

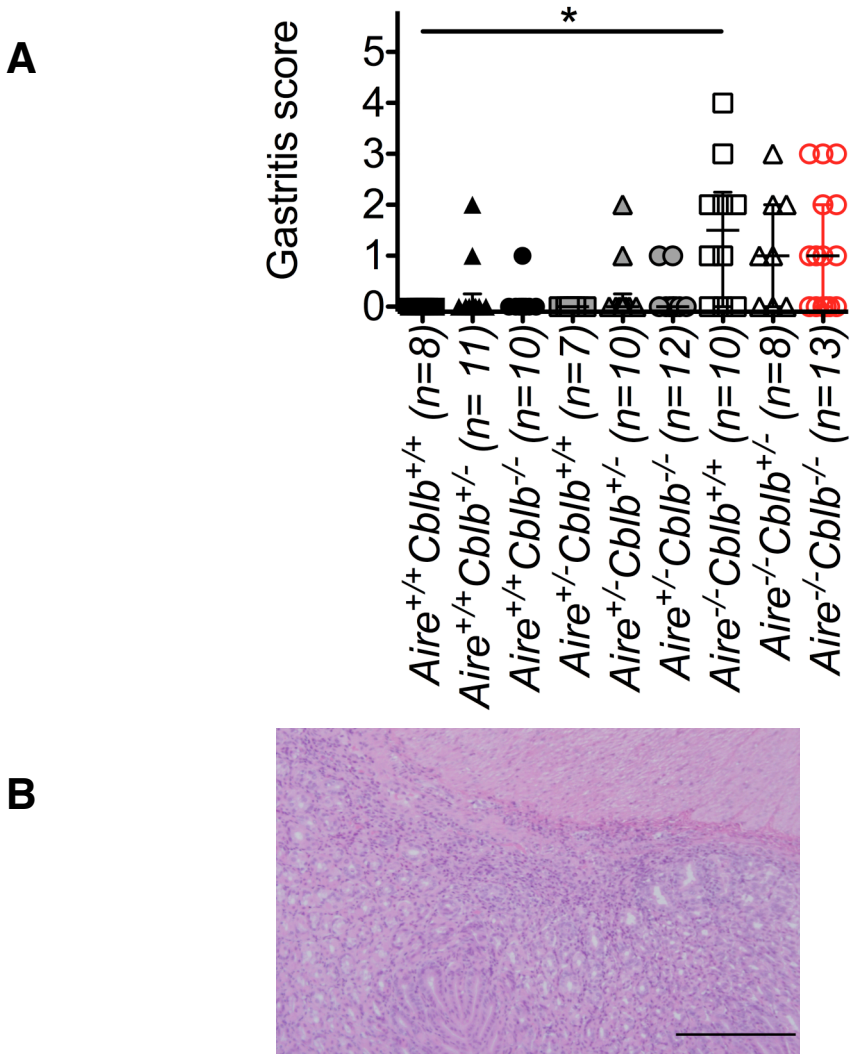

Figure 3.8 Lymphocytic infiltration targeted towards stomach of *Aire*$^{-/-}$*Cblb*$^{-/-}$ mice.

A. Histology scores for the stomach from 3-6 week old *Aire*$^{-/-}$ *Cblb*$^{-/-}$ mice (taken at time of death or euthanasia) and 20 week old control counterparts (endpoint of study) of the indicated genotypes. Bars represent medians and interquartile ranges. Data were analysed by a Kruskal-Wallis and Dunn's Multiple Comparison test to compare the medians of each group.

B. Higher power images of the stomach from *Aire*$^{-/-}$*Cblb*$^{-/-}$ mice grade 3 gastritis. Bars: 200 μm.

prone to lymphocytic infiltration in the stomach regardless of the *Cblb* genotype. By contrast, the majority of mice harbouring the *Aire*$^{-/-}$*Cblb*$^{-/-}$ and single *Aire*$^{-/-}$ or *Cblb*$^{-/-}$ mutations remained free of inflammatory infiltrates in other organs tested, which include the eye, thyroid, lung, heart, liver, kidney and testis or ovary (Fig. 3.4 and 3.5). It is however noted that the *Aire*$^{-/-}$ (regardless of *Cblb* genotype) mice frequently develop blindness in one eye, either due to autoimmunity or retro-orbital bleeding of the mice. In this study, the overtly healthy eye was taken for histological analysis.

3.5.2 Indirect immunofluorescence evidence of IgG autoantibody directed towards the exocrine pancreas

Another characteristic feature previously observed in *Aire*$^{-/-}$ mice on various strain backgrounds was the presence of IgG autoantibodies that targeted specific organs mirroring the pattern of lymphocyte infiltration (Anderson et al., 2002; Jiang et al., 2005; Niki et al., 2006). Serum was collected from 3-6 week old *Aire*$^{-/-}$*Cblb*$^{-/-}$ mice and 20 week old control counterparts. Autoantibodies were detected by applying sera diluted 1:30 to frozen cryosections of tissue sections of the pancreas, salivary glands, lung, kidney, liver, stomach, thyroid, heart eye and testis or ovary from *Rag1*-deficient mice. *Rag1*-deficient mice tissue sections were used so that the sections were free from endogenous IgG, thereby decreasing the background staining with the secondary anti-IgG antibody. Binding of IgG in the serum was detected by the application of an anti-mouse IgG-Alexa-488 fluorescent antibody. Counter-staining was performed using DAPI to allow visualisation of the nucleus in each cell and the stained sections were visualised by epifluorescence microscopy or confocal microscopy. Representative staining and disease scores for all organs tested are seen in Fig. 3.9 and Fig. 3.10.

In line with the results in section 3.5.1, autoantibodies reacting with pancreas and salivary gland were detected in the sera of *Aire*$^{-/-}$*Cblb*$^{-/-}$ mice and not in single mutant controls when tested against frozen organ cryosections (Figs. 3.9 and 3.10).

In the pancreas, *Aire*$^{-/-}$*Cblb*$^{-/-}$ autoantibodies reacted with exocrine acinar cells in pancreas and not with beta cells within the islets of Langerhans, correlating with the specificity of inflammatory destruction seen in histology (Fig. 3.11*A*). Autoantibody

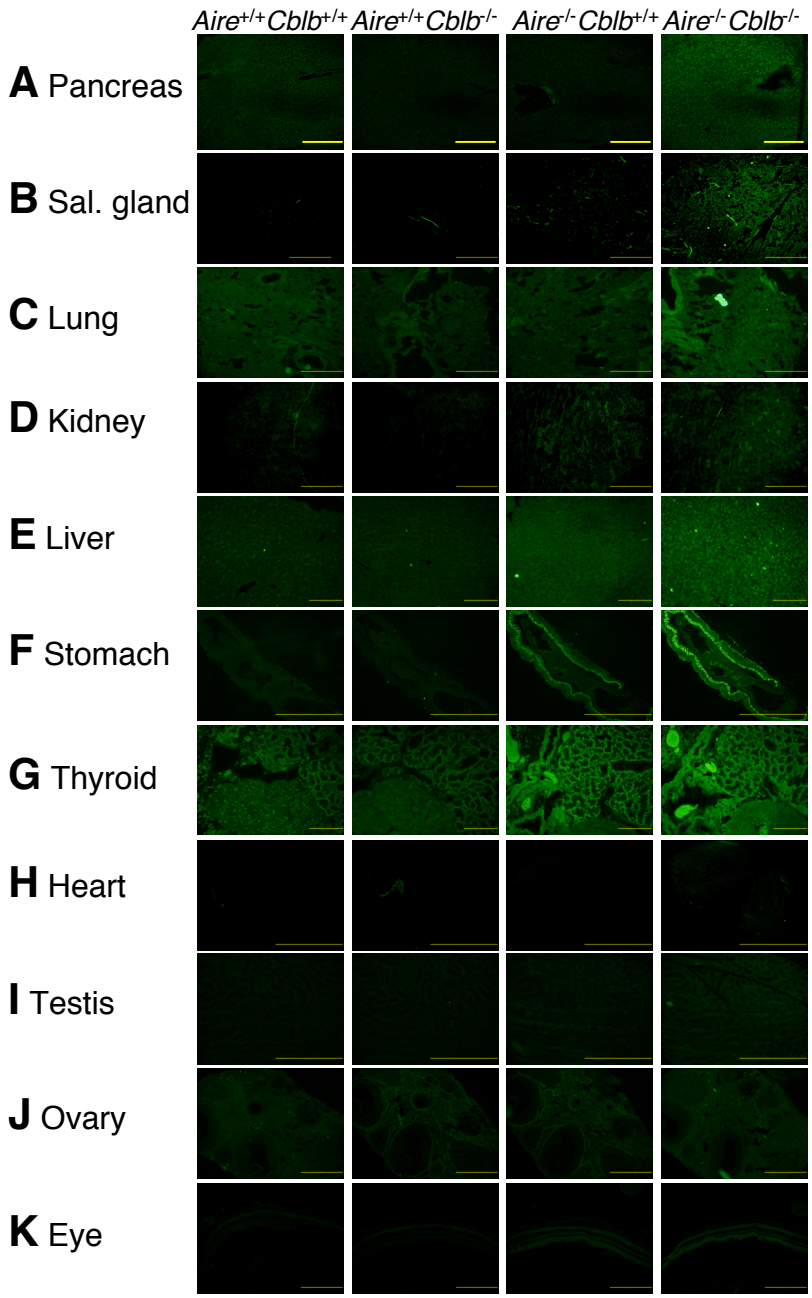

Figure 3.9 Representative immunofluorescence staining of organs with serum IgG from *Aire*$^{+/+}$*Cblb*$^{+/+}$, *Aire*$^{+/+}$*Cblb*$^{-/-}$, *Aire*$^{-/-}$*Cblb*$^{+/+}$ and *Aire*$^{-/-}$*Cblb*$^{-/-}$ mice.
Representative sections of immunofluorescent testing of sera from individual *Aire*$^{+/+}$*Cblb*$^{+/+}$, *Aire*$^{+/+}$*Cblb*$^{-/-}$, *Aire*$^{-/-}$*Cblb*$^{+/+}$ and *Aire*$^{-/-}$*Cblb*$^{-/-}$ mice, tested against frozen sections of *Rag1*$^{-/-}$ pancreas (A), salivary gland (B), lung (C), kidney (D), liver (E), stomach (F), thyroid (G), heart, (H) testis, (I) ovary (J) and eye (K). All mice were 20 weeks of age except *Aire*$^{-/-}$*Cblb*$^{-/-}$ mice that were 3-6 weeks old. Original magnification: x200 magnification, bars: 200 μm for pancreas, liver and thyroid; x100 magnification, bars: 500 μm for salivary glands, lung, kidney, ovary and eye; x40 magnification, bars: 2 mm for stomach, heart and testis.

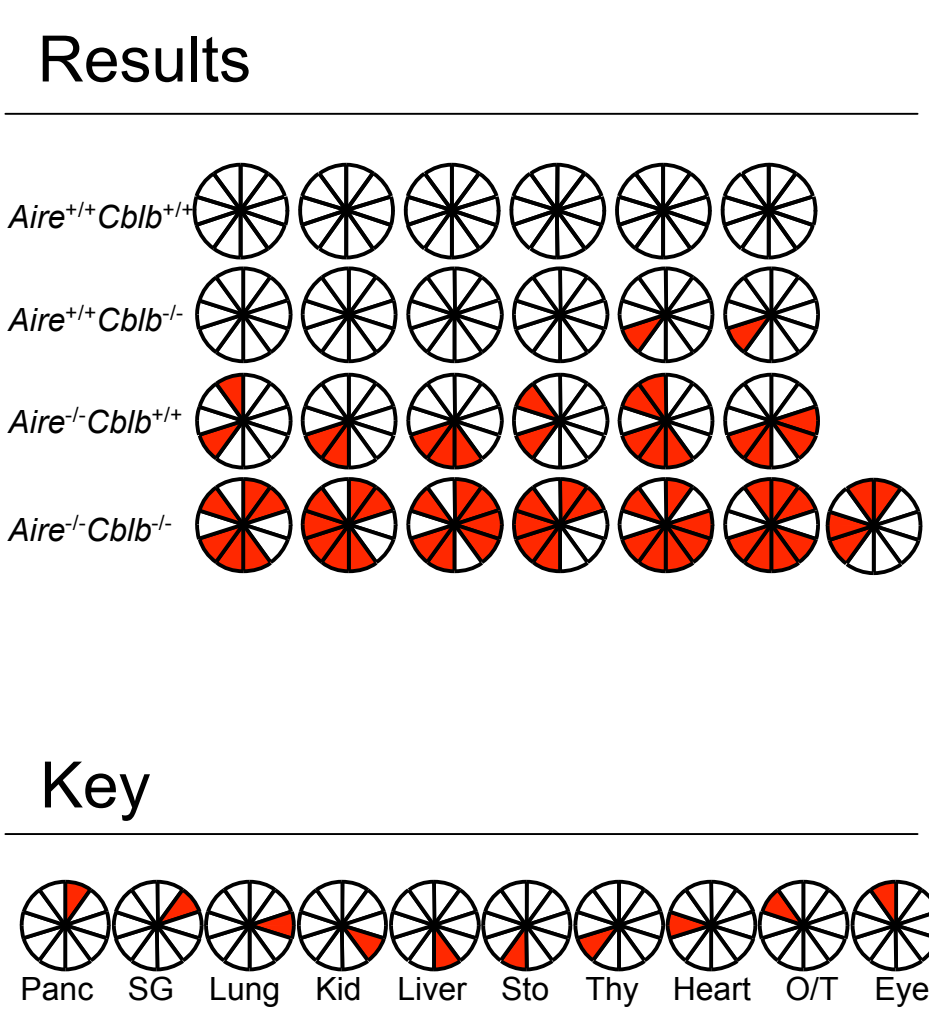

Figure 3.10 Summary of the patterns of organ specific autoantibodies detected in *Aire*$^{-/-}$*Cblb*$^{-/-}$ mice and littermate counterparts.
Each pie chart represents a single mouse and shaded sections denote the detection of autoantibodies in a given organ as indicated by the key above. Panc, pancreas; SG, salivary gland; Kid, kidney; Sto, stomach; Thy, thyroid; O/T, ovary or testis.

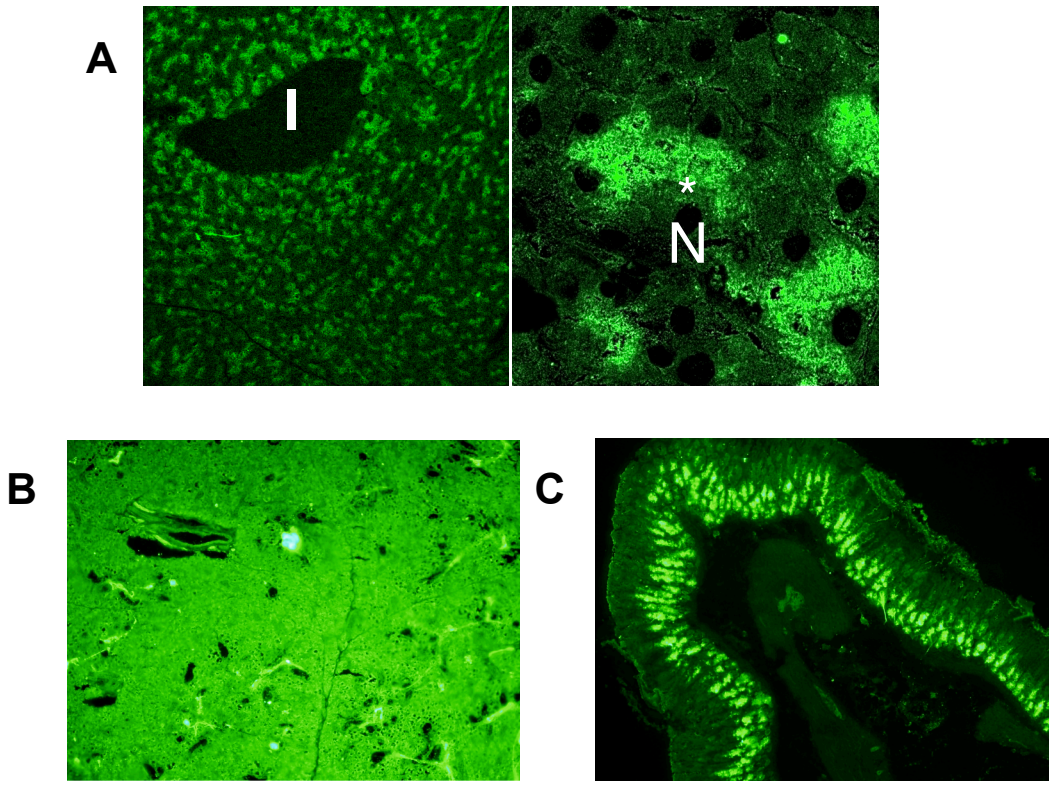

Figure 3.11 Pattern of staining of organ specific autoantibodies in *Aire*$^{-/-}$*Cblb*$^{-/-}$

Representative immunofluorescent staining of frozen sections of pancreas from *Rag1*$^{-/-}$ mice by anti-IgG in serum from *Aire*$^{-/-}$*Cblb*$^{-/-}$ mice.

A. In the pancreas, islet of Langerhans is marked by "I". High power view shows granular pattern of staining most intensely in the apical cytoplasm of exocrine acinar cells, marked by "*". Nuclei are marked by "N". Original magnification: x200 for left panel and x600 for right panel.

B. In the salivary gland, *Aire*$^{-/-}$*Cblb*$^{-/-}$ sera yielded diffuse cytoplasmic staining of most cells in salivary gland. Original magnification: x100.

C. In the stomach, *Aire*$^{-/-}$*Cblb*$^{-/-}$ sera selective stained crypt epithelium. Original magnification: x100.

staining was most intense in the apical, zymogen granule-rich cytoplasm of the pancreatic acinar cells (Fig. 3.11*A*). On the contrary, the pattern of staining in the salivary gland appeared to be more diffuse – strong straining was observed in the cytoplasm of the cells, with no particular structures being stained more intensely (Fig. 3.11*B*). In the stomach, autoantibodies were detected in mice harbouring the *Aire*$^{-/-}$ allele, regardless of the *Cblb* genotype. The stomach autoantibodies targeted the mucosal cells in the basal half of the crypts in the stomach wall (Fig. 3.11*C*). Hence, the pattern of autoantibody reactivity was consistent with the pattern of lymphocyte infiltration seen in section 3.5.1.

3.6 Hematopoietic *Cblb*-deficiency combines with non-hematopoietic *Aire*-deficiency to cause rapid onset disease

Bone marrow chimeras were constructed to further characterize the pancreatic autoimmunity in the *Aire*$^{-/-}$*Cblb*$^{-/-}$ double deficient mice. The experimental design is schematically illustrated in Fig. 3.12. Wild-type or *Aire*$^{-/-}$ mice were lethally irradiated, killing rapidly dividing cells, such as hematopoietic stem cells and cells of the immune system which were replaced by a bone marrow transplant. Different mixtures of donor bone marrow cells were transplanted by intravenous injection: 100% wild-type; 100% *Cblb*$^{-/-}$ marrow or an equal mixture of wild-type and *Cblb*$^{-/-}$ marrow. The donor derived bone marrow stem cells were allowed to reconstitute the hematopoietic system for six weeks. In the bone marrow chimeras, the pancreas and other radioresistant tissues would have had a normal *Cblb* gene, while the T cells would either be normal or lack *Cblb*. On the other hand, *Aire*-deficiency would be present only in the radioresistant non-haematopoietic cells. Previous studies have shown that *Aire* is expressed in non-hematopoietic thymic epithelium where it is crucial for expression of organ specific antigens (Anderson et al., 2002; Gardner et al., 2008; Liston et al., 2003).

The purpose of the chimeras was three-fold. Firstly, it aimed to determine if the selective exocrine pancreas destruction precipitated by the combination of *Cblb* and *Aire* deficiency could have reflected a function of *Cblb* in the pancreas itself, as opposed to its established function in peripheral T cell regulation. Secondly, if the wasting syndrome were recapitulated in the bone marrow chimeras, it would allow the

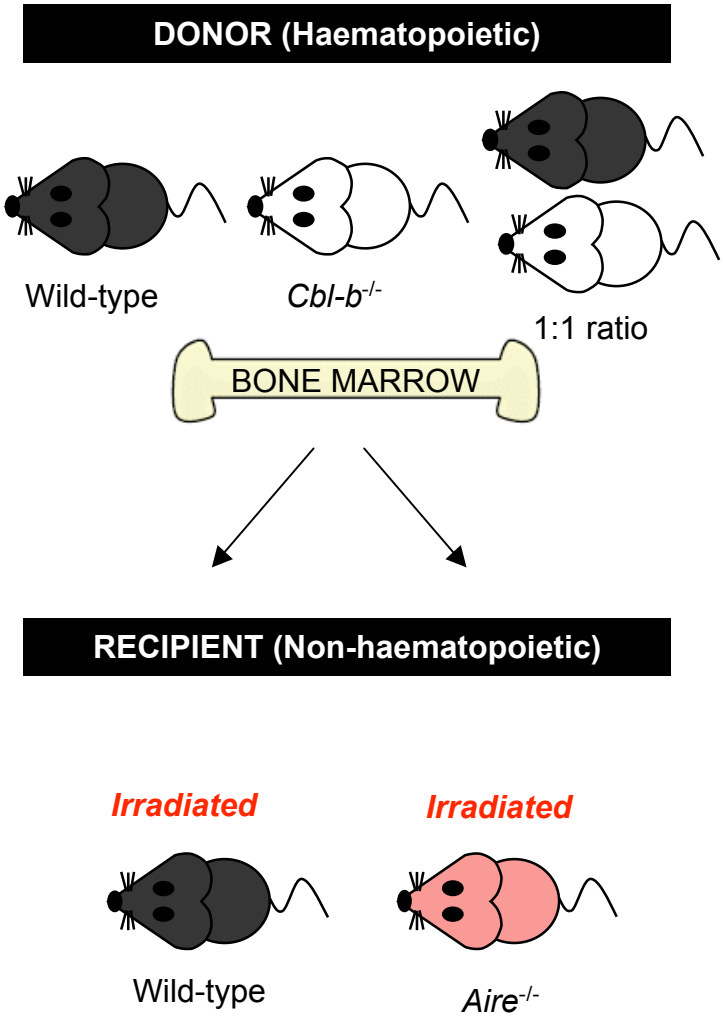

Figure 3.12 Design of the competitive bone marrow chimera experiment.
Aire-deficient or wild-type recipients were lethally irradiated and reconstituted with bone marrow from wild-type or *Cblb*$^{-/-}$ mice in the following three combinations: 100% *Aire*$^{-/-}$, 100% *Cblb*$^{-/-}$ or an equal mixture of both. Each combination was introduced into five recipients.

generation of *Aire*$^{-/-}$*Cblb*$^{-/-}$ double deficient mice in a systematic and synchronized way to facilitate the analysis of lymphocyte development and frequencies. In our breeding strategy, it proved difficult to obtain reasonable numbers of *Aire*$^{-/-}$*Cblb*$^{-/-}$ and age-matched littermate controls for experimentation. Thirdly, it allowed the determination of intrinsic quantitative defects in lymphocyte maturation or survival in competition with wild-type cells (in the 1:1 mixed bone marrow chimera).

3.6.1 Survival, pancreatitis and sialoadenitis in chimeras

A summary of survival results from three independent bone marrow chimera experiments are shown in Table 3.2.. Six weeks post-reconstitution, thirteen out of the nineteen chimeras of *Aire*$^{-/-}$ recipients of *Cblb*$^{-/-}$ marrow developed a cachectic appearance and either died suddenly or were euthanased due to weight lost or ill-health. *Aire*$^{-/-}$ recipients of *Cblb*$^{+/+}$ and wild type recipient of *Cblb*$^{-/-}$ remained relatively healthy as indicated by one death in the ten and thirteen recipients monitored, respectively. Four out of the nine *Aire*$^{-/-}$ chimeras reconstituted with equal mixtures of *Cblb*$^{-/-}$ and *Cblb*$^{+/+}$ marrow also developed wasting establishing that the cooperative autoimmunity was not suppressed in the presence of wild-type T cells.

A representative result from Experiment 2 is seen in Fig 3.13. All *Aire*$^{-/-}$ recipients of *Cblb*$^{-/-}$ marrow did not survive beyond 42 days post reconstitution (Fig 3.13*A*). The *Aire*$^{-/-}$ recipients of a 1:1 mixture of wild-type:*Cblb*$^{-/-}$ marrow, began to appear cachectic by 35 days, and over the course of the experiment two recipients needed to be euthanased (Fig 3.13*A*). Histologically, *Aire*$^{-/-}$ recipients of *Cblb*$^{-/-}$ marrow exhibited severe exocrine pancreatitis and moderate sialoadenitis with extensive or complete loss of acinar cells, whereas their single defect counterparts had limited pancreatitis and sialoadenitis with a disease score of ≤3 for the pancreas and ≤1 for the salivary glands, (Fig 3.13*B* and *C*).

Taken together, the development of the lethal wasting syndrome accompanied by exocrine pancreatitis and sialoadenitis in *Aire*$^{-/-}$ recipients of *Cblb*$^{-/-}$ marrows confirmed

Table 3.2 Results of transplanting *Cblb*$^{-/-}$ or wild-type bone marrow, or an equal mixture of the two, into *Aire*-deficient or wild-type recipients. In the mixed chimeras, the wild-type marrow carried a CD45.1 allelic marker, enabling flow cytometric analysis to confirm equal reconstitution. Numerator, numbers of mice that died suddenly or were sacrificed when moribund or had lost 20% of the body weight; denominator, total number of mice tested; n.d, not done.

Recipients	***Aire*$^{-/-}$**			***Aire*$^{+/+}$**		
Donors	***Cblb*$^{-/-}$**	***Cblb*$^{+/+}$**	***Cblb*$^{-/-}$: *Cblb*$^{+/+}$**	***Cblb*$^{-/-}$**	***Cblb*$^{+/+}$**	***Cblb*$^{-/-}$: *Cblb*$^{+/+}$**
Experiment 1	2/5	n.d.	2/4	0/3	0/3	n.d.
Experiment 2	5/5	1/5	2/5	1/5	0/5	0/5
Experiment 3	6/10	0/5	n.d.	0/5	0/10	n.d.
Total	13/19	1/10	4/9	1/13	0/18	0/5

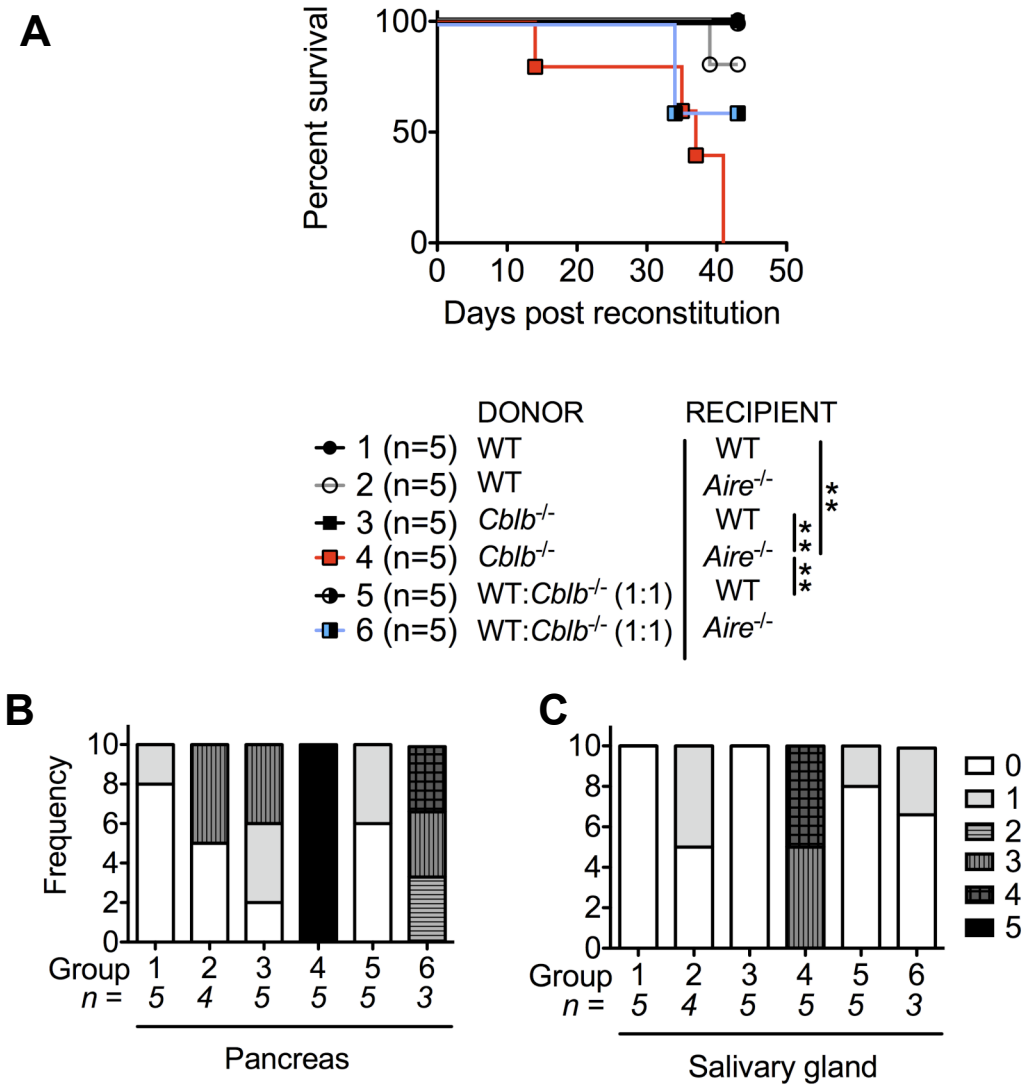

Figure 3.13 Pancreatitis and sialoadenitis results from *Cblb*-deficiency in the haematopoietic compartment and *Aire*-deficiency in the non haematopoietic system.

A. Survival of *Aire*-deficient or wild-type recipients after reconstitution with *Cblb*$^{-/-}$ or wild-type bone marrow, or an equal mixture of the two. ** indicates a P<0.01 calculated using a log-rank Mantel-Cox test.

B. Pancreatitis scores of recipient mice

C. Sialoadenitis scores of recipient mice.

the non-hematopoietic requirement for *Aire*$^{-/-}$ and hematopoietic requirement for *Cblb*$^{-/-}$ in the development of the disease.

3.6.2 Analysis of lymphocyte development in bone marrow chimeras

To understand the effects of the single and double deficiency in *Aire* and *Cblb*, T lymphocyte populations in the thymus, spleen and lymph nodes were analysed. For all results in this section, wild-type or *Cblb*$^{-/-}$ into wild-type or *Aire*$^{-/-}$ bone marrow chimeras were generated, and the mice were euthanised 29 days post-reconstitution before any of the mice succumbed to the lethal wasting syndrome.

3.6.2.1 Lymphocyte populations in the central lymphoid organ, the thymus

Representative analysis of the lymphocyte populations in the thymus are shown in Fig. 3.14 and quantified in Table 3.3. The different subpopulations were identified based on the expression of the cell surface markers CD4 and CD8 to distinguish double negative (DN, CD4$^-$CD8$^-$), double positive (DP, CD4$^+$CD8$^+$), CD4 single positive (CD4$^+$CD8$^-$) and CD8 single positive (CD4$^-$CD8$^+$) cells. Compared to the wild-type and single mutant controls, there were no significant differences in these populations (Table 3.4).

The DN populations were further divided into four subpopulations, DN1 (CD25$^-$CD44^{high}), DN2 (CD25$^+$CD44^{high}), DN3 (CD25$^+$CD44^{low}) and DN4 (CD25$^-$ CD44^{low}), representing successive stages of maturity. As seen in Table 3.3 and 3.4, higher numbers of DN1 cells appeared to be present in *Aire*$^{-/-}$ mice. Likewise, a similar trend of increase in DN4 in the *Aire*$^{-/-}$ groups compared to wild-type was also observed when comparing their percentage but not their absolute number (Table 3.4). Given the multiple tests performed, these subtle abnormalities in the DN1 and DN4 population would need to be tested in independent experiments to determine if they are indeed reproducible.

Further subdivision of the CD4 cells into CD4$^+$FoxP3$^-$ cells and CD4$^+$FoxP3$^+$ natural T regulatory cells (nTreg) demonstrated comparable total numbers and percentages of

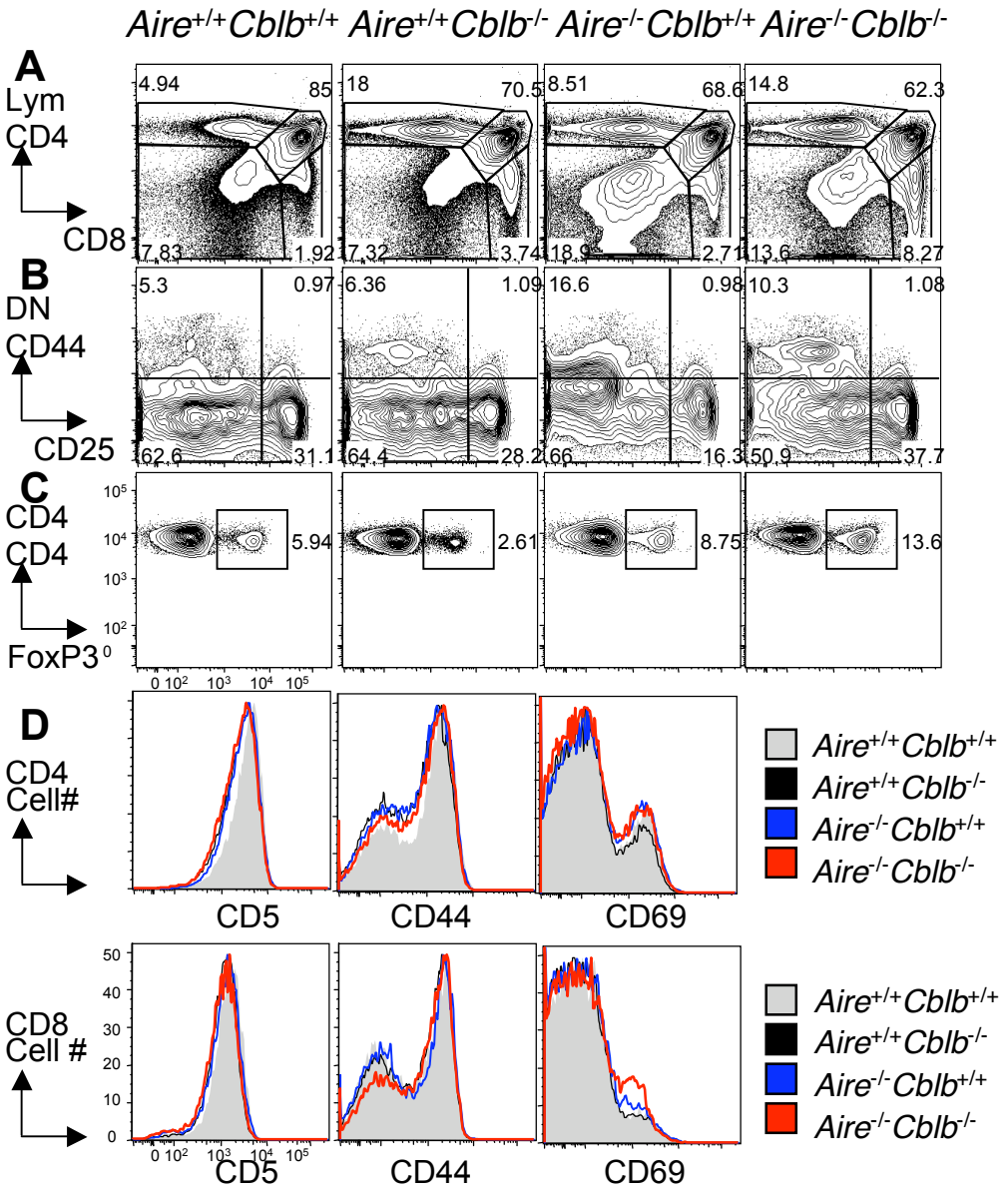

Figure 3.14 Representative flow cytometric analysis of the thymus from *Aire*$^{+/+}$*Cblb*$^{+/+}$, *Aire*$^{+/+}$*Cblb*$^{-/-}$, *Aire*$^{-/-}$*Cblb*$^{+/+}$ and *Aire*$^{-/-}$*Cblb*$^{-/-}$ bone marrow chimeras.

A. Gated on lymphocytes (Lym), showing the percentage of DN, DP, CD4 and CD8 subsets

B. Gated on DN cells (DN), showing the percentages of DN1, DN2, DN3, DN4 subsets

C. Gated on CD4^{+} single positive cells, showing the percentages of CD4^{+}FoxP3^{+} subsets

D. Gated on CD4^{+} (top) or CD8^{+} (bottom), showing CD5, CD44 and CD69 expression on each subset.

Table 3.3 Table shows the means and standard deviations of lymphocyte populations in the thymus, spleen, inguinal/axillary and pancreatic lymph nodes of the different bone marrow chimera groups.

	Aire$^{+/+}$*Cblb*$^{+/+}$	*Aire*$^{+/+}$*Cblb*$^{-/-}$	*Aire*$^{-/-}$*Cblb*$^{+/+}$	*Aire*$^{-/-}$*Cblb*$^{-/-}$
Thymus				
Total cells (x10^6)				
All lymphocytes	14.93±5.993	7.054±5.029	5.33±3.845	10.16±7.448
CD25$^-$CD44^{high} (DN1)	0.047±0.011	**0.031±0.014**	**0.128±0.079**	0.074±0.056
CD25$^+$CD44^{high} (DN2)	0.007±0.002	0.005±0.002	0.006±0.002	0.009±0.007
CD25$^+$CD44^{low} (DN3)	0.219±0.065	0.153±0.097	0.134±0.059	0.202±0.116
CD25$^-$CD44^{low} (DN4)	0.548±0.201	0.391±0.226	0.522±0.198	0.51±0.254
CD4$^+$CD8$^+$ (DP)	12.91±5.265	5.682±4.653	3.661±3.399	8.21±6.756
CD4$^+$ (SP)	0.902±0.493	0.599±0.334	0.647±0.297	0.875±0.408
CD8$^+$ (SP)	0.265±0.114	0.168±0.089	0.181±0.06	0.239±0.08
CD4$^+$FoxP3$^+$ (SP)	0.036±0.018	0.025±0.018	0.04±0.014	0.041±0.015
% from total lymphocytes				
CD25$^-$CD44^{high} (DN1)	**0.331±0.062**	**0.557±0.321**	**2.824±1.823**	1.186±1.188
CD25$^+$CD44^{high} (DN2)	0.051±0.019	0.079±0.032	0.131±0.058	0.119±0.072
CD25$^+$CD44^{low} (DN3)	1.578±0.599	2.246±0.448	2.859±0.803	2.675±1.58
CD25$^-$CD44^{low} (DN4)	**3.772±1.11**	6.528±3.489	**11.18±3.63**	6.186±2.815
CD4$^+$CD8$^+$ (DP)	86.36±0.94	73.9±13.67	62.58±13.61	74.52±10.99
CD4$^+$ (SP)	5.902±0.987	12.79±8.433	14.9±10.01	10.91±4.005
CD8$^+$ (SP)	1.794±0.34	3.412±2.182	4.404±2.971	3.736±2.701
CD4$^+$FoxP3$^+$ (SP)	0.245±0.059	0.506±0.381	0.948±0.457	0.811±0.76
Spleen				
Total cells (x10^6)				
All lymphocytes	13.04±1.708	10.04±4.698	8.538±2.247	9.53±4.369
B cells	5.996±1.116	4.026±1.711	3.231±1.206	5.144±3.722
CD4$^+$	0.798±0.047	0.703±0.399	0.638±0.176	0.674±0.238
CD8$^+$	0.255±0.056	0.269±0.114	0.354±0.18	0.278±0.085
CD4$^+$FoxP3$^+$	0.296±0.032	0.256±0.142	0.215±0.066	0.234±0.096
CD4$^+$CD5$^+$	0.766±0.044	0.667±0.384	0.598±0.159	0.643±0.232
CD4$^+$CD44$^+$	0.578±0.033	0.504±0.32	0.445±0.161	0.45±0.136
CD4$^+$CD69$^+$	0.192±0.028	0.187±0.123	0.156±0.048	0.173±0.065
CD8$^+$CD5$^+$	0.237±0.051	0.249±0.104	0.308±0.149	0.256±0.081
CD8$^+$CD44$^+$	0.158±0.03	0.174±0.069	0.266±0.163	0.177±0.046
CD8$^+$CD69$^+$	0.042±0.016	0.038±0.024	0.068±0.081	0.049±0.017
% from total lymphocytes				
B cells	46.27±8.288	40.58±3.154	38.55±11.76	48.01±18.48
CD4$^+$	6.178±0.595	6.815±1.486	7.508±0.708	7.751±2.748
CD8$^+$	1.942±0.206	2.799±0.857	3.976±1.236	3.305±1.239

$CD4^+FoxP3^+$	2.287±0.296	2.476±0.382	2.497±0.145	2.592±0.753
$CD4^+CD5^+$	5.934±0.591	6.435±1.226	7.026±0.527	7.335±2.426
$CD4^+CD44^+$	4.489±0.581	4.747±0.941	5.101±0.599	5.191±1.66
$CD4^+CD69^+$	1.485±0.245	1.741±0.456	1.808±0.087	1.921±0.429
$CD8^+CD5^+$	1.807±0.19	2.596±0.774	3.474±1.004	3.013±1.062
$CD8^+CD44^+$	**1.207±0.148**	1.801±0.403	**2.912±1.353**	2.169±0.911
$CD8^+CD69^+$	0.318±0.1	0.365±0.102	0.705±0.654	0.597±0.271
	$Aire^{+/+}Cblb^{+/+}$	$Aire^{+/+}Cblb^{-/-}$	$Aire^{-/-}Cblb^{+/+}$	$Aire^{-/-}Cblb^{-/-}$
Lymph nodes				
Total cells ($x10^6$)				
All lymphocytes	0.596±0.207	0.706±0.265	0.428±0.358	0.54±0.173
B cells	0.329±0.112	0.324±0.194	0.22±0.199	0.259±0.124
$CD4^+$	0.132±0.056	0.16±0.059	0.098±0.079	0.139±0.03
$CD8^+$	0.043±0.015	0.062±0.026	0.043±0.034	0.054±0.01
$CD4^+FoxP3^+$	0.047±0.023	0.063±0.018	0.036±0.033	0.052±0.012
$CD4^+CD5^+$	0.125±0.051	0.153±0.054	0.091±0.071	0.128±0.028
$CD4^+CD44^+$	0.074±0.037	0.102±0.032	0.057±0.042	0.083±0.014
$CD4^+CD69^+$	0.038±0.019	0.056±0.023	0.031±0.022	0.048±0.01
$CD8^+CD5^+$	0.042±0.014	0.06±0.025	0.04±0.031	0.05±0.011
$CD8^+CD44^+$	0.018±0.007	0.039±0.013	0.024±0.019	0.031±0.003
$CD8^+CD69^+$	0.008±0.002	0.015±0.007	0.01±0.006	0.013±0.004
% from total lymphocytes				
B cells	55.37±3.634	43.3±15.65	49.59±4.345	46.2±8.663
$CD4^+$	21.75±3.001	23.08±3.182	23.14±2.186	26.82±6.31
$CD8^+$	7.369±1.299	8.767±0.8824	10.5±2.338	10.56±2.626
$CD4^+FoxP3^+$	7.704±1.508	9.356±2.039	8.587±2.336	10.08±2.636
$CD4^+CD5^+$	20.62±2.549	22.1±3.297	22.01±2.278	24.76±5.611
$CD4^+CD44^+$	12.09±2.439	15.13±3.655	13.73±1.428	16.18±4.218
$CD4^+CD69^+$	6.242±1.226	8.14±1.664	7.735±1.736	9.274±2.55
$CD8^+CD5^+$	7.215±1.294	8.494±1.005	10.03±2.359	9.802±2.493
$CD8^+CD44^+$	**3.025±0.7179**	5.538±0.5836	**6.119±1.988**	**6.199±2.01**
$CD8^+CD69^+$	**1.331±0.2847**	2.141±0.1832	**2.836±1.202**	2.554±0.7777
Pancreatic lymph nodes				
Total cells ($x10^6$)				
All lymphocytes	0.908±0.549	0.588±0.297	0.794±0.27	0.782±0.257
B cells	0.403±0.291	0.182±0.218	0.224±0.123	0.349±0.175
$CD4^+$	0.221±0.139	0.161±0.067	0.194±0.072	0.191±0.046
$CD8^+$	0.046±0.031	0.033±0.015	0.046±0.021	0.046±0.007
$CD4^+FoxP3^+$	0.056±0.037	0.046±0.025	0.04±0.012	0.042±0.017
$CD4^+CD5^+$	0.216±0.134	0.158±0.065	0.184±0.068	0.183±0.046
$CD4^+CD44^+$	0.175±0.115	0.134±0.063	0.154±0.064	0.15±0.041
$CD4^+CD69^+$	0.077±0.048	0.062±0.03	0.082±0.036	0.075±0.011
$CD8^+CD5^+$	0.043±0.029	0.031±0.015	0.04±0.019	0.042±0.006

$CD8^+CD44^+$	0.028±0.022	0.024±0.011	0.033±0.018	0.032±0.008
$CD8^+CD69^+$	0.011±0.007	0.01±0.006	0.013±0.006	0.013±0.003
% from total lymphocytes				
B cells	41.94±13.25	24.15±20.27	32.84±20.71	43.39±6.876
$CD4^+$	24.11±3.206	28.26±6.273	24.06±1.784	24.85±1.723
$CD8^+$	4.958±0.791	6±2.407	5.59±1.477	6.109±0.999
$CD4^+FoxP3^+$	5.94±1.457	7.719±1.7	5.06±0.29	5.364±0.313
$CD4^+CD5^+$	23.54±3.123	27.74±6.343	22.89±1.693	23.82±1.47
$CD4^+CD44^+$	18.7±3.365	23.3±7.575	18.96±2.065	19.45±1.171
$CD4^+CD69^+$	8.302±1.818	10.59±3.096	10.01±1.303	9.913±1.391
$CD8^+CD5^+$	4.722±0.736	5.633±2.398	4.986±1.47	5.663±0.98
$CD8^+CD44^+$	2.863±0.836	4.345±1.593	3.897±1.51	4.232±0.319
$CD8^+CD69^+$	1.233±0.291	1.664±0.721	1.551±0.482	1.722±0.282

Table 3.4 Table shows the statistical analysis of total cell numbers and percentages from Table 3.3 calculated from a One-way ANOVA followed by Bonferroni's Multiple Comparison Test comparing each group. Test are shown only for groups that display statistical significance in either total cell numbers of percentages.

Description	Population	Bonferroni's Multiple Comparison Test	t value	Significance	Summary
Total cells ($x10^6$)	$CD25^-CD44^{high}$ (DN1)	$Aire^{+/+}Cbl\text{-}b^{+/+}$ vs $Aire^{+/+}Cbl\text{-}b^{-/-}$	0.5226	No	ns
Thymus		$Aire^{+/+}Cbl\text{-}b^{+/+}$ vs $Aire^{-/-}Cbl\text{-}b^{+/+}$	2.5790	No	ns
		$Aire^{+/+}Cbl\text{-}b^{+/+}$ vs $Aire^{-/-}Cbl\text{-}b^{-/-}$	0.8490	No	ns
		$Aire^{+/+}Cbl\text{-}b^{-/-}$ vs $Aire^{-/-}Cbl\text{-}b^{+/+}$	**3.1020**	**Yes**	*
		$Aire^{+/+}Cbl\text{-}b^{-/-}$ vs $Aire^{-/-}Cbl\text{-}b^{-/-}$	1.3720	No	ns
		$Aire^{-/-}Cbl\text{-}b^{+/+}$ vs $Aire^{-/-}Cbl\text{-}b^{-/-}$	1.7300	No	ns
% from total lymphocytes	$CD25^-CD44^{high}$ (DN1)	$Aire^{+/+}Cbl\text{-}b^{+/+}$ vs $Aire^{+/+}Cbl\text{-}b^{-/-}$	0.3255	No	ns
Thymus		**$Aire^{+/+}Cbl\text{-}b^{+/+}$ vs $Aire^{-/-}Cbl\text{-}b^{+/+}$**	**3.5830**	**Yes**	*
		$Aire^{+/+}Cbl\text{-}b^{+/+}$ vs $Aire^{-/-}Cbl\text{-}b^{-/-}$	1.2290	No	ns
		$Aire^{+/+}Cbl\text{-}b^{-/-}$ vs $Aire^{-/-}Cbl\text{-}b^{+/+}$	**3.2580**	**Yes**	*
		$Aire^{+/+}Cbl\text{-}b^{-/-}$ vs $Aire^{-/-}Cbl\text{-}b^{-/-}$	0.9038	No	ns
		$Aire^{-/-}Cbl\text{-}b^{+/+}$ vs $Aire^{-/-}Cbl\text{-}b^{-/-}$	2.3540	No	ns
Total cells ($x10^6$)	$CD25^-CD44^{low}$ (DN4)	$Aire^{+/+}Cbl\text{-}b^{+/+}$ vs $Aire^{+/+}Cbl\text{-}b^{-/-}$	1.1260	No	ns
Thymus		$Aire^{+/+}Cbl\text{-}b^{+/+}$ vs $Aire^{-/-}Cbl\text{-}b^{+/+}$	0.1826	No	ns
		$Aire^{+/+}Cbl\text{-}b^{+/+}$ vs $Aire^{-/-}Cbl\text{-}b^{-/-}$	0.2744	No	ns
		$Aire^{+/+}Cbl\text{-}b^{-/-}$ vs $Aire^{-/-}Cbl\text{-}b^{+/+}$	0.9435	No	ns
		$Aire^{+/+}Cbl\text{-}b^{-/-}$ vs $Aire^{-/-}Cbl\text{-}b^{-/-}$	0.8517	No	ns
		$Aire^{-/-}Cbl\text{-}b^{+/+}$ vs $Aire^{-/-}Cbl\text{-}b^{-/-}$	0.0918	No	ns
% from total lymphocytes	$CD25^-CD44^{low}$ (DN4)	$Aire^{+/+}Cbl\text{-}b^{+/+}$ vs $Aire^{+/+}Cbl\text{-}b^{-/-}$	1.4830	No	ns
Thymus		**$Aire^{+/+}Cbl\text{-}b^{+/+}$ vs $Aire^{-/-}Cbl\text{-}b^{+/+}$**	**3.9890**	**Yes**	**
		$Aire^{+/+}Cbl\text{-}b^{+/+}$ vs $Aire^{-/-}Cbl\text{-}b^{-/-}$	1.3000	No	ns
		$Aire^{+/+}Cbl\text{-}b^{-/-}$ vs $Aire^{-/-}Cbl\text{-}b^{+/+}$	2.5060	No	ns
		$Aire^{+/+}Cbl\text{-}b^{-/-}$ vs $Aire^{-/-}Cbl\text{-}b^{-/-}$	0.1839	No	ns
		$Aire^{-/-}Cbl\text{-}b^{+/+}$ vs $Aire^{-/-}Cbl\text{-}b^{-/-}$	2.6900	No	ns
Total cells ($x10^6$)	$CD8^+CD44^+$	$Aire^{+/+}Cbl\text{-}b^{+/+}$ vs $Aire^{+/+}Cbl\text{-}b^{-/-}$	0.2755	No	ns
Spleen		$Aire^{+/+}Cbl\text{-}b^{+/+}$ vs $Aire^{-/-}Cbl\text{-}b^{+/+}$	1.8480	No	ns
		$Aire^{+/+}Cbl\text{-}b^{+/+}$ vs $Aire^{-/-}Cbl\text{-}b^{-/-}$	0.3342	No	ns
		$Aire^{+/+}Cbl\text{-}b^{-/-}$ vs $Aire^{-/-}Cbl\text{-}b^{+/+}$	1.5730	No	ns
		$Aire^{+/+}Cbl\text{-}b^{-/-}$ vs $Aire^{-/-}Cbl\text{-}b^{-/-}$	0.0587	No	ns
		$Aire^{-/-}Cbl\text{-}b^{+/+}$ vs $Aire^{-/-}Cbl\text{-}b^{-/-}$	1.5140	No	ns
% from total lymphocytes	$CD8^+CD44^+$	$Aire^{+/+}Cbl\text{-}b^{+/+}$ vs $Aire^{+/+}Cbl\text{-}b^{-/-}$	1.1150	No	ns
Spleen		**$Aire^{+/+}Cbl\text{-}b^{+/+}$ vs $Aire^{-/-}Cbl\text{-}b^{+/+}$**	**3.1970**	**Yes**	*
		$Aire^{+/+}Cbl\text{-}b^{+/+}$ vs $Aire^{-/-}Cbl\text{-}b^{-/-}$	1.8050	No	ns

		$Aire^{+/+}Cbl\text{-}b^{-/-}$ vs $Aire^{-/-}Cbl\text{-}b^{+/+}$	2.0820	No	ns
		$Aire^{+/+}Cbl\text{-}b^{-/-}$ vs $Aire^{-/-}Cbl\text{-}b^{-/-}$	0.6900	No	ns
		$Aire^{-/-}Cbl\text{-}b^{+/+}$ vs $Aire^{-/-}Cbl\text{-}b^{-/-}$	1.3920	No	ns
Total cells ($x10^6$)	$CD8^+CD44^+$	$Aire^{+/+}Cbl\text{-}b^{+/+}$ vs $Aire^{+/+}Cbl\text{-}b^{-/-}$	2.6830	No	ns
Lymph node		$Aire^{+/+}Cbl\text{-}b^{+/+}$ vs $Aire^{-/-}Cbl\text{-}b^{+/+}$	0.8503	No	ns
		$Aire^{+/+}Cbl\text{-}b^{+/+}$ vs $Aire^{-/-}Cbl\text{-}b^{-/-}$	1.6690	No	ns
		$Aire^{+/+}Cbl\text{-}b^{-/-}$ vs $Aire^{-/-}Cbl\text{-}b^{+/+}$	1.8330	No	ns
		$Aire^{+/+}Cbl\text{-}b^{-/-}$ vs $Aire^{-/-}Cbl\text{-}b^{-/-}$	1.0140	No	ns
		$Aire^{-/-}Cbl\text{-}b^{+/+}$ vs $Aire^{-/-}Cbl\text{-}b^{-/-}$	0.8186	No	ns
% from total lymphocytes	$CD8^+CD44^+$	$Aire^{+/+}Cbl\text{-}b^{+/+}$ vs $Aire^{+/+}Cbl\text{-}b^{-/-}$	2.6710	No	ns
Lymph node		**$Aire^{+/+}Cbl\text{-}b^{+/+}$ vs $Aire^{-/-}Cbl\text{-}b^{+/+}$**	**3.2890**	**Yes**	*
		$Aire^{+/+}Cbl\text{-}b^{+/+}$ vs $Aire^{-/-}Cbl\text{-}b^{-/-}$	**3.3740**	**Yes**	*
		$Aire^{+/+}Cbl\text{-}b^{-/-}$ vs $Aire^{-/-}Cbl\text{-}b^{+/+}$	0.6181	No	ns
		$Aire^{+/+}Cbl\text{-}b^{-/-}$ vs $Aire^{-/-}Cbl\text{-}b^{-/-}$	0.7030	No	ns
		$Aire^{-/-}Cbl\text{-}b^{+/+}$ vs $Aire^{-/-}Cbl\text{-}b^{-/-}$	0.0850	No	ns
Total cells ($x10^6$)	$CD8^+CD69^+$	$Aire^{+/+}Cbl\text{-}b^{+/+}$ vs $Aire^{+/+}Cbl\text{-}b^{-/-}$	2.2630	No	ns
Lymph node		$Aire^{+/+}Cbl\text{-}b^{+/+}$ vs $Aire^{-/-}Cbl\text{-}b^{+/+}$	0.7440	No	ns
		$Aire^{+/+}Cbl\text{-}b^{+/+}$ vs $Aire^{-/-}Cbl\text{-}b^{-/-}$	1.6660	No	ns
		$Aire^{+/+}Cbl\text{-}b^{-/-}$ vs $Aire^{-/-}Cbl\text{-}b^{+/+}$	1.5190	No	ns
		$Aire^{+/+}Cbl\text{-}b^{-/-}$ vs $Aire^{-/-}Cbl\text{-}b^{-/-}$	0.5971	No	ns
		$Aire^{-/-}Cbl\text{-}b^{+/+}$ vs $Aire^{-/-}Cbl\text{-}b^{-/-}$	0.9222	No	ns
% from total lymphocytes	$CD8^+CD69^+$	$Aire^{+/+}Cbl\text{-}b^{+/+}$ vs $Aire^{+/+}Cbl\text{-}b^{-/-}$	1.7410	No	ns
Lymph node		**$Aire^{+/+}Cbl\text{-}b^{+/+}$ vs $Aire^{-/-}Cbl\text{-}b^{+/+}$**	**3.2350**	**Yes**	*
		$Aire^{+/+}Cbl\text{-}b^{+/+}$ vs $Aire^{-/-}Cbl\text{-}b^{-/-}$	2.6290	No	ns
		$Aire^{+/+}Cbl\text{-}b^{-/-}$ vs $Aire^{-/-}Cbl\text{-}b^{+/+}$	1.4940	No	ns
		$Aire^{+/+}Cbl\text{-}b^{-/-}$ vs $Aire^{-/-}Cbl\text{-}b^{-/-}$	0.8882	No	ns
		$Aire^{-/-}Cbl\text{-}b^{+/+}$ vs $Aire^{-/-}Cbl\text{-}b^{-/-}$	0.6060	No	ns

these subsets between all groups. These data indicate that overall T cell development in the thymus was not measurably altered in the *Aire*$^{-/-}$*Cblb*$^{-/-}$ bone marrow chimeras.

3.6.2.2 Lymphocyte populations in the secondary lymphoid organs, the spleen and lymph nodes

Following development in the thymus, T lymphocytes migrate to different secondary lymphoid organs, including the spleen and various lymph nodes. In this section "lymph nodes" refer to pooled lymphocytes from the inguinal and axillary subcutaneous lymph nodes, whereas "pancreatic lymph nodes" refers to lymphocytes harvested from the lymph node that drains the pancreas – the organ that was affected by lymphocytic infiltration in *Aire*$^{-/-}$*Cblb*$^{-/-}$ mice. Hence, it was interesting to compare the status of activation using flow cytometric cell surface markers between the pancreas-draining lymph node close to the site of infiltration and subcutaneous lymph nodes that were present at a distant site.

In all three peripheral organs (spleen, subcutaneous lymph nodes and pancreatic lymph nodes), there appeared to be no significant differences in the numbers of B cells, T cells, CD4, CD8 and nTreg cells (Figs. 3.15, 3.16, 3.17 and Tables 3.3 and 3.4). Similarly, the total numbers of CD4 and CD8 cells that upregulated the activation markers CD44 and CD69 were comparable between groups. Increases were observed in the percentages of CD8^{+}CD44^{+} cells in the spleen (*Aire*$^{-/-}$ compared to wild-type) and subcutaneous lymph nodes (*Aire*$^{-/-}$ and *Aire*$^{-/-}$*Cblb*$^{-/-}$ compared to wild-type). Besides CD44, the *Aire*$^{-/-}$ also displayed higher percentages of CD8^{+}CD69^{+} cells. Nevertheless, these increases in percentage of CD8 cells upregulating the CD44 and CD69 marker did not translate to an increase in the corresponding total number of cells. Taken together, the data suggest that the overall T cell subsets and activation status in the *Aire*$^{-/-}$*Cblb*$^{-/-}$ chimeric mice were relatively comparable to the single mutant and wild-type control chimeras.

3.6.3 Analysis of lymphocyte development in mixed bone marrow chimeras

There is a possibility that quantitative abnormalities in lymphocyte maturation and survival would be masked unless the mutant T cells were placed in competition with the wild-type T cells. These differences would not have been detected in the flow cytometry

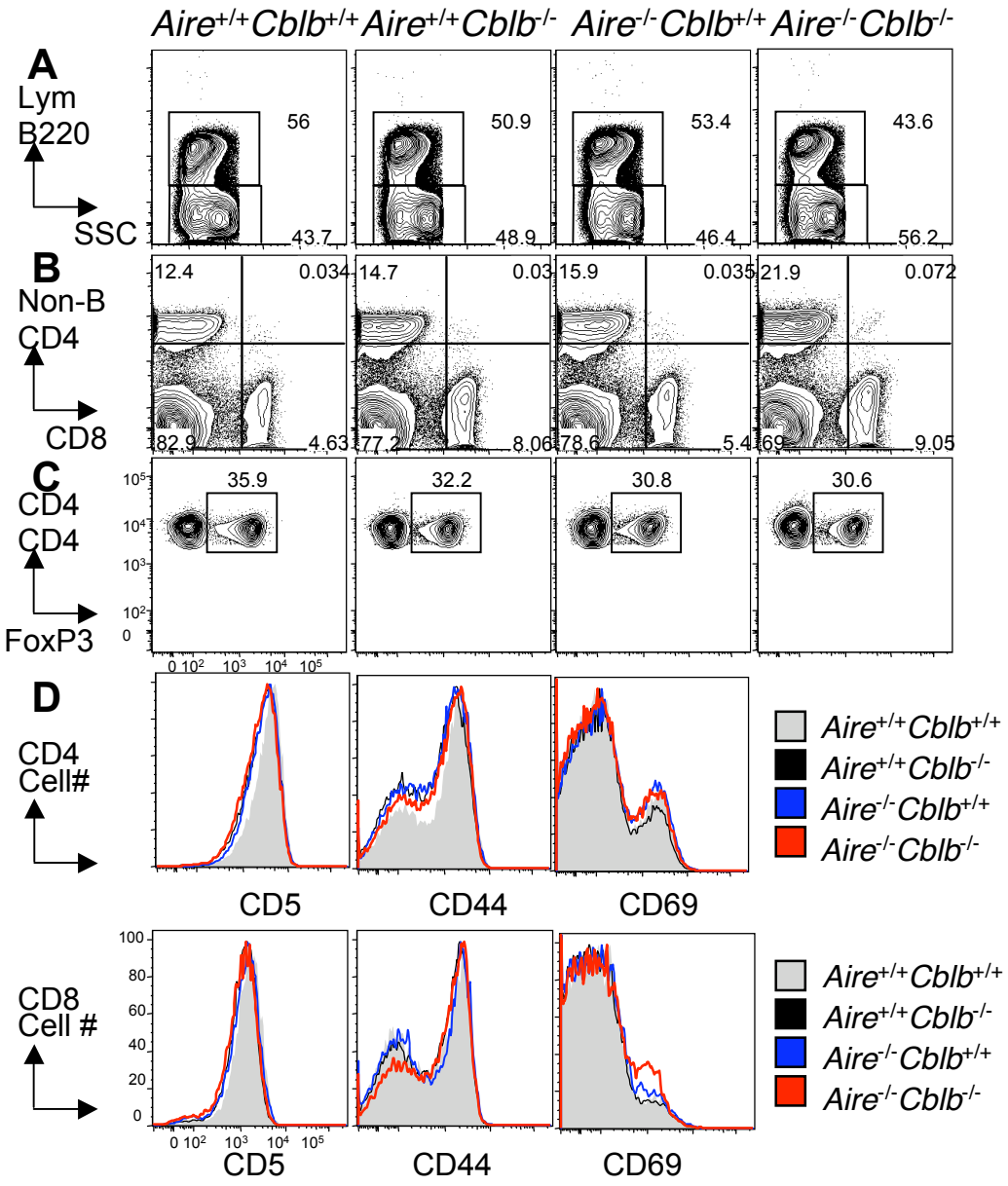

Figure 3.15 Representation of flow cytometry plots from splenocytes of from *Aire*$^{+/+}$*Cblb*$^{+/+}$, *Aire*$^{+/+}$*Cblb*$^{-/-}$, *Aire*$^{-/-}$ *Cblb*$^{+/+}$ and *Aire*$^{-/-}$*Cblb*$^{-/-}$ bone marrow chimeras.

A. Gated on lymphocytes (Lym), showing the percentage of B cell subsets

B. Gated on non-B cells, showing the percentage of CD4 and CD8 subsets

C. Gated on CD4^{+} cells, showing the percentage of CD4^{+}FoxP3^{+} subsets

D. Gated on CD4^{+} (top) or CD8^{+} (bottom), showing CD5, CD44 and CD69 expression on each subset.

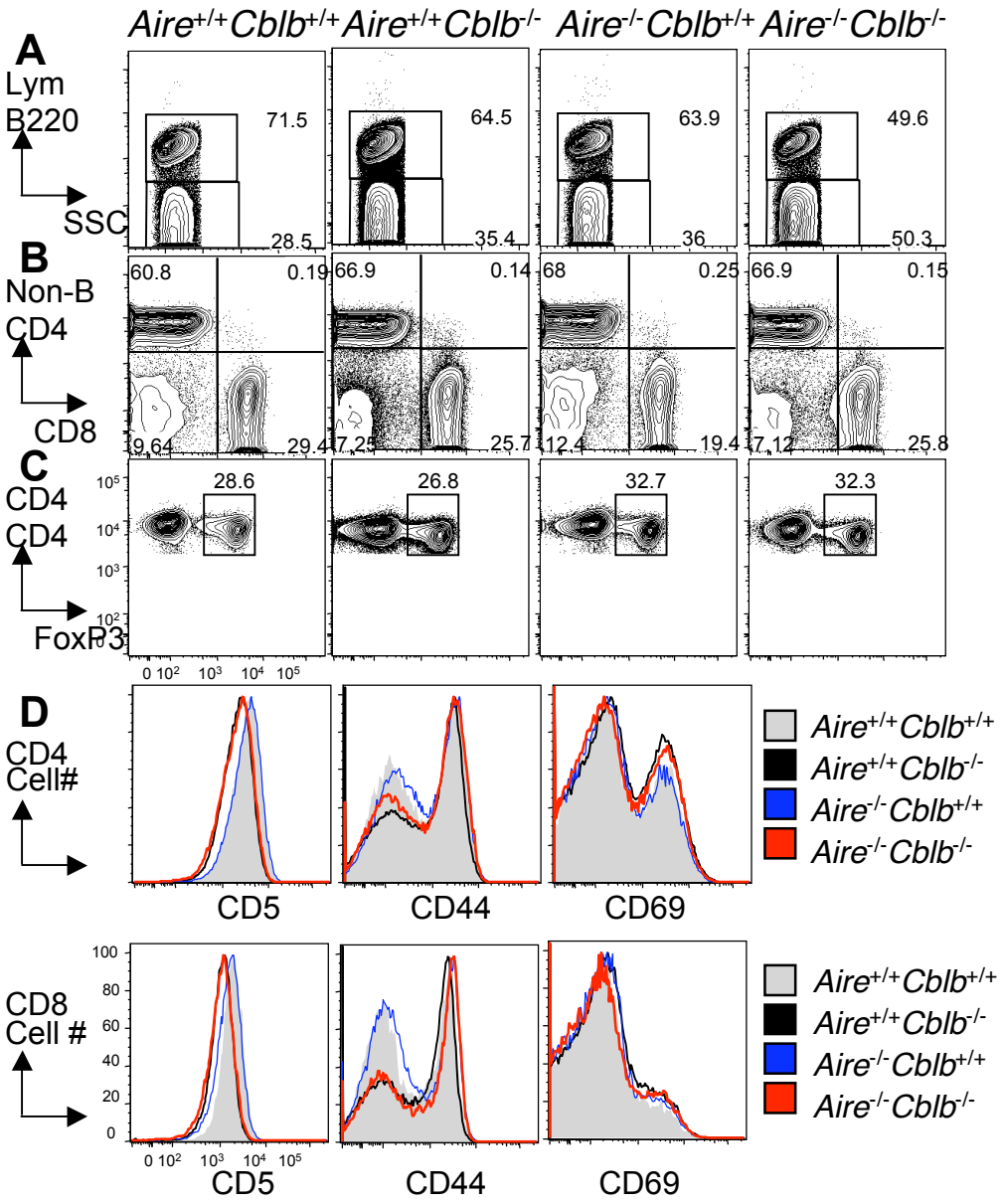

Figure 3.16 Representation of flow cytometry plots from lymphocytes of the lymph nodes from *Aire*$^{+/+}$*Cblb*$^{+/+}$, *Aire*$^{+/+}$*Cblb*$^{-/-}$, *Aire*$^{-/-}$*Cblb*$^{+/+}$ and *Aire*$^{-/-}$*Cblb*$^{-/-}$ bone marrow chimeras.

A. Gated on lymphocytes (Lym), showing the percentage of B cell subsets

B. Gated on non-B cells, showing the percentage of CD4 and CD8 subsets

C. Gated on CD4^{+} cells, showing the percentage of CD4^{+}FoxP3^{+} subsets

D. Gated on CD4^{+} (top) or CD8^{+} (bottom), showing CD5, CD44 and CD69 expression on each subset.

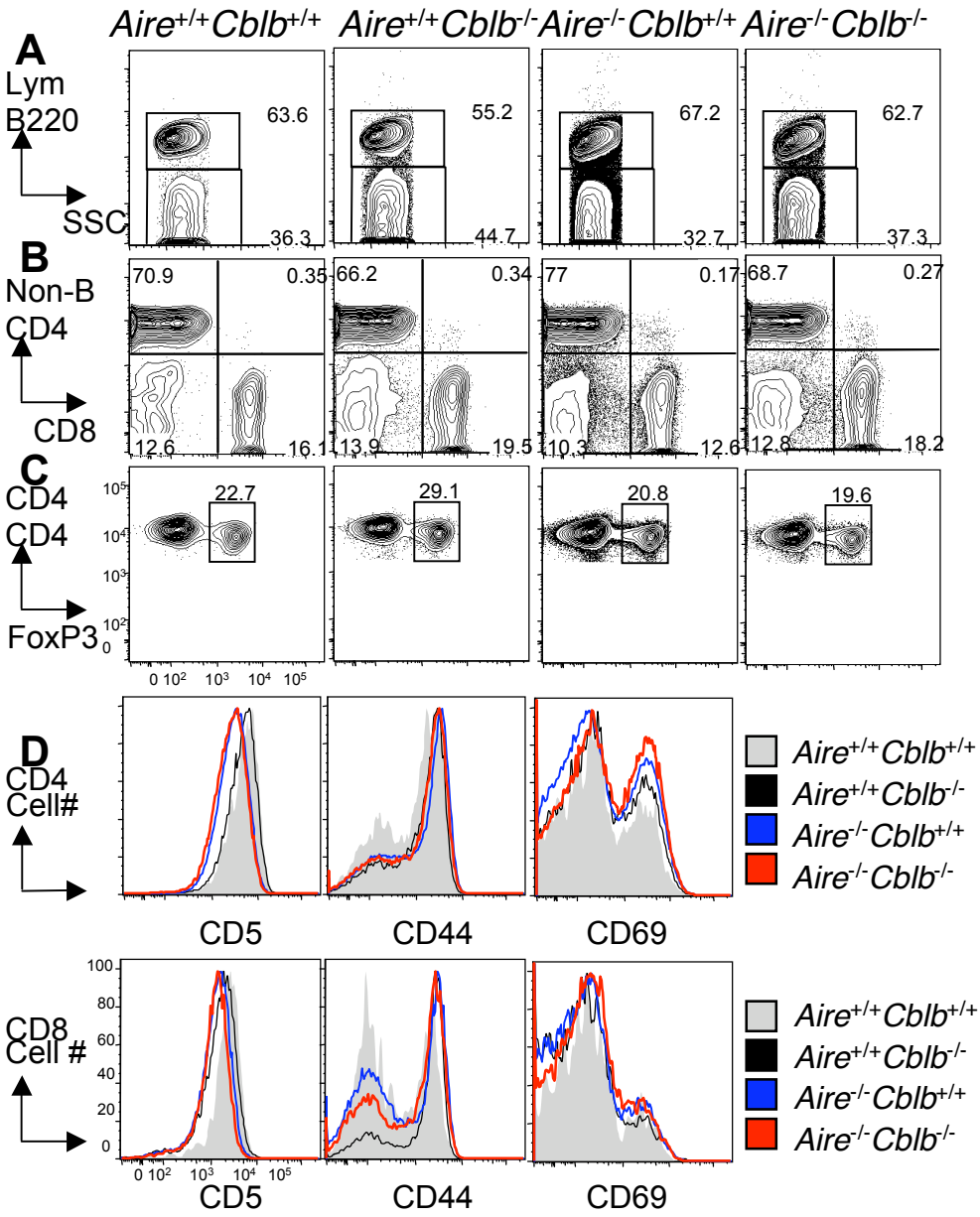

Figure 3.17 Representation of flow cytometry plots from lymphocytes of the pancreatic lymph nodes from *Aire*$^{+/+}$*Cblb*$^{+/+}$, *Aire*$^{+/+}$*Cblb*$^{-/-}$, *Aire*$^{-/-}$*Cblb*$^{+/+}$ and *Aire*$^{-/-}$*Cblb*$^{-/-}$ bone marrow chimeras.

A. Gated on lymphocytes (Lym), showing the percentage of B cell subsets

B. Gated on non-B cells, showing the percentage of CD4 and CD8 subsets

C. Gated on CD4^{+} cells, showing the percentage of CD4^{+}FoxP3^{+} subsets

D. Gated on CD4^{+} (top) or CD8^{+} (bottom), showing CD5, CD44 and CD69 expression on each subset.

analysis in section 3.6.2 but could be detected by analysing the chimeras which have been reconstituted with equal ratios of *Cblb*$^{-/-}$ and wild-type bone marrow. The experimental design of the mixed bone marrow chimeras was illustrated in Fig. 3.12. The genotype of the hematopoietic cells that engrafted and differentiated can be tracked by monoclonal antibody staining for the surface markers CD45.1 and CD45.2 (corresponding to different CD45 allotypes). The wild-type bone marrow was obtained from a B10.BR.CD45.1 congenic mice that expressed the CD45.1 marker. In contrast, the recipient mice and *Cblb*$^{-/-}$ bone marrow expresses the CD45.2 marker.

Twenty-nine days post-reconstitution, the mice were euthanised and tested for the repopulation of B cells, T cells and other lymphocyte subsets. The relative percentages are seen in Fig. 3.18, Fig 3.19, Fig, 3.20 and Table 3.5, showing the relative reconstitution of the CD45.1 and CD45.2 components in the bone marrow chimeras. There was no measurable preferential expansion of *Cblb*$^{-/-}$ T cells in *Aire*$^{-/-}$ recipients. CD45.2^{+} cells preferentially contributed to the peripheral T cells in the spleen and blood relative to the frequency in thymocytes or B cells in the same animal in all regardless of recipient *Aire* genotype. Since the recipient mice were CD45.2, and memory T cells and Tregs were radioresistant, it is likely the excess CD45.2 peripheral T cells were recipient or host derived.

3.7 Splenocyte precursors are able to transfer the disease

Following the establishment that the pancreatic-wasting syndrome was a result of *Cblb*-deficiency in the hematopoietic system, it was of interest to determine if lymphocytes could transfer the disease to another mouse. To test this, 1, 3 or 8.5 × 10^6 splenocytes from either wild-type or *Aire*$^{-/-}$*Cblb*$^{-/-}$ mice were intravenously injected into pairs of B10.BR.*Rag1*-deficient mice (Fig. 3.21*A*). *Rag1*-deficient mice were used as recipients as the absence of *Rag1* eliminates all mature T and B cell from the repertoire. Thus, any autoimmunity observed in these mice could be attributed to the effect of adoptively transferred cells.

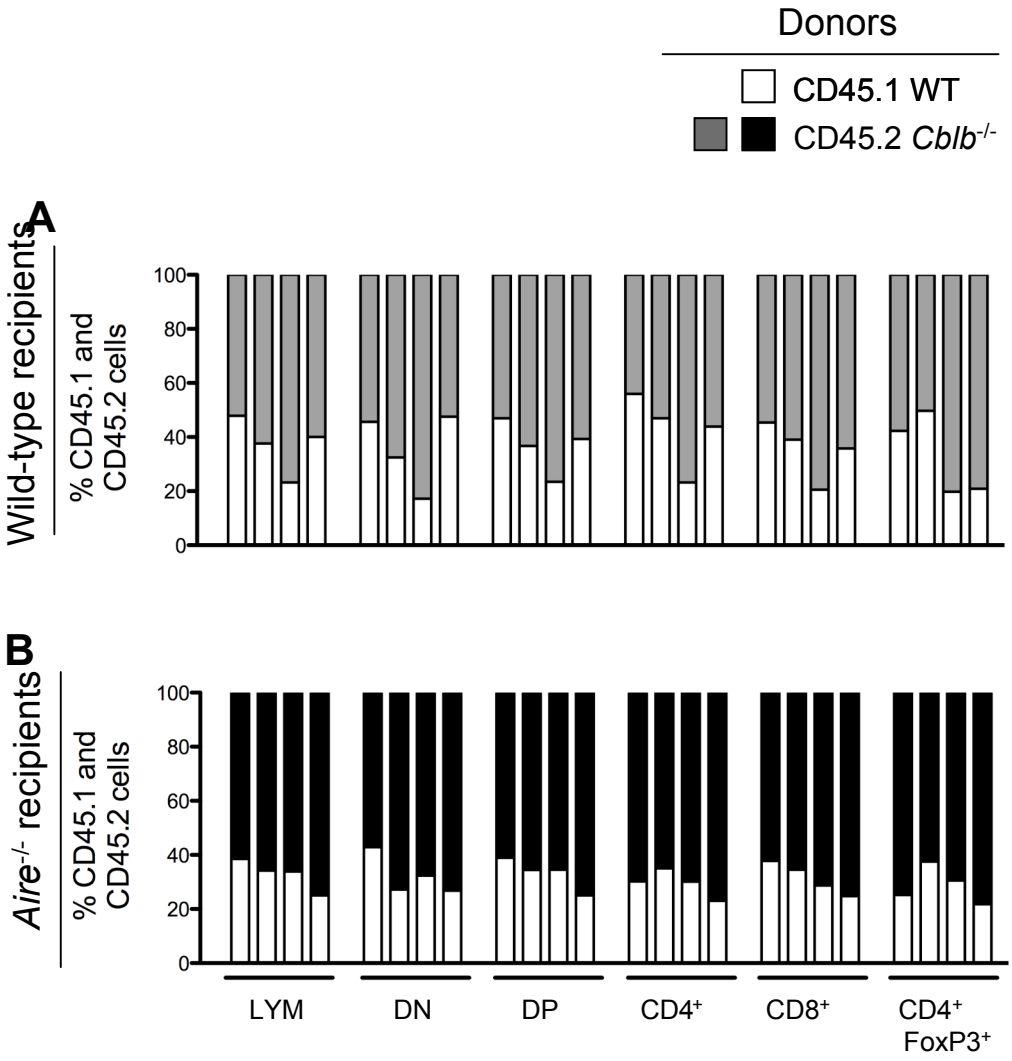

Figure 3.18 Contribution of CD45.1 and CD45.2 cells to thymus subsets in individual chimeric mice.
Irradiated wild-type recipients (A) or *Aire*$^{-/-}$ recipients (B) received equal mixtures of wild-type marrow carrying the CD45.1 allelic marker and *Cblb*$^{-/-}$ marrow carrying the CD45.2 allelic marker .The vertical axis denotes the percentage of CD45.1 or CD45.2 allotype cells in the indicated cell type. Every bar represents a single mouse and these are listed in the same order for each cell type analysed. Lymphocytes (lym); double negative (DN); double positive (DP); single positive CD4 cells (CD4^{+}); single positive CD8 cells (CD8^{+}) and T regulatory cells (CD4^{+}FoxP3^{+}) cells.

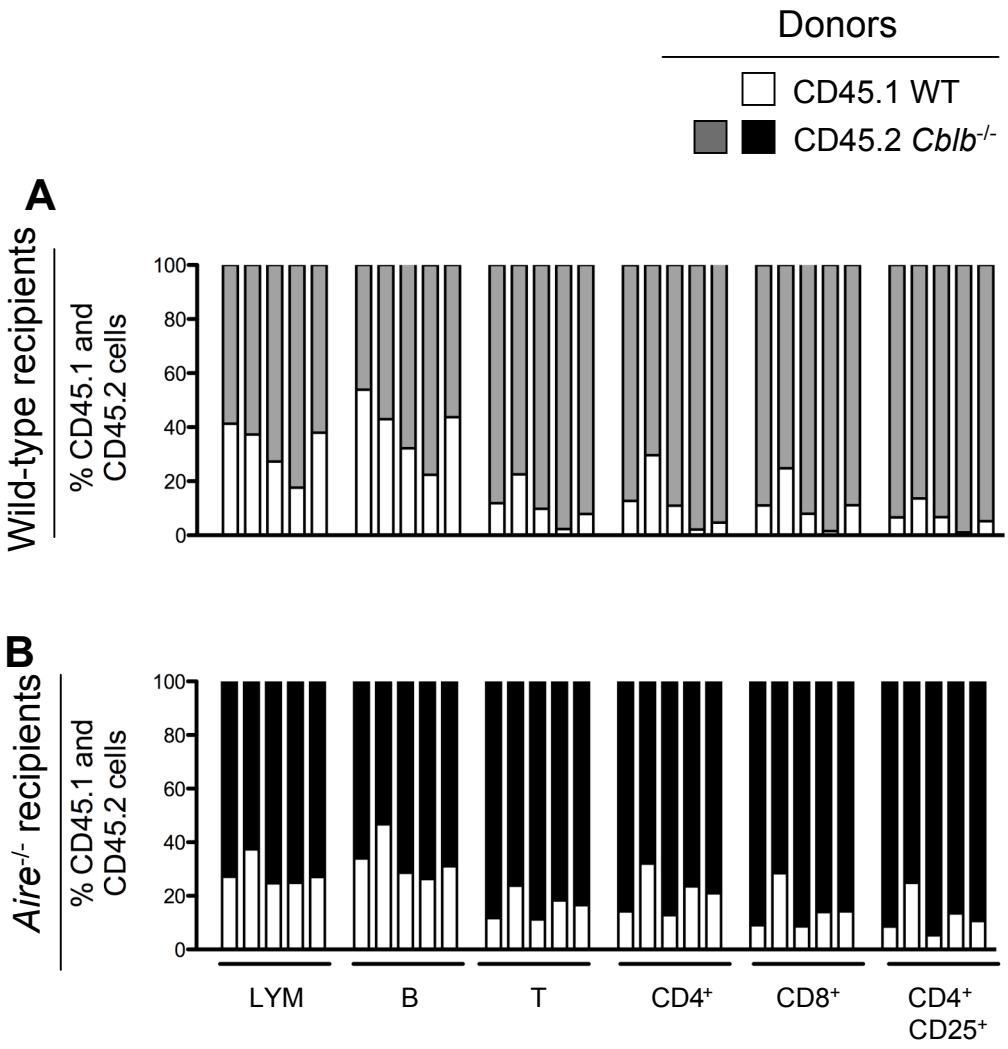

Figure 3.19 Contribution of CD45.1 and CD45.2 cells to blood lymphocyte subsets in individual chimeric mice.
Irradiated wild-type recipients (A) or *Aire*$^{-/-}$ recipients (B) received equal mixtures of wild-type marrow carrying the CD45.1 allelic marker and *Cblb*$^{-/-}$ marrow carrying the CD45.2 allelic marker .The vertical axis denotes the percentage of CD45.1 or CD45.2 allotype cells in the indicated cell type. Every bar represents a single mouse and these are listed in the same order for each cell type analysed. Lymphocytes (lym), B cells (B), T cells (T), CD4 cells (CD4^{+}), CD8 cells (CD8^{+}) and Treg (CD4^{+}CD25^{+}) cells.

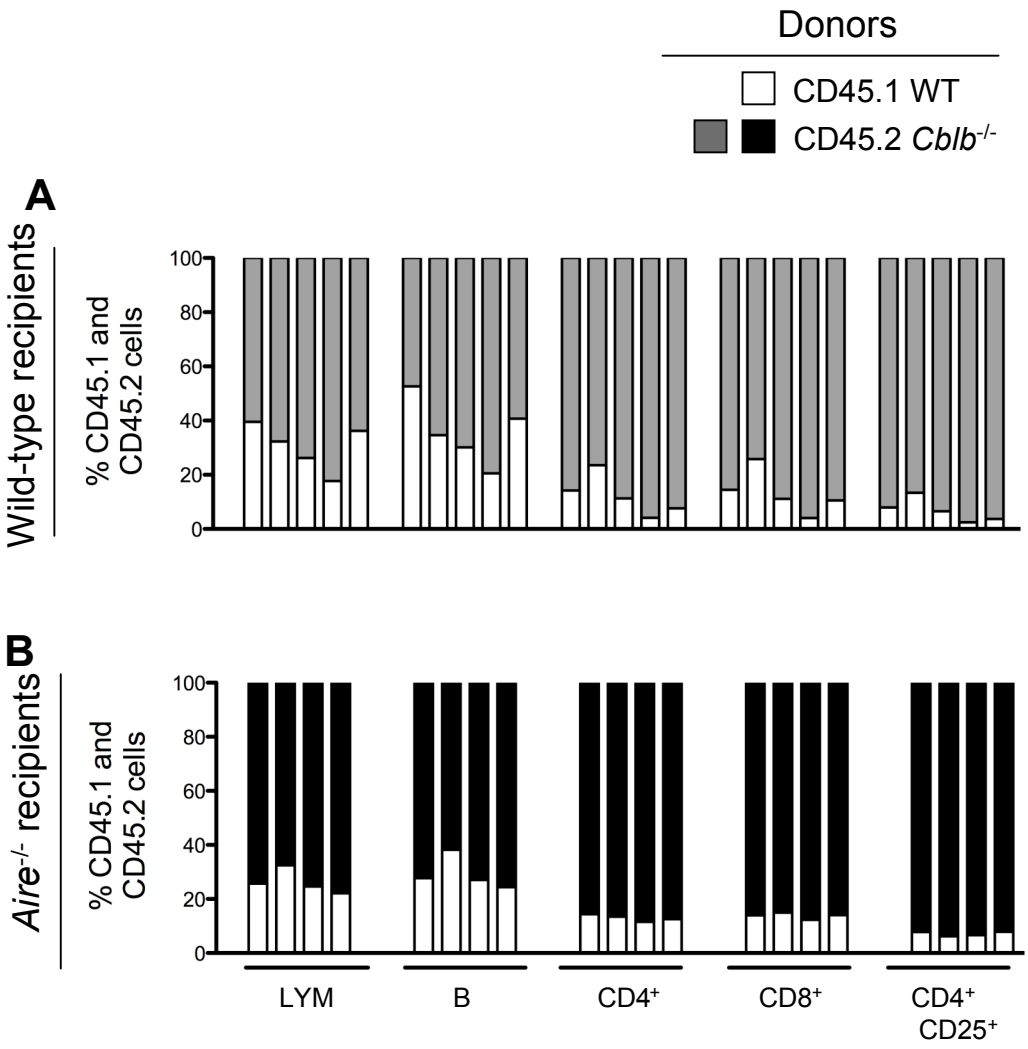

Figure 3.20 Contribution of CD45.1 and CD45.2 cells to splenocyte subsets in individual chimeric mice.
Irradiated wild-type recipients (A) or *Aire*$^{-/-}$ recipients (B) received equal mixtures of wild-type marrow carrying the CD45.1 allelic marker and *Cblb*$^{-/-}$ marrow carrying the CD45.2 allelic marker .The vertical axis denotes the percentage of CD45.1 or CD45.2 allotype cells in the indicated cell type. Every bar represents a single mouse and these are listed in the same order for each cell type analysed. Lymphocytes (lym), B cells (B), T cells (T), CD4 cells (CD4^{+}), CD8 cells (CD8^{+}) and Treg (CD4^{+}CD25^{+}) cells.

Table 3.5 Statistical analysis of the mixed bone marrow chimeras. For this analysis, the lymphocyte population was used as a reference population and the percentages of CD45.1 and CD45.2 lymphocytes were taken to be the "expected" frequency in all other subsets of the same mouse. The expected frequencies were compared to the CD45.1 and CD45.2 allotype percentages for other subpopulations in the same organ (the "observed" frequencies). The p value for the chi-squared test for independence are taken to be significant when $p<0.05$ as seen in the shaded background.

Organ	Population	Allotype	Chi-squared P Values		Significance
			Aire$^{+/+}$	*Aire*$^{-/-}$	
Thymus	DN	CD45.1	0.2881	0.5511	No
		CD45.2	0.5885	0.7711	No
	DP	CD45.1	0.9966	0.9993	No
		CD45.2	0.9980	0.9997	No
	CD4	CD45.1	0.2568	0.4944	No
		CD45.2	0.4090	0.7043	No
	CD8	CD45.1	0.8092	0.8481	No
		CD45.2	0.9057	0.9374	No
	Tregs	CD45.1	0.0025	0.1280	No
		CD45.2	0.0258	0.3377	No
Blood	B cells	CD45.1	0.0997	0.2577	No
		CD45.2	0.3568	0.6516	No
	T cells	CD45.1	<0.0001	<0.0001	Yes
		CD45.2	<0.0001	0.0300	Yes
	CD4 cells	CD45.1	<0.0001	0.0068	Yes
		CD45.2	<0.0001	0.2683	No
	CD8	CD45.1	<0.0001	<0.0001	Yes
		CD45.2	<0.0001	0.0110	Yes
	CD4 CD25	CD45.1	<0.0001	<0.0001	Yes
		CD45.2	<0.0001	0.0014	Yes
Spleen	B cells	CD45.1	0.1920	0.6521	No
		CD45.2	0.4727	0.8779	No
	CD4	CD45.1	<0.0001	<0.0001	Yes
		CD45.2	<0.0001	0.0146	Yes
	CD8	CD45.1	<0.0001	<0.0001	Yes
		CD45.2	<0.0001	0.0265	Yes
	Tregs	CD45.1	<0.0001	<0.0001	Yes
		CD45.2	<0.0001	0.0001	Yes

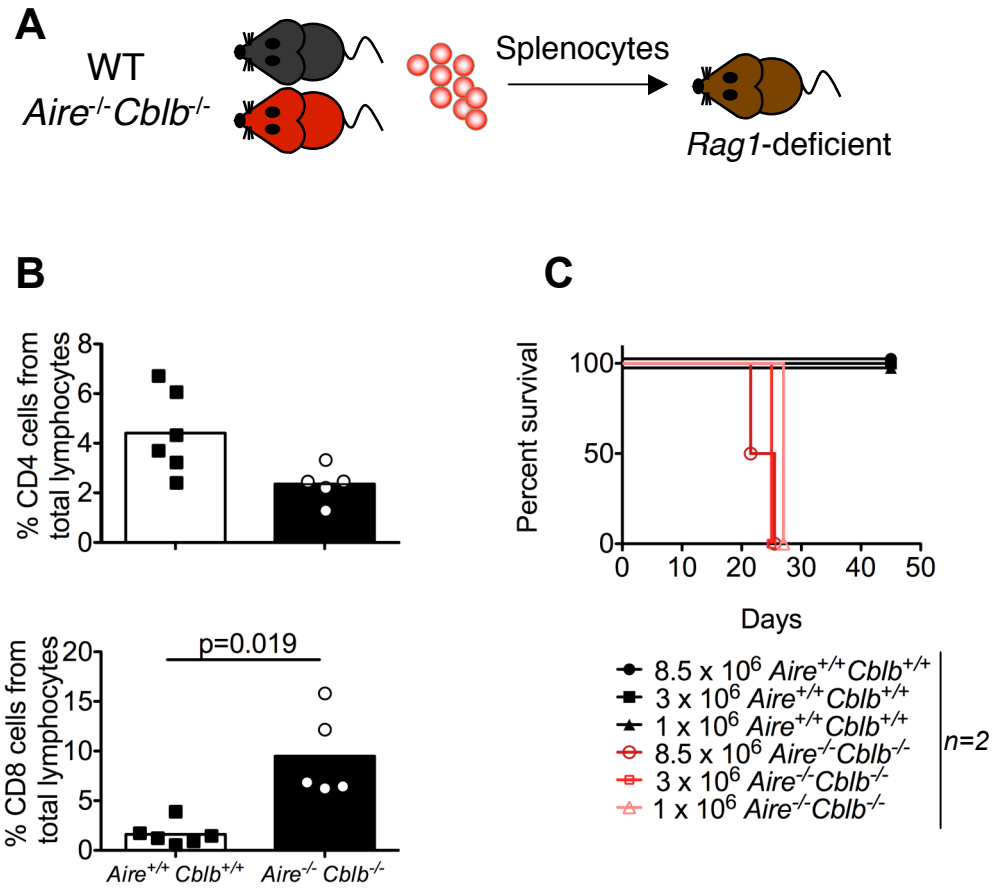

Figure 3.21 Transfer of cachectic disease by splenocytes from *Aire*$^{-/-}$*Cblb*$^{-/-}$ mice to lymphopenic *Rag1*-deficient recipients.

A. 1, 3 and 8.5 x 10^6 splenocytes from *Aire*$^{-/-}$*Cblb*$^{-/-}$ or wild-type B10.BR mice were injected into *Rag1*-deficient B10.BR recipients.

B. Percentage of $CD4^+$ and $CD8^+$ cells in the blood of mice 12 days post-transfer of the indicated splenocytes.

C. Survival of *Rag1*-deficient B10.BR mice after adoptive transfer of the indicated splenocytes.

Flow cytometric analysis of peripheral blood lymphocytes in the recipients twelve days post transfer revealed a marked over-representation of the CD8 T cell subset in recipients of *Aire*$^{-/-}$*Cblb*$^{-/-}$ spleen cells, although this difference was not statistically significant (Fig. 3.21*B*). All mice receiving *Aire*$^{-/-}$*Cblb*$^{-/-}$ spleen cells became cachectic and moribund by 28 days following adoptive transfer, regardless of the number of transferred cells, while all mice receiving wild-type splenocytes remained healthy (Fig. 3.21*C*). At necropsy, the only gross pathology detected was a small translucent pancreas in recipients of *Aire*$^{-/-}$*Cblb*$^{-/-}$ spleen cells, and histology demonstrated extensive lymphocytic infiltration of the exocrine pancreas and loss of most or all acinar cells (Fig. 3.22*A* and *B*). The pancreas pathology appeared to be more severe for recipients that received higher number of *Aire*$^{-/-}$*Cblb*$^{-/-}$ spleen cells. The data indicated that as few as one million *Aire*$^{-/-}$*Cblb*$^{-/-}$ splenocytes were able to transfer the disease to *Rag1*-deficient recipients.

3.8 CD4 T helper cells and CD8 T cytotoxic cells are necessary to transfer the disease

Having established that splenocytes could transfer disease, we now had to establish if CD4 or CD8 T cells were required to adoptively transfer disease. Thus, the cell transfer experiment in 3.7 was repeated with CD4 and CD8 T cell-enriched or T cell depleted subsets of spleen cells. Spleen cells were obtained from bone marrow chimeras with both tolerance defects (*Aire* deficient recipients of *Cblb*-deficient marrow; abbreviated as *Aire*$^{-/-}$*Cblb*$^{-/-}$) and from control chimeras with neither defect (abbreviated as wild-type), because insufficient T cell subsets could be obtained from the 3 week old very small, cachectic *Aire*$^{-/-}$*Cblb*$^{-/-}$ mice. The cells were pooled and divided into three groups. Two of the groups were MACS-enriched for the CD4 or CD8 population, respectively, and both the positive and negative fractions of the enrichment were used for further transfers. The non-enriched splenocytes served as a positive control for the experiment, whereby, the cells were known to be able to transfer disease.

Groups of *Rag1*-deficient mice received either 2×10^6 whole splenocytes, 2×10^6 CD4- or CD8-depleted spleen cells, or 2×10^5 CD4 or 1×10^5 CD8 enriched cells. These numbers

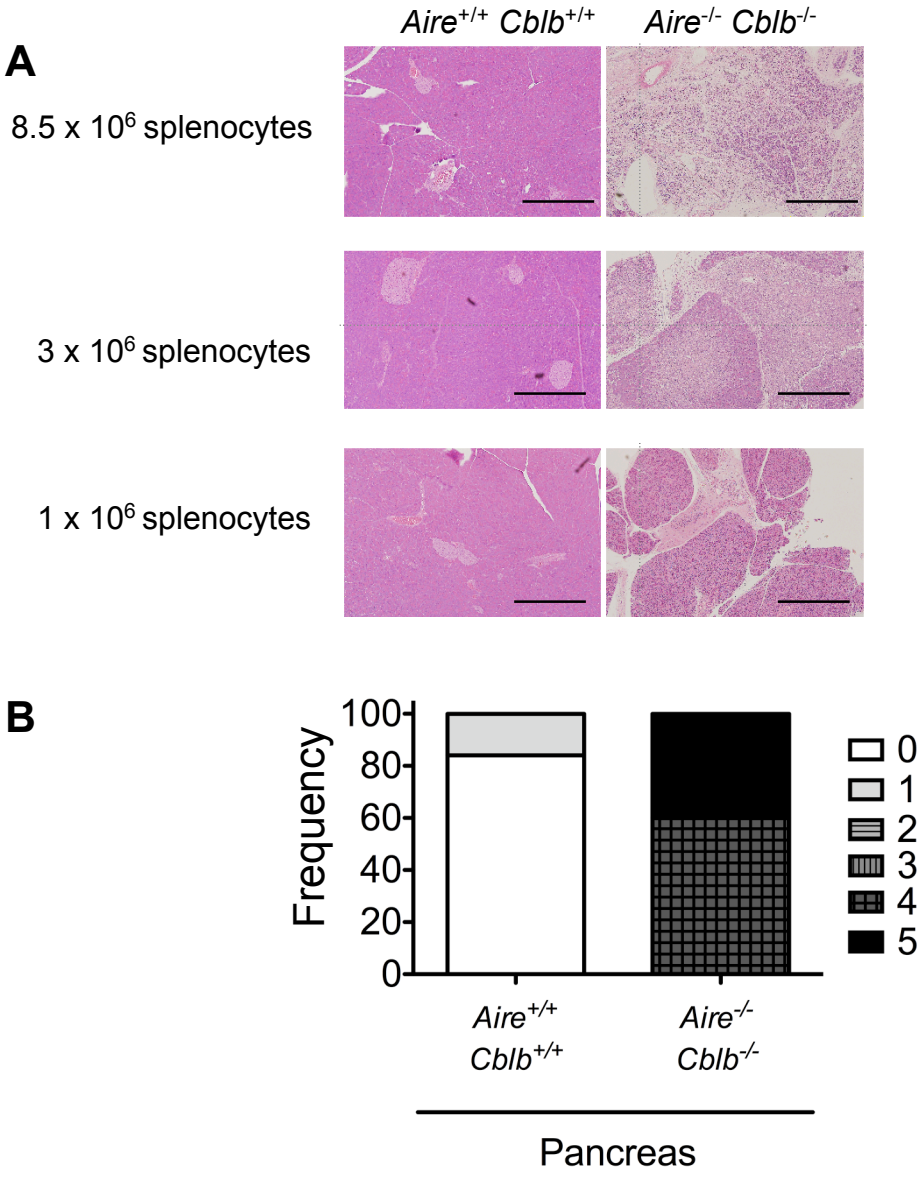

Figure 3.22 Transfer of pancreatitis disease by limiting numbers of splenocytes from *Aire*$^{-/-}$*Cblb*$^{-/-}$ mice to lymphopenic *Rag1*-deficient recipients.

A. Representative haematoxylin and eosin-stained sections of the pancreas from mice in each group. Original magnification: x100, Bars: 500 μm.

B. Percentage of recipient mice with different grades of pancreatitis (*n=6*/group).

were chosen as they approximated the numbers of CD4 and CD8 T cells within 2×10^6 total lymphocytes (Fig. 3.23). To ensure complete deletion of the residual irrelevant subset, the recipients of CD4-enriched and CD8-depleted cells were treated with depleting antibody to CD8; and recipients of the CD8-enriched and CD4-depleted cells were treated with depleting antibody to CD4 on days zero, one, seven and fourteen of the experiment. Flow cytometric staining of the peripheral blood samples taken nineteen days post-transfer determined that the CD4-enriched and CD8 -depleted group had only CD4 cells; and the CD8-enriched and CD4-depleted group had only CD8 cells. This established that efficient subset deletion had been achieved.

All *Rag1*-deficient mice that received unfractionated splenocytes from *Aire*$^{-/-}$*Cblb*$^{-/-}$ donors died or were euthanased due to cachexia by 45 days post transfer (Fig. 3.24 *A*). By contrast, the cachectic syndrome did not develop in recipients of CD8- or CD4-depleted splenocytes from *Aire*$^{-/-}$*Cblb*$^{-/-}$ donors nor in recipients of CD8- or CD4-enriched cells, establishing that both T cell subsets were required to transfer lethal autoimmunity. Severe exocrine pancreatitis was observed in recipients of whole *Aire*$^{-/-}$ *Cblb*$^{-/-}$ splenocytes, while the different combinations of CD4- or CD8- enriched and CD4- or CD8-depleted cells displayed varying degrees of histological severity scores. On the contrary, the recipients of all groups of wild-type cells displayed negligible infiltrations (Fig. 3.2.24*B*). These results imply that pancreatitis can be initiated either by CD4 or CD8 cells, but both cell types are required for efficient autoimmune destruction of this organ.

The histological analysis of the submandibular salivary gland in mice that received *Aire*$^{-/-}$*Cblb*$^{-/-}$ whole splenocytes, or CD4-enriched or CD8-depleted splenocytes revealed infiltration in the salivary glands with histological scores from 2 to 5 in majority of the recipients (Fig. 3.24*C*). By contrast, no sialoadenitis was observed in recipients of CD4-depleted or CD8-enriched cells. From these results, it can be inferred that CD4 cells from *Aire*$^{-/-}$*Cblb*$^{-/-}$ chimeras are necessary for the development of sialoadenitis in lymphopenic *Rag1*-deficient recipients.

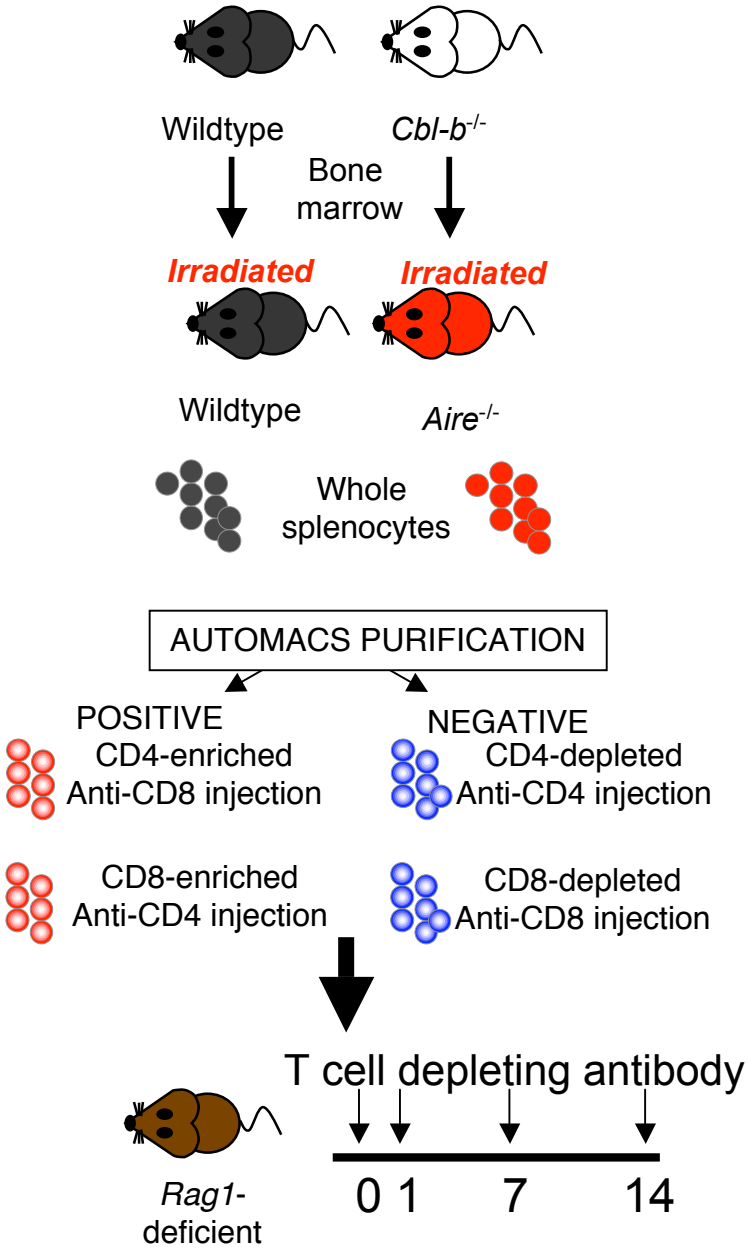

Figure 3.23 Schematic explaining the experimental design to determine the role of T cells in adoptive transfer of pancreatitis. Adoptive transfer of $2x10^6$ unfractionated spleen cells (containing approximately $2x10^5$ CD4- or $1x10^5$ CD8 cells), $2x10^6$ spleen cells selectively depleted of CD4- or CD8-cells, or $2x10^5$ CD4- or $1x10^5$ CD8- enriched spleen cells, obtained from bone marrow chimeras of the indicated genotypes. Recipients of CD4-depleted or CD8-enriched cells, and recipients of CD8-depleted or CD4-enriched cells, were also treated with depleting antibody to CD4 or CD8, respectively, on days 0, 1, 7 and 14 to deplete any residual T cells of the relevant subset.

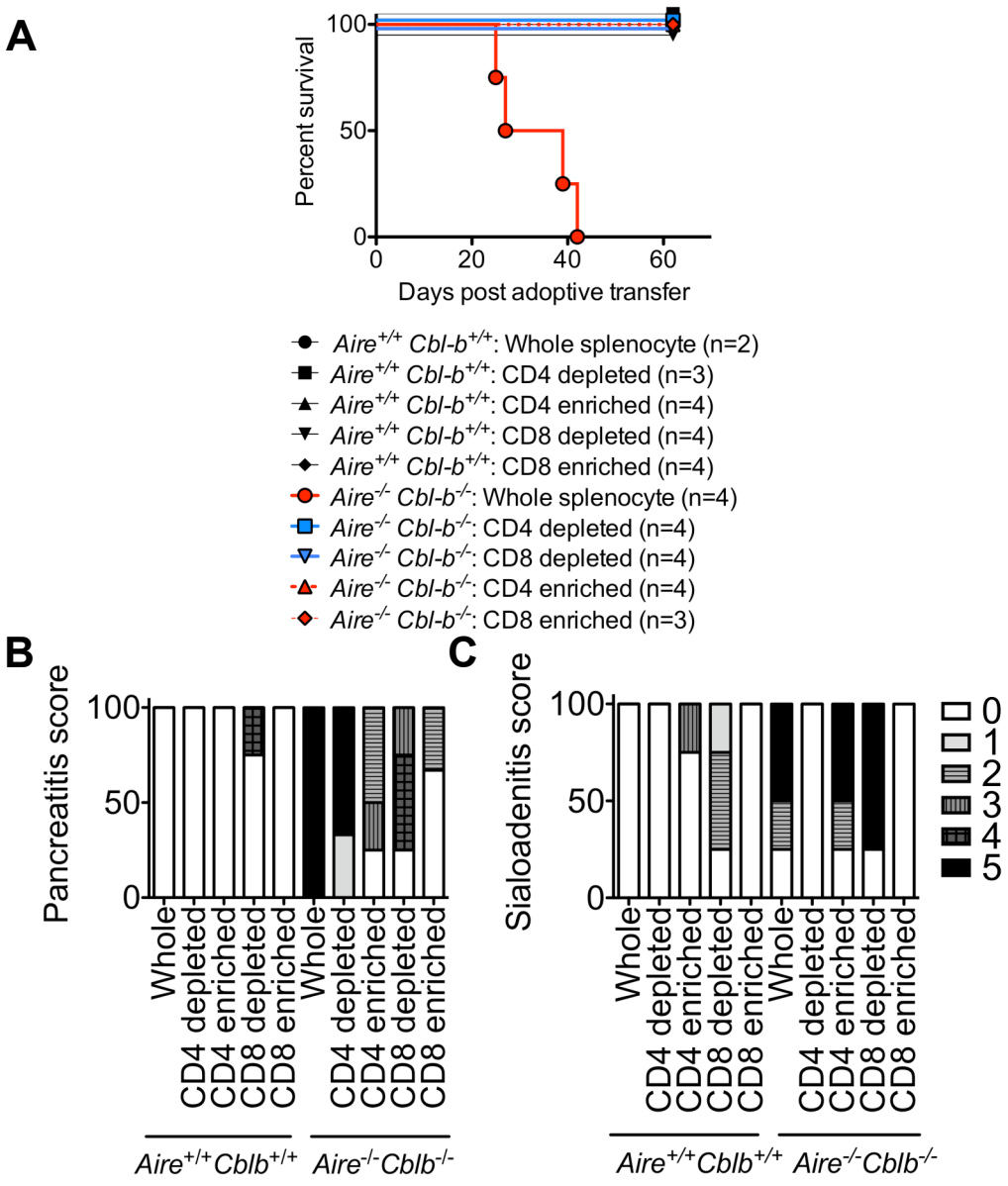

Figure 3.24 *Aire*$^{-/-}$*Cblb*$^{-/-}$ CD4 and CD8 cells are necessary to transfer the wasting syndrome to lymphopenic *Rag1*-deficient recipients.

A. Survival of *Rag1*-deficient B10.BR mice after adoptive transfer of the indicated subsets of splenocytes.

B. Percentage of recipient mice with different grades of pancreatitis.

C. Percentage of recipient mice with different grades of sialoadenitis.

These experiment established that both CD4 and CD8 cells are necessary for development of pancreatitis and CD4 cells are necessary for development of sialoadenitis. It still remains to be tested if these populations are sufficient to drive the disease. There is a possibility that other lymphocyte populations may also be required to precipitate or promulgate the disease. Several studies have indicated that there is a possible role for B cells (Gavanescu et al., 2008) and B-cell-activating factor to the tumour necrosis factor family (BAFF)-secreting dendritic cells (Lindh et al., 2008) in the development of autoimmunity in *Aire*$^{-/-}$ mice. Since the pattern of disease was mirrored by the presence of autoantibodies against these same organs, it would be interesting to test if B cells were also needed to transfer the disease using a similar experimental set-up in the future.

3.9 Wild-type T regulatory cells confer protection from lethal wasting and pancreatitis in *Aire*$^{-/-}$*Cblb*$^{-/-}$ mice

As indicated in section 3.8, the CD4 population is necessary for the development of both pancreatitis and sialoadenitis. However, there are many different subpopulations of CD4 cells such as CD4 helper cells and T regulatory cells. Notably, besides the conventional role of *Aire* in mediating negative selection of antigen-specific CD8 and CD4 helper cells in the thymus, it has been suggested to play a role in positive selection and formation of organ-specific nTreg cells. Mice that have deficiencies in the master transcription factor of Treg cells, FoxP3, frequently present with multiorgan specific autoimmunity (Fontenot et al., 2003; Hori et al., 2003; Khattri et al., 2003). It could be possible that the multiorgan autoimmunity caused by *Aire*-deficiency, at least in part is due to a defect in Tregs. This section will investigate if wild-type nTregs that have been positively selected in an *Aire*-dependent fashion are able to control the lethal pancreatitis mediated by the double genetic defects in *Aire* and *Cblb*.

To do this, 3×10^6 *Aire*$^{-/-}$*Cblb*$^{-/-}$ splenocytes (CD45.2 and CD45.1/2, for simplicity will be refered to as CD45.2$^+$) and adjusted numbers of wild-type CD45.1$^+$CD4$^+$CD25$^+$ MACS-enriched CD45.1 nTreg cells were intra-venously introduced into groups of ten *Rag1*-deficient recipients in the following ratios: 1:0, 1:1/9: 1:1/3 and 1:1 (*Aire*$^{-/-}$*Cblb*$^{-/-}$:wild-type CD4$^+$CD25$^+$) (Fig. 3.25). The CD45.2$^+$ *Aire*$^{-/-}$*Cblb*$^{-/-}$ splenocytes were

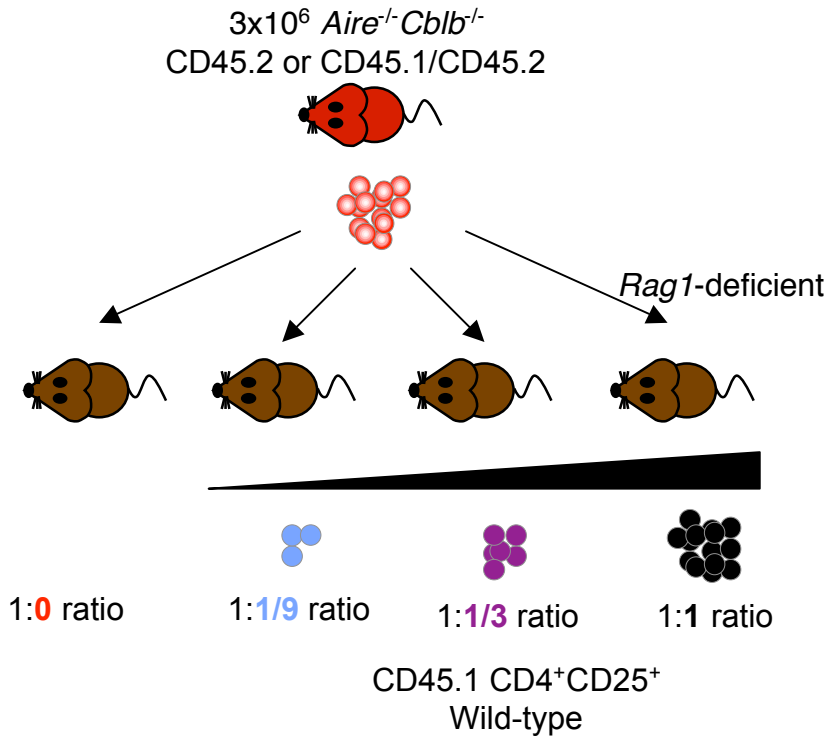

Figure 3.25 Schematic representation of the T regulatory cell adoptive transfer assay.
Rag1-deficient recipients of *Aire*$^{-/-}$*Cblb*$^{-/-}$ splenocytes were given CD4^{+}CD25^{+} wild-type cells in different ratios as indicated.

obtained from bone marrow chimeras to circumvent potential problems of obtaining insufficient cell numbers from small cachectic wasting *Aire*$^{-/-}$*Cblb*$^{-/-}$ mice obtained via breeding.

The mice were bled 22 days post-adoptive transfer to verify the engraftment and expansion of the CD45.2^{+} *Aire*$^{-/-}$*Cblb*$^{-/-}$ splenocytes and the CD45.1^{+}CD4^{+}FoxP3^{+} population. As seen in Fig. 3.26*A*, 0.16±0.04, 0.45±0.07, 0.52±0.11 and 0.28±0.08 (mean±s.d.)% of CD4^{+}FoxP3^{+} cells were detected in recipients of 1:0, 1:1: 1:1/3 and 1:1/9 (*Aire*$^{-/-}$*Cblb*$^{-/-}$:wild-type CD4^{+}CD25^{+}), respectively. Statistical analysis indicated that all groups receiving co-transferred CD4^{+}CD25^{+} cells had significantly elevated frequencies of circulating Foxp3^{+} CD4 cells compared to the frequency in the control (1:0) group, and that the frequency was higher in the groups receiving higher numbers of co-transferred CD25^{+} cells (groups 1:1 and 1:1/3) compared to the recipients of the lowest number (group 1:1/9). When the Foxp3^{+}CD4^{+} cells in the recipients were subdivided according to whether they came from the *Aire*$^{-/-}$*Cblb*$^{-/-}$ donor (CD45.2^{+}) or the wild-type donor (CD45.1^{+}), CD45.1^{+} cells represented 94.7±2.2, 90.9±2.43 and 79.4±3.79 (mean±s.d.) % of the FoxP3^{+} cells in the 1:1: 1:1/3 and 1:1/9 (*Aire*$^{-/-}$*Cblb*$^{-/-}$:wild-type CD4^{+}CD25^{+}) groups (Fig. 3.26*B*(top panel)). Thus, the co-transferred wild-type Tregs increased the overall numbers of circulating Tregs and accounted for the majority of circulating Tregs.

To establish the extend to which the wild-type CD45.1^{+} cells contributed to the FoxP3^{-} T cell pool within the mice, the percentages of CD45.1^{+}CD4^{+}FoxP3^{-} and CD8 cells in each group was enumerated: group 1:1 (25.3±3.9 CD4^{+} FoxP3^{-} and 13.34±6.04 CD8); group 1:1/3 (13.84±4.1 CD4^{+} FoxP3^{-} and 2.68±1.37 CD8) and 1:1/9 (8.08±7.3 CD4^{+} FoxP3^{-} and 1.79±1.83), whereby percentages are expressed from total CD4^{+} FoxP3^{-} or CD8 cells, respectively. Similar to the Foxp3^{+}CD4^{+}, there appears to be a dose-dependent appearance of CD4^{+} FoxP3^{-} and CD8 cells in the following order group 1:1 < group 1:1/3 < group 1:1/9, although ≥75% of FoxP3^{-} T cells in each group represented disease-driving *Aire*$^{-/-}$*Cblb*$^{-/-}$ CD45.2^{+} cells. This verified that most of the FoxP3^{-}CD4 and CD8 cells were CD45.2^{+} and hence derived from the *Aire*$^{-/-}$*Cblb*$^{-/-}$ donor.

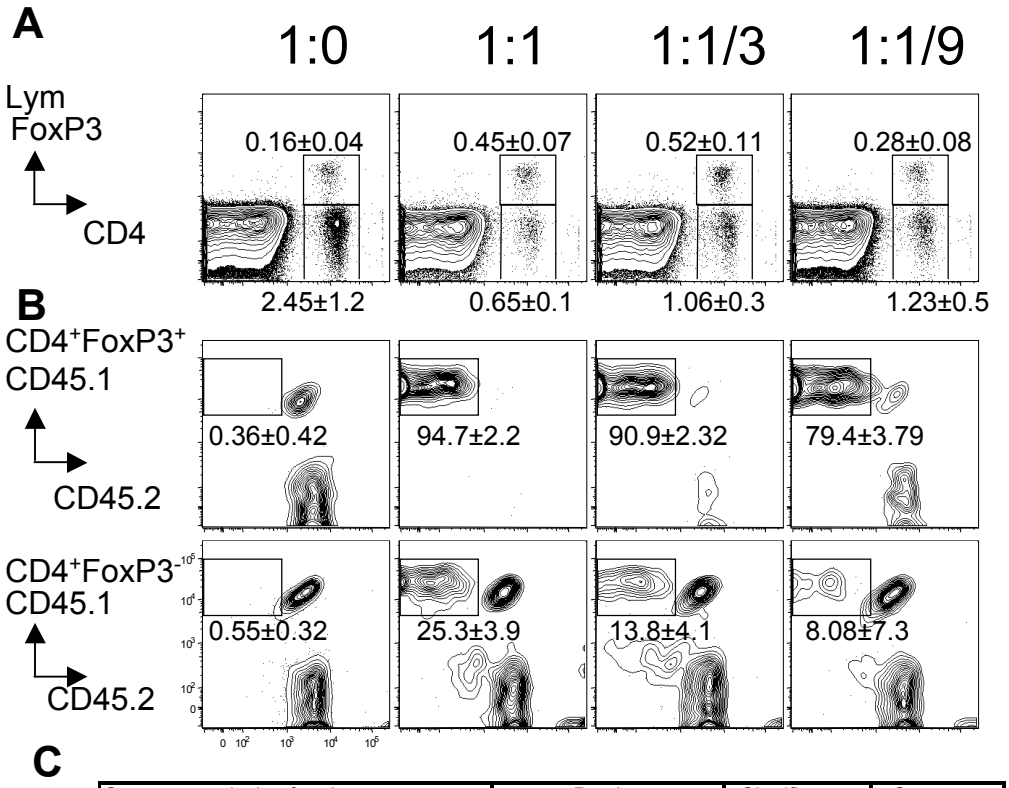

C

One-way analysis of variance	P value	Significance	Summary
All groups	< 0.0001	Yes	***
Bonferroni's Multiple Comparison Test	t value	Significance	Summary
1:0 vs 1:1	13.02	Yes	***
1:0 vs 1:1/3	14.45	Yes	***
1:0 vs 1:1/9	6.95	Yes	***
1:1 vs 1:1/3	1.432	No	n.s.
1:1 vs 1:1/9	6.071	Yes	***
1:1/3 vs 1:1/9	0.2433	Yes	***

Figure 3.26 Representative flow cytometry plots of recipients analysed 22 days post transfers show detectable levels of CD45.1 FoxP3^{+} cells in the blood.

A. Representation of flow cytometric plots of FoxP3^{+} and FoxP3^{-} CD4 cells gated on total lymphocytes in blood from recipients of the indicated groups.

B. Division of the CD4^{+}FoxP3^{+} (top) and CD4^{+}FoxP3^{-} (bottom) cells into CD45.1 and CD45.2.

C. One-way ANOVA and Bonferronni post-test comparing percentages of CD45.1 FoxP3^{+} T regulatory cells from total lymphocytes between all groups.
Percentages for (A) and (B) show the means and standard deviation of each group for *n*=10 mice per group.

All the *Rag1*-deficient mice receiving *Aire*$^{-/-}$*Cblb*$^{-/-}$ splenocytes alone (1:0 group) either died spontaneously or were sacrificed due to 20% weight loss by 56 days post-adoptive transfer (Fig. 3.27). By contrast, recipients of *Aire*$^{-/-}$*Cblb*$^{-/-}$ cells that received equal amounts of wild-type CD4^{+}CD25^{+} and *Aire*$^{-/-}$*Cblb*$^{-/-}$ splenocytes remained healthy for the duration of the experiment (108 days) as determined by gross observation and survival. Sixty percent and 70% of the *Rag1*-deficient recipients in the 1:1/3 and 1:1/9 groups also survived for the 108-day course of the experiment. Statistical analysis supported the conclusion that there was a dose-response relationship, in that survival in the 1:1/9 recipient group was unlikely to be the same as in the 1:1 group. Thus, co-transfer of wild-type CD4^{+}CD25^{+} conferred protection from the lethality in a dose dependent manner.

To determine the effect of co-transferred CD25^{+} CD4 cells on exocrine pancreatitis and sialoadenitis, the remaining recipients that survived on day 108 were sacrificed and analysed histologically. As seen in Fig. 3.28*A*, while 6 or the 10 recipient mice in the 1:1/9 group survived, all of these animals had developed pancreatitis with median pancreatitis scores of 5. By contrast, less severe pancreatitis was observed in the recipients that received higher numbers of Tregs, with median scores of 2 in the 1:1/3 group and zero in the 1:1 group. Thus, there was a dose-response relationship between the number of wild-type Tregs transferred and suppression of exocrine pancreatitis. A similar trend was observed for the salivary gland (Fig. 3.28*B*), albeit all recipient mice displayed less severe sialoadenitis scores compared to the pancreatitis. The differences seen in the salivary gland histology between the experimental groups were not statistically significant.

Overall, this experiment demonstrates that the addition of wild-type T regulatory cells were able to suppress the pancreatitis in *Rag1*-recipients of *Aire*$^{-/-}$*Cblb*$^{-/-}$ cells and its progression to lethal disease, although further experimentation will be needed to accurately delineate the role of Tregs in the progression of the disease. In particular, it will be important to determine whether suppression of disease reflected a unique quality of wild-type Tregs, the overall increase in Tregs or if the addition of wild-type T cells displaced or diluted the disease-driving *Aire*$^{-/-}$*Cblb*$^{-/-}$ cells.

A

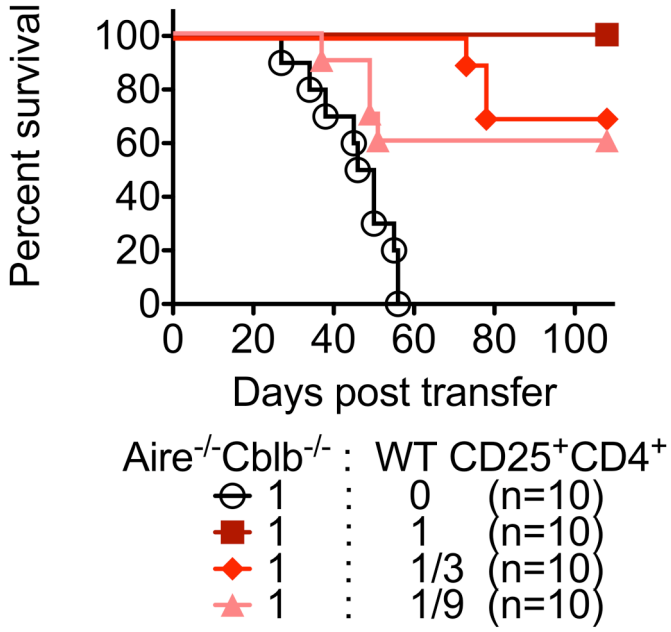

B

Group comparision	P value	Significance	Summary
1:0 Tregs vs 1:1 Tregs	<0.0001	Yes	***
1:0 Tregs vs 1:1/3 Tregs	<0.0001	Yes	***
1:0 Tregs vs 1:1/9 Tregs	0.0091	Yes	**
1:1 Tregs vs 1:1/3 Tregs	0.0675	No	n.s.
1:1 Tregs vs 1:1/9 Tregs	0.0291	Yes	*
1:1/3 Tregs vs 1:1/9 Tregs	0.4512	No	n.s.

Figure 3.27 Wild-type CD4$^+$CD25$^+$ cells are able to suppress cachectic wasting syndrome in *Rag1*-deficient recipients of *Aire*$^{-/-}$*Cblb*$^{-/-}$ splenocytes in a dose-dependent manner (Experiment 1).

A. Survival measured post-transfer of *Aire*$^{-/-}$*Cblb*$^{-/-}$ and CD4$^+$CD25$^+$ wild-type cells, *n* = 10 per group for Experiment 1.

B. Summary of statistical analysis for survival calculated using a log rank Mantel-Cox test.
Results are representative of two independent experiments with *n*=10 in each group.

A

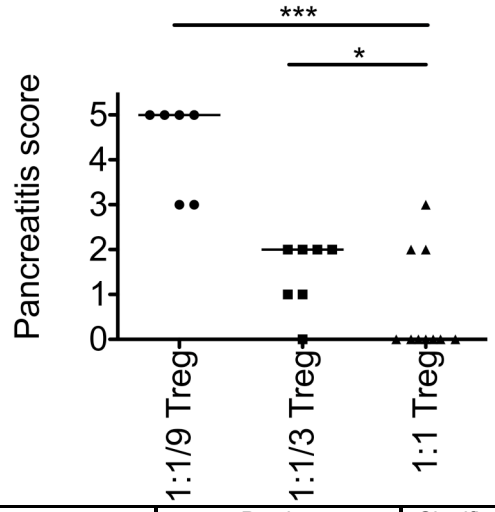

Kruskal-Wallis test	P value	Significance	Summary
All groups	0.0008	Yes	***
Dunn's Multiple Comparison Test	Difference in rank sum	Significance	Summary
1:1/9 Treg vs 1:1/3 Treg	9.262	Yes	*
1:1/9 Treg vs 1:1 Treg	12.68	Yes	***
1:1/3 Treg vs 1:1 Treg	3.421	No	n.s.

B

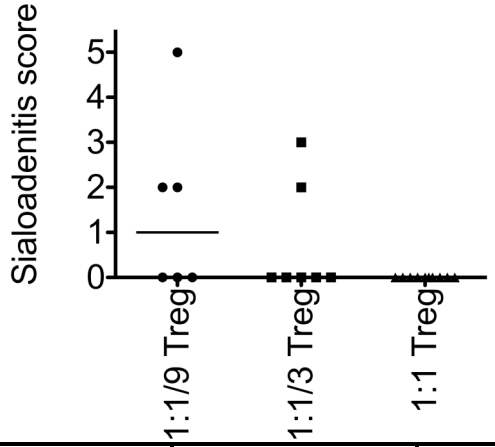

Kruskal-Wallis test	P value	Significance	Summary
All groups	0.0655	No	n.s.
Dunn's Multiple Comparison Test	Difference in rank sum	Significance	Summary
1:1/9 Treg vs 1:1/3 Treg	2.464	No	n.s.
1:1/9 Treg vs 1:1 Treg	5.75	No	n.s.
1:1/3 Treg vs 1:1 Treg	3.286	No	n.s.

Figure 3.28 Wild-type CD4^{+}CD25^{+} cells are able to suppress development of pancreatitis ad sialadenitis in *Rag*1-deficient recipients of *Aire*$^{-/-}$*Cblb*$^{-/-}$ splenocytes in a dose-dependent manner.

A. Pancreatitis scores for *Rag*1-deficient recipients sacrificed at Day 108 of Experiment 1.

B. Sialoadenitis scores for *Rag*1-deficient recipients sacrificed at Day 108 of Experiment 1.

The P values and significance comparing the different groups was determined by a Kruskal-Wallis test comparing all columns and Dunn's Multiple Comparison test comparing pairs of columns. Results are representative of two independent experiments with *n*=10 in each group.

3.10 Chapter summary and key findings

3.10.1 CBL-B, a key failsafe for AIRE-mediated autoimmunity

The findings in this chapter, obtained both by breeding or bone marrow transplantation, established that variations in the latent period and organ specificity of autoimmune disease in *Aire*-deficiency reflected the activity of a fail-safe tolerance mechanism mediated by the ubiquitin ligase Cbl-b. Single deficiencies in *Aire* and *Cblb* resulted in no clinical autoimmune disease in the animals studied here on a genetic background not particularly prone to autoimmunity, and resulted in variable autoimmune disease with a long latent phase when studied on other genetic backgrounds (Anderson et al., 2002; Bachmaier et al., 2000; Chiang et al., 2000; Ramsey et al., 2002b; Yokoi et al., 2007). When both tolerance mechanisms were crippled, an emergent phenotype of complete autoimmune destruction of the exocrine pancreas occurred within weeks after T cells began emigrating from the thymus. The cooperation between *Aire* and *Cblb* was unique: while the $Fasl^{gld}$ and $Rc3h1^{san}$ mutations gave rise to more fully penetrant autoimmunity on their own, when compounded with $Aire^{-/-}$ they yielded autoimmune phenotypes that appear simply to be the sum of each individual defect. Reasons for this will be discussed in chapter 6. These findings are the first to reveal a higher-level architecture assembling individual tolerance mechanisms together for robust resistance to autoimmunity.

Cbl-b has a well-defined role in the regulation of mature T cell activation. Cbl-b is only expressed at low levels in immature T lymphocytes (Naramura et al., 2002; Thien and Langdon, 2005) and consequently *Cblb*-deficiency does not alter thymic selection or *Aire*-dependent thymic deletion (Hoyne et al., 2011b). Cbl-b is upregulated in mature and anergic T cells, where it inhibits the PI3K and NF-κB signalling pathways activated by TCR-CD28 co-stimulation and is required for T cell anergy to prevent proliferation of T cells that have recognized peripheral antigens with insufficient affinity or in the absence of adequate CD28 co-stimulation (Bachmaier et al., 2000; Chiang et al., 2000; Fang and Liu, 2001; Gronski et al., 2004; Heissmeyer et al., 2004; Jeon et al., 2004; Naramura et al., 2002; Qiao et al., 2008; Thien and Langdon, 2005). Hence, a simple explanation for the rapid progression to pancreatic autoimmune disease observed here is that pancreas-specific T cells escape thymic deletion due to *Aire*-deficiency and then

escape anergy and the normal requirement for CD28 co-stimulation due to *Cblb*-deficiency, allowing them to proliferate and differentiate into tissue-damaging effector T cells.

3.10.2 Defects in nTreg and iTregs may exacerbate autoimmunity in *Aire*$^{-/-}$*Cblb*$^{-/-}$ mice

The simple explanation was made based on the assumption that *Aire* and *Cblb* only crippled two different tolerance pathways. However, the results in section 3.9 demonstrated that wild-type nTreg were able to confer protection from the lethal pancreatitis precipitated by adoptively transferring *Aire*$^{-/-}$*Cblb*$^{-/-}$ cells into lymphopenic recipients. An attractive explanation for this rescue is that *Aire*$^{-/-}$*Cblb*$^{-/-}$ mice exhibit additional deficiencies in FoxP3^{+} T regulatory cells besides the deficiency in negative selection associated with *Aire*$^{-/-}$ and T cell anergy associated with *Cblb*$^{-/-}$. Hence, although the combination of *Aire*$^{-/-}$ and *Cblb*$^{-/-}$ represents two genetic defects, it may cripple more than two tolerance pathways. There has been growing evidence that *Aire* might also promote formation of FoxP3^{+} natural T regulatory cells (nTregs) that develop in the thymus (Hinterberger et al., 2010; Kekalainen et al., 2007b; Laakso et al., 2011; Ryan et al., 2005; Wolff et al., 2010), and that *Cblb* promotes differentiation of inducible T regulatory (iTregs) cells that upregulate FoxP3 in response to TGF-β stimulation (Harada et al., 2010; Hoyne et al., 2011b; Wohlfert et al., 2004; Wohlfert et al., 2006). Coupling *Aire*-deficiency with *Foxp3*-deficiency further accelerated the already rapidly lethal effect of *Foxp3*-deficiency on its own (Chen et al., 2005).

The possibility that a qualitative deficiency of iTregs is necessary for autoimmune pancreatitis in *Aire*$^{-/-}$*Cblb*$^{-/-}$ mice is addressed by the mixed bone marrow chimera experiments (Section 3.6). Here it was observed that *Aire*$^{-/-}$ recipient mice that received wild-type marrow (and could therefore develop normal iTreg cells) in addition to the *Cblb*$^{-/-}$ marrow still developed lethal pancreatitis, although this appeared to be less severe than *Aire*$^{-/-}$ recipient mice that received only *Cblb*$^{-/-}$ cells. The result contrasted with autoimmunity entirely due to nTreg defects, which are fully corrected by mixtures of defective and wild-type T cells (Sakaguchi et al., 2009). This suggests that the disease was not mediated simply by defects in the nTreg component. However *Aire*

deficiency in these mixed chimeras could potentially decrease thymic formation of organ-specific nTregs from both the mutant and wild-type marrow, particularly given the potent suppression of pancreatitis by co-transfer of nTregs that had developed in a wild-type thymus (Figure 3.27 and 3.28). It would be valuable in a future experiment to test whether or not co-transfer of nTregs from an *Aire*-deficient donor could suppress pancreatitis to the same extent. Along these lines, the presence of normal Tregs did not suppress organ-specific autoimmunity when Anderson and colleagues (Anderson et al., 2005) transferred 50:50 mixtures of splenocytes from *Aire*-deficient and *Aire* wild-type mice into *Rag*-deficient mice.

Another way of providing a source of normally educated nTregs would be to repeat the mixed bone marrow chimera experiment in thymectomized recipients that had been grafted with two thymi: a wild-type thymus as well as an Aire-deficient thymus. Anderson and colleagues (Anderson et al., 2005) performed this experiment in mice that were singly deficient in *Aire* and found that autoimmunity still developed, again providing compelling evidence against a substantial role for a qualitative defect in nTregs. Understanding how *Aire* and *Cblb* co-operate mechanistically will be further explored using transgenic mice in chapter 4, allowing accurate tracking and measurements of a single self-reactive clone in the *Aire*$^{-/-}$*Cblb*$^{-/-}$ mice.

3.10.3 Only two organs targeted in *Aire*$^{-/-}$*Cblb*$^{-/-}$ mice: the pancreas and salivary glands

It is striking that the immediate autoimmune destruction in *Aire*$^{-/-}$*Cblb*$^{-/-}$ double mutant animals was not more generalized but remained limited to exocrine acinar cells in the pancreas and mucous acinar cells in the submandibular salivary gland. The pancreatic endocrine tissues and other organs (lung, kidney, liver, thyroid, heart, eye, ovaries/testis) remained virtually unaffected by autoimmunity in the double-deficient animals, although *Aire* deficiency interferes with thymic deletion against hundreds of autoantigens that are highly expressed in different organs (Anderson et al., 2005; Anderson et al., 2002; Liston et al., 2003), and *Cblb* deficiency can predispose to pancreatic islet autoimmune destruction (Gronski et al., 2004; Yokoi et al., 2007; Yokoi et al., 2002). Since both the pancreas and salivary gland have similarities in structure

(exocrine and endocrine) and function (production of digestive enzymes), it is possible that the same autoreactive immune cell clone from the *Aire*$^{-/-}$*Cblb*$^{-/-}$ mice is targeting a common autoantigen in the acinar cells in the two organs (common immunogenicity). However, adoptive transfer assays from section 3.8 suggest that pancreatitis is both CD8- and CD4-dependent, while the sialoadenitis is predominantly CD4 -dependent. Furthermore, the pattern of autoantibody detection from the sera of *Aire*$^{-/-}$*Cblb*$^{-/-}$ seemed to be largely targeted towards the apical surface of the pancreatic acinar cells, while a more diffuse pattern is observed for the salivary gland. Hence, experiments in chapter 5 will set out to isolate CD8- and CD4-dependent disease driving cells in *Aire*$^{-/-}$*Cblb*$^{-/-}$ mice and utilize this information to understand the nature and immunogenicity of the driver autoantigen(s) in this double-deficient mouse strain.

Chapter 4

Varying the T cell repertoire in *Aire*$^{-/-}$ *Cblb*$^{-/-}$ double deficient mice

Acknowledgements of assistance in the work described in this chapter: The mice were genotyped by the Australian Phenomics Facility, while I performed most of the Aire genotyping. Glucosuria scoring in sections 4.4.1 and 4.4.2 were performed by Ken Chau and Luke Walker (Animal technicians). Technical assistance for mouse takedown in section 4.4.2 was obtained from Jennifer Koffler (IGL laboratory technician). The experiments in section 4.5 were a collaborative effort between Dr. Stephen Daley and me. Results from section 4.5.3 were published in (Hoyne et al., 2011b). *All in vitro and in vivo experiments described in this section were designed in collaboration with Dr. Stephen Daley and performed by me with some help from Debbie Howard (IGL laboratory technician) for injections and diabetes testing. The optimised peripheral proliferation assay has been published (Silva et al., 2011). All hematoxylin and eosin section cutting and staining was done by Ms. Anne Prins (Flow Cytometry and Microscopy, John Curtin School of Medical Research).*

4.1 Preamble

Chapter 3 poses a mechanistic question: why is autoimmunity in *Aire*$^{-/-}$*Cblb*$^{-/-}$ double deficient mice selectively targeted towards the acinar cells in the pancreas and salivary gland while other organs remained relatively untouched? This is intriguing as Aire regulates the expression of numerous peripheral tissue antigens (Anderson et al., 2002). It is hypothesized that the spectrum of the organs targeted is determined by variations in the T cell repertoire (repertoire/presentation hypothesis). According to this hypothesis, by varying the repertoire, the *Aire*$^{-/-}$*Cblb*$^{-/-}$ double deficient mice are predicted to still present with infant onset autoimmune disease but targeted towards a different organ. In this chapter, the T cell repertoire was varied using two strategies. Section 4.3 introduced variations in the repertoire by changing the MHC. Sections 4.4 and 4.5 examined the consequence of producing high numbers of T cell precursors specific for a different pancreatic cell-type.

4.1.1 Substituting the MHC

MHC haplotypes account for the strongest genetic effects on autoimmune diseases in humans and mice although the basis for this remains unresolved (Todd and Wicker, 2001; Wandstrat and Wakeland, 2001). One explanation is that particular MHC haplotypes may be particularly selective for positive selection of certain driver T cells. A second explanation is that particular MHC alleles may be better at presenting the driver autoantigen that provokes autoimmunity in peripheral tissues (McDevitt, 1980). It is also possible that the driver autoantigens are poorly presented to reduce effective negative selection during development in the thymus, peripheral anergy or other peripheral tolerance mechanisms.

Thus, in the *Aire*$^{-/-}$*Cblb*$^{-/-}$ double deficient mice it is possible that the driver autoantigen from pancreas or salivary gland presented by the *H2*^{k}-encoded MHC: (i) happens to cross-react with T cells that are efficiently positively selected in the thymus of *H2*^{k} mice; (ii) efficiently presented by the T cells to induced autoimmunity or (iii) poorly presented for tolerance in the thymus and periphery. There is evidence that varying MHC haplotype in *Aire*$^{-/-}$ mice alters the spectrum of the organs targeted. For example,

on the NOD background (but not on the NOD.$H2^b$ background) the mice are prone to developing pancreatitis and sialoadenitis, while on the C57BL/6 background the mice develop uveitis and on the BALC/c background the mice develop gastritis (Jiang et al., 2005; Niki et al., 2006). Therefore, it seemed reasonable to test if changing the MHC haplotype would change the spectrum of the disease in *Aire*$^{-/-}$*Cblb*$^{-/-}$ mice.

4.1.2 Changing the starting frequency of cells recognising particular MHC:peptide complexes produced in the pancreas

The pattern of autoimmunity in *Aire*$^{-/-}$*Cblb*$^{-/-}$ mice is most likely highly influenced by the starting frequencies of T cells recognising the acinar structures in the pancreas and salivary gland that were positively selected during maturation in the thymus. In *Aire*$^{-/-}$ *Cblb*$^{-/-}$ mice these driver T cells may be elevated due to the genetic deficiencies in *Aire* (failure of negative selection in the thymus) and *Cblb* (failure of a peripheral anergy control mechanism). These high frequencies of exocrine pancreas-specific cells may have out-competed other T cell clones causing severe autoimmunity in the pancreas before any other autoimmunity could develop. It is possible to vary the starting frequencies of the autoreactive TCR without changing the MHC haplotye using TCR transgenic mice. In the $H2^k$ TCR^{3A9} transgenic mice, the TCR repertoire is skewed to contain high numbers of T cells that efficiently target the hen-egg-lysozyme (HEL) antigen. If the repertoire/presentation hypothesis holds true, this would change the course of disease in the *Aire*:*Cblb* double deficient mice when HEL is expressed in pancreatic islet β cells, so that the mice would develop early onset diabetes instead of pancreatitis. The system has several advantages: (i) it provides high numbers of driver autoreactive cells that are scarce under physiological conditions; (ii) the autoreactive cells are traceable using a clonotypic antibody throughout TCR^{3A9} T cell development and function and (iii) the pattern of HEL-self antigen is varied to target specific organs in the body mirroring the expression of the *bona fide* autoantigens by controlling expression under the tissue-specific promoter (in this study the insulin or thyruglobulin promoter was used).

4.2 Mice used in this chapter

4.2.1 *H2^b Cblb$^{-/-}$* and *Aire$^{-/-}$* mice

The *Cblb$^{-/-}$* (*H2^b*) mouse used in this chapter was generated by backcrossing a *Cblb$^{-/-}$* B10.BR.C57BL/6.N_2F_6 mouse to a C57BL/6 mouse, and intercrossing the offspring for three filial generations to fix the *H2^b* MHC allele before being used for experimentation. The *Aire$^{-/-}$* (*H2^b*) mouse was generated by crossing a B10.BR.C57BL/6.N_5F_7 that was homozygous for the *Aire$^{-/-}$* and heterozygous for *Rag1*-deficiency (*H2^b*) to a C57BL/6 mouse. Offspring from this cross were intercrossed for at least four filial generations before being used for experimentation.

4.2.2 TCR^{3A9}, insHEL and thyrHEL transgenic mice

The TCR^{3A9} transgenic mice inherited rearranged TCR chains, utilizing the variable regions Vα3 and Vβ8.2 (Ho et al., 1994) that caused most T cells in the thymus to have high affinity for a peptide generated from position 46-61 of hen HEL, complexed to the MHCII molecule I-A^k (Allen et al., 1987). TCR^{3A9} cells are positively selected and can be detected in B10.BR (*H2^k*) mice by the clonotypic anti-mouse TCR^{1G12} antibody (Peterson and Unanue) (Van Parijs et al., 1998). The strain has been maintained in the laboratory on the B10.BR genetic background. *Cblb$^{-/-}$*TCR^{3A9} mice were produced by crossing a *Cblb$^{-/-}$* B10.BR.C57BL/6/129.N_3 mouse with the B10.BR.TCR^{3A9} mouse and intercrossing the offspring for at least seven generations prior to use in experimentation.

The insHEL transgenic strain, ILK-3, expresses HEL as a self-protein under the control of the pancreas-specific rat insulin promoter. The pattern of HEL expression mirrors that of insulin. These mice express high concentrations of HEL in the beta cells of the pancreatic islets (140-400 ng/mg tissue), low concentrations of HEL (10-20 ng/ mL) in blood plasma (Akkaraju et al., 1997b) and trace levels are made by the thymic epithelium in a manner that is dependent on *Aire* (Liston et al., 2003). The *Aire$^{-/-}$* insHEL mouse that was used to establish the crosses studied here had a mixed B10.BR×C57BL/6.N_3F_3 background. The mouse was crossed to the insHEL strain

maintained in the laboratory and intercrossed for at least four filial generations prior to analysis.

In double-transgenic (Dbl-Tg) TCR^{3A9}:insHEL mice, the TCR^{3A9} cells were tolerized despite their high prevalence. This occurred through deletion of the high avidity $IG12^{+}$ T cells during development in the thymus and export of residual T cells that were either functionally anergic or are $FoxP3^{+}$ nTregs (Akkaraju et al., 1997b; Lesage et al., 2002). The anergic cells expressed low HEL-specific TCR and CD3 and increased amounts of CD5 (Akkaraju et al., 1997b; Lesage et al., 2002). The mice developed insulitis, but this remained sub-clinical or benign in a large fraction of the animals (Akkaraju et al., 1997b). On the B10.BR background, ~20% of the Dbl-Tg mice developed diabetes by 24 weeks of age (Lesage et al., 2002). In the absence of *Aire*, TCR^{3A9} cells escaped negative selection in the thymus of Dbl-Tg mice and were exported into the peripheral circulation in large numbers causing 50% of the $Aire^{-/-}$ TCR^{3A9}:insHEL mice to present with diabetes by 15 weeks of age (Liston et al., 2004a).

ThyrHEL mice, TLK-2, produced membrane-bound HEL protein at high levels in the thyroid epithelium (140/400 ng/mL), approximately 0.5 ng/mL levels of soluble HEL protein in the circulation (Akkaraju et al., 1997a; Akkaraju et al., 1997b) and higher levels of HEL in thymic epithelial cells than found in insHEL mice (Liston et al., 2004a). The higher expression of HEL in the thymus of thyrHEL mice resulted in more severe deletion of thymocytes than in the insHEL mice (Akkaraju et al., 1997b). In the thymus of *Aire*-deficient mice, the deletion of self-reactive thyrHEL cells was completely abolished (Liston et al., 2004a). Crossing a B10.BR.C57BL/6.N3F2 mouse homozygous for *Aire*- and *Rag1*-deficiency to the B10.BR.thyrHEL strain available in the laboratory generated this strain.

To generate $Aire^{-/-}Cblb^{-/-}$ deficient double transgenic mice, B10.BR.C57BL/6/129.N_3F_{14} $Cblb^{-/-}TCR^{3A9}$ mice were crossed with *Aire* heterozygous mice derived from the *Aire* insHEL, *Aire* thyrHEL or *Aire* TCR^{3A9} strains described above.

4.3 Substituting the MHC allele that presents the driver autoantigen to T cells

At the start of the chapter, three hypotheses were put forward to explain the pattern of autoimmunity based on MHC haplotype. To assess the contribution of MHC alleles on in the pattern of autoimmunity in *Aire*$^{-/-}$*Cblb*$^{-/-}$ double deficient mice, the *H2*^{k} MHC haplotype (I-A^{k}, I-E^{k}, K^{k}, D^{k} & L^{k}) from the original *Aire*$^{-/-}$*Cblb*$^{-/-}$ double deficient mice was substituted with the *H2*^{b} MHC haplotype (K^{b}, I-A^{b}, I-E^{null}, D^{b}, L^{null}). The B10.BR, (*H2*^{k}) and C57/BL6, (*H2*^{b}) are congenic strains, and genetically vary only at the MHC and at a small number of other background loci that differed between the B10.BR and C57BL/6 substrains.

Bone marrow chimeras were constructed whereby T cell-depleted wild-type or *Cblb*$^{-/-}$ (*H2*^{b}) bone marrow were used to reconstitute sub-lethally irradiated wild-type or *Aire*$^{-/-}$ (*H2*^{b}) recipients. T cell depletion was performed to eliminate mature T cells from the marrow so that only hematopoietic stem cell-derived T cells developed in the recipient mice. The donor bone marrow stem cells were allowed to reconstitute the recipient hematopoietic system for six weeks to test the effect of MHC substitution on survival and development of pancreatitis in *Aire*$^{-/-}$*Cblb*$^{-/-}$ chimeras (Fig. 4.1).

Fig. 4.2 compares the survival curves of two separate chimeric experiments: experiment 2 from section 3.4 for *Aire*$^{-/-}$*Cblb*$^{-/-}$ *H2*^{k} bone marrow chimeras, and experiment 1 for the *H2*^{b} bone marrow chimeras. The survival curves focus on four groups in each chimera – wild-type or *Aire*$^{-/-}$ recipients of wild-type marrow and wild-type or *Aire*$^{-/-}$ recipients of *Cblb*$^{-/-}$ marrow. In the *H2*^{k} chimeras, *Aire*$^{-/-}$ recipients of *Cblb*$^{-/-}$ marrow exhibit a median survival of 35 days and the mice either died suddenly or were euthanised because of cachexia by 41 days post reconstitution (Fig. 4.2*A*). On the other hand, *Aire*$^{-/-}$ recipients of *Cblb*$^{-/-}$ marrow in the *H2*^{b} chimeras, had a median survival of 63 days, and there were still 2 of 7 mice surviving 165 days post reconstitution (Fig. 4.2*B*). This result suggested that the *H2*^{b} background delayed the onset of the wasting disease.

To determine the spectrum of organs targeted by autoimmunity in the *H2*^{b} chimeras, a histological survey of the pancreas, salivary gland, lung, liver, stomach, heart, thyroid,

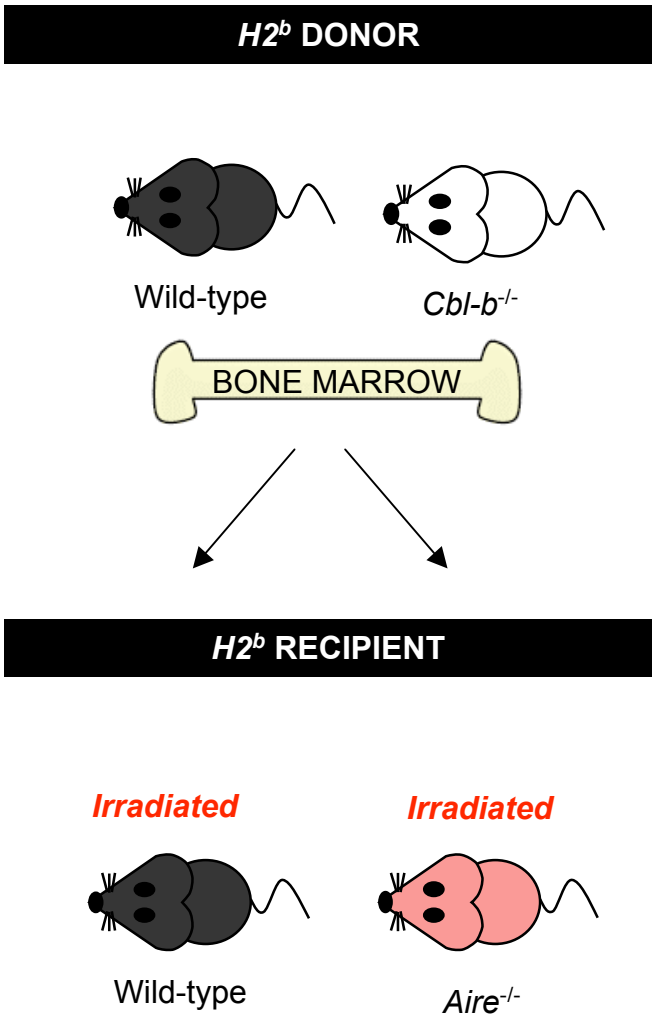

Figure 4.1 Combining the *Aire*$^{-/-}$ and *Cblb*$^{-/-}$ mutations on the *H2*^{b} background.
Aire-deficient or wild-type irradiated recipients were reconstituted with bone marrow from wild-type or *Cblb*$^{-/-}$ mice in the following three combinations: 100% wild-type, 100% *Cblb*$^{-/-}$ or an equal mixture of both. Each combination was introduced into five recipients.

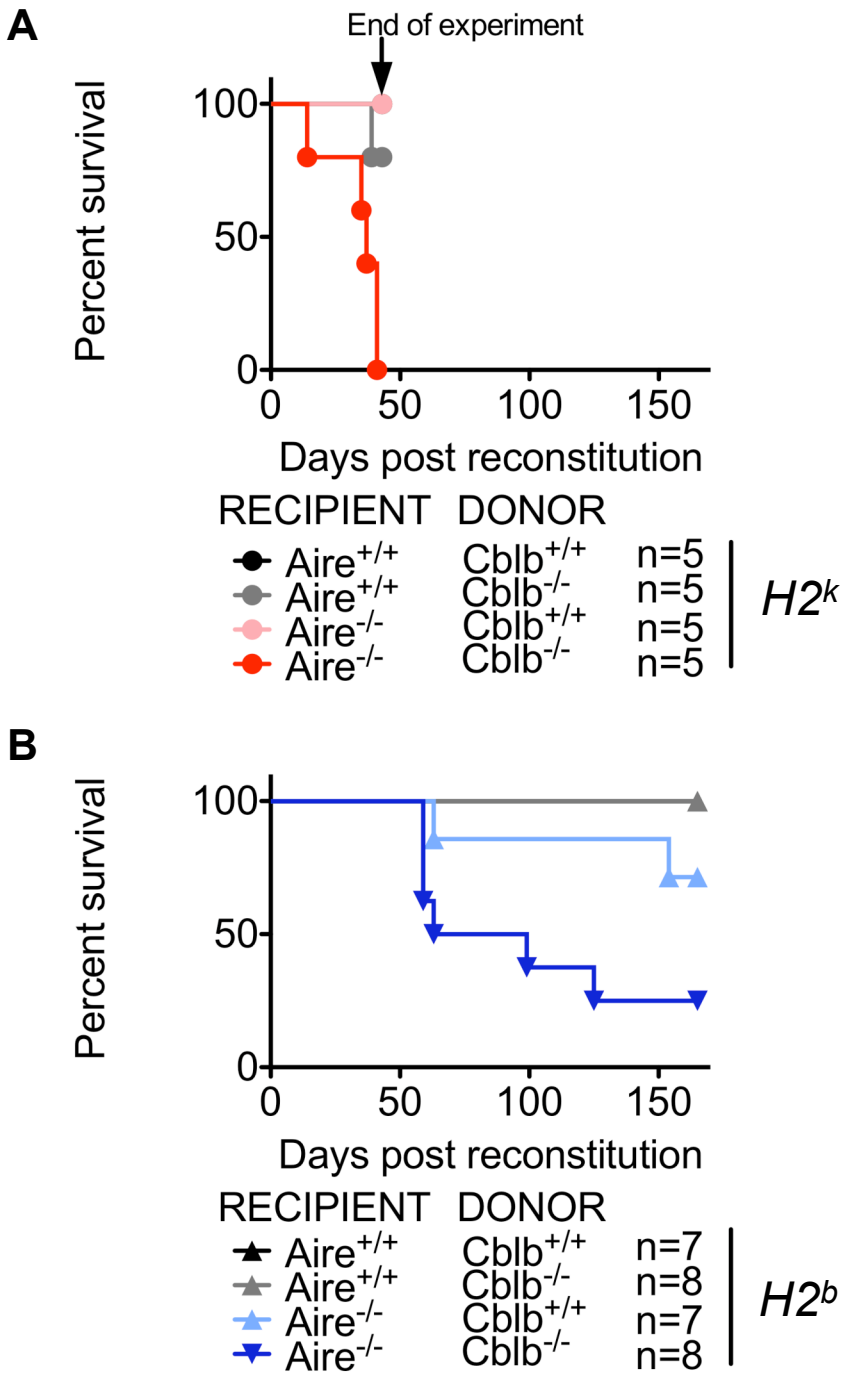

Figure 4.2 Combining the *Aire*$^{-/-}$ and *Cblb*$^{-/-}$ mutations on the *H2*^{b} background causes lethal autoimmunity, but at a slower onset and incidence compared to *H2*^{k} mice.
Comparison of survival of *Aire* deficient or wild-type recipients post-reconstitution with *Cblb*$^{-/-}$ or wild-type bone marrow on the *H2*^{k} (A, chapter 3) and the *H2*^{b} (B) genetic backgrounds. All mice from the *H2*^{k} experiment were sacrificed by 41 days post-reconstitution. Statistical analysis of the *Aire*$^{-/-}$*Cblb*$^{-/-}$ *H2*^{k} and *H2*^{b} groups using a log-rank Mantel-Cox test gave a P value of 0.0002.

eye, testis/ovaries was performed on a second cohort of chimeric mice 14 weeks after reconstitution. Like the first cohort, there was little evidence as cachexia during the first eight weeks after reconstitution. Similar to that of the *Aire*$^{-/-}$*Cblb*$^{-/-}$ *H2*^{k} 5-6 week post-reconstitution bone marrow chimeras, lymphocytic infiltration targeting the acinar cells of the pancreas and submandibular salivary gland were observed. The histological scores are shown in Fig. 4.3. All other organs remained relatively free of infiltration.

These results indicated that *Aire*$^{-/-}$ and *Cblb*$^{-/-}$ deficiencies co-operated on the *H2*^{b} background but compared to the *H2*^{k} background the target organs remained the same but the tempo of the disease was slower.

4.4 Changing the starting frequency of T cell recognising peptide/MHC complexes targeted towards a different self-tissue.

4.4.1 Effect of introducing *Aire*- and *Cblb*-deficiencies to TCR^{3A9}:insHEL transgenic model by breeding

The effect of increasing the frequency of T cell, recognising a particular pancreatic autoantigen in *Aire*$^{-/-}$*Cblb*$^{-/-}$ *H2*^{k} mice were analysed using TCR^{3A9}:insHEL Dbl-Tg mice. This system had been used in the laboratory to study the effect of single mutations in *Aire* and *Cblb*, both of which accelerated the age and incidence of autoimmunity (Hoyne et al., 2011b; Liston et al., 2004a). Depending on the availability of mice, mice that were either heterozygous for *Aire* or *Cblb,* and hemizygous for TCR^{3A9} or insHEL were intercrossed.

Based on the repertoire hypothesis, it was predicted that the introduction of high numbers of HEL-specific TCR^{3A9} cells in the *Aire*$^{-/-}$*Cblb*$^{-/-}$ *H2*^{k} mice would change the specificity of autoimmunity from the exocrine to endocrine pancreas. As expected, the introduction of large numbers of CD4 TCR^{3A9} cells reactive to insHEL increased the lifespan of *Aire*$^{-/-}$*Cblb*$^{-/-}$ mice, from a median survival of 31 days for non-transgenic mice to 110 days for Dbl-Tg mice in the same cross (Fig. 4.4*A*, P value of 0.0114). This lengthening of lifespan was accompanied by a change in the target cell type within the same organ: non-transgenic mice displayed severe destruction of the exocrine pancreas,

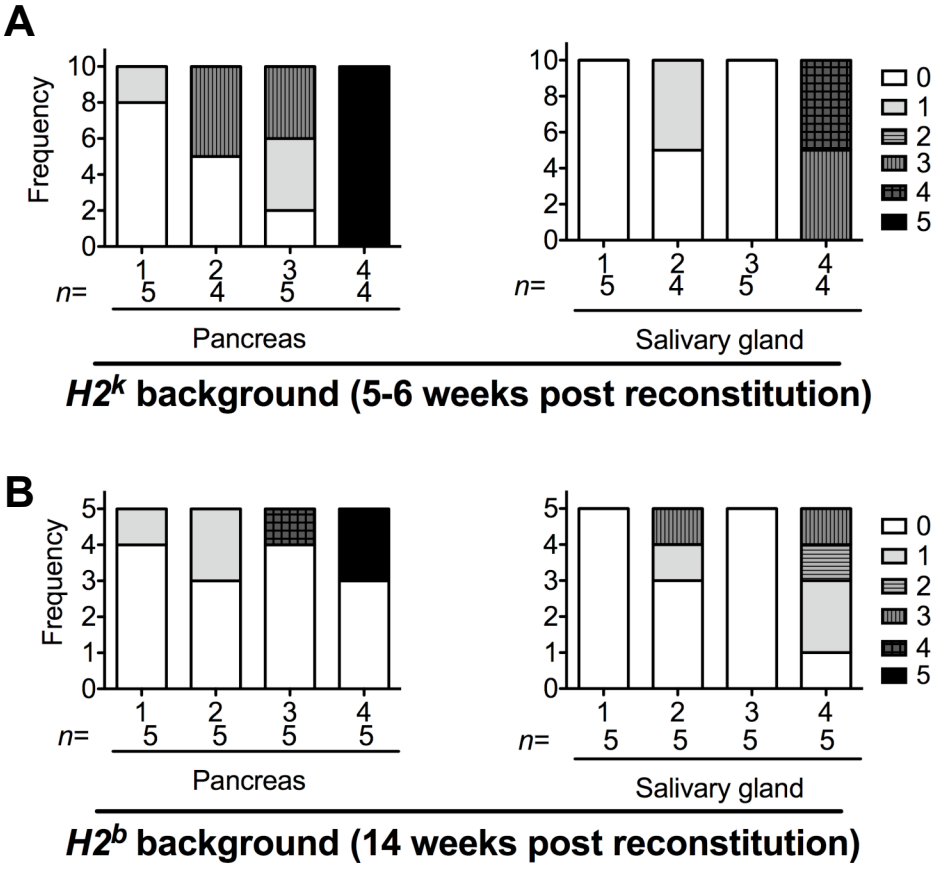

Group	Donor	Recipient
1	WT	WT
2	*Cblb*$^{-/-}$	WT
3	WT	*Aire*$^{-/-}$
4	*Cblb*$^{-/-}$	*Aire*$^{-/-}$

Figure 4.3 Combining the *Aire*$^{-/-}$ and *Cblb*$^{-/-}$ mutations of the *H2*^{b} background results in infiltration of the pancreas and salivary glands.

A. Percentage of recipient mice with different grades of pancreatitis and sialoadenitis 6 weeks post-reconstitution on the *H2*^{k} genetic background.

B. Percentage of recipient mice with different grades of pancreatitis and sialoadenitis 14 weeks post-reconstitution on the *H2*^{b} genetic background.

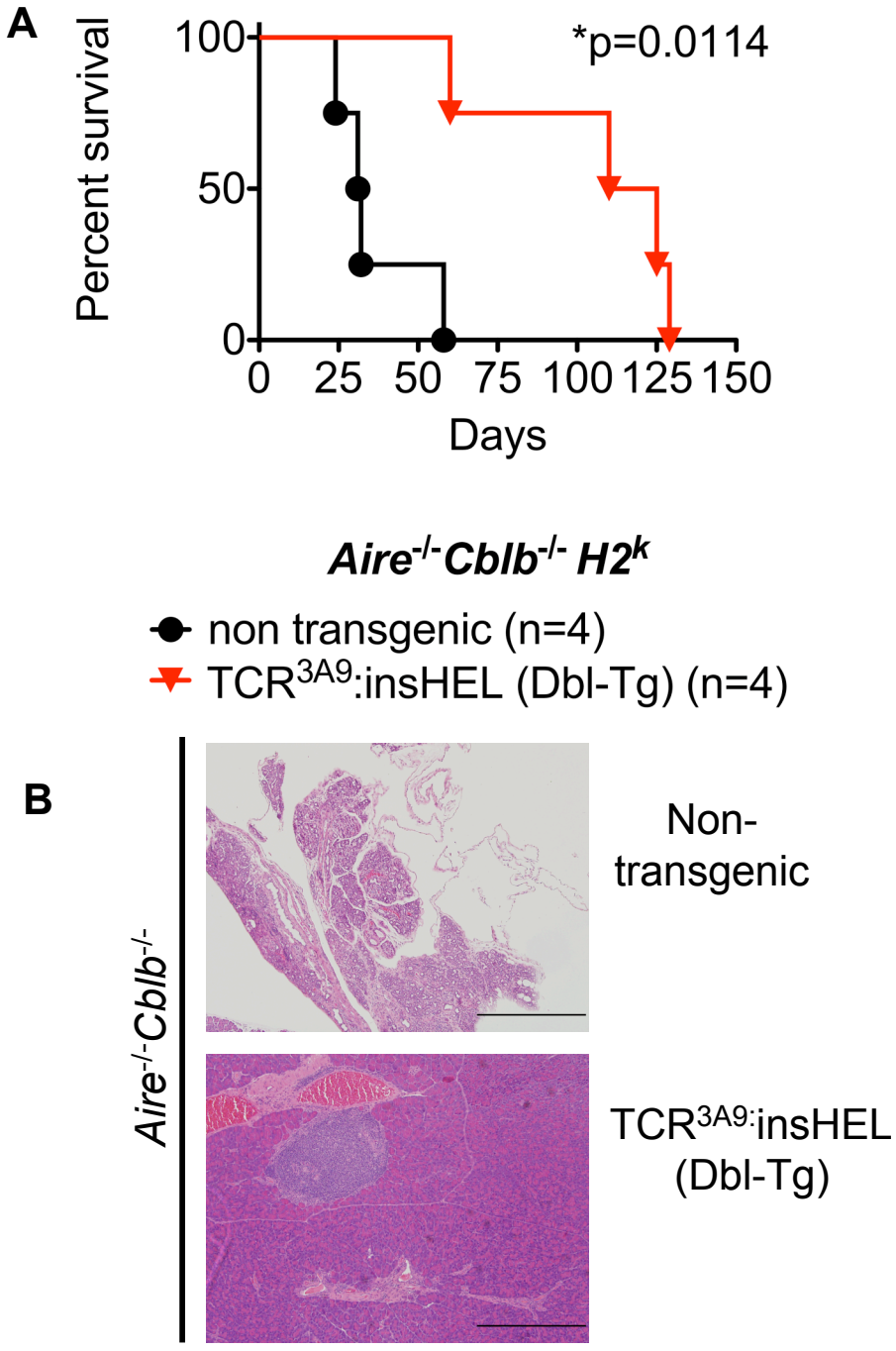

Figure 4.4 Effect of introducing the TCR^{3A9} and insHEL transgenes on autoimmunity in *Aire*$^{-/-}$*Cblb*$^{-/-}$ *H2*^{k} mice.

A. Survival of the *Aire*$^{-/-}$*Cblb*$^{-/-}$ non-transgenic and Dbl-Tg mice measured until 20 weeks of age.

B. Representative hematoxylin and eosin staining of the pancreas from 20 weeks old non-transgenic and Dbl-Tg *Aire*$^{-/-}$*Cblb*$^{-/-}$ mice euthanised when mice were cachectic. Bars: 500 µm, 100x magnification.

whereas *Aire*$^{-/-}$*Cblb*$^{-/-}$ double transgenic TCR^{3A9}:insHEL mice presented with infiltration targeted towards the islet structures in the pancreas (Fig. 4.4*B*). Hence, increasing the CD4 TCR^{3A9} islet-specific precursors slowed the course of the exocrine pancreatic disease and lethality in the *Aire*$^{-/-}$*Cblb*$^{-/-}$ *H2*^{k} mice.

As islet-specific autoimmunity would manifest clinically as diabetes development, a cohort of TCR^{3A9}:insHEL Dbl-Tg, with either single or double deficiencies in *Aire*$^{-/-}$ and *Cblb*$^{-/-}$ were monitored for glucose in the urine (glucosuria) weekly from 2 weeks of age (Fig. 4.5). Consistent with previous studies (Hoyne et al., 2011b; Liston et al., 2004a), no glucosuria was detected in mice carrying the TCR^{3A9} or insHEL transgene alone. The results in Fig. 4.5 focused on the TCR^{3A9}:insHEL Dbl-Tg mice. With the exception of the *Aire*$^{+/+}$*Cblb*$^{+/+}$ wild-type group (which was a small group, *n*=3), all groups developed diabetes throughout the time course of the experiment (140 days). Combined *Aire*- and *Cblb*-deficiencies appeared to cause little or no increase in diabetes development compared to the other groups tested. While insufficient *Aire*$^{-/-}$*Cblb*$^{+/+}$ Dbl-Tg mice were available in this experiment, previous studies showed these have diabetes onset and incidences similar to the *Aire*$^{-/-}$*Cblb*$^{-/-}$ Dbl-Tg mice here (Liston et al., 2004a). Diabetes in *Aire*$^{-/-}$*Cblb*$^{-/-}$ Dbl-Tg mice was relatively comparable to *Aire* or *Cblb* single deficient Dbl-Tg mice.

Consistent with diabetes development, the mice that developed diabetes presented with islet-specific infiltration (Fig 4.6). This infiltration appeared comparable between mice from each *Aire* and *Cblb* genotypic group. A caveat in this assay is that not all groups were available - *Aire*$^{+/-}$*Cblb*$^{+/+}$, *Aire*$^{-/-}$*Cblb*$^{+/+}$ and *Aire*$^{-/-}$*Cblb*$^{+/-}$ groups were missing from the analysis, some of which are key control groups in the study. Due to the difficulty in breeding mice of the appropriate genotype, the next step was to construct bone marrow chimeras to achieve the desired mouse genotypes and confirm the observations from this section.

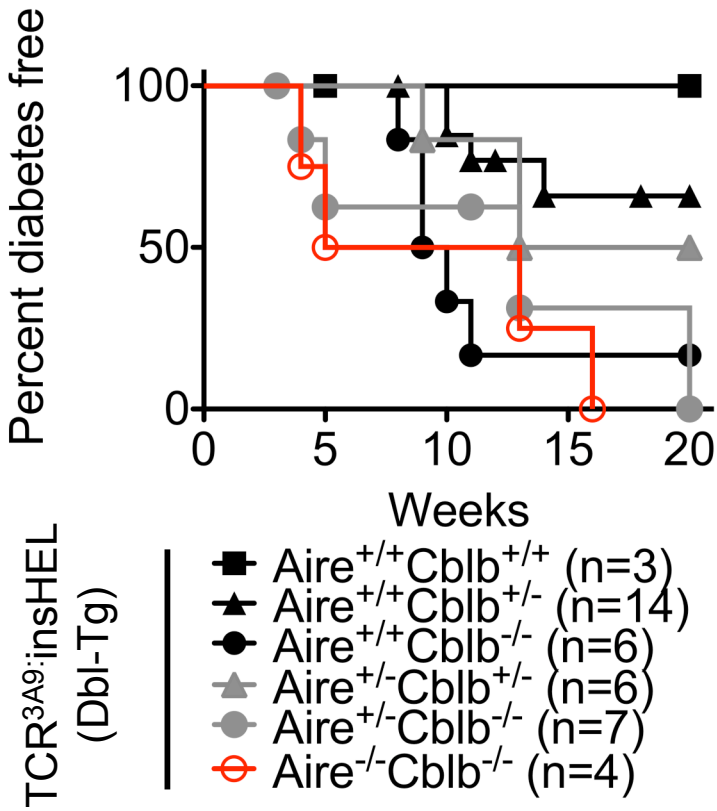

Figure 4.5 Effect of introducing the *Aire*$^{-/-}$ and *Cblb*$^{-/-}$ mutations into TCR^{3A9}:insHEL (Dbl-Tg) mice.
Mice of the indicated genotypes were tracked for diabetes from birth to 20 weeks. Glucosuria was monitored weekly and mice were considered diabetic after the first evidence of diabetes if a positive reading (diastix score of ≥2) is also obtained on the successive reading.

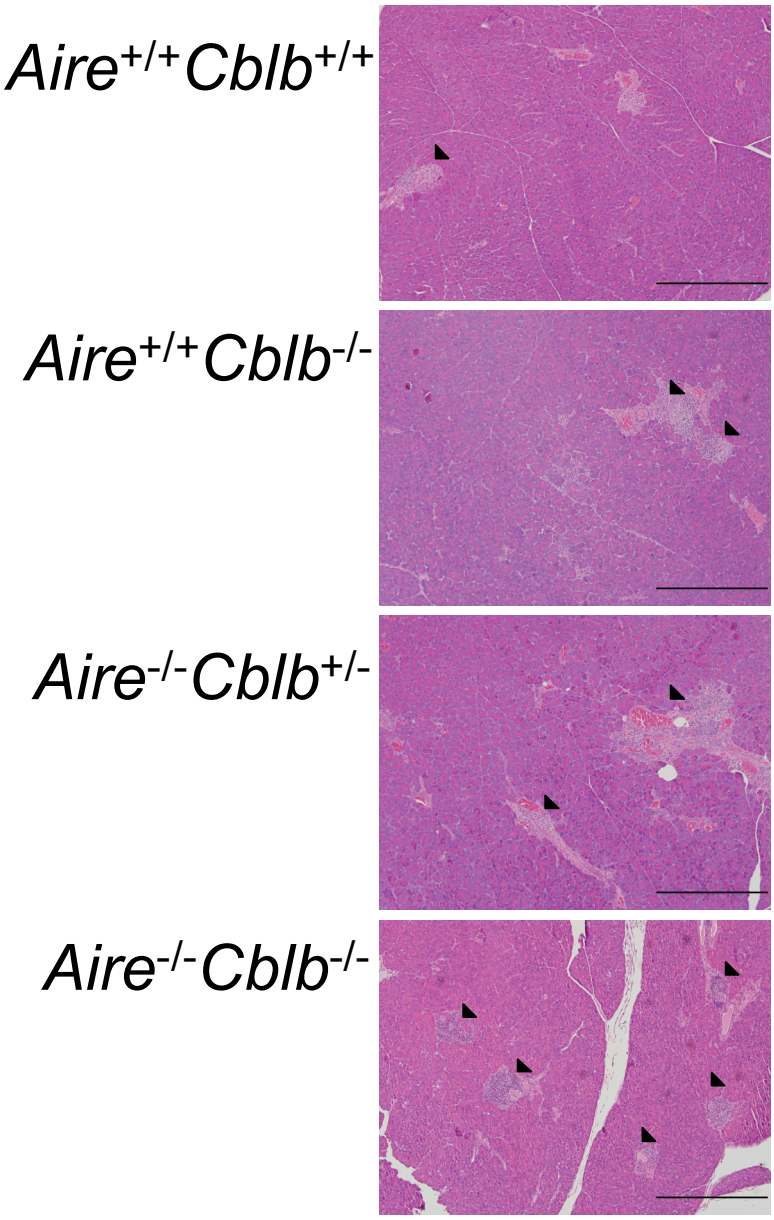

Figure 4.6 Representative hematoxylin and eosin staining of the pancreas from Dbl-Tg mice of the indicated genotype either at 20 weeks of age or earlier if mice were taken down after losing 20% of their body weight.
The arrows indicate the position of lymphocyte infiltrated islets. Bars: 500 µm, Magnification: 100x.

4.4.2 Bone marrow chimeras

Bone marrow from non-transgenic, wild-type TCR^{3A9} or *Cblb*$^{-/-}$ TCR^{3A9} mice were used to reconstitute the hematopoietic system of 10 groups of irradiated wild-type or *Aire*$^{-/-}$ mice which were insHEL negative, *Aire*$^{+/+}$*Cblb*$^{+/+}$ insHEL^{+} or *Aire*$^{-/-}$insHEL^{+} (Fig 4.7). Half the recipient mice were females and the other half were males. Again, the mice were monitored for diabetes development. Consistent with the results in section 4.4.1, only TCR^{3A9}→insHEL^{+} (double transgenic) chimeras that had both TCR^{3A9} and insHEL transgenes (groups 8-10) developed glucosuria (Fig 4.8*A*). In both the *Aire*$^{-/-}$*Cblb*$^{-/-}$ Dbl-Tg (group 10) and *Aire*$^{+/+}$*Cblb*$^{-/-}$ Dbl-Tg (group 9) groups, 3 out of 10 mice had developed diabetes after 42 days of reconstitution at comparable rates (Fig 4.8*A*). One out of 10 mice from the *Aire*$^{-/-}$*Cblb*$^{+/+}$ Dbl-Tg group (group 8) developed diabetes.

However, it is also important to note that the onset of diabetes in the chimeric mice occurred as early as 14 and 21 days post-reconstitution. This time seemed to be too fast for T cell development and emigration from the thymus in these chimeras. It is therefore possible that some mature TCR^{3A9} cells were present in the donor bone marrow, and these caused diabetes rapidly in the irradiated recipients in groups 9 and 10, the groups that received *Cblb*$^{-/-}$ donor marrow.

Pancreas histology was examined for all male mice in the experiment Figs. 4.9 and 4.10. In contrast to the islet-specific destruction of TCR^{3A9}:insHEL double transgenic mice obtained via breeding, the bone marrow chimeras had lymphocytic infiltration targeting exocrine pancreas in addition to the islets (Fig. 4.10). The exocrine-specific infiltration was particularly obvious in the *Aire*$^{-/-}$*Cblb*$^{-/-}$ group, whereby two of the five mice had complete destruction of the acinar cells, akin to the non-transgenic *Aire*$^{-/-}$*Cblb*$^{-/-}$ ($H2^{k}$) bone marrow chimeras described in chapter 3. In addition, 4 of the 10 mice in the *Cblb*$^{-/-}$ TCR^{3A9}→ *Aire*$^{-/-}$ insHEL group (group 10), but not in other groups, showed signs of cachectic wasting 42 days post-reconstitution and needed to be sacrificed moribund due to extensive loss of body weight, mirroring the non-transgenic *Aire*$^{-/-}$ *Cblb*$^{-/-}$ $H2^{k}$ chimeras (chapter 3) (Fig. 4.8*B*).

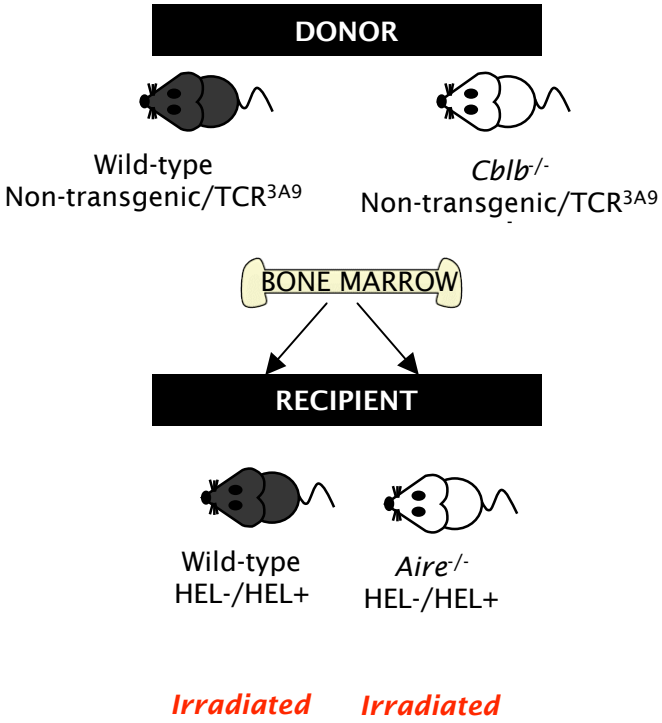

DONOR / RECIPIENTS	non-transgenic	TCR3A9	Cblb-/- TCR3A9
non-transgenic	3	5	5
Aire-/- non-transgenic		5	5
insHEL		10	10
Aire-/- insHEL	5	10	10

Numbers of mice in each experimental group

Figure 4.7 Schematic representation of experimental plan to construct *Aire*$^{-/-}$*Cblb*$^{-/-}$ TCR^{3A9}:insHEL bone marrow chimeras and control counterparts.
Irradiated *Aire*$^{-/-}$ or wild-type insHEL or non-transgenic mice were reconstituted with *Cblb*$^{-/-}$ or wildtype TCR^{3A9} or non-transgenic bone marrow, yielding 10 distinct experimental groups of chimeric mice.

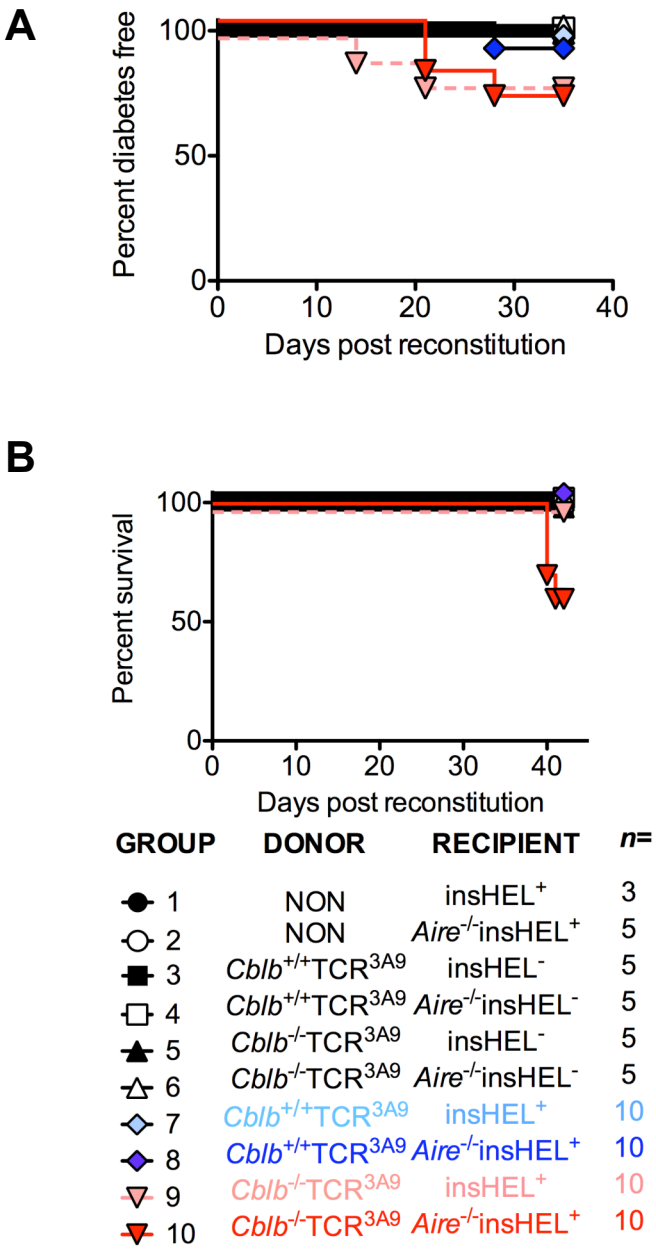

Figure 4.8 Glucosuria measurements and survival of TCR^{3A9}:insHEL bone marrow chimeras and control counterparts of the indicated *Aire* and *Cblb* genotypes.

A. Percentage of diabetes free mice. Mice of the indicated genotypes were tracked for diabetes up to 42 days post-reconstitution. Glucosuria was monitored weekly and mice were considered diabetic after the first evidence of diabetes if a positive reading (diastix score of ≥2) is also obtained on the successive reading.

B. Survival of recipients up to 42 days post-reconstitution.

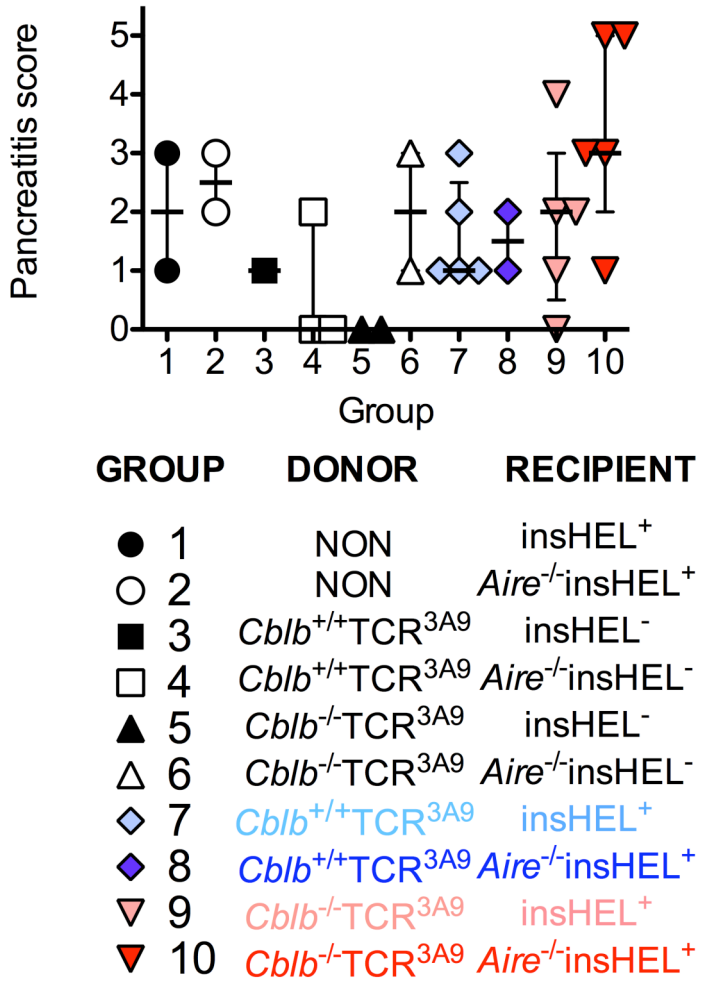

Figure 4.9 Exocrine pancreatitis development in *Aire*$^{-/-}$*Cblb*$^{-/-}$ TCR^{3A9}→insHEL bone marrow chimeras and control counterparts.
Bars represent the median histological scores for each group and error bars indicate the interquartile range.

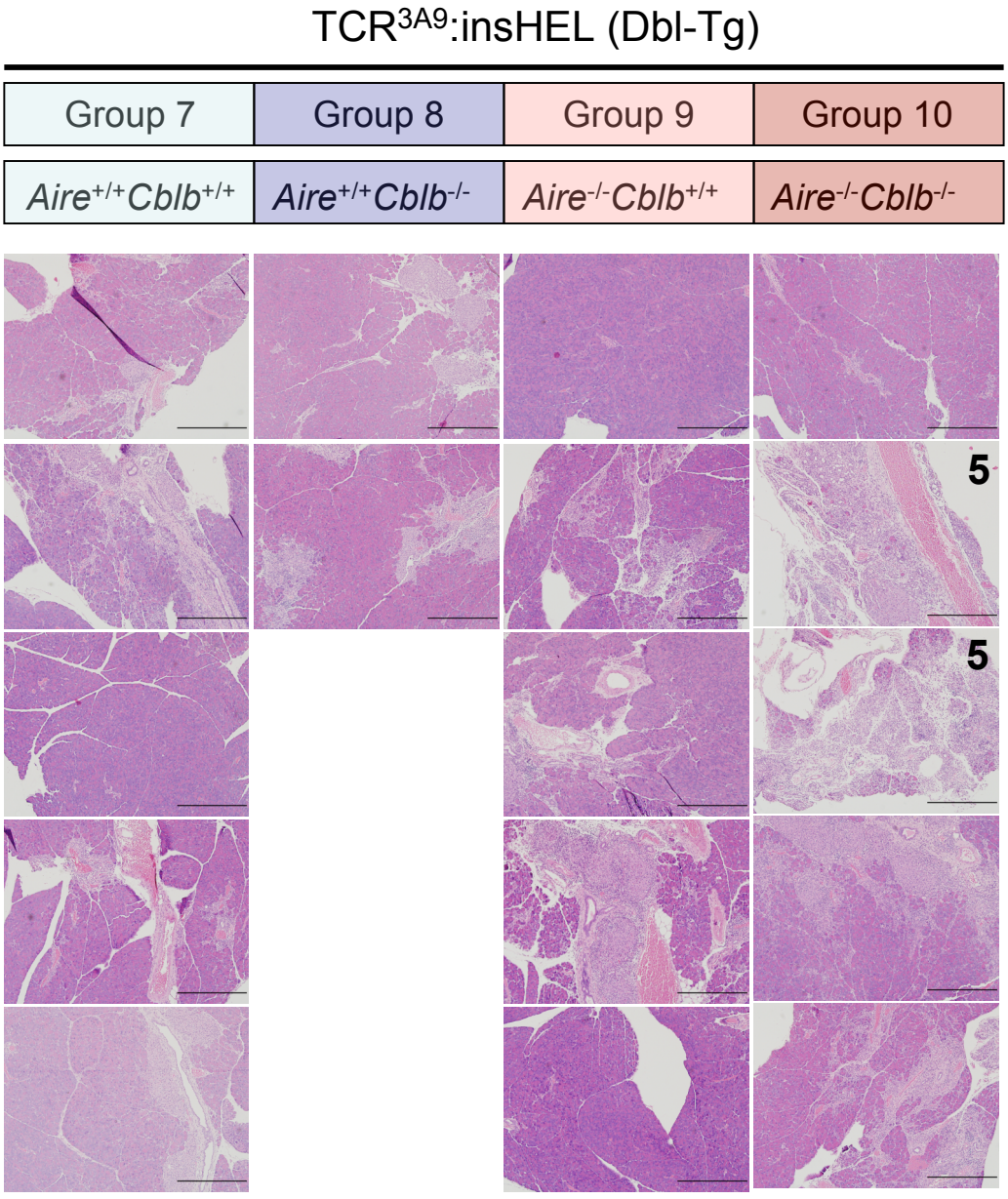

Figure 4.10 Representative hematoxylin and eosin staining of the pancreas from the respective groups.
Groups refer to the Dbl-Tg groups 7, 8, 9 and 10 in Fig. 4.8 and 4.9. The number of the left side of the figure corresponds to the disease score. Bars: 500 µm, Magnification: x100.

The increased incidences of exocrine pancreatitis in *Cblb*$^{-/-}$ TCR^{3A9}→ *Aire*$^{-/-}$ insHEL Dbl-Tg chimeras compared to animals bred with the genotype could be attributed to several reasons. Firstly, it is possible that in addition to the transgenic CD4 TCR^{3A9} cells, a small number of exocrine pancreas-specific mature T cells (CD4 or CD8 cells) were transferred in the donor marrow and these developed in the *Aire*$^{-/-}$*Cblb*$^{-/-}$ chimera group when the cells were placed in a lymphopenic environment induced by the sub-lethal irradiation. An alternative explanation is that radioresistant memory CD8 T cells in the *Aire*$^{-/-}$ co-operated with donor CD4 cells to cause exocrine pancreatitis. Thus, TCR^{3A9} negative T cells from the donor marrow or the recipients could have been able to cause an exocrine-pancreas specific effect autoimmunity not seen in TCR^{3A9}:insHEL bred mice where fewer TCR specificities arise as most of the T cells were islet-specific T cells.

4.4.3 Pancreas autoimmunity in mixed chimeras where only a fraction of T cells were *Cblb*-deficient

If exocrine pancreatitis in TCR^{3A9}→insHEL chimeras were due to other T cells in the *Cblb*$^{-/-}$ bone marrow inoculum, T cell depleting the donor marrow and diluting the numbers of *Cblb*$^{-/-}$ cells could change the pattern of autoimmunity. To achieve this, T cell-depleted *Cblb*$^{+/+}$ bone marrow were mixed in a 1:1 ratio to produce either *Cblb*$^{-/-}$ TCR^{3A9}:*Cblb*$^{+/+}$ TCR^{3A9} or *Cblb*$^{+/+}$TCR^{3A9}:*Cblb*$^{+/+}$TCR^{3A9} control mixtures where all the T cells had wild-type *Cblb*. The mixtures were transplanted into irradiated insHEL or *Aire*$^{-/-}$ insHEL recipients. All *Aire*$^{-/-}$ insHEL mice receiving the control (TCR^{3A9}: TCR^{3A9}) mixture developed diabetes by 21 days post transfer, and 3 of 4 *Aire*$^{-/-}$insHEL mice receiving the *Cblb*$^{-/-}$TCR^{3A9}:TCR^{3A9} developed diabetes at a slightly slower pace in this experiment by 28 days post reconstitution (Fig. 4.11*A*). All other mice tested remained free of diabetes for the duration of the experiment. The *Cblb*$^{-/-}$ TCR^{3A9}:TCR^{3A9}→*Aire*$^{-/-}$insHEL group developed exocrine pancreatitis scores ranging from 2 to 5, whereas the control TCR^{3A9}:TCR^{3A9} into *Aire*$^{-/-}$insHEL group developed scores of 0 to 3. All other groups had a score of 1 or below (Fig. 4.11*B*).

Taken together, the results from the 100% and 50% *Cblb*-deficient chimera experiments, when *Cblb*$^{-/-}$ was combined with *Aire*$^{-/-}$ in TCR^{3A9}→insHEL Dbl-Tg

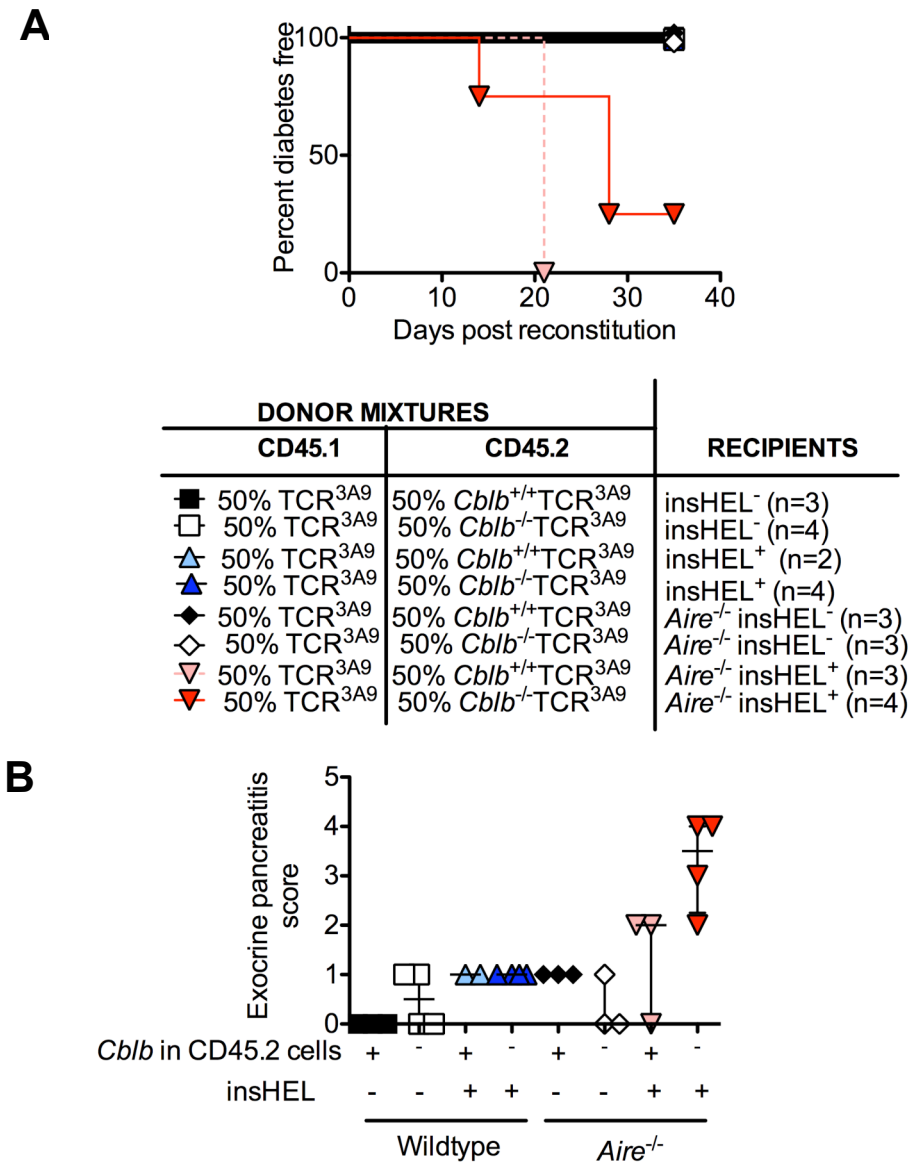

Figure 4.11 Consequence of *Cblb*-deficiency in only a subset of TCR^{3A9} T cells.

Irradiated *Aire*$^{-/-}$ or wild-type insHEL or non transgenic counterparts were reconstituted with 50:50 mixture of CD45.1 TCR^{3A9} and CD45.2 *Cblb*$^{-/-}$ or *Cblb*$^{+/+}$ TCR^{3A9} bone marrow.

A. Percentage diabetes free mice. Mice were tracked for diabetes for 42 days post-reconstitution. Glucosuria was monitored weekly and mice were considered diabetic after the first evidence of diabetes if a positive reading is also obtained on the successive reading.

B. Pancreatitis scores for recipient mice. Bars indicate median value for each group and error bars indicate interquatile range.

transgenic animals (data from 4.4.2, 4.4.3), there was surprisingly no evidence of enhanced endocrine pancreas autoimmune destruction compared to single *Aire*$^{-/-}$ or *Cblb*$^{-/-}$ double transgenic controls. By contrast, exocrine pancreatic autoimmunity exhibited an intriguing 3-way interaction. It was most severe in *Aire*$^{-/-}$ recipients that received *Cblb*$^{-/-}$ TCR^{3A9} bone marrow, but only when the recipients were insHEL^{+}. A possible explanation for this result is that islet-reactive CD4^{+} T cells in *Aire*$^{-/-}$ insHEL recipients may provide help for exocrine pancreas-specific CD8^{+} cells. The latter must express endogenous TCRs, and perhaps these are drawn from radioresistant memory T cells in the recipient mice. The nature and role of CD8 cells in the exocrine pancreatitis is explained further in the next chapter.

4.5 Studying the combinatorial role of Aire and Cblb in tolerance at a cellular level

The interaction between *Aire* and *Cblb* was next analysed at the cellular level, using the TCR^{3A9} transgenic system to track autoreactive CD4 T cells in both central and peripheral tolerance to organ-specific HEL antigen produced by the insHEL or thyrHEL transgenes.

4.5.1 Studying the combined effect of Aire- and Cblb-deficiencies in central tolerance (thymic selection)

The role of *Aire* as a transcription regulator during negative selection in the thymus has been firmly established (Anderson et al., 2002; Liston et al., 2003). Although Cbl-b is ubiquitously expressed in many tissues in the body, it has not been shown to play a role in thymic development, but its homologue c-cbl inhibits T cell signalling to determine the fate of thymocytes during development (Naramura et al., 1998; Thien et al., 1999). Studies have shown that Cbl-b mediates its function in mature peripheral T cells (Bachmaier et al., 2000; Chiang et al., 2000), but it is nevertheless unclear at what stage in thymic T cell maturation Cbl-b becomes necessary. Hence it was valuable to test the consequence of *Cblb*-deficiency in positive and negative selection of the CD4 TCR^{3A9} transgenic cells, alone and combined with *Aire*-deficiency.

To investigate the combined effect of *Aire*- and *Cblb*-deficiency on self-reactive CD4 cells expressing HEL-specific TCR^{3A9}, the 100% TCR^{3A9} transgenic bone marrow chimeras in section 4.4.2 were analysed by flow cytometry 42 days post reconstitution. As expected for TCR^{3A9} cells undergoing positive selection, in the thymus of TCR^{3A9}→insHEL-negative bone marrow chimeras (on the left side of Fig 4.12*A*), there were high frequencies of $CD4^+CD8^-$ single positive (SP) T cells bearing the TCR^{3A9} receptor stained brightly with the 1G12 anti-clonotype antibody. No 1G12 staining occurred on CD4 SP thymocytes from control chimeras reconstituted with non-transgenic bone marrow, establishing the specificity of detecting T cells expressing the TCR^{3A9} receptor.

Negative selection was observed in TCR^{3A9}→$insHEL^+$ chimeras that were *Aire*-sufficient, reflected by a 50% decrease in the frequency of $1G12^+CD4^+$ SP thymocytes (Figure 4.12*A*, 4.14 and Fig 4.15). There was no measurable effect of *Cblb*-deficiency on thymic negative selection measured in this way. By contrast, no decrease in frequency of $1G12^+CD4^+$ SP thymocytes occurred in TCR^{3A9}→$insHEL^+$ chimeras that were *Aire*-deficient, as has been found previously (Liston et al., 2003), and this deficiency of negative selection appeared unaltered by combining it with *Cblb*-deficiency. Hence there was no discernable evidence for cooperation between *Cblb*-deficiency and *Aire*-deficiency at the level of islet-reactive CD4 cells developing in the thymus.

Analysis of the pancreatic lymph node and spleen also gave no evidence for a compounding effect of *Cblb*-deficiency when combined with the failure of thymic negative selection in TCR^{3A9}→$insHEL^+$ chimeras that were *Aire*-deficient (Fig. 4.12*B* and *C*, 4.14, 4.16, 4.16). The frequency of TCR^{3A9}-expressing $CD4^+Foxp3^-$ T cells revealed by the 1G12 clonotypic antibody in pancreatic node or spleen was decreased ~90% in $insHEL^+$ chimeras that were *Aire*-sufficient compared to $insHEL^-$ chimeras, reflecting thymic negative selection in the former and positive selection in the latter. *Aire*-deficiency in the $insHEL^+$ chimeras prevented the drop in frequency of TCR^{3A9}-expressing $CD4^+Foxp3^-$ T cells in the spleen and pancreatic node, so that these were almost as high as the frequency in $insHEL^-$ chimeras (Fig. 4.12*B* and *C*, 4.15, 4.16, 4.17, 4.18). There was nevertheless no evidence that the frequency of TCR^{3A9}-

Figure 4.12 Representative flow cytometry plots showing the percentages of $CD4^+$ and $CD8^+$ cells from total lymphocytes (upper rows) and $FoxP3^+$ and TCR^{3A9} cells from total CD4 cells (lower row) in bone marrow chimeras with the indicated donor and recipient genotypes.

A. Thymus (percentages in Figures 4.14 and 4.15)
B. Pancreatic lymph node (percentages in Figures 4.16 and 4.17)
C. Spleen (percentages in Figures 4.19 and 4.20)

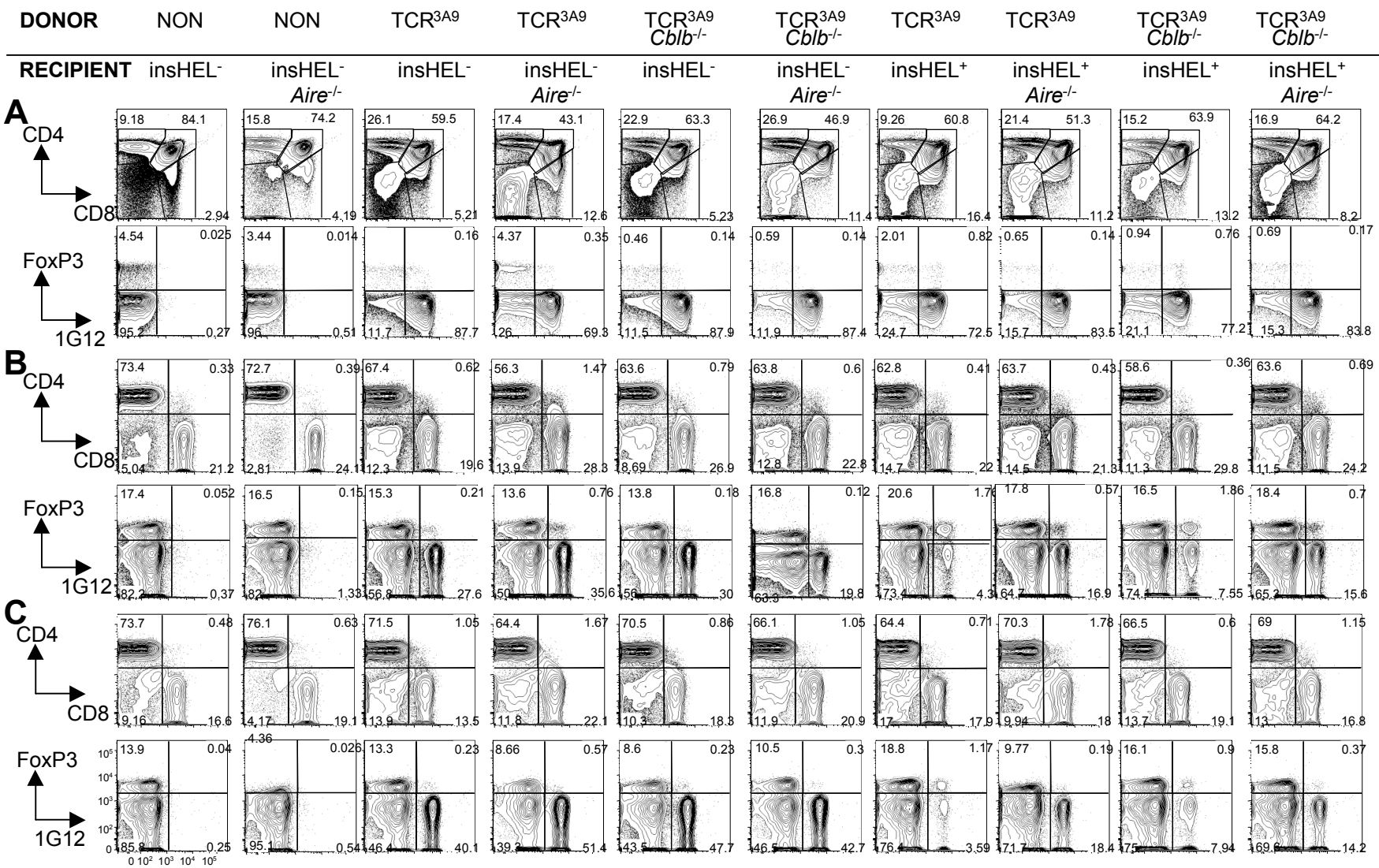
DONOR
NON
NON
TCR3A9
TCR3A9
TCR3A9 Cblb-/-
TCR3A9 Cblb-/-
TCR3A9
TCR3A9
TCR3A9 Cblb-/-
TCR3A9 Cblb-/-
RECIPIENT
insHEL-
insHEL- Aire-/-
insHEL-
insHEL- Aire-/-
insHEL-
insHEL- Aire-/-
insHEL+
insHEL+ Aire-/-
insHEL+
insHEL+ Aire-/-
A
CD4
CD8
FoxP3
1G12
B
CD4
CD8
FoxP3
1G12
C
CD4
CD8
FoxP3
1G12

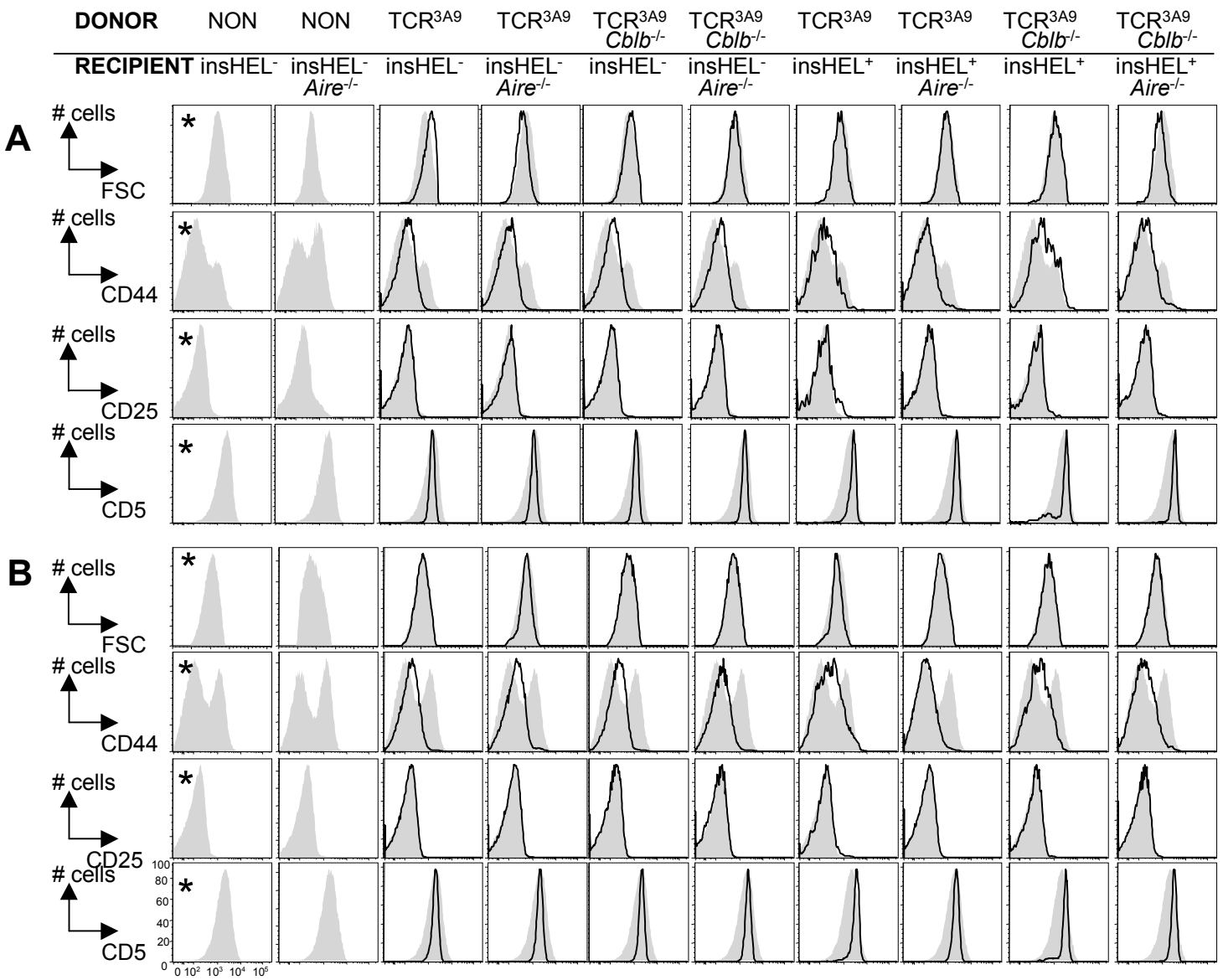

CD4⁺1G12⁺

CD4⁺1G12⁻ Group 1

*CD4⁺1G12⁻ Group 1

Figure 4.13 Representative histograms of forward side scatter (FSC), CD44, CD25 and CD5 expression on TCR^{3A9}1G12^{+}CD4^{+} cells (blank unshaded) in bone marrow chimeras with the indicated donor and recipient genotypes overlaid on 1G12^{-}CD4^{+} cells from non-transgenic (Group 1) chimeras (grey shaded).

A.Pancreatic lymph node (mean fluorescence intensity in Figure 4.18) B.Spleen (mean fluorescence intensity in Figure 4.21).

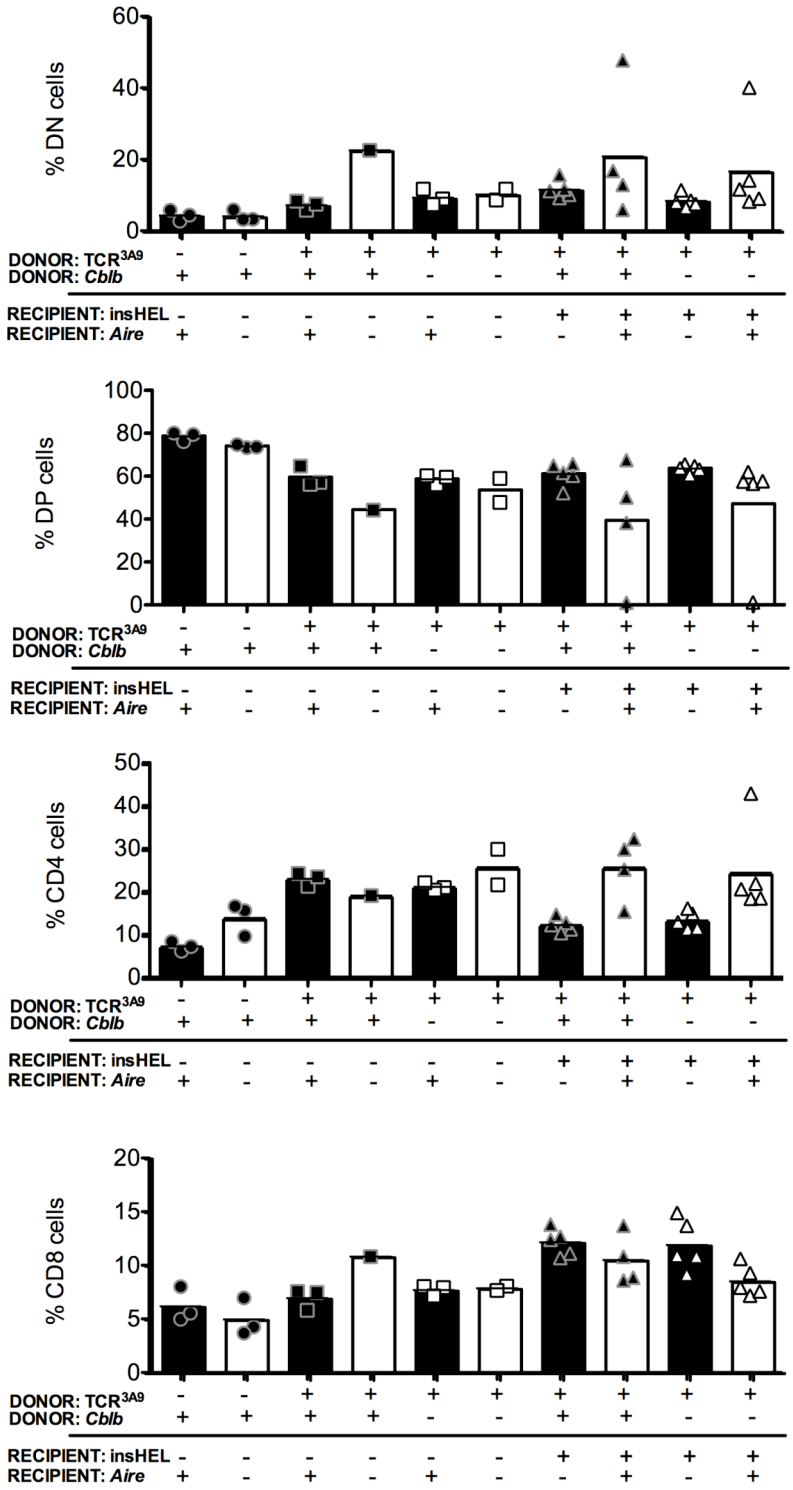

Figure 4.14 Percentages of double negative (DN), double positive (DP), CD4 and CD8 cells from total lymphocytes in the thymus of bone marrow chimeras.
The bars represent the means and each point represents a single mouse.

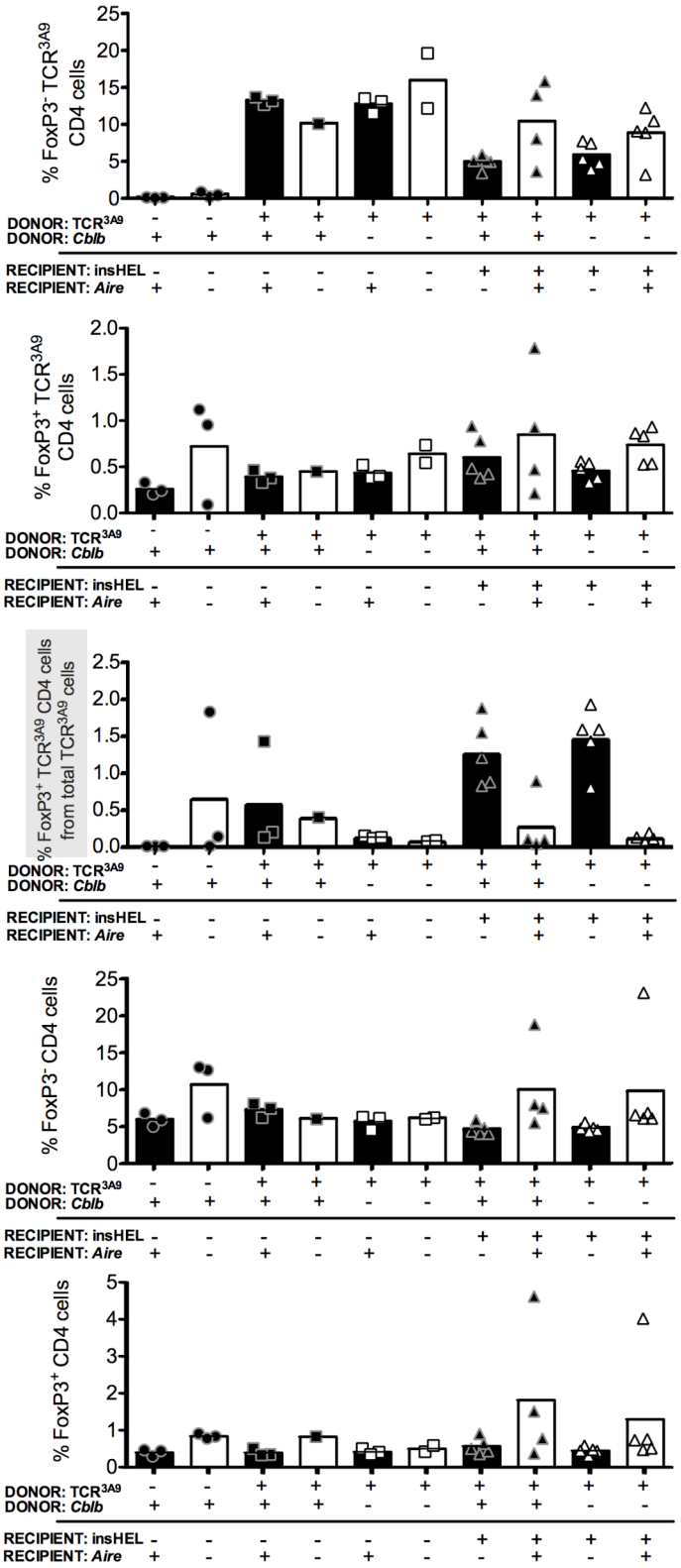

Figure 4.15 Percentages of FoxP3$^-$ TCR^{3A9}, FoxP3$^+$ TCR^{3A9}, FoxP3$^-$ and FoxP3$^+$ cells in the thymus of bone marrow chimeras.

The bars represent the means and each point represents a single mouse. All percentages are expressed from total lymphocytes except for the third panel where the FoxP3$^+$TCR^{3A9} percentages are expressed from total TCR^{3A9} cells.

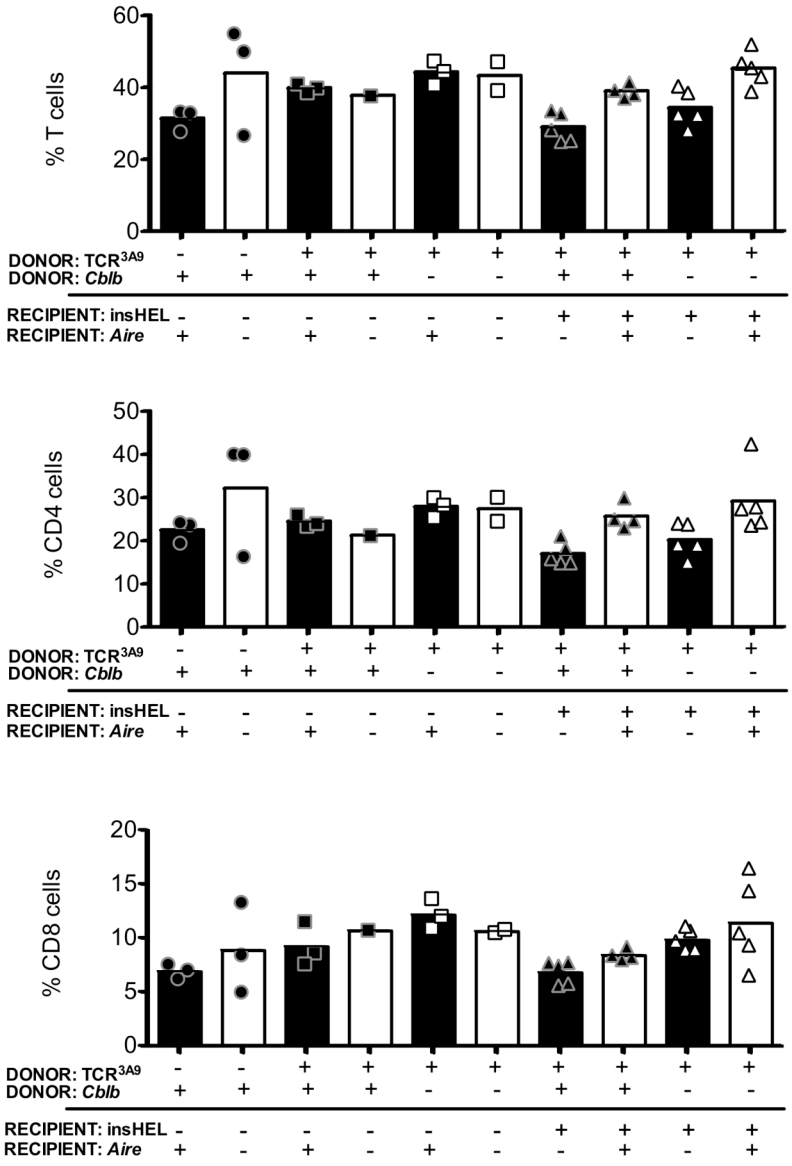

Figure 4.16 Percentages of T cells, CD4 cells and CD8 cells from total lymphocytes in the pancreatic lymph node of bone marrow chimeras.
The bars represent the means and each scatter represents a single mouse.

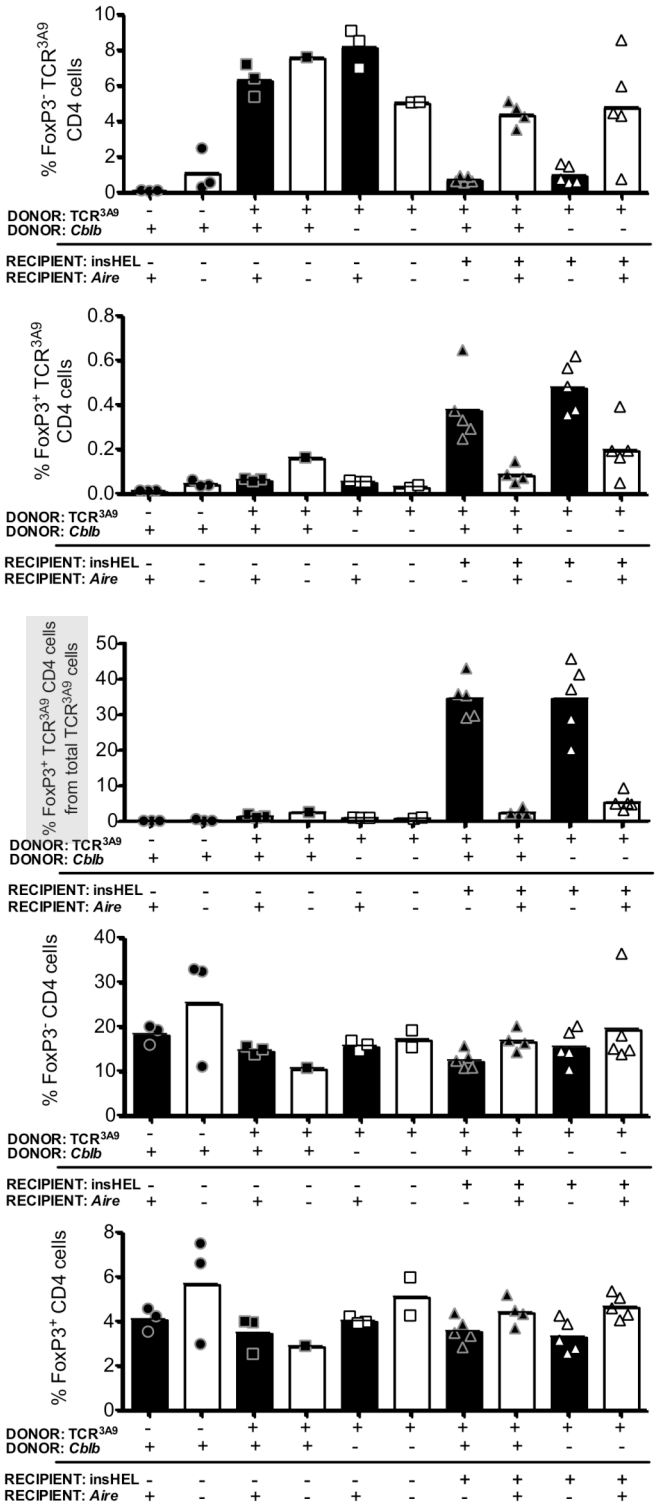

Figure 4.17 Percentages of FoxP3^{-} TCR^{3A9}, FoxP3^{+} TCR^{3A9}, FoxP3^{-} and FoxP3^{+} cells in the pancreatic lymph node of bone marrow chimeras.

The bars represent the means and each scatter represents a single mouse. All percentages are expressed from total lymphocytes except for the third panel where the FoxP3^{+}TCR^{3A9} percentages are expressed from total TCR^{3A9} cells.

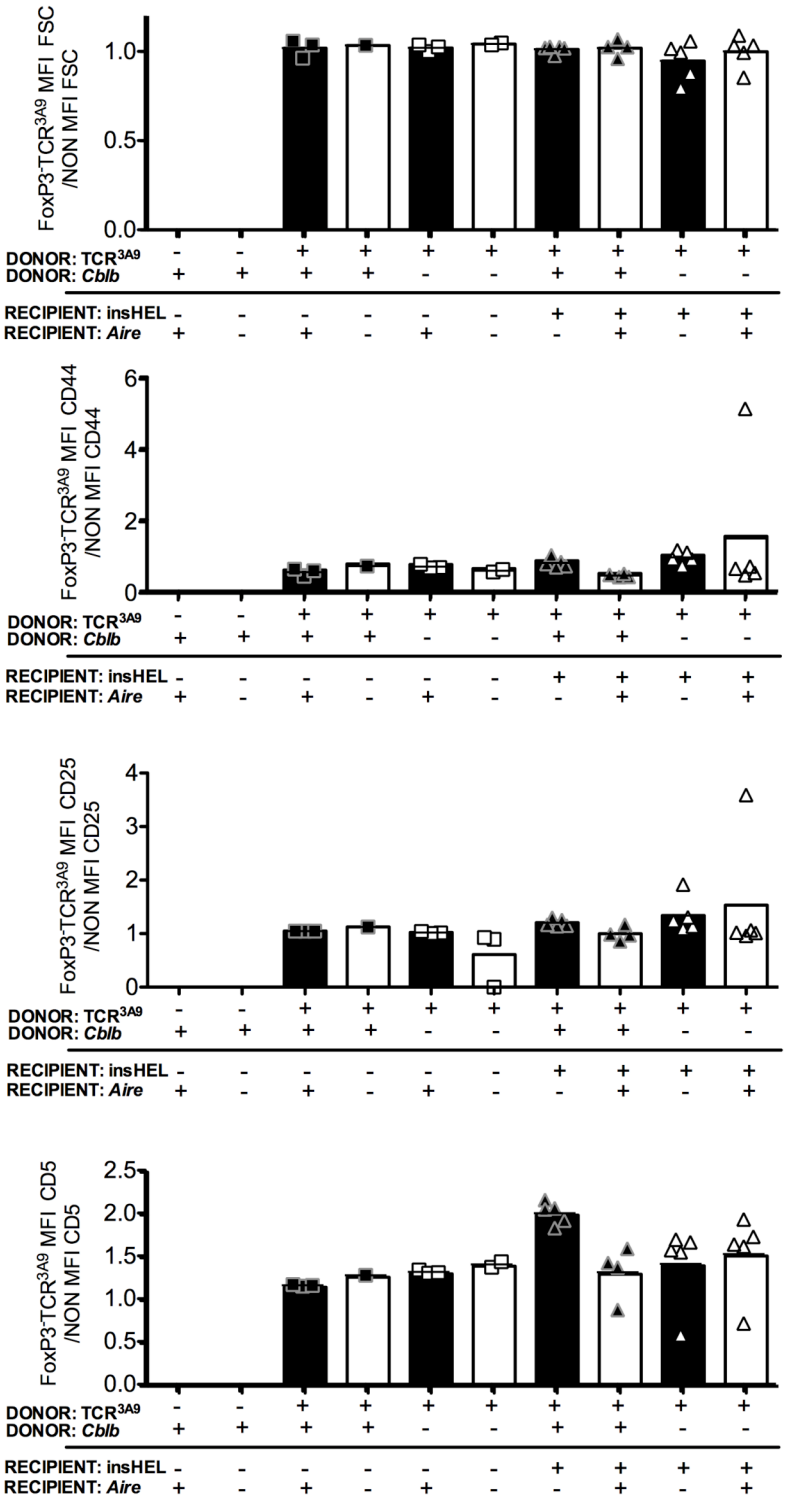

Figure 4.18 MFI of FSC,CD44, CD25 and CD5 in the pancreatic lymph node of bone marrow chimeras in each group relative to average MFI of respective markers in non-transgenic controls. The bars represent the means and each point represents a single mouse.

expressing $CD4^+Foxp3^-$ T cells was further increased by combining *Cblb*-deficiency with *Aire*-deficiency in either the pancreatic node or spleen, as might have been expected if these cells were induced to proliferate by HEL-antigen reaching the pancreatic node from the pancreatic islets. Analysis of markers of T cell activation, including forward scatter as a measure of cell size, CD44, CD25 and CD5, also showed no difference between *Cblb*-deficient or sufficient $TCR^{3A9+}CD4^+Foxp3^-$ T cells in $TCR^{3A9}\rightarrow insHEL^+$ $Aire^{-/-}$ chimeras (Fig. 4.19, 4.20 and 4.21).

4.5.2 Impact of *Aire* and *Cblb*-deficiency on the formation of islet-specific $Foxp3^+$ CD4 cells.

Co-operation between *Aire* and *Cblb* deficiency could be hypothesized to occur at the level of the $Foxp3^+$ T cell subset, since *Cblb*-deficiency diminishes Foxp3 induction in mature T cells (Harada et al., 2010). In TCR^{3A9}:insHEL double-transgenic mice, like many other MHC II-restricted TCR transgenic models (Jordan et al., 2001; Kawahata et al., 2002; Lerman et al., 2004; Liston et al., 2007), a subset of autoreactive CD4 cells escape thymic negative selection and become $Foxp3^+CD25^+$ natural T regulatory cells. The numbers of T regulatory cells in the bone marrow chimeras were quantified by intracellular staining for $FoxP3^+$ in $CD4^+$ TCR^{3A9} clonotype positive ($1G12^+$) cells. In the thymus of insHEL-negative recipients, very few TCR^{3A9} CD4 cells expressed Foxp3, and those that did had lower staining with the 1G12 anti-clonotypic antibody compared to Foxp3-negative cells (Fig 4.12). This is likely to be due to co-expression of an endogenous TCR alpha chain on these cells. By contrast, in the thymus of $insHEL^+$ recipients with wild-type *Aire*, a small but distinct population of $1G12^{high}Foxp3^+$ cells was formed that accounted for a higher percentage of the TCR^{3A9} CD4 cells (Fig 4.12*A* and Fig 4.14). This population of $1G12^{high}Foxp3^+$ CD4 cells was more dramatically increased in the spleen and pancreatic lymph node of the $TCR^{3A9}\rightarrow$insHEL chimeras, both as a percentage of all lymphocytes and as a percentage of $1G12^{high}$ CD4 cells (Fig. 4.14, 4.16 and 4.18). *Cblb* deficiency in the donor marrow did not interfere with the accumulation of $1G12^{high}$ $Foxp3^+$ CD4 cells in the thymus, spleen and pancreatic node of $insHEL^+$ $Aire^{+/+}$ recipients, and there was a tendency for *Cblb*-deficient nTreg cells to be more frequent in these animals. By contrast, *Aire*-deficiency greatly reduced the frequency of $1G12^{high}$ $Foxp3^+$ CD4 cells in the thymus, spleen and pancreatic node of $insHEL^+$ $Aire^{+/+}$ recipients, although their frequency was slightly increased when *Aire*-

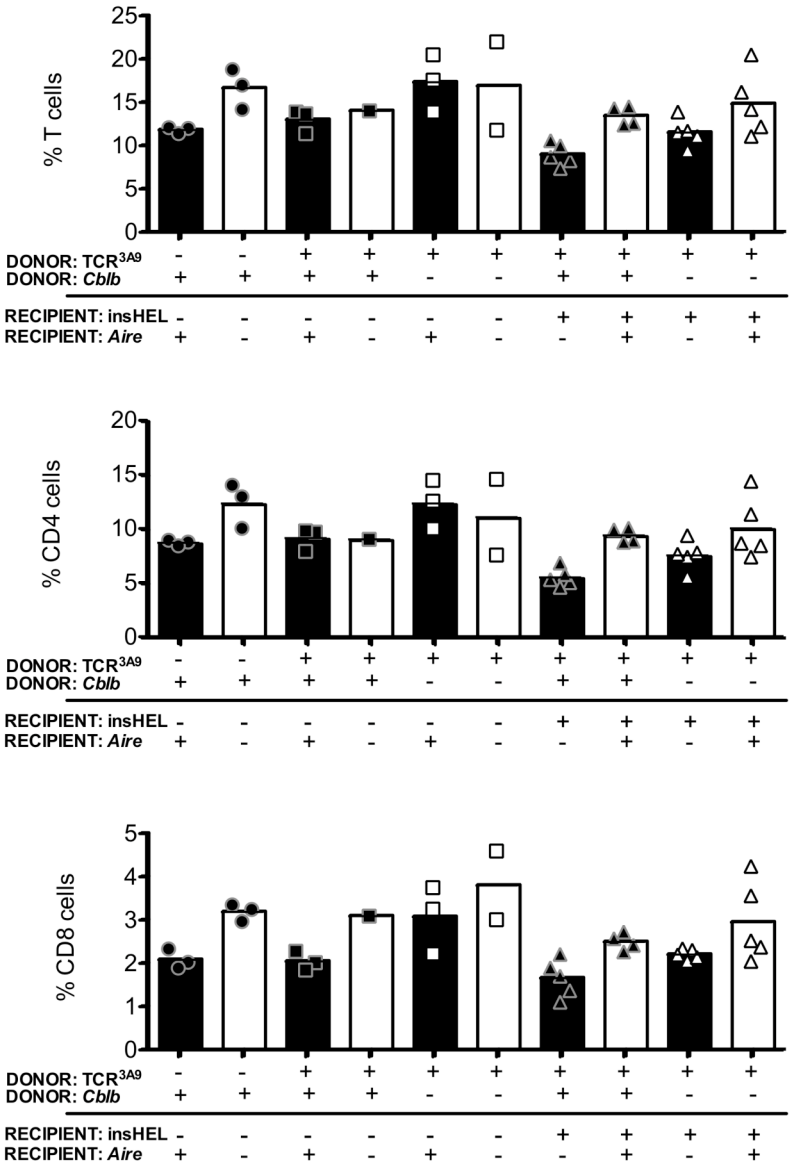

Figure 4.19 Percentages of T cells, CD4 cells and CD8 cells from total lymphocytes in the spleen of bone marrow chimeras. The bars represent the means and each point represents a single mouse.

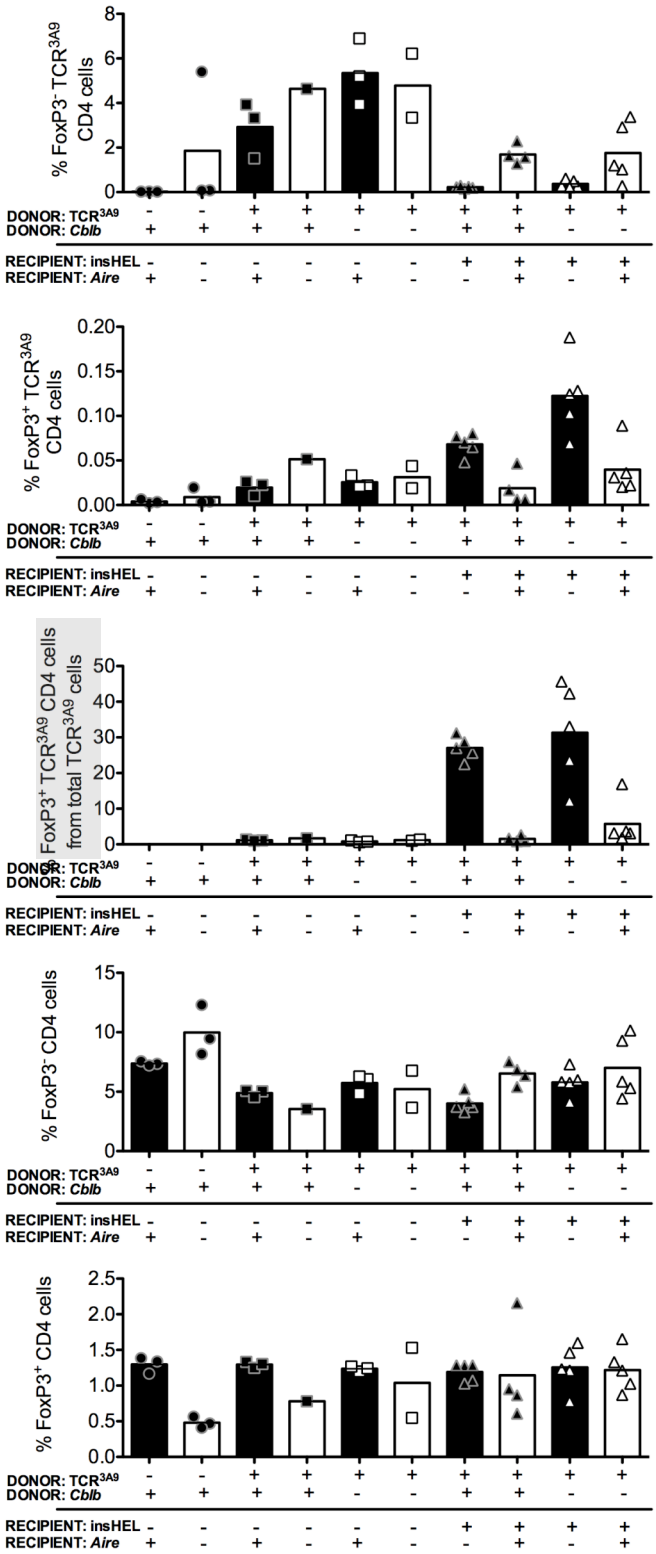

Figure 4.20 Percentages of FoxP3^{-} TCR^{3A9}, FoxP3^{+} TCR^{3A9}, FoxP3^{-} and FoxP3^{+} cells in the spleen of bone marrow chimeras.

The bars represent the means and each point represents a single mouse. All percentages are expressed from total lymphocytes except for the third panel where the FoxP3^{+}TCR^{3A9} percentages are expressed from total TCR^{3A9} cells.

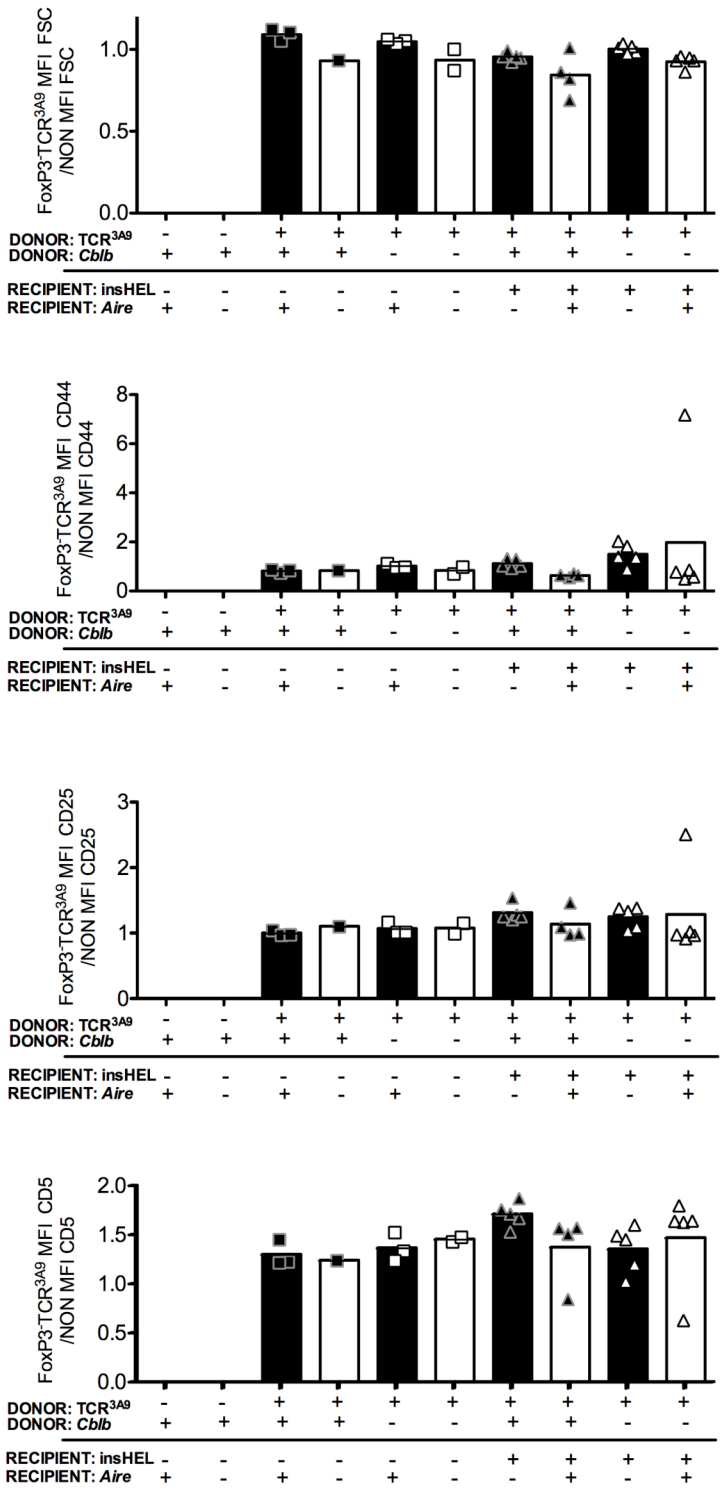

Figure 4.21 MFI of FSC,CD44, CD25 and CD5 in the spleen of bone marrow chimeras in each group relative to average MFI of respective markers in non-transgenic controls.
The bars represent the means and each point represents a single mouse.

and *Cblb*- deficiency were combined. Collectively, the data above indicate that *Cblb*-deficiency had little measurable effect on the regulation of self-reactive CD4 cells that recognized HEL expressed in the endocrine pancreas, even when it is combined with *Aire*-deficiency.

Cblb-deficiency nevertheless had been shown to inhibited the formation of iTreg cells (Harada et al., 2010). This was tested in the TCR^{3A9} transgenic system with the experimental strategy illustrated in Fig, 4.22. Naïve CD4 cells from non-transgenic and TCR^{3A9} mice that were *Cblb*-sufficient and deficient were stimulated with anti-CD3 and anti-CD28 in the absence and presence of varying 0.1 ng/ mL or 0.5 ng/ mL TGFβ. Wild-type and TCR^{3A9} transgenic mice induced upregulation of the iTreg transciption factor FoxP3 by 20.3% and 12.4% of the cells following 0.1 ng/ mL TGFβ stimulation and 62.5% and 42.5% after 0.5 ng/ mL TGFβ stimulation. By contrast, the induction of FoxP3 was severely impaired in the $Cblb^{-/-}$ mutants cells with only 1.57% and 7.95% of cells expressing the marker after stimulation with 0.1 ng/ mL or 0.5 ng/ mL TGFβ, respectively (Fig 4.23). In Fig. 4.24, when the iTregs were tested for functional activity suppress proliferation of CFSE-labelled $CD4^{+}CD62L^{+}CD25^{-}$ T effector cells co-cultures with antigen presenting cells, wild-type and TCR^{3A9} iTregs were able to mediated suppression of T effector as measured by CFSE-dilution. However, $Cblb^{-/-}$ TCR^{3A9} iTregs were less suppressive demonstrating that $Cblb^{-/-}$ organ specific T cells displayed impaired ability to form functional iTreg cells following stimulation by TGFβ. It is unclear if this *in vitro* observation is physiologically relevant and may contribute to the disease observed in the $Aire^{-/-}Cblb^{-/-}$ mice.

The finding here that the individual defects caused by *Aire*- and *Cblb*-deficiency do not result in a co-operative breakdown of tolerance in insHEL-reactive CD4 T cells from double mutant chimeras may mean that additional peripheral tolerance mechanisms exist to prevent activation of TCR^{3A9}–expressing T cells. By contrast, these additional peripheral tolerance mechanisms may not apply to the T cells that caused exocrine pancreatitis in the double mutant mice, and this possibility is explored further in the next chapter.

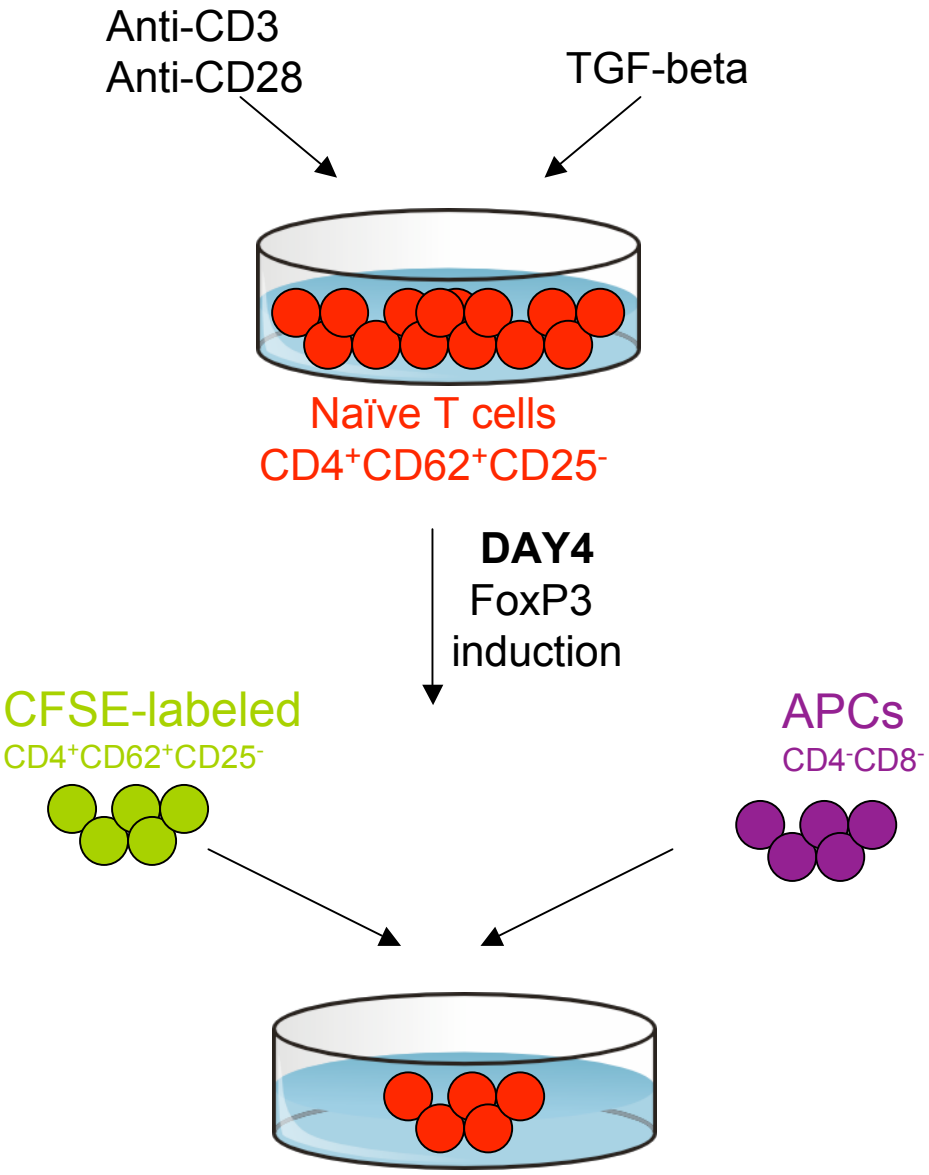

Figure 4.22 Schematic representation of experimental set-up for induction of FoxP3 and functionality of wild-type and *Cblb*$^{-/-}$ cells.
Sorted naïve T cells ($CD4^+CD62^+CD25^-$) were stimulated with anti-CD3 and anti-CD28, together with TGF-ß to induce FoxP3 expression. Four days after initial culture, the cells were co-cultured with CFSE-labelled naïve T cells and antigen presenting cells to assay for suppression of proliferation.

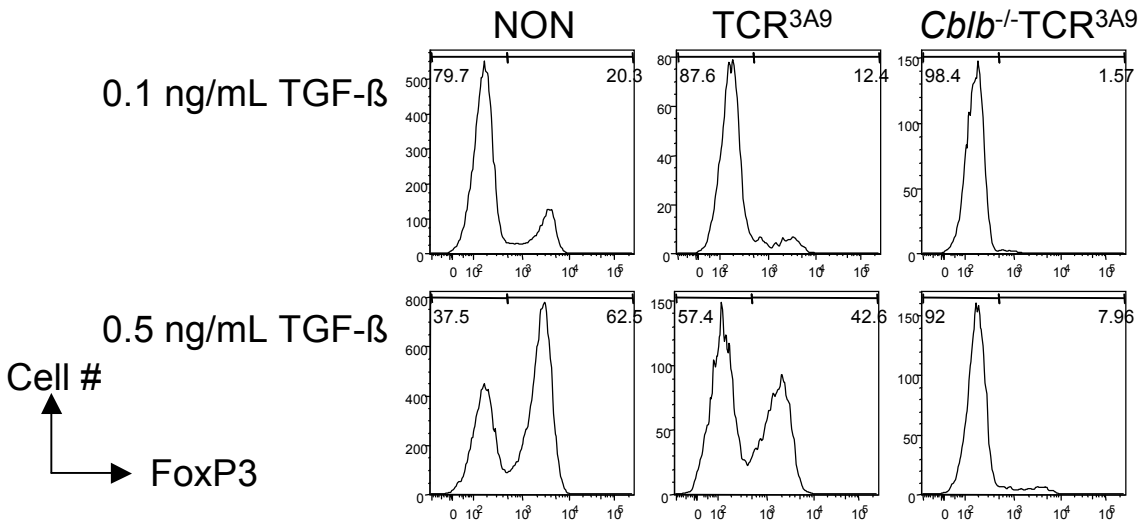

Figure 4.23 *Cblb*-deficient TCR^{3A9} cells are resistant to TGF-ß induced iTreg formation.
Naive CD4^{+}CD62L^{+}CD25^{-} T cells from non-transgenic or *Cblb*$^{+/+}$ and *Cblb*$^{-/-}$ TCR^{3A9} transgenic mice were stimulated with anti-CD3 and anti-CD28 in the presence of the indicated concentrations of TGF-ß. Development of Foxp3^{+} iTreg cells was assessed by flow cytometry after 5 days.

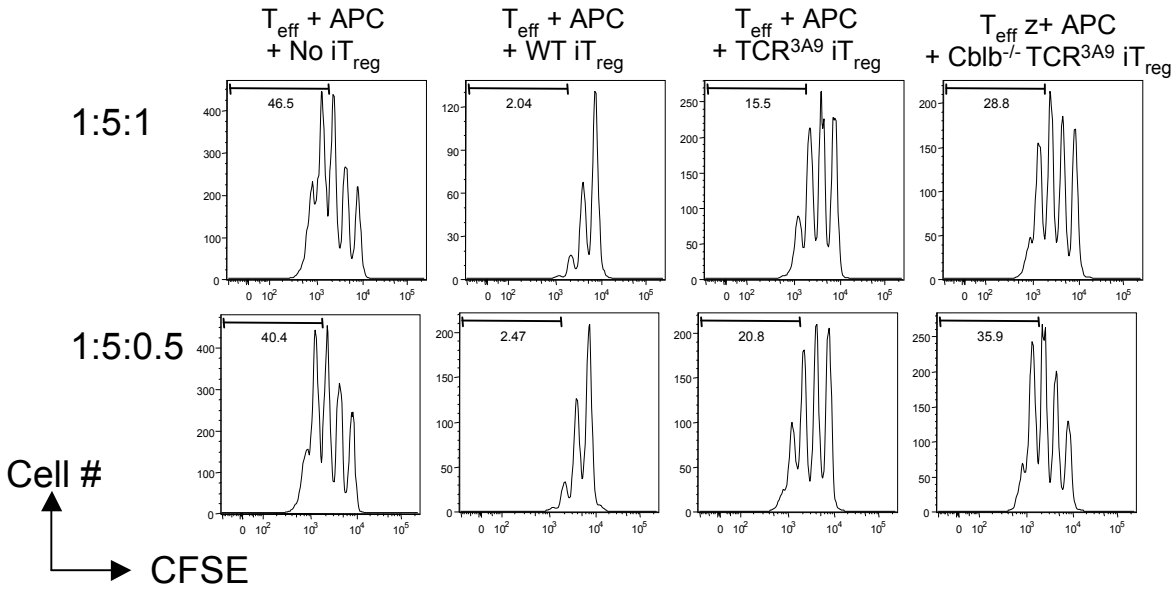

Figure 4.24 iTreg assay showed *Cblb*-deficient TCR^{3A9} cells are resistant to TGF-ß induced iTreg formation.
CFSE-labelled CD4^{+}CD62L^{+}CD25^{-} naive T cells from *Cblb*$^{+/+}$ TCR^{3A9} mice were used as responder cells in suppression assays, mixed with irradiated T cell-depleted splenocytes as a source of antigen presenting cells and with the cultured CD4 cells shown in Fig. 4.23. The cells were mixed in the two indicated ratios (CFSE-labelled responder cells:APCs:TGF-ß treated CD4 cells). Anti-CD3 antibody was added to the cultures and CFSE dilution was assessed by flow cytometry 3 days later.

4.5.3 Impact of *Aire*- and *Cblb*-deficiencies on peripheral tolerance in CD4 T cells

While the following chapter develops a new retrogenic experimental model to examine the T cells responsible for exocrine pancreatitis in *Aire*$^{-/-}$*Cblb*$^{-/-}$ double deficient mice, the remainder of this chapter describes a set of preliminary experiments focussing on the role of *Aire* and *Cblb* in CD4 T cell peripheral tolerance using the TCR^{3A9} transgenic system. Although *Aire* is predominantly expressed in the medullary thymic epithelial cells, it is also expressed in dendritic cells and extrathymic splenic and lymph node cells in the periphery (Adamson et al., 2004; Gardner et al., 2008; Halonen et al., 2001; Lee et al., 2007; Ramsey et al., 2006). Hence in this section I explored how deficiency of *Aire* affected the fate of mature peripheral HEL-specific CD4 T cells, and how it interacted with a defect in *Cblb* in this context.

4.5.4 *Aire*-deficiency interferes with mature CD4 T cell activation by organ-specific antigen.

To focus on the role of AIRE in peripheral CD4 T cell tolerance, an *in vivo* adoptive transfer T cell activation assay was developed. Spleen cells from CD45.1 TCR^{3A9} transgenic mice were labelled with carboxyfluorescein succinimidyl ester (CFSE) and intravenously transferred into unirradiated CD45.2 insHEL-transgenic recipient mice or into non-transgenic control recipients (Fig 4.25). This regime enabled a trace number of organ-specific CD4 T cells to be tracked at a single cell level (Fig. 4.26*A*) in a host with a normal lymphocyte repertoire and tolerance mechanisms. Three to four days post-transfer, the mice were sacrificed and the transferred cells were analysed by flow cytometry. Measurement of CFSE dilution and intracellular staining for Ki-67, a cell cycle protein, showed that a large fraction of the HEL-reactive T cells bearing the clonotypic receptor were stimulated into proliferation (Fig. 4.26*B*,*C*,*D*). This was observed in the pancreatic lymph node, which was expected due to drainage of the islet-HEL neo-self antigen either free in the lymph or transported by antigen presenting dendritic cells. Interestingly, many CD4 TCR^{3A9} cells in the spleen were also stimulated into cycle, albeit to a lesser extent than in the pancreatic node (Fig. 4.27). This was surprising given that previous studies have indicated that HEL expression in the recipient mice was limited to the pancreas and thymus. When the insHEL-transgenic recipients were *Aire*-deficient, fewer CD4 TCR^{3A9} cells were induced to divide in the

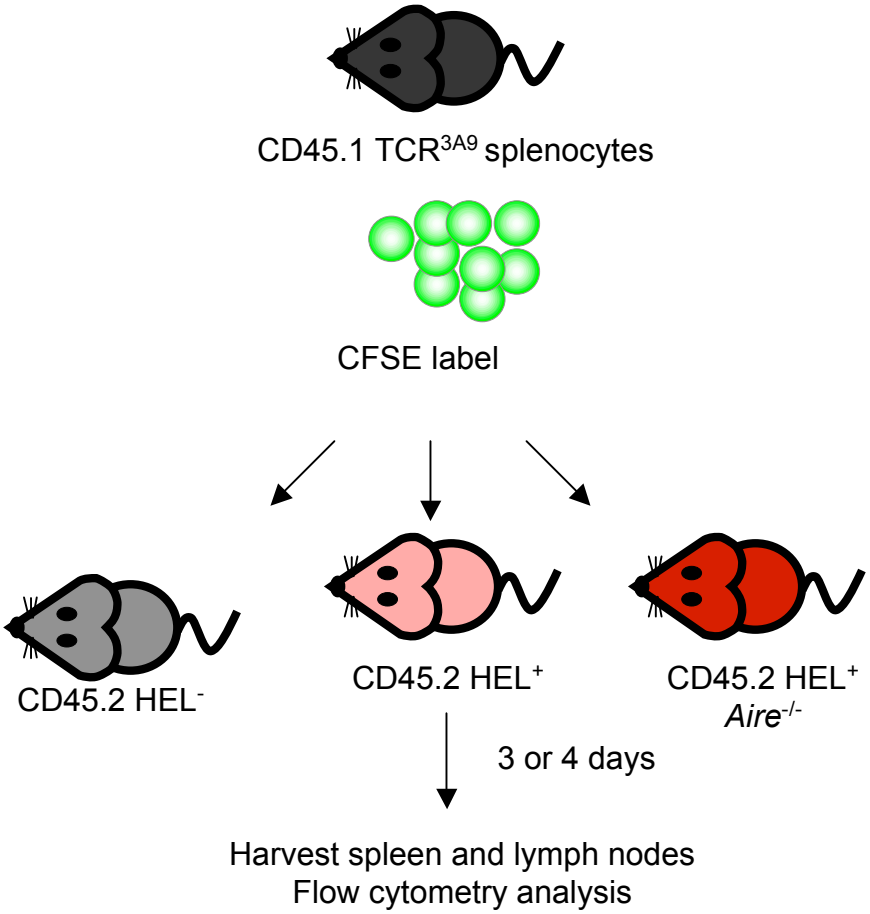

Figure 4.25 Adoptive transfer of CFSE-labelled T cells: experimental strategy.
Splenocytes from CD45.1 TCR^{3A9} transgenic or non-transgenic control mice, were labelled with CFSE before adoptive transfer into CD45.2 $insHEL^{+}$ recipient mice expressing HEL controlled by insulin or thyroglobulin intravenously. 10 - 20 x 10^{6} cells were injected into each recipient. Three or four days post-injection, the mice were sacrificed and spleen, subcutaneous lymph nodes and pancreatic lymph nodes were analysed for cell division by flow cytometry.

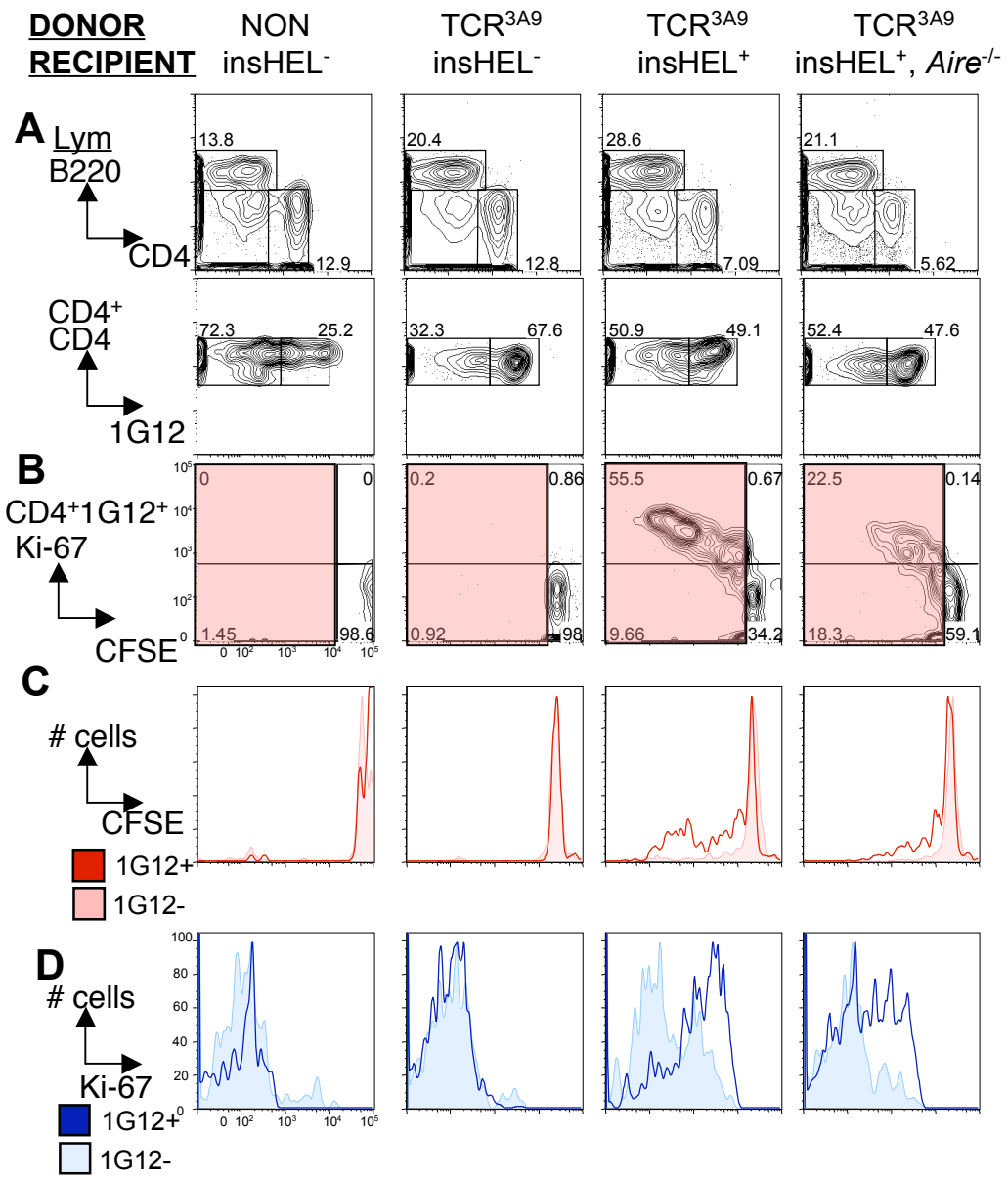

Figure 4.26 *Aire*-deficiency causes decreased activation of HEL-specific CD4 pancreatic lymph node T cells by insHEL transgene.

A. Representative flow cytometry plots of B cells and CD4 cells from donor CD45.1 cells (upper panels) and TCR^{3A9} cells from total CD4 cells in recipient mice four days after cell transfer gated on $CD45.1^{+}CD4^{+}$ (lower panels)

B. CFSE dilution and Ki-67 upregulation of $1G12^{+}TCR^{3A9}$ cells. Percentages of divided cells seen in Figure 4.28 are calculated from quadrants seen in red.

C. Histograms gated on CD4 cells showing CFSE dilution of $1G12^{+}TCR^{3A9}$ (unshaded dark red) and $1G12^{-}$ counterparts (shaded light red) in the same recipient.

D. Histograms gated on CD4 cells showing Ki-67 upregulation of $1G12^{+}$ TCR^{3A9} (unshaded dark blue) and $1G12^{-}$ counterparts (shaded light blue) in the same recipient.

Data are representative of two independent experiments with *n* = 1-3 mice per group (see Figure 4.28: Experiment 1).

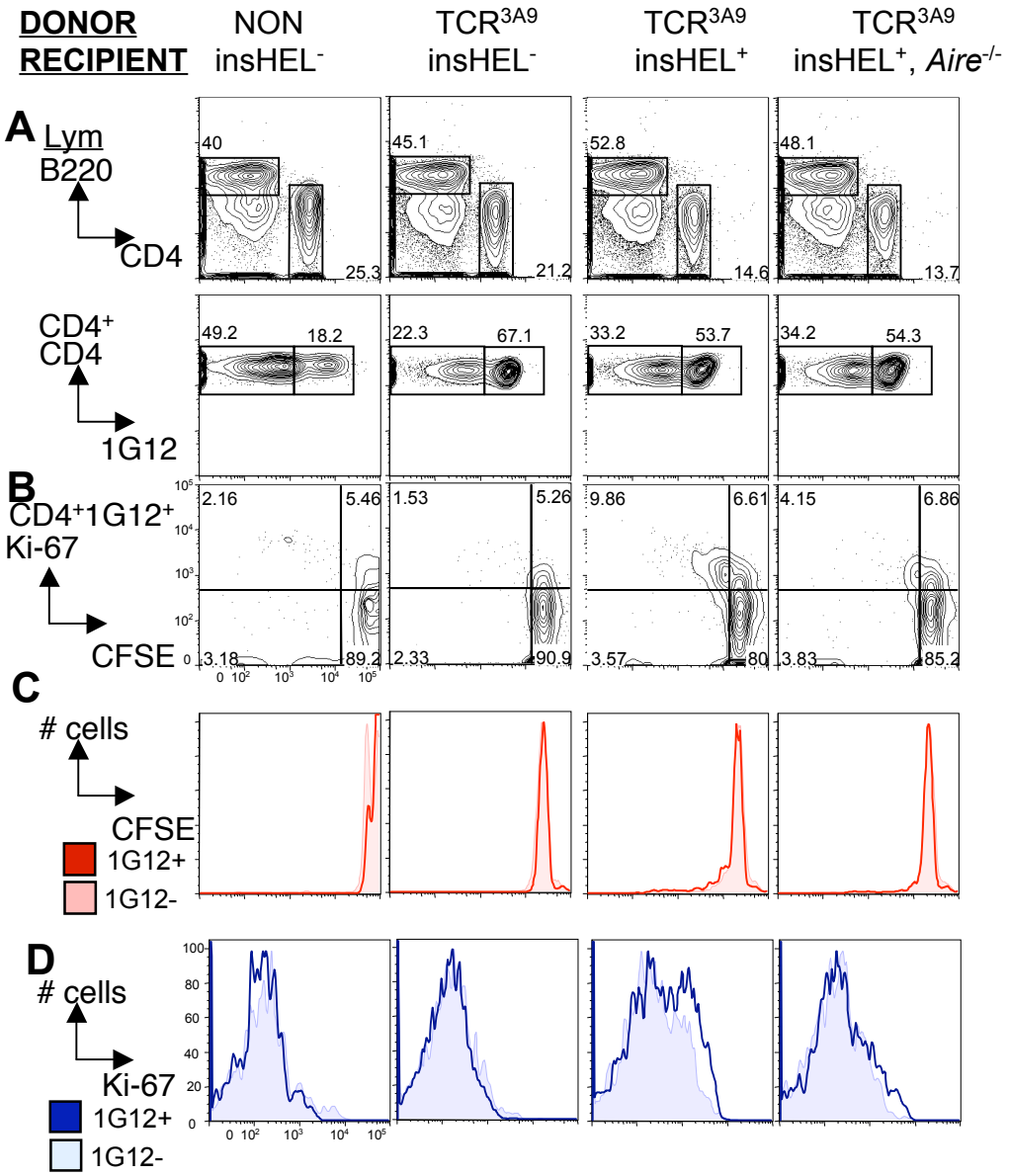

Figure 4.27 *Aire*-deficiency causes decreased activation of HEL-specific CD4 splenic T cells by insHEL transgene.

A. Representative flow cytometry plots of B cells and CD4 cells from donor CD45.1 cells (upper panels) and TCR^{3A9} cells from total CD4 cells in recipient mice four days after cell transfer gated on $CD45.1^{+}CD4^{+}$ (lower panels).

B. CFSE dilution and Ki-67 upregulation of $1G12^{+}TCR^{3A9}$ cells.

C. Histograms gated on CD4 cells showing CFSE dilution of $1G12^{+}TCR^{3A9}$ (unshaded dark red) and $1G12^{-}$ counterparts (shaded light red) in the same recipient.

D. Histograms gated on CD4 cells showing Ki-67 upregulation of $1G12^{+}$ TCR^{3A9} (unshaded dark blue) and $1G12^{-}$ counterparts (shaded light blue) in the same recipient

Data are representative of two independent experiments with *n* = 1-3 mice per group (see Figure 4.28: Experiment 1).

pancreatic node (Fig 4.26) and in the spleen (Fig 4.27). The effect of *Aire*-deficiency on peripheral activation of the CD4 cells was consistent, although somewhat variable, in multiple insHEL-transgenic recipients in two independent experiments (Fig 4.28).

To determine if the peripheral expression of the insHEL transgene occurred in hemopoietic cells (e.g. dendritic cells) or in non-hemopoietic cells such as pancreatic beta cells and lymph node stromal cells, the T cell transfer experiments were repeated in bone marrow chimeras. Irradiated insHEL-transgenic or non-transgenic mice were reconstituted with bone marrow from either insHEL-transgenic or non-transgenic donors. This experiment created four different groups of chimeric mice, where the insHEL transgene was present only in the hematopoietic cells, only in non-hematopoietic cells, in both or not present at all (Fig 4.29). Twelve weeks after bone marrow transplantation, CFSE-labelled spleen cells from CD45.1 TCR^{3A9} transgenic mice were injected into the bone marrow chimeric mice. Four days later, flow cytometry revealed proliferation of $1G12^{+}CD45.1^{+}$CD4 T cells only in recipient mice (in pancreatic lymph node and spleen) with the insHEL transgene in the non-hematopoietic compartment, whereas no proliferation was induced by the insHEL transgene when present exclusively in the hematopoietic compartment (Fig 4.30). Thus, the autoantigen responsible for peripheral activation of naïve TCR^{3A9} CD4 T cells is made and presented exclusively in non-hematopoietic cells. These could either be pancreatic islet beta cells, whose HEL-expression is unaffected by *Aire*-deficiency, or the $Aire^{+}$ peripheral antigen expressing lymph node stromal cells (Gardner et al., 2008).

The peripheral T cell activation studies above were extended to animals bearing a second transgene driven by a different organ-specific promoter: thyrHEL transgenic mice where the thyroglobulin promoter causes HEL expression in thyroid epithelium and, in an *Aire*-dependent manner, in thymic medullary epithelium. After four days of transfer of CFSE-labelled spleen cells from $CD45.1^{+}TCR^{3A9}$ mice, flow cytometry showed that $1G12^{+}$ HEL-specific T cells were stimulated to divide in the lymph nodes (Fig 4.31) and spleen (Fig 4.32) of thyrHEL-transgenic mice. Fewer T cells were induced to divide in *Aire*-deficient thyrHEL-transgenic mice (Fig. 4.31, 4.32 and 4.33). When the donor cells were left for 14 days prior to analysis in recipient mice, it was difficult to trace any $1G12^{+}$ and $1G12^{+}$ cells in the mice. This indicated that *Aire* is

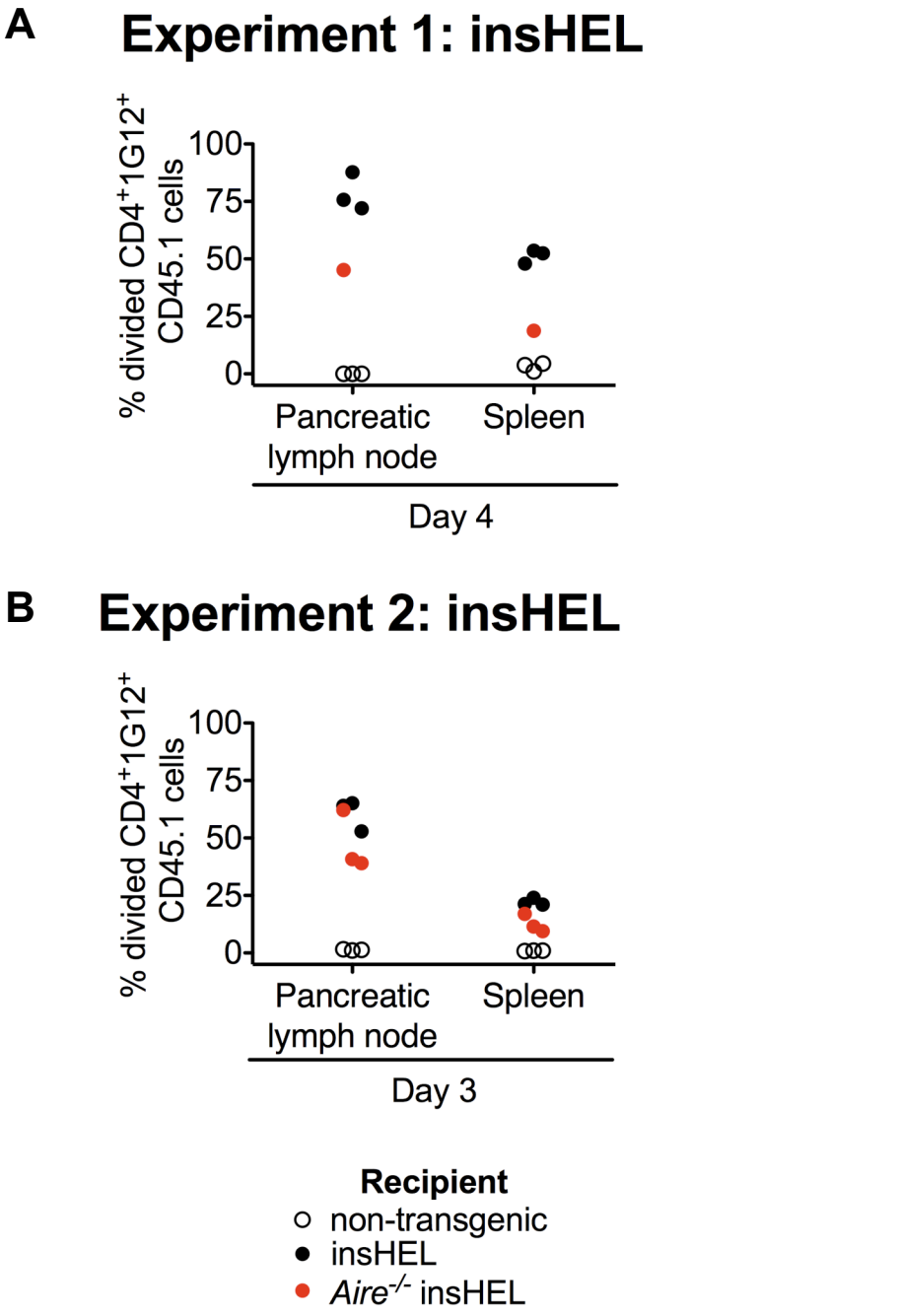

Figure 4.28 *Aire*-deficiency reduces proliferation of TCR^{3A9} cells induced by the insHEL transgene.
Graph shows the percentage of CD4^{+}1G12^{+}CD45.1 donor cells that have divided four (A) and three (B) days after adoptive transfer in CFSE^{low} cells. Data show two independent experiments (A and B) with *n* = 1-3 mice per group.

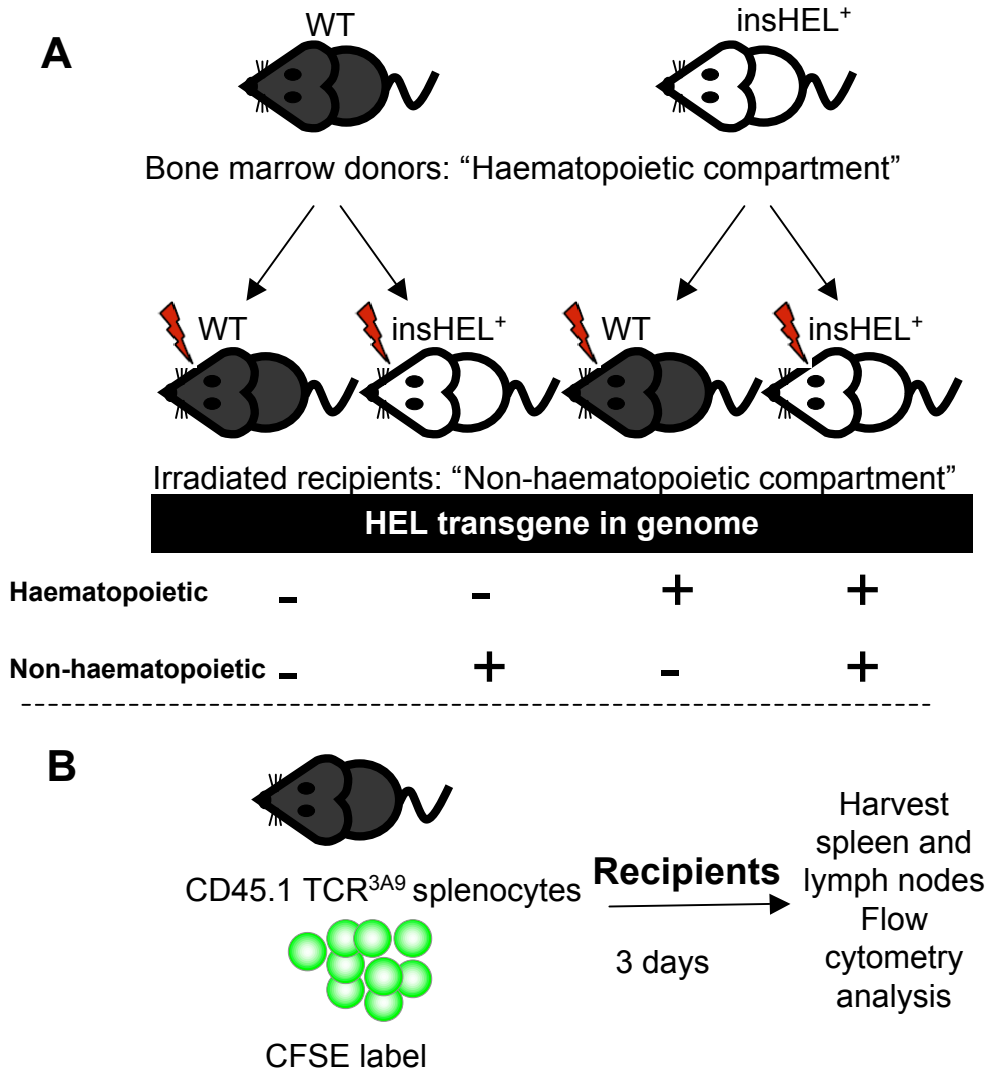

Figure 4.29 Adoptive transfer of CFSE labelled T cells into HEL-chimeric mice experimental strategy.

A. Bone marrow chimeras with HEL transgene restricted to the haematopoietic or non-haematopoietic cells were generated by reconstituting irradiated wild-type or insHEL$^+$ CD45.2$^+$ recipients with wild-type or insHEL$^+$ bone marrow from CD45.2$^+$ donors.

B. Splenocytes from CD45.1 TCR^{3A9} or non-transgenic control mice were labelled with CFSE, and 10 - 20 x 10^6 cells were injected into each chimeric recipient. Three days post-injection, the mice were sacrificed and spleen, subcutaneous lymph nodes and pancreatic lymph nodes were analysed for cell division by flow cytometry.

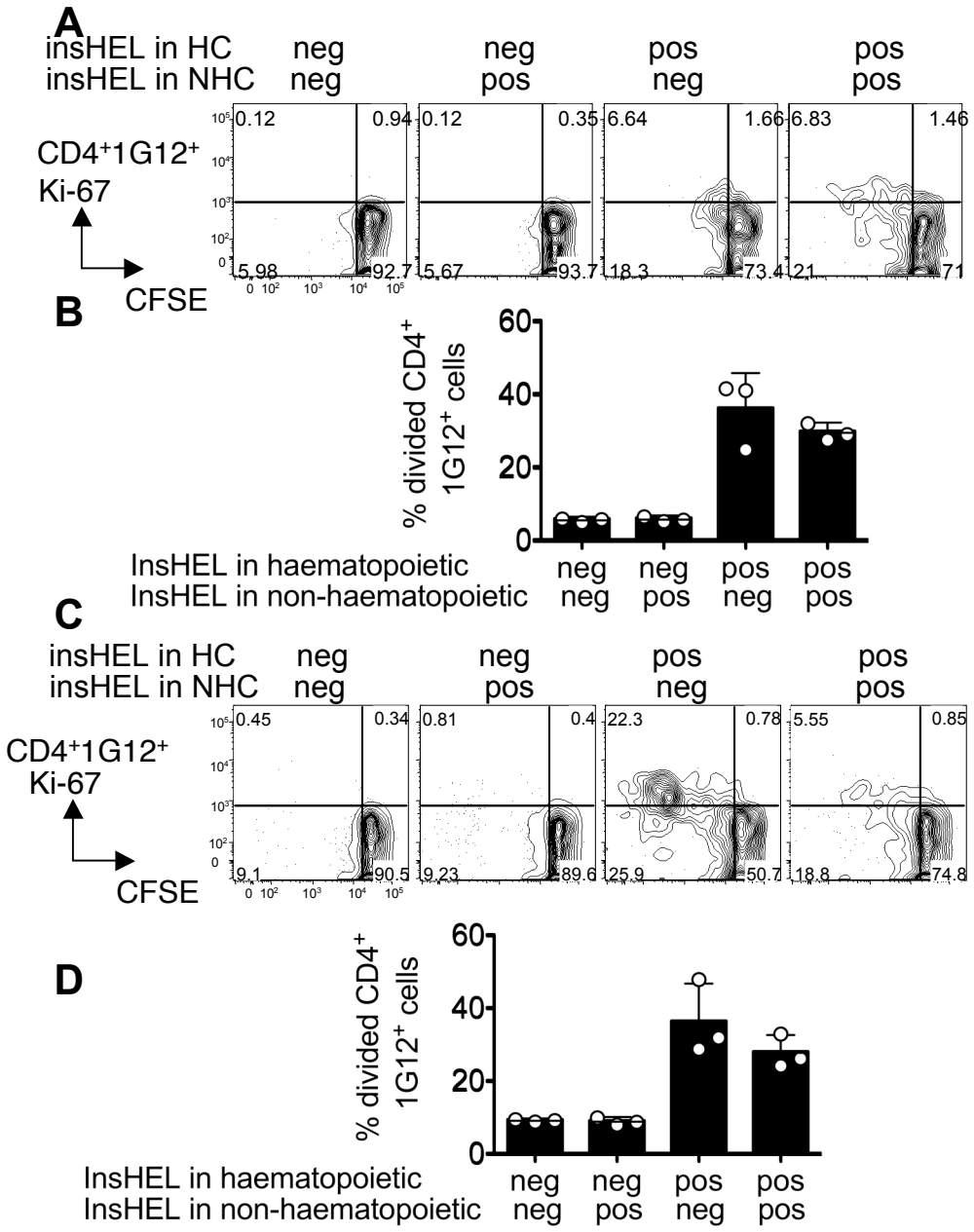

Figure 4.30 Induction of division in TCR^{3A9} donor cells require the insHEL transgene in the haematopoietic compartment.

A. Profiles gated on CD45.1^{+}CD4^{+}1G12^{+} showing CFSE dilution and Ki-67 upregulation of TCR^{3A9} cells in the pancreatic lymph node.

B. Percentage of donor CD45.1^{+}CD4^{+}1G12^{+} cells three days post adoptive transfer in the quadrants that have diluted CFSE in the pancreatic lymph node.

C. As (A) in the spleen.

D. As (B) in the spleen

Data are representative of two independent experiments with *n* = 3 mice per group. HC, haematopoietic component; NHC, non-haematopoietic component.

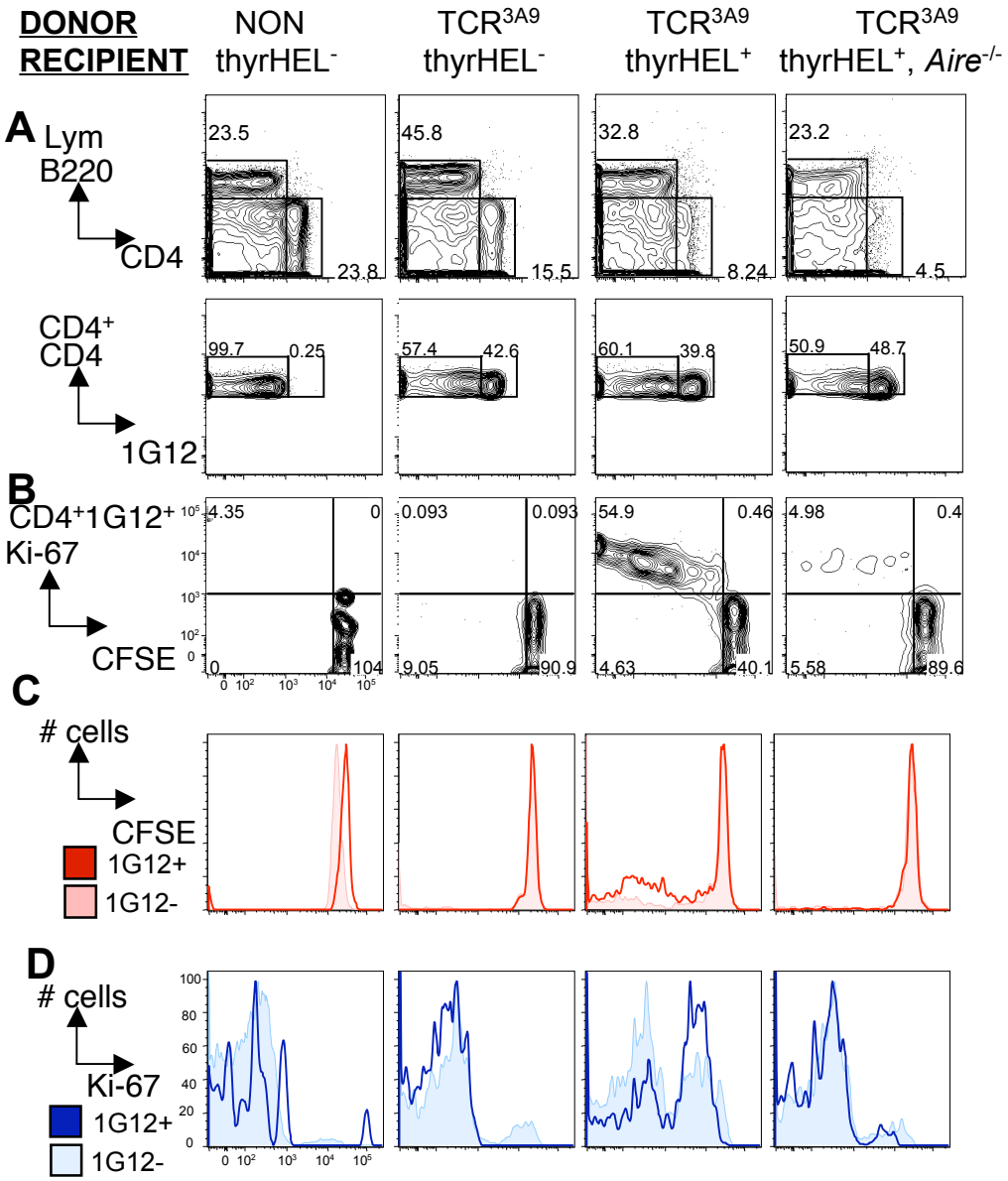

Figure 4.31 *Aire*-deficiency causes decreased activation of HEL-specific CD4 splenic T cells by thyrHEL transgene.

A. Representative flow cytometry plots of B cells and CD4 cells from donor CD45.1 cells and TCR^{3A9} cells from total CD4 cells in recipient mice four days after cell transfer gated on CD45.1^{+}CD4^{+}1G12^{+}.

B. CFSE dilution and Ki-67 upregulation of 1G12^{+}TCR^{3A9} cells.

C. Histograms gated on CD4 cells showing CFSE dilution of 1G12^{+}TCR^{3A9} (unshaded dark red) and 1G12^{-} counterparts (shaded light red) in the same recipient.

D. Histograms gated on CD4 cells showing Ki-67 upregulation of 1G12^{+} TCR^{3A9} (unshaded dark blue) and 1G12^{-} counterparts (shaded light blue) in the same recipient.

Data are representative of two independent experiments with *n* = 3-5 mice per group (see Figure 4.33: Experiment 1).

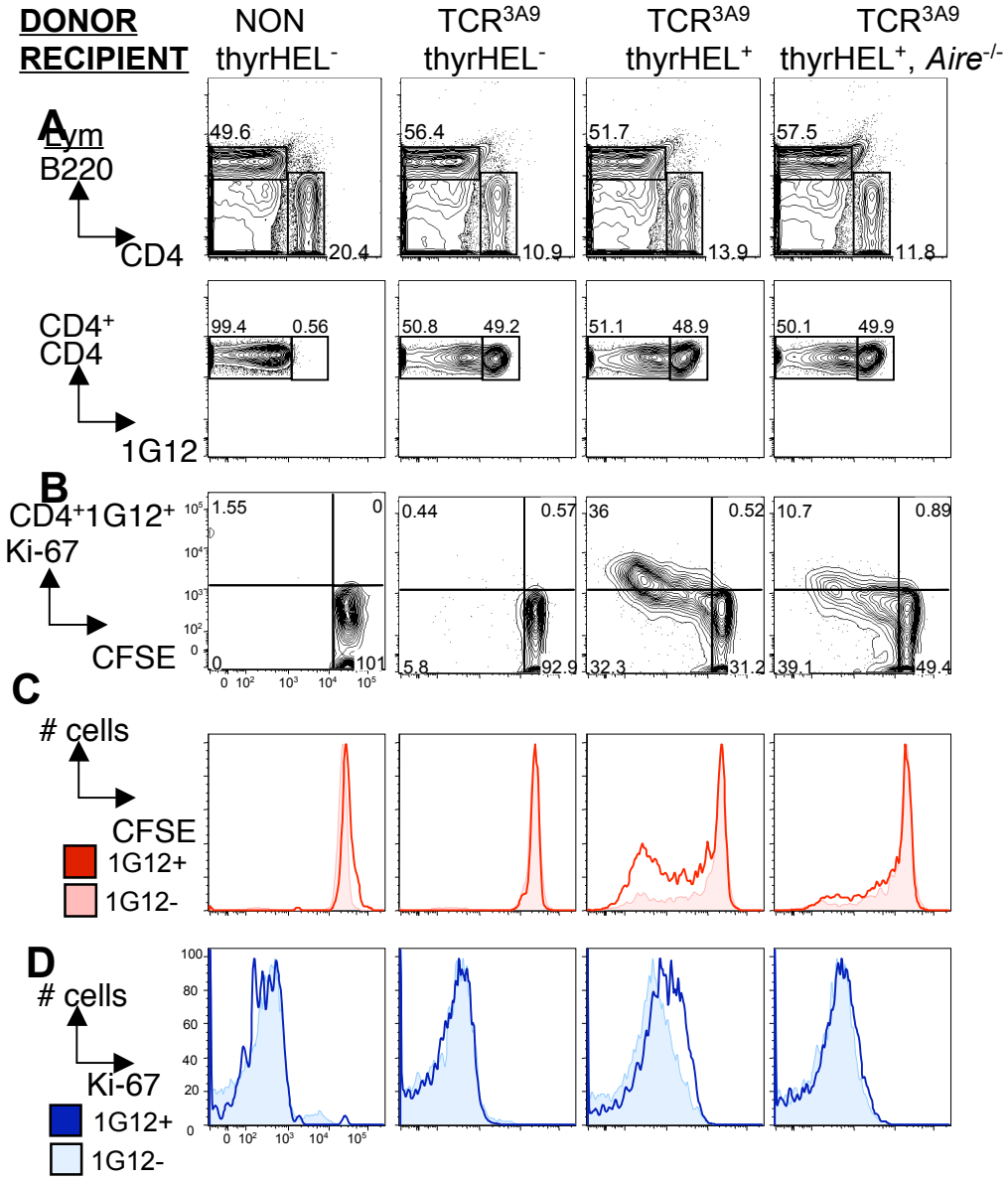

Figure 4.32 *Aire*-deficiency causes decreased activation of HEL-specific CD4 subcutaneous lymph node T cells by thyrHEL transgene.

A. Representative flow cytometry plots of B cells and CD4 cells from donor CD45.1 cells and TCR^{3A9} cells from total CD4 cells in recipient mice four days after cell transfer gated on $CD45.1^{+}CD4^{+}1G12^{+}$.

B. CFSE dilution and Ki-67 upregulation of $1G12^{+}TCR^{3A9}$ cells.

C. Histograms gated on CD4 cells showing CFSE dilution of $1G12^{+}TCR^{3A9}$ (unshaded dark red) and $1G12^{-}$ counterparts (shaded light red) in the same recipient.

D. Histograms gated on CD4 cells showing Ki-67 upregulation of $1G12^{+}$ TCR^{3A9} (unshaded dark blue) and $1G12^{-}$ counterparts (shaded light blue) in the same recipient.

Data are representative of two independent experiments with *n* = 3-5 mice per group (see Figure 4.33: Experiment 1).

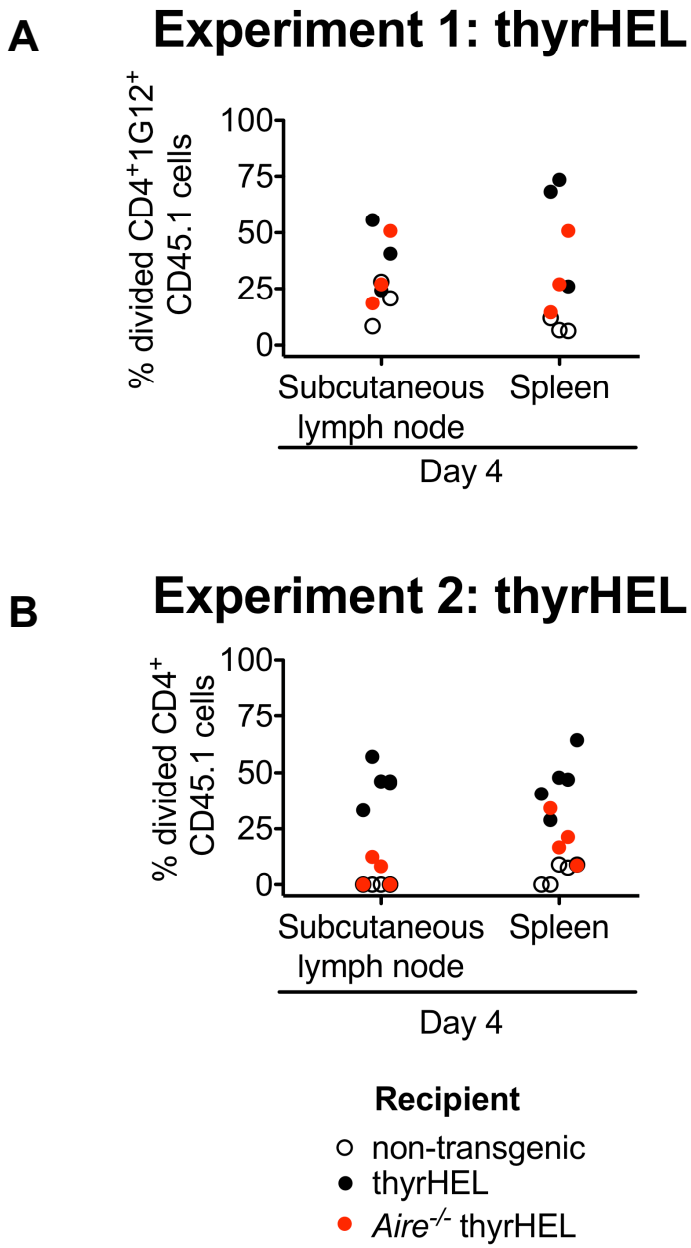

Figure 4.33 *Aire*-deficiency reduces proliferation of TCR^{3A9} cells induced by the thyrHEL transgene.
Graph shows the percentage of CD4^{+}1G12^{+}CD45.1 donor cells four (A and B) days days after adoptive transfer of CFSE^{low} cells. Data show two independent experiments with *n* = 3-5 mice per group.

required for efficient activation of organ-specific T cells in peripheral lymphoid tissues of two different transgenic strains (insHEL and thyrHEL). The activation observed could be suggested to cumulate in activation induced cell death of antigen-specific cells by 14 days post-transfer.

4.5.5 Impact of *Cblb*-deficiency on peripheral tolerance in CD4 T cells

To test the effect of *Cblb*-deficiency, alone or combined with *Aire*-deficiency, in the transfer assay for peripheral T cell proliferation, CD45.2 $Cblb^{-/-}$ TCR^{3A9} spleen cells were mixed in a 1:1 ratio with CD45.1 $Cblb^{+/+}$ TCR^{3A9} spleen cells. The mixture was labelled with CFSE and injected into CD45.1/CD45.2 wild-type or $Aire^{-/-}$insHEL recipients. After four days, flow cytometry was used to compare CFSE-dilution and Ki-67 expression in wild-type and $Cblb^{-/-}$ TCR^{3A9} cells in the same recipients. In the pancreatic lymph node and spleen of $insHEL^{+}$ $Aire^{+/+}$ recipients, divided T cell progeny accounted for a larger percentage of the $Cblb^{-/-}$ T cells compared to their *Cblb*-sufficient counterparts (Fig. 4.34 and 4.35), consistent with published studies of *Cblb*-deficient T cells (Jeon et al., 2004). In the *Aire*-deficient insHEL recipients in this experiment, the percent of the wild-type or $Cblb^{-/-}$ TCR^{3A9} cells that had divided varied greatly from mouse to mouse (Fig. 4.35). While this variability made it impossible to interpret the results from the *Aire*-deficient experimental group accurately, there appeared to be no consistent enhancement of proliferation of *Cblb*-deficient T cells within individual recipients. Due to limited numbers of mice and time, repeating this experiment was not deemed a sufficiently high priority at this time compared with the retrogenic experiments described in the next chapter.

4.5.6 The consequences of adding an adjuvant on peripheral tolerance

In the experiments above, organ-specific CD4 cells were activated into several rounds of cell division as a result of endogenous HEL antigen presentation. This proliferation was nevertheless self-limiting and did not precipitate diabetes. Since autoimmune disease may also require an inflammatory trigger, the adoptive transfer system was varied by giving the recipient mice exogenous HEL emulsified in a strong adjuvant several days after TCR^{3A9} T cell transfer.

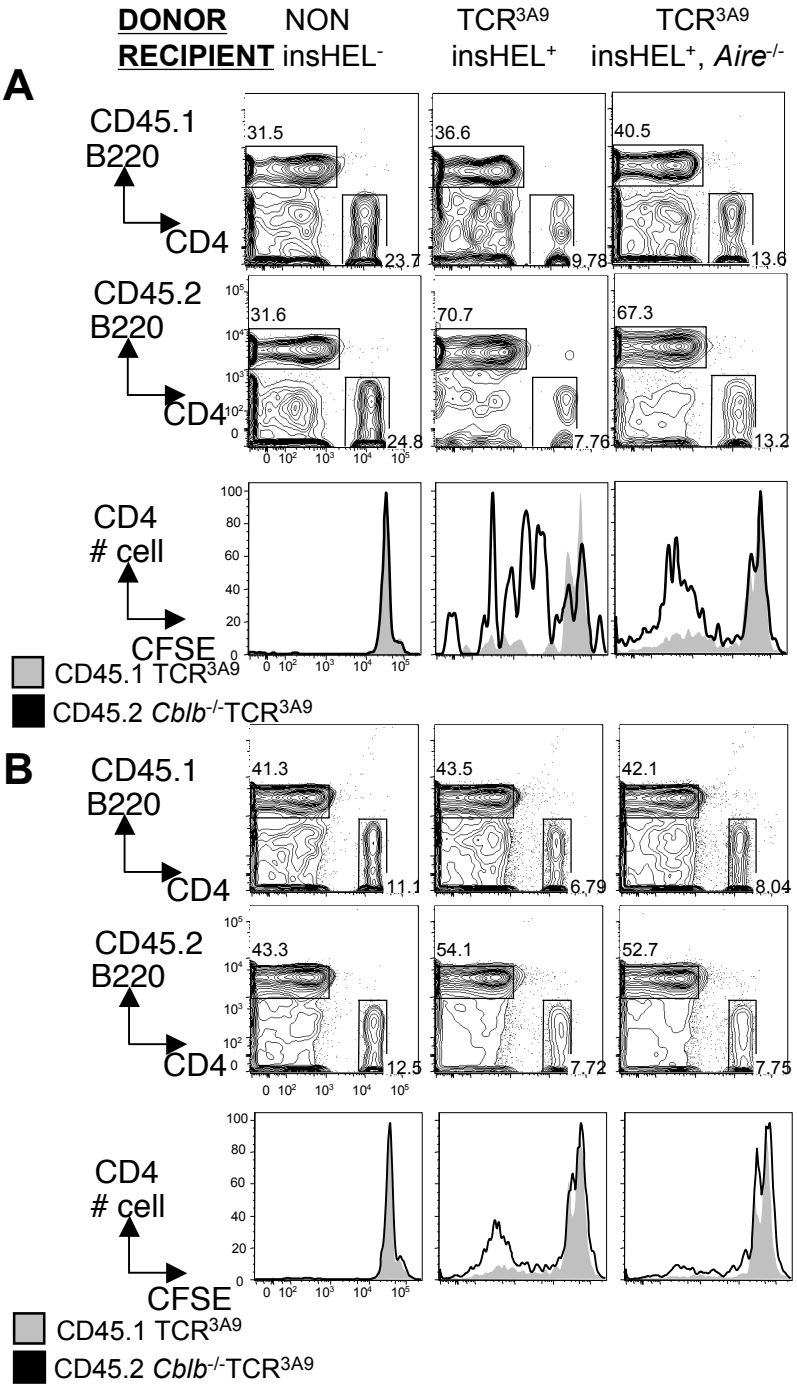

Figure 4.34 *Aire*- and *Cblb*-deficiency do not co-operate to alter the proliferation of pancreas specific TCR^{3A9} cells.
Representative flow cytometry plots of B cells and CD4 cells from donor CD45.1 TCR^{3A9} (top panel) and CD45.2 *Cblb*$^{-/-}$ TCR^{3A9} cells (middle panel) in recipient mice four days after cell transfer. The bottom panel shows representative histograms gated on CD4 cells showing CFSE dilution of CD45.1^{+}CD4^{+} (shaded grey) and CD45.2^{+}CD4^{+} *Cblb*$^{-/-}$ (unshaded black) cells in the pancreatic lymph node (A) and spleen (B) of the same recipient.

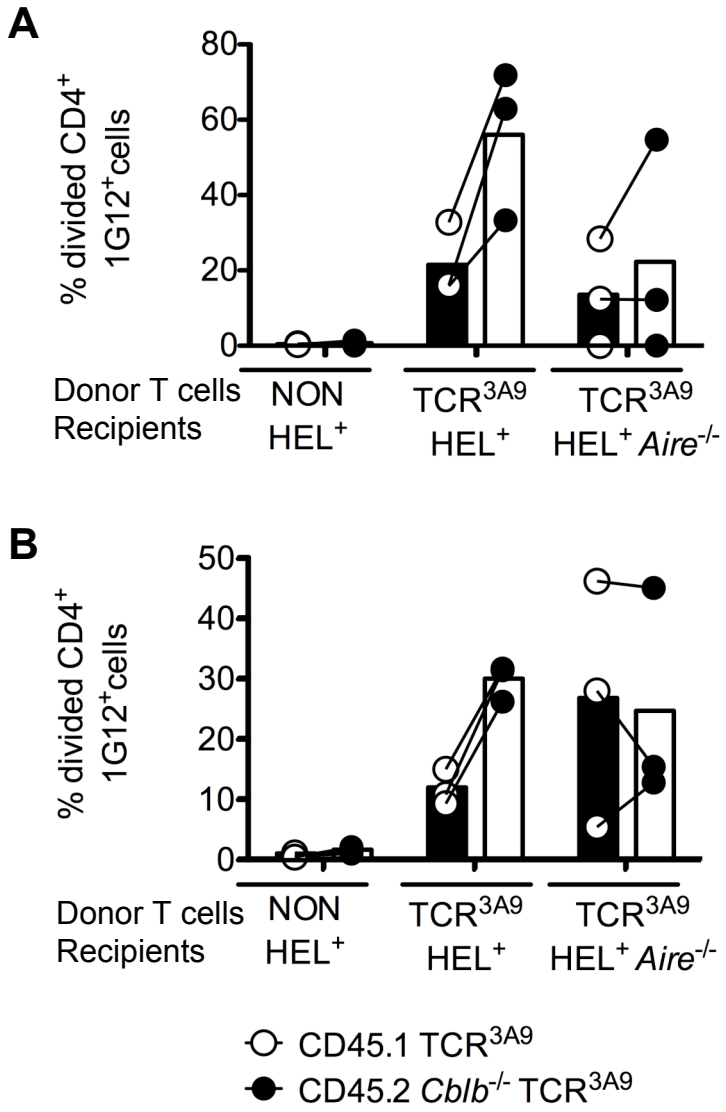

Figure 4.35 *Aire*- and *Cblb*-deficiency do not co-operate to alter the proliferation of pancreas specific TCR^{3A9} cells.
Graph represent the percentage of donor CD45.1^{+}CD4^{+}1G12^{+} wild-type and CD45.2 *Cblb*$^{-/-}$ donor cells that has diluted CFSE four days post adoptive transfer. The lines join connect the samples from the same recipient mouse.

A. Pancreatic lymph node
B. Spleen

Dose optimisation experiments were performed to establish the number of wild-type TCR^{3A9} CD4 cells needed to precipitate diabetes in insHEL-transgenic recipients. 3×10^5, 1×10^6 or 3×10^6 MACS-enriched CD4 cells from TCR^{3A9} single transgenic mice were intravenously transferred into groups of 4-5 insHEL-transgenic recipients. On the same day, the recipients were intraperitoneally immunised with HEL protein emulsified in complete Freund's adjuvant (CFA) and the mice were monitored for glucosuria three times a week (Fig. 4.36). As seen in Fig. 4.37*A*, all mice receiving TCR^{3A9} CD4 cells developed glucosuria within 2-3 weeks after immunization, whereas no diabetes occurred in control animals that were immunized with HEL in CFA but did not receive TCR^{3A9} cells. While the immunized control recipients developed HEL-specific IgG antibodies compared to nonimmunized animals, transfer of TCR^{3A9} CD4 cells increased the titres of these autoantibodies ~20-fold (Fig. 4.37*B*). The diagnosis of diabetes in recipients of TCR^{3A9} cells, and not in the immunized control recipients, was confirmed by elevated blood glucose 36 days after transfer (Fig. 4.37*C*). This experiment established that as few as 3×10^5 TCR^{3A9} CD4 cells were sufficient to induce diabetes when stimulated with exogenous HEL in Freund's adjuvant.

The next step was to delay the HEL/CFA immunization until three days after transferring 3×10^5 MACS-enriched CD4 TCR^{3A9} cells. During this tolerisation period, the transferred T cells would be exposed only to endogenous HEL, which in the previous section 4.5.4 was established to induce an abortive round of proliferation that was followed theoretically by T cell anergy and deletion. As seen in Fig. 4.38*A*, delaying HEL/CFA immunisation ameliorated the development of diabetes and recipient mice presented with only trace amounts of glucose in the urine. HEL-specific IgG Fig. 4.38*B* and blood glucose levels Fig. 4.38*C* tested 50 days after T cell transfer were also reduced when HEL/CFA immunization was delayed. These effects may reflect active tolerance to endogenous HEL during the 3 days delay period, or the short-lived nature of unstimulated TCR^{3A9} CD4 cells. To evaluate the latter possibility, a third group of animals were immunized on day 0 but received ten times fewer TCR^{3A9} CD4 cells. These also developed less glucosuria and did not have elevated blood glucose on day 50, but their serum titres of anti-HEL IgG were comparable to animals receiving the higher T cell dose. Regardless, these experiments established an experimental system to

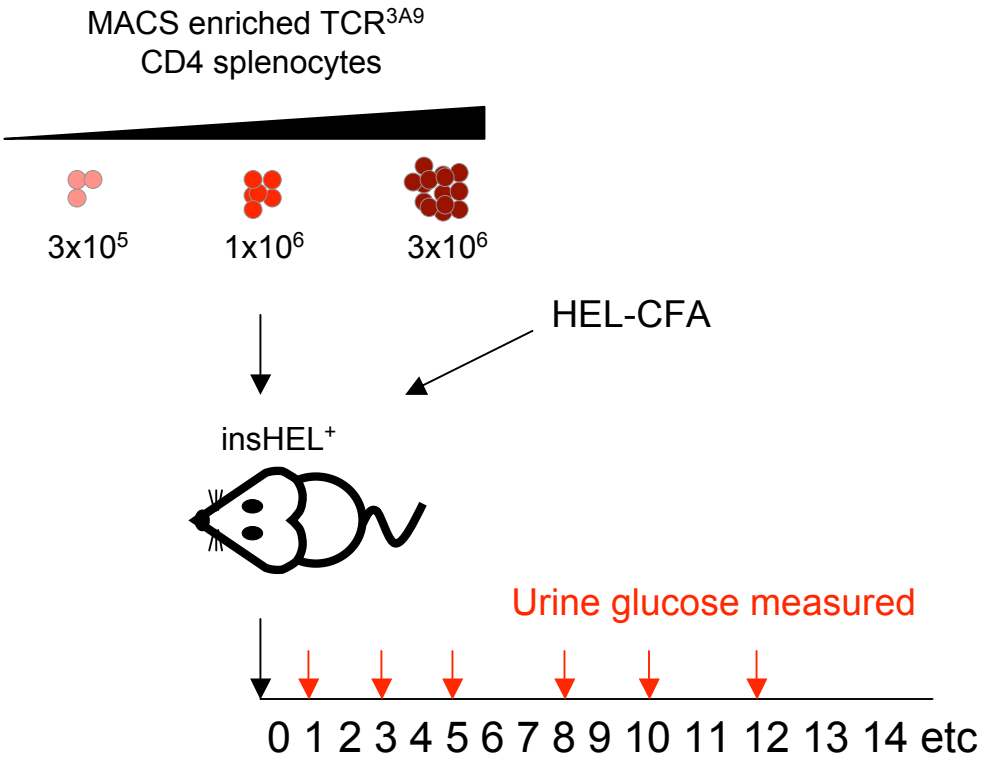

Figure 4.36 Experimental design to test organ destruction by TCR^{3A9}CD4 cells
Varying numbers of MACS-enriched CD4 cells from single transgenic TCR^{3A9} mice were injected intravenously into groups of 4-5 insHEL transgene recipients. On the same day, the recipients were intraperitoneally immunised with HEL protein emulsified in complete Freund's adjuvant (CFA). Urine glucose was measured three times a week for the duration of the experiment.

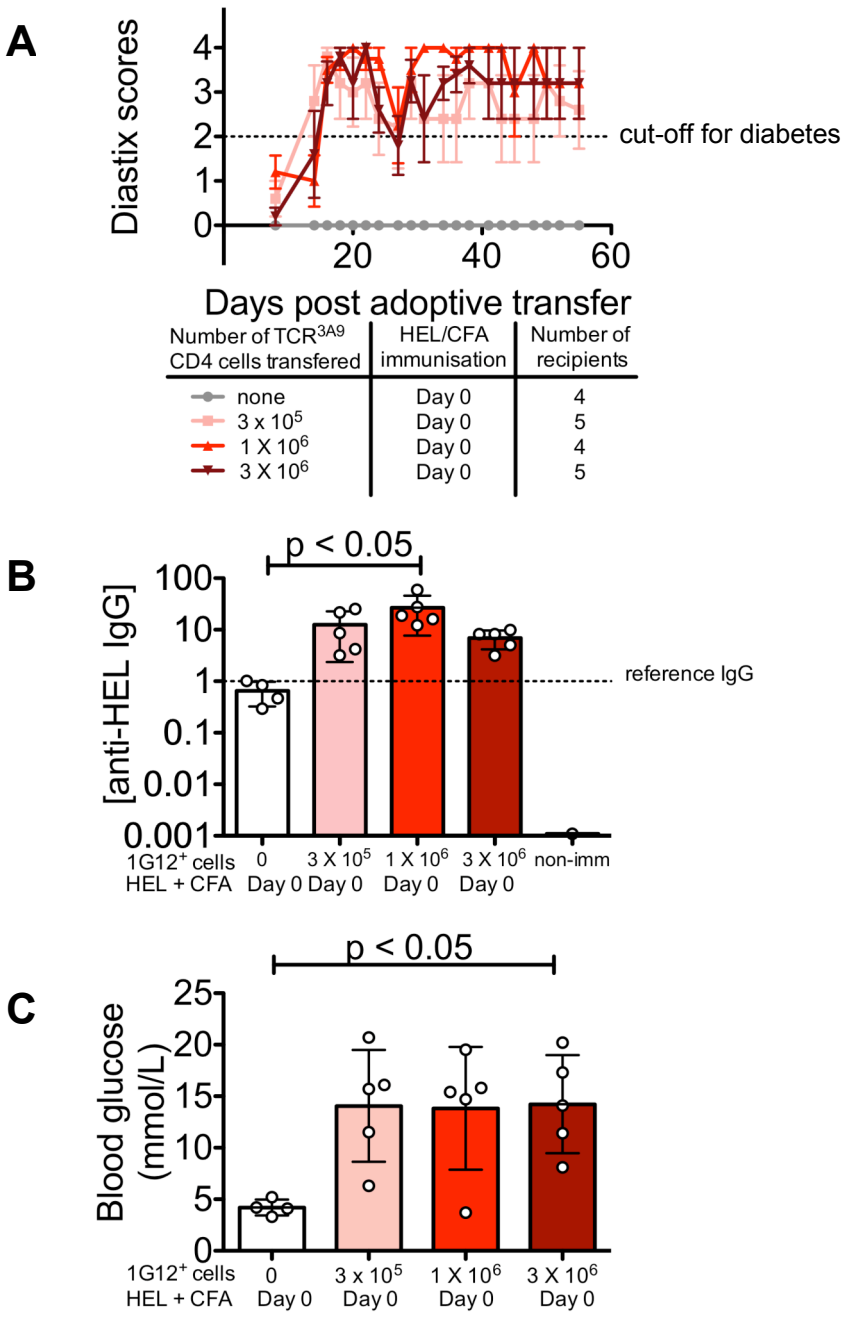

Figure 4.37 Effect of titrating the number of donor TCR^{3A9}CD4 cells to be used for an adoptive transfer model of islet destruction.

A. The indicated numbers of CD4-enriched splenocytes from TCR^{3A9} transgenic mice were intravenously injected into insHEL-transgenic recipients which then received 200 µg HEL protein emulsified in CFA intraperitoneally on day 0. Glucosuria was monitored twice a week and mice were considered diabetic after two subsequent positive readings (Diastix score of ≥2).

B. Measurement of HEL-specific IgG in the serum of mice in day 36. Concentrations are expressed in arbitrary units relative to reference anti-HEL IgG serum from the Porthos IgG^{HEL} transgenic strain.

C. Measurement of blood glucose in the mice on day 36.

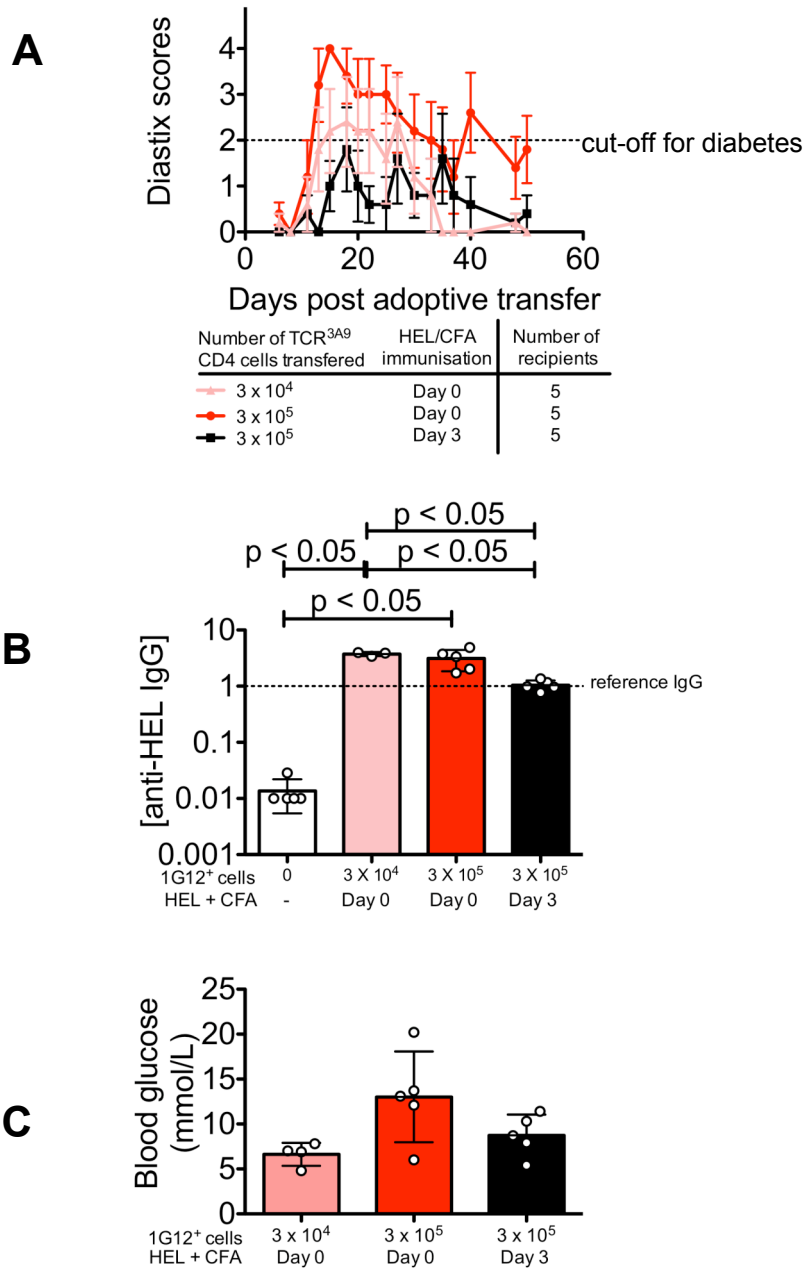

Figure 4.38 Effect of delaying HEL+CFA injection after adoptive transfer of islet-specific TCR^{3A9}CD4 cells.

A. The indicated numbers of CD4-enriched splenocytes from TCR^{3A9} transgenic mice were intravenously injected into insHEL-transgenic recipients which then received 200 µg HEL protein emulsified in CFA intraperitoneally on day 0 or day 3. Glucosuria was monitored twice a week and mice were considered diabetic after two subsequent positive readings (Diastix score of ≥2).

B. Measurement of HEL-specific IgG in the serum of mice on day 50. Concentrations are expressed in arbitrary units relative to reference anti-HEL IgG serum from the Porthos IgG^{HEL} transgenic strain.

C. Measurement of blood glucose in the mice on day 50.

examine the effects of *Aire*- and *Cblb*-deficiencies on pancreatic islet destruction mediated by limiting numbers of CD4 T cells.

The experimental design established above was next used to compare $Cblb^{-/-}$ deficient TCR^{3A9} CD4 cells with *Cblb*–wild-type controls, after transfer into insHEL-transgenic recipients that were either *Aire*-deficient or *Aire*-wild-type creating 7 different groups. Most of the recipients were immunized with HEL in CFA, but a subset was immunized at the time of T cell transfer (day 0). The groups immunized on day 0 developed comparable urine glucose scores in the following weeks when they received 3×10^5 TCR^{3A9} CD4 cells that were either $Cblb^{-/-}$ deficient or *Cblb*-wildtype (Fig. 4.39). In the groups where immunization was delayed, there also appeared to be no difference in the induction of glucosuria between groups of recipients receiving $Cblb^{-/-}$ deficient or *Cblb*-wild-type T cells, nor between groups of recipients that were *Aire*-deficient or *Aire*-wild-type. Hyperglycemia >15mM occurred only in the experimental group comprising *Aire*-deficient recipients of $Cblb^{-/-}$ deficient T cells: in two of the four animals on day 14 and one of the four on day 36 (Fig. 4.40*B*) consistent with the time course results of glucosuria detection in Fig. 4.39. There were no detectable differences in HEL-specific IgG antibodies in the serum of mice from all groups receiving TCR^{3A9} cells (Fig. 4.40*A*). Thus, even under the pressure of acute stimulation by antigen in adjuvant, combining *Aire* and *Cblb* defects did not display a significant co-operative effect leading to the breakdown of peripheral CD4 T cell tolerance to pancreatic islet beta cells, although there was a possible trend to precipitate diabetes in a subset of animals that would require further analysis in much larger experimental groups than were available for these preliminary studies.

4.6 Chapter summary and key findings

4.6.1 Changing the strain background from B10.BR $H2^k$ to C57BL/6 $H2^b$

The experiments in this chapter aimed to understand the pattern of autoimmune disease that occurred spontaneously in $Aire^{-/-}Cblb^{-/-}$ double-deficient mice. The experiments in the first section tested the hypothesis that variations in the efficiency of antigen presentation by MHC molecules determined the spectrum of organs targeted in an

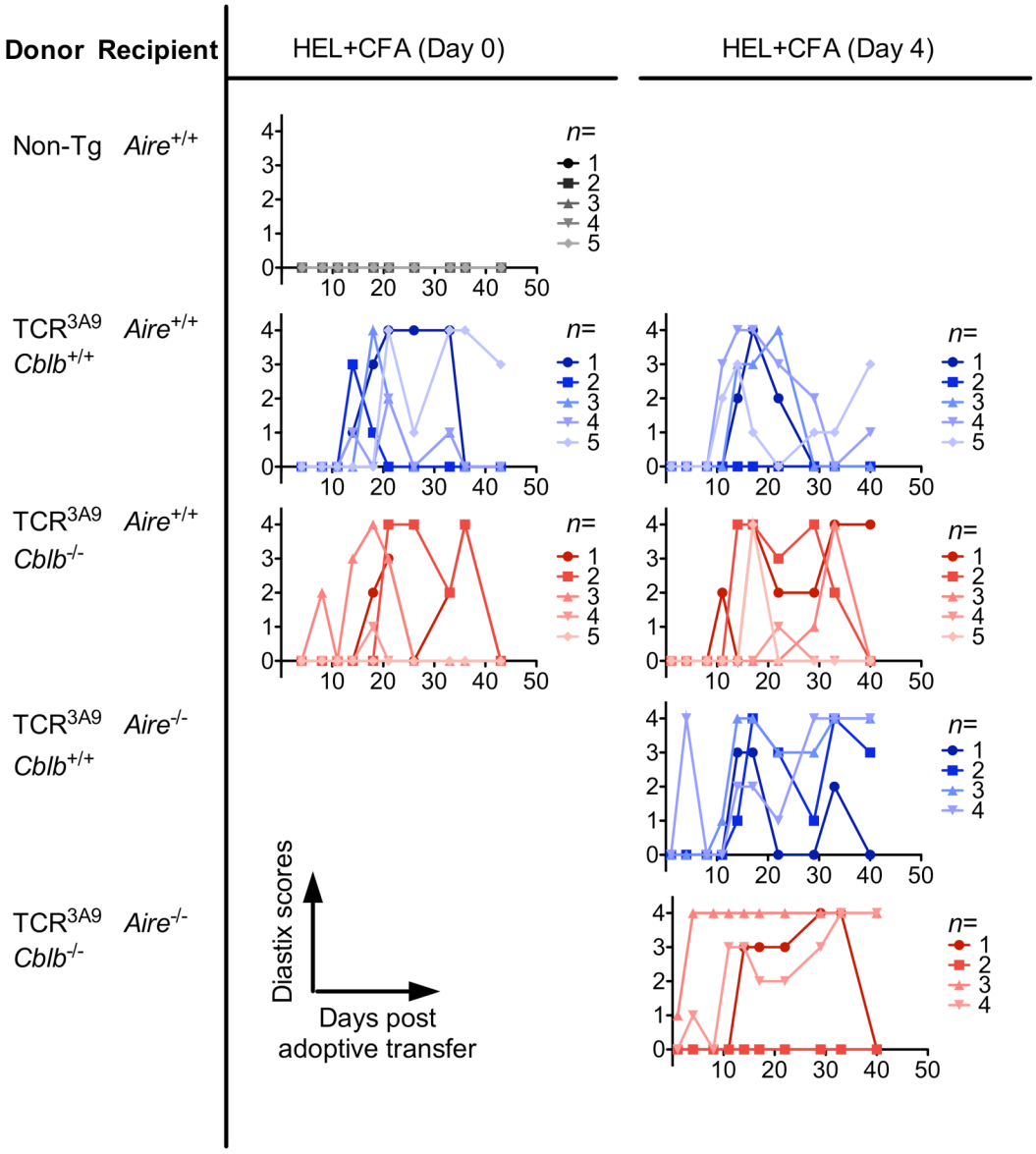

Figure 4.39 *Aire* and *Cblb*-deficiencies have little effect on islet destruction by TCR^{3A9}CD4 T cells.
3x10^5 of CD4-enriched splenocytes from TCR^{3A9} *Cblb*$^{+/+}$ or TCR^{3A9} *Cblb*$^{-/-}$ transgenic mice were injected intravenously into *Aire*$^{+/+}$ or *Aire*$^{-/-}$ insHEL-transgenic recipients which then received 200 µg HEL protein emulsified in CFA intraperitoneally on day 0 or 4. Glucosuria was monitored twice a week and mice were considered diabetic after two subsequent positive readings (Diastix score of ≥2).

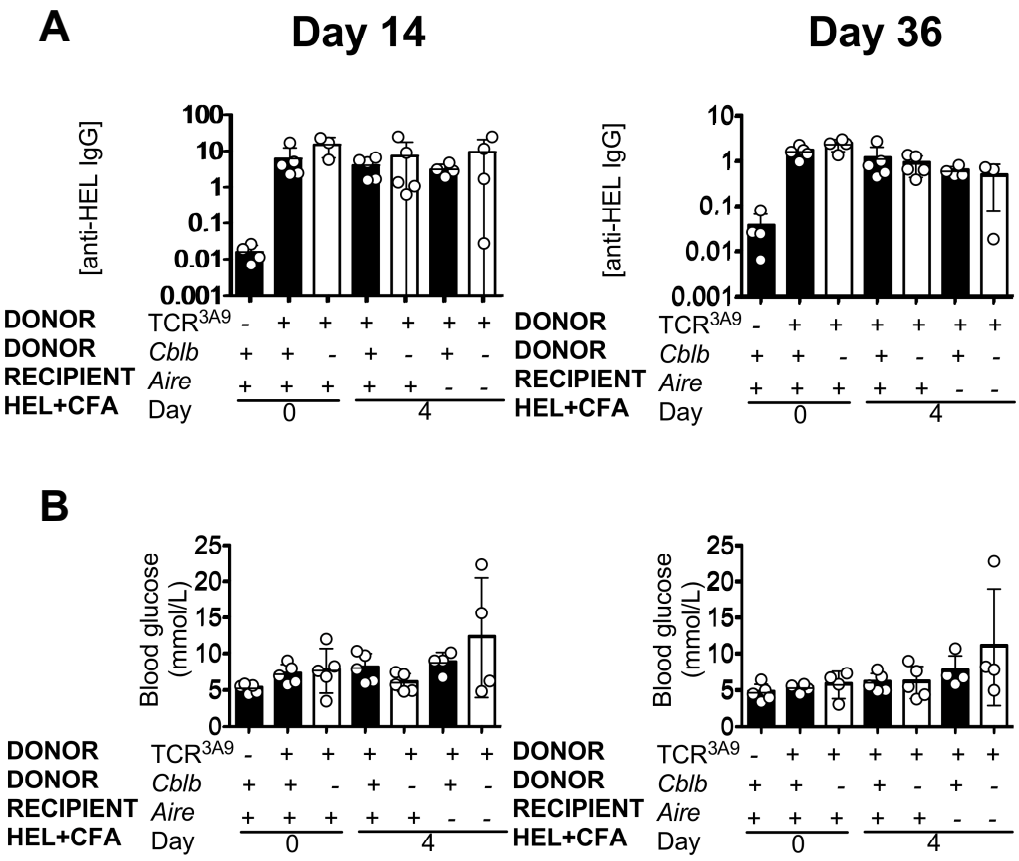

Figure 4.40 *Aire* and *Cblb*-deficiencies have little effect on autoantibody (HEL-specific IgG) formation or islet destruction by TCR^{3A9}CD4 T cells.

A. Measurement of HEL-specific IgG in the serum of mice on days 14 and 36.

B. Measurement of blood glucose in the mice on days 14 and 36.

autoimmune disease. As a test, the MHC of the *Aire*- and *Cblb*-deficient mice was changed from $H2^k$ haplotype, with *k* alleles of Class II I-A & I-E and Class I molecules K, D & L, to the $H2^b$ haplotype, with the alleles K^b, $I\text{-}A^b$, $I\text{-}E^{null}$, D^b, L^{null}. Surprisingly, the change in MHC haplotype did not change the organs that were targeted by spontaneous autoimmune disease, but it reduced the incidence, intensity and severity of pancreatitis. There are several possible explanations for the differing severity but not specificity of autoimmune disease in *Aire*- and *Cblb*-deficient mice with the two MHC haplotypes. These explanations could be broadly divided into differences in MHC:peptide interactions between the strains (section 4.6.1.1) and non-MHC differences (section 4.6.1.2).

4.6.1.1 Differences in MHC:peptide-dependent interactions

Firstly, it is possible that the MHC molecules encoded by $H2^k$ and $H2^b$ may both present the same driver autoantigen(s) from the pancreas and salivary glands, resulting in autoimmunity in the same organs, but the efficiency of presentation varied between the two MHCs. It is possible that thymic presentation of the driver antigen(s) on the MHC molecules encoded by the susceptible $H2^k$ MHC molecule interacted highly efficiently with the driver T cell. In the thymus, this more efficient interaction would have resulted in more efficient positive selection of the driver T cells. In the periphery, the highly efficient $H2^k$ MHC:driver T cell interaction would provoke more severe autoimmune disease in the $Aire^{-/-}Cblb^{-/-}$ mice. Mathis and colleagues have demonstrated that T cells recognising the HEL_{46-61} peptide in the context of MHC Class II were strongly selected when both A^{α} and A^{β} MHC molecules were derived from the CBA $H2^k$ genetic background, but not the C57BL/6 $H2^b$ genetic background (Tourne et al., 1999), highlighting the particular MHCs can be more efficient for positive selection of the particular T cells.

The reverse is also equally likely, where the same "driver antigen could be less efficiently presented by MHC molecules encoded by susceptible $H2^k$ compared to $H2^b$, resulting in less efficient presentation of the driver-antigens for peripheral tolerance - the classical *Ir* (Immune response)-gene effect (McDevitt and Chinitz, 2004; McDevitt and Sela, 1965). It would be interesting to test this further on other MHC backgrounds

such as the B10.NOD-*H2*^{g7} background (*H2*^{g7} haplotype, encoding K^{d}, I-A^{g7}, I-E^{null}, D^{b}, L^{null}). The NOD *H2*^{g7} haplotype is of particular interest because lethal exocrine pancreatitis occurred when *Aire*-deficiency was bred to the NOD strain background, and on this background homozygosity for *H2*^{g7} caused a high incidence of the disease whereas heterozygosity or homozygosity for *H2*^{b} was powerfully protective (Jiang et al., 2005). The dominant behaviour of the resistant *H2*^{b} haplotype in the *Aire*-/- NOD.*H2*^{g7} × *H2*^{b} cross would be consistent with the *Ir* (Immune response)-gene effect.

Other examples of weakened or less efficient MHC:peptide-TCR interactions are those where one of two weakening mutations in the driver peptides result in major changes in tolerance and autoimmunity. For example, the hemagglutinin-specific CD4 that is usually fully activated is induced into a long-lived tolerant state by an alanine to serine substitution (Sloan-Lancaster et al., 1993). Another example is that a natural polymorphism in the insulin gene promoter that causes only a twofold to threefold decrease in thymic insulin gene expression but is strongly linked to diabetes susceptibility (Pugliese et al., 1997; Vafiadis et al., 1997). Similarly, a splice variant in proteolipid protein lacking the 116-151 region in thymus results in high frequencies of PLP-specific cells in the peripheral repertoire, increasing experimental autoimmune encephalitis susceptibility (Anderson et al., 2000). In theory, this weakened peptide:MHC interaction cause by mutations in the peptide would have the same effect as a weakened interactions caused by the present of absence of particular MHC alleles in different strains, suggesting that less efficient binding of peptide:MHC to driver T cells could cause rapid autoimmunity.

Explanation of the MHC haplotype effects along these lines must also take into account the finding in the previous chapter that both CD8 and CD4 cells were required to transfer pancreatitis from *Aire*- and *Cblb*- double-deficient mice into lymphopaenic recipients, anticipating a role for MHC I and MHC II molecules. To examine the role of specific MHC I and MHC II molecules, it would be interesting to cross the *Aire*- and *Cblb*-deficiencies onto C57BL/6 mouse strains with MHC Class I mutations (eg *K*^{bm1}) or MHC Class II mutations (eg *I-A*^{bm12}). If the severity of pancreatitis persist in the presence of the MHC Class I mutation or MHC Class II mutation, it would suggest that

the driver antigen is presented in the context of MHC Class I or MHC Class II, respectively.

4.6.1.2 Differences in MHC:peptide-independent susceptibility loci

A complexity in the MHC congenic crosses is the possibility that any disease suppression might result from differences in immune regulatory genes on the different C57BL/6 and C57BL/10 backgrounds. Although genetically, the strains should have very little genetic variation except at the MHC loci, these strains have been maintained as separate lines for many generations, making it plausible that they have accumulated single nucleotide polymorphisms or genetic variations in other immune regulatory genes that might influence the timing of disease onset. These variations in non-MHC immune regulatory loci could be detected by performing an *Aire*$^{-/-}$*Cblb*$^{-/-}$ B10.BR *H2*^{k} and C57BL/6 *H2*^{b} intercross. If the pancreatitis and sialoadenitis susceptibility occurred in the F1 *H2*^{kb} offspring, the dominant susceptibility effect would be consistent with effects of MHC alleles presenting the autoantigen(s) more efficiently to induce autoimmunity in the periphery. However, if the susceptibility is absent in F1 offspring but present in a minor selection of F2 offspring (recessive susceptibility), it could be indicative of less efficient presentation by the *H2*^{k} MHC for central and peripheral tolerance, which is usually recessive. Alternatively, as the F2 offspring also contain random shuffles of the B10.BR and C57BL/6 genomes at this stage, a genome wide scan could be performed to samples DNA from pancreatitis or sialoadenitis susceptible mice to identify susceptible non-MHC alleles that contribute towards development of pancreatitis of sialoadenitis. An F2 cross performed between the NOD.*Aire*$^{-/-}$ pancreatitis prone strain and the non-pancreatitis prone C57BL/5.*Aire*$^{-/-}$ strain established five regions that were responsible for pancreatitis, none of which spanned the *Cblb* gene (Jiang et al., 2005). This result, however demonstrated that the combination of *Aire*$^{-/-}$ and other genetic homozygous genetic deficiencies, perhaps in the same pathway as the *Cblb* gene, could precipitate rapid pancreatitis.

A second possible explanation for the MHC effects is that entirely different driver autoantigen peptides are being presented by the *H2*^{k} and *H2*^{b} haplotypes, but some other factor accounts for the targeting of autoimmunity against the exocrine pancreas in both strains. For example, the content of digestive enzymes in the exocrine pancreas and

salivary gland acinar cells could serve as an inflammatory co-factor that serves as a positive feedback when rare autoreactive T cells become activated. In support of this possibility, inspection of the $H2^k$, $H2^{g7}$ and $H2^b$ haplotypes reveals no shared classical MHC molecules between the first two pancreatitis susceptible haplotypes. Likewise, the exocrine pancreas is also a major target of spontaneous autoimmune disease in BALB/c ($H2^d$) mice that lack CTLA-4 (Ise et al., 2010; Waterhouse et al., 1995). However, the same highly abundant, pancreas-specific autoantigen – PDIA2 – has been identified as a target autoantigen in *Ctla4*-deficient BALB/c mice and in *Aire*-deficient NOD mice (Ise et al., 2010; Niki et al., 2006). Clearly, a key issue for future studies is to identify the driver autoantigen(s) in $H2^k$ $Aire^{-/-}Cblb^{-/-}$ double-deficient mice.

4.6.2 Effect of T cell frequency in the primary repertoire using transgenic mice.

This chapter also tested a second, related *repertoire/presentation* hypothesis to explain the pattern of autoimmunity in $Aire^{-/-}Cblb^{-/-}$ double-deficient mice: that the targeting of the exocrine pancreas and submandibular salivary gland reflects an underlying elevated frequency of T cells produced in the thymus that happen to have TCRs that recognize an autoantigen that is abundant in these cell types. This hypothesis was tested by breeding the *Aire*- and *Cblb*-deficiencies to a TCR:insHEL double-transgenic strain that produced high frequencies of a CD4 T cells that recognised an efficiently presented $HEL_{45\text{-}61}$/I-A^k complex expressed in the endocrine pancreas beta cells. This increased the precursor frequency of self-reactive CD4 T cells, but recognizing the endocrine islets instead of the exocrine acinar cells in the pancreas. Double transgenic mice devoid of both *Aire* and *Cblb* were protected from exocrine pancreatitis, establishing that specific T cells against the exocrine acinar cells are required for this spontaneous disease. However, there was no drastic acceleration of diabetes development in *Aire*- and *Cblb*- double-deficient mice with the high frequency of islet-reactive T cells compared to counterparts with single deficiency of *Aire* or *Cblb*. Although introducing high frequencies of TCR^{3A9} cells into insHEL recipients could result in severe insulitis instead of pancreatitis and TCR^{3A9} cells have been shown to be regulated by both *Aire* and *Cblb* individually (Hoyne et al., 2011a; Liston et al., 2003), the spontaneous autoimmunity in $Aire^{-/-}Cblb^{-/-}$ TCR^{3A9}:insHEL mice did not display the strong epistatic

co-operation of *Aire*- and *Cblb*- deficiencies observed in the pancreatitis prone *Aire*$^{-/-}$ *Cblb*$^{-/-}$ non-transgenic mice.

One explanation for the failure to redirect the specificity of robust autoimmunity in the TCR^{3A9} transgenic mice is that the antigen is highly efficiently presented in the thymus and periphery to induce tolerance. It would be interesting to extend the experimental approach by breeding *Aire*$^{-/-}$*Cblb*$^{-/-}$ to the TCR7 transgenic strain, which produces high frequencies of CD4 T cells recognizing a sub-dominant HEL$_{74-88}$ peptide that is less efficiently presented by I-A^b. TCR7 T cells do not encounter sufficient peptide in TCR:insHEL animals to be deleted within the thymus. Whereas peripheral 3A9 T cells transferred into insHEL transgenic mice are triggered into an abortive cycle of proliferation and activation-induced cell death (AICD) or anergy, there is insufficient pMHC in pancreatic lymph node to activate TCR7 cells. In insHEL$^+$ mice, the TCR7 cells develop in a state of "immunological ignorance" representative of many T cells that recognize self-pMHC with too low an abundance or avidity for actively acquired tolerance. In contrast to the TCR^{3A9}:insHEL strain that develops diabetes spontaneously, this TCR7:insHEL strain is resistant to diabetes development unless it is coupled to a simultaneous block in CTLA-4 signalling (Neighbors et al., 2006). The strain thus would serve as a valuable transgenic model to analyse the co-operation between tolerance defects where the driver antigen is inefficiently presented.

Another explanation for the failure to redirect autoimmunity in the TCR^{3A9} transgenic is that the autoreactive repertoire was only enriched for CD4 cells, whereas the adoptive transfer experiments in chapter 3 demonstrated that both CD4 and CD8 cells were necessary to precipitate the lethal pancreatitis seen in non-transgenic *Aire*$^{-/-}$*Cblb*$^{-/-}$ mice. It would thus be valuable to extend the transgenic experiments to include a TCR that recognizes an MHC I-restricted islet autoantigen, such as the TCR^{OT-1} transgenic strain where many CD8 cells would recognise the ovalbumin peptide SIINFEKL complexed with the Class I protein, K^b (Hogquist et al., 1994). The OVA self-antigen could be presented in the islets under the control of the rat-insulin promoter (Kurts et al., 1996). This system would provide valuable insight to determine if changes in driver autoreactive precursor CD8 cells were able to redirect spontaneous autoimmunity to the endocrine pancreas when *Aire* and *Cblb* were deficient. Since single deficiency for *Aire*

precipitates diabetes within a few days after birth in TCR^{OT-1} × Rip-OVA transgenic mice (Anderson et al., 2005) the experiments would require lowering the frequency of islet-reactive CD8 cells using mixed bone marrow chimeras.

A third explanation for the failure to redirect autoimmunity in the TCR^{3A9}:insHEL transgenic animals was suggested by the results of the flow cytometric analyses in this chapter, which showed that islet-reactive CD4 T cells remained quiescent in the pancreatic node of *Aire*$^{-/-}$*Cblb*$^{-/-}$ double deficient chimeras, despite escaping thymic deletion and having an intrinsically lower activation threshold. Since the peripheral transfer experiments demonstrate that insHEL is being presented in the draining node in a way that can promote T cell activation, these T cells appeared to be kept quiescent by other mechanisms. It may be that the driver T cells that recognize the exocrine pancreas in *Aire*$^{-/-}$*Cblb*$^{-/-}$ double deficient mice are not able to be controlled by these other mechanisms, due either to some special characteristic of the autoantigen they recognize or the exocrine pancreas as discussed above. Rather than attempt to emulate these factors with available TCR transgenic mice, a better strategy to understand how *Aire*$^{-/-}$ and *Cblb*$^{-/-}$ interact to precipitate lethal autoimmunity devoid of a latent period would be to isolate the driver T cells themselves and use their TCRs to construct transgenic animals. The following chapter will describe efforts to isolate the exocrine pancreas-specific T cells responsible for spontaneous disease in the *Aire*$^{-/-}$*Cblb*$^{-/-}$ mice, and begin tracing their control by AIRE and CBL-B in TCR retrogenic mice.

Chapter 5

Clonal expansion of pancreas-specific T cells in *Aire*$^{-/-}$*Cblb*$^{-/-}$ mice

Acknowledgements of assistance in the work described in this chapter: Mice were genotyped for Cblb by the Australian Phenomics Facility. For the analysis of plates in section 5.2, DNA sequence traces for 10/29 plates were translated by Nadine Barthel (IGL technical staff) and 1/29 were translated and assigned to unique TCRαs or TCRβs by Mandeep Singh (IGL PhD student). All hematoxylin and eosin section cutting and staining was done by Ms. Anne Prins (Flow Cytometry and Microscopy, John Curtin School of Medical Research).

5.1 Preamble

The previous chapter explored the hypothesis that the acinar pancreas- and submandibular salivary gland-specific autoimmunity in *Aire*$^{-/-}$*Cblb*$^{-/-}$ mice was due to variations in the frequency of T cells that recognise different autoantigens. However, varying either the MHC in which the T cells were selected upon or increasing the precursor frequency of self-reactive CD4 T cells against the pancreatic islets using transgenic mice altered the incidence but failed to change the specificity of the autoimmunity. These results indicate that there is something unique about the antigen(s), tissues or T cells that escape tolerance in *Aire*$^{-/-}$*Cblb*$^{-/-}$ mice. This chapter analyses the T cells responsible for autoimmunity in the *Aire*$^{-/-}$*Cblb*$^{-/-}$ mice, and establishes an experimental system to determine their specificity and track their fate in wild-type animals.

To enrich for the T cells responsible for exocrine pancreatitis or sialoadenitis in *Aire*$^{-/-}$ *Cblb*$^{-/-}$ mice, I made use of the finding in Chapter 3 that spleen cells could adoptively transfer the disease into lymphopaenic *Rag1*-deficient mice. When normal T cells are transferred into *Rag1*-deficient recipients, the T cells proliferate in two characteristic phases. Initially, rapid expansion occurs in a subset of T cells which are driven to proliferate by gut commensal antigens (Kieper et al., 2005). There is also a slower homeostatic proliferation of clones driven by self-MHC restricted T cells (Ernst et al., 1999; Goldrath and Bevan, 1999; Moses et al., 2003). Based on the rapid onset of pancreas destruction after adoptive transfer, it was assumed that the pancreas-damaging T cells would rapidly proliferate in the *Rag1*-deficient recipients, forming larger clones than any triggered by homeostatic proliferation, and preferentially accumulate in the pancreas. By conducting serial adoptive transfers of T cells obtained from the pancreas of *Aire*$^{-/-}$*Cblb*$^{-/-}$ mice, it would therefore be possible to enrich for the T cell(s) against the driver autoantigen(s) in *Aire*$^{-/-}$*Cblb*$^{-/-}$ mice.

The serial transfer strategy was combined with a powerful new approach to analyse individual T cells in immune or autoimmune responses by a multiplex RT-PCR method that simultaneously amplifies the TCRα and TCRβ chains from single T cells (Dash et al., 2011). This method was selected as it allowed for an unbiased analysis of the clonal

diversity and recurring motifs by looking at the complete nucleotide sequence of the TCRα and TCRβ in single cells. It also enabled specific TCRs to be cloned and expressed in retrogenic mice (Holst et al., 2006a; Holst et al., 2006b; Lennon et al., 2009), opening up a way to analyse their antigen specificity and regulation by Aire and Cbl-b.

5.2 TCR profiling of original donor, primary and secondary recipients from serial adoptive transfers of *Aire*$^{-/-}$*Cblb*$^{-/-}$ and wild-type cells

5.2.1 Serial transfer system to enrich pancreas-reactive T cells from using bone marrow chimeric *Aire*$^{-/-}$*Cblb*$^{-/-}$ mice

The *in vivo* serial adoptive transfer assay to enrich for autoimmune driver T cells in exocrine pancreatitis is shown systematically in Fig, 5.1. In the experiment described in this section, the original donor mice were bone marrow chimeras. Two chimeric *Aire*$^{-/-}$ recipients of *Cblb*$^{-/-}$ bone marrow (termed MUT1 and MUT2 donors) and two corresponding chimeric wild-type recipients of wild-type bone marrow (termed WT1 and WT2 donors) were used. Cells from each of the four original donors were transferred separately to different recipients, although it is important to note that the donor chimeras were constructed from the same *Cblb*$^{-/-}$ or wild-type bone marrow.

Cells were harvested for the primary transfer six weeks after bone marrow reconstitution, by which time the MUT donor chimeras had developed exocrine pancreatitis while the WT donor mice were free of pancreatic lymphocyte infiltration (Fig. 5.2). Both CD4 and CD8 cells were detected in the pancreas of MUT donor mice, with a CD4/CD8 ratio of 2 (MUT1:7.44%/3.55% ; MUT2: 11.9%/5.76%), while spleen from WT mice showed a CD4/CD8 ratio of 3 (WT1: 9.08%/2.95%) and 2.6 (WT2: 8.74%:3.06%), respectively (Figure 5.3*A*). For the primary transfer, 0.5×10^6 pancreas-infiltrating lymphocytes (P_0 cells) isolated from MUT donors or 2×10^6 splenocytes (S_0 cells) isolated from WT counterparts were injected into the bloodstream of individual *Rag1*-deficient recipients.

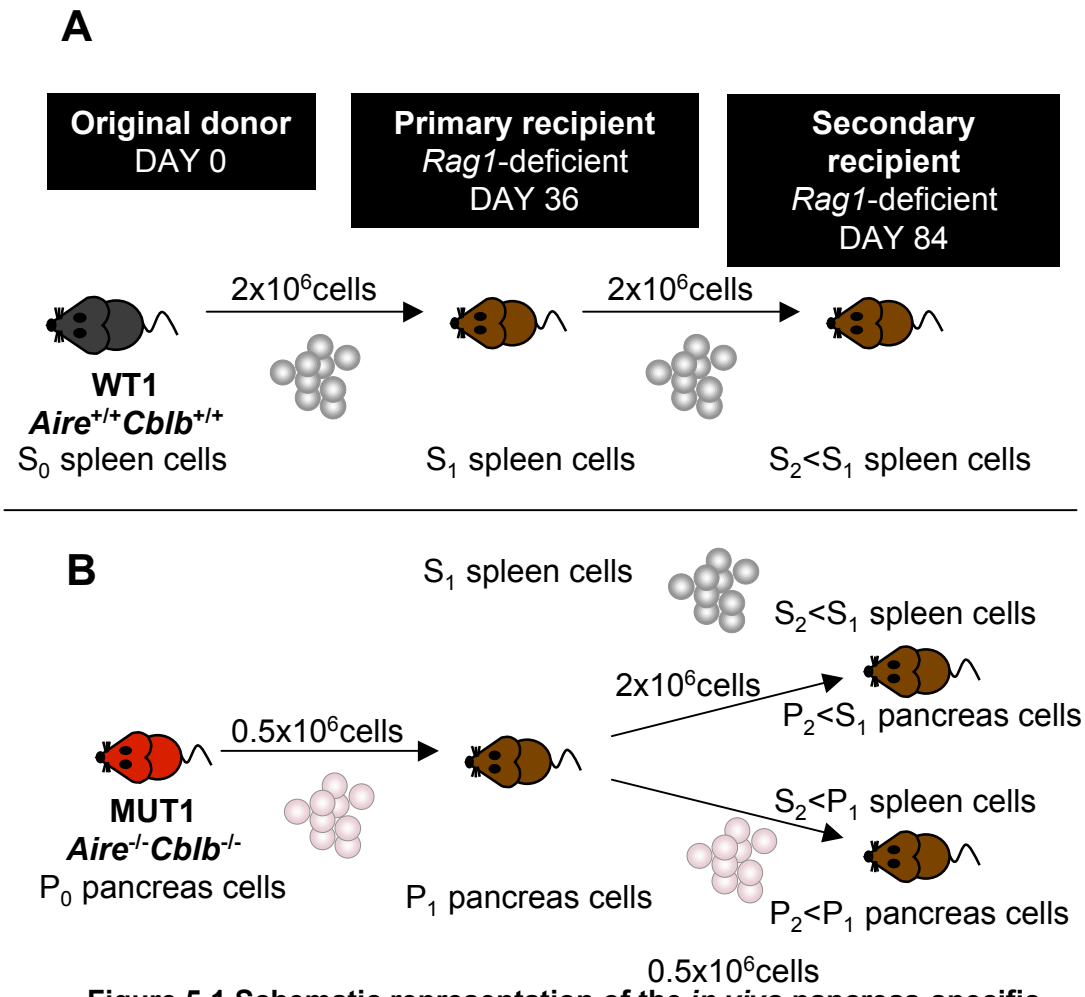

Figure 5.1 Schematic representation of the *in vivo* pancreas-specific T cell enrichment assay.

A. $2x10^6$ splenocytes from wild-type recipients of wild-type bone marrow were adoptively transferred into primary *Rag1*-deficient recipients

B. Half of the pancreas infiltrating lymphocytes from *Cblb*$^{-/-}$ recipients of *Aire*$^{-/-}$ bone marrow were adoptively transferred into primary *Rag1*-deficient recipients. When the *Aire*$^{-/-}$*Cblb*$^{-/-}$ recipients began to lose weight, $2x10^6$ splenocytes and one third of the pancreas infiltrating lymphocytes were harvested and transferred to a second group of *Rag1*-deficient recipients.

For both A. and B. single cells from all groups were sorted for muliplex sequencing analysis. 0, original donors; 1, primary recipients; 2, secondary recipients; P, pancreas; S, spleen. For secondary recipients, the first letter indicates the organs the cells were recovered from while the second letter indicates origin of the transferred cells.

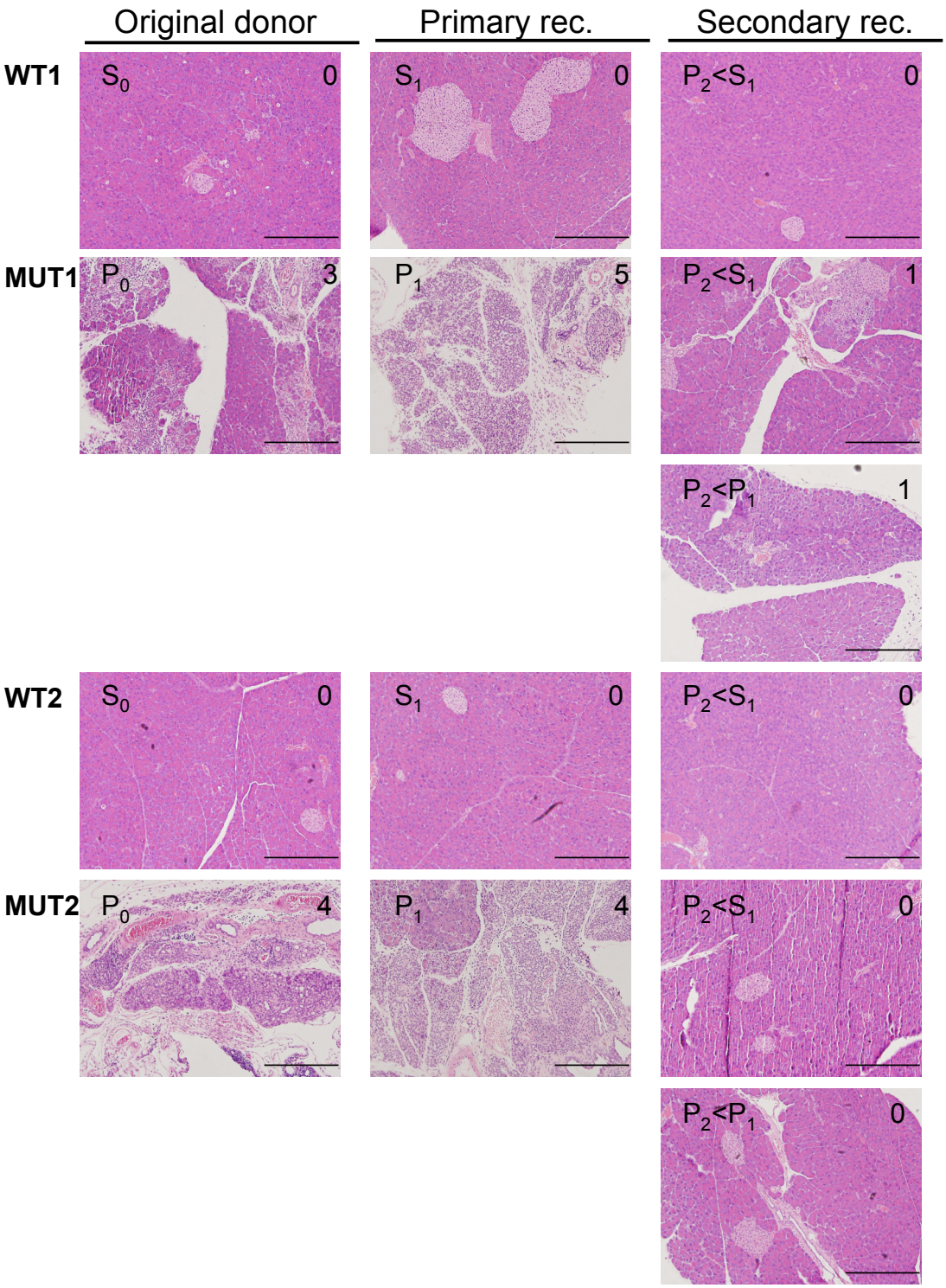

Figure 5.2 Hematoxylin and eosin sections of the pancreas of mice of Figure 5.1 at time of takedown.
Images were taken at x100 magnification and bars represent 500 μm. The respective pancreatitis scores are quantified and listed at the top right corner of each image. 0, original donors; 1, primary recipients; 2, secondary recipients; P, pancreas; S, spleen. For secondary recipients, the first letter indicates the organs the cells were recovered from while the second letter indicates origin of the transferred cells.

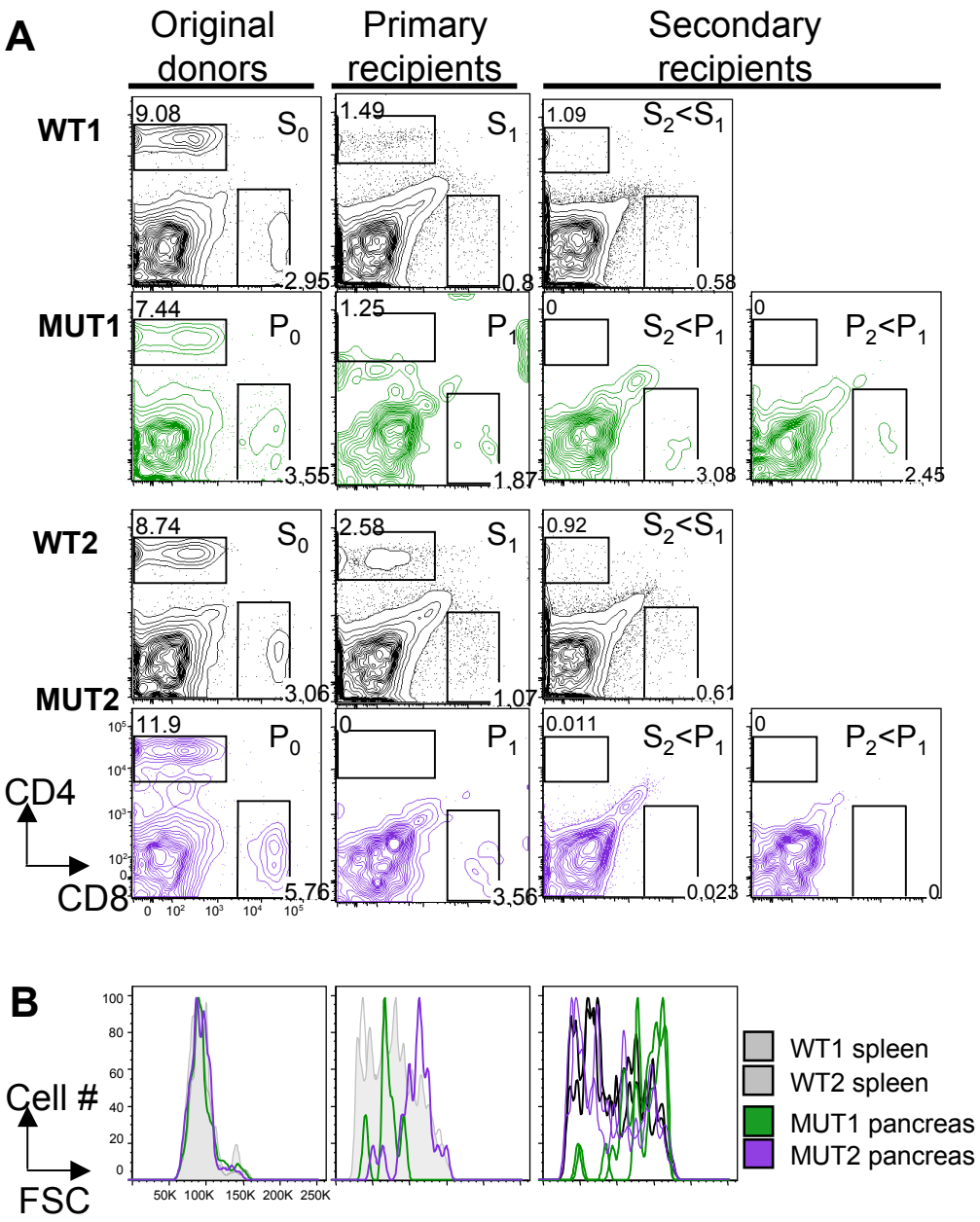

Figure 5.3 Flow cytometric plots and histograms of lymphocytes from mice used in the single cell sorts.

A. CD4 and CD8 cells from total lymphocytes in spleen and pancreas of recipient mice. 0, original donors; 1, primary recipients; 2, secondary recipients; P, pancreas; S, spleen. For secondary recipients, the first letter indicates the the organs the cells were recovered from while the second letter indicates origin of the transferred cells.

B. Forward side scatter on the CD8 cells in the pancreas of secondary recipients.

In the primary recipients, the animals that received MUT pancreas (P_0) cells began to display signs of rough coats and weight lost on day 36 of the experiment, whereas the recipients of WT spleen (S_0) cells remained healthy. The mice were sacrificed and spleen (S_1) and pancreas (P_1) were harvested. Consistent with their weight loss, the MUT1 and MUT2 primary recipient mice had developed severe pancreatitis with a score of ≥4, while no pancreatitis was present in the WT1 and WT2 primary recipients (Fig. 5.2). The pancreatic infiltration in MUT1 comprised of both CD4 and CD8 cells, while only CD8 cells were detected in MUT2 (Fig. 5.3*A*). From each primary recipient 2×10^6 S_1 spleen cells were transferred to each secondary *Rag1*-deficient recipient. As the numbers of pancreatic infiltrating cells recovered from each MUT primary recipient mice varied, each pancreas was divided into three portions – 1/3 for histological analysis, 1/3 for single cell sorting and 1/3 was used to prepare pancreatic lymphocytes (P_1 cells) that were injected into the circulation of single *Rag1*-deficient secondary recipients.

The secondary recipients were sacrificed 48 days following secondary transfer, before gross signs of weight loss had developed, with the aim of catching the early infiltrating T cells in the pancreas. The secondary recipients of MUT1 S_1 splenocytes or MUT1 P_1 pancreatic lymphocytes displayed mild pancreatitis with a score of 1, while no pancreatitis had developed in secondary recipients of MUT2 cells (Fig. 5.2). The pancreas of secondary recipients of WT cells remained free of infiltration. CD4 and CD8 T cells were present at the normal ratio in the spleen ($S_2<S_1$) of WT secondary recipients, while only CD8 cells were detected in spleen ($S_2<P_1$) and pancreas ($P_2<P_1$) of the MUT1 secondary recipients and in the spleen ($S_2<P_1$) of the MUT2 secondary recipient. Additionally, the CD8 cells that were detected within the pancreas ($P_2<P_1$) of the MUT1 secondary recipient appeared to be larger as indicated by an increase in forward scatter of the cells (Fig.5.3*B*).

Single CD4 and CD8 cells were sorted for TCR sequencing from the original donors, and from the primary and secondary recipients. For all spleen and pancreatic lymphocyte samples from each mouse, 80 CD4 and CD8 cells were sorted unless lower numbers of cells were recovered. For the pancreas samples in primary and secondary recipients, all CD4 and CD8 cells that could be recovered were sorted.

5.2.2 Strategy for analysis of TCRα and TCRβ chains in single T cells from donors and recipients

The variable regions of individual TCRα and TCRβ chains from each sorted T cell were PCR amplified and sequenced. The work-flow for the process in shown systematically in Fig 5.4. The mRNA of sorted single cells was first reverse-transcribed into cDNA, and TCR-encoding cDNA was selectively amplified through two rounds of nested PCR with degenerate internal and external primer combinations. The first round amplified TCRα and TCRβ cDNAs together, and the second round amplified TCRα and TCRβ cDNAs separately. A total of 23 nested forward primers complementary to different T cell receptor alpha chain variable (*Trav*) sequences and 19 nested forward primers complementary to different T cell receptor beta chain variable (*Trbv*) sequences were coupled with single, nested reverse primers complementary to the 5' ends of the T cell receptor alpha chain constant region (*Trac*) and T cell receptor beta chain constant region (*Trbc*). The final PCR products were resolved by gel electrophoresis and were scored for successful amplification of TCRα, TCRβ or both (Fig. 5.5). For MUT1;WT1 and MUT2:WT2 combination a total of 669 (64.01% of total PCRs) and 573 (53.75% of total PCRs) samples, respectively, yielded products for both TCRα and TCRβ (Tables 5.1 and 5.2). The PCR products were Sanger sequenced by priming with the internal constant region reverse primers, yielding the unique VJ or VDJ junction sequences of the TCRα and TCRβ chains, respectively in each sorted single cell.

For each T cell, the T cell receptor alpha chain variable (*Trav*) and joining (*Traj*) segments, and the T cell receptor beta chain variable (*Trbv*) and joining (*Trbj*) segments were translated and assigned by comparison with known genomic sequences available from the International ImMunoGeneTics information system (IMGT) database (Giudicelli et al., 2006). The complementarity determining region three (CDR3) sequence and length were also determined. Sequences in which not all components could be assigned to a particular Trav/Traj or Trbv/Trbj were excluded from further analysis with some exceptions discussed in section 5.5.2. A caveat in this assignment is that some families of Trav elements display very similar 3' sequences close to the CDR3 region that was amplified, making it difficult to accurately assign it to a particular Trav. In instances where this occurred, two or more Travs were listed as

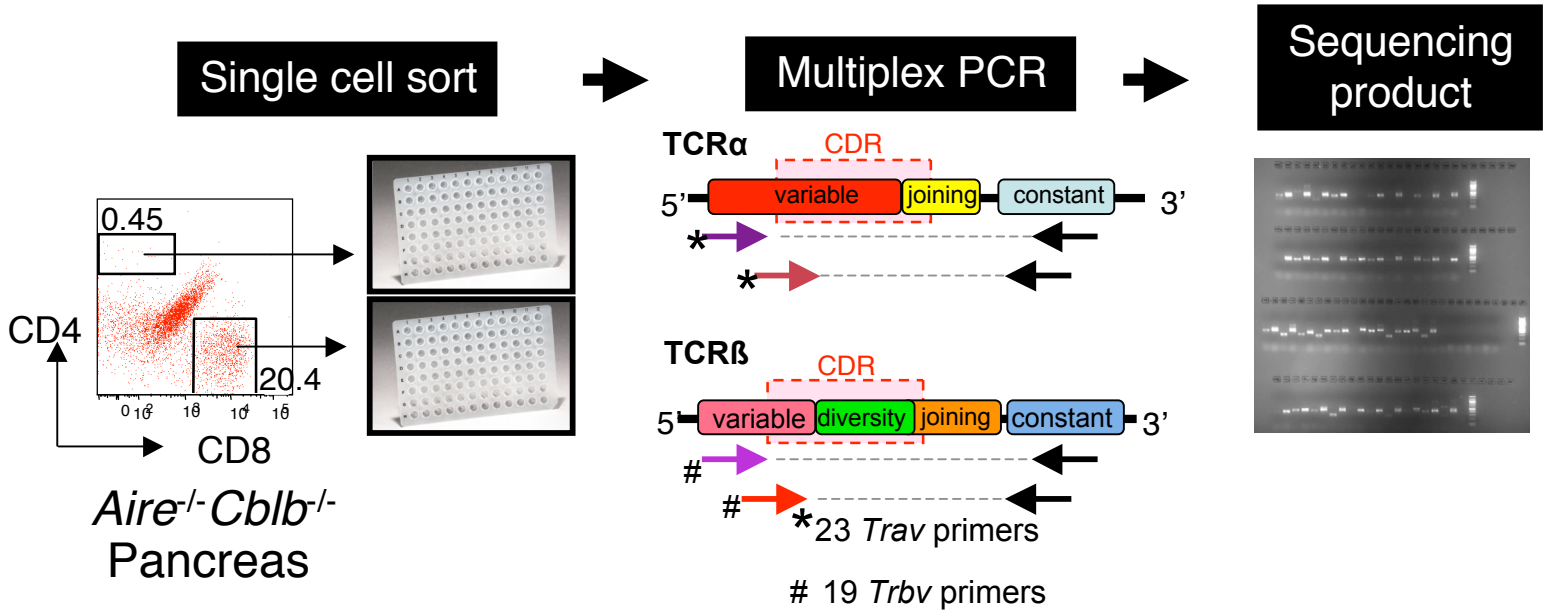

Figure 5.4 Illustration of the work flow for single cell sequencing of T cells from *Rag1*-deficient mice. CD4 and CD8 cells were singly sorted. cDNA was made from the mRNA in the cells. The cells were then subjected to two rounds of nested PCR using degenerate primers.The first round amplified both TCRα and TCRβ together, while the second round amplified TCRα and TCRβ separately. Products were electrophorised on a gel and subsequently sequenced.

A

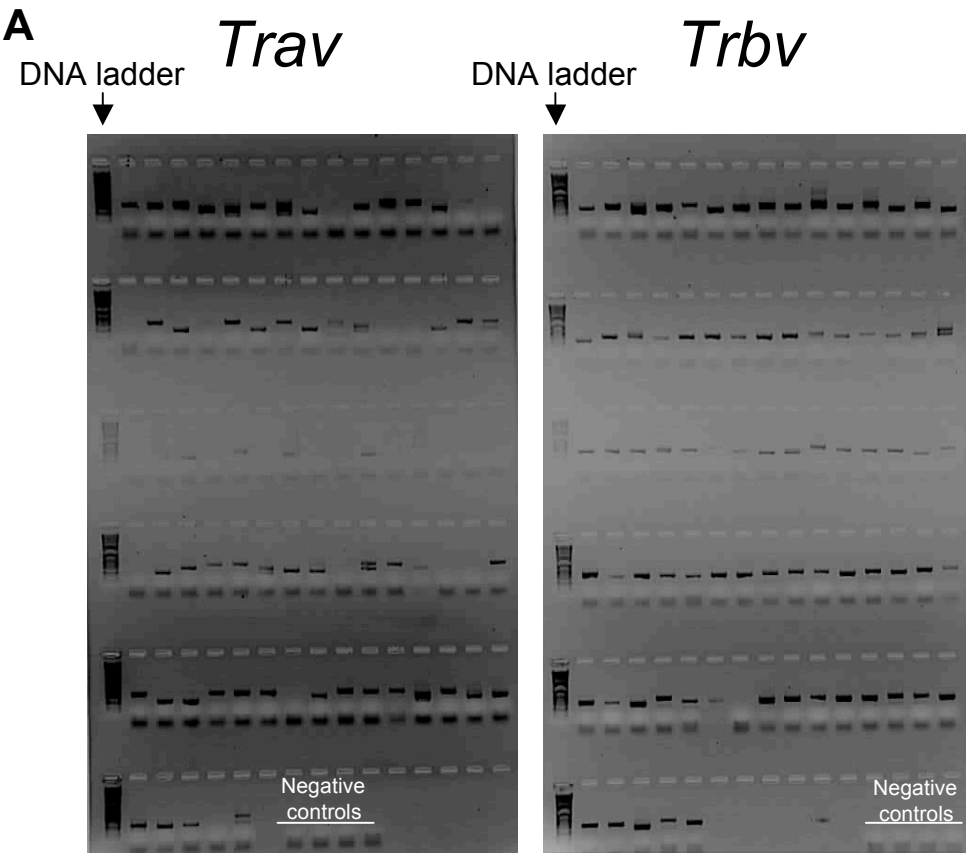

B

Chain	Frequency
Trav only	0/80
Trbv only	21/80
Trav* and *Trbv	**58/80**

Figure 5.5 Confirmation of product in single cell multiplex PCR reactions.

A. Resolution on a 2% agarose gel electrophoresis of the *Trav* (left) and corresponding *Trbv* (right) products from the single cell multiplex secondary nested PCR reaction. The negative controls are indicated on the gel. The 1kb DNA ladder is ran on the far left.

B. Score of the number of *Trav* and *Trbv* reactions which yielded a product on each plate. The products for each cell were sequenced only when both *Trav* and *Trbv* yeilded a product.

Table 5.1 Frequency of *Trav* and *Trbv* reactions that yielded a product for each sample from the WT1 and MUT1 mice. For secondary recipients, in instances where there are two fractions, the first fraction is recipients of S_1 and the second recipients of P_1.

Wild-type spleen

Plate	Chain	Frequency
CD4WT S_0	*Trav*	0/80
	Trbv	21/80
	Trav* and *Trbv	**58/80**
CD4WT S_1	*Trav*	1/20
	Trbv	4/20
	Trav* and *Trbv	**10/20**
CD4WT S_2	*Trav*	1/80
	Trbv	13/80
	Trav* and *Trbv	**55/80**
CD8WT S_0	*Trav*	1/80
	Trbv	16/80
	Trav* and *Trbv	**53/80**
CD8WT S_1	*Trav*	0/20
	Trbv	5/20
	Trav* and *Trbv	**7/20**
CD8WT S_2	*Trav*	2/80
	Trbv	6/80
	Trav* and *Trbv	**24/80**

Aire$^{-/-}$ *Cblb*$^{-/-}$ spleen

Plate	Chain	Frequency
CD4WT S_0	*Trav*	8/80
	Trbv	16/80
	Trav* and *Trbv	**47/80**
CD4WT S_1	*Trav*	N.D.
	Trbv	N.D.
	Trav* and *Trbv	**N.D.**
CD4WT S_2	*Trav*	4/80, 2/80
	Trbv	13/50, 8/80
	Trav* and *Trbv	**48/80, 41/80**
CD8WT S_0	*Trav*	7/80
	Trbv	19/80
	Trav* and *Trbv	**37/80**
CD8WT S_1	*Trav*	N.D.
	Trbv	N.D.
	Trav* and *Trbv	**N.D.**
CD8WT S_2	*Trav*	2/80, 2/80
	Trbv	15/80, 8/80
	Trav* and *Trbv	**50/80, 38/80**

Aire$^{-/-}$ *Cblb*$^{-/-}$ pancreas

Plate	Chain	Frequency
CD4WT P_0	*Trav*	1/40
	Trbv	6/40
	Trav* and *Trbv	**31/40**
CD4WT P_1	*Trav*	1/8
	Trbv	1/8
	Trav* and *Trbv	**3/8**
CD4WT P_2	*Trav*	0/5, 0/20
	Trbv	0/5, 0/20
	Trav* and *Trbv	2/5, 3/20
CD8WT P_0	*Trav*	2/40
	Trbv	4/40
	Trav* and *Trbv	**32/40**
CD8WT P_1	*Trav*	0/5
	Trbv	0/5
	Trav* and *Trbv	**0/5**
CD8WT P_2	*Trav*	2/75, 2/79
	Trbv	5/75, 1/79
	Trav* and *Trbv	**51/75, 79/95**

Table 5.2 Frequency of *Trav* and *Trbv* reactions that yielded a product for each sample from the WT2 and MUT2 mice. For secondary recipients, in instances where there are two fractions, the first fraction is recipients of S_1 and the second recipients of P_1.

Wild-type spleen

Plate	Chain	Frequency
CD4WT S_0	*Trav*	3/80
	Trbv	15/80
	Trav* and *Trbv	**61/80**
CD4WT S_1	*Trav*	4/40
	Trbv	3/40
	Trav* and *Trbv	**14/40**
CD4WT S_2	*Trav*	3/80
	Trbv	14/80
	Trav* and *Trbv	**50/80**
CD8WT S_0	*Trav*	0/80
	Trbv	11/80
	Trav* and *Trbv	**69/80**
CD8WT S_1	*Trav*	2/40
	Trbv	10/40
	Trav* and *Trbv	**14/40**
CD8WT S_2	*Trav*	0/80
	Trbv	10/80
	Trav* and *Trbv	**16/80**

Aire$^{-/-}$ *Cblb*$^{-/-}$ spleen

Plate	Chain	Frequency
CD4WT S_0	*Trav*	3/80
	Trbv	10.80
	Trav* and *Trbv	**65/80**
CD4WT S_1	*Trav*	N.D.
	Trbv	N.D.
	Trav* and *Trbv	**N.D.**
CD4WT S_2	*Trav*	2/80, 6/80
	Trbv	15/80, 16/80
	Trav* and *Trbv	**25/80, 35/80**
CD8WT S_0	*Trav*	3/80
	Trbv	5/80
	Trav* and *Trbv	**66/80**
CD8WT S_1	*Trav*	N.D.
	Trbv	N.D.
	Trav* and *Trbv	**N.D.**
CD8WT S_2	*Trav*	2/80. 1/80
	Trbv	1/80, 0/80
	Trav* and *Trbv	**4/80, 12/80**

Aire$^{-/-}$ *Cblb*$^{-/-}$ pancreas

Plate	Chain	Frequency
CD4WT P_0	*Trav*	1/80
	Trbv	7/80
	Trav* and *Trbv	**72/80**
CD4WT P_1	*Trav*	no cells
	Trbv	no cells
	Trav* and *Trbv	**no cells**
CD4WT P_2	*Trav*	0/1, 0/1
	Trbv	0/1, 0/1
	Trav* and *Trbv	0/1, 0/1
CD8WT P_0	*Trav*	0/80
	Trbv	10.80
	Trav* and *Trbv	**69/80**
CD8WT P_1	*Trav*	5/20
	Trbv	1/20
	Trav* and *Trbv	**1/20**
CD8WT P_2	*Trav*	0/4
	Trbv	0/4
	Trav* and *Trbv	**0/4**

possibilities.

5.2.3 Results of analysis of TCRα or TCRβ chains from single CD4 cells in original donors, primary and secondary recipients

A summary of the results from the serial transfer experiment is shown in Fig. 5.6. Each unique Trav/CDR3α/Traj paired to Trbv/CDR3β/Trbj combination is termed a single TCR "clonotype" and those that occurred in two or more T cells within a recipient or donor mouse were shaded in colour and listed in Table 5.3 (for WT1 and MUT1) and Table 5.4 (for WT2 and MUT2), along with the fraction of T cells that displayed this TCR clonotype. Raw data are seen in the Appendix Tables 5.10 to 5.26.

For the original MUT or WT donor spleen or pancreatic cells (S_0 or P_0), the sorted CD4 T cells exhibited a diverse range of TCR clonotypes, with no two cells bearing the same TCR. In the primary recipients, very few cells were recovered from each group, although the TCR clonotypes detected in WT1 S_1 spleen CD4 cells (*n*=5) and MUT1 P_1 pancreas CD4 cells (*n*=2) were unique (Fig. 5.6). In WT2 S_1 CD4 cells, one clonotype (2.1) was found in 2/12 cells, while all other CD4 cells from the same mouse carried unique TCRs. No cells were recovered from the pancreas of the MUT2 primary recipient (Fig. 5.6), consistent with the absence of histological evidence of lymphocytic infiltration in this mouse (Fig 5.2).

Expansion or enrichment of particular CD4 clones became apparent in both MUT and WT secondary recipients. In MUT1 secondary recipients of P_1 pancreas-infiltrating cells, seven TCR clonotypes were detected in two or more of the 34 CD4 cells analysed in the spleen (S_2<P_1): clonotypes 1.4, 1.5, 1.6, 1.7, 1.8, 1.9 and 1.10 (Fig. 5.6). One of these, clonotype 1.4, was also carried by two of four P_2<P_1 pancreas CD4 cells in the same mouse, compared to 6/34 S_2<P_1 spleen CD4 cells. The MUT1 secondary recipient of S_1 splenocytes had five TCR clonotypes, clonotypes 1.11, 1.12, 1.13, 1.14 and 1.15, which were carried by two or three CD4 cells from 23 CD4 cells sequenced in the S_2<S_1 spleen (Fig. 5.6). TCR sequence data was only obtained for two CD4 cells in the P_2<S_1 pancreas of the same recipient, and both carried TCRs that differed from the TCRs detected in the spleen CD4 cells (Fig. 5.6). Thus, the MUT1 secondary recipients

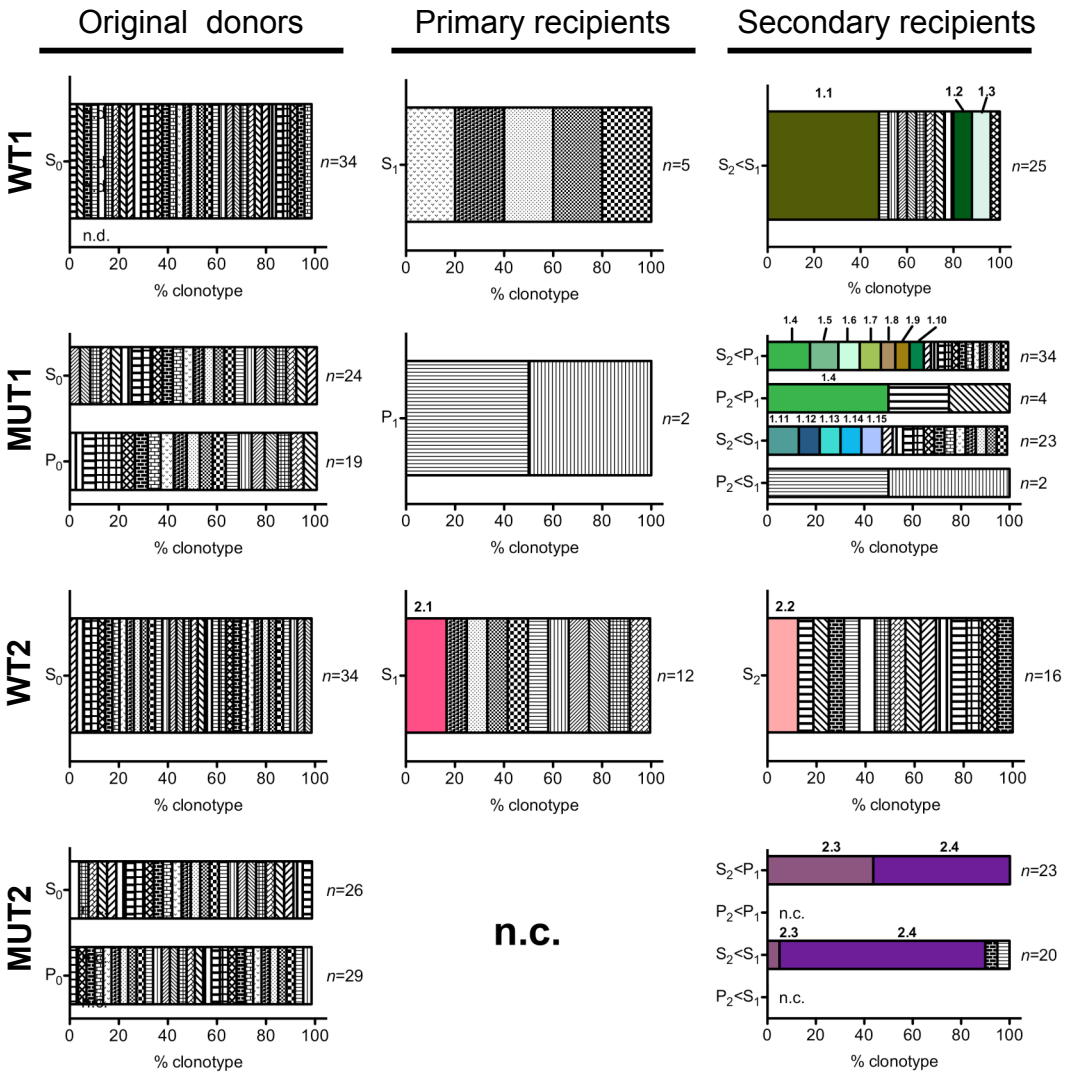

Figure 5.6 Analysis of distinct TCRα and TCRβ combinations found in CD4 cells of original donor and primary/secondary *Rag1*$^{-/-}$ recipients of wild-type or *Aire*$^{-/-}$*Cblb*$^{-/-}$ lymphocytes. Segment sizes are proportional to the percentages of different clones with a unique combination of Vα, Jα, Vß, Jß and complementarity determining regions. For the wild-type donor and recipient mice, only splenocytes were transferred and assayed. For the *Aire*$^{-/-}$*Cblb*$^{-/-}$, both pancreas infiltrating lymphocytes and splenocytes were assayed. n.c. indicated no detection of cells. Clones that were represented ≥2 times are represented by a coloured region and given a unique identification number. 0, original donors; 1, primary recipients; 2, secondary recipients; P, pancreas; S, spleen. For secondary recipients, the first letter indicates the organs the cells were recovered from while the second letter indicates origin of the transferred cells.

Table 5.3 The frequencies of recurring (≥2) CD4 clones and their respective Trav, CDR3α, Traj and Trbv, CDR3β, Trbj regions from WT1 and MUT1 mice. Each clonotype of interest is given a unique "clonotype number". Numerator represents number of clones of the respective clonotype and denominator represents the total number of clones isolated.

Trav	Va	CDR3a	Ja	Traj	Trbv	Vb	CDR3b	Jb	Trbj	Clonotype	S_0	P_0	P_1	S_2<S_1	P_2<S_1	S_2<P_1	P_2<P_1	
Trav7-6 or 7D-6	YLCAV	RGNMGYKL	TFGTGTSLLVDP	Traj9	Trbv14	YLCAS	SKTGINQAP	LFGEGTRLSVL	Trbj1-5	1.1				12/25				WT1
Trav8-2	YFCAT	DDTNTGKL	TFGDGTVLTVKP	Traj27	Trbv13-2	YFCAS	GGTGGAETL	YFGSGTRLTVL	Trbj2-3	1.2				2/25				WT1
Trav10, 10D	YFCAA	SNYGNEKI	TFGAGTKLTIKP	Traj48	Trbv5	YFCAS	SPDRGGWEQ	YFGPGTRLTVL	Trbv2-7	1.3				2/25				WT1
Trav5-1	YFCSA	SGTGNYKY	VFGAGTRLKVIA	Traj40	Trbv13-3	YFCAS	RAGVAEQ	FFGPGTRLTVL	Trbj2-1	1.4						6/34	2/4	MUT1
Trav13-1 or 13D-4	YLCAM	HQGGSAKL	IFGEGTKLTVSS	Traj57	Trbv13-2	YFCAS	GGPGQGANERL	FFGHGTKRSVL	Trbj1-4	1.5						4/34		MUT1
Trav12D-1, 12-2, 12D-2, 12-3, 12D-3	YYCAL	SDQGGSAKL	IFGEGTKLTVSS	Traj57	Trbv3	YFCAS	SLGLGIQNTL	YFGAGTRLSVL	Trbj2-4	1.6						3/34		MUT1
Trav8-2	YFCAT	DNNYAQGL	TFGLGTRVSVFP	Traj26(1)	Trbv29	YFCAS	STGDAGQL	YFGEGSKLTVL	Trbj2-2	1.7						3/34		MUT1
Trav7-5, 7D-5	YLCAP	LSSNTDKV	VFGTGTRLQVSP	Traj34	Trbv13-2	YFCAS	GDRPGRAEV	FFGKGTRLTVV	Trbj1-1	1.8						2/34		MUT1
Trav7-3, 7D-3	YLCAV	SDNNNAP	RFGAGTKLSVKP	Traj43	Trbv13-2	YFCAS	GDAGTGGYEQ	YFGPGTRLTVL	Trbv2-7	1.9						2/34		MUT1
Trav13-2	YFCAI	NYGSSGNKL	IFGIGTLLSVKP	Traj32	Trbv13-2	YFCAS	GAGQSNTEV	FFGKGTRLTVV	Trbj1-1	1.10						2/34		MUT1
Trav6-1, 6-2, 6-4, 6D-04, 6-5, 6D-5, 6-6, 6D-6, 6-7/DV9	YYCVL	ATGNTGKL	IFGLGTTLQVQP	Traj37	Trbv13-2	YFCAS	GDAGLGDTGQL	YFGEGSKLTVL	Trbj2-2	1.11				3/23				MUT1
Trav6-6 or D-6	YYCAL	ARNNNNAP	RFGAGTKLSVKP	Traj43	Trbv19	FLCAS	RTQGNTEV	FFGKGTRLTVV	Trbj1-1	1.12				2/23				MUT1
Trav7-5 or D-5	YLCAP	LSSNTDKV	VFGTGTRLQVSP	Traj34	Trbv13-2	YFCAS	GDRPGRAEV	FFGKGTRLTVV	Trbj1-1	1.13				2/23				MUT1
Trav8-2	YFCAT	DNNYAQGL	TFGLGTRVSVFP	Traj26(1)	Trbv29	YFCAS	STGDAGQL	YFGEGSKLTVL	Trbj2-2	1.14				2/23				MUT1
Trav12D-1, 12-2, 12D-2, 12-3	YYCAL	SDQGGSAKL	IFGEGTKLTVSS	Traj57	Trbv3	YFCAS	SLGLGIQNTL	YFGAGTRLSVL	Trbj2-4	1.15				2.23				MUT1

Table 5.4 The frequencies of recurring (≥2) CD4 clones and their respective Trav, CDR3α, Traj and Trbv, CDR3β, Trbj regions from WT2 and MUT2 mice. Each clonotype of interest is given a unique "clonotype number". Numerator represents number of clones of the respective clonotype and denominator represents the total number of clones isolated.

Trav	Va	CDR3a	Ja	Traj	Trbv	Vb	CDR3b	Jb	Trbj	Clonotype	S_0	P_0	P_1	S_2<S_1	P_2<S_1	S_2<P_1	P_2<P_1	
Trav8D-2	YFCAT	DNTNTGKL	TFGDGTVLTVKP	Traj27	Trbv31	YLCAW	IRDNQDTQ	YFGPGTRLLVL	Trbj2-5	2.1			2/12					WT2
Trav14-1	YFCAA	YTGGLSGKL	TFGEGTQVTVIS	Traj2	Trbv31	YLCAW	SPRDGSAETL	YFGSGTRLTVL	Trbj2-3	2.2				2/16				WT2
Trav4-3 or 4D-3	YFCAA	ENYAQGL	TFGLGTRVSVFP	Traj26(1)	Trbv5	YFCAS	SQDRGQDTDV	FFGKGTRLTVV	Trbj1-1	2.3				1/20		10/23		MUT2
Trav6D-7, 6-5	YFCAL	SKGHKCLP-HPEPRTCCA			Trbv5	YFCAS	SQDRGQDTEV	FFGKGTRLTVV	Trbj1-1	2.4				17/20		13/23		MUT2

displayed an oligoclonal CD4 expansion, but these TCRs did not appear to share any specific features in common (Table 5.3).

By contrast, in the spleen of MUT2 secondary recipients two TCR combinations accounted for most of the CD4 cells for which sequence data was obtained. Clonotype 2.3 was carried by 10 of 23 CD4 spleen cells in the mouse that received P_1 pancreas infiltrating cells (recipient $S_2<P_1$), but only 1 of 20 CD4 splenocytes in the recipient of S_1 spleen cells (recipient $S_2<S_1$). Clonotype 2.4 was carried by 13/23 CD4 spleen cells in the recipient of P_1 pancreas cells (recipient $S_2<P_1$) and also carried by 17/20 CD4 splenocytes in the recipient of S_1 cells (recipient $S_2<S_1$) (Fig. 5.6). No cells were detected in the pancreas of the MUT2 secondary recipient, consistent with the absence of pancreatitis in this animal.

Expanded clones of CD4 cells were also evident in the secondary recipients of WT cells. In the WT1 secondary recipient, the spleen CD4 repertoire was dominated by clonotype 1.1 (frequency of 12/25 cells), with two other clonotypes also recurring: 1.2 (frequency of 2/25) and 1.3 (frequency of 2/25) (Fig. 5.6). Similarly, in the secondary recipient of WT2 spleen cells, clonotype 2.2 occurred at a frequency of 2/16 CD4 cells in the spleen (Fig. 5.6). No similarities could be discerned between the expanded clonotypes in MUT or WT secondary recipients, with respect to TCRα or TCRβ element usage or sequence motifs in the complementarity determining regions (Table 5.3 and Table 5.4).

These results indicate that particular CD4 clones become selectively expanded after two-rounds of serial transfers for both WT and MUT mice, and hence clonal expansion per se is unlikely to be sufficient to identify autoimmune driver clones. The autoimmune driver TCRs would be best selected as clonotypes that accumulated preferentially in the pancreas relative to the spleen of the same MUT mouse or accumulated in the pancreas in more than one recipient mouse. In this experiment only one TCR, clonotype 1.4 from MUT1, met both those criteria.

5.2.4 Analysis of TCRα or TCRβ chains on CD8 cells in original donor, primary recipient and secondary recipients

Fig. 5.7, Tables 5.5, 5.6 and Appendix Tables 5.27 – 5.34 summarizes the results for the analysis of the CD8 clones within the repertoire. Consistent with the CD4 repertoire, the original WT and MUT donors had a diverse repertoire of TCRs among CD8 cells with each TCR only occurring once (Fig. 5.7). No TCR PCR products or sequence data was obtained from the few CD8 cells isolated from the pancreas of MUT1 primary recipients, while all eight cells analysed in the MUT2 primary recipient (P_1) carried an identical TCR, clonotype 1.17 (Fig. 5.7 and Table 5.6). Remarkably, an identical TCR clonotype 1.17 was also detected on one of the 22 CD8 cells analysed in the pancreas of the MUT1 original donor (P_0). Although complete TCR sequence data was only obtained from a few CD8 cells in the WT1 and WT2 primary recipients (S_1), the two and nine cells analysed, respectively, each carried unique TCRs (Fig. 5.7).

As with the CD4 cells above, oligoclonal repertoires were evident in the CD8 cells from secondary recipients of MUT or WT cells (Fig. 5.7 and Table 5.5). The MUT1 secondary recipients displayed a striking increase in three TCR clonotypes that were present in both the recipient of P_1 pancreas and the recipient of S_1 spleen cells. Clonotype 1.17 was present in 1/31 CD8 cells in $S_2<P_1$ spleen, 30/73 CD8 cells in $P_2<P_1$ pancreas, and 2/38 CD8 cells in $S_2<S_1$ spleen. The high frequency of CD8 cells bearing this TCR in the pancreas makes it a strong candidate for an autoimmune driver. Clonotype 1.18 also represents a driver candidate, because it was present in 5/31 cells in $S_2<P_1$ spleen, 42/73 in $P_2<P_1$ pancreas, 14/38 CD8 cells in $S_2<S_1$ spleen, and 21/51 cells in $P_2<S_1$ pancreas. Clonotype 1.19 was present in 8/38 CD8 cells in $S_2<S_1$ spleen and in $S_2<P_1$ spleen. Other clones that were represented only in one organ of the secondary recipient mice occurring at a frequency of more than one were clonotypes 1.20, 1.21, 1.22 and 1.23 (Fig. 5.7 and Table 5.5).

Intriguingly, two TCRs detected in MUT1 were also dominant clones in MUT2 secondary recipients. Clonotype 1.17 was carried by 100% of CD8 cells analysed in the pancreas of the MUT2 P_1 primary recipient (n=8) and in the spleen of the secondary recipient of MUT2 $S_2<S_1$ spleen cells (n=3). It was also detected at a frequency of 1/5

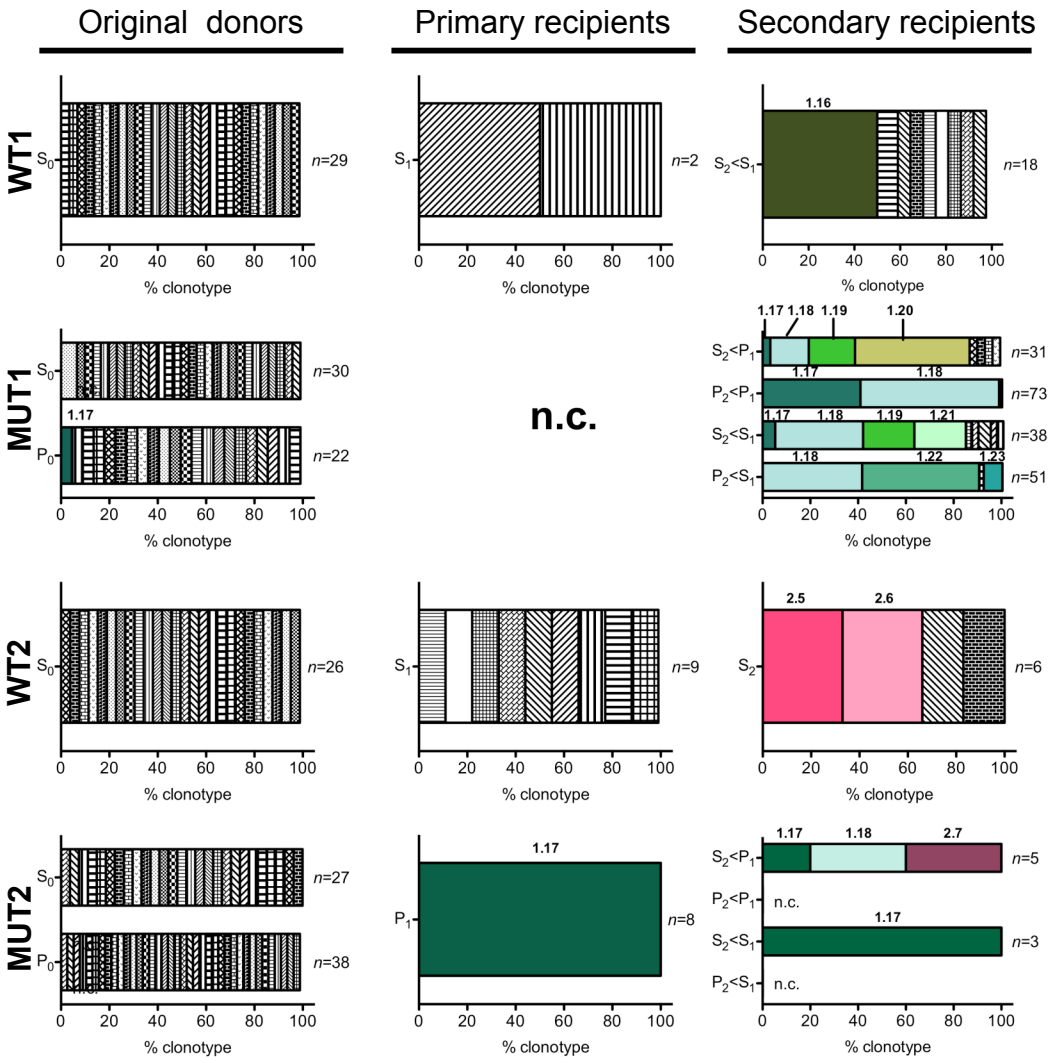

Figure 5.7 Analysis of of distinct TCRα and TCRβ combinations found in CD4 cells of original donor and primary/secondary *Rag1*$^{-/-}$ recipients of wild-type or *Aire*$^{-/-}$*Cblb*$^{-/-}$ lymphocytes. Segment sizes are proportional to the percentages of different clones with a unique combination of Vα, Jα, Vß, Jß and complementarity determining regions. For the wild-type donor and recipient mice, only splenocytes were transferred and assayed. For the *Aire*$^{-/-}$*Cblb*$^{-/-}$, both pancreas infiltrating lymphocytes and splenocytes were assayed. n.c. indicated no detection of cells. Clones that were represented ≥2 times are represented by a coloured region and given a unique identification number. 0, original donors; 1, primary recipients; 2, secondary recipients; P, pancreas; S, spleen. For secondary recipients, the first letter indicates the organs the cells were recovered from while the second letter indicates origin of the transferred cells.

Table 5.5 The frequencies of recurring (≥2) CD8 clones and their respective Trav, CDR3α, Traj and Trbv, CDR3β, Trbj regions from WT1 and MUT1 mice. Each clonotype of interest is given a unique "clonotype number". Numerator represents number of clones of the respective clonotype and denominator represents the total number of clones isolated.

Trav	Va	CDR3a	Ja	Traj	Trbv	Vb	CDR3b	Jb	Trbj	Clonotype	S_0	P_0	P_1	S_2<S_1	P_2<S_1	S_2<P_1	P_2<P_1	
Trav3-1	YFCAV	GNSGGSNAKL	TFGKGTKLSVKS	Traj42	Trbv13-3	YFCAS	RDRDTQ	YFGPGTRLLVL	Trbj2-5	1.16				9/18				WT1
Trav6-4, 6D-4	YFCAL	VDSNYQL	IWGSGTKLIIKP	Traj33	Trbv13-2	YFCAS	GGNSSYEQ	YFGPGTRLTVL	Trbv2-7	1.17		1/22		2/38		1/31	30/73	MUT1
Trav7-3, 7D-3	YLCAV	NTGANTGKL	TFGHGTILRVHP	Traj52	Trbv1	LYCTC	SADREGHEQ	YFGPGTRLTVL	Trbv2-7	1.18				14/38	21/51	5/31	42/73	MUT1
Trav8-2	YFCAT	DNNYAQGL	TFGLGTRVSVFP	Traj26(1)	Trbv29	YFCAS	STGDAGQL	YFGEGSKLTVL	Trbj2-2	1.19				8/38		6/31		MUT1
Trav9-3,9-4, 9D-4	YFCVL	TINSAGNKL	TFGIGTRVLVRP	Traj17	Trbv13-2	YFCAS	GDNNERL	FFGHGTKLSVL	Trbj1-4	1.20						15/31		MUT1
Trav7-4., 7D-4	YFCAA	SDANKM	IFGLGTILRVRP	Traj47	Trbv19	FLCAS	RKLGNQDTQ	YFGPGTRLLVL	Trbj2-5	1.21				8/38				MUT1
Trav7-3, 7D-3	YLCAV	IDYANKM	IFGLGTILRVRP	Traj47	Trbv13-1	YFCAS	TGQNYAEQ	FFGPGTRLTVL	Trbj2-1	1.22					25/51			MUT1
Trav7-1	YFCAV	RVGDNSKL	IWGLGTSLVVNP	Traj38	Trbv1	LYCTC	SADRGGNTL	YFGEGSRLIVV	Trbj1-3	1.23					4/51			MUT1

Table 5.6 The frequencies of recurring (≥2) CD8 clones and their respective Trav, CDR3α, Traj and Trbv, CDR3β, Trbj regions from WT2 and MUT2 mice. Each clonotype of interest is given a unique "clonotype number". Numerator represents number of clones of the respective clonotype and denominator represents the total number of clones isolated.

Trav	Va	CDR3a	Ja	Traj	Trbv	Vb	CDR3b	Jb	Trbj	Clonotype	S_0	P_0	P_1	S_2<S_1	P_2<S_1	S_2<P_1	P_2<P_1	
Trav6-6	YYCAL	GDYGNEKI	TFGAGTKLTIKP	Traj48	Trbv29	YFCAS	SRQGNTGQL	YFGEGSKLTVL	Trbj2-2	2.5				2/6				WT2
Trav13-2	YLCAL	ELDYANKM	IFGLGTILRVRP	Traj47	Trbv13-3	YFCAS	SDAGGANERL	FFGHGTKLSVL	Trbj1-4	2.6				2/6				WT2
Trav6-4 or Trav6D-4	YFCAL	VDSNYQL	IWGSGTKLIIKP	Traj33	Trbv13-2	YFCAS	GGNSSYEQ	YFGPGTRLTVL	Trbv2-7	1.17			8/8	3/3		1/5		MUT2
Trav7-3 or 7D-3	YLCAV	NTGANTGKL	TFGHGTILRVHP	Traj52	Trbv1	LYCTC	SADREGHEQ	YFGPGTRLTVL	Trbv2-7	1.18						2/5		MUT2
Trav7-3 or 7D-3	YLCAV	NTGANTGKL	TFGHGTILRVHP	Traj52	Trbv5	YFCAS	SQDRGQDTEV	FFGKGTRLTV	Trbj1-1	2.7						2/5		MUT2

CD8 cells in the MUT2 S_2<P_1 spleen, representing the secondary recipient of P_1 pancreas cells. The second TCR that was detected in both MUT1 and MUT2 secondary recipients was clonotype 1.18 that was present at a frequency of 2/5 in MUT2 S_2<P_1 spleen cells. This clone was of interest because the nucleotide sequencing chromatograms revealed two or more overlapping DNA sequences in the TCRα PCR product but a single DNA sequence for the TCRβ product from each of these CD8 cells. This is likely to reflect expression of two rearranged TCRα alleles in this clone, and will be discussed in the discussion section 5.5.2. The only clone detected in MUT2 that was not detected in MUT1 was clonotype 2.7 that represented 2/5 of the CD8 cells analysed in the S_2<P_1 spleen cells from the MUT2 secondary recipient.

In WT1 secondary recipients, there was an expansion of clonotype 1.16, which was present in 9/18 CD8 cells in the S_2<S_1 spleen. Two other independent TCRs, clonotypes 2.5 and 2.6, were each present at a frequency of 2/6 in spleen CD8 cells of the WT2 secondary recipient mouse.

Taken together, data from sections 5.2.3 and 5.2.4 indicate that serial adoptive transfer experiments enriched for clonally expanded CD4 and CD8 cells from both WT and MUT donors. Within the pancreas and spleen of secondary recipients, the clonal expansion appeared to be selective for a number of dominant clones. Although expansion occurred in both WT and MUT secondary recipients, the presence of two MUT CD8 clones (clonotype 1.17 and 1.18) in more than three different recipient mice, occurring at higher frequencies in the pancreas compared to the spleen is suggestive that these clones might have been repeatedly selected for clonal expansion by driver autoantigen(s) in the pancreas.

There were two drawbacks in this experiment. Firstly, the donor mice were bone marrow chimeras and this could have skewed the T cell repertoire in the original donor. The transplanted wild-type or *Cblb*$^{-/-}$ bone marrow given to these chimeras could contain residual mature T cells in addition to haematopoietic stem cells. Likewise, the irradiated wild-type or *Aire*$^{-/-}$ marrow recipients would have a pool of radioresistant memory T cells. The presence of residual T cells from donor marrow or host may have

skewed the T cell repertoire. Furthermore, for the first several weeks following bone marrow transplantation, any residual mature T cells from the marrow donor or the host will undergo strong lymphopenia-induced homeostatic expansion. The occurrence of the same TCR in the CD8 cells that expand in recipients of pancreas cells from two separate original chimera donors, MUT1 and MUT2, could best be explained by a pre-existing CD8 clone present in the *Cblb*$^{-/-}$ bone marrow that underwent proliferation in both of the chimeras. The possibility of contamination of PCR products can be firmly excluded because this shared TCR clonotype was never detected in CD4 cells or WT cells that were sorted and amplified in parallel on the same 96-well plates.

The second caveat was that very small numbers of lymphocytes were adoptively transferred in some cases, particularly during secondary transfer of pancreatic cells. This may create a population bottleneck that exaggerates the oligoclonality of the CD4 and CD8 T cell repertoire in the secondary recipients. Indeed, the small sample size of two to five sorted T cells yielding complete TCR sequences for some experimental groups made it difficult to draw meaningful conclusions at those time points. In MUT1 primary recipients, TCRs from only two CD4 and no CD8 cells were analysed, while ≥30 CD8 cells were analysed in the secondary recipients although the number of CD4 cells remained low. However for MUT2 recipients, TCR sequences could only be obtained for CD8 cells in the pancreas of the primary recipients, while no CD4 or CD8 cells were detected in the pancreas of the secondary recipients either because these animals were euthanased before the onset of autoimmune pancreatitis or because these recipients lacked the necessary mix of CD4 and CD8 cells shown both to be required for disease progression in Chapter 3.

5.3 Serial transfer system for enrichment of autoreactive T cell clones using pooled lymphocytes from *Aire*$^{-/-}$*Cblb*$^{-/-}$ mice

To validate the observations from section 5.2 and circumvent the caveats of bone marrow chimeras, the serial transfer experiment was repeated with a few changes. Firstly, instead of using bone marrow chimeras, in this experiment the original donors were a pair of unmanipulated, age-matched 24-day-old mice, one of the B10.BR.*Aire*$^{-/-}$ *Cblb*$^{-/-}$ genotype (MUT3) and the other B10.BR wild-type genotype (WT3) (Fig. 5.8).

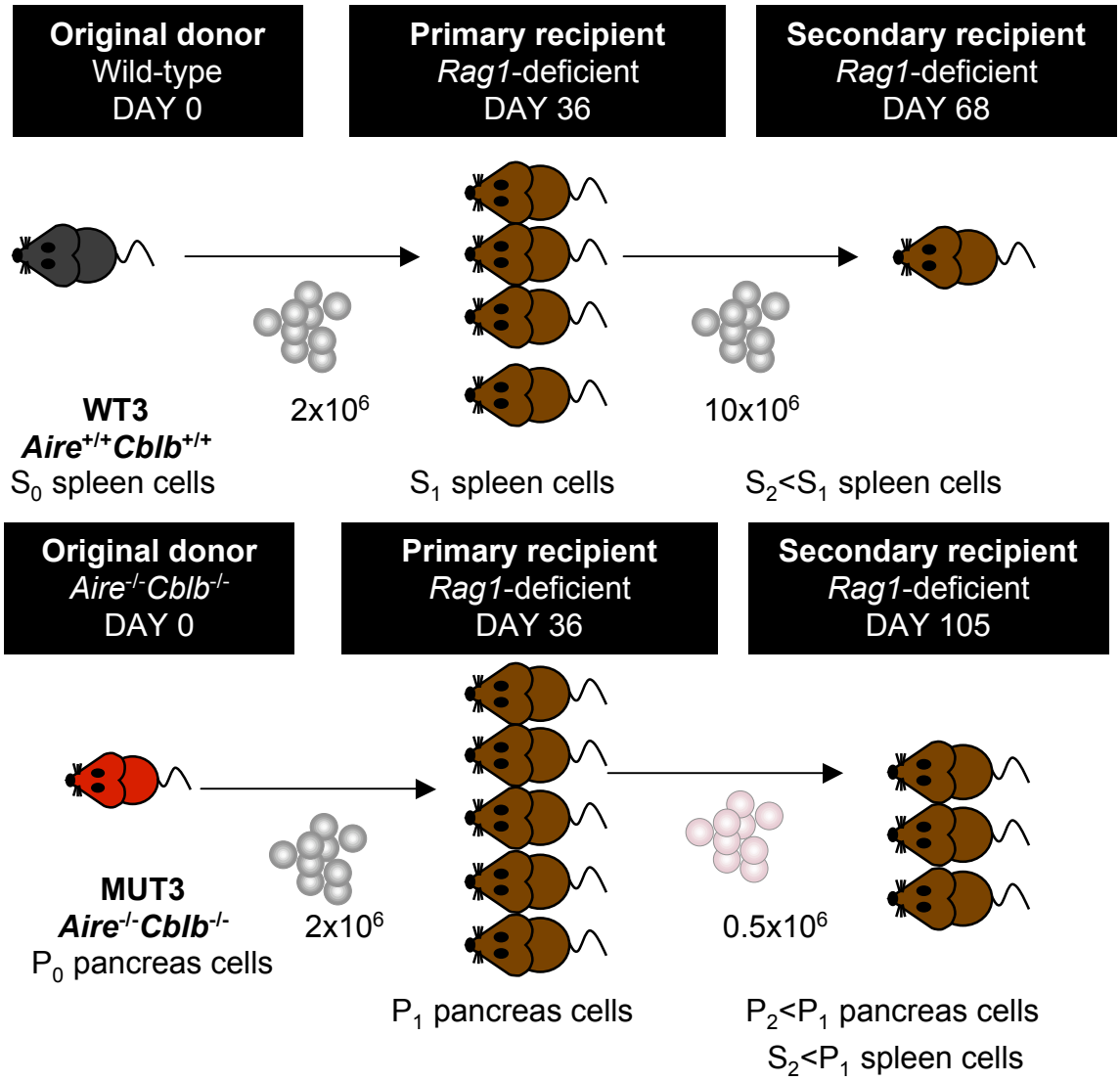

Figure 5.8 Schematic representation of the *in vivo* pancreas-specific T cell enrichment assay.
Splenocytes from *Aire*$^{-/-}$*Cblb*$^{-/-}$ and wild-type mice were adoptively transferred into *Rag1*-deficient recipients. When the *Aire*$^{-/-}$*Cblb*$^{-/-}$ recipients began to lose weight,the wild-type splenocytes and mutant pancreas infiltrating lymphocytes were harvested, pooled and transferred to a second group of *Rag1*-deficient recipients. Single cells from the secondary recipients were sorted for TCR sequencing. 0, original donors; 1, primary recipients; 2, secondary recipients; P, pancreas; S, spleen. For secondary recipients, the first letter indicates the organs the cells were recovered from while the second letter indicates origin of the transferred cells.

At the time of euthanasia to harvest cells for the primary adoptive transfer, the MUT3 original donor mouse had a cachectic appearance typical of B10.BR.*Aire*$^{-/-}$*Cblb*$^{-/-}$ mice, and histological analysis revealed grade 5 exocrine pancreatitis (Fig. 5.9). The second variation to the design was that 2×10^6 spleen cells were used for the primary transfer of both WT and MUT cells, and these were given to multiple primary recipients in parallel so that larger numbers of pancreas-infiltrating lymphocytes were available for secondary transfers. A total of 2×10^6 WT3 or MUT3 splenocytes (S_0) were adoptively transferred to groups of four and five *Rag*-1-deficient primary recipients, respectively (Fig 5.8).

The primary recipients were euthanased 36 days after adoptive transfer, by which time the recipients of MUT3 cells were exhibiting cachexia. As seen in Fig. 5.9, all MUT3 primary recipients had developed destructive exocrine pancreatitis with a score of ≥3, whereas all of the WT3 primary recipients were free of lymphocytic infiltration in the pancreas. In order to minimise T cell population bottlenecks in the secondary transfer and ensure the maximum numbers of cells were transferred to the secondary recipients, pooled populations of cells from multiple primary recipients were used. All splenocytes (S_1) from the four WT3 primary recipients were pooled and 10×10^6 cells were transferred into a secondary recipient. For the MUT3 group, pancreas-infiltrating lymphocytes (P_1) from the five primary recipients were pooled and 0.5×10^6 cells were transferred to each of three secondary *Rag*-1-deficient recipients (Fig. 5.8).

The WT3 secondary recipient was sacrificed for analysis on Day 68 of the experiment. This mouse did not show any signs of autoimmunity in the pancreas (Fig. 5.9). Both CD4 and CD8 cells were present in the spleen of WT3 in a 20.7%:3.29% (CD4:CD8) ratio (Fig.5.10*A*).

By contrast, MUT3 secondary recipients were sacrificed on Day 105 of the experiment when the mice began to show signs of cachectic wasting. The MUT3 secondary recipients were sacrificed later than WT3 secondary recipients to allow more time for the development of pancreatitis in the mice. Histological analysis revealed varying degrees of exocrine pancreatitis, with disease scores of 5, 3 and 2 (Fig. 5.9). All

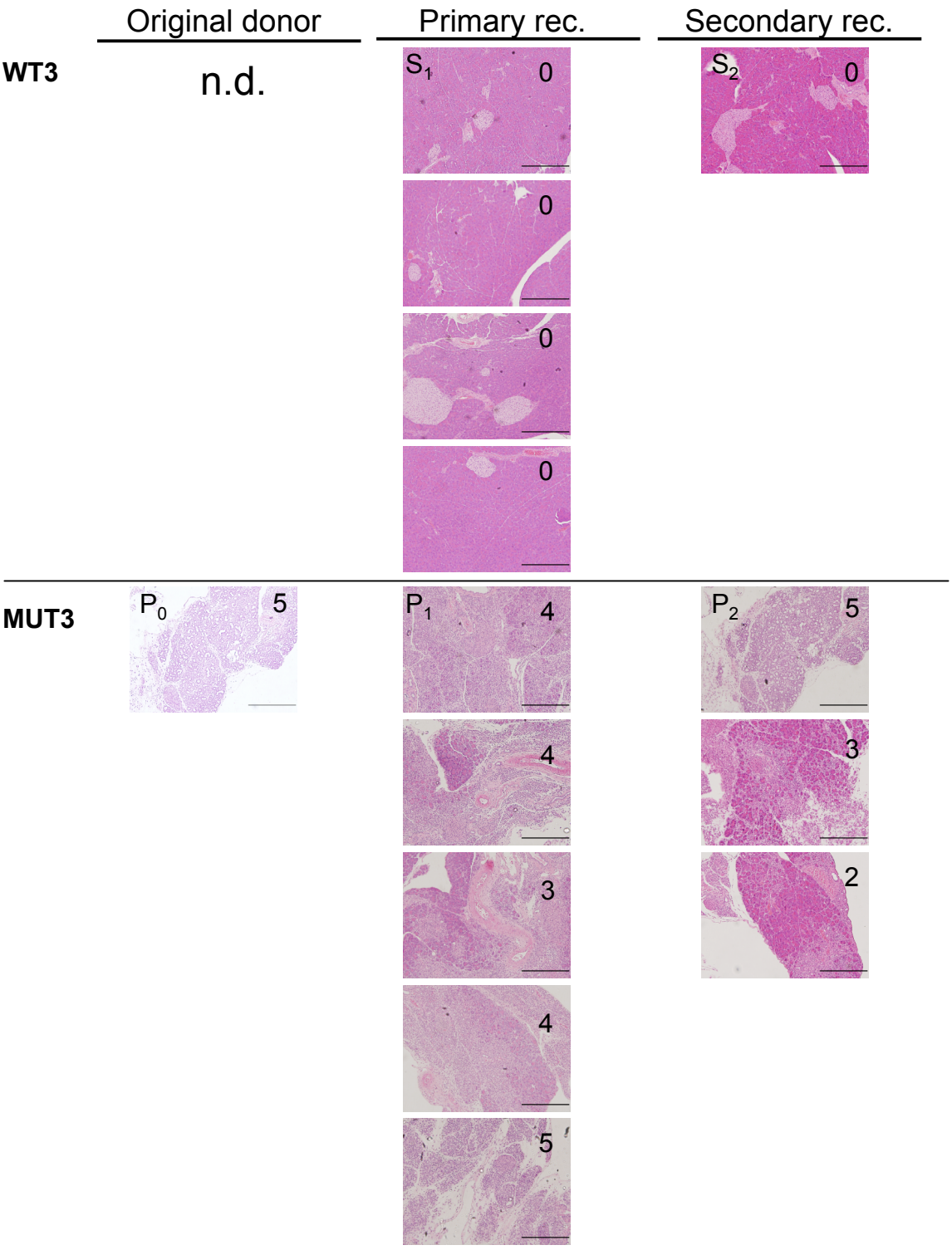

Figure 5.9 Hematoxylin and eosin sections of the pancreas in donor and recipient mice.
Pancreatitis scores between 0 and 5 are shown for each animal. Images were taken at x100 magnification and bars represent 500 µm.

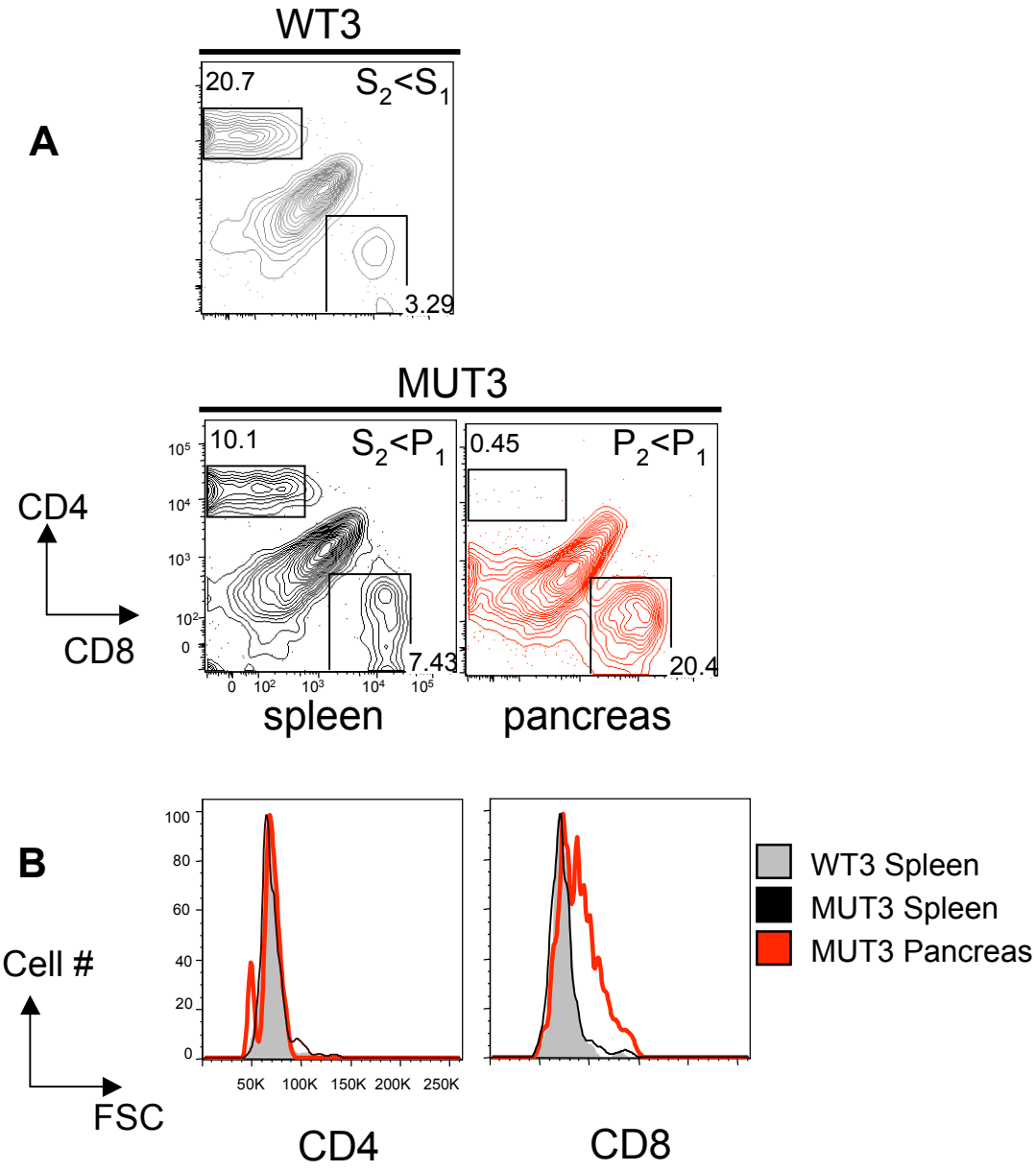

Figure 5.10 Flow cytometric analysis of lymphocytes isolated from the secondary WT3 and MUT3 recipients.

A. Percentage of pooled CD4 and CD8 cells gated on total lymphocytes in the indicated tissues of secondary recipients.

B. Forward side scatter as a measure of size of CD4 and CD8 cells.

splenocytes (S_2<P_1) or pancreas infiltrating lymphocytes (P_2<P_1) from each recipient were pooled for subsequent analysis. Flow cytometric analysis of the spleen of the MUT3 secondary recipients revealed both CD4 and CD8 cells present at a ratio of 10.1%:7.43% (CD4:CD8) (Fig.5.10*A*). T cells in the pancreas were strongly skewed in favour of CD8 cells, however, with only 0.45% of lymphocytes bearing CD4 while 20.4% carried CD8 Fig.5.10*A*. Additionally, consistent with the results for MUT1 in the previous section, the CD8 cells within the pancreas appeared blasted as measured by an increase in forward scatter of the cells Fig.5.10*B*.

In this transfer, single CD4 and CD8 cells from only the secondary recipients were sorted into 96-well plates for TCR analysis. The corresponding TCRα and TCRβ variable regions sequences for each WT3 or MUT3 T cell were determined using the strategy detailed in the previous section. As observed in Table 5.7, the success rate for amplification of both TCRα and TCRβ chains from each sorted T cell was 49.7% (293 of 480 samples) for this experiment.

The results for the CD4 repertoire analysis in WT3 and MUT3 secondary recipients are summarised in Fig. 5.11, Table 5.8, Appendix Table 5.44, 5.45 and 5.46. In the spleen (S_2<S_1) of the WT3 secondary recipient, most of the CD4 cells that were sequenced carried a unique TCR clonotype with the exception of two TCRs that each occurred on two separate CD4 cells (clonotypes 3.1 and 3.2). Similarly, the majority of the CD4 cells isolated from the spleen (S_2<P_1) (13/16) and pancreas (P_2<P_1) (15/15) of the MUT3 secondary transfer recipients carried unique TCRs. Only one TCR, clonotype 3.3, was carried by three separate CD4 cells in the spleen of the MUT3 recipients, and this was not found among the CD4 cells isolated from the pancreas. Thus, the CD4 repertoire in both WT3 and MUT3 secondary recipients did not appear to be strongly dominated by any CD4 clone.

The repertoire of TCRs carried by CD8 T cells in the WT3 and MUT3 secondary recipients is summarised in Fig. 5.12, Table 5.9, Appendix Table 5.47, 5.48 and 5.49. The CD8 repertoire of the WT3 secondary recipient revealed diverse TCRs with the expansion of one clonotype, 3.4, found in 5/24 T cells that were successfully sequenced.

Table 5.7 Frequency of *Trav* and *Trbv* reactions that yielded a product for each sample from the WT3 and MUT3 mice.

Plate	Chain	Frequency
CD4WT $S_2<S_1$	*Trav*	0/80
	Trbv	8/80
	Trav* and *Trbv	**50/80**
CD4MUTS $S_2<P_1$	*Trav*	0/80
	Trbv	20/80
	Trav* and *Trbv	**38/80**
CD4MUTP $P_2<P_1$	*Trav*	0/80
	Trbv	19/80
	Trav* and *Trbv	**49/80**
CD8WTS $S_2<S_1$	*Trav*	Jan-80
	Trbv	13/80
	Trav* and *Trbv	**51/80**
CD8MUTS $S_2<P_1$	*Trav*	0/80
	Trbv	19/80
	Trav* and *Trbv	**55/80**
CD8MUTP $P_2<P_1$	*Trav*	2/80
	Trbv	13/80
	Trav* and *Trbv	**50/80**

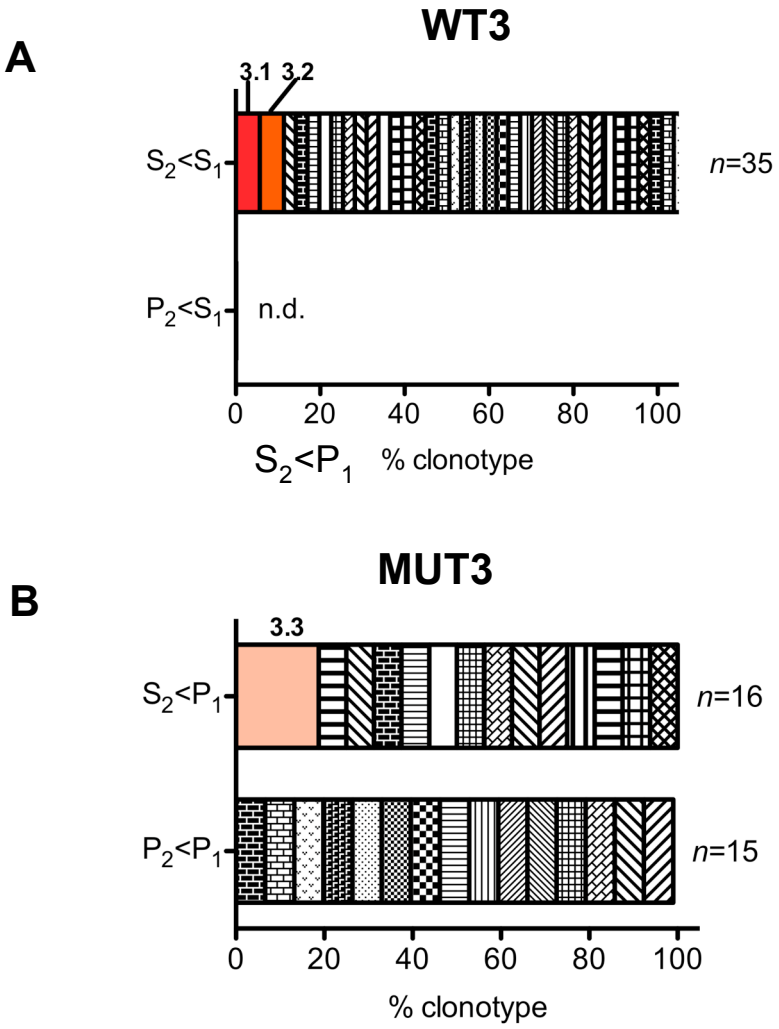

Figure 5.11 Unique TCRα and TCRβ combinations found in single CD4 cells in the indicated tissue of WT3 (A) and MUT3 (B) secondary *Rag1*$^{-/-}$ recipients.
Segment sizes are proportional to the percentages of CD4 cells with a unique TCR clonotype based on the combination of Vα, Jα, Vß, Jß and complementarity determining region sequences. Clones that were represented ≥2 times are represented by a coloured region and given a unique identification number. 1, primary recipients; 2, secondary recipients; P, pancreas; S, spleen. The first letter indicates the organs the cells were recovered from while the second letter indicates origin of the transferred cells.

Table 5.8 The frequencies of recurring (≥2) CD4 clones and their respective Trav, CDR3α, Traj and Trbv, CDR3β, Trbj regions from WT3 and MUT3 mice. Each clonotype of interest is given a unique "clonotype number". Numerator represents number of clones of the respective clonotype and denominator represents the total number of clones isolated.

Trav	Va	CDR3a	Ja	Traj	Trbv	Vb	CDR3b	Jb	Trbj	Clonotype	S_2	P_2	
Trav14-1	YFCAA	SGVSGGSNYKL	TFGKGTLLTVTP	Traj53	Trbv26	YLCAS	SQGSQNTL	YFGAGTRLSVL	Trbj2-4	**3.1**	2/35		WT3
Trav14-2	YFCAA	SSTGNYKY	VFGAGTRLKVI	Traj40	Trbv26	YLCAS	SLQGTNERL	FFGHGTKLSV	Trbj1-4	**3.2**	2/35		WT3
Trav13D-1	YLCAM	GDNNAGAKL	TFGGGTRLTVRP	Traj39	Trbv20	YLCGA	RDNYAEQ	FFGPGTRLTVL	Trbj2-1	**3.3**	3/16		MUT3

Table 5.9 The frequencies of recurring (≥2) CD8 clones and their respective Trav, CDR3α, Traj and Trbv, CDR3β, Trbj regions from WT3 and MUT3 mice. Each clonotype of interest is given a unique "clonotype number". Numerator represents number of clones of the respective clonotype and denominator represents the total number of clones isolated. Note that clonotype 3.8 was included in this table although only occurring once as it is highly related to clonotype 3.5.

Trav	Va	CDR3a	Ja	Traj	Trbv	Vb	CDR3b	Jb	Trbj	Clonotype	S_2	P_2	
Trav4-3 or Trav4D-3	YFCAA	EGGSAKL	IFGEGTKLTVSS	Traj57	Trbv19	FLCAS	SMGLGYEQ	YFGPGTRLTV	Trbv2-7	3.4	5/24		WT3
Trav7-1	YFCAV	SSSGSWQL	IFGSGTQLTVMP	Traj22	Trbv1	LYCTC	SGDSSGNTL	YFGEGSRLIVV	Trbj1-3	3.5	12/39	29/42	MUT3
Trav7-1	YFCAV	SGGSNYQL	IWGSGTKLIIKP	Traj33	Trbv1	LYCTC	SGDRGGNTL	YFGEGSRLIVV	Trbj1-3	3.6	8/39	9/42	MUT3
Trav12D-1, 2, D-2, 3	YYCAL	SDTSSGQKL	VFGQGTILKVYL	Traj16	Trbv14	YLCAS	SFGTGAYAEQ	FFGPGTRLTVL	Trbj2-1	3.7	7/39		MUT3
Trav12D-1, 2, D-2, 3	YYCAL	SGNTGYQNF	YFGKGTSLTVIP	Traj49	Trbv1	LYCTC	SGDSSGNTL	YFGEGSRLIVV	Trbj1-3	3.8	1/39		MUT3

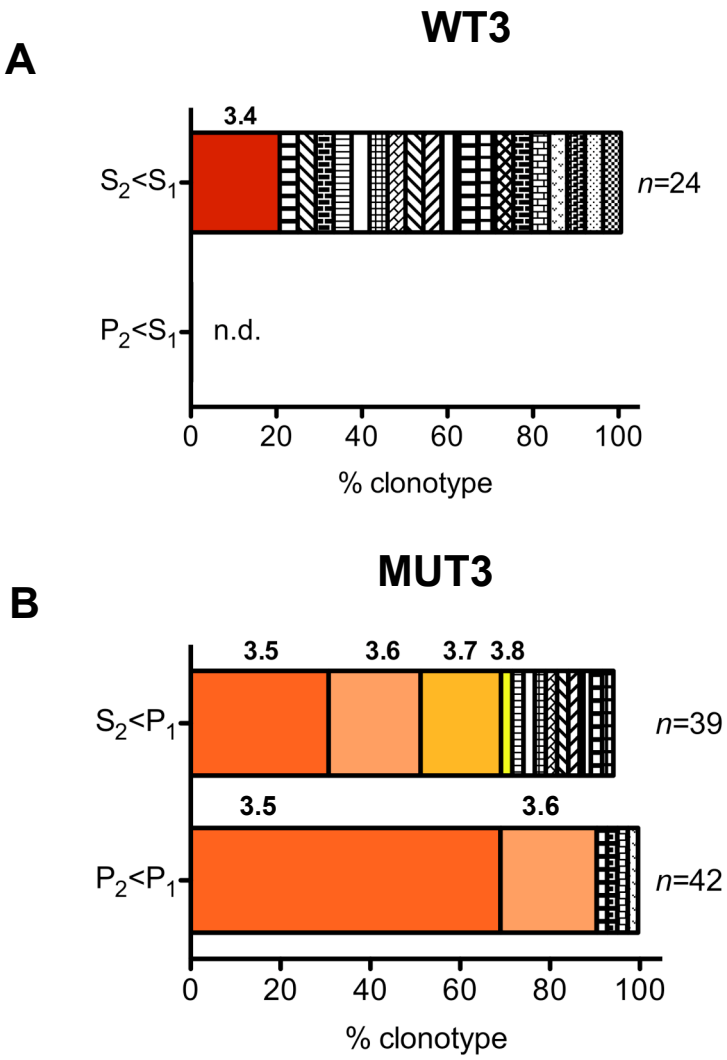

Figure 5.12 Unique TCRα and TCRβ combinations found in single CD8 cells in the indicated tissue of WT3 (A) and MUT3 (B) secondary *Rag1*$^{-/-}$ recipients.
Segment sizes are proportional to the percentages of CD8 cells with a unique TCR clonotype based on the combination of Vα, Jα, Vß, Jß and complementarity determining region sequences. Clones that were represented ≥2 times are represented by a coloured region and given a unique identification number. 1, primary recipients; 2, secondary recipients; P, pancreas; S, spleen. The first letter indicates the organs the cells were recovered from while the second letter indicates origin of the transferred cells. Note that clonotype 3.8 only occurs once but was shaded as it is highly similar to clonotype 3.5.

This degree of clonal expansion among CD8 cells was consistent with that observed in WT1 and WT2 secondary recipients analysed in section 5.2, and reinforces the conclusion that clonal expansion per se cannot be taken as an accurate indicator of autoimmune driver TCRs.

Thirteen unique TCRs were identified among 39 sequenced CD8 cells from the spleen ($S_2<P_1$) of MUT3 secondary recipients (Fig 5.12*B* and Table 5.8). Three TCRs were carried by two or more separate CD8 T cells: clonotype 3.5 was present in 12/39 CD8 cells, clonotype 3.6 in 8/39 cells and clonotype 3.7 in 7/39 cells. Interestingly, the two most frequent TCRs, clonotypes 3.5 and 3.6, had identical Trav, Trbv, Trbj segments and differed only in their Traj gene segment and in the sequence of their CDR3α (S…..QL, dots represent differences) and CDR3β (SG…GNTL, dots represent differences). These two similar TCRs made up 30.7% and 20.5% of the CD8 splenic repertoire that was sequenced. Clonotype 3.8 shared exactly the same TCRß chain as clonotype 3.5 and occurred once. Even more impressive was the discovery of the same TCRs, clonotypes 3.5 and 3.6, at high frequencies in the pancreas ($P_2<P_1$) infiltrating CD8 cells of the same secondary recipients with an occurrence of 29/42 (69%) and 9/42 (21.4%), respectively. Only four other TCRs were detected in the pancreatic CD8 cells from MUT3 secondary recipients, all of which were only found once. These clones were different from that observed to be expanded in the CD8 repertoire of WT3 secondary recipients. All TCRs detected in this experiment were also different from the TCRs detected in the experiment described in section 5.2, and from TCRs detected in CD4 cells of the MUT3 secondary recipients.

The findings from this experiment demonstrate a clear selective expansion of two similar CD8 clones, differing only in the CDR3α, TRAJ region and CDR3β sequences in the MUT3 secondary recipients. The two clones made up 51.2% and 90.4% of the CD8 repertoire analysed for spleen ($S_2<P_1$) and pancreas ($P_2<P_1$) of MUT3, respectively. The enrichment of two very similar clones in the pancreas and to a lesser extend in the spleen suggested that the clones were repeatedly selected most likely attributed to their ability to bind the driver pancreas-specific autoantigen(s) with high affinity. To test this hypothesis, the dominant TCR clonotype 3.5 was used to generate retrogenic mice as described in the following section.

5.4 Production and preliminary characterization of TCR retrogenic mice expressing the putative pancreatic autoimmunity driver TCR 3.5 clonotype

5.4.1 Construction of a retroviral vector bearing TCRα and TCRβ chains of MUT3 CD8 TCR 3.5 clonotype

To test if the TCRs that were found enriched in pancreas-infiltrating T cells recognised *bona fide* exocrine pancreatic antigens and were capable of driving pancreatitis, CD8 clonotype 3.5 from section 5.3 was selected as a promising clone and used to create a multicistronic retroviral vector encoding the TCRα and TCRβ chains of clonotype 3.5. For this purpose, the unique junctional nucleotide sequences of the Trav7-1/SSSGSWQL/Traj22 and Trbv1/GDSSGNTL/Trjb1-3 segments were obtained from the sequence analysis of the PCR products of multiple CD8 MUT3 cells in section 5.3. The remaining 5' untranslated and coding sequence of *Trav7-1* and *Trbv1*, and the sequence of the *Trac* and *Trbc*-1 constant regions was obtained from ImMunoGeneTics (IMGT) and ENSEMBL databases, since these regions were not covered by the sequencing primers in section 5.3. The accurate *Trbc-1* sequence proved difficult to obtain from online bioinformatic tools, and was taken directly from the original sequencing of genomic clones of the TCRβ chain (Gascoigne et al., 1984). The TCRα and TCRβ chains were designed to share a single open reading frame (Fig 5.13), separated from each other by a self-cleaving 2A peptide sequence to serve as a *cis*-acting hydrolase element mediating cleavage between the translated TCRα and TCRβ chains (Holst et al., 2006a). The 1824 base pair insert encompassing clonotype 3.5 TCRα-2A peptide-TCRβ chains sequences was flanked by restriction enzymes sites *Eco*RI and *Xho*I allowing the insertion into the mouse stem cell virus (MSCV)-based retroviral vector, pMIGII (Holst et al., 2006a). The vector contained an internal ribosome entry sequence followed by green fluorescent protein (IRES-GFP) cassette to identify transfected cells. The nucleotide sequence and translation of the insert designed are seen in Fig. 5.13.

The 1824 bp TCRα-2A peptide-TCRβ sequence was chemically synthesized and cloned into the pMIGII vector by Biomatik Corporation and the sequence was verified using two primers flanking the insert and one internal primer. For simplicity, the construct was abbreviated as pMIGII-TCRαβ3.5 for the remainder of this chapter.

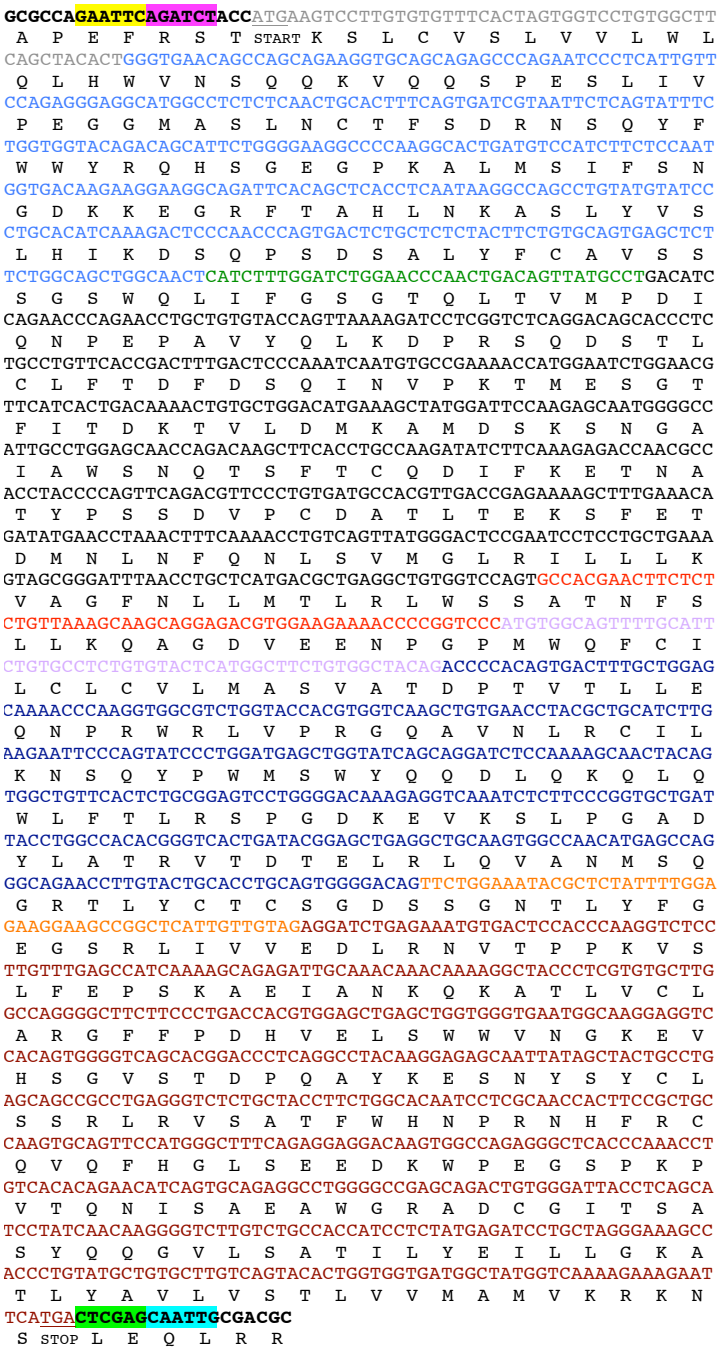

Figure 5.13 The nucleotide sequence and corresponding translated open reading frame of the TCRαß3.5 vector insert synthesized by Biomatik Corporation.

The portion of the sequence indicated by each colour is as follows: TRAV7.1 Leader sequence, TRAV7.1, TRAJ22, TRAC, 2A self cleaving peptide, TRBV1 Leader sequence, TRBV1, TRBJ1.3, TRBC1. In-frame translation initiation and termination codons are underlined. Restriction sites: *EcoR*I, *Bgl*II, *Xho*I, *Mfe*I. The *EcoR*I and *Xho*I sites were utilised for cloning into the pMIGII vector.

5.4.2 Verification of TCRα-2A-TCRβ 3.5 expression on the cell surface and stable transfection into the GP+E86 retroviral producer cell line

The TCRα and TCRβ expression on the cell surface was determined by transient transfection of the pMIGII-empty vector or pMIGII-TCRαβ3.5, with or without the pMIGII-CD3βγεζ co-receptor components, into 293T human embryonic kidney cells. As seen in Fig 5.14*A*, *B* and *C*, transfection of the pMIGII vector, with or without the TCRαβ3.5 insert resulted in GFP expression detected by confocal microscopy and flow cytometry. However, only the 293T cells that were transfected with both pMIGII-TCRαβ3.5 and pMIGII-CD3βγεζ showed TCRβ expression on the cell surface as seen in Fig. 5.14*D*. This result verified that the vector successfully produced TCRα and TCRβ chains that assembled with CD3βγεζ subunits, since these steps are a pre-requisite for surface TCR expression.

The pMIGII-TCRαβ3.5 was used to stably transduce a retroviral packaging cell line, GP+E86. GP+E86 is a 3T3-based cell line. It constitutively expresses the Moloney Leukaemia virus *gag* and *pol* genes from one stably transfected plasmid and the Moloney ecotropic *env* gene from another transfected plasmid, providing a safe packaging vector to produce replication defective retroviral vector particles (Markowitz et al., 1988). These packaging cells were stably transduced with the pMIGII-TCRαβ3.5 vector by repeatedly co-culturing the GP+E86 cell line with defective retrovirus-containing supernatant harvested from 293T cells that were transiently co-transfected with pMIGII-TCRαβ3.5 together with *gag*, *pol* and *env* retroviral genes in separate vectors. This transduction system resulted in 99.9% transduction efficiency of the GP+E86 cell line (Fig. 5.15). The titres for the GP+E86 transduced cells were determined to be 2.693×10^5cells/mL for the pMIGII-empty vector and 3.727×10^5cells/mL for the pMIGII-TCRαβ3.5 (Figures 5.16 and 5.17). The high titres obtained here were imperative for the construction of TCRαβ3.5 retrogenic mice.

5.4.3 Autoimmune pancreatitis in TCRαβ3.5 retrogenic mice

To determine if CD8 T cells expressing TCRαβ3.5 were able to drive autoimmune pancreatitis and recapitulate the phenotype of the original MUT3 donor and secondary

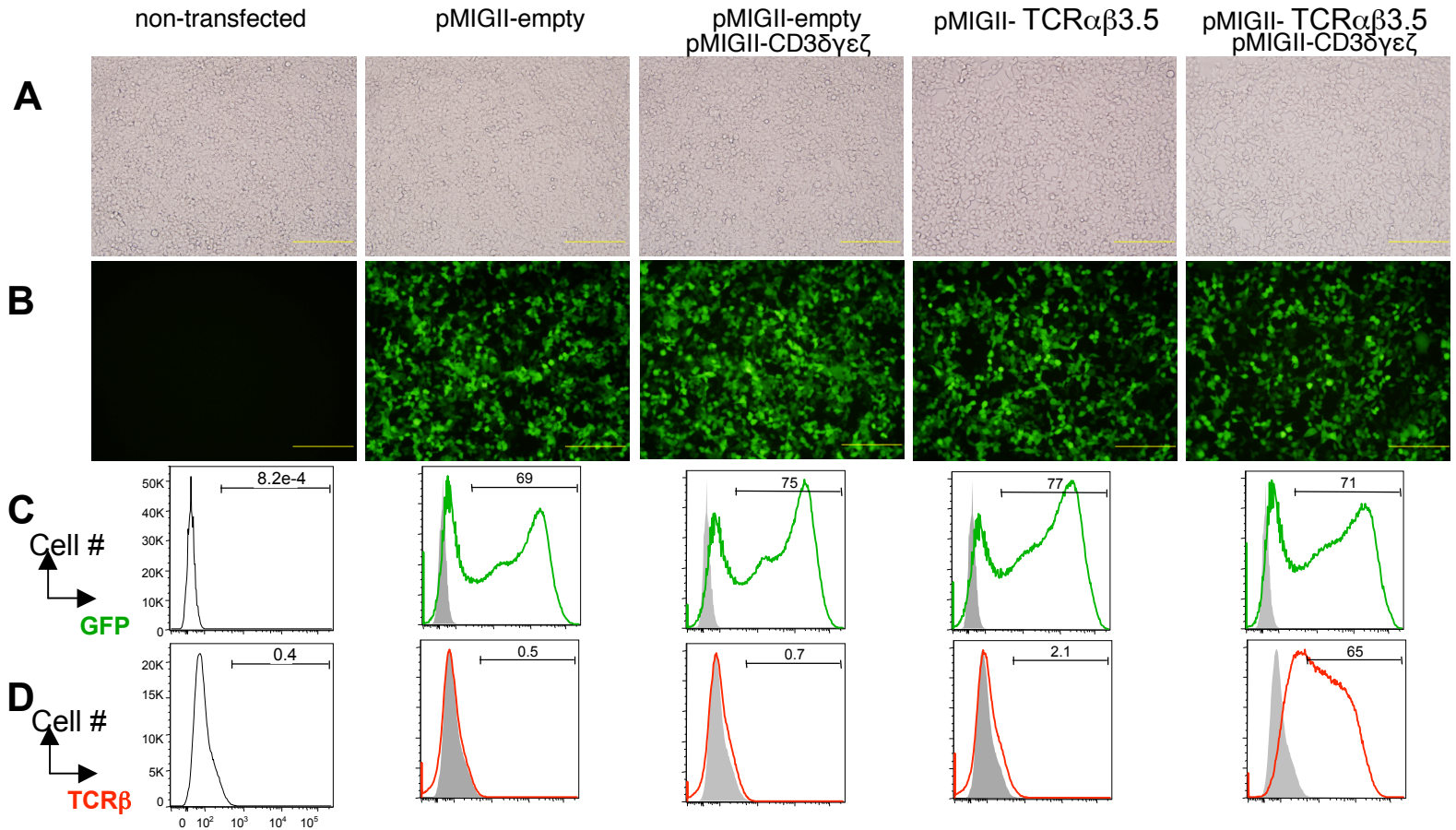

Figure 5.14 Verification of TCR expression 48 hours after transfection of 293T cells with pMIGII-TCRαβ3.5 and pMIGII-CD3δγεζ or controls.

A. Brightfield images of the cells in culture viewed at x200 magnification; bars represent 200 μm.
B. GFP detection of cells under UV light viewed at x200 magnification; bars represent 200 μm.
C. Expression of GFP (green) detected by flow cytometry. Grey solid histogram is the non-transfected control.
D. Expression of cell surface TCRß (red) detected by flow cytometry. Grey solid histogram is the non-transfected control.

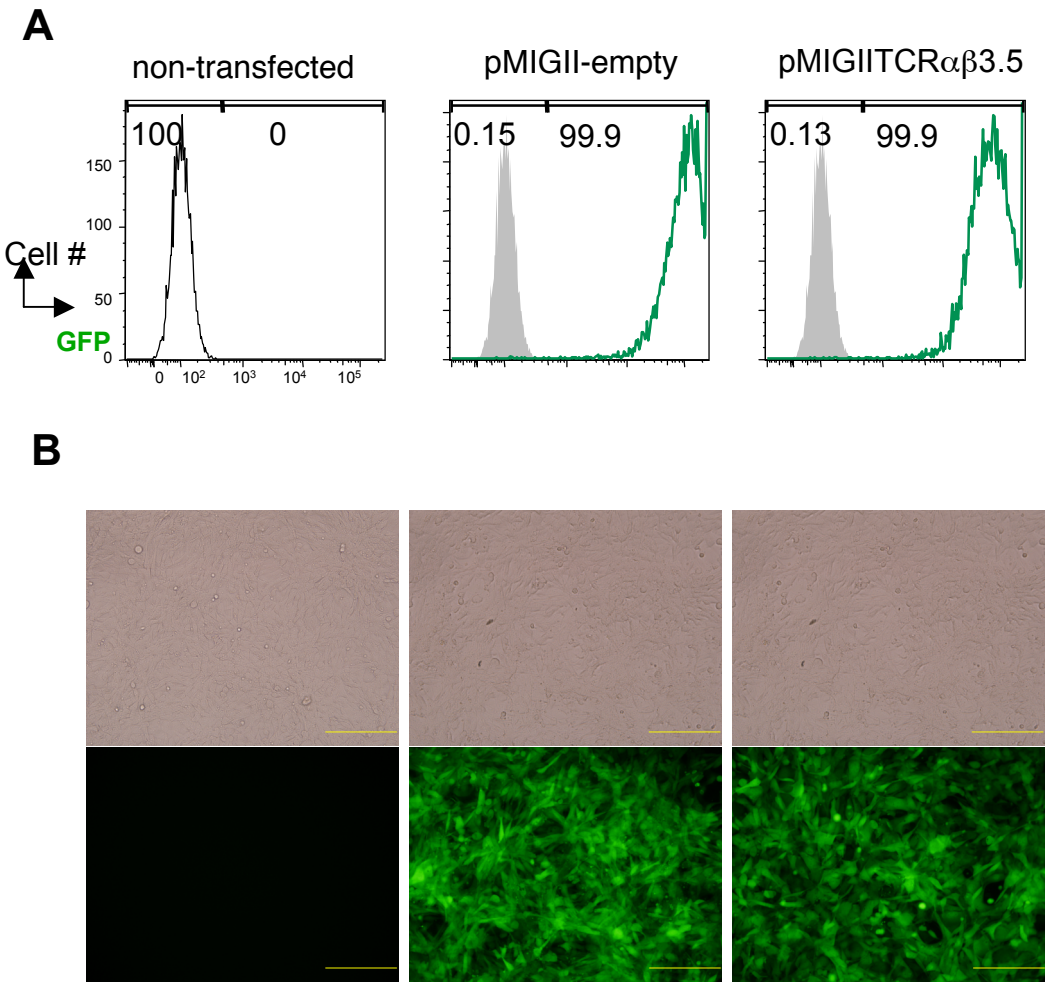

Figure 5.15 The generation of stably transfected retroviral GP+E86 producer cell lines.

A. GPF expression detected by flow cytometry for GP+E86 cells that have been repeatedly transduced with supernatant from 293T cells that had been transiently transfected with pMIGII or pMIGII-TCRαβ3.5 after 72 hours of culture.

B. Brightfield images of the cells in culture after cells have grown to confluency (48 hours after (A)) viewed at x200 magnification; bars represent 200 μm.

C. GFP detection of cells under UV light viewed at x200 magnification; bars represent 200 μm.

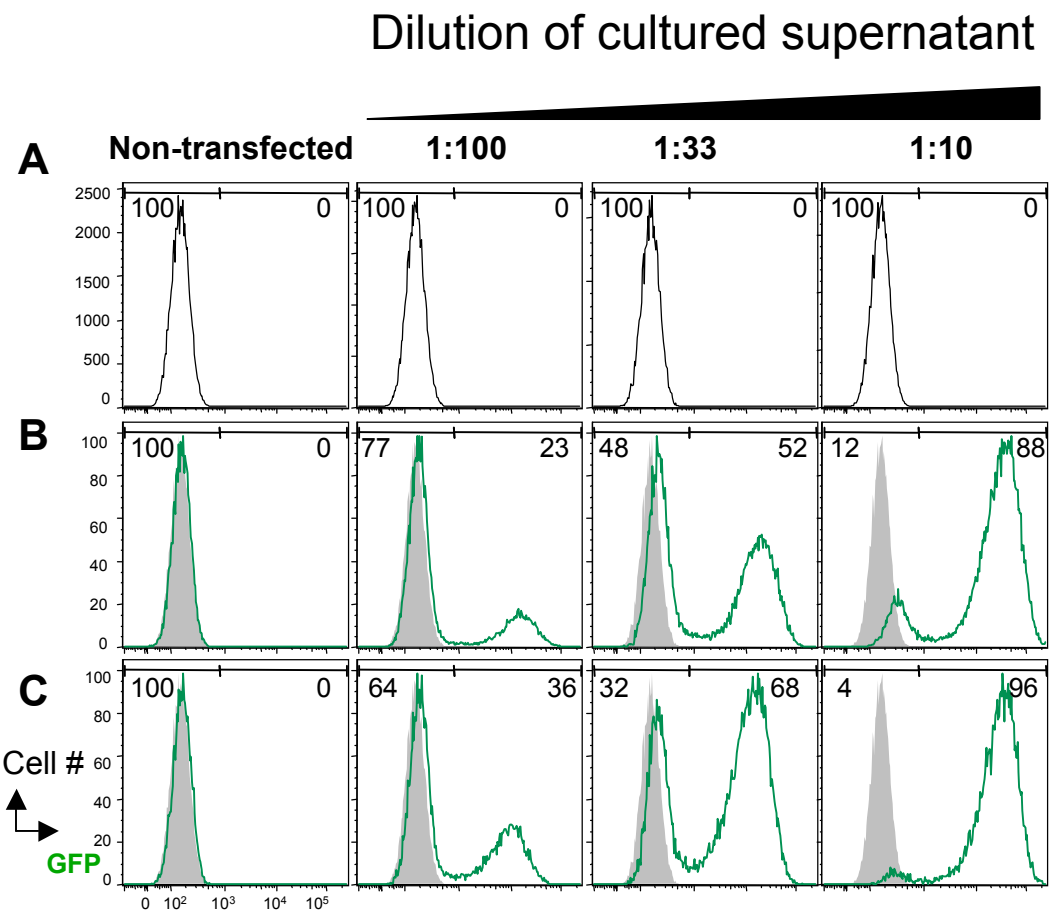

Figure 5.16 Determination of retroviral titres for the stably transduced retroviral GP+E86 producer cell line.
GPF expression detected by flow cytometry for 3T3 cells transduced with the indicated dilutions of retroviral supernatant harvested from GP+E86 after 48 hours of culture.

A. Non transfected
B. pMIGII-empty vector
C. pMIGII-TCR$\alpha\beta$3.5

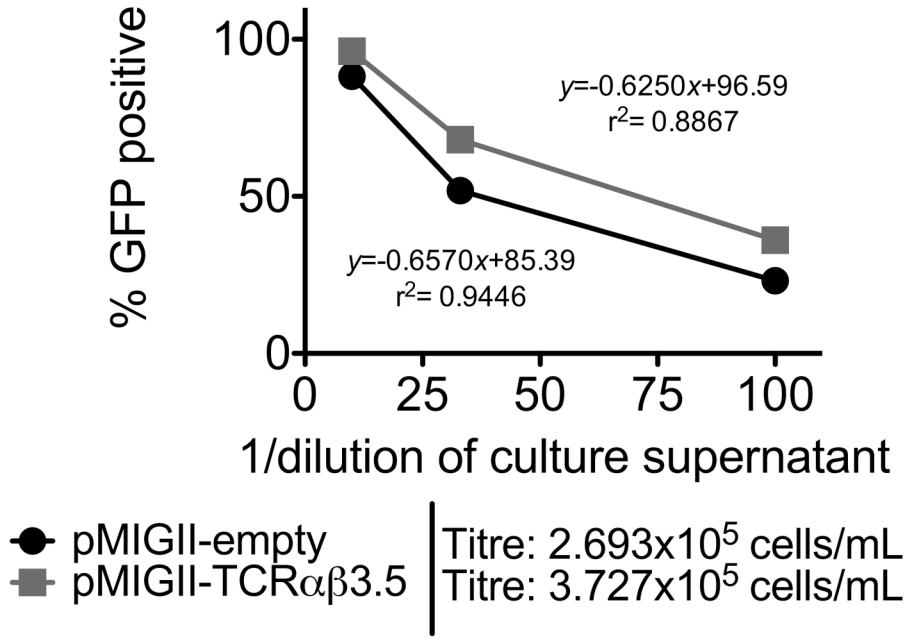

Figure 5.17 Determination of retroviral titres for the stably transduced retroviral GP+E86 producer cell line.
Graph shows the percentage of GFP+ cells resulting from exposure to 1:10, 1:33 and 1:100 dilutions of retroviral supernatant harvested from GP+E86 and applied onto 3T3 cells for 48 hours. A linear regression was performed and the equation and r^2 values for each line of best fit is shown. For determination of titres, the dilution that results in 50% GFP+ cells is interpolated from the equation and used to calculate the total number of GFP+ transduced cells per mL of supernatant using the formula: percent positive × 0.01 × dilution factor × 10^4 cells.

recipient B10.BR.*Aire*$^{-/-}$*Cblb*$^{-/-}$ mice, TCRαβ3.5 retrogenic bone marrow chimeras were generated. The retroviral GP+E86 cell lines expressing pMIGII-TCRαβ3.5 or the control pMIGII-empty vector was used to transduce B10.BR.wild-type or B10.BR.*Cblb*$^{-/-}$ bone marrow. The transduced marrow was used to reconstitute the hemopoietic system of irradiated *Rag1*$^{-/-}$*Aire*$^{+/+}$ or *Rag1*$^{-/-}$*Aire*$^{-/-}$ recipients. This experimental design resulted in TCRαβ3.5 retrogenic chimeras with four relevant genotypic combinations: wild-type T cells and thymic epithelium, *Cblb*$^{-/-}$ T cells with wild-type thymic epithelium, wild-type T cells with *Aire*$^{-/-}$ thymic epithelium, or *Cblb*$^{-/-}$ T cells combined with *Aire*$^{-/-}$ thymic epithelium. Two control groups of chimeras were constructed in parallel, by reconstituting *Rag1*$^{-/-}$*Aire*$^{+/+}$ recipients with B10.BR wild-type bone marrow that was either non-transduced or transduced with pMIGII-empty vector. A detailed schematic of the experimental design is shown in Fig. 5.18.

The bone marrow chimeras were closely monitored for weight loss. By 22 days post reconstitution, all recipients of pMIGII-TCRαβ3.5 transduced marrow began to lose weight regardless of their *Aire* or *Cblb* genotypes. The weight loss appeared to be more severe for the groups receiving the *Cblb*$^{-/-}$ bone marrow, although larger group sizes would be needed to test this inference statistically. By contrast, the recipients of the empty vector transduced bone marrow maintained relatively consistent body weight throughout the 29 days time course (Fig. 5.19). The severe weight loss in the *Aire*$^{-/-}$ *Cblb*$^{-/-}$ retrogenic group may simply reflect the autoimmunity in B10.BR.*Aire*$^{-/-}$*Cblb*$^{-/-}$ bone marrow chimeras described in Chapter 3, since the transplanted bone marrow would generate a polyclonal T cell repertoire. However, the trend towards weight loss in the fully wild-type retrogenic chimeras can be directly compared to the control group which was transduced with pMIGII-empty vector, and suggests that the TCRαβ3.5 cells were able to drive weight loss even with wild-type *Aire* and *Cblb*.

Definitive evidence that TCR3.5-expressing cells drive pancreatic autoimmunity came from histological analysis of the retrogenic animals Fig 5.20. Empty vector transduced wild-type chimeras remained relatively free of pancreatitis, whereas corresponding wild-type chimeras that received TCRαβ3.5-transduced bone marrow displayed severe exocrine pancreatic lymphocytic infiltration (pancreatitis scores ranging from 3 to 5).

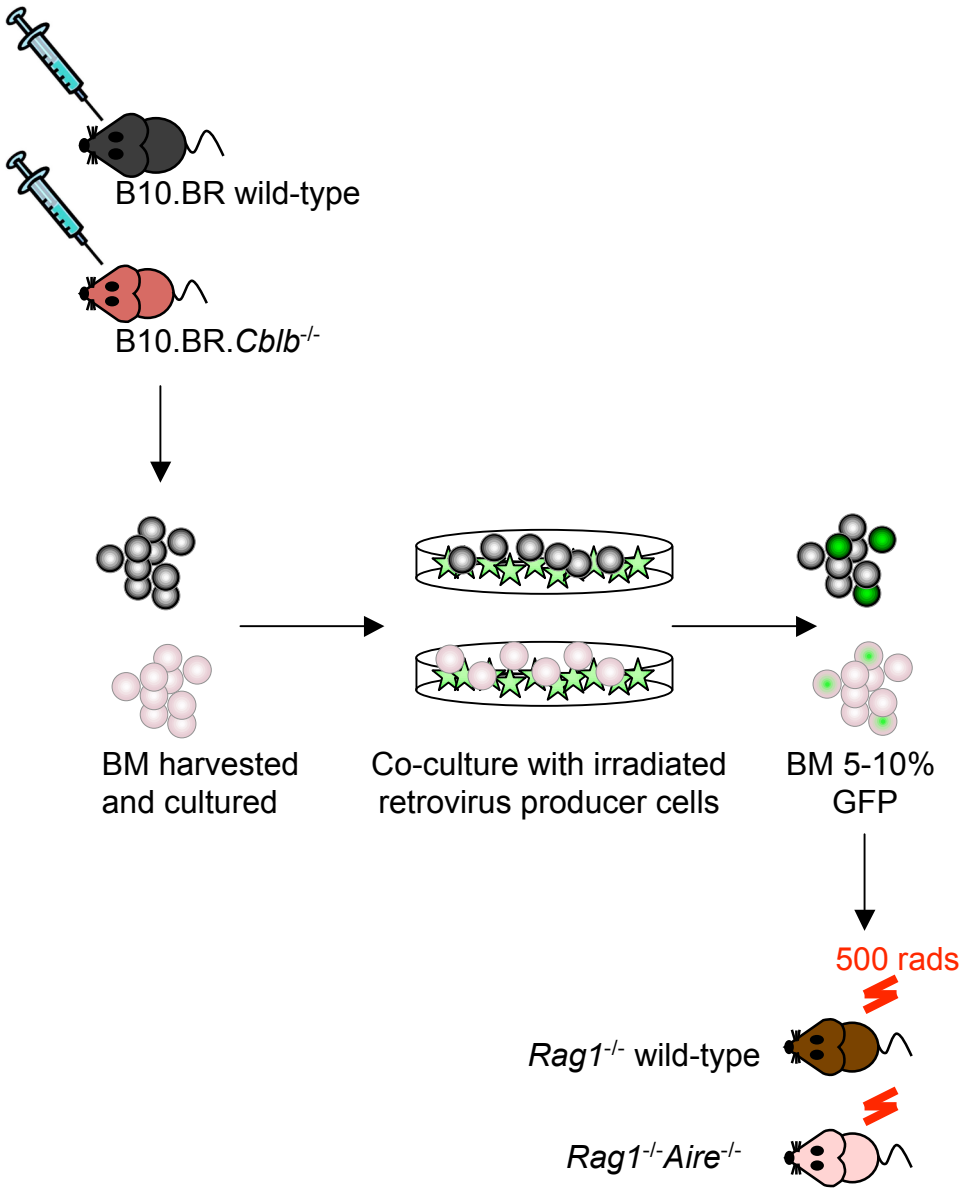

Figure 5.18 Retroviral transduction of bone marrow stem cells. Bone marrow stem cells from 5-fluorouracil-treated wild-type or *Cblb*$^{-/-}$ donor mice were transduced by co-culture with TCRαß3.5 transfected GP+E86 retroviral producer cells and used to reconstitute sub-lethally irradiated *Rag1*$^{-/-}$ wild-type or *Rag1*$^{-/-}$*Aire*$^{-/-}$ recipient mice. This experimental design creates retrogenic chimeras of wild-type, *Aire*$^{-/-}$, *Cblb*$^{-/-}$ and *Aire*$^{-/-}$*Cblb*$^{-/-}$ genotypes.

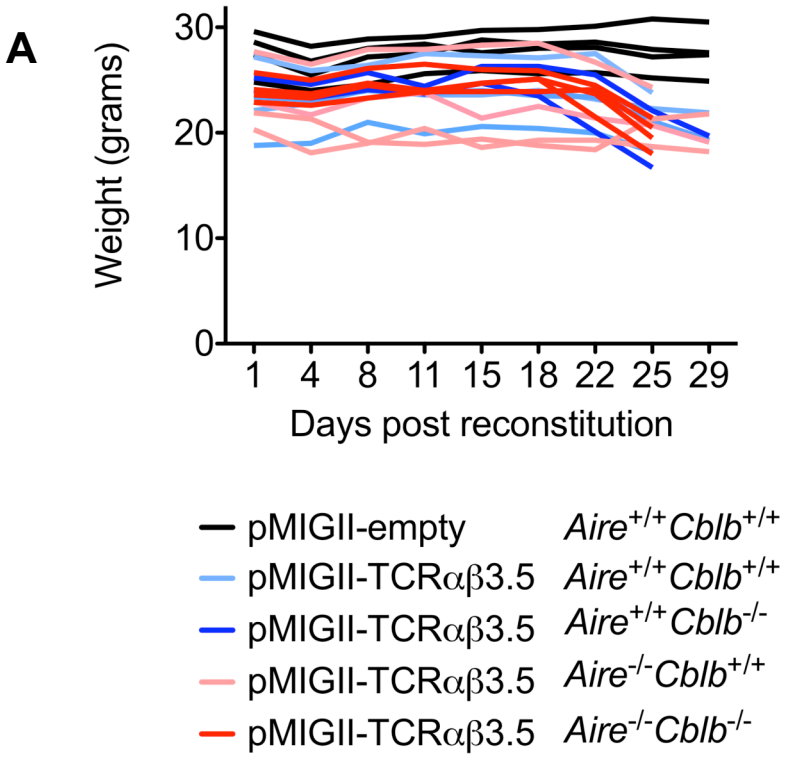

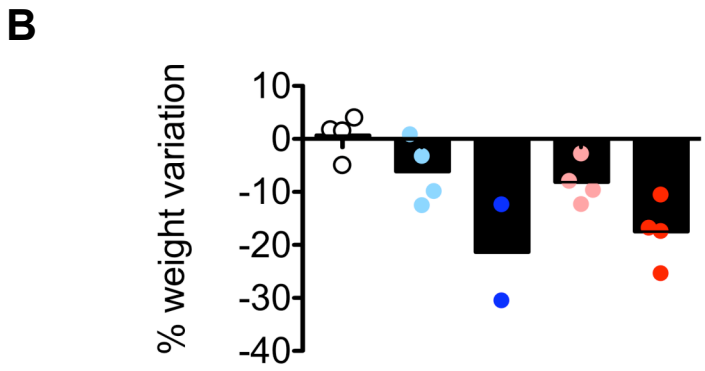

Figure 5.19 TCRαβ3.5 retrogenic mice lose weight within 25 days post-reconstitution.

A. Weight of retrogenic mice monitored for 29 days. Every line represents a single recipient mouse. Mice in the same groups are coded with the same colour.

B. Percentage of weight variation comparing the weight of mice on day 0 and day 25 (when the first group of mice were sacrificed after losing >15% of their body weight). Each dot represents a single mouse, bars represent means.

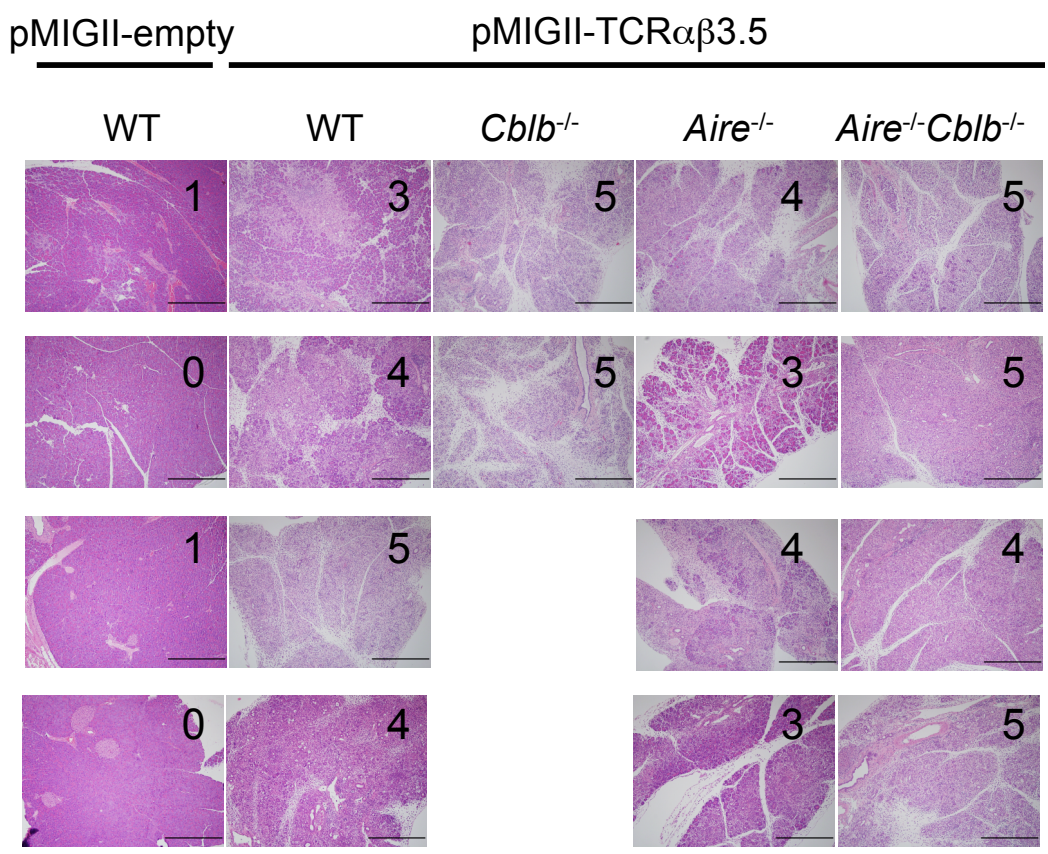

Figure 5.20 TCRαβ3.5 retrogenic mice displayed pancreatitis within 25 days post-reconstitution.
Haematoxylin and eosin stained pancreas sections from retrogenic mice. Magnification: x100, Bars: 500μm. Pancreatitis scores are indicated on the top right corner of each sample.

The fact that pancreatitis was induced by TCRαβ3.5 despite the presence of normal *Aire* in the recipients' thymic epithelium and normal *Cblb* in the T cells may reflect the high frequency of self-reactive T cells or dysregulated expression of the retrogenic TCR, as discussed at the end of this chapter. Regardless, this result validated the adoptive transfer enrichment assays described in section 5.3 by showing that one of the TCR clonotypes that accumulated in the pancreas was indeed an exocrine pancreas-specific driver clone.

Severe pancreatitis was also present in the other TCRαβ3.5-transduced marrow recipient groups Fig 5.20, with those receiving *Cblb*$^{-/-}$ bone marrow displaying marginally more severe disease scores. This trend was consistent with the weight loss observation but is more problematic to interpret because of the occurrence of exocrine pancreatitis in conventional *Rag1*$^{-/-}$ bone marrow chimeras that receive *Cblb* deficient bone marrow or lack *Aire* in their thymic epithelium (unpublished data).

5.4.4 Flow cytometric analysis of TCRαβ3.5 retrogenic mice

To determine the impact of negative and positive selection on T cells expressing TCRαβ3.5 during development in the thymus, the TCRαβ3.5 retrogenic mice were analysed by flow cytometry at the time of sacrifice. Expression of GFP was used to identify T cells that expressed the retroviral vector. The intensity of GFP per cell varied by more than two orders of magnitude within individual chimeras, as well as from one chimera to another (Fig 5.21*A*). This is likely to be caused by variation in the permissiveness for retroviral transcription between different chromosomal sites of retroviral integration, which will be unique in each transduced hemopoietic stem or progenitor cell (Klug et al., 2000). Since the level of retroviral expression in any given cell would influence the amount of TCRαβ3.5 that was produced, the developing thymocytes and mature T cells in all TCRαβ3.5 retrogenic mice were divided into three populations – GFP^{neg}, GFP^{low} and GFP^{hi}. The percentage of cells within each population varied from mouse to mouse, but standardizing cells for the level of retroviral expression allowed cells with high expression (GFP^{hi}) to be compared to those with none (GFP^{neg}). For all the cellular phenotypes described in the remainder of this section, there appeared to be no observable effects of the *Aire*- and *Cblb*-deficiencies in

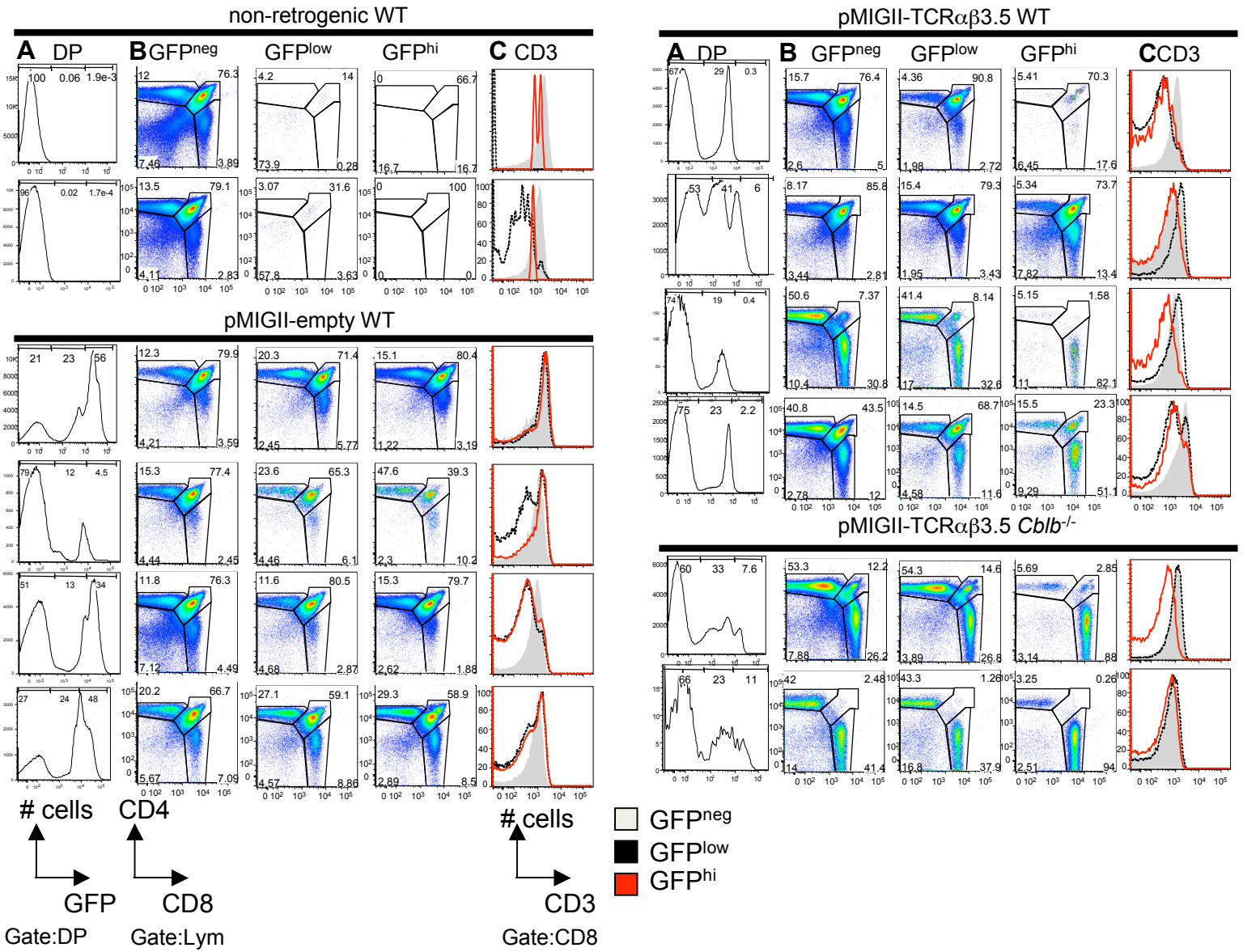
non-retrogenic WT
A DP
B GFPneg
GFPlow
GFPhi
C CD3
pMIGII-empty WT
pMIGII-TCRαβ3.5 WT
pMIGII-TCRαβ3.5 Cblb-/-
cells
CD4
GFP
CD8
Gate:DP
Gate:Lym
cells
CD3
Gate:CD8
GFPneg
GFPlow
GFPhi

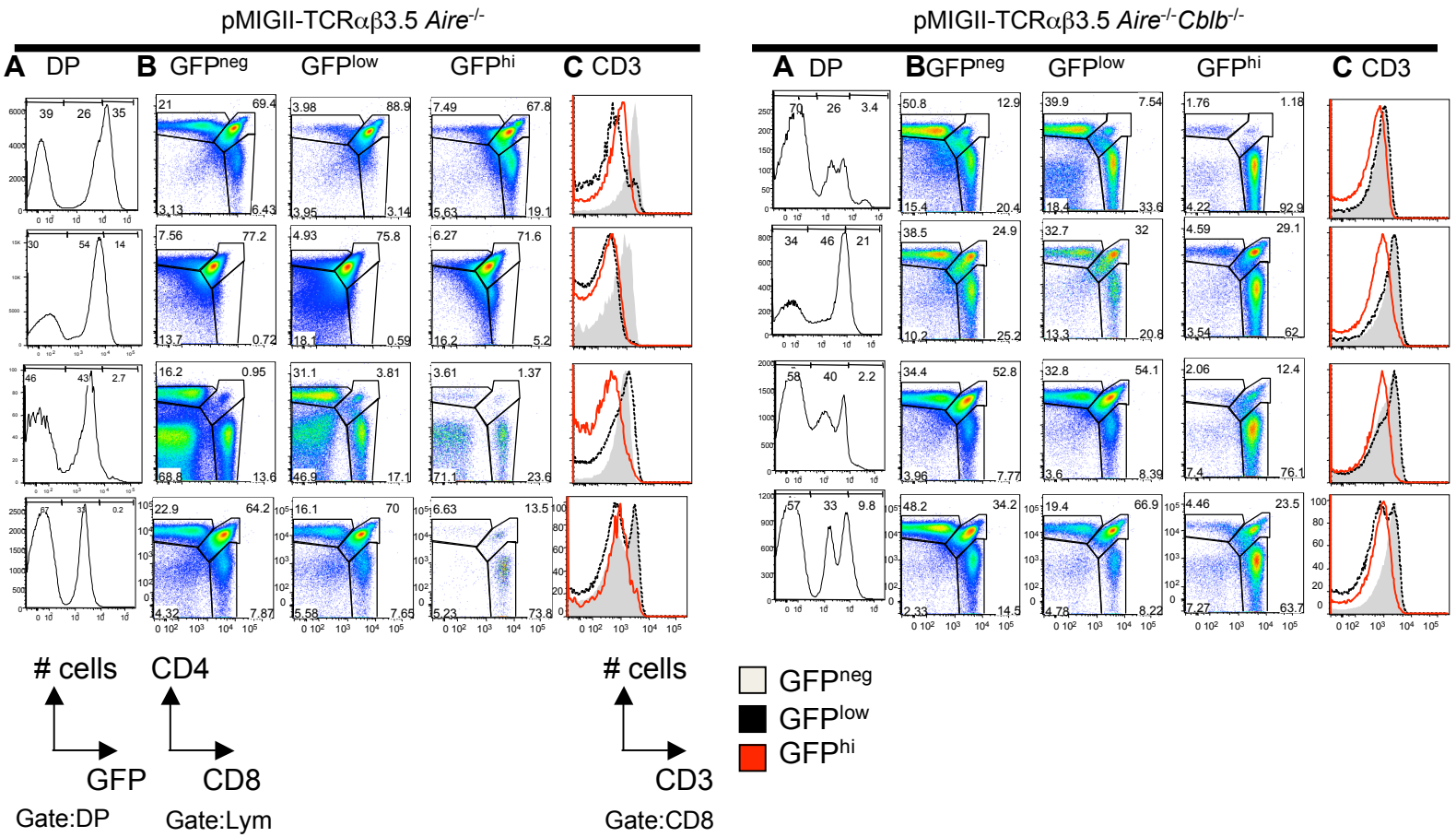

Figure 5.21 Flow cytometry plots of thymocytes in retrogenic mice.

A. Gated on double positive cells, histograms show the distribution of GFP expression on DP cells in each of the indicated experimental groups. The percentage of GFP^{neg}, GFP^{low} and GFP^{hi} cells are shown.

B. CD4 versus CD8 plots gated on GFP^{neg}, GFP^{low} and GFP^{hi} thymocytes. Percent of cells in each window is shown.

C. Overlaid histograms gated on GFP^{neg}, GFP^{low} and GFP^{hi} CD8 cells showing CD3 expressions.

development and activation of T cells expressing high levels of pMIGII-TCRαβ3.5. Hence, for simplicity, all recipient genotypes would be described as a single retrogenic TCRαβ3.5 group unless otherwise stated.

Since the TCR3.5 clonotype was isolated from $CD8^+$ T cells, it would be expected that thymocytes expressing the pMIGII-TCRαβ3.5 vector at high levels would be positively selected into the CD8 single positive (SP) subset. Comparing the percentages of GFP^{hi} thymocytes that developed into $CD4^+$SP or $CD8^+$SP cells tested this hypothesis. As seen in Fig. 5.21 and 5.22, the GFP^{neg} DP T cells that did not express the TCRαβ3.5 receptor formed a lower percentage of $CD8^+$SP than $CD4^+$SP cells, in an ~1:3 ratio that was comparable to that of control chimeras reconstituted with non-transduced or empty vector-transduced bone marrow recipients. Likewise, GFP^{hi} cells expressing the pMIGII-empty vector differentiated into $CD4^+$SP and $CD8^+$SP cells at the normal ratio. By contrast, $CD8^+$SP cells were produced in marked excess to $CD4^+$SP cells in the GFP^{hi} cells expressing pMIGII-TCRαβ3.5 (Fig. 5.22*A*). Thus, expression of TCR3.5 promotes positive selection into the CD8 lineage.

The CD8 SP GFP^{hi} cells expressing pMIGII-TCRαβ3.5 differed from GFP^{hi} CD8 SP cells expressing pMIGII-empty vector, and from CD8 SP cells that were GFP^{neg}, in that they carried less CD3 on their cell surface (Fig 5.21*C* and Fig 5.22*B*). This trait may reflect active downregulation of the 3.5 TCR as a result of its reactivity with self antigens, or it may reflect inefficient cleavage and surface expression of the retrovirally-encoded TCR, as discussed at the end of the chapter.

The accumulation of GFP^{hi} thymocytes within the CD8 SP subset in the retrogenic animals also implied that DP and CD8 SP cells expressing the pancreas-specific autoreactive TCRαβ3.5 were not subjected to pronounced thymic negative selection regardless of the *Aire* or *Cblb* genotype. This contrasted with the marked decrease in CD4 SP cells bearing the insulin-specific TCR^{3A9}:insHEL described in chapter 4, which underwent *Aire*-dependent negative selection, and with published studies of retrogenic mice expressing other self-reactive TCRs (Holst et al., 2006b).

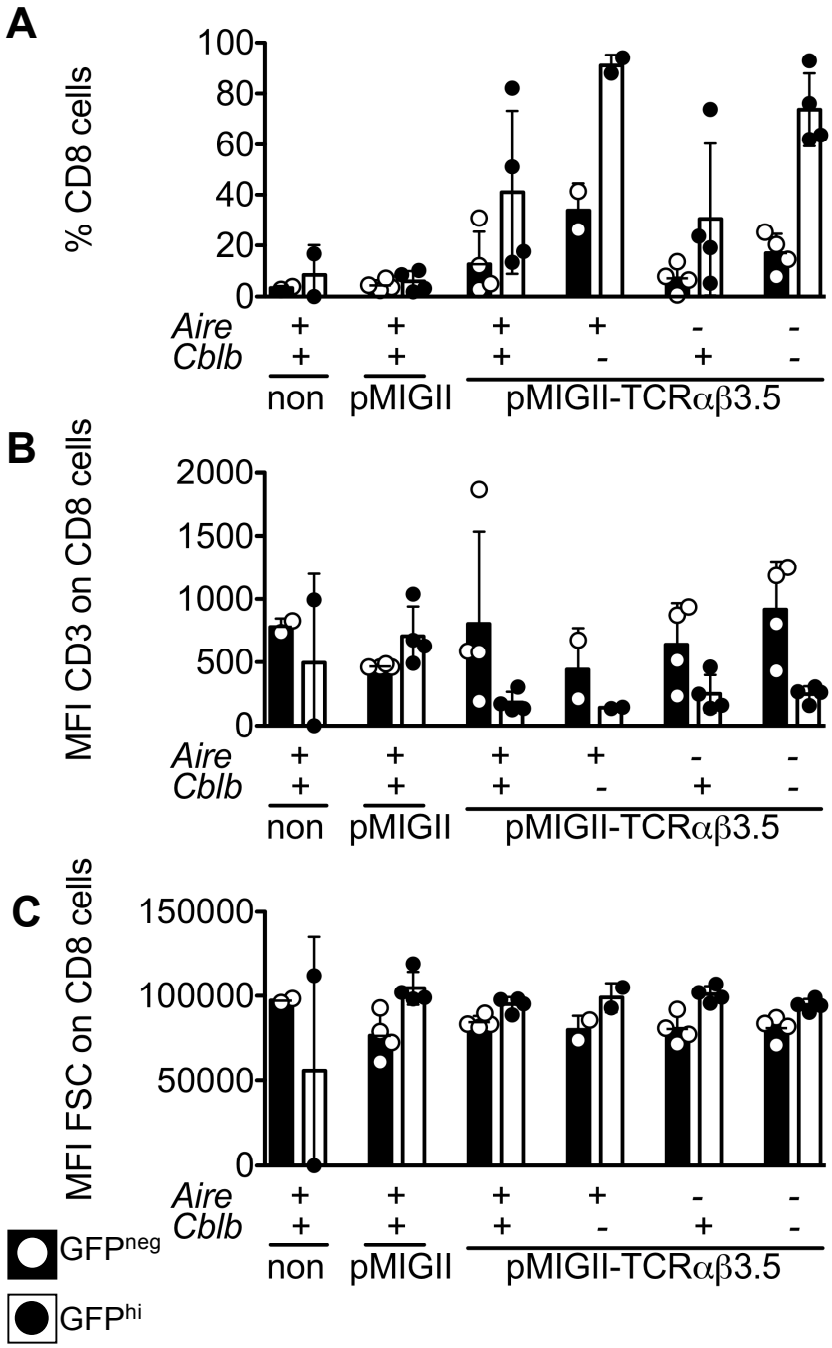

Figure 5.22 Graphs show the comparisons for GFP^{neg} (black bars) and GFP^{hi} (white bars) cells for:

A. Percentages of CD8 cells from total thymocytes
B. CD3 geometric fluorescent mean intensity for CD8 cells
C. Forward light scatter geometric mean intensity for CD8 cells

The conclusion that TCRαβ3.5 expressing cells were not subject to thymic negative selection was reinforced by the finding of high frequencies of $GFP^{hi}CD8^{+}$ T cells in the peripheral lymph nodes and spleen of each of the retrogenic TCRαβ3.5 groups. A normal frequency of $CD8^{+}$ cells, representing ~25% of gated T cells, was observed in $GFP^{neg}CD3^{+}$ T cells in the lymph nodes of all retrogenic animals (Fig. 5.23*A-F*, GFP^{neg} panels; 5.24*A*, upper panel). Likewise, there was a normal frequency of $CD8^{+}$ cells among $GFP^{hi}CD3^{+}$ T cells in control retrogenic animals expressing the pMIGII-empty vector (Fig. 5.23*B* and 5.24*A*). This normal apportioning between CD4 and CD8 subsets is consistent with these T cells lacking TCRαβ3.5 and expressing a normal, polyclonal repertoire of TCRs. By contrast, in $GFP^{hi}CD3^{+}$ T cells expressing the pMIGII-TCRαβ3.5 vector at high levels, $CD8^{+}$ T cells accounted for more than 80% of $GFP^{hi}CD3^{+}$ T cells in the lymph nodes regardless of *Aire* or *Cblb* genotype (Fig. 5.23*C-F* and 5.24*A* lower panel).

Analysis of CD3 expression revealed only a subtle decrease in CD3 expression on the $GFP^{hi}CD8^{+}$ T cells in lymph nodes of the TCRαβ3.5 retrogenic mice (Fig. 5.23*C-F* and 5.24*B* lower panel). This contrasted with the much more marked decrease observed for $GFP^{hi}CD8^{+}$ SP cells in the thymus, suggesting that surface expression of the retroviral-encoded TCR recovered by the time the thymocytes had emigrated and fully matured.

Further analysis of the $GFP^{hi}CD8^{+}$ T cells accumulating in the various peripheral lymph nodes of the retrogenic animals provided evidence that these were not tolerant but were activated selectively in the lymph nodes that drain the pancreas and intestinal tract. In the axillary and inguinal lymph nodes of TCRαβ3.5 retrogenic mice the mean geometric intensity of forward scatter for $GFP^{hi}CD8^{+}$ T cells was comparable to that of GFP^{hi} $CD8^{+}$ T cells from the empty vector control retrogenic animals (Fig. 5.23*C-F* , 5.25 and 5.27*A* lower panel). This measure of T cell size increased in the pancreatic lymph node and mesenteric lymph node of the TCRαβ3.5 retrogenic mice but not in the empty vector controls (Fig. 5.23*C-F* , 5.25 and 5.27*A* lower panel).

The difference in CD8 T cell activation between pancreatic versus inguinal and axillary lymph nodes was most clearly revealed when CD44 expression was used as a measure

Figure 5.23 Representative flow cytometry plots and histograms of peripheral lymphocytes in retrogenic mice.

For each sample, flow cytometric plots represent CD45.2, B cells, T cells, CD4 cells, CD8 cells, FSC, CD3 expression and CD44 expression on GFP^{neg}, GFP^{low} and GFP^{hi} expressors from experimental groups.

A. Non-retrogenic control
B. Wild-type pMIGII vector control
C. Wild-type pMIGII-TCRαß3.5
D. *Cblb*$^{-/-}$ pMIGII-TCRαß3.5
E. *Aire*$^{-/-}$ pMIGII-TCRαß3.5
F. *Aire*$^{-/-}$ Cblb$^{-/-}$ pMIGII-TCRαß3.5

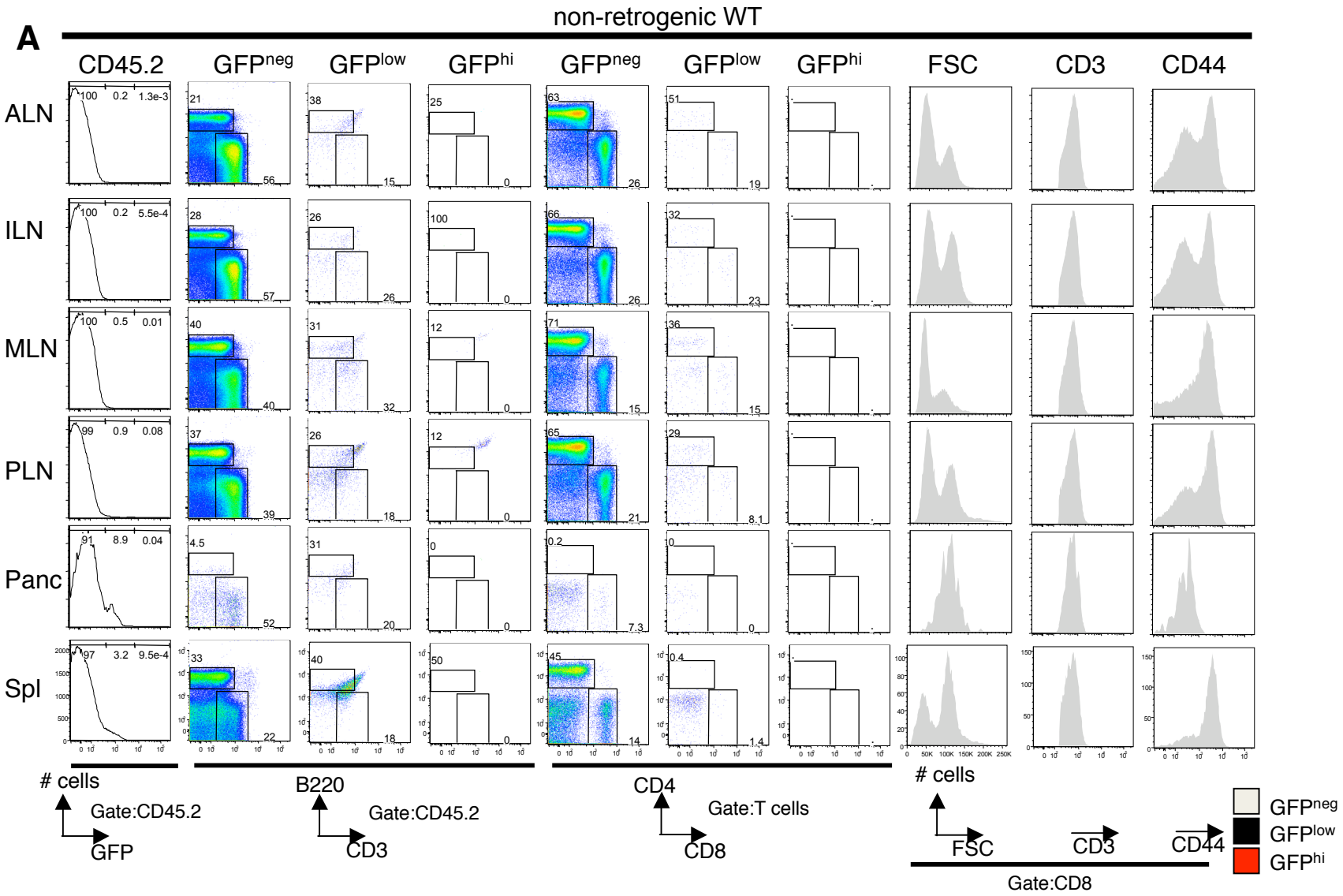
A
non-retrogenic WT
CD45.2
GFPneg
GFPlow
GFPhi
GFPneg
GFPlow
GFPhi
FSC
CD3
CD44
ALN
ILN
MLN
PLN
Panc
Spl
cells
Gate:CD45.2
GFP
B220
Gate:CD45.2
CD3
CD4
Gate:T cells
CD8
cells
FSC
CD3
CD44
Gate:CD8
GFPneg
GFPlow
GFPhi

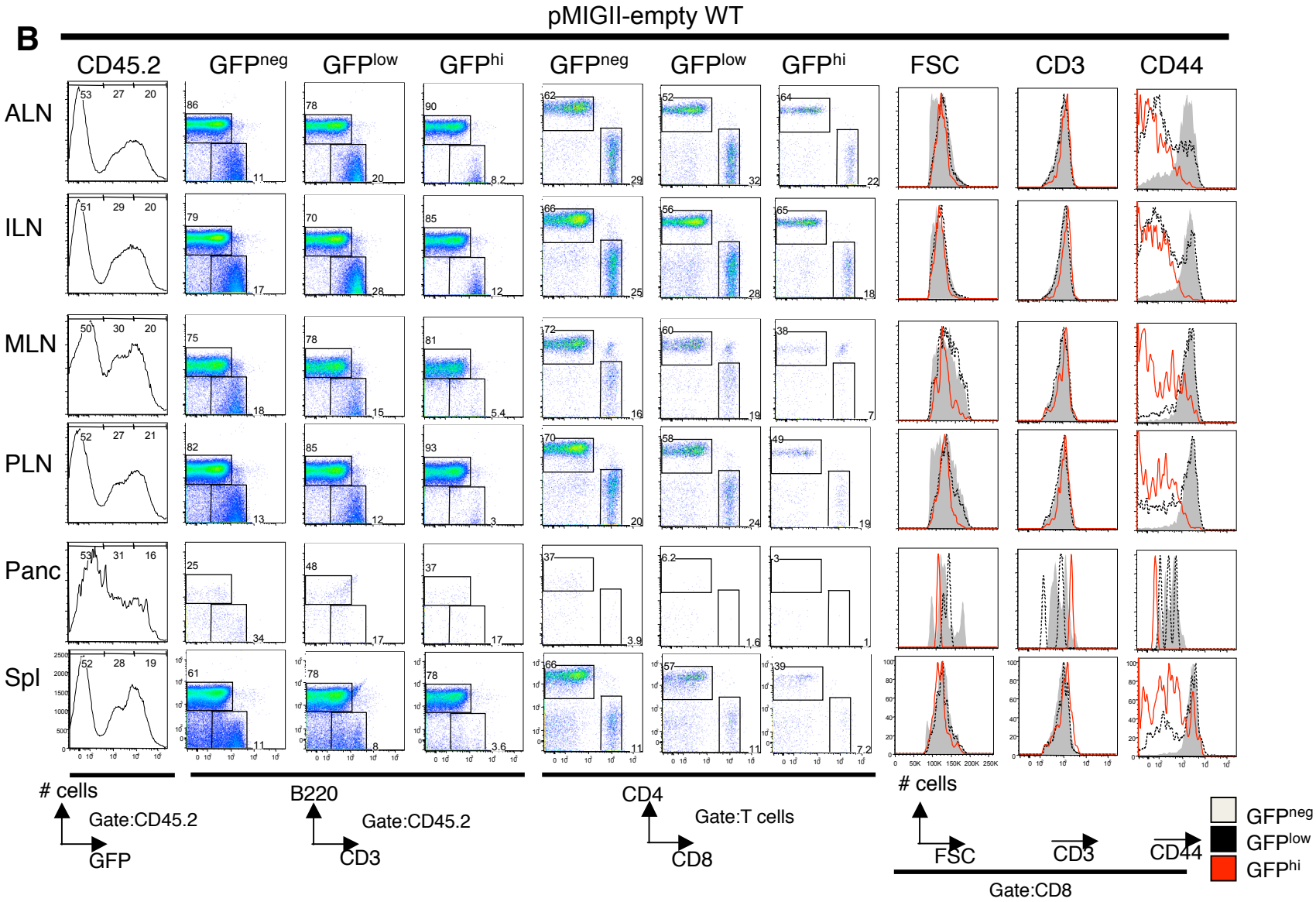
B
pMIGII-empty WT
CD45.2
GFPneg
GFPlow
GFPhi
GFPneg
GFPlow
GFPhi
FSC
CD3
CD44
ALN
ILN
MLN
PLN
Panc
Spl
cells
Gate:CD45.2
GFP
B220
Gate:CD45.2
CD3
CD4
Gate:T cells
CD8
cells
FSC
CD3
CD44
Gate:CD8
GFPneg
GFPlow
GFPhi

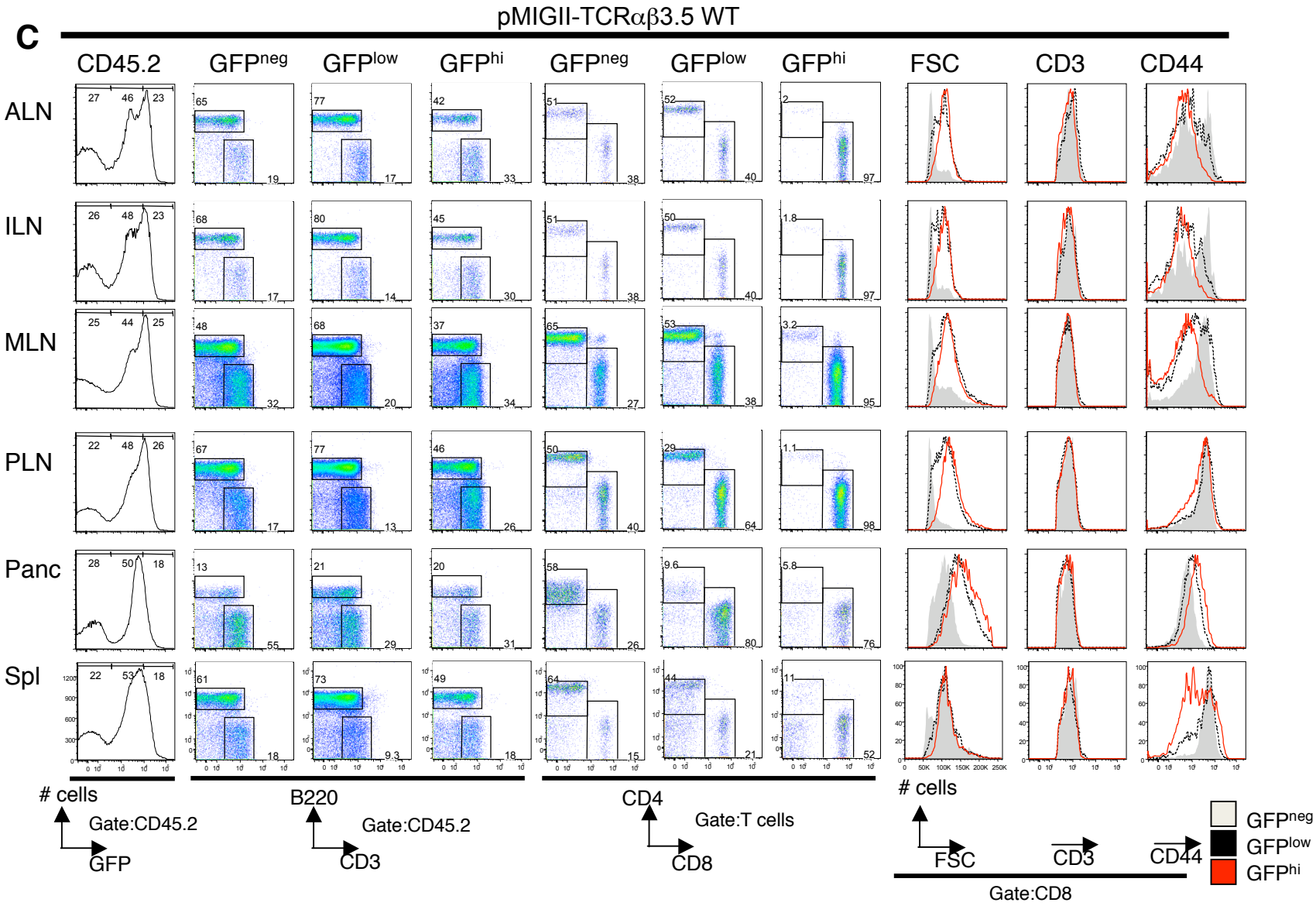
C
pMIGII-TCRαβ3.5 WT
CD45.2
GFPneg
GFPlow
GFPhi
GFPneg
GFPlow
GFPhi
FSC
CD3
CD44
ALN
ILN
MLN
PLN
Panc
Spl
cells
Gate:CD45.2
GFP
B220
Gate:CD45.2
CD3
CD4
Gate:T cells
CD8
cells
FSC
CD3
CD44
Gate:CD8
GFPneg
GFPlow
GFPhi

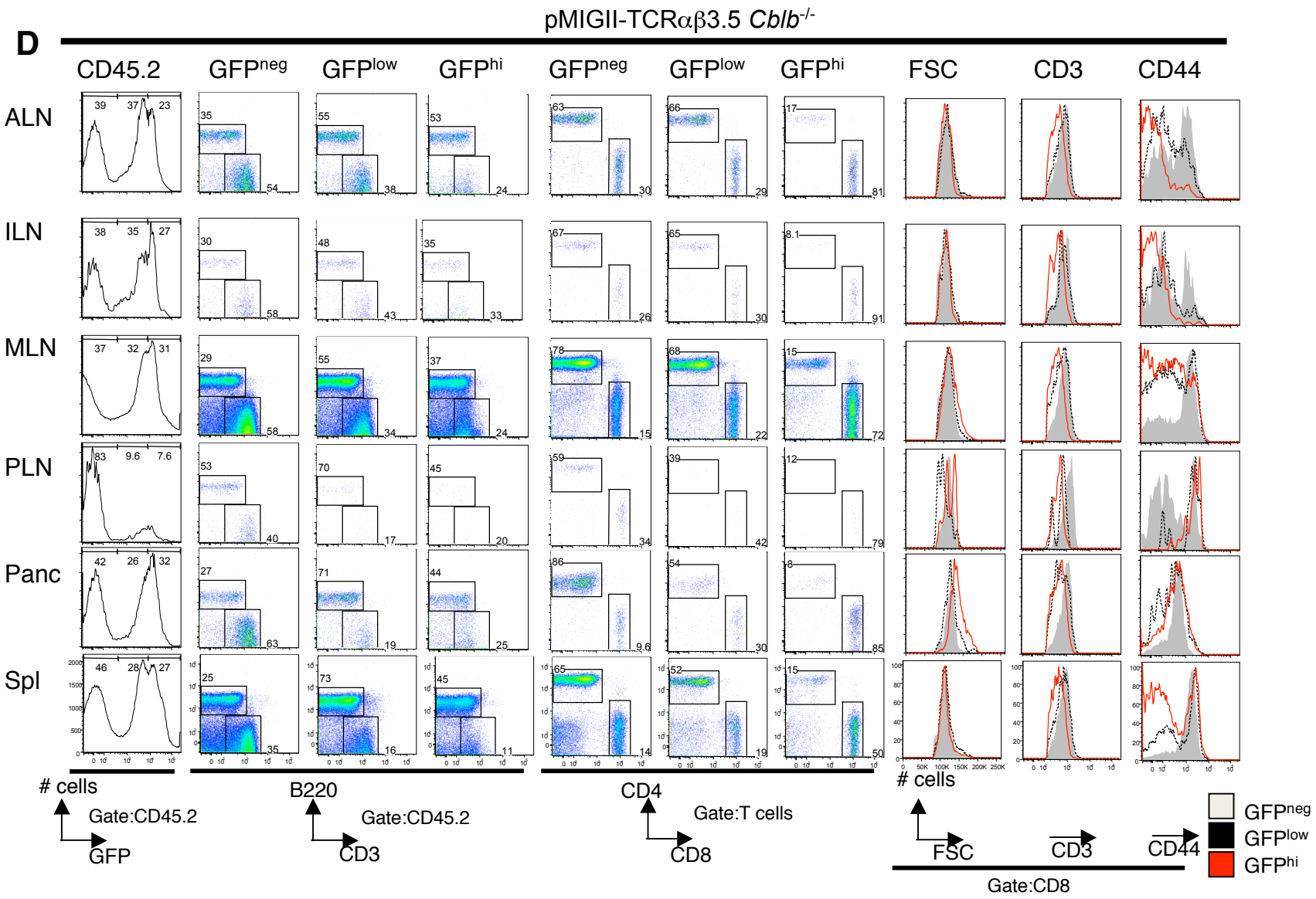
D
pMIGII-TCRαβ3.5 Cblb-/-
CD45.2
GFPneg
GFPlow
GFPhi
GFPneg
GFPlow
GFPhi
FSC
CD3
CD44
ALN
ILN
MLN
PLN
Panc
Spl
cells
Gate:CD45.2
GFP
B220
Gate:CD45.2
CD3
CD4
Gate:T cells
CD8
cells
FSC
CD3
CD44
Gate:CD8
GFPneg
GFPlow
GFPhi

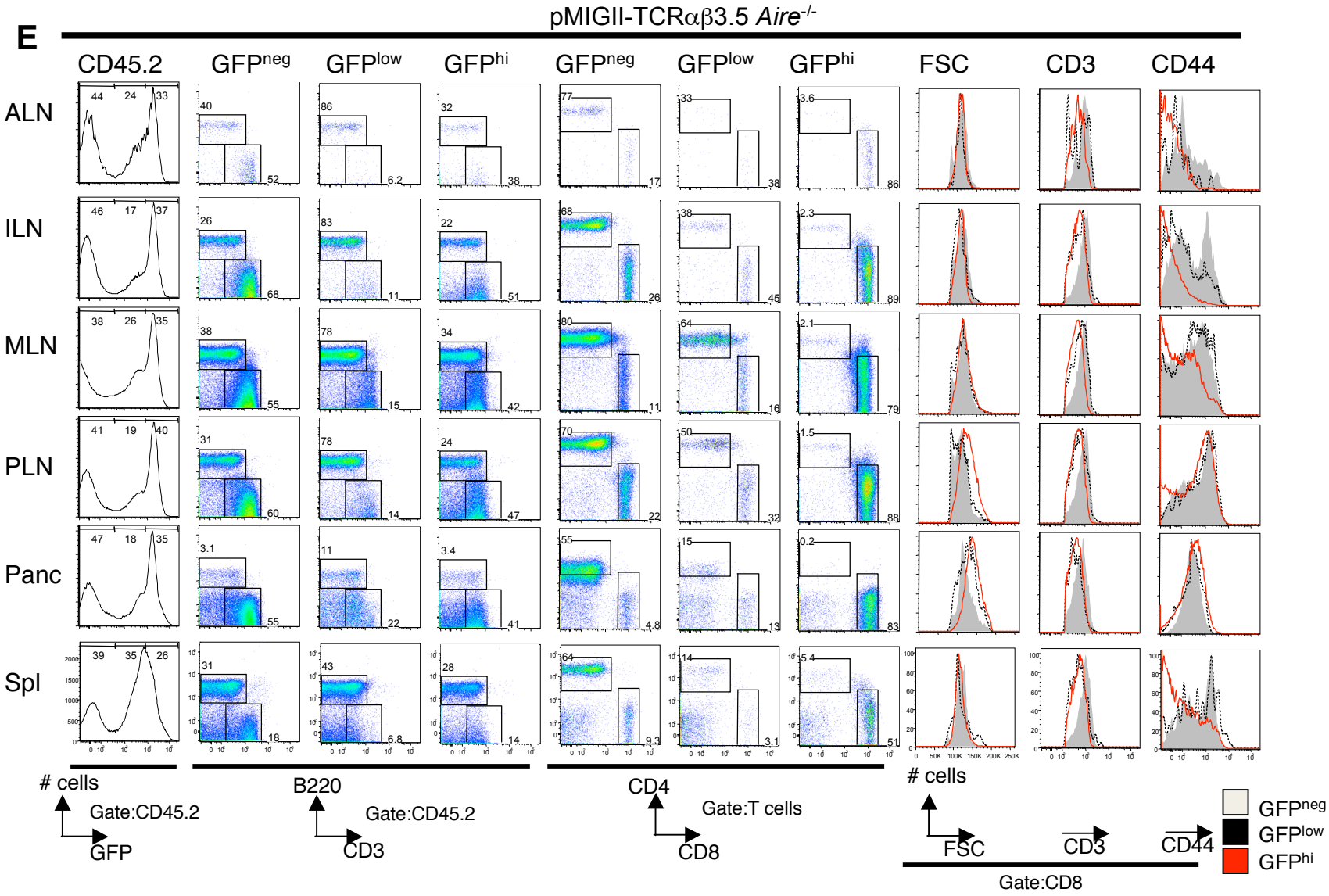
E
pMIGII-TCRαβ3.5 Aire-/-
CD45.2
GFPneg
GFPlow
GFPhi
GFPneg
GFPlow
GFPhi
FSC
CD3
CD44
ALN
ILN
MLN
PLN
Panc
Spl
cells
Gate:CD45.2
GFP
B220
Gate:CD45.2
CD3
CD4
Gate:T cells
CD8
cells
FSC
CD3
CD44
Gate:CD8
GFPneg
GFPlow
GFPhi

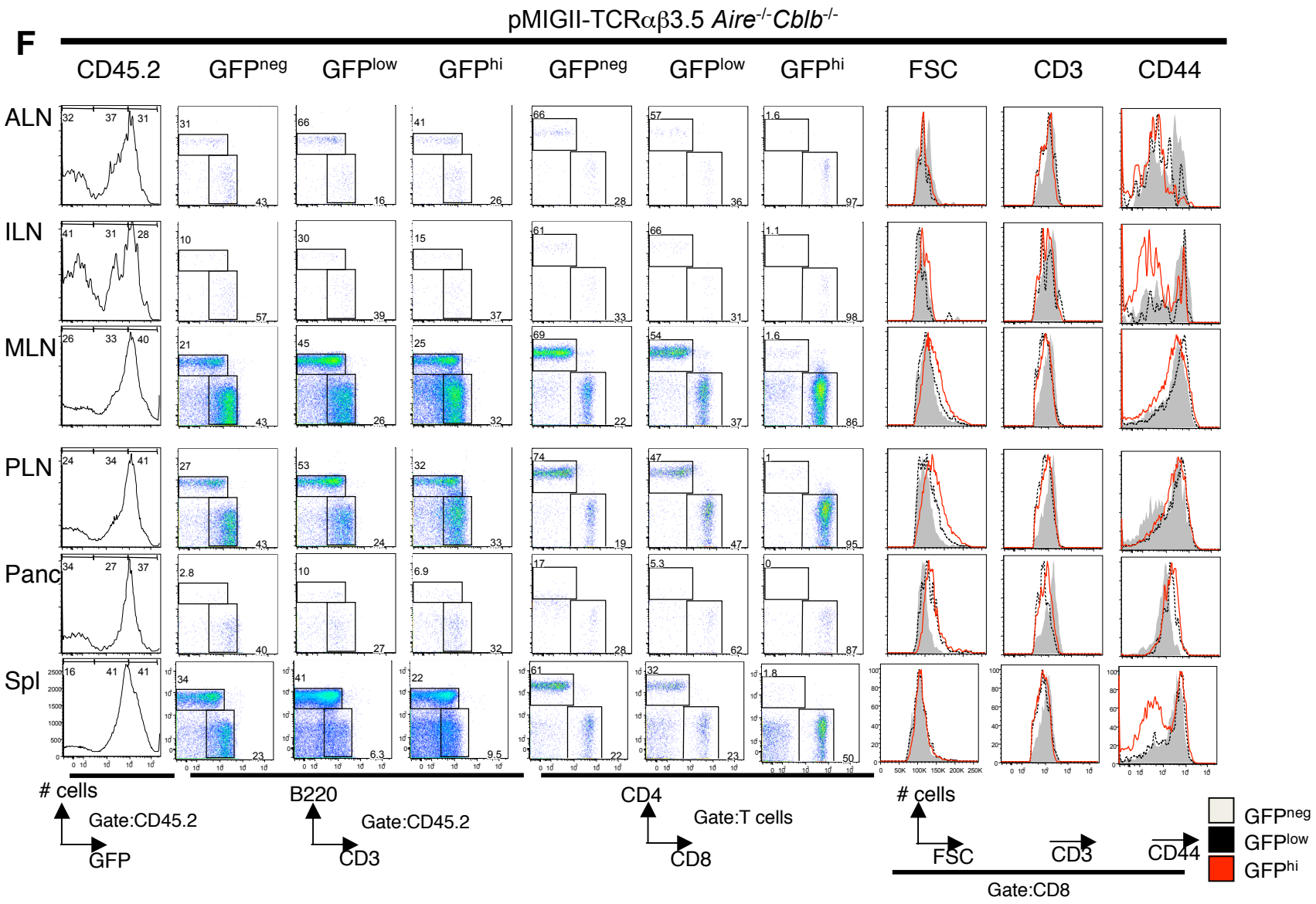
F
pMIGII-TCRαβ3.5 Aire-/-Cblb-/-
CD45.2
GFPneg
GFPlow
GFPhi
GFPneg
GFPlow
GFPhi
FSC
CD3
CD44
ALN
ILN
MLN
PLN
Panc
Spl
cells
Gate:CD45.2
GFP
B220
Gate:CD45.2
CD3
CD4
Gate:T cells
CD8
cells
FSC
CD3
CD44
Gate:CD8
GFPneg
GFPlow
GFPhi

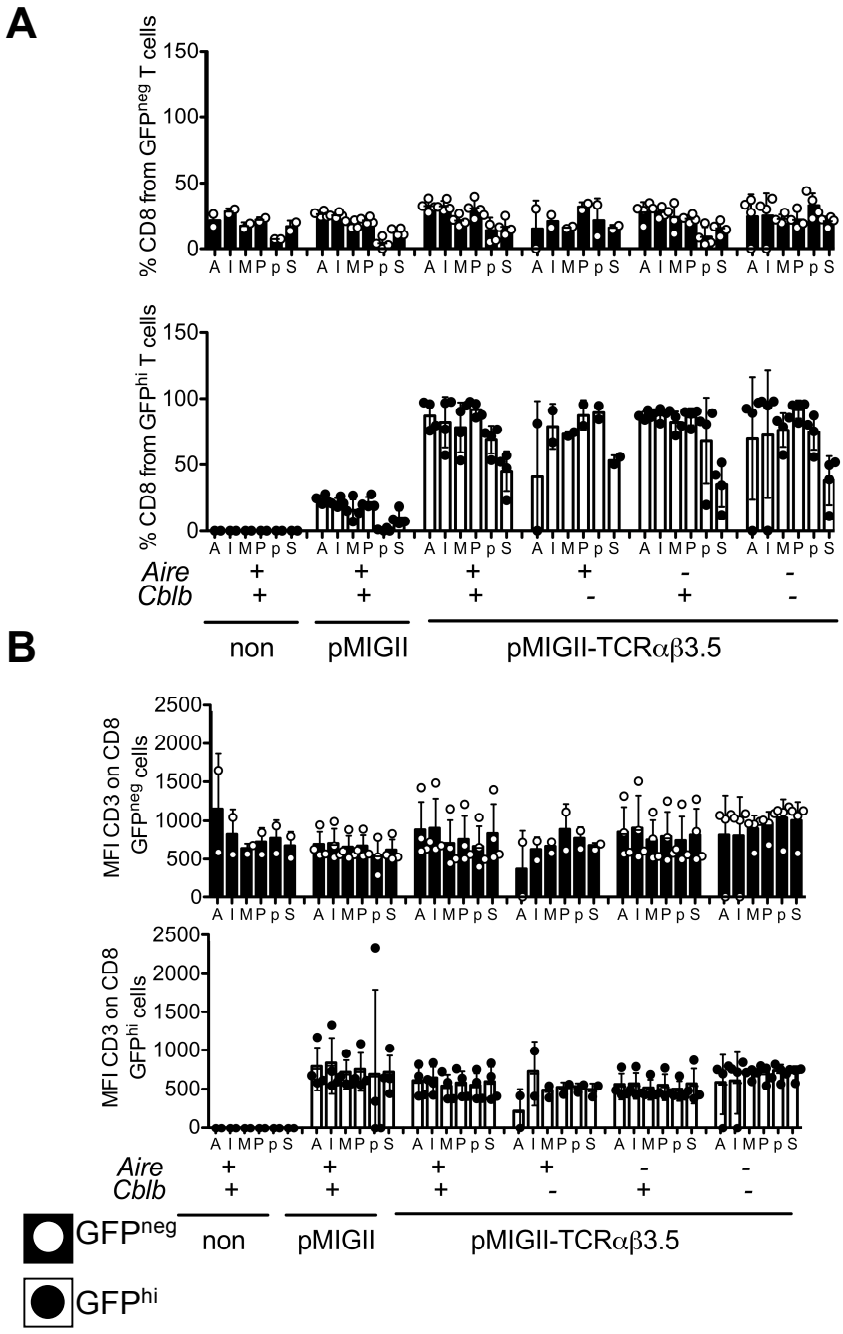

Figure 5.24 Graphs show the comparisons for GFP^{neg} (black bars) and GFP^{hi} (white bars) cells for:

A. Percentages of CD8 cells from total T cells

B. CD3 geometric fluorescent mean intensity for CD8 cells

Each dot represents a single mouse. Bars represent means and error bars represents standard deviations. A: Axillary lymph node, I: Inguinal lymph node, M: messenteric lymph node, P: Pancreatic lymph node, p: pancreas, S: spleen

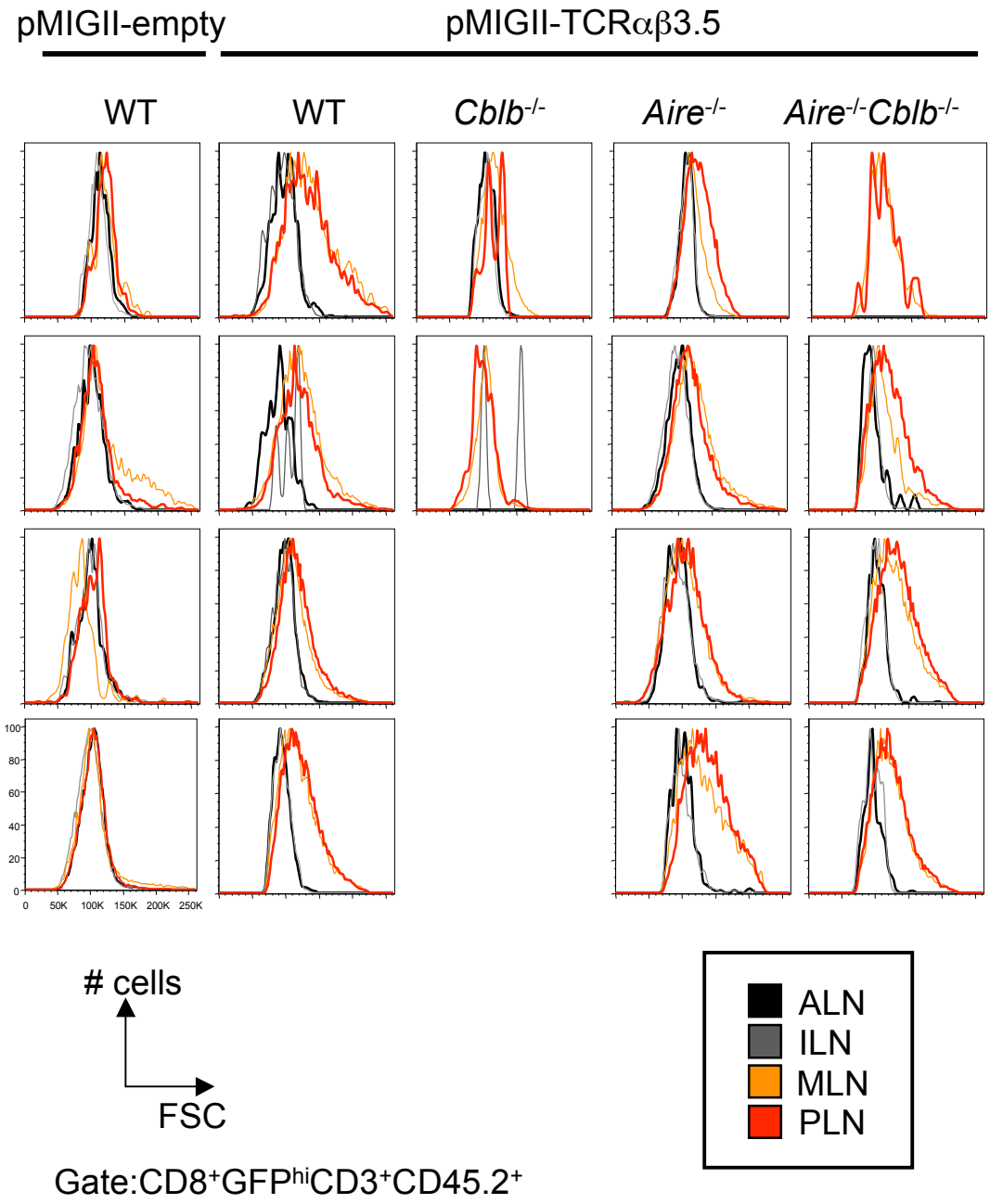

Figure 5.25 Histograms of forward size scatter measurement on $CD8^{+}GFP^{hi}CD3^{+}CD45.2^{+}$ cells in axillary (ALN), inguinal (ILN), messenteric (MLN), pancreatic (PLN) lymph nodes.

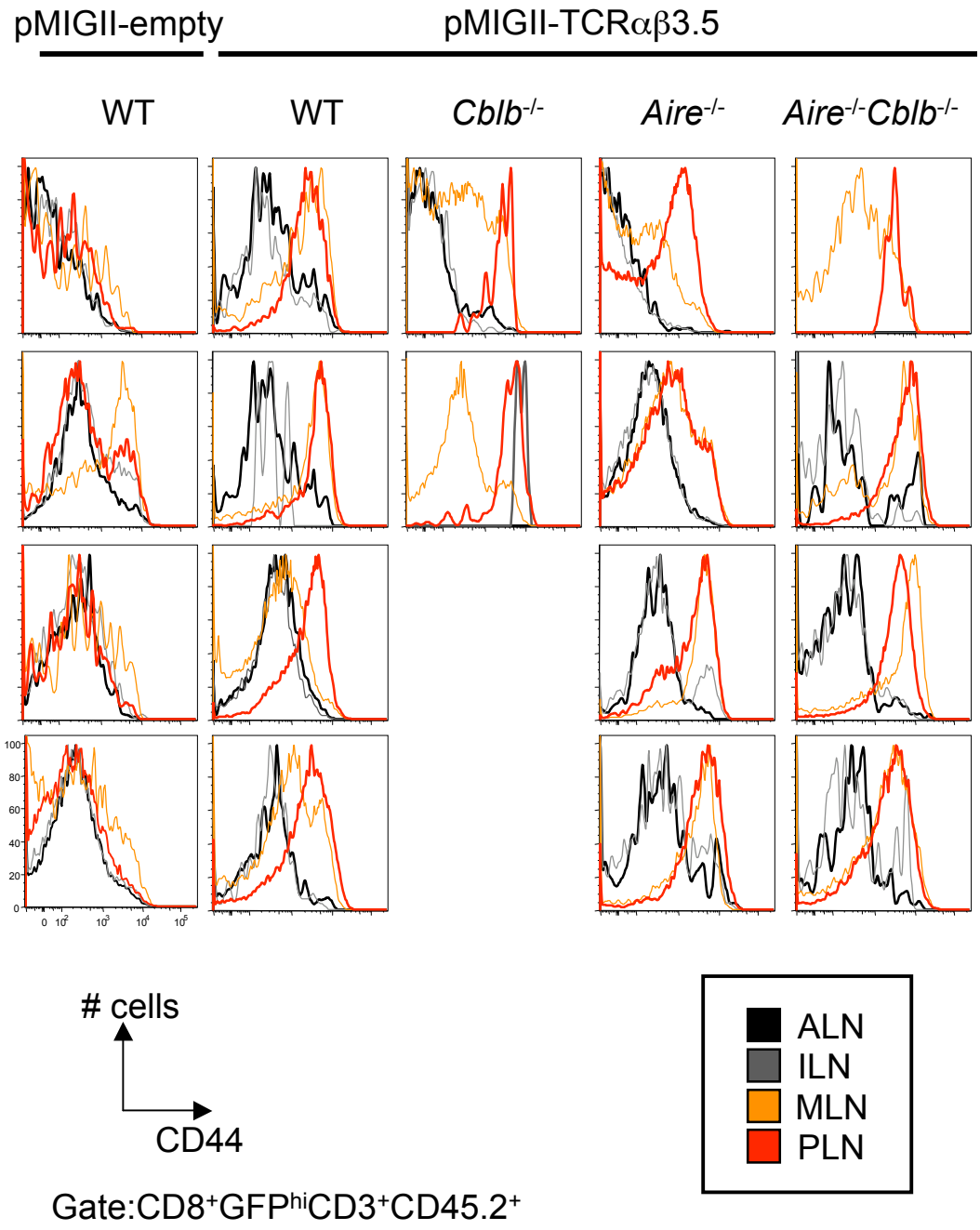

Figure 5.26 Histograms of CD44 expression on $CD8^+GFP^{hi}CD3^+CD45.2^+$ cells in axillary (ALN), inguinal (ILN), messenteric (MLN), pancreatic (PLN) lymph nodes.

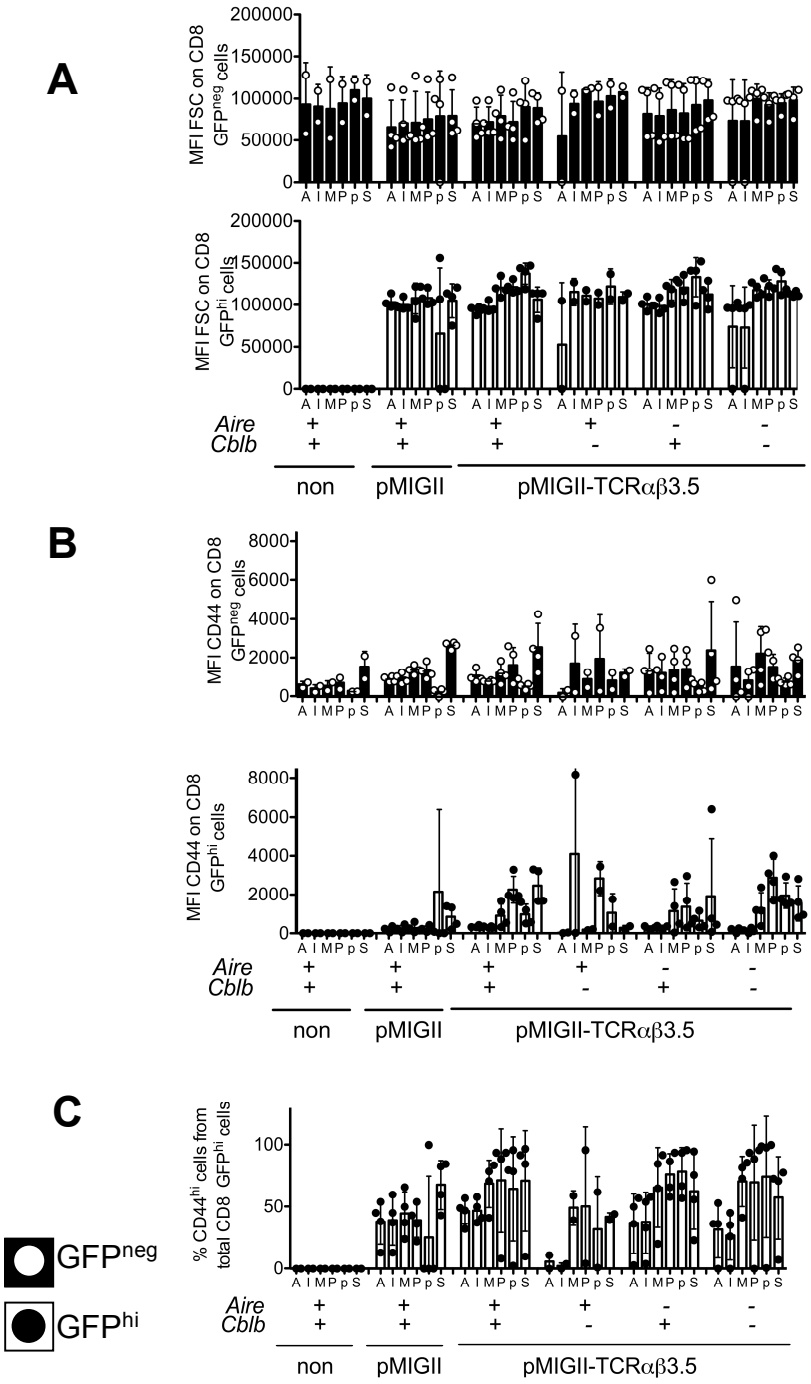

Figure 5.27 Graphs show the comparisons for GFP^{neg} (black bars) and GFP^{hi} (white bars) cells for:

A. Forward light scatter geometric mean intensity

B. CD44 mean geometric intensity for

C. (B) represented as percentage of CD8 GFP^{hi} cells that are CD44^{hi}

Each dot represents a single mouse. Bars represent means and error bars represents standard deviations. A: Axillary lymph node, I: Inguinal lymph node, M: messenteric lymph node, P: Pancreatic lymph node, p: pancreas, S: spleen

of T cell activation (Fig. 5.23*C-F* , 5.26 and 5.27*B-C* lower panel). In the axillary and inguinal lymph nodes of TCRαβ3.5 retrogenic mice the majority of $GFP^{hi}CD8^{+}$ T cells were $CD44^{low}$, bearing levels of CD44 comparable to those of antigenically naïve CD8 T cells. By contrast, the majority of $GFP^{hi}CD8^{+}$ T cells were $CD44^{hi}$ in the pancreatic lymph nodes of the same chimeras, consistent with their having encountered pancreas-derived autoantigen on dendritic cells in the pancreatic lymph node. In the mesenteric lymph nodes and spleen of the retrogenic animals, there were intermediate frequencies of activated $CD44^{hi}$ activated T cells among the GFP^{hi} CD8 cell subset. In the case of the spleen, these activated T cells are likely to have migrated to the organ via the bloodstream after activation in the pancreatic lymph node, since the downregulation of CD62L lymph node homing receptors that occurs on activated T cells still allows their migration to the spleen whereas migration to other lymph nodes is normally blocked. By the same reasoning, the activated GFP^{hi} CD8 cells in the mesenteric lymph node are likely to have been activated *in situ*. This observation raises two possibilities. One possibility is that the pancreatic autoantigen recognized by $TCR3.5^{+}$ CD8 cells was also made in the intestine, where it was captured and presented by dendritic cells that migrate via intestinal lymph to the mesenteric node. Evidence for pancreatic enzyme expression by intestinal epithelial cells exists (Ponnuraj and Hayward, 2001). Alternatively, some dendritic cells or activated T cells that originate in the pancreas may migrate to the mesenteric node, for example via the peritoneal cavity, which is known to drain especially to the pancreatic lymph nodes and thence to the mediastinal intrathoracic lymph nodes, but also to the mesenteric lymph nodes (Andrade et al., 1996; Parungo et al., 2007; Turley et al., 2005; Watanabe et al., 2000).

5.5 Chapter summary and key findings

5.5.1 Multiplex single cell sequencing to isolate autoimmune driver clones in *Aire*$^{-/-}$*Cblb*$^{-/-}$ mice.

The aim of this chapter was to further understand the cellular basis for co-operative interaction between *Aire* and *Cblb*-deficiencies by establishing an experimental system to determine the specificity and regulation of the autoimmune driver T cell clone(s) in *Aire*$^{-/-}$*Cblb*$^{-/-}$ mice. To achieve this, two rounds of adoptive transfer of *Aire*$^{-/-}$*Cblb*$^{-/-}$ splenocytes into lymphopenic *Rag1*-deficient were used, followed by single cell TCR

profiling, to isolate putative pancreas-specific TCRα and TCRβ chains carried by driver CD4 and CD8 clones.

Following secondary transfers, there were cellular phenotypic differences between the wild-type and *Aire*$^{-/-}$*Cblb*$^{-/-}$ cell recipients. Flow cytometry analysis (Figs. 5.3 and 5.10) showed an over-representation of the CD8 cells or under-representation of CD4 cells in the *Aire*$^{-/-}$*Cblb*$^{-/-}$ recipients compared to wild-type counterparts. Additionally, forward side scatter measurements indicated that the *Aire*$^{-/-}$*Cblb*$^{-/-}$ recipient CD8 cells were enlarged, a common indication of activation. Although the splenic adoptive transfer assays in Chapter 3 indicated that both CD4 and CD8 cells were necessary for lethal autoimmunity in the recipients, transfer of CD4-depleted or CD8-enriched spleen cells was sufficient to induce extensive exocrine pancreatitis measured histologically. Thus, it is possible that pancreas-specific CD8 cells are responsible for the major insult to the exocrine pancreas cells while CD4 cells provide help to augment CD8 cell accumulation and differentiation into cytotoxic effectors. This scenario is supported by evidence of co-operation between CD8 and CD4 cells in adoptive transfer and depletion studies in NOD mice (Bendelac et al., 1987; Miller et al., 1988; Mora et al., 1999; Nagata et al., 1994; Peterson and Haskins, 1996; Santamaria et al., 1995; Serreze et al., 2001; Verdaguer et al., 1997; Wang et al., 1996; Wong et al., 1996; Wong et al., 1998; Yagi et al., 1992). Direct evidence that autoreactive CD4 cells help CD8 cell expansion and autoimmune destruction comes from adoptive co-transfer of autoreactive CD8 and CD4 cells recognizing ovalbumin or influenza haemagglutinin expressed as transgenic self antigens in pancreatic islet beta cells (Hernandez et al., 2002; Kurts et al., 1997a). CD8 T cells may also possess the ability to undergo greater clonal expansion compared to CD4 cells. My results have parallels with the observation that CD8-antigen specific but not CD4 T cells were over-represented in peripheral blood in Hashimoto's thyroiditis patients, and there was a trend for a more CD8 skewed repertoire in patients who had suffered with the disease for an extended period of time compared to newly diagnosed patients (Okajima et al., 2009).

Surprisingly, despite cellular differences in wild-type and *Aire*$^{-/-}$*Cblb*$^{-/-}$ CD8 cells isolated from secondary recipients, single-cell TCR sequencing from recipients of either

displayed clonally expanded CD4 and CD8 cells, albeit enrichment was less pronounced in recipients of wild-type compared to *Aire*$^{-/-}$*Cblb*$^{-/-}$ spleen cells. It can be suggested that the expansion seen in the wild-type secondary recipients may be a response to commensal flora within the gut (Kieper et al., 2005), a phenomenon that frequently occurs when lymphoid cells are initially transferred into lymphopenic recipients. It seemed reasonable to predict that the expansion in *Aire*$^{-/-}$*Cblb*$^{-/-}$-recipients was "driven" by a pancreatic antigen for those expanded T cell clones that accounted for a higher fraction of T cells in the pancreas compared to the spleen. Several CD8 TCR clonotypes fulfilled this criteria and one dominant clone, TCR 3.5, was chosen initially for further analysis because it represented 30.7% of the splenic and 69.0% of the pancreatic CD8 T cell repertoire in secondary MUT3 recipients. The spontaneous development of exocrine pancreatitis in retrogenic mice expressing TCR3.5, and selective activation of TCR3.5-expressing CD8 cells in the pancreatic but not axillary or inguinal lymph nodes, confirmed that this was indeed a driver clone capable of causing extensive exocrine pancreatitis, as will be discussed further in section 5.5.3.

5.5.2 Discussion of other expanded T cell clones revealed by single-cell sequence analysis.

5.5.2.1. TCRs 1.17 and 1.18 shared in recipients from two separate donors. It was interesting that the MUT1 and MUT2 secondary recipients revealed clonal expansion of CD8 cells bearing identical TCRs – clonotype 1.17 and 1.18 – despite receiving spleen cells that originated from separate MUT1 and MUT2 donor chimeric animals (section 5.2). The possibility of contamination during the sorting, PCR and sequencing steps seemed unlikely, as there was no overlap with the TCRs amplified from CD4 cells in the MUT1 and MUT2 recipients. Contamination during processing or staining would have been predicted to result in the same TCRs being detected in both CD4 and CD8 cells.

Convergent evolution is another theoretical explanation: that the two clones arose independently in the MUT1 and MUT2 donors but were selected to have an identical TCR sequence based on binding to the same exocrine-specific antigens with high affinities. The likelihood of two pancreas-infiltrating CD8 clones with the same TCRα-

TCRβ pairing and exact same CDR3s evolving independently in MUT1 and MUT2 seems small. It would seem difficult to explain the complete identity of the TCR junctional nucleotide sequences by selection for TCR specificity, since antigenic selection can only operate on the protein sequence and not on the redundant nucleotides such as those in +3 positions within each codon, which would be expected to yield synonymous differences at the nucleotide level. In diabetogenic CD8 T cells cloned from the pancreatic islets of NOD mice such as NY7.2 and NY8.3 (Santamaria et al., 1995), however, recurrent use of TCRβ and TCRα chains that were identical at the nucleotide level was indeed shown to result from selection for autoantigen specificity because the T cells were isolated from independent mice and differed at the level of co-expressed TCR transcripts from out-of-frame rearrangements. The efficient ability of clonal selection to arrive at identical TCRα chain nucleotide sequences in many independent animals was reinforced by *Tra* sequence analysis of islet-infiltrating CD8 cells from NOD mice bearing a rearranged *Trb* transgene from the NY8.3 clone but unconstrained *Tra* diversity (Verdaguer et al., 1996). In this light, it is noteworthy that the TCRα chain sequence in TCR clonotype 1.18 was also found in TCR clonotype 2.7 but in the latter it was paired with a different TCRβ chain sequence. This again resembles the patterns that arose from convergent evolution in independent diabetogenic CD8 T cell clones (Santamaria et al., 1995). However the presence of an identical TCRα chain but different TCRβ chains may also have arisen in clonotype 2.7 by divergent evolution of progeny from a single CD8 T cell, through re-expression of *Rag1* and *Rag2* genes allowing secondary *Trb* rearrangements as has been shown to occur in diabetogenic CD8 cells from NOD mice (Serra et al., 2002).

The possibility of convergent evolution of exocrine pancreas-specific CD8 cells, comparable to that described for pancreatic islet-specific CD8 cells by Santamaria's group (Santamaria et al., 1995; Verdaguer et al., 1997), is also supported by the similarities within expanded CD8 clones in MUT3 recipients. Thus clonotype 3.5, which used to construct retrogenic mice and shown to be a driver of exocrine pancreatitis, uses identical α chain and β chain V and J elements to clonotype 3.6 and have similar but nevertheless distinct junctional sequences, indicating that these clones must have arisen independently yet have been selected to have very similar TCRs (Table 5.9). Clonotype 3.8 has an identical beta chain sequence to clonotype 3.5 but a

different alpha chain. It is conceivable that these two clonotypes have arisen from divergent evolution of daughter cells derived from the same founder CD8 cell as a result of secondary alpha chain rearrangements (Serra et al., 2002), although convergent evolution appears equally plausible given the evidence from Santamaria's analyses.

It is potentially significant that clonotype 3.5 was more frequent in pancreas than in spleen, whereas the related clonotype 3.6 was equally frequent in both tissues and the other related clonotype 3.8 was only detected in spleen. Recent analysis of recurring TCR clonotypes among islet-reactive CD8 T cells by Santamaria's group (Han et al., 2005b; Tsai et al., 2010) has revealed that T cells with small differences in their alpha chain but identical beta chains have identical pMHC specificity but nevertheless differ approximately 10-fold in affinity. The high affinity CD8 cells mediate pancreatic destruction provided they escape activation-induced death and their frequency becomes sufficiently high so that they dominate the CD8 infiltrates within the pancreatic islets. By contrast, the low affinity CD8 cells preferentially accumulated in the blood, spleen and pancreatic lymph node as activated $CD44^{hi}$ $CD122^{hi}$ $CD62L^{hi}$ memory cells that were unable to make IL-2 or proliferate *in vitro* but potently suppressed proliferation of high affinity CD8 cells either *in vitro* or in the pancreatic lymph node, and powerfully suppressed diabetes in NOD mice. The suppressive function of low affinity islet-specific CD8 cells was ascribed to inhibition of antigen presentation by dendritic cells through interferon gamma and the immunoregulatory enzyme idoleamine 2,3-dioxygenase, and elimination of islet antigen-presenting dendritic cells by perforin-mediated killing (Tsai et al., 2010). These results raise the possibility that clonotypes 3.8 and 3.6 may similarly have lower affinity than clonotype 3.5, so that they accumulate equally or primarily in lymphoid tissues as regulatory memory CD8 cells. It should be possible to test this hypothesis in future experiments, by comparing retrogenic mice expressing clonotypes 3.5, 3.6 and 3.8.

A third explanation for the occurrence of CD8 T cells with identical TCRs in MUT1 and MUT2 but not MUT3 recipients is based on the fact that a single pool of $Cblb^{-/-}$ bone marrow was transplanted into irradiated $Aire^{-/-}$ recipients to generate the original bone marrow chimera donors MUT1 and MUT2, whereas the MUT3 donor was entirely independent (and was not a bone marrow chimera). Mature CD8 T cells bearing TCR

clonotypes 1.17 and 1.18 may already have been present in the *Cblb*$^{-/-}$ bone marrow, which was not depleted of T cells before transplantation, and these "passenger" T cells clonally expanded in both the irradiated *Aire*$^{-/-}$ MUT1 and MUT2 chimeras and in the primary and secondary recipients of spleen or pancreas cells from MUT1 and MUT2. For this explanation to apply, CD8 T cells bearing TCR clonotypes 1.17 and 1.18 must have evaded clonal deletion in the *Aire*$^{+/+}$ thymus of the *Cblb*$^{-/-}$ marrow donor, so that these CD8 T cells were present in the bone marrow. This inference has interesting parallels with the observation that the dominant CD8 T cell clonotype from MUT3, TCRαβ3.5, did not appear to undergo clonal deletion in retrogenic mice with a wild-type *Aire*$^{+/+}$ thymus. Taken together, these data raise the possibility that the CD8 T cells responsible for exocrine pancreatitis in *Aire*$^{-/-}$*Cblb*$^{-/-}$ double mutant mice are not regulated by *Aire*, and that the effects of *Aire*-deficiency may act through co-operating CD4 helper T cells or antagonistic Foxp3^{+} Tregs.

5.5.2.2. Analysis of TCRs 1.18, 1.22 and 1.23 confounded by two co-expressed chains. The multiplex single cell PCR method is a powerful strategy to accurately detect clonal expansion in the T cell repertoire. However, this method did produce several recurring TCR clonotypes where assignment to particular TCRα or TCRβ gene segments proved challenging. One example is clonotype 1.18 where a large fraction of the single CD8 cells analysed in MUT1 recipients could only be assigned to a complete TCRβ but not a TCRα. The nucleotide sequence chromatogram of the TCRα region sequence for a typical T cell bearing clonotype 1.18 is shown in Fig 5.28 and displayed in the 3'→5' direction as the *Trac* reverse primer was used for the sequencing. The sequence was characterized by a region of homogeneous nucleotide sequence that corresponded to the 5' end of the *Trac* (constant) region, followed by many overlapping dual peaks in the *Traj* and *Trav* regions indicating the presence of two different variable domain nucleotide sequences on the single T cell (Petrie et al., 1993). Dual-TCRs occur at a frequency of 30% of T cells in normal mice (Casanova et al., 1991) and this dual specificity could result in an autoreactive TCR bypassing negative selection during thymic development due to the presence of a second non-autoreactive receptor (Zal et al., 1996). Besides clonotype 1.18, clonotypes 1.22 and 1.23 also appeared to have two peaks within the *Trbj* and *Trbv* regions, while each bearing a unique TCRα, highly suggestive of the presence of two TCRβs on each clone (Fig. 5.29). The nature of the

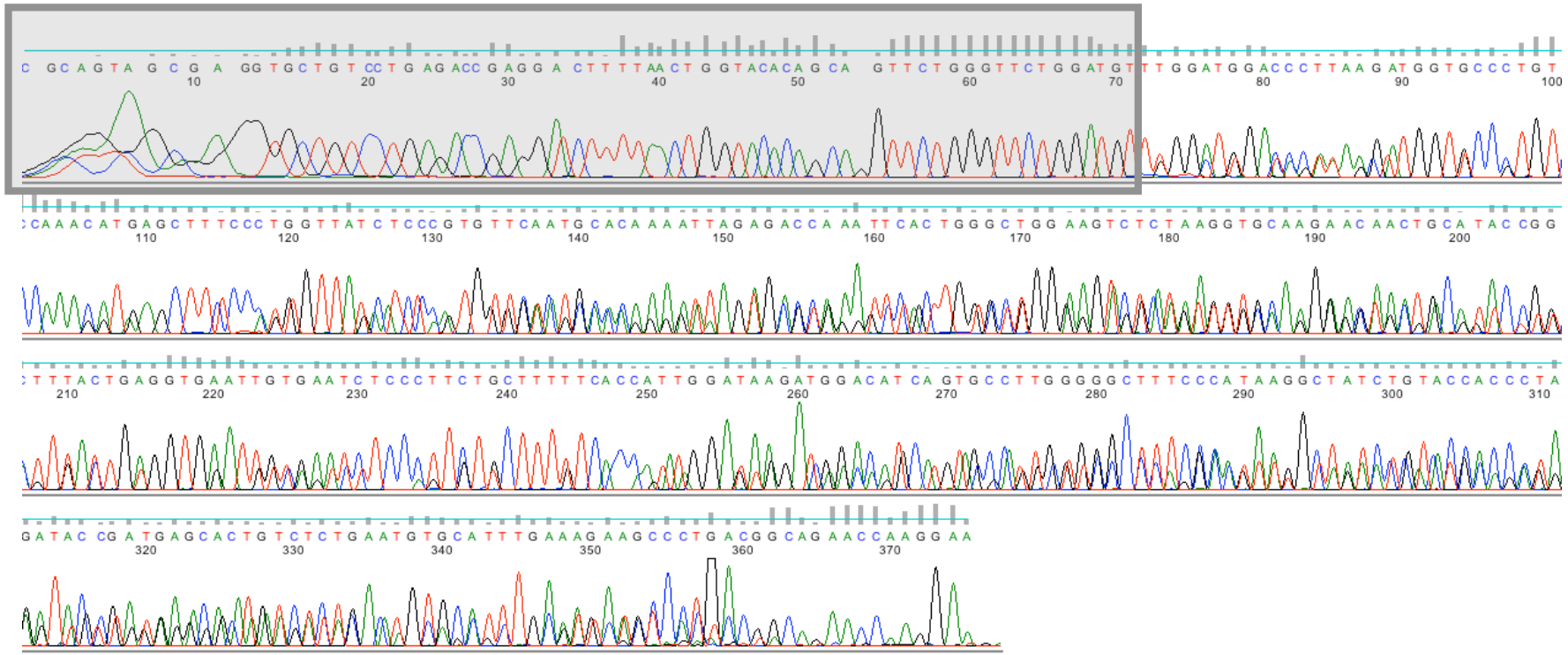

Figure 5.28 Nucleotide chromatogram sequences for clonotype 1.18.
The 3’ to 5’ nucleotide chromatogram sequences obtained by sequencing the TCRα chain using the *Trac* internal reverse primer. The shaded areas correspond to the sequences of the TCRα constant region. After the shaded region, double peaks are present throughout the sequence.

second TCRα or TCRβ in clonotype 1.18, 1.22 and 1.23 could be resolved by blunt-end cloning of the PCR product into an expression vector, transformation into competent bacterial cells and PCR screening the bacterial colonies for the detection of the two in frame TCRα or TCRβ sequences. Cloning of the individual TCRs from these clonally expanded T cells would enable an accurate sequence to be obtained for each *Tra* or *Trb* expressed, to determine if the co-expressed sequences are both in-frame or if one of the sequences derives from an out-of-frame rearrangement on the other TRA or TRB allele. It is noteworthy that a subset of T cells with clonotypes 1.18, 1.22 and 1.23 lacked amplification of a second *Tra* or *Trb* cDNA (Fig. 5.29). These T cells may represent independent clones arriving at the same TCR sequence by convergent evolution, as discussed above, or the second mRNA may simply have been present at lower abundance and failed to be co-amplified from all of the T cells.

5.5.2.3. Analysis of TCR 2.4 confounded by apparent failure to amplify the in-frame alpha chain. Another interesting clone, clonotype 2.4 consistently displayed a TCRβ similar to that of clonotype 2.1. However, the TCRα could only be assigned to a *Trav*6D-7 or 6-5. Following the *Trav* sequence, there appeared to be a stop codon after 13 codons, making it impossible to assign it to the appropriate *Traj* gene segment. The nucleotide chromatogram traces did not have dual-peaks and could clearly be assigned to a particular bases without any ambiguity. This sequence could be translated into three reading frames as seen in Fig. 5.29. The frames are seen in the 3'→5' direction as the *Trac* reverse primer was utilised for sequencing. As seen in the Fig. 5.30, when translated in "Frame 2", *Trav*6D-7 or 6-5 could be assigned as the appropriate *Trav* sequence but when translated in "Frame 3" the sequence matched *Traj*30. Thus, the TCRα detected during sequencing represented an mRNA from an out-of-frame non-productive TCRα rearrangement present within the cell. It is likely that there was a functional TCRα that was not amplified by the multiplex PCR strategy used here either due to the dominance of the out-of-frame TCR in the cell, no coverage of the in-frame TCRα by the 23 *Trav* forward primers used or suboptimal primer binding condition for the in-frame *Trav* forward TCRα primer. It would be useful to utilise the cloning strategy described in the previous paragraph to search for another in-frame TCR for this clone.

	WT1 & MUT1 GROUP							
Clonotype	S_0	P_0	P_1	$S_2<S_1$	$P_2<S_1$	$S_2<P_1$	$P_2<P_1$	
1.18				14/38	21/51	5/31	42/73	
1.22					25/51			
1.23					4/51			
Clonotype	S_0	P_0	P_1	$S_2<S_1$	$P_2<S_1$	$S_2<P_1$	$P_2<P_1$	
1.18				**7/38**	**16/51**	0/31	**35/73**	**Trav**
1.22					**22/51**			**Trbv**
1.23					**2/51**			**Trbv**

Figure 5.29 Figure shows the frequencies of clonotypes 1.18, 1.22 and 1.23 and the number of clones in which double peaks were observed (in red).

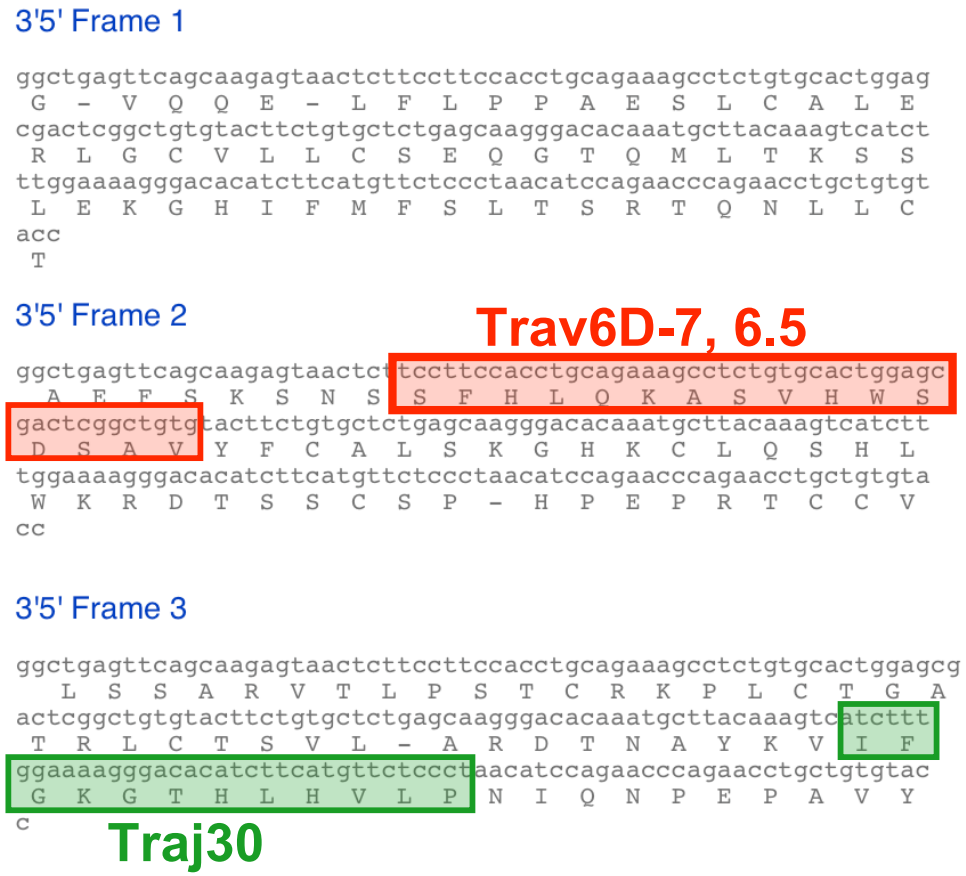

Figure 5.30 Translation of the nucleotide sequence of clonotype 2.4 in three different reading frames.
The translation of the nucleotide sequenced obtained by sequencing the TCRα sequence using the *Trac* internal reverse primer. Translation with reading frame 2 detects usage of Trav6D-7 or 6.5 (red) and translation with reading frame 3 detects the usage of Traj30 (green).

5.5.3 Evidence for positive but not negative selection the TCRαβ3.5 clonotype in retrogenic mice

Given the issues complicating simple interpretation of TCR sequence data, a key advance established here is the use of retrogenic mice to examine *in vivo* the fate and function of the different clonally expanded TCR clonotypes revealed by the multiplex sequence analysis. In order to achieve this, a stably transduced retroviral producer cell line expressing CD8 TCR 3.5 clonotype was generated. This cell line served as a valuable tool to examine the mechanism of organ-specific autoimmune disease in the *Aire*$^{-/-}$*Cblb*$^{-/-}$ mouse model as it allowed for T cells expressing the putative organ specific TCR to be tracked based on their expression of GFP, because TCRα-2A-TCRβ 3.5 and GFP were encoded by a single, tricistronic mRNA. A preliminary retrogenic experiment verified that clonotype 3.5 isolated from the adoptive transfer enrichment assay was pancreas-specific and able to recapitulate in mice with wild-type *Aire* and *Cblb* the exocrine pancreatic autoimmunity caused by polyclonal CD8 T cells from B10.BR.*Aire*$^{-/-}$*Cblb*$^{-/-}$ mice.

Because of the tricistronic mRNA produced in a subset of hemopoietic cells in the retrogenic mice, expression of GFP would be expected to correlate with the expression of TCRαβ3.5. Consistent with this expectation, GFP^{hi} thymocytes and peripheral T cells were greatly skewed towards the CD8 subset consistent with positive selection on MHC Class I, whereas GFP^{neg} and GFP^{low} T cells apportioned normally to yield ~75% CD4 cells and only ~25% CD8 T cells. Accumulation of large numbers of GFP^{hi} CD8 T cells occurred in the thymus and peripheral lymph nodes of all TCRαβ3.5 retrogenic mice regardless of their *Aire* or *Cblb* genotypes. Thus there was no evidence that T cells expressing this TCR were negatively selected medulla after positive selection in the thymic cortex, nor after emigration to spleen, axillary and inguinal lymph nodes. While negative selection occurs efficiently in many TCR transgenic mice bearing self-reactive TCRs against trace antigens expressed in the thymic medulla, it is nevertheless formally possible that the high numbers of exocrine pancreas autoimmune driver TCRαβ3.5 cells overwhelmed the *Aire*-dependent negative selection that was usually in place to keep this clone in-check. Hence, reducing the starting concentration of the TCRαβ3.5 cells

using mixed retrogenic chimeras (WT: TCRαβ3.5, 50:50 ratio) may reveal a requirement for *Aire*-deficiency in negative selection of TCRαβ3.5 cells.

Alternatively, it could be suggested that T cells expressing the TCRαβ3.5 receptor escaped thymic deletion by deviating to the atypical CD8αα intraepithelial lymphocytes (IEL), rather than adopting a conventional CD8αβ lineage (Yamagata et al., 2004). Although these IEL cells usually home to the gut (Leishman et al., 2001), they have been found in the pancreatic infiltrate in B6 and NOD BDC2.5 transgenic mice (Holler et al., 2007). In BDC2.5 transgenic mice, the frequency of the IELs detected in the pancreas correlated strongly with the aggressively of insulitis particularly in early stages of the disease indicating the cells have the potential of escaping the gut, homing to a different tissue and inducing pathogenicity (Holler et al., 2007). However, further analysis of the retrogenic mice in a subsequent experiment showed that majority of the GFP^{hi} CD8 cells expressed both CD8α and CD8β (Fig. 5.31).

While the data here show that $TCR3.5^{+}$ CD8αβ T cells escaped thymic deletion even in $Aire^{+/+}$ retrogenic mice, this may be due to the low surface expression of CD3 observed on GFP^{hi} CD8 SP thymocytes compared either with GFP^{neg} CD8 SP thymocytes in TCRαβ3.5 retrogenic mice or to GFP^{hi} CD8 SP thymocytes from empty vector retrogenic mice (Figure 5.22*B*). CD3 and TCR expression normally increases following positive selection of DP thymocytes into CD8 SP cells, but this did not appear to occur in the positively selected GFP^{hi} cells expressing the retroviral TCR3.5 until the CD8 cells had matured in the periphery (Figure 5.24*B*). The delayed surface accumulation of the retroviral-encoded TCR may stem from inefficient cleavage of the 2A peptide sequence that links the TCR alpha and beta chains (Holst J, personal communication and (Holst et al., 2006b)), resulting in sufficient cleavage and TCR expression to support the low levels of surface TCR on DP cells and positive selection but insufficient to trigger deletion of CD8 SP cells in the thymic medulla. The efficiency of 2A-mediated cleavage of different TCRα and β chains has been found to vary, and for some TCRs efficient cleavage required inclusion of a flexible Gly-Ser-Gly spacer between the C-terminus of the alpha chain and the 2A peptide that presumably allows the 2A peptide to adopt its catalytic conformation. In future studies, it will be important to test this

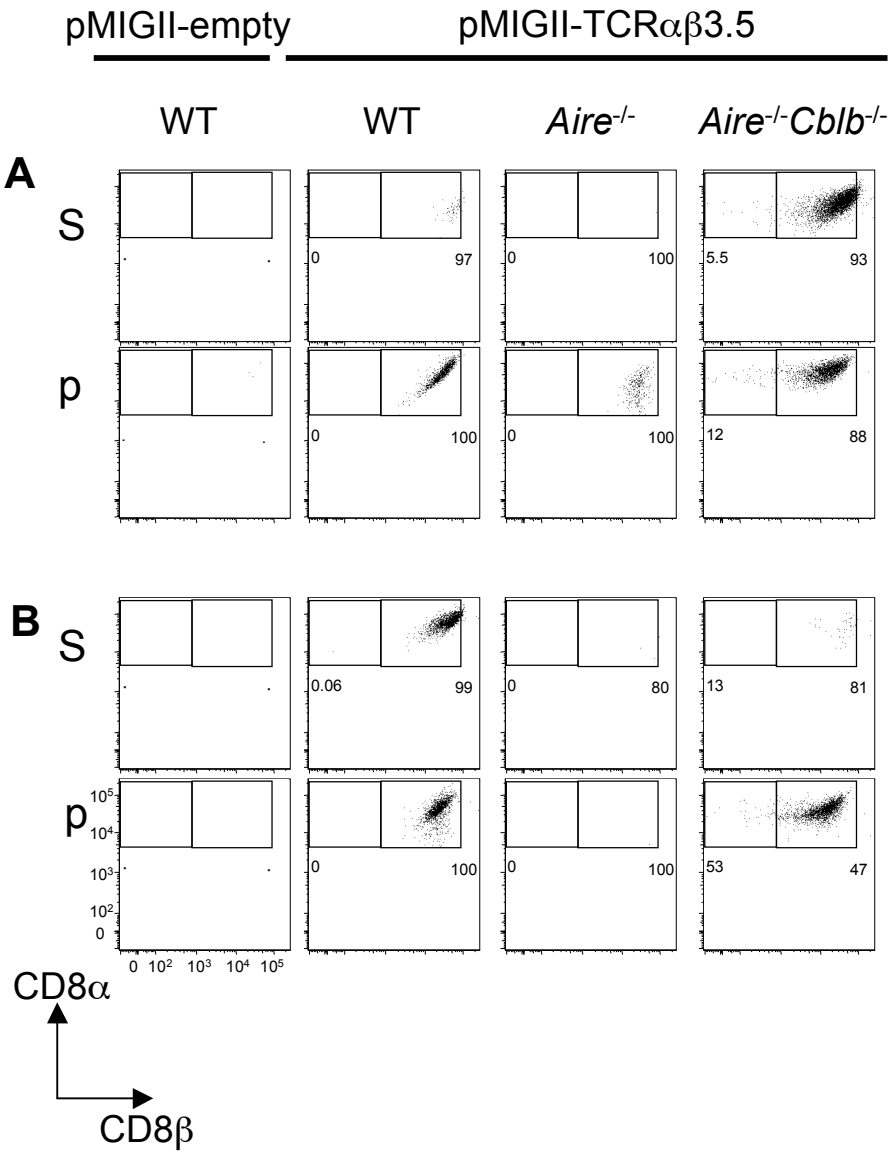

Gate:CD8^{+}GFP^{hi}CD3^{+}CD45.2^{+}

Figure 5.31 Flow cytometry plots of CD8α and CD8β populations in retrogenic mice of the indicated genotype from an independent experiment.

Plots were gated on CD8^{+}GFP^{hi}CD3^{+}CD45.2^{+}cells. For each group, two mice were analysed (A and B). S: spleen, p: pancreas. Note that in this experiment, the pMIGII-TCRαβ3.5 *Cblb*$^{-/-}$ retrogenic chimera was not analysed.

possibility by constructing a second generation of TCR3.5 retrogenic mice using a construct that contains a Gly-Ser-Gly spacer.

5.5.4 Are TCR3.5+ CD8 cells sufficient to induce exocrine pancreatitis?

The ability of the TCR3.5 to serve as an autoimmune driver was established by finding extensive histological destruction of the exocrine pancreas in TCR3.5 retrogenic mice with wild-type *Aire* and *Cblb* genes, compared to completely normal pancreas histology in empty vector retrogenic mice of the same wild-type genotype. While there were high frequencies of GFP^{hi} CD8 T cells presumably expressing TCR3.5 in these retrogenic mice, these developed among many more donor and host derived CD8 and CD4 T cells that did not express GFP and presumably carried a diverse, polyclonal TCR repertoire. Given the requirement for CD8 and CD4 cells discussed above, it is conceivable that these endogenous CD4 cells may have cooperated with the $TCR3.5^{+}$ CD8 cells to enhance their activation in the pancreatic lymph node and accumulation and destruction of the exocrine pancreas. Cooperation with helper cells may be more critical when the frequency of $TCR3.5^{+}$ cells is not at the extraordinarily elevated frequencies present in the retrogenic chimeras. These issues could be addressed in future studies where the TCR3.5 retrogenic construct is transduced into $Rag1^{-/-}$ bone marrow, and then used to reconstitute $Rag1^{-/-}$ recipients alone or to reconstitute $Rag1^{+/+}$ recipients after mixing the transduced $Rag1^{-/-}$ marrow with progressively increasing proportions of non-transduced $Rag1^{+/+}$ marrow. The finding of relatively little weight loss in the wild-type TCR3.5 retrogenic chimeras, compared to $Cblb^{-/-}$ or $Aire^{-/-}Cblb^{-/-}$ retrogenic animals, may also suggest that one or both mutations are required to allow full activation of pancreatic destruction, and this will need to be addressed in mixed chimeras where the frequency of $TCR3.5^{+}$ cells is decreased as described above.

5.5.5 What is the autoantigen recognized by $TCR3.5^{+}$ CD8 cells?

The selective destruction of the exocrine pancreas and selective activation of GFP^{hi} CD8 cells in the pancreatic lymph node in TCR3.5 retrogenic mice indicates that the TCR 3.5 recognises an autoantigen that is specifically expressed in the exocrine pancreatic epithelium. Candidate autoantigens include the pancreas-specific protein

encoded by *Pdia2*, which has been shown to be a target of autoimmunity in NOD.*Aire*$^{-/-}$ mice (Niki et al., 2006) and in Balb/c.*Ctla4*-deficient mice (Ise et al., 2010). Testing the specificity of TCR3.5 will be facilitated by the availability of this TCR either as a retroviral vector that can be introduced into T cell hybridomas or expressed on CD8 T cells isolated from lymph nodes and spleen of retrogenic mice. The same approach would also conceivably allow definition of the autoantigen(s) recognized by the other pancreas and salivary gland expanded CD8 and CD4 T cell clonotypes.

5.5.6 Summary.

This chapter described the isolation and rapid analysis of an autoimmune driver T cell using single cell multiplex RT-PCRs and construction of retrogenic mice. Extending this strategy to the other CD8 and CD4 TCR clonotypes in the pancreas and to those from salivary gland T cells would allow detailed characterization of other pancreas- and salivary gland-specific clones from B10.BR.*Aire*$^{-/-}$*Cblb*$^{-/-}$ mice. Considering the data from this chapter and previous chapters, it can be suggested that pancreas- and salivary gland-specific clones in B10.BR.*Aire*$^{-/-}$*Cblb*$^{-/-}$ mice have different CD4 and CD8 cell requirements. The resulting autoimmunity in the mice may also be a result of a complex co-operation between *Aire*- or *Cblb*-deficiencies in antigen-specific CD4 or CD8 cells (retrogenic experiment and CD4/CD8 adoptive transfer assays, Chapter 3), non-antigen specific CD4 helper T cells (50% TCR^{3A9}→insHEL^{+} bone marrow chimeras, Chapter 4), nTregs (wildtype nTregs adoptive transfer assay, Chapter 3) and iTregs (*Cblb*$^{-/-}$ TCR^{3A9}insHEL^{+} iTreg assay, Chapter 4). The retrogenic strategy would permit further study of a *complex co-operative autoimmunity pathogenesis model* as the strategy allows for complete control over the specific T cell receptor and *Aire*- or *Cblb*- genetic deficiencies in each T cell population present in the retrogenic mice. This, coupled with the ability to track, manipulate and isolate the retrogenic T cells for further analysis would serve as a valuable tool enriching the current understanding of the epistatic co-operation between *Aire*- and *Cblb*-deficiencies.

Chapter 6

Discussion

6.1 Introductory comments

A large body of work has aimed to provide a coherent genetic architecture that explains the pathogenesis of autoimmune diseases. While rare autoimmune diseases could result from single gene variants with a simple Mendelian pattern of inheritance (Bennett et al., 2001; Bjorses et al., 1998; Fisher et al., 1995), more common and complex diseases have been shown to result from interactions between multiple alleles, each harbouring only a weak effect on its own but in combination would synergise to cause severe autoimmunity. Genome wide association studies have identified many genetic markers associated with autoimmune diseases (Barrett et al., 2009; Hyttinen et al., 2003; Todd and Wicker, 2001; Wandstrat and Wakeland, 2001), but it is unclear which genes are causative or how these genes interact with each other. An even more distant goal is to explain, with the aid of genotype, the mechanisms that account for the occurrence of autoimmune diseases and use that information to predict individuals at risk of the disease and target treatment.

This study hypothesised that there may be a minimum set of defects that are needed in combination before the emergence of autoimmunity – a *multistep model* for the development of autoimmune disease. Since multiple tolerance mechanisms function to keep autoimmunity in-check and each mechanism is governed by a unique set of genes, it seemed reasonable to consider genes within the same molecular pathway as *functionally equivalent* and treat them as equal from the perspective of autoimmune disease pathogenesis. This assumption simplified the polygenic nature of autoimmune diseases and allowed robust testing for additive effects between combinations of pathways. With this pathway stratification in mind, mice harbouring mild genetic defects in two tolerance pathways were examined for the ability to develop severe autoimmunity, in absence of a latent phase. Specifically, *Aire*-deficient mice – with crippled thymic deletion of organ-specific T cells - were crossed with mice carrying genetic defects in one of four key peripheral tolerance mechanisms: decreased T regulatory cells (*Card11*$^{unm/unm}$), apoptosis (*Fasl*$^{gld/gld}$), anergy (*Cblb*$^{-/-}$), or dysregulated T follicular helper cells (*Rc3h1*$^{san/san}$). *Cblb*-deficiency was unique among these four in precipitating rapid clinical autoimmunity when combined with *Aire*-deficiency, resulting in lethal destruction of the exocrine pancreas and salivary gland within weeks

after birth. These findings are the first to reveal a higher-level architecture assembling individual tolerance mechanisms together for robust resistance to autoimmunity in support of a *multi-step model* for the progression of autoimmunity. In the following sections, the discussion will focus on the construction of a mechanistic model to understand why the combination of *Aire* and *Cblb*-deficiencies synergised strongly and relate the principles highlighted in this mouse model to the general pathogenesis of autoimmunity.

6.2 Mechanistic basis for the strong epistatic co-operation between *Aire*- and *Cblb*-deficiencies

The potency of the *Aire*$^{-/-}$*Cblb*$^{-/-}$ combination could be illustrated by considering an *autoimmune threshold model* to examine the interaction between genetic defects in central and peripheral tolerance pathways on development of autoimmunity. This can be modelled as either a binomial distribution or a linear progression of disease state. When using this model to calculate relative risk of autoimmunity, several parameters were taken into consideration: the precursor frequency of self-reactive T cells or *forbidden clones* and the presence of tolerance pathways that buffer and control these *forbidden clones*. The balance of these two parameters determines if an individual falls below or above the risk threshold for autoimmunity (Fig. 6.1). As seen in the figure, there is a positive correlation between the number of self-reactive *forbidden clones* (represented by the *y* axis) and the risk of developing autoimmunity (represented by the *x* axis), whereby higher frequencies of self-reactive precursors increase the likelihood of developing autoimmunity (Fig. 6.1*A*). The scatter dot represents the disease-state in any individual while the *autoimmune threshold* determines the risk for an individual to develop an autoimmune disease. Multiple tolerance pathways regulate the threshold. Under normal conditions, when all tolerance pathways are working effectively, there are low frequencies of self-reactive cells and multiple tolerance pathways regulating the low number of self-reactive cells.

Arguably, the most prominent feature of an organ-specific autoimmune disease is the existence of self-reactive (*forbidden*) organ-specific cell(s) that can recognise and elicit an immune response targeted towards tissue-specific antigens. In the *Aire*$^{-/-}$*Cblb*$^{-/-}$

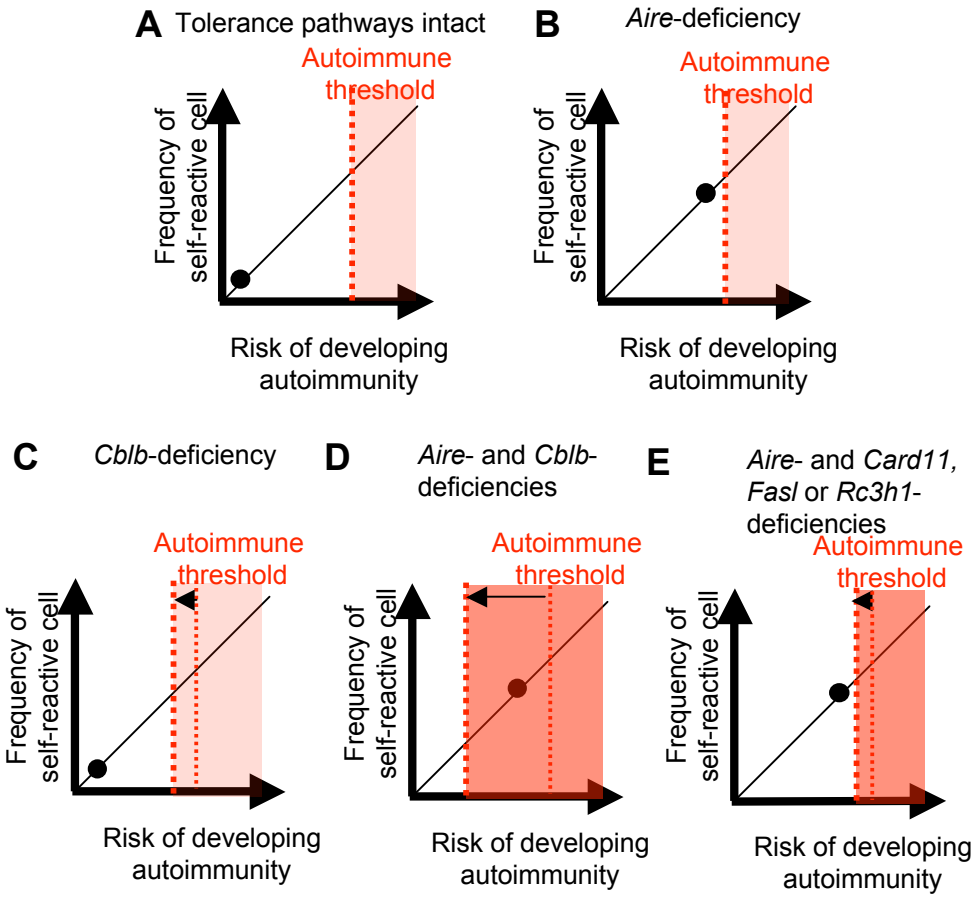

Figure 6.1. Schematic illustrating the relationship between the frequency of self-reactive cells and the risk of developing autoimmunity, and how this relationship is altered by different tolerance mechanisms.

A. The frequency of self-reactive cells is directly proportional to the risk of developing autoimmunity.

B. *Aire*-deficiency increases the burden of self-reactive cells although the this still falls below the high autoimmune threshold risk in B10.BR.*Aire*$^{-/-}$ mice.

C. *Cblb*-deficiency decreases the threshold risk for autoimmunity, although mice still do not present with severe autoimmunity.

D. The combination of *Aire*- and *Cblb*-deficiencies are able to break tolerance because of the altered frequency of self-reactive cells and changes in the autoimmune risk threshold.

E. The *Aire*$^{-/-}$ and *Cblb*$^{-/-}$ co-operation is unique as other combinations seem to display comparable autoimmunity to the single deficiency in *Aire*$^{-/-}$ mice seen in (B).

mouse model, the *forbidden clones* recognise self-antigens in the pancreas and salivary glands. In the pancreas, the self-reactive cells comprised primarily of CD8 cells with more than one dominant TCR being detected and different TCRs detected in different mice (interindividual variability). Indeed, CD4 cells and B cells (autoantibodies) also contribute towards the disease pathogenesis. The potency of the *forbidden clones* in *Aire*$^{-/-}$*Cblb*$^{-/-}$ mice is demonstrated by the observation that one dominant CD8 (clonotype 3.5) chosen from the single cell TCR analysis could precipitate extensive pancreatic destruction when present at high frequencies (30-50% from total T cells) in retrogenic mice without the need for defects in *Aire* or *Cblb*. This indicates that high frequencies of *forbidden clones* release the dependence of the clone from control by tolerance mechanisms (chapter 5). This paradigm is further exemplified by the finding that the pancreas infiltration could be re-directed from exocrine to endocrine pancreas in *Aire*$^{-/-}$*Cblb*$^{-/-}$ mice by simply changing the frequency of the predominant TCR using TCR^{3A9}:insHEL transgenic models (chapter 4). Hence, as demonstrated by the model, high numbers of autoreactive T cells would result in skewing towards a high autoimmune risk zone.

What increases the burden of self-reactive *forbidden clones*? During the development of thymocytes, *forbidden* T cells clones harbouring self-reactive TCRs that bind strongly to an array of self-antigens complexed to MHC are triggered to die. *Aire* is thought to play a vital role in this process by regulating the expression of selective tissue-specific antigens in the thymus, mediating negative selection of T cell recognising these antigens. However, when this process of negative selection is crippled by *Aire*-deficiency, it increases the numbers of forbidden clones that escape deletion (Anderson et al., 2002; Liston et al., 2003). This could have increased the burden of pancreas- or salivary gland-specific clones in the *Aire*$^{-/-}$*Cblb*$^{-/-}$ mice, posing a higher risk for the mice to develop pancreatitis or sialoadenitis (Fig. 6.1*B*).

The second feature of the model, that sets the threshold for developing autoimmunity is the presence of central and peripheral tolerance mechanism that control the numbers and functions of the forbidden clones. As thymic deletion is not full-proof, and perhaps more severely affected in absence of *Aire*, self-reactive clones require further control by other peripheral tolerance failsafe mechanisms to so the individual remains within the

low autoimmune risk zone (Fig. 6.1*B*). If there is a defect in one peripheral tolerance pathway, such as *Cblb*, it decreases the *autoimmune threshold*, increasing the risk of developing autoimmune disease (Fig. 6.1*C*). A predisposition to high amounts of forbidden clones coupled with defects in peripheral tolerance pathways may act synergistically to cause autoimmune diseases although the defects do not manifest as a simple addition but some combinations (combination of *Aire*$^{-/-}$ with *Cblb*$^{-/-}$) (Fig. 6.1*D*) interact more strongly than others (combination of *Aire*$^{-/-}$ with *Fasl*$^{gld/gld}$, *Rc3h1*$^{san/san}$ or *Card11*$^{unm/unm}$) (Fig. 6.1*E*). This observation begs the question: why is the combination between *Aire*- and *Cblb*-deficiencies so potent?

In order for the peripheral tolerance mechanism to create a large shift in the threshold for autoimmune development when combined with high numbers of *forbidden clones*, there are several possible explanations that have been highlighted by the *Aire*$^{-/-}$*Cblb*$^{-/-}$ mouse model in this study discussed below.

6.2.1 *Aire*- and *Cblb*-deficiencies act on two complimentary pathways that control the same autoreactive clone(s)

In order for multiple tolerance mechanisms to co-operate, the mechanisms must act upon non-redundant pathways that control the same autoreactive cell(s). It can be hypothesized that the interaction between *Aire* and *Cblb* appears to be strong as both confer protection against organ-specific autoimmunity, whereas the *Fasl* and *Rc3h1* are essential in protection against systemic forms of autoimmunity. *Aire*-deficiency disrupts expression of organ-specific antigens in medullary epithelial cells of the thymus, and this indirectly affects thymic clonal deletion of organ-specific T cells (Anderson et al., 2002; Liston et al., 2003). *Cblb* is only expressed at low levels in immature T lymphocytes (Naramura et al., 2002; Thien and Langdon, 2005) and consequently *Cblb*-deficiency has not been shown to alter thymic selection or *Aire*-dependent thymic deletion (Hoyne et al., 2011b). In the periphery, Cbl-b is upregulated in mature and anergic T cells, where it inhibits the PI3K and NFκB signalling pathways activated by TCR-CD28 co-stimulation and is required for T cell anergy to prevent proliferation of T cells that have recognised peripheral antigens with insufficient affinity or in the absence of adequate CD28 co-stimulation (Bachmaier et al., 2000; Chiang et al., 2000; Fang and

Liu, 2001; Gronski et al., 2004; Heissmeyer et al., 2004; Jeon et al., 2004; Naramura et al., 2002; Qiao et al., 2008; Thien and Langdon, 2005). Hence, the two pathways that are guarded by the *Aire* and *Cblb* genes are separate but complimentary pathways that regulate organ-specific T cells. The rapid progression to pancreatic autoimmune disease observed here can be inferred to result from pancreas-specific T cells escaping thymic deletion due to *Aire*-deficiency and then escaping anergy and the normal requirement for CD28 costimulation due to *Cblb*-deficiency, allowing them to proliferate and differentiate into high numbers of tissue-damaging effector T cells (Fig. 6.2*B*).

On the other hand, the autoimmunity manifested by *Fasl* and *Rc3h1*-deficient mice did not appear to selectively target particular organs but are of a more lymphoproliferative nature, characterized by splenomegaly, lymphodenopathy and the presence of anti-nuclear antibodies (Roths et al., 1984; Vinuesa et al., 2005a). Thus, it would be reasonable to assume that *Fasl* and *Rc3h1* would only be an important failsafe for thymic deletion when the TCR reacts with a systemic autoantigen and not an organ-specific autoantigen. In this study, *Fasl* was chosen to represent a key regulator in apoptosis. As indicated in the introduction (1.3.1.1), there are two different pathways that lead to apoptosis: *Fas/Fasl*- and *Bim*-dependent pathways. Deletion of organ-specific T cells that bind to both systemic and organ-specific antigens in the thymus is thought to be predominantly dependent on *bim* (Bouillet et al., 2002). However, in the periphery, both *bim* and *fas/fasl* may regulate apoptosis of self-reactive T cell depending on T cell specificity and/or the duration and strength of TCR stimulation. Fas/Fasl is primarily important for aborting T cells that receive chronic recurrent TCR signals (Alderson et al., 1995; Brunner et al., 1995), as would occur mainly for systemic antigens, whereas Bim appears to be the main pathway that eliminates T cells that are activated by transient exposure to antigens (Bouillet et al., 1999) like organ-specific T cells that encounter antigen in one peripheral lymph node. Mice lacking both the pro-apoptotic Bcl-2 family member *bim* and *Fas* developed a modest increase in lymphadenopathy (Fortner et al., 2010). This suggests that *Fas* control systemic self-reactive cells that fail to delete in the thymus of *bim*-deficient mice in the periphery. To test if this hypothesis is accurate, the synergy between *bim* and *Fasl* or *Rc3h1*-deficient mice in response to both an organ-specific and systemic antigen could be compared. Using the TCR^{3A9} model, the *Bim* and *Fasl* double mutations could be introduce on

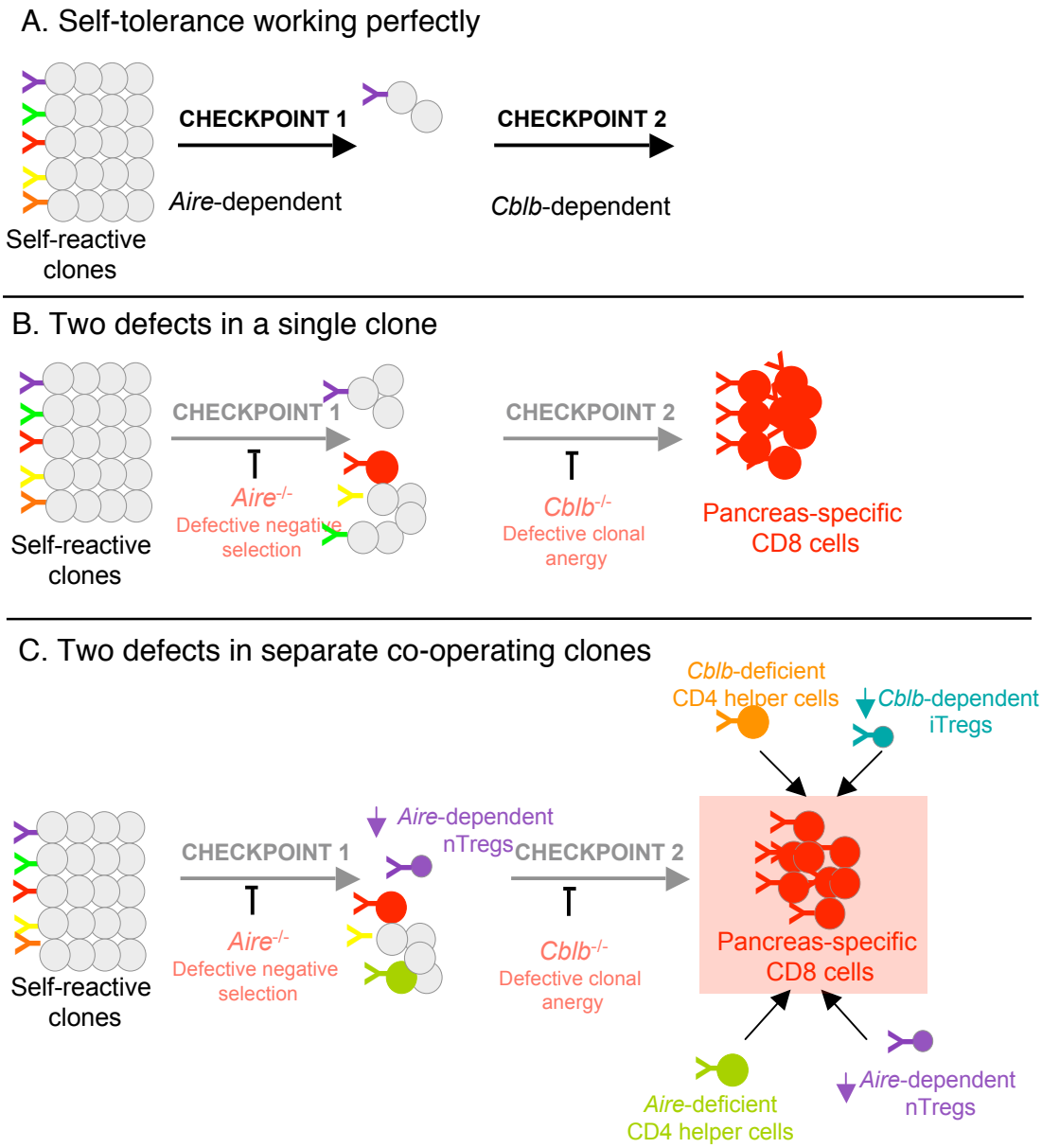

Figure 6.2. Multistep models for the pathogenesis of autoimmune disease in the *Aire*$^{-/-}$*Cblb*$^{-/-}$ mouse model.

A. Normally, self-reactive clones are controlled by multiple tolerance pathways.

B. Two defects in two sequential checkpoints allows a single clone pancreas-specific CD8 clone to bypass tolerance.

C. Two defects in two tolerance genes affecting many cell types that regulate self-reactive cells both intrinsically and extrinsically affecting more than two checkpoints.

transgenic mice harboring CD4 TCR^{3A9} (Ho et al., 1994) coupled with either an organ-specific (low concentration insHEL or high concentration thyrHEL) (Akkaraju et al., 1997a; Akkaraju et al., 1997b) or systemic (low concentration ML4 or high concentration ML5 soluble HEL) (Goodnow et al., 1988) autoantigen. If the prediction holds true, the organ-specific combination would display no or mild signs of increases autoimmunity -diabetes (for the insHEL) or thyroiditis (for the thyrHEL) compared to wild-type counterparts, while the "systemic" soluble antigen would precipitate a drastic increase in lymphoproliferation.

The combination of *Card11*$^{unm/unm}$ and *Aire*$^{-/-}$ was set up to reflect the combination of defects in the $FoxP3^{+}$ T regulatory cells and central tolerance. As the FoxP3-deficient *scurfy* mice exhibit a severe lethal phenotype on its own (Fontenot et al., 2003; Hori et al., 2003; Khattri et al., 2003), the *Card11*$^{unm/unm}$ represented a milder defect in the natural T regulatory component, making it possible to identify a strong interaction between the two mild defects. The *Card11*$^{unm/unm}$ hypomorphic allele compromised the formation of $Foxp3^{+}$ Treg cells in the thymus and the cells were found at one seventh the frequency of wild-type control animals in the periphery. Although there were low numbers of nTreg cells, T cells were able to retain the function of preventing autoimmunity but resulted in dysregulation of T_H2 cells leading to the expansion of this particular cell type (Altin et al., 2011). Mechanistically the defect in *Card11*$^{unm/unm}$ could be suggested to still produce sufficient numbers of nTreg cells to confer protection against organ-specific autoimmunity in this system even in the absence of *Aire*.

This concept of interdependence and non-redundancy of tolerance pathways being a requirement for increasing the risk of severe autoimmunity development could be extended by exploring if coupling any gene defect in thymic negative selection of organ-specific T cells and athymic T cell anergy/co-stimulation would recapitulate the phenotype of the *Aire*$^{-/-}$*Cblb*$^{-/-}$ mice (Fig 6.3). Other molecules that play pivotal roles in the *Aire*-related negative selection pathway such as the differentiation receptors on the mTEC cells including CD40, RANK and LTbR, which signal mTEC differentiation through NIK and the RelB/NFκB2 transcription factors (Gray et al., 2006; Seach et al., 2008; Venanzi et al., 2007) could be coupled with *Cblb*-deficiency and monitored for

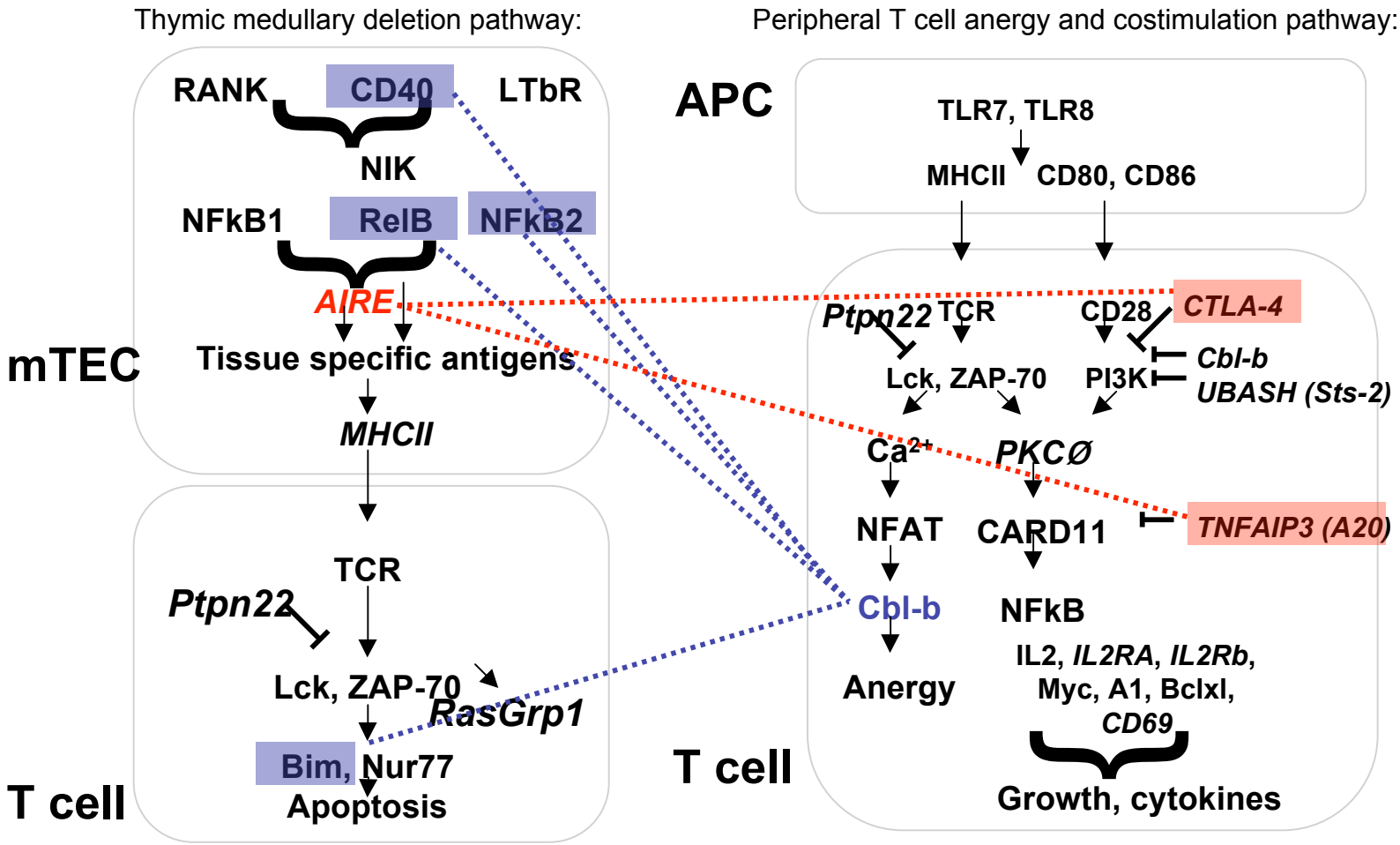

Figure 6.3. Key genes involved in the negative selection and peripheral T cell anergy pathways.

The lines combine defects that could be tested to determine if any "functionally equivalent" gene involved in negative selection could co-operate with any "functionally equivalent" gene involved in peripheral T cell anergy.

development of severe autoimmunity. Likewise, it would be also interesting to test if other genes involved in peripheral T cell anergy or co-stimulation such as CTLA-4 or A20 (*Tnfaip3*) (Graham et al., 2008; Musone et al., 2008; Nair et al., 2009; Plenge et al., 2007; Thomson et al., 2007; Trynka et al., 2009) would co-operate with *Aire*-deficiency to yield similar outcomes of accelerated autoimmunity, devoid of a latent phase (Fig 6.3).

6.2.2 Although representing two genetic lesions, *Aire*- and *Cblb*-deficiencies may affect more than one tolerance pathway.

The discussion in section 6.2.1 assumed a simplistic model to explain the potency of the *Aire*- and *Cblb*-deficient combination, whereby two genetic lesions affect two pathways (negative selection and anergy) within the same autoreactive clone, precipitating autoimmunity. However, it is also important to consider that the two different failsafes could affect two interacting cells: one affecting the *forbidden clone* and the other affecting a cell that enhances or inhibits the *forbidden clone*. Data from adoptive transfer experiments in chapter 3 provide compelling evidence that both CD4 and CD8 cells were necessary to adoptively transfer lethal pancreatitis from $Aire^{-/-}Cblb^{-/-}$ mice to lymphopenic recipients, although CD8 cells alone appeared able to cause substantial subclinical damage to the pancreas. Additionally, single cell multiplex PCRs in chapter 5 detected a large clonal expansion of CD8 cells in the pancreas, and one of the clones isolated was sufficient to recapitulate pancreatitis when present in high numbers (together with a polyclonal repertoire of other T cell specificities) in retrogenic chimeras without the need for *Aire* or *Cblb* deficiency (chapter 5). On the other hand, CD4 cells appeared to be less frequently detected in the pancreas, suggesting, albeit not completely ruling out the possibility that the CD4 T cells may not be self-reactive in the $Aire^{-/-}Cblb^{-/-}$ mice. The results from the TCR^{3A9}→insHEL bone marrow chimeras, especially the ones where only 50% of the TCR-transgenic marrow was *Cblb*-deficient also illustrated this. Lethality and exocrine pancreatitis was observed here when three variables were in alignment: *Aire*-deficiency, *Cblb*-deficiency and the presence of HEL in the islets. This could imply that the CD4 TCR^{3A9} T cells that home to the HEL-expressing pancreatic islets were helping the small amount of exocrine-specific CD8 cells to damage the acinar cells. Thus, although the CD4 cells may not be exocrine-specific, these cells could still act as helper cells in mediating the disease by

extrinsically contributing to the immune microenvironment of exocrine-specific CD8 cells. In the NOD diabetes mouse model, it has been clearly demonstrated that autoreactive CD8 T cells are the first to infiltrate the pancreas, the first wave of cell recognising insulin derived epitopes (Wong et al., 1999), followed by highly diabetogenic T cells recognising other antigens such as islet-associated glucose-6-phosphatase with high avidity (Verdaguer et al., 1997; Verdaguer et al., 1996). The role of CD4 cell help to precipitate diabetes in this model remains unclear, however multiple studies have suggested that CD4 T cell help may be required for the antigen-specific CD8 cells to reach their maximum diabetogenic potential (Bendelac et al., 1987; Christianson et al., 1993; DiLorenzo and Serreze, 2005; Yagi et al., 1992), most likely by activating the APCs (CD40 on CD4/CD154 on APC ligation) that present antigen to the CD8 antigen-specific cells (Amrani et al., 2002). Thus, it is entirely possible that *Aire*-deficiency is only acting on non-antigen specific CD4 T helper cells, and *Cblb* deficiency only on antigen-specific CD8 cells with cell-to-cell cooperation explaining the strong genetic epistasis in the $Aire^{-/-}Cblb^{-/-}$ mouse model.

A further potential layer of complexity is added by experimental data that suggest *Aire* may play a role in the education of antigen-specific nTreg cells (Hinterberger et al., 2010; Kekalainen et al., 2007b; Laakso et al., 2010; Ryan et al., 2005; Wolff et al., 2010), and that *Cblb* promotes TGFβ-induced FoxP3 upregulation by naïve $CD4^+$ cells to form iTregs cells (data from Chapter 4 and (Harada et al., 2010)). Interestingly, several mouse models that have deficiencies in Tregs have been shown to develop early lethality and multiorgan autoimmunity similar to $Aire^{-/-}Cblb^{-/-}$ mice. (i) Neonatal mice thymectomized 2 to 4 days post-birth develop thyroiditis, gastritis, orchitis, prostatitis, and sialoadenitis (Kojima and Prehn, 1981; Nishizuka and Sakakura, 1969). This disease was preventable by inoculation of normal cells, containing what we currently know as T regulatory cells (Sakaguchi et al., 1982). (ii) Deficiency in the key transcription factor for Treg cells - FoxP3. In mice (Fontenot et al., 2003; Hori et al., 2003; Khattri et al., 2003) and humans (Bennett et al., 2001; Chatila et al., 2000; Wildin et al., 2001) the deficiency resulted in a lymphoproliferative wasting disease accompanied by multi-organs lymphocytic infiltration. (iii) Mice with abolished production of a key Treg-related immunomodulatory cytokine - TGFβ (Li et al., 2007; Shull et al., 1992) demonstrated lymphoproliferative wasting disease accompanied by

multi-organ lymphocytic infiltration. The parallels between the autoimmunity without a latent phase and multiorgan infiltration, in the well-studied *FoxP3*-deficient *scurfy* mouse model and *Aire*$^{-/-}$*Cblb*$^{-/-}$ mice suggested that the autoimmune phenotype in *Aire*$^{-/-}$ *Cblb*$^{-/-}$ could occur, at least partly, as a result of defective T regulatory cells.

Thus, it is also plausible that a co-factor for pancreatitis development is a deficiency in nTreg caused by the absence of *Aire* and/or deficiency in iTreg cells in the absence of *Cblb*. In support of this is the observation that transfer of varying doses of wild-type Tregs suppressed the wasting syndrome and pancreatitis in adoptive transfer recipients of *Aire*$^{-/-}$*Cblb*$^{-/-}$ cells in a dose dependent manner, although I have not tested if this suppression will still be observed if *Cblb*-deficient or *Aire*-deficient Tregs were used instead (chapter 3). In contrast to that, it is also noteworthy that *Aire*$^{-/-}$ recipients that received equal mixtures of wild-type and *Cblb*$^{-/-}$ bone marrow still developed pancreatitis although this appeared to be less severe than *Aire*$^{-/-}$ recipient mice that received only *Cblb*$^{-/-}$ cells. This failure to correct autoimmunity with wild-type Tregs *in trans* contrasts with autoimmunity due to nTreg defects, which is fully corrected in animals or humans with mixtures of defective and wild-type T cells (Sakaguchi et al., 2009). Hence the mixed chimera experiments suggest that the disease was not mediated simply by defects in the nTreg component but must have primarily an effector T cell-autonomous basis.

Taken together, although *Aire* and *Cblb*-deficiencies represented two genetic lesions in autoimmunity, the pleiotropic nature of the two genes suggest that the defects may have potentially crippled more than two failsafes or tolerance checkpoints for organ-specific autoimmunity in the *Aire*$^{-/-}$*Cblb*$^{-/-}$ mice (Fig. 6.2*C*). Future work could provide further resolution of how the respective genotypic deficiencies (in *Aire* or *Cblb*) within each cell type contributes to the development of autoimmunity. The retrogenic technology described in Chapter 5 will be an invaluable tool to tackle this question as it allows for the introduction of defects in different tolerance genes within different cell types. The genotypic contribution of CD4 helper and CD8 cells could be tested by restricting *Aire*- and *Cblb*-deficiencies to different immune cell types and observe which combinations recapitulated the disease. Alternatively, in light of the TCR^{3A9}→insHEL chimera result on the requirement for TCR^{3A9} cells in the development of exocrine pancreatitis, it is

also possible to combine this system with the CD8-retrogenic system. Simply, a low frequency of CD8 wild-type or *Cblb*-deficient retrogenic donor marrow could be introduced together equal numbers of non-transgenic:wild-type TCR^{3A9} marrow. In this system, *Cblb*-deficienct would be restricted to rare exocrine pancreas specific CD8 cells, while *Aire*-deficiency would affect the frequency of TCR^{3A9} cells available to serve as helpers in insHEL recipients and wild-type cells would provide a buffer so autoimmunity does not develop rapidly. If the notion for CD4 and CD8 was correct, this experiment should see the requirement for three variables before the development of lethal exocrine pancreatitis: *Cblb*-deficiency in the retrogenic bone marrow, *Aire*-deficiency and insHEL in the recipients.

6.3 Comparing the *Aire*$^{-/-}$*Cblb*$^{-/-}$ mouse model with other mouse models

The main characteristic features of the *Aire*$^{-/-}$*Cblb*$^{-/-}$ mouse model is the lethal wasting disease and autoimmunity targeted towards the pancreas and salivary gland. This section provides a comparison of the *Aire*$^{-/-}$*Cblb*$^{-/-}$ mouse model with other mice harbouring similar histopathological characteristics that could provide insights on understanding the molecular basis of the severe autoimmunity in the B10.BR.*Aire*$^{-/-}$ *Cblb*$^{-/-}$ mouse model. The mouse strains discussed are summarised in Table 6.1 and can be divided into three categories: mice with defects in the *Aire*-related pathway; in the *Cblb*-related pathway; and defects in cytokine pathways.

Table 6.1. Comparing the *Aire*$^{-/-}$*Cblb*$^{-/-}$ mouse model with mice that display similar phenotypes.

Mouse model	*Aire*$^{-/-}$*Cblb*$^{-/-}$	*Aire*$^{-/-}$	*Map3k14*^{aly}	*Cd28*$^{-/-}$	*Ctla4*$^{-/-}$
Background	B10.BR	NOD	B6×AEJ	NOD (BDC2.5 Treg-treated)	BALB/c, (DO11.10 TCRβ × *Ctla4*$^{-/-}$)
Pathway	AIRE, CBL-B	AIRE	AIRE	CBL-B	CBL-B
Median survival	3.5 weeks	10 weeks	>48 weeks	>24 weeks	7 weeks

Histopathological infiltration	Exocrine pancreas, salivary gland, stomach	Exocrine pancreas, eye, salivary gland, stomach	Exocrine salivary gland, lacrimal gland, pancreas, lung	Exocrine pancreas	Heart, lungs exocrine pancreas
Organ-specific autoantibody	Exocrine pancreas, salivary gland, stomach	Pancreas, eye, salivary gland, stomach, lung, thyroid	Not detected (mice had defect in humoral immunity)	Exocrine pancreas	Not done
Autoantigen identification	Not identified	Protein disulfide isomerase family 2	Not identified	Pancreatic amylase	Protein disulfide isomerase family 2
Autoimmunity driving cell (determined by adoptive transfer of disease to lymphopaenic recipients)	CD4 and CD8 dependent (pancreatitis), CD4-dependent (sialoadenitis)	Not done	CD4-dependent (Vβ1 in pancreas and Vβ1 & Vβ5 in salivary glands)	CD4-dependent	CD4-dependent
Model for human disease	Autoimmune pancreatitis	Autoimmune pancreatitis	Sjogren's syndrome	Autoimmune pancreatitis	
Other comments	Wild-type Treg cells confer protection for pancreatitis	*H2*^{b} MHC and *Idd3*/ *Idd5* protective for pancreatitis		Disease attributed to a defect in peripheral survival of Treg cells	CTLA-4 expression by Treg enough to control disease
References	(Teh et al., 2010)	(Jiang et al., 2005; Niki et al., 2006)	(Tsubata et al., 1996; Yamamichi et al., 1997)	(Meagher et al., 2008)	(Ise et al., 2010; Tivol et al., 1995)

6.3.1 Mice with deficiencies in functionally equivalent genes to *Aire*

The first group of mice that exhibited a similar co-occurrence of autoimmune T cell mediated exocrine pancreatitis and sialoadenitis is a group of mice with deficiencies in the *Aire*-related pathway of autoantigen presentation by medullary thymic epithelium. B6×AEJ.*Map3k14*^{aly} mice harbor a mutation in the NFκB-inducing kinase (NIK), an upstream activator of Rel-B through the non-canonical NFκB pathway involved in the

development of AIRE-expressing thymic medullary epithelial cells (Fletcher et al., 2009). The mice survived for more than 48 weeks of age but displayed striking autoimmunity targeted towards the exocrine pancreas, salivary glands, lacrimal glands and lung (Tsubata et al., 1996). The CD4 cells that infiltrated the pancreas or salivary gland appeared oligoclonal, with recurrent use of particular Vβ elements and sequencing evidence for expansion of particular CD4 T cell clones that were distinct in pancreas and salivary gland of the same mouse (Yamamichi et al., 1997). Although similar organs were targeted in the *Map3k14*^{aly} and *Aire*$^{-/-}$*Cblb*$^{-/-}$ mouse model, CD4 cells mediated disease in the former while both CD8 and CD4 cells were needed for the adoptive transfer of pancreatitis in the latter.

Another similar mouse was the NOD mouse sub-strain lacking AIRE (Jiang et al., 2005; Niki et al., 2006). Wild-type NOD mice are a well-recognised model for studying autoimmune diabetes and displayed severe insulitis but not exocrine pancreatitis. Interestingly, when *Aire* mutations were intercrossed to the NOD mouse strain, the mice presented with accelerated and modified autoimmunity targeted towards the exocrine instead of endocrine pancreas. In comparison to the B10.BR.*Aire*$^{-/-}$*Cblb*$^{-/-}$ mice, the mice had a longer median of survival (10 weeks compared to 3.5 weeks) but display similar B and T cell autoimmunity directed toward the exocrine pancreatitis, salivary gland and stomach. In the study from the Mathis laboratory (Jiang et al., 2005), congenic crosses made between the B6 and NOD backgrounds showed that the NOD *H2*^{g7} MHC haplotype together with the *Idd3* and *Idd5* haplotypes on chromosome 3 and 1, respectively, were key determinants of exocrine pancreas autoimmunity in this mouse (Jiang et al., 2005). While B10.BR *Aire*$^{-/-}$*Cblb*$^{-/-}$ mice do not utilise the *H2*^{g7} MHC haplotype and *Cblb* is not located within the *Idd3* or *Idd5* chromosomal regions, it is noteworthy that the NOD *Idd5* locus alters the relative splicing of Ctla-4 isoforms (Ueda et al., 2003), a molecule within the *Cblb* pathway in that Ctla-4, like Cbl-b, negatively regulates CD28 signalling.

6.3.2 Mice with deficiencies in functionally equivalent genes to *Cblb*

The second group of mice that displayed striking similarities to the *Aire*$^{-/-}$*Cblb*$^{-/-}$ mice are groups of mice with mutations in the "*Cblb*-related pathway": that is, other

mutations in negative regulators of CD28 co-stimulation. Similar to the NOD.*Aire*$^{-/-}$ mouse stain describe above, another manipulation to the NOD strain that precipitated exocrine pancreatitis was CD28-deficiency, which was revealed provided the animals were protected from diabetes by either adoptive transfer of BDC2.5 islet-specific Treg cells or by insulin treatment (Meagher et al., 2008). In these animals, the exocrine pancreas infiltration was adoptively transferable by CD4 cells that were shown to target the pancreatic amylase antigen, which is expressed in the pancreatic acinar cells and in the salivary gland (Meagher et al., 2008). On face value, Cbl-b deficiency and CD28 deficiency should be considered as having opposite polarity: Cbl-b deficiency exaggerates CD28 signalling or renders T cells CD28 independent (Bachmaier et al., 2000; Chiang et al., 2000), whereas CD28 deficiency eliminates this source of co-stimulation. However the Bluestone group demonstrated that CD28 deficient NOD mice have greatly diminished Tregs, explaining the paradoxical acceleration of type 1 diabetes in these animals (Salomon et al., 2000) and by extension also explaining the development of exocrine pancreatitis. An important function of Tregs is expression of Ctla-4, and Ctla-4 deficiency on exocrine pancreas-specific Tregs partly explains pancreatitis in *Ctla4* knockout mice (Ise et al., 2010). Hence Treg deficiency results in greater or prolonged display of CD80 and CD86 on antigen presenting cells (Ise et al., 2010; Qureshi et al., 2011; Schmidt et al., 2009; Wing et al., 2008). However, in NOD.*Cd28*$^{-/-}$ mice this mechanism cannot explain the development of exocrine pancreatitis, since no matter how much CD80 and CD86 are displayed there is no CD28 receptor to receive these co-stimulatory signals. Deficiency of Tregs in NOD.*Cd28*$^{-/-}$ mice may nevertheless enhance T cell stimulation through other pathways such as the TCR itself. IL-10, which is an important product of Tregs, downregulates surface MHC II display on dendritic cells and macrophages through induction of MHC II ubiquitination by MARCH1 (Tze et al., 2011). Since MHC II binds to the TCR, decreases in IL-10 would lead to a converse increase in MHC II-TCR binding and T cell stimulation. Data from this mouse strain coupled with information from the NOD.*Aire*$^{-/-}$ mouse suggest that modifying the NOD mouse strain to have defects either in thymic selection (AIRE) or T cell co-stimulation (CD28) precipitates a similar disease to the B10.BR.*Aire*$^{-/-}$*Cblb*$^{-/-}$ mouse.

As pointed out above, one of the molecules that could be influenced by the NOD background is Ctla-4. The role of Cbl-b has a number of parallels with the inhibitory cell surface receptor, Ctla-4, suggesting they are both part of a single peripheral T cell tolerance pathway for suppressing pancreatic and salivary gland autoimmunity. Ctla-4 is also induced by sustained antigen exposure on mature and anergic T cells and opposes CD28 co-stimulation, in part by binding more avidly to the CD28 ligands CD80 and CD86 (Linsley and Nadler, 2009; Pentcheva-Hoang et al., 2009) and stripping these molecules from the surface of antigen-presenting cells (Qureshi et al., 2011). Moreover, autoimmune exocrine pancreatic and salivary gland destruction are prominent features of the multi-organ inflammation that occurs in Ctla-4 deficient 129/Sv mice or BALB/c DO11.10 TCRβ transgenic mice (Ise et al., 2010; Tivol et al., 1995; Waterhouse et al., 1995). The autoimmune inflammation was seen to be CD4-dependent and Ctla-4 was shown to oppose accumulation of pancreas-specific T cells by two routes: intrinsically by its expression on pancreas-specific effector T cells that showed strong reactivity towards the PDIA2 antigen (Ise et al., 2010) and extrinsically by its expression on $Foxp3^+$ Treg cells where it down-regulated CD86 on antigen presenting cells to mediate their suppressive effects (Ise et al., 2010; Qureshi et al., 2011; Schmidt et al., 2009; Wing et al., 2008). Since *Cblb*-deficiency relieves T cells of their dependence on CD80 and CD86, it may have a similar effect to *Ctla4*-deficiency by allowing pancreas-reactive T cells to proliferate vigorously despite stimulation by immature dendritic cells with low MHC II, CD80 and CD86. Experiments *in vitro* showed that *Cblb*-deficient T effector cells were refractory to growth inhibition by $CD4^+CD25^+$ T regulatory cells, although the basis of this effect is unresolved (Wohlfert et al., 2004; Wohlfert et al., 2006).

6.3.3 Mice with deficiencies in genes that alter the "microenvironment" of the self-reactive cells

The third group of mice developing exocrine pancreatitis and sialoadenitis are animals with an altered cytokine environment in the pancreas. NOD mice treated with interferon-gamma (IFNγ) and tumour necrosis factor-alpha (TNFα) demonstrated a reduction in insulitis and a propensity towards exocrine pancreatitis (Campbell et al., 1991). Besides this mouse model, LP-BM5 murine leukemia virus-treated C57BL/6 mice developed exocrine pancreatitis and sialoadenitis (Watanabe et al., 2003). The

infiltrating cells were CD4 T cells, Mac-1^+ cells and B cells, of which most cells were apoptotic cells characterized by expression of Fas ligand and TNFα. The major inflammatory cytokines found in the exocrine pancreas were IFNγ and interleukin-10 (Watanabe et al., 2003). *Aire*-deficiency also could cause general dysregulation of a constellation of pro-inflammatory cytokines, changing the cytokine milieu and environment within the mice. Evidence for this comes from APECED patients that present with high titres of neutralising auto-antibodies against type I interferons (IFN-α and -ω (Husebye et al., 2009; Meager et al., 2006; Meloni et al., 2008) and IL-17A, IL-17F and/or IL-22 (Kisand et al., 2010; Puel et al., 2011; Puel et al., 2010). In mouse models, IL-17 cytokines seemed to be important for the control of various other pathogens, particularly in the lungs and gastrointestinal track (Khader et al., 2009). Th17 cells, especially their downstream cytokines, mediate major pathogenic functions in many other autoimmune diseases such as multiple sclerosis, rheumatoid arthritis, inflammatory bowel disease and psoriasis (Hu et al., 2010), providing evidence that accumulation of these cytokines can contribute towards the development of autoimmunity. This represents another layer of dysregulation that could influence the phenotype of the *Aire*$^{-/-}$*Cblb*$^{-/-}$ double-deficient mouse.

Comparing the mouse models in sections 6.3.1, 6.3.2 and 6.3.3 to double-deficient *Aire*$^{-/-}$*Cblb*$^{-/-}$ highlighted several themes that reinforced the conclusions or hypotheses that were drawn about the mechanistic interactions between *Aire*$^{-/-}$ and *Cblb*$^{-/-}$ in section 7.2. Firstly, most of the mouse models that shared similar histopathological characteristics to *Aire*$^{-/-}$*Cblb*$^{-/-}$ harbour genetic deficiencies in the genes associated with *Aire* or *Cblb* pathways on various mouse genetic backgrounds. This provides compelling evidence that the *Aire* and *Cblb* pathways may represent important failsafes for pancreas- and salivary gland-specific autoimmunity. Secondly, the data from these different mouse models suggest that the genetic deficiencies in the mice affect the self-reactive cells and cells that affect the microenvironment of the self-reactive cells (e.g. Tregs or cytokines). It is however interesting to note that adoptive transfer of only CD4 cells from the B6×AEJ.*Map3k14*^{aly}, NOD.*Cd28*$^{-/-}$ and BALB/c.DO11.10TCRβ×*Ctla4*$^{-/-}$ mouse models to lymphopenic recipients caused pancreatitis. This contrasted with the *Aire*$^{-/-}$*Cblb*$^{-/-}$ mouse model whereby the pancreatitis was largely CD8-dependent. It would thus be

interesting to further characterize the CD8 cells that are mediating pancreatitis in this model and identify the target antigen recognised by these self-reactive clones.

Overall, the observations from mouse models with similar autoimmunity to *Aire*$^{-/-}$*Cblb*$^{-/-}$ mice support the notion that lethal autoimmunity, devoid of a latent phase resulted from unifying genetic defects affecting both self-reactive cell intrinsic and cell extrinsic regulation of the self-reactive cells.

6.4 Exploring organ specificity in *Aire*$^{-/-}$*Cblb*$^{-/-}$ mice

6.4.1 Why is the pancreas and salivary gland specifically targeted?

An intriguing feature of the *Aire*$^{-/-}$*Cblb*$^{-/-}$ mice is that the mice present with autoimmunity targeted towards the exocrine pancreas and salivary glands. This specific, reproducible pattern contrasts with the single gene deficiency in *Aire* in both man and mice that affects multiple organs. Although, APS1 patients are diagnosed by the clinical triad of mucocutaneous candidiasis, hypoparathyroidism and adrenal insufficiency, they also displayed wide variability in secondary autoimmune manifestations including type I diabetes, premature ovarian failure, alopecia, vitiligo, malabsorption, and pancreatic insufficiency (Betterle et al., 1998; Perheentupa, 2006; Peterson and Peltonen, 2005). Consistent with numerous organ-specific genes that depend upon *Aire* for expression in thymic medullary epithelium (Anderson et al., 2002), mice with *Aire*-deficiency gradually develop autoantibodies and lymphocytic infiltration in numerous organs, including the salivary glands, eye, liver, kidney, stomach, lungs, thyroid gland and reproductive organs. Thus, it is intriguing that *Aire* and *Cblb* double-deficient mice would display autoimmunity targeted so aggressively towards just the exocrine pancreas and submandibular salivary glands, yet no evidence of acceleration against other tissues such as the stomach.

In this study, one hypothesis tested was that the organ-specificity is determined by the frequency of different T cells formed and positively selected in the T cell repertoire. Evidence supporting this hypothesis comes from experiments in NOD.*Cd28-/-* mice, where a depleted repertoire of Tregs was experimentally restored by adoptively

transferring islet-specific Tregs that had been expanded in culture (Meagher et al., 2008). By manipulating the repertoire in this way, the accelerated insulitis and diabetes in the animals was suppressed while accelerated exocrine pancreatitis was unaffected and became the dominant clinical feature. Chapter 4 described two complimentary methods that were used to test if this kind of variation in the nascent T cell repertoire redirected autoimmunity in *Aire*$^{-/-}$*Cblb*$^{-/-}$ mice to other organs. Firstly, the *H2*^{k} haplotype (*k* alleles of Class II I-A & I-E and Class I molecules K, D & L) MHC upon which T cells were positively and negatively selected in the thymus was substituted with *H2*^{b} (I-A^{b}, I-E^{null}, K^{b}, D^{b}, L^{null}). This change did not alter the target organs but diminished the onset and incidence of the cachectic wasting, pancreatitis and sialoadenitis. The fact that these animals lived much longer argues against the possibility that the rapidly lethal course of pancreatic autoimmunity in *H2*^{k} *Aire*$^{-/-}$*Cblb*$^{-/-}$ mice obscured accelerated autoimmunity against other organs because the latter might require a few more weeks to develop. A second approach was to keep the MHC constant but skew the repertoire to form high numbers of T cells bearing a HEL-specific TCR^{3A9} that recognized HEL in pancreatic islets. This also diminished the incidence and severity of exocrine pancreatitis in *Aire*$^{-/-}$*Cblb*$^{-/-}$ TCR^{3A9}-transgenic mice, but extensive exocrine pancreatitis still developed in a clear subgroup of the animals generated by bone marrow chimeras despite the skewing of the TCR repertoire towards recognizing the pancreatic islets. Moreover, there was no dramatic increase in the onset or incidence of diabetes compared to TCR^{3A9} × insHEL mice with single deficiency of either Aire or Cbl-b alone. Hence, these two approaches used to test the "*repertoire/presentation hypothesis*" failed to satisfactorily explain the organ specificity of the disease in the *Aire*- and *Cblb*-deficient mice.

An alternative explanation for acinar-specific autoimmune destruction is that each peripheral organ is protected by a specific set of fail-safe mechanisms that control self-reactive organ-specific T cells that escape negative selection in the thymus. In this view, different target organs would arise by combining *Aire*-deficiency with defects in different peripheral tolerance pathways regardless of the *H2* haplotype (*peripheral pathway hypothesis*). This hypothesis is compatible with the observation that mice of various *H2*-types harbouring gene defects in *Aire*- or *Cblb*-related pathways displayed autoimmune exocrine pancreatitis or sialoadenitis as discussed in section 6.3. Further

support for this hypothesis comes from studies of NOD mice with unaltered MHC but lacking CD86 or congenic for two non-MHC chromosomal segments, wherein autoimmunity was redirected from the pancreatic islets to peripheral nerves or the biliary ducts (Irie et al., 2006; Salomon et al., 2001). Although preliminary data from breeding B10.BR mice with combinations of *Aire*$^{-/-}$ and either *Fasl*$^{gld/gld}$, *Roquin*$^{san/san}$ or *Card11*$^{unm/unm}$ have not revealed co-operative autoimmunity, it would be of interest to test the effect of combining *Aire*-deficiency with defects in other peripheral tolerance pathways such as peripheral inhibition by PD-1 (Keir et al., 2007; Sharpe et al., 2007) or non-*Aire* dependent peripheral deletion (Cohen et al., 2010; Yip et al., 2009). It is also possible that most tissues are guarded by two or more peripheral tolerance failsafe mechanisms. To test this, it would be possible to breed *Aire*-deficient mice with defects in two different peripheral tolerance pathways – triple mutant mice, whereby the mutations could either occur in one or both copies of the tolerance gene (heterozygous or homozygous) and observe if any of these deficiencies could change the spectrum of organs targeted for autoimmune destruction.

It is intriguing that two organs were targeted in combination and this may be attributed to common features present in both the organs. Since both the exocrine pancreas and salivary gland have similarities in structure and function (production of digestive enzymes), it is possible that the T cells from the *Aire*$^{-/-}$*Cblb*$^{-/-}$ mice were targeting a shared autoantigen in the two organs, such as amylase (Meagher et al., 2008). However, the results of adoptive transfer assays in section 3 indicated that pancreatitis was both CD8- and CD4-dependent, while the sialoadenitis was predominantly CD4-dependent. Furthermore, the pattern of autoantibody detection from the sera of *Aire*$^{-/-}$*Cblb*$^{-/-}$ seemed to be largely targeted towards the apical cytoplasmic granules of the pancreatic acinar cells, while a more diffused pattern was observed for the salivary gland acinar cells. An antigen-independent common feature of these organs is that they are sensitive to initial insult, promoting the secretion of pro-inflammatory cytokines including type I interferons, TNF-α and IL-1 mediating hastened destruction of the exocrine organs (Mavragani and Crow, 2010; Patel and Fine, 2005). This could explain the link between the destruction on both organs. Since the early destruction of both organs may be lethal due to the abolished production of digestive enzymes needed for nutrient absorption and/or the release of digestive enzymes and inflammatory cytokines from acute

pancreatic damage, the mice had to be sacrificed before other organs damage might have been observed. Prolonging the survival of the mice, perhaps by the introduction of exocrine pancreas specific Tregs (Meagher et al., 2008), may unveil autoimmunity in additional organs.

6.4.2 Identifying the target antigen in *Aire*$^{-/-}$*Cblb*$^{-/-}$ mice

To further understand the autoimmune-specificity in *Aire*$^{-/-}$*Cblb*$^{-/-}$ mice, a key next step will be to determine the target autoantigen(s) in both the pancreas and salivary glands. This could be achieved by testing the related TCRs isolated by PCR from multiple CD8 T cells in the pancreas (chapter 5) and the distinct TCRs isolated from multiple CD4 T cells in the salivary gland (data from Singh, M. – PhD student in the laboratory) form the secondary adoptive transfer recipients of *Aire*$^{-/-}$*Cblb*$^{-/-}$ mice. These TCRs could be tested for reactivity towards peptide-autoantigens by two approaches: a candidate autoantigen testing approach, or a screening and mass spectrometry approach.

The candidate antigen testing approach would test pancreas-specific T cells isolated from retrogenic mice for their ability to proliferate and produce interleukin-2 following stimulation with antigen presenting cells expressing candidate autoantigens. As the pancreatitis was largely mediated by CD8 cells, the antigens would require MHC Class I-dependent presentation. To achieve this, the appropriate APCs could be generated by retroviral transduction of candidate autoantigen cDNAs into LPS-activated B cells or GM-CSF expanded bone marrow derived dendritic cells. *In vitro* cultures could be set up to determine reactivity of the retrogenic antigen-specific T cells. A good candidate autoantigen in the pancreas is the abundant endoplasmic reticulum protein, pancreas-specific protein disulfide isomerase (PDIp, gene symbol *Pdia2*; (Ise et al., 2010; Niki et al., 2006)) that was identified as a causative autoantigen in *Ctla4*-deficient mice and in *Aire*-deficient NOD mice. Interestingly, a similar pattern of autoantibody reactivity with apical exocrine pancreatic cells to that described in NOD.*Aire*$^{-/-}$ mice (Niki et al., 2006) was observed in sera from *Aire*$^{-/-}$*Cblb*$^{-/-}$ mice. Another likely candidate is pancreatic amylase expressed in the granules of the exocrine pancreas and also expressed in salivary gland, since this autoantigen was targeted by pancreatic autoimmunity in NOD.*CD28*$^{-/-}$ mice (Meagher et al., 2008). Other possible autoantigens that could be

tested are autoantigens identified based on high autoantibody titres in autoimmune pancreatitis patients such as lactoferrin (Jin et al., 2009), carbonic anhydrase (CA)-II (Aparisi et al., 2005), CA-IV (Nishimori et al., 2005), pancreatic secretory trypsin inhibitor (Asada et al., 2006), heat shock protein-10 (Takizawa et al., 2009) and plasminogen-binding protein (Frulloni et al., 2009). Besides these *bona fide* autoantigens, molecular mimicricy amongst microbes and target antigens could also result in a break down of tolerance. Commonly, *Helicobacter pylori* antigens have been shown to display cross reactivity with carbonic anhydrase (CA)-II and ubiquitin-protein ligase E3 component n-recognin 2 expressed in the acinar cells of the pancreas (Guarneri et al., 2005).

A caveat in the candidate antigen testing strategy is that it is a biased approach and unlikely to unravel novel autoantigens. Thus, an unbiased strategy could be utilised to tackle the problem by screening pools of peptides from pancreas or salivary gland extracts for T cell stimulatory activity, followed by chromatographic separation and mass spectrometry to identify the reactive peptides. More specifically, the pathogenic TCR-of-interest could be co-transfected together with a nuclear factor of activated T-cells (NFAT) transcription factor-reporter gene construct into the $58\alpha^{-}\beta^{-}$ T cell hybridoma line. The line lacks endogenous TCR chains albeit carrying CD3 molecules needed to respond to TCR stimulation. The system allows for the screening of candidate autoantigens with NFAT expression and IL-2 production as readouts for successful TCR-specific stimulation (Ise et al., 2010). The autoantigens could be presented to the pathogenic T cells as peptide libraries of fractionated pancreas or salivary gland extracts. The target antigen could then be identified via mass spectrometry to the reactive pool of autoantigens (Lieberman et al., 2003). Construction of retrogenic mouse models with immune cells specific for peptide autoantigens identified could shed light on how *Aire* and *Cblb* deficiencies contributes to the autoimmunity associated with *bona fide* autoantigens *in vivo*.

6.4.3 Potential for pancreas- and salivary gland-specific targeted treatment

Chapter 5 established that single cell multiplex sequencing coupled with the construction of retrogenic mice is a valuable tool for further understanding organ

specificity in the *Aire*$^{-/-}$*Cblb*$^{-/-}$ mice. With the current technology, particular clones of self-reactive T cells that could be important in the pathogenesis of autoimmunity could be easily identified and targeted for tolerisation or selective deletion. Although it seems logical that autoreactive T cells clones that are clonally expanded in an organ-specific autoimmune disease would provide further insights about the disease, it has proved difficult to identify the driver clones. In humans, TCR bias has been observed in numerous diseases such as multiple sclerosis (Hong et al., 1999; Oksenberg et al., 1993; Wucherpfennig et al., 1990), inflammatory bowel disease (Saubermann et al., 1999), ulcerative colitis (Probert et al., 2001), Sjögren's Syndrome (Sasaki et al., 2000), systemic lupus erythematosus (Desai-Mehta et al., 1995) and rheumatoid arthritis (Sun et al., 2005). In most cases, however, only the TCRβ but not the TCRα chain was identified and the target of the TCR was unknown. With current technology readily available to provide a more complete analysis of TCR repertoire, it would be useful to revisit and mine for autoimmune-driving T cell clones in human diseases and study the behaviour of these clones when coupled with one or more deficiencies in tolerance genes. This may provide insights on how antigen-specific pathogenic T cell can be selectively identified and purged or tolerised in the repertoire using APC-coupled-antigen treatment.

By identifying the driver self-reactive T cells, targeted treatment could also be attempted using the specific autoantigen they recognised as exemplified by the progress that has been made in the type I diabetes field. One of the key autoantigens identified as a target of driver CD8 T cell clones in NOD mice was islet-specific glucose-6-phosphatase catalytic subunit related protein (IGRP). Similar to the results in *Aire*$^{-/-}$ *Cblb*$^{-/-}$ mice, recurrent clonal expansion of CD8 T cells with similar islet-specific TCRs was found and shown to cause pancreatic islet destruction in NOD mice. Many of these T cells expressed highly homologous T cell receptor chains (Valpha17-Jalpha42) that recognised the IGRP peptide sequence $IGRP_{206–214}$ in the context of the MHC molecule K^d and were present on the earliest T cell infiltrates into the islets during the development of diabetes (Amrani et al., 2001; Anderson et al., 1999; DiLorenzo et al., 1998; Lieberman et al., 2003; Santamaria et al., 1995; Verdaguer et al., 1997). Treatment of NOD mice with IGRP peptides that expand low affinity IGRP CD8 cells with suppressive activity was shown to be effective in reversing diabetes progression

(Han et al., 2005b; Tsai et al., 2010). In the human population, the IGRP-encoding gene resides in a TID susceptibility locus on chromosome 2 (Pociot and McDermott, 2002) and the effectiveness of this peptide for therapy for TID could be considered (Han et al., 2005a). This example indicates that target antigens found in mice are translatable to human diseases.

Indeed the *Aire*-deficient mice have started to unveil a list single autoantigens that can target specific organs for spontaneous destruction. The first to be identified was the *Aire*-dependent eye-specific interphotoreceptor retinoid-binding protein (IRBP) that trigger eye-specific autoimmunity (DeVoss et al., 2006). Transplantation of IRBP knockout thymi into athymic IRBP sufficient mice trigger spontaneous autoimmune uveitis demonstrating that expression of single eye antigen during T cell development in the thymus is crucial in preventing eye-specific autoimmunity (DeVoss et al., 2006). Similarly, single *Aire*-dependent self-antigens have been identified as targets for destruction in single organs such as the pancreas-specific PDIA2 (Niki et al., 2006), lacrimal gland odorant binding protein 1a (DeVoss et al., 2010), prostate seminal vesicle secretory protein 2 (Hou et al., 2009), stomach mucin 6 (Gavanescu et al., 2007) and H/Kβ subunit of the H^+K^+ ATPase (Laurie et al., 2004) and lung vemeromulin (Shum et al., 2009). The identification of particular organ-specific autoantigens targeted in the *Aire*-deficient mice is a useful tool for identifying clinically relevant autoantigens for diagnosis and treatment of organ-specific autoimmune diseases.

As we continue to build upon this list of autoantigens and further understand how each of these antigens is controlled, it would help build clearer opportunities to target treatment more specifically in autoimmune diseases. There have already been attempts to treat autoimmune diseases using self-antigenic peptide to modulate autoimmune responses based on leads from mouse models. Originally identified in NOD mice (Daniel and Wegmann, 1996; Nakayama et al., 2005), the altered peptide ligand of the insulin $B_{9\text{-}23}$ epitope, NBI-6024, that was recognised by the interferon-gamma T_H1 inflammatory cells, was used to modulate the T cell response in type I diabetes. The results of a phase I trial indicated that the peptide treatment cause a shift in T_H1 pathogenic immune response to a protective T_H2 response (Alleva et al., 2006), although a phase II trial indicated that there were no significant effects on pancreatic

beta-cell function (Walter et al., 2009). Similarly, a two phase trial myelin basic protein$_{83-99}$ altered peptide ligand for the treatment of multiple sclerosis was prematurely terminated because the treatment led to hypersensitive reaction and disease exacerbation (Bielekova et al., 2000; Kappos et al., 2000). It is possible that the little success in these trials could be attributed to ineffective dose delivery and the underlying altered peptide ligand-T cell specific precursor frequency, avidity, activation status, all of which would influence the outcome of a robust immune response that could also vary from patient to patient as autoimmune diseases are extremely heterogenous (Genain and Zamvil, 2000). Perhaps the full potential of this therapy could be realised by better understanding the mechanism that are involved in self-antigen regulation in the laboratory in *in vitro* models and animal models and considering tailored therapy for each patient depending on the state of the disease. Hence, augmenting the expression of autoantigens or administering doses of autoantigen that could induce tolerance could still be a valuable strategy for controlling autoimmunity towards the specific antigen, without inducing alternative autoimmune disorders by using broad-spectrum immunosupressions to treat autoimmunity that is only targeted towards one or two organs. However, there is still broad scope for research to understand the precise mechanism to create an effective immune response with this strategy.

6.5 *Aire*$^{-/-}$*Cblb*$^{-/-}$ mice as a mouse model for the human diseases autoimmune pancreatitis, Sjogren's syndrome and Mikulicz disease

6.5.1 Autoimmune pancreatitis, Sjögren's syndrome and Mikulicz disease share similar histopathological features as *Aire*$^{-/-}$*Cblb*$^{-/-}$ mice

The ultimate goal for using animal models to study autoimmunity is to characterise disease pathogenesis, allowing better understanding of the disease and targets for immunotherapies that can alter the course of disease. The features of the *Aire*$^{-/-}$*Cblb*$^{-/-}$ mice are histopathologically most similar to the human conditions Sjögren's syndrome, Mikulicz disease and exocrine pancreatitis.

Of the three, Sjögren's Syndrome or sicca syndrome is the most extensively studied (Goransson et al., 2006). It is an autoimmune disorder affecting the exocrine salivary and lacrimal glands, clinically characterized by xerostomia (dry mouth) and

keratoconjunctivitis sicca (dry eyes). The disease affects approximately 3.1 million people worldwide with 90% of patients being female (Helmick et al., 2008). It exists in two forms, either primary of secondary. Primary Sjögren's Syndrome affects salivary and/or lacrimal glands in the absence of other rheumatic diseases, while its more common secondary form occurs in the presence of other rheumatic diseases, such as systemic lupus erythematosus (Prabu et al., 2003), rheumatoid arthritis (Reader et al., 1951), scleroderma (Kirkham, 1969), and primary biliary cirrhosis (Culp et al., 1982). The diagnosis of this syndrome includes detection of lymphocytes within the salivary glands (a feature of the *Aire*$^{-/-}$*Cblb*$^{-/-}$ mouse model), ocular and oral dryness, and the presence of anti-SSA/Ro, anti-SSB/La and antinuclear antibodies in the serum (Vitali, 2003). A similar disease to Sjögren's Syndrome, also characterized by infiltration in the salivary and lacrimal glands is Mikulicz's disease. The difference between the two diseases is that Mikulicz's disease exhibits a male dominance, no detection of anti-SSA/Ro, anti-SSB/La antibodies, and demonstrates a good response to corticosteroid treatment (Yamamoto et al., 2005). Besides that, Mikulicz's disease is characterised by high concentrations of serum IgG4, a feature shared with autoimmune pancreatitis.

Autoimmune pancreatitis is a rare condition twice as likely to develop in men compared to women. It is frequently associated with several autoimmune diseases including Sjögren's syndrome (Montefusco et al., 1984) and was only considered a separate disease when cases of pancreatitis without systemic autoimmunity were reported (Yoshida et al., 1995). The challenge in diagnosis is differentiating the disease from other forms of non-autoimmune pancreatitis (usually associated with chronic alcohol consumption or infections with Epstein-Barr virus, hepatitis virus or cytomegalovirus) and pancreatic cancer. The characteristic features include histological detection of pancreatic infiltration, hypergammaglobulinemia, elevated serum IgG4 levels, elevated plasma concentrations of carbonic anhydrase II and lactoferrin and antinuclear antibodies (Asada et al., 2006; Niki et al., 2006; Okazaki et al., 2001; Uchida et al., 2002). In humans, the condition rarely proceeds to total pancreatic insufficiency, but it is a relatively common syndrome that proceeds to pancreatic insufficiency and malabsorption in dogs (Wiberg et al., 2000). Recently, there have been suggestions of a new clinical entity and classification – IgG4-related diseases that encompasses Mikulicz's disease and autoimmune pancreatitis (Takahashi et al., 2011).

There is still much to understand about the etiology and pathogenesis of these diseases and the emergence of new mouse models that accurately resemble the human diseases would be a valuable tool in the advancement of the field. As the histological features of the *Aire*$^{-/-}$*Cblb*$^{-/-}$ mouse model fits with these diseases, exhibiting very specific destruction of the exocrine pancreas and salivary glands, it would be interesting to further investigate other key characteristics of the human disease in the mouse model. This would include the measurements of mouse-IgG1 antibodies (equivalent to human IgG4 (Hussain et al., 1995)) and detection of target antigens in the mouse that could unravel new biomarkers to be used for diagnosis of the disease or therapeutic treatment using coupled-cell-tolerance strategies (APCs coupled with autoantigens for tolerising autoreactive cell).

Currently there is little evidence about a connection between *Aire*- and *Cblb*-deficiencies in humans with pancreatitis/sialoadenitis. The well-characterized APECED disease has been associated with a simple monogenic recessive deficit in the *Aire* gene. It is notable that malabsorption and/or steatorrhoea occur as a secondary feature in 15-22% of APECED patients, and pancreatic insufficiency has been demonstrated in a fraction of these individuals (Betterle et al., 1998; Perheentupa, 2006). On the other hand, single gene deficiencies in *Cblb* have been identified in type 1 diabetes (Hoyne et al., 2011b; Yokoi et al., 2007; Yokoi et al., 2002). Single nucleotide polymorphisms that are linked to the *Cblb* gene have also been identified in a range of polygenic autoimmune diseases such as multiple sclerosis (Corrado et al., 2010; Sanna et al., 2010) and systemic lupus erythematosus (Doniz-Padilla et al., 2011). To date, there have not been reports of double deficiencies in both genes in autoimmune patients. Considering that many of the mouse models described in section 7.4 share deficiencies in *Aire*-dependent or *Cblb*-dependent tolerance pathways, this provides a compelling basis for analysing genetic variants within these pathways in Sjögren's syndrome syndrome, Mikulicz disease and exocrine pancreatitis autoimmune diseases.

6.6 Comparing the *multistep pathogenesis* for autoimmune disease with cancer

This study began by examining a *multistep pathogenesis model* to unravel a genetic basis for the clinical latency and heterogeneity in autoimmune diseases. Conventionally,

the latent phase in autoimmune disease have been attributed to environmental triggers. However, the presence of a latent phase in diabetes development in NOD mice (Alam et al., 2011) and autoimmunity in the MRL/lpr mice housed in germ-free conditions (Maldonado et al., 1999) provided scope for alternative explanations. Furthermore, NOD.*Aire*$^{-/-}$ mice housed in germ-free conditions developed comparable rates of exocrine pancreatitis to their specific-pathogen free-housed counterparts (Gray et al., 2007), supporting the notion that environmental triggers cannot fully explain variations in tempo and progression of autoimmune disease.

The co-operation between the two self-tolerance defects has striking parallels with the co-operative onset of cancer without a latent phase with combined defects in particular cancer checkpoints such as activation of an oncogene and inactivation of a failsafe tumor suppressor gene (Hanahan and Weinberg, 2000, 2011). Like the multi-step pathogenesis of different cancers, specific combinations of defects in compensating mechanisms of tolerance may be required to precipitate different autoimmune diseases. These findings provide a framework for understanding the latency and heterogeneity in clinical autoimmune disease and the complexity of its inheritance. There are several features that differ in the *multistep model* for autoimmunity to that of cancer pathogenesis. In cancer, multiple mutations accumulate in genes that regulate different pathways that control cell survival and growth in any cell type, resulting in multiple kinds of cancers able to metastasise to different areas. On the other hand, autoimmunity occurs as a results of multiple mutations occuring in genes involved in central of peripheral tolerance pathways and act either cell intrinsically or cell extrinsically on self-reactive lymphocyte clone(s), usually affecting haematopoietic progenitors of developing lymphocytes that are continuously produced throughout life. Cancer of the immune cells, or lymphoma (T and B cells) or leukaemia (myeloid cells), affect the immune cells but contrary to autoimmunity, these cancerous cells do not usually mediate severe destruction of specific organs.

Intriguingly, there is an increased occurrence of lymphoma in individuals with pre-existing autoimmune conditions such as lupus, rheumatoid arthritis and Sjögren's Syndrome (Bernatsky et al., 2005; Smedby et al., 2006; Zintzaras et al., 2005). As highlighted above, unifying features of the two diseases is that both are heterogenous in

nature, present with a latent phase (presumed to be a period of accumulating additional mutations) and result from inhibitions of normal pathways that keep cell growth/clonal expansion in check. These features suggest that the co-relation could be attributed to shared genetic defects between the two. A prominent example is that mutations in Fas, the molecule involved in apoptosis are associated with autoimmune diseases in mice and humans. Recent studies in chronic lymphocytic leukaemia demonstrated that monoclonal antibodies from the lymphoma react with autoantigens present in apoptotic cells and bacteria, providing preliminary indication that autoreactivity may play a role in lymphoma pathogenesis (Catera et al., 2008; Chu et al., 2010).

As both lymphoma and autoimmunity share numerous similarities in etiology and pathogenesis, findings or concepts from lymphoma may be applied to autoimmunity, and vice versa. Similar therapeutic strategies could potentially be used to treat autoimmune diseases and lymphoma or leukaemia. Administration of *ex vivo*-generated antibodies, such as CD25-specific antibody (daclizumab) has been used to treat noninfectious autoimmune uveitis, multiple sclerosis and adult T cell leukaemia (Waldmann, 2007). Another example is the monoclonal CD20-specific antibody (rituximab) has been approved for treatment of non-Hodgkin lymphoma and chronic lymphocytic leukemia, as well as some non-malignant autoimmune conditions like rheumatoid arthritis (Keating, 2010).

6.7 Concluding remarks

This study highlights the importance of studying the synergistic interactions between two alleles as some combinations could prove more or less potent than predicted based on the knowledge of the individual gene function. Perhaps the easiest way to continue tackling this would be to construct a detailed map of gene groups and molecular pathways needed to execute each tolerance mechanisms based on autoimmune driver genes found in genome wide association studies. As genes within the same group could be considered functionally equivalent, synergistic effects between defects in two pathways could be easily tested. In time, it is hoped that these genes will be joined by many others to yield a detailed map of the gene groups or molecular pathways needed

to execute immune tolerance to particular organs and understand how each pathway interacts to prevent autoimmunity.

Because of the potential collaborative nature of these tolerance defects, it could also be suggested that heterozygous mutations in tolerance genes may also contribute to pathogenesis and should be given more consideration. Deleterious inherited mutations are predicted to occur at a frequency of 1 in every 100 000 genes (Haag-Liautard et al., 2007). As there are 25 000 genes in each individual, 1 in every 4 children are predicted to carry 1 deleterious mutations, that could easily occur in one of the many tolerance genes in a rapidly outbreeding population. There is thus a high likelihood that many carry deleterious mutations of tolerance genes in a heterozygous state. A second hit in the functional copy of the tolerance allele could easily occur given that 10^{-6} somatic mutations occur per gene per cell division (Araten et al., 2005) and lymphocytes are continuously produced.

To summarise, organ-specific autoimmune disease is extremely complex in nature. As we continue to build a logical genetic framework for understanding the pathogenesis, it is important to not only draw information from genome wide association studies, but refine the information by strategically testing particular gene-gene combinations coupled with lymphocyte receptor reactivity to understand how these interactions orchestrate autoimmunity. A clearer picture of the genotypic contribution to autoimmune disease would not only provide insights to explain the mechanisms that account for human diseases but aid in predicting individual at risk of disease and effectively target treatments.

Chapter 7

Appendix

7.1 Supplementary figure and table for Chapter 3

Appendix 3.1 Table shows the RAW DATA of litter sizes for the 9 breeder pairs, the number of offspring of each genotype from each breeder pair (TOTAL OBTAINED) and the expected Mendelian ratios of each genotype based on the genotype of the parent breeder (TOTAL EXPECTED). Summary is seen in Table 3.1.

RAW DATA | **TOTAL OBTAINED** | TOTAL EXPECTED

F4, Breeder pair 1

Litters	Female	Male
1	2	5
2	2	5
3	1	
4	6	
5	6	2
6	5	5
7	5	4
8	2	7
9	5	3
10	8	5
11	2	2
12	1	1
13	1	3
14	3	5
15		2
16	Lost	
17	3	

Obtained	*Aire*$^{+}$ /+	*Aire*$^{+}$ /-	*Aire*$^{-}$ /-
Cblb +/+	8	17	5
Cblb +/-	6	27	12
Cblb^{-} /-	12	1	4

Expected	*Aire*$^{+}$ /+	*Aire*$^{+}$ /-	*Aire*$^{-}$ /-
Cblb +/+	5.75	11.5	5.75
Cblb +/-	11.5	23	11.5
Cblb^{-} /-	5.75	11.5	5.75

F4, Breeder pair 2

Litters	Female	Male
1	Lost	

Obtained	*Aire*$^{+}$ /+	*Aire*$^{+}$ /-	*Aire*$^{-}$ /-
Cblb +/+	2	1	1

Expected	*Aire*$^{+}$ /+	*Aire*$^{+}$ /-	*Aire*$^{-}$ /-
Cblb +/+	0.88	1.75	0.88

2	4	2
3	1	4
4	2	4
5	Lost	

Cblb $^{+/-}$	1	3	4
Cblb $^{-/-}$		1	1

Cblb $^{+/-}$	1.75	3.51	1.75
Cblb $^{-/-}$	0.88	1.75	0.88

F5, Breeder pair 1

Litters	Female	Male
1	5	2
2	1	2
3	1	3
4		1
5	2	3
6	Lost	
7	2	4
8	5	5
9	3	3
10	1	2

Obtained	*Aire* $^{+}$ $^{/+}$	*Aire* $^{+}$ $^{/-}$	*Aire* $^{-}$ $^{/-}$
Cblb $^{+/+}$		6	6
Cblb $^{+/-}$		9	10
Cblb $^{-/-}$		6	3

Expected	*Aire* $^{+}$ $^{/+}$	*Aire* $^{+}$ $^{/-}$	*Aire* $^{-}$ $^{/-}$
Cblb $^{+/+}$		5	5
Cblb $^{+/-}$		10	10
Cblb $^{-/-}$		5	5

RAW DATA **TOTAL OBTAINED** TOTAL EXPECTED

F5, Breeder pair 2

Litters	Female	Male
1	3	5
2	3	4
3	Lost	

Obtained	*Aire* $^{+}$ $^{/+}$	*Aire* $^{+}$ $^{/-}$	*Aire* $^{-}$ $^{/-}$
Cblb $^{+/+}$			4
Cblb $^{+/-}$			8
Cblb $^{-/-}$			3

Expected	*Aire* $^{+}$ $^{/+}$	*Aire* $^{+}$ $^{/-}$	*Aire* $^{-}$ $^{/-}$
Cblb $^{+/+}$			3.75
Cblb $^{+/-}$			7.5
Cblb $^{-/-}$			3.75

F5, Breeder pair 3

Litters	Female	Male
1	3	1
2	2	5
3	1	2

Obtained	*Aire* $^{+}$ $^{/+}$	*Aire* $^{+}$ $^{/-}$	*Aire* $^{-}$ $^{/-}$
Cblb $^{+/+}$		1	2
Cblb $^{+/-}$		3	1
Cblb $^{-/-}$	1	4	3

Expected	*Aire* $^{+}$ $^{/+}$	*Aire* $^{+}$ $^{/-}$	*Aire* $^{-}$ $^{/-}$
Cblb $^{+/+}$		2.5	2.5
Cblb $^{+/-}$		2.5	2.5
Cblb $^{-/-}$		2.5	2.5

F6, Breeder pair 2

Litters	Female	Male
1	2	1
2	4	3

Obtained	*Aire* $^{+}$ $^{/+}$	*Aire* $^{+}$ $^{/-}$	*Aire* $^{-}$ $^{/-}$
Cblb $^{+/+}$			6
Cblb $^{+/-}$			5

Expected	*Aire* $^{+}$ $^{/+}$	*Aire* $^{+}$ $^{/-}$	*Aire* $^{-}$ $^{/-}$
Cblb $^{+/+}$			3.25
Cblb $^{+/-}$			6.5

3	Lost	
4	1	2

Cblb^{-} /-			2

Cblb^{-} /-			3.25

F6, Breeder pair 4

Litters	Female	Male
1	5	2
2	1	5
3	5	6
4	2	5

Obtained	*Aire*$^{+}$ /+	*Aire*$^{+}$ /-	*Aire*$^{-}$ /-
Cblb +/+		4	
Cblb +/-	11	6	
Cblb^{-} /-		8	

Expected	*Aire*$^{+}$ /+	*Aire*$^{+}$ /-	*Aire*$^{-}$ /-
Cblb +/+	3.65	3.65	
Cblb +/-	7.3	7.3	
Cblb^{-} /-	3.65	3.65	

F7, Breeder pair 1

Litters	Female	Male
1	4	5
2	5	2

Obtained	*Aire*$^{+}$ /+	*Aire*$^{+}$ /-	*Aire*$^{-}$ /-
Cblb +/+			1
Cblb +/-			13
Cblb^{-} /-			2

Expected	*Aire*$^{+}$ /+	*Aire*$^{+}$ /-	*Aire*$^{-}$ /-
Cblb +/+			4
Cblb +/-			8
Cblb^{-} /-			4

F9, Breeder pair 1

Litters	Female	Male
1	Lost	
2	4	3
3	3	8
4	5	2

Obtained	*Aire*$^{+}$ /+	*Aire*$^{+}$ /-	*Aire*$^{-}$ /-
Cblb +/+			
Cblb +/-	6	5	
Cblb^{-} /-	7	5	

Expected	*Aire*$^{+}$ /+	*Aire*$^{+}$ /-	*Aire*$^{-}$ /-
Cblb +/+			
Cblb +/-	5.75	5.75	
Cblb^{-} /-	5.75	5.75	

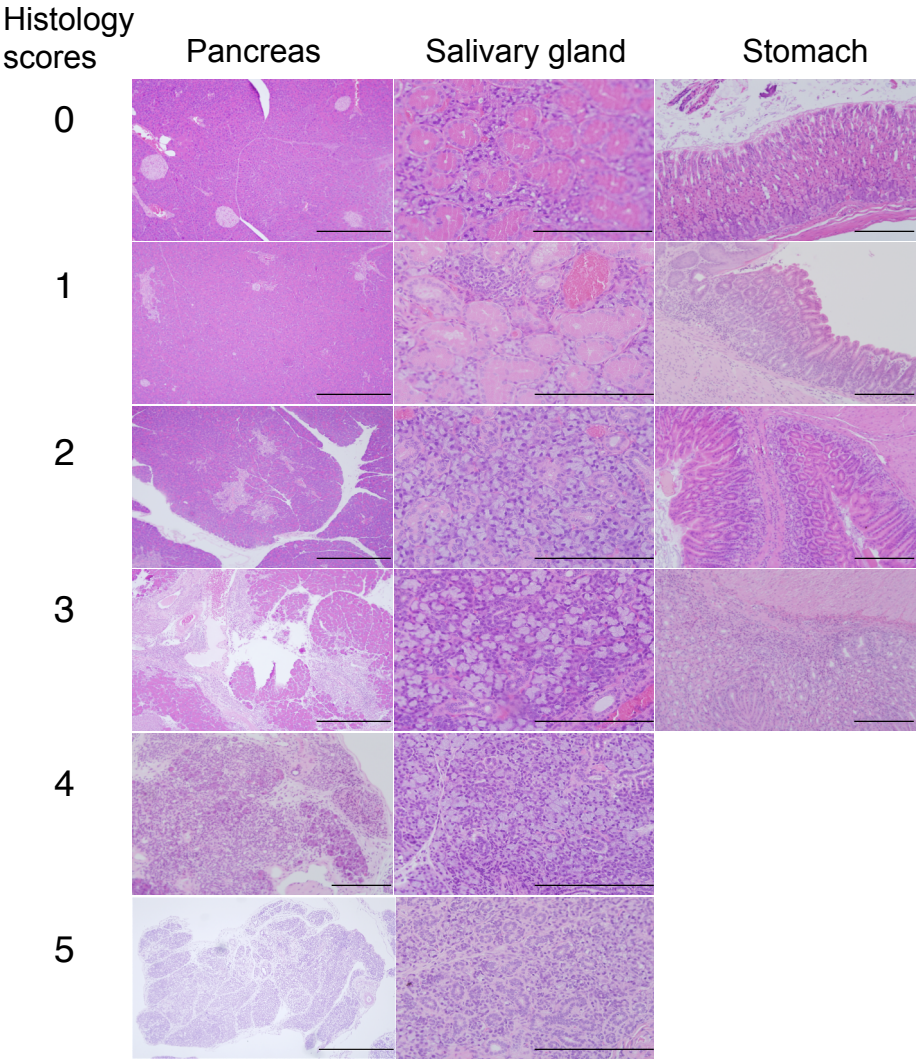

Appendix 3.2. Histology scores for histopathology.
Pancreas: (0) No pancreatitis detected; (1) Perivascular lymphocyte infiltration; (2) Small patches of lymphocyte infiltration in the exocrine tissue; (3) Extensive infiltration in the exocrine pancreatic tissue and destruction of <50% of the exocrine acinar tissue; (4) Extensive infiltration in the exocrine pancreatic tissue and destruction of 50%-90% of the exocrine acinar tissue; (5) Extensive infiltration in the exocrine pancreatic tissue and complete absence of exocrine acinar tissue. Original magnification: x100. Bars: 500 μm.
Submandibular salivary gland: (0) No sialoadenitis detected; (1) Perivascular lymphocyte infiltration; (2) Small patches of lymphocyte infiltration in the supporting tissue, decrease in mucous acini; (3) Extensive lymphocytic infiltration and destruction of <50% of the mucous acinar tissue; (4) Extensive lymphocytic infiltration and destruction of 50%-90% of the mucous acinar tissue; (5) Extensive lymphocytic infiltration and complete absence of mucous acinar tissue. Original magnification: x400. Bars: 200 μm.
Varying lymphocytic infiltration in the stomach. Original magnification: x200. Bars: 200 μm.

7.2 Supplementary tables for Chapter 5

Tables on the following pages show raw data from the multiplex RT-PCR sequencing of mRNA isolated from paired TCRα and β chains in *Aire*$^{-/-}$*Cblb*$^{-/-}$ donors, adoptive transfer primary and secondary recipients.

Table 5.10 The analysis of CD4 clones in the spleen of original donors of WT1 mice (S_0, Plate CT32).

Trav	Va	N	Ja	Traj	Length, aa	Trbv	Vb	N	Jb	Trbj	Length, aa	Frequency
Trav3-4	YFCAV	SANYNQGKL	IFGQGTKLSIKP	Traj23	9	Trbv20	YLCGA	RDRANSD	YTFGSGTRLLV	Trbj1-2	7	1
Trav5D-4	YFCAA	SSNNRIP	FFGDGTQLVVK	Traj31	7	Trbv3	YFCAS	SPGTGYEQ	YFGPGTRLTVL	Trbv2-7	8	1
Trav5D-4	YFCAA	SEQGGSAKL	IFGEGTKLTVSS	Traj57	9	Trbv13-3	YFCAS	SDGTGEKAP	LFGEGTRLSVL	Trbj1-5	9	1
Trav6?	YFCAL	LCGSFNKL	TFGAGTRLAVCP	Traj4	8	Trbv13-2	YFCAS	GEQNTEV	FFGKGTRLTVV	Trbj1-1	7	1
Trav6-1, 2	YCVLA	VSSNTNKV	VFGTGTRLQVLP	Traj34	8	Trbv13-2	YFCAS	GDATGRDTQ	YFGPGTRLLVL	Trbj2-5	9	1
Trav6-1, 6-2	YYCVL	VDSNYQL	IWGSGTKLIIKP	Traj33	7	Trbv29	YFCAS	SSTGRNTEV	FFGKGTRLTVV	Trbj1-1	9	1
Trav6-3, 6D-3	YYCAM	RDAYGSSGNKL	IFGIGTLLSVKP	Traj32	11	Trbv13-2	YFCAS	GDAGQGYAEQ	FFGPGTRLTVL	Trbj2-1	10	1
Trav6-4, 6D-4	YFCAL	DYTGANTGKL	TFGHGTILRVHP	Traj52	10	Trbv13-2	YFCAS	GDRNTGQL	YFGEGSKLTVL	Trbj2-2	8	1
Trav6-5, D-6, D-7,	YYCAL	GEGTGSKL	SFGKGAKLTVSP	Traj58	8	Trbv26	YLCAS	SPLGPYYEQ	YFGPGTRLTVL	Trbv2-7	9	1
Trav6-5, D-6, D-7,	YYCAQ	SGSFNKL	TFGAGTRLAVCP	Traj4	7	Trbv20	YLCGA	RDNYAEQ	FFGPGTRLTVL	Trbj2-1	7	1
Trav6-6	YYCAL	GASMNYNQGKL	IFGQGTKLSIKP	Traj23	11	Trbv31	YLCAW	SLGGDQDTQ	YFGPGTRLLVL	Trbj2-5	9	1
Trav7?	YLCAV	NYNQGKL	IFGQGTKLSIKP	Traj23	7	Trbv31	YLCAW	SSDWGGYEQ	YFGPGTRLTVL	Trbv2-7	9	1
Trav7-1	YFCAV	TDRGSALGRL	HFGAGTQLIVIP	Traj18	10	Trbv19	FLCAS	RLGNQDTQ	YFGPGTRLLVL	Trbj2-5	8	1
Trav7-1	YFCAV	RGMTTASLGKL	QFGTGTQVVVTP	Traj24	11	Trbv13-1	YFCAS	SGPKDTQ	YFGPGTRLLVL	Trbj2-5	7	1
Trav7-2, 3, D-3	YLCAV	SPGGSNAKL	TFGKGTKLSVKS	Traj42	9	Trbv13-1	YFCAS	SGLTSQNTL	YFGAGTRLSVL	Trbj2-4	9	1
Trav7-3	YLCAA	SPGGNYKP	TFGKGTSLVVHP	Traj6	8	Trbv1	YCTCS	AEAGDTGQL	YFGEGSKLTVL	Trbj2-2	9	1
Trav8-1, 8D-1	YFCAT	NTNTGKL	TFGDGTVLTVKP	Traj27	7	Trbv31	YLCAW	SLEGGQNTL	YFGAGTRLSVL	Trbj2-4	9	1
Trav9?	YFCVL	RMQQGTGSKL	SFGKGAKLTVSP	Traj58	10	Trbv13-2	YFCAS	VLGGRGEQ	YFGPGTRLTVL	Trbv2-7	8	1
Trav9-3,D-3, 4	YFCAV	SAGSNYNVL	YFGSGTKLTVEP	Traj21	9	Trbv1	YCTCS	VQGNQDTQ	YFGPGTRLLVL	Trbj2-5	8	1
Trav9D-4	YFCVL	SASGGSNAKL	TFGKGTKLSVKS	Traj42	10	Trbv13-2	YFCAS	GALTGSYEQ	YFGPGTRLTVL	Trbv2-7	9	1
Trav10, 10D	YFCAA	RITGNTGKL	IFGLGTTLQVQP	Traj37	9	Trbv19	FLCAS	SIWGAQDTQ	YFGPGTRLLVL	Trbj2-5	9	1
Trav11, 11D	YICVVG	DRGSALGRL	HFGAGTQLIVIP	Traj18	9	TRVB1	YCTCS	ADRDTQ	YFGPGTRLLVL	Trbj2-5	6	1
Trav12D-1, 2, D-2, 3, D-3	YYCAL	SRVGDNSKL	IWGLGTSLVVNP	Traj38	9	Trbv26	YLCAS	SQDSGNT	LYFGEGSRLIVV	Trbj1-3	7	1
Trav12D-1, 2, D-2, 3, D-3	YYCAL	GANYGNEKI	TFGAGTKLTIKP	Traj48	9	Trbv2	YFCPS	IQAGGGWRQ	SFGPGTRLTVL	Trbj2-1	9	1
Trav13-1, D-1	LCAM	DQGGRAL	IFGTGTTVSVSP	Traj15	7	Trbv19	FLCAS	SKRGAETL	YFGSGTRLTVL	Trbj2-3	8	1
Trav13-2	YFCAI	ESSAGNKL	TFGIGTRVLVRP	Traj17	8	Trbv2	YFCAS	SQDRDTQ	YFGPGTRLLVL	Trbj2-5	7	1
Trav13D-1	YLCAL	EGNNNAP	RFGAGTKLSVKP	Traj43	7	Trbv5	YFCAS	SQEGLGYAEQ	FFGPGTRLTVL	Trbj2-1	10	1
Trav14-1	YFCAA	RGSNAKL	TFGKGTKLSVKS	Traj42	7	Trbv4(2)	YLCAS	SSGQGYERL	FFGHGTKLSVL	Trbj1-4	9	1
Trav14-2	YFCAA	SDTNTGKL	TFGDGTVLTVKP	Traj27	8	Trbv5	YFCAS	SQAREGEQ	YFGPGTRLTVL	Trbv2-7	8	1
Trav14-2	YFCAA	TSNTNKV	VFGTGTRLQVLP	Traj34	7	Trbv3	YFCAS	SFDRGGSAETL	YFGSGTRLTVL	Trbj2-3	11	1
Trav14D-3/DV8	YFCAA	SGGSALGRL	HFGAGTQLIVIP	Traj18	9	Trbv13-1	YFCAS	SERTGTSAETL	YFGSGTRLTVL	Trbj2-3	11	1
Trav16, 16D/DV11	YFCAM	REGRGYQNF	YFGKGTSLTVIP	Traj49	9	Trbv5	YFCAS	SQDRGSYEQ	YFGPGTRLTVL	Trbv2-7	9	1
Trav21/DV12	YHCIL	RNNNNAP	RFGAGTKLSVKP	Traj43	7	Trbv1	YCTCS	ADTGGNTL	YFGAGTRLSVL	Trbj2-4	8	1
Trav21/DV12	YHCIL	NSGYQNF	YFGKGTSLTVIP	Traj49	7	Trbv19	FLCAS	SRQGEA	YFGPGTRLTVL	Trbv2-7	6	1
												34

Table 5.11 The analysis of CD4 clones in the spleen of WT1 primary recipient mice (S_1, Plate CT43).

Trav	Va	N	Ja	Traj	Length, aa	Trbv	Vb	N	Jb	Trbj	Length, aa	Frequency
Trav4-3, D-3	YFCAA	EANNAGAKL	TFGGGTRLTVRP	Traj39	9	Trbv1	LYCTC	SDWGGNTGQL	YFGEGSKLTVL	Trbj2-2	10	1
Trav7D-5	YLCAV	SSNTGYQNF	YFGKGTSLTVIP	Traj49	9	Trbv4(2)	YLCAS	SDWGDQNTL	YFGAGTRLSVL	Trbj2-4	9	1
Trav6D-4, Trav6D-6, Trav6D-7	YFCAL	STGNYKY	VFGAGTRLKVIA	Traj40	7	Trbv30	YFCSP	YFGEGSKLTVL	YFGEGSKLTVL	Trbj2-2	11	1
Trav7-4, D-4	YFCAV	SGGNMGYKL	TFGTGTSLLVDP	Traj9	9	Trbv2	YFCAS	SQDGGLRGQNTL	YFGAGTRLSVL	Trbj2-4	12	1
Trav7D-2	YLCAA	SMGTGSNRL	TFGKGTKFSLIP	Traj28	9	Trbv13-2	YFCAS	GELGGDTQ	YFGPGTRLLVL	Trbj2-5	8	1
												5

Table 5.12 The analysis of CD4 clones in the spleen of WT1 secondary recipient mice (S_2, Plate CT60).

Trav	Va	N	Ja	Traj	Length, aa	Trbv	Vb	N	Jb	Trbj	Length, aa	Frequency
TRAV3-4	YFCAV	SRNSGTYQ	RFGTGTKLQVVP	Traj13	8	Trbv4(2)	YLCAS	VLGNQDTQ	YFGPGTRLLVL	Trbj2-5	8	1
TRAV4-3, 4D-3	YFCAA	ANMDYANKM	IFGLGTILRVRP	Traj47	9	Trbv1	LYCTC	SADPTYSGNTL	YFGEGSRLIVV	Trbj1-3	11	1
TRAV7-5, 7D-5	YLCAD	TGYQNF	YFGKGTSLTVIP	Traj49	6	Trbv3	YFCAS	SLDQGGEV	FFGKGTRLTVV	Trbj1-1	8	1
TRAV7-6 or 7D-6	YLCAV	RGNMGYKL	TFGTGTSLLVDP	Traj9	8	Trbv14	YLCAS	SKTGINQAP	LFGEGTRLSVL	Trbj1-5	9	12
TRAV8-2	YFCAT	DDTNTGKL	TFGDGTVLTVKP	Traj27	8	Trbv13-2	YFCAS	GGTGGAETL	YFGSGTRLTVL	Trbj2-3	9	2
TRAV9-1, D-1, 2, D-2, 3, D-3, 4, D-4	YFCVL	SVTGSGGKL	TLGAGTRLQVNL	Traj44	9	Trbv13-1	YFCAS	SDQDSAEQ	FFGPGTRLTVL	Trbj2-1	8	1
TRAV9-1, TRAV9D-3	YFCAV	SSGTGGYKV	VFGSGTRLLVSP	Traj12	9	Trbv31	YLCAW	SPLGGREQ	YFGPGTRLTVL	Trbv2-7	8	1
TRAV10, 10D	YFCAA	SNYGNEKI	TFGAGTKLTIKP	Traj48	8	Trbv5	YFCAS	SPDRGGWEQ	YFGPGTRLTVL	Trbv2-7	9	2
TRAV13-2	YLCAL	ERNNYAQGL	TFGLGTRVSVFP	Traj26(1)	9	Trbv20	YLCGA	RDPGFDERL	FFGHGTKLSVL	Trbj1-4	9	1
TRAV14D-3/DV8	YFCAA	KSAGNKL	TFGIGTRVLVRP	Traj17	7	Trbv20	YLCGA	RDPGFDERL	FFGHGTKLSVL	Trbj1-4	9	1
TRAV14D-3/DV8	YFCAA	SEGNMGYKL	TFGTGTSLLVDP	Traj9	9	Trbv2	YFCAS	SPTGTNSD	YTFGSGTRLLVI	Trbj1-2	8	1
TRAV16, 16D/DV11	YFCAM	REGRTGNYKY	VFGAGTRLKVIA	Traj40	10	Trbv13-2	YFCAS	GGTGGAETL	YFGSGTRLTVL	Trbj2-3	9	1
												25

Table 5.13 The analysis of CD4 clones in the spleen of original donors of MUT1 mice (S_0, Plate CT38).

Trav	Va	N	Ja	Traj	Length, aa	Trbv	Vb	N	Jb	Trbj	Length, aa	Frequency
Trav4-4/DV10	YFCAA	TGNTGKL	IFGLGTTLQVQP	Traj37	7	Trbv20	YLCGA	STDNNQAP	LFGEGTRLSVL	Trbj1-5	8	1
Trav5-1	YFCSA	GNYAQGL	TFGLGTRVSVFP	Traj26(1)	7	Trbv26	YLCAS	RYWGGNQDTQ	YFGPGTRLLVL	Trbj2-5	10	1
Trav5D-4	YFCAA	SENNNNAP	RFGAGTKLSVKP	Traj43	8	Trbv13-1	YFCAS	SGGGAETL	YFGSGTRLTVL	Trbj2-3	8	1
Trav5D-4	YFCAA	SGGSNAKL	TFGKGTKLSVKS	Traj42	8	Trbv17	YLCAS	SGGTGGTQ	YFGPGTRLLVL	Trbj2-5	8	1
Trav6-1, 6-2, 6-4, 6D-4, 6-5, 6D-5, 6, 6D-6, 6-7/DV9, 6D-7	YYCAL	GWAGSFNKL	TFGAGTRLAVCP	Traj4	9	Trbv13-3	YFCAS	GTGGTNTGQL	YFGEGSKLTVL	Trbj2-2	10	1
Trav6-5, 6D-5	YYCAL	RFNYGNEKI	TFGAGTKLTIKP	Traj48	9	Trbv19	FLCAS	SIVGLYEQ	YFGPGTRLTVL	Trbv2-7	8	1
Trav6-7/DV9	YYCAL	GNSGGSNYKL	TFGKGTLLTVTP	Traj53	10	Trbv5	YFCAS	SPTGRNTS	YFGAGTRLSVL	Trbj2-4	8	1
Trav6D-5, 6-6, 6-7/DV9	YYCAL	GVNTNTGKL	TFGDGTVLTVKP	Traj27	9	Trbv1	LYCTC	SAGGSAETL	YFGSGTRLTVL	Trbj2-3	9	1
Trav7-5	YLCAV	ENRGSALGRL	HFGAGTQLIVIP	Traj18	10	Trbv4(2)	YLCAS	TKDRRQDTQ	YFGPGTRLLVL	Trbj2-5	9	1
Trav7-6	YLCAV	SSGSWQL	IFGSGTQLTVMP	Traj22	7	Trbv13-1	YFCAS	SARDNSGNTL	YFGEGSRLIVV	Trbj1-3	10	1
Trav7-6	YLCAV	GNNAGAKL	TFGGGTRLTVRP	Traj39	8	Trbv3	YFCAS	SWDWGDAEQ	FFGPGTRLTVL	Trbj2-1	9	1
Trav9-1, 9D-1, 9-2, 9D-3	YFCAA	GNTRKL	IFGLGTTLQVQP	Traj37	6	Trbv20	YLCGA	RVVGVQDTQ	YFGPGTRLLVL	Trbj2-5	9	1
Trav9-1, 9D-1, 9-2, 9D-3	YFCAV	SAYGSSGNKL	IFGIGTLLSVKP	Traj32	10	Trbv3	YFCAS	SSGAETL	YFGSGTRLTVL	Trbj2-3	7	1
Trav9-1, 9D-1, 9-2, 9D-3	YFCAV	RDYSNNRL	TLGKGTQVVVLP	Traj7	8	Trbv4(2)	YLCAS	SPRGQNTL	YFGAGTRLSVL	Trbj2-4	8	1
Trav9-3, 9-4, 9D-4	YFCAV	SALGSSGNKL	IFGIGTLLSVKP	Traj32	10	Trbv15	YLCAS	SPDTSGNTL	YFGEGSRLIVV	Trbj1-3	9	1
Trav9-3, 9-4, 9D-4	YFCAV	SIASSSFSKL	VFGQGTSLSVVP	Traj50	10	Trbv31	YLCAR	RGGERL	FGHGTKLSVLGL	Trbj1-4	6	1
Trav12D-1, 12-2, 12D-2, 12-3, 12D-3	YYCAL	SDNNAGAKL	TFGGGTRLTVRP	Traj39	9	Trbv13-1	YLCAS	SPWGGSAETL	YFGSGTRLTVL	Trbj2-3	10	1
Trav13D-4	YLCAM	ANTGYQNF	YFGKGTSLTVIP	Traj49	8	Trbv14	YLCAS	SLGGNTGQL	YFGEGSKLTVL	Trbj2-2	9	1
Trav14-1	YFCAA	SDYQGGRAL	IFGTGTTVSVSP	Traj15	9	Trbv13-1	YFCAS	SDGTGGQDTQ	YFGPGTRLLVL	Trbj2-5	10	1
Trav14-1	YFCAA	SGSQGGSAKL	IFGEGTKLTVSS	Traj57	10	Trbv31	YLCAW	TGGTSAETL	YFGSGTRLTVL	Trbj2-3	9	1
Trav14-3	YFCAA	MNYNQGKL	IFGQGTKLSIKP	Traj23	8	Trbv14	YLCAS	SFRDSGNTL	YFGEGSRLIVV	Trbj1-3	9	1
Trav14-3	YFCAA	SAGNTGKL	IFGLGTTLQVQP	Traj37	8	Trbv29	YFCAS	SKGGLGGYEQ	YFGPGTRLTVL	Trbv2-7	10	1
Trav16, 16D/DV11	YFCAM	REGTNTNKV	VFGTGTRLQVLP	Traj34	9	Trbv14	YLCAS	SLGSSD	YTFGSGTRLLVI	Trbj1-2	6	1
Trav19	YLCAA	GANTGYQNF	YFGKGTSLTVIP	Traj49	9	Trbv2	YFCAS	SPQGNERL	FFGHGTKLSVL	Trbj1-4	8	1
												24

Table 5.14 The analysis of CD4 clones in the pancreas of original donors of MUT1 mice (P_0, Plate CT25).

Trav	Va	N	Ja	Traj	Length, aa	Trbv	Vb	N	Jb	Trbj	Length, aa	Frequency
Trav4-3, 4D-3	YFCAA	MSGGSNYKL	TFGKGTLLTVTP	Traj53	9	Trbv2	YFCAS	SQGNSD	YTFGSGTRLLVI	Trbj1-2	6	1
Trav5D-4	YFCAA	TASLGKL	QFGTGTQVVVTP	Traj24	7	Trbv5	YFCAS	SQGAQNTL	YFGAGTRLSVL	Trbj2-4	8	1
Trav6-4, 6D-4	YCVLG	DLSSGSWQL	ILGSGTQVTVMP		9	Trbv29	YFCAS	SPRTGDTL	YFGAGTRLSVL	Trbj2-4	8	1
Trav6-4, 6D-4, 6-5, 6D-5, 6-6, 6D-6, 6-7/DV9, 6D-7	YYCAL	AYYAQGL	TFGLGTRVSVFP	Traj26(1)	7	Trbv1	LYCTC	SANSAETL	YFGSGTRLTVL	Trbj2-3	8	1
Trav6-6, 6D-6	YYCAL	SVVSGSFNKL	TFGAGTRLAV**C**P	Traj4	10	Trbv3	YFCAS	SLGGGSAETL	YFGSGTRLTVL	Trbj2-3	10	1
Trav6-7, 6-7/DV9	YYCAL	GVYNQGKL	IFGQGTKLSIKP	Traj23	8	Trbv13-2	YFCAS	GDLGSSQNTL	YFGAGTRLSVL	Trbj2-4	10	1
Trav6D-5, 6-6, 6-7/DV9	YYCAL	GDNNRI	FFGDGTQLVVKP	Traj31	6	Trbv29	YFCAS	SFQTGNTL	YFGEGSRLIVV	Trbj1-3	8	1
Trav7-2, 7D-2	YLCAA	SRGGSNAKL	TFGKGTKLSVKS	Traj42	9	Trbv19	FLCAS	SRDREDTQ	YFGPGTRLLVL	Trbj2-5	8	1
Trav7-4, 7D-4	YFCAA	RAITGNTGKL	IFGLGTTLQVQP	Traj37	10	Trbv1	LYCTC	SALTGGNSPL	YFAAGTRLTVT	Trbj1-6	10	1
Trav7D-5, 7-6	YFCAV	SYSNYQL	IWGSGTKLIIKP	Traj33	7	Trbv13-1	YFCAS	SPSSYEQ	YFGPGTRLTVL	Trbv2-7	7	1
Trav8-1, 8D-1	YFCAT	TFGKGTLLTVTP	TFGKGTLLTVTP	Traj53	12	Trbv4	YLCAS	SPTGGYEQ	YFGPGTRLTVL	Trbv2-7	8	1
Trav13-2, 13D-2	YLCAM	NGGSNYKL	TFGKGTLLTVTP	Traj53	8	Trbv5	YFCAS	SQQGANERL	FFGHGTKLSVL	Trbj1-4	9	1
Trav13D-1, 13-2	YLCAL	EQNAGAKL	TFGGGTRLTVRP	Traj39	8	Trbv20	YLCGA	RDRGAEQ	FFGPGTRLTVL	Trbj2-1	7	1
Trav14-3	YFCAA	NNNAGAKL	TFGGGTRLTVRP	Traj39	8	Trbv3	FCAS	SLDRGREQ	YFGPGTRLTVL	Trbv2-7	8	1
Trav16, 16D/DV11	YFCAM	REGSPGTGSNRL	TFGKGTKFSLIP	Traj28	12	Trbv13-2	GPQDSGNTL	GPQDSGNTL	YFGEGSRLIVV	Trbj1-3	9	1
Trav16, 16D/DV11	YFCAM	REGTGSGGKL	TLGAGTRLQVNL	Traj44	10	Trbv13-2	YFCAS	GDPGQNSGNTL	YFGEGSRLIVV	Trbj1-3	11	1
Trav17	YFCAL	DTNAYKV	IFGKGTHLHVLP	Traj30	7	Trbv5	YFCAS	SQGWGGEYTQ	YFGPGTRLLVL	Trbj2-5	10	1
Trav19	YLCAA	GEAGAKL	TFGGGTRLTVRP	Traj39	7	Trbv13-1	YFCAS	SGTGQNTL	YFGAGTRLSVL	Trbj2-4	8	1
Trav21/DV12	YHCIL	RVGGGSAKL	IFGEGTKLTVSS	Traj57	9	Trbv2	YFCAS	SHRLGSSYEQ	YFGPGTRLTVL	Trbv2-7	10	1
												19

Table 5.15 The analysis of CD4 clones in the pancreas of MUT1 primary recipient mice (P_1). Note that no CD8 cells were identified (Plate CT40)

Trav	Va	N	Ja	Traj	Length, aa	Trbv	Vb	N	Jb	Trbj	Length, aa	Frequency
Trav8-1, 8D-1	YFCAT	DAAGYQNF	YFGKGTSLTVIP	Traj49	8	Trbv1	LYCTC	SARAGNTL	YFGEGSRLIVV	Trbj1-3	8	1
Trav13-2, 13D-2	YFCAI	DLNYNQGKL	IFGQGTKLSIKP	Traj23	9	Trbv20	YLCGA	KRGPSYEQ	YFGPGTRLTVL	Trbv2-7	8	1
												2

Table 5.16 The analysis of CD4 clones in the spleen of MUT1 secondary recipient mice (S_2<S_1, Plate CT48).

Trav	Va	N	Ja	Traj	Length, aa	Trbv	Vb	N	Jb	Trbj	Length, aa	Frequency
Trav3-3 or D-3	YFCAV	RNTGANTGKL	TFGHGTILRVHP	Traj52	10	Trbv5	YFCAS	SLQNTEV	FFGKGTRLTVV	Trbj1-1	7	1
Trav5D-4	YFCAA	SRNYNVL	YFGSGTKLTVEP	Traj21	7	Trbv3	YFCAS	SSTGGQDTQ	YFGPGTRLLVL	Trbj2-5	9	1
Trav5D-4	YFCAA	SRNYNVL	YFGSGTKLTVEP	Traj21	7	Trbv3	YFCAS	SSTGGQDTQ	YFGPGTRLLVL	Trbj2-5	9	1
Trav6-1, 6-2, 6-4, 6D-04, 6-5, 6D-5, 6-6, 6D-6, 6-7/DV9	YYCVL	ATGNTGKL	IFGLGTTLQVQP	Traj37	8	Trbv13-2	YFCAS	GDAGLGDTGQL	YFGEGSKLTVL	Trbj2-2	11	3
Trav6-6 or D-6	YYCAL	ARNNNNAP	RFGAGTKLSVKP	Traj43	8	Trbv19	FLCAS	RTQGNTEV	FFGKGTRLTVV	Trbj1-1	8	2
Trav6D-6	YYCAL	SDSNYQL	IWGSGTKLIIKP	Traj33	7	Trbv13-3	YFCAS	SDLGQGDAETL	YFGSGTRLTVL	Trbj2-3	11	1
Trav7-5 or D-5	YLCAP	LSSNTDKV	VFGTGTRLQVSP	Traj34	8	Trbv13-2	YFCAS	GDRPGRAEV	FFGKGTRLTVV	Trbj1-1	9	2
Trav7-6	YLCAV	KGNMGYKL	TFGTGTSLLVDP	Traj9	8	Trbv19	FLCAS	SIRGLGGVNTGQL	YFGEGSKLTVL	Trbj2-2	13	1
Trav8-2	YFCAT	DNNYAQGL	TFGLGTRVSVFP	Traj26(1)	8	Trbv29	YFCAS	STGDAGQL	YFGEGSKLTVL	Trbj2-2	8	2
Trav9D-3	YFCAV	SAQSNNRI	FFGDGTQLVVKP	Traj31	8	Trbv3	YFCAS	SLRSSYEQ	YFGPGTRLTVL	Trbv2-7	8	1
Trav12D-1, 12-2, 12D-2, 12-3, 12D-3	YYCAL	SENYGNEKI	TFGAGTKLTIKP	Traj48	9	Trbv13-1	YFCAS	TGTLSSYEQ	YFGPGTRLTVL	Trbv2-7	9	1
Trav12D-1, 12-2, 12D-2, 12-3, 12D-3	YYCAL	DSGGSNAKL	TFGKGTKLSVKS	Traj42	9	Trbv13-2	YFCAS	GDASANTEV	FFGKGTRLTVV	Trbj1-1	9	1
Trav12D-1, 12-2, 12D-2, 12-3, 12D-3	YYCAL	SDQGGSAKL	IFGEGTKLTVSS	Traj57	9	Trbv3	YFCAS	SLGLGIQNTL	YFGAGTRLSVL	Trbj2-4	10	2
Trav14-1	YFCAA	PSTGGNNKL	TFGQGTVLSVIP	Traj56	9	Trbv5	YFCAS	SQDRANTGQL	YFGEGSKLTVL	Trbj2-2	10	1
Trav14D-1	YFCAA	SAIYGNEKI	TFGAGTKLTIKP	Traj48	9	Trbv13-1	YFCAS	SEDRVEQ	YFGPGTRLTVL	Trbv2-7	7	1
Trav14D-3/DV8	YFCAA	RMNYNQGKL	IFGQGTKLSIKP	Traj23	9	Trbv31	YLCAW	SLPGGGEQ	YFGPGTRLTVL	Trbv2-7	8	1
Trav21/DV12	YHCIL	RVAMATGGNNKL	TFGQGTVLSVIP	Traj56	12	Trbv13-2	YFCAS	GDGWDWGDTQ	YFGPGTRLLVL	Trbj2-5	10	1
												23

Table 5.17 The analysis of CD4 clones in the pancreas of MUT1 secondary recipient mice (P_2<S_1, Plate CT62, 63).

Trav	Va	N	Ja	Traj	Length, aa	Trbv	Vb	N	Jb	Trbj	Length, aa	Frequency
Trav8-1	YFCAT	DAAGYQNF	YFGKGTSLTVIP	Traj49	8	Trbv1	LYCTC	SARAGNTL	YFGEGSRLIVV	Trbj1-3	8	1
Trav7-2, 7D-2	YLCAA	LSGGN	TFGKGTSLVVHP	Traj6	5	Trbv19	FLCAS	SISGGLSYEQ	YFGPGTRLTVL	Trbv2-7	10	1
												2

Table 5.18 The analysis of CD4 clones in the spleen of MUT1 secondary recipient mice (S_2<P_1, Plate CT60).

Trav	Va	N	Ja	Traj	Length, aa	Trbv	Vb	N	Jb	Trbj	Length, aa	Frequency
Trav4-2	YFCAA	HQGGRAL	IFGTGTTVSVSP	Traj15	7	Trbv20	YLCGA	SDNSAETL	YFGSGTRLTVL	Trbj2-3	8	1
Trav4-3, 4D-3	YFCAA	PSNYNVL	YFGSGTKLTVEP	Traj21	7	Trbv13-3	YFCAS	RAGVAEQ	FFGPGTRLTVL	Trbj2-1	7	1
Trav5-1	YFCSA	SGTGNYKY	VFGAGTRLKVIA	Traj40	8	Trbv13-3	YFCAS	RAGVAEQ	FFGPGTRLTVL	Trbj2-1	7	6
Trav5-1	YFCSA	KYSGTGNY	VFGAGTRLKVIA	Traj40	8	Trbv13-3	YFCAS	RAGVAEQ	FFGPGTRLTVL	Trbj2-1	7	1
Trav6-2	YYCVL	GETGNTGKL	IFGLGTTLQVQP	Traj37	9	Trbv24	YFCAS	SPVRDRNSGNTL	YFGEGSRLIVV	Trbj1-3	12	1
Trav6-2	YYCVL	GETGNTGKL	IFGLGTTLQVQP	Traj37	9	Trbv4(2)	YLCAS	SLQGASDY	TFGSGTRLLVI	Trbj1-2	8	1
Trav7-3, 7D-3	YLCAV	SDNNNAPR	FGAGTKLSVKP	Traj43	8	Trbv13-2	YFCAS	GDAGTGGYEQ	YFGPGTRLTVL	Trbv2-7	10	1
Trav7-3, 7D-3	YLCAV	SDNNNAP	RFGAGTKLSVKP	Traj43	7	Trbv13-2	YFCAS	GDAGTGGYEQ	YFGPGTRLTVL	Trbv2-7	10	2
Trav7-5, 7D-5	YLCAP	LSSNTDKV	VFGTGTRLQVSP	Traj34	8	Trbv13-2	YFCAS	GDRPGRAEV	FFGKGTRLTVV	Trbj1-1	9	2
Trav7D-2	YLCAA	LSGGNYKP	TFGKGTSLVVHP	Traj6	8	Trbv19	FLCAS	SISGGLSYEQ	YFGPGTRLTVL	Trbv2-7	10	1
Trav8-2	YFCAT	DNNYAQGL	TFGLGTRVSVFP	Traj26(1)	8	Trbv29	YFCAS	STGDAGQL	YFGEGSKLTVL	Trbj2-2	8	3
Trav9-1, 9D-3	YFCAV	SAQSNNRI	FFGDGTQLVVKP	Traj31	8	Trbv3	YFCAS	SLRSSYEQ	YFGPGTRLTVL	Trbv2-7	8	1
Trav10, 10D	YFCAA	RRTNAYKV	IFGKGTHLHVLP	Traj30	8	Trbv5	YFCAS	SQGGANTGQL	YFGEGSKLTVL	Trbj2-2	10	1
Trav12D-1, 12-2, 12D-2, 12-3, 12D-3	YYCAL	SDQGGSAKL	IFGEGTKLTVSS	Traj57	9	Trbv3	YFCAS	SLGLGIQNTL	YFGAGTRLSVL	Trbj2-4	10	3
Trav13-1 or 13D-4	YLCAM	HQGGSAKL	IFGEGTKLTVSS	Traj57	8	Trbv13-2	YFCAS	GGPGQGANERL	FFGHGTKRSVL	Trbj1-4	11	4
Trav13-2	YFCAI	NYGSSGNKL	IFGIGTLLSVKP	Traj32	9	Trbv13-2	YFCAS	GAGQSNTEV	FFGKGTRLTVV	Trbj1-1	9	2
Trav13D-1, 13-2	YLCAP	RTGGYKV	VFGSGTRLLVSP	Traj12	7	Trbv19	FLCAS	RTGDYAEQ	FFGPGTRLTVL	Trbj2-1	8	1
Trav14-2	YFCAA	SSGGSNAKL	TFGKGTKLSVKS	Traj42	9	Trbv29	YFCAS	SFANTEV	FFGKGTRLTVV	Trbj1-1	7	1
Trav16, 16D/DV11	YFCAM	REGEGGSAKL	IFGEGTKLTVSS	Traj57	10	Trbv29	YFCAS	SLDSEQ	YFGPGTRLTVL	Trbv2-7	6	1
												34

Table 5.19 The analysis of CD4 clones in the pancreas of MUT1 secondary recipient mice (P_2<P_1, Plate CT63, 64).

Trav	Va	N	Ja	Traj	Length, aa	Trbv	Vb	N	Jb	Trbj	Length, aa	Frequency
Trav5-1	YFCSA	SGTGNYKY	VFGAGTRLKVIA	Traj40	8	Trbv13-3	YFCAS	RAGVAEQ	FFGPGTRLTVL	Trbj2-1	7	2
Trav8-1, 8D-1	YFCAT	DASGGNYKP	TFGKGTSLVVHP	Traj6	9	Trbv4(2)	YLCAS	LRSRDWGNTGQ	YFGEGSKLTVL	Trbj2-2	11	1
Trav8-1, 8D-1	YFCAT	DASGGNYKP	TFGKGTSLVVHP	Traj6	9	Trbv4(2)	YLCAS	RSRDWGNTGQL	YFGEGSKLTVL	Trbj2-2	11	1
												4

Table 5.20 The analysis of CD4 clones in the spleen of original donors of WT2 mice (S_0, Plate CT28).

Trav	Va	N	Ja	Traj	Length, aa	Trbv	Vb	N	Jb	Trbj	Length, aa	Frequency
Trav3-4	YFCAV	SAHYNQGKL	IFGQGTKLSIKP	Traj23	9	Trbv17	YLCAS	SRQGNQDTQ	YFGPGTRLLVL	Trbj2-5	9	1
Trav4-4/DV10	YFCAA	ENQGKL	IFGQGTKLSIKP	Traj23	6	Trbv1	LYCTCS	ADRWGGSAETL	YFGSGTRLTVL	Trbj2-3	11	1
Trav5D-4	YFCAA	RPSGTYQ	RFGTGTKLQVVP	Traj13	7	Trbv19	FLCAS	SIGWGEDTQ	YFGPGTRLLVL	Trbj2-5	9	1
Trav6D-5	YYCAL	RGSSGNKL	IFGIGTLLSVKP	Traj32	8	Trbv5	YFCAS	SQEAGGYEQ	YFGPGTRLTVL	Trbv2-7	9	1
Trav6D-5, 6-6, 6-7/DV9	YFCAL	RGSALGRL	HFGAGTQLIVIP	Traj18	8	Trbv1	LYCTC	SETDLSNERL	FFGHGTKLSVL	Trbj1-4	10	1
Trav6D-5, 6-6, 6-7/DV9	YYCAL	GGNNNAP	RFGAGTKLSVKP	Traj43	7	Trbv20	YLCGA	CRDWGGSNTGQL	YFGEGSKLTVL	Trbj2-2	12	1
Trav6D-5, 6-6, 6-7/DV9	YYCAL	GDRNSAGNKL	TFGIGTRVLVRP	Traj17	10	Trbv3	YFCAS	SLGTGVTGQL	YFGEGSKLTVL	Trbj2-2	10	1
Trav6D-7	YYCAL	SDWAYKV	IFGKGTHLHVLP	Traj30	7	Trbv13-2	YFCAS	GDAGGSQDTQ	YFGPGTRLLVL	Trbj2-5	10	1
Trav7-2, 7D-2	YLCAA	STASLGKL	QFGTGTQVVVTP	Traj24	8	Trbv1	LYCTC	SAEWENTL	YFGAGTRLSVL	Trbj2-4	8	1
Trav7-3, 7D-3	YLCAV	DYNVL	YFGSGTKLTVEP	Traj21	5	Trbv13-1	YFCAS	SVDRGSNERL	FFGHGTKLSVL	Trbj1-4	10	1
Trav7-3, 7D-3	YLCAV	AAGNTGKL	IFGLGTTLQV	Traj37	8	Trbv5	YFCAS	SQDWEQDTQ	YFGPGTRLLVL	Trbj2-5	9	1
Trav7-4, 7D-4	YFCAA	SMSNYNVL	YFGSGTKLTVEP	Traj21	8	Trbv20	YLCGV	SRDSQDTQ	YFGPGTRLLVL	Trbj2-5	8	1
Trav7-5, 7D-5	YLCAA	TSGGNYKP	TFGKGTSLVVHP	Traj6	8	Trbv31	YLCAW	RSGGYAEQ	FFGPGTRLTVL	Trbj2-1	8	1
Trav7D-5	YLCAV	RDSNYQL	IWGSGTKLIIKP	Traj33	7	Trbv1	LYCTC	SADWGGDAETL	YFGSGTRLTVL	Trbj2-3	11	1
Trav8-1, 8D-1	YFCAT	DDTNTGKL	TFGDGTVLTVKP	Traj27	8	Trbv1	LYCTC	SSGLGGQDTQ	YFGPGTRLLVL	Trbj2-5	10	1
Trav8-1, 8D-1	YFCAT	GANTGKL	TFGHGTILRVHP	Traj52	7	Trbv31	YLCAC	FPGQSSYEQ	YFGPGTRLTVL	Trbv2-7	9	1
Trav8-1, 8D-1	YFCAT	FNNNNAP	RFGAGTKLSVKP	Traj43	7	Trbv5	YFCAS	SQEGGQNTL	YFGAGTRLSVL	Trbj2-4	9	1
Trav8-2	YFCAT	DRGTASLGKL	QFGTGTQVVVTP	Traj24	10	Trbv13-2	YFCAS	GDAGGEDTEV	FFGKGTRLTVV	Trbj1-1	10	1
Trav8-2	YFCAT	DDDTNAYKV	IFGKGTHLHVLP	Traj30	9	Trbv31	YLCAW	SLQNSYNSPL	YFAAGTRLTVT	Trbj1-6	10	1
Trav8D-2	YFCAT	YQGGRAL	IFGTGTTVSVSP	Traj15	7	Trbv31	YLCAW	SPGQGRGTL	YFGSGTRLTVL	Trbj2-3	9	1
Trav9D-3	YFCAV	SYNAGAKL	TFGGGTRLTVRP	Traj39	8	Trbv4(2)	YLCAS	SLTGGSAETL	YFGSGTRLTVL	Trbj2-3	10	1
Trav10, 10D	YFCAA	SGTGNYKY	VFGAGTRLKVIA	Traj40	8	Trbv13-2	YFCAS	GVGTGGSPL	YFAAGTRLTVT	Trbj1-6	9	1
Trav10,10D	YFCAA	SNSNNRI	FFGDGTQLVVKP	Traj31	7	Trbv5	YFCAS	SRGTGIDERL	FFGHGTKLSVL	Trbj1-4	10	1
Trav11, 11D	YICVV	GATNTNKV	VFGTGTRLQVLP	Traj34	8	Trbv31	YLCAW	SSGTGGFEQ	YFGPGTRLTVL	Trbv2-7	9	1
Trav12D-1, 12-2, 12D-2, 12-3, 12D-3	YYCAL	ILNTGNYKY	VFGAGTRLKVIA	Traj40	9	Trbv5	YFCAS	SQGQGRAEQ	FFGPGTRLTVL	Trbj2-1	9	1
Trav13-2	YLCAL	DYSAGNKL	TFGIGTRVLVRP	Traj17	8	Trbv13-1	YFCAS	SDADTQ	YFGPGTRLLVL	Trbj2-5	6	1
Trav14-1	YYCAL	AYYAQGL	TFGLGTRVSVFP	Traj26(1)	7	Trbv1	LYCTC	SANSAETL	YFGSGTRLTVL	Trbj2-3	8	1
Trav14-1	YFCAA	SDTGNYKY	VFGAGTRLKVIA	Traj40	8	Trbv26	YLCAS	SLTGGNSAETL	YFGSGTRLTVL	Trbj2-3	11	1
Trav14-3	YFCAA	SRNNNAP	RFGAGTKLSVKP	Traj43	7	Trbv29	YFCAS	SFSGLGSYEQ	YFGPGTRLTVL	Trbv2-7	10	1
Trav14-3	YFCAA	SANTGNYKY	VFGAGTRLKVIA	Traj40	9	Trbv4(2)	YLCAS	SSTGANNQAP	LFGEGTRLSVL	Trbj1-5	10	1
Trav16, 16D/DV11	YFCAM	REGSTGYQNF	YFGKGTSLTVIP	Traj49	10	Trbv15	YLCAS	SLGVGGYEQ	YFGPGTRLTVL	Trbv2-7	9	1
Trav16, 16D/DV11	YFCAM	REGNSGGSNAKL	TFGKGTKLSVKS	Traj42	12	Trbv26	YLCAS	SLGTGPGTGQL	YFGEGSKLTVL	Trbj2-2	11	1
Trav16, 16D/DV11	YFCAM	REGGQGGRAL	IFGTGTTVSVSP	Traj15	10	Trbv5	YFCAS	SQDLSYNYAEQ	FFGPGTRLTVL	Trbj2-1	11	1
Trav21/DV12	YHCIL	NTGYQNF	YFGKGTSLTVIP	Traj49	7	Trbv19	FLCAS	SRTGYNSPL	YFAAGTRLTVT	Trbj1-6	9	1
												34

Table 5.21 The analysis of CD4 clones in the spleen of WT2 primary recipient mice (S_1, Plate CT42).

Trav	Va	N	Ja	Traj	Length, aa	Trbv	Vb	N	Jb	Trbj	Length, aa	Frequency
Trav4-3	YFCAA	ERNTGKL	IFGLGTTLQVQP	Traj37	7	Trbv13-2	YFCAS	GDRGGNSPL	YFAAGTRLTVT	Trbj1-6	9	1
Trav4-3	YFCAA	GSGGSNAKL	TFGKGTKLSVKS	Traj42	8	Trbv19	FLCAS	SIRVEQ	YFGPGTRLTVL	Trbv2-7	6	1
Trav6-3, 6D-3	YYCAM	ITGNTGKL	IFGLGTTLQVQP	Traj37	8	Trbv31	YLCAW	SLGTPNERL	FFGHGTK**R**SVL	Trbj1-4	9	1
Trav6-5, 6D-6, 6D-7	YFCAL	SSNTNKV	VFGTGTRLQVLP	Traj34	7	Trbv1	YCTCS	AETGNYAEQ	FFGPGTRLTVL	Trbj2-1	9	1
Trav8D-2	YFCAT	DNTNTGKL	TFGDGTVLTVKP	Traj27	8	Trbv31	YLCAW	IRDNQDTQ	YFGPGTRLLVL	Trbj2-5	8	2
Trav9-3, 4, 4-D	YFCVL	SANTGGLSGKL	TFGEGTQVTVIS	Traj2	11	Trbv29	YFCAS	SRTGIAETL	YFGSGTRLTVL	Trbj2-3	9	1
Trav10, 10D	YFCAA	SISSNNR	IFFGDGTQLVVKF	Traj31	7	Trbv19	FLCASS	SRDWGVEQ	YFGPGTRLTVL	Trbv2-7	8	1
Trav13-2	YLCAM	ERSYGNEKI	TFGAGTKLTIKP	Traj48	9	Trbv20	YLCGA	RWGHPYEQ	YFGPGTRLTVL	Trbv2-7	8	1
Trav13D-1, 13-2, 13D-2	YLCAL	NYGSSGNKL	IFGIGTLLSVKP	Traj32	9	Trbv5	YFCAS	SQGRGGQDTQ	YFGPGTRLLVL	Trbj2-5	10	1
Trav14-2	YFCAA	KATGGNNKL	TFGQGTVLSVIP	Traj56	9	Trbv20	YLCGA	RGTYEQ	YFGPGTRLTVL	Trbv2-7	6	1
Trav14-2	YFCAA	SRGGSAKL	IFGEGTKLTVSS	Traj57	8	Trbv20	YLCGA	RELGNYAEQ	FFGPGTRLTVL	Trbj2-1	9	1
												12

Table 5.22 The analysis of CD4 clones in the spleen of WT2 secondary recipient mice (S_2, Plate CT58).

Trav	Va	N	Ja	Traj	Length, aa	Trbv	Vb	N	Jb	Trbj	Length, aa	Frequency
Trav5D-4	YFCAA	SERGSALGRL	HFGAGTQLIVIP	Traj18	10	Trbv13-3	YFCAS	SNREGQNTL	YFGAGTRLSVL	Trbj2-4	9	1
Trav6-6, 6D-6	YYCAL	GDTGNYKY	VFGAGTRLKVIA	Traj40	8	Trbv20	YLCGA	RDRAQNTL	YFGAGTRLSVL	Trbj2-4	8	1
Trav6-6, 6D-6	YYCAL	AKRNNNNAP	RFGAGTKLSVKP	Traj43	9	Trbv4(2)	YLCAS	SQDWGANQDTQ	YFGPGTRLLVL	Trbj2-5	11	1
Trav6-7/DV9, 6-7	YYCAR	NSGGSNYKL	TFGKGTLLTVTP	Traj53	9	Trbv20	YLCGA	SRDGNYAEQ	FFGPGTRLTVL	Trbj2-1	9	1
Trav6D-5, 6-6, 6-7/DV9	YYCAL	GETSSGQKL	VFGQGTILKVYL	Traj16	9	Trbv2	YFCAS	SQDSGGTYEQ	YFGPGTRLTVL	Trbv2-7	10	1
Trav6D-6	YYCAL	SENNNAP	RFGAGTKLSVKP	Traj43	7	Trbv4(2)	YLCAS	SLRTPNTGQL	YFGEGSKLTVL	Trbj2-2	10	1
Trav6D-7	YYCAL	AKRNNNNAP	RFGAGTKLSVKP	Traj43	9	Trbv4(2)	YLCAS	SQDWGANQDTQ	YFGPGTRLLVL	Trbj2-5	11	1
Trav7-4, 7D-4	YFCAA	NTNAYKV	IFGKGTHLHVLP	Traj30	7	Trbv13-1	YFCAS	SDFTSAETL	YFGSGTRLTVL	Trbj2-3	9	1
Trav7-4, 7D-4	YFCAA	SEHNAGAKL	TFGGGTRLTVRP	Traj39	9	Trbv13-1	YFCAS	RTGGASQNTL	YFGAGTRLSVL	Trbj2-4	10	1
Trav7D-2	YLCAA	SIIAGGYKV	VFGSGTRLLVSP	Traj12	9	Trbv20	YLCGA	REGGGSDY	TFGSGTRLLVI	Trbj1-2	8	1
Trav9-1, D-1, 2, D-3	YFLIT	GNTGKL	IFGLGTTLQVQP	Traj37	6	Trbv20	YLCGA	RDQGRNAEQ	FFGPGTRLTVL	Trbj2-1	9	1
Trav10, 10D	YFCAA	SKAGTGSNRL	TFGKGTKFSLIP	Traj28	10	Trbv20	YLCGA	REGGGSDY	TFGSGTRLLVI	Trbj1-2	8	1
Trav14-1	YFCAA	YTGGLSGKL	TFGEGTQVTVIS	Traj2	9	Trbv31	YLCAW	SPRDGSAETL	YFGSGTRLTVL	Trbj2-3	10	2
Trav14-3	YFCAA	SSGTGSKL	SFGKGAKLTVSP	Traj58	8	Trbv4(2)	YLCAS	SLRTPNTGQL	YFGEGSKLTVL	Trbj2-2	10	1
Trav16, 16D/DV11	YFCAM	RDDTNAYKV	IFGKGTHLHVLP	Traj30	9	Trbv20	YLCGA	RDQGRNAEQ	FFGPGTRLTVL	Trbj2-1	9	1
												16

Table 5.23 The analysis of CD4 clones in the spleen of original MUT2 donors (S_0, Plate CT34).

Trav	Va	N	Ja	Traj	Length, aa	Trbv	Vb	N	Jb	Trbj	Length, aa	Frequency
Trav4-3 or 4D-3	YFCAA	EANNNAP	RFGAGTKLSVKP	Traj43	7	Trbv29	YFCAS	SLVGQYAEQ	FFGPGTRLTVL	Trbj2-1	9	1
Trav5D-4	YFCAA	STNSGGSNYKI	TFGKGTLLTVTP	Traj53	11	Trbv5	YFCAS	SQARGAGEV	LFGKGTRLTVV	Trbj1-5	9	1
Trav6-2	YYCVL	GYNTNTGKL	TFGDGTVLTVKP	Traj27	9	Trbv2	YFCAS	SLDTGVYNSPL	YFAAGTRLTVT	Trbj1-6	11	1
Trav6-4 or 6D-4	YFCAL	VDRTGYQNF	YFGKGTSLTVIP	Traj49	9	Trbv15	YLCAS	SPGGGTEV	FFGKGTRLTVV	Trbj1-1	8	1
Trav6-6	YYCAL	GDNTGANTGKI	TFGHGTILRVHP	Traj52	11	Trbv31	YLCAW	SLLGVSYEQ	YFGPGTRLTVL	Trbv2-7	9	1
Trav6-7/DV9 or 6D-7	YYCAP	YNTNTGKL	TFGDGTVLTVKP	Traj27	8	Trbv20	YLCGA	GTGSDTQ	YFGPGTRLLVL	Trbj2-5	7	1
Trav6D-5	YYCAL	TYNTNTGKL	TFGDGTVLTVKP	Traj27	9	Trbv29	YFCAS	SIQDNNQAP	LFGEGTRLSVL	Trbj1-5	9	1
Trav7-3, 7D-3	YLCAV	RRNYKY	VFGAGTRLKVIA	Traj40	6	Trbv31	YLCAW	SKTSSQNTL	YFGAGTRLSVL	Trbj2-4	9	1
Trav7D-2	YLCAA	SGAGNTGKL	IFGLGTTLQVQP	Traj37	9	Trbv13-1	YFCAS	SDAGRQDTQ	YFGPGTRLLVL	Trbj2-5	9	1
Trav8-1 or 8D-1	YFCAT	DATNSAGNKL	TFGIGTRVLVRP	Traj17	10	Trbv13-2	YFCAS	GDAGGAEQ	FFGPGTRLTVL	Trbj2-1	8	1
Trav8-1 or 8D-1	YFCAS	NSGGSNYKL	TFGKGTLLTVTP	Traj53	9	Trbv13-2	YFCAS	GDGGDAEQ	FFGPGTRLTVL	Trbj2-1	8	1
Trav8-1 or D-1	YFCAT	QSGSFNKL	TFGAGTRLAVCP		8	Trbv5	YFCAS	SPQGANSD	YTFGSGTRLLVI	Trbj1-2	8	1
Trav9-1, D-1, 2, D-3	YFCAA	SGNEKI	TFGAGTKLTIKP	Traj48	6	Trbv13-1	YFCAS	SDTGGAHETL	YFGSGTRLTVL	Trbj2-3	10	1
Trav9D-2, 3, 4	YFCAV	SNNNNAP	RFGAGTKLSVKP	Traj43	7	Trbv13-2	YFCAS	GDRGEGSDY	TFGSGTRLLVI	Trbj1-2	9	1
Trav9D-2. 3. 4	YFCAV	SLQGGSAKL	IFGEGTKLTVSS	Traj57	9	Trbv31	YLCAW	SLGRGDTQ	YFGPGTRLLVL	Trbj2-5	8	1
Trav11 or 11D	YICVV	GDRGSALGRL	HFGAGTQLIVIP	Traj18	10	Trbv13-2	YFCAS	GDEGQINSD	YTFGSGTRLLVI	Trbj1-2	9	1
Trav12D-1, 2, D-2, 3, D-3	YYCAL	TWTGGYKV	VFGSGTRLLVSP	Traj12	8	Trbv5	YFCAS	SQEGTGGGAETL	YFGSGTRLTVL	Trbj2-3	12	1
Trav13D-1 or 13-2	YLCAP	SSNTNKV	VFGTGTRLQVLP		7	Trbv13-2	YFCAS	GDALGEDTQ	YFGPGTRLLVL	Trbj2-5	9	1
Trav14-3	YFCAA	SDTNAYKV	IFGKGTHLHVLP	Traj30	8	Trbv13-2	YFCAS	GEWYSGNTL	YFGEGSRLIVV	Trbj1-3	9	1
Trav14-3	YFCAA	VNTGNYKY	VFGAGTRLKVIA	Traj40	8	Trbv2	YFCAS	SQDNYEQ	YFGPGTRLTVL	Trbv2-7	7	1
Trav14-3	YFCAA	SVVTGSGGKL	TLGAGTRLQVNL	Traj44	10	Trbv31	YLCAW	SLGLGSEQ	YFGPGTRLTVL	Trbv2-7	8	1
Trav14D-1	YFCAA	SEKSNNRI	FFGDGTQLVVKP	Traj31	8	Trbv1	LYCTC	SADNYEQ	YFGPGTRLTVL	Trbv2-7	7	1
Trav14D-1	YFCAA	SRVYTGNYKY	VFGAGTRLKVIA	Traj40	10	Trbv13-3	YFCAS	SDVGSDY	TFGSGTRLLVI	Trbj1-2	7	1
Trav14D-1	YFCAA	SNYAQGL	TFGLGTRVSVFP	Traj26(1)	7	Trbv31	YLCAW	SNYNNRAP	LFGEGTRLSVL	Trbj1-5	8	1
Trav14D-3/DV8	YFCAA	ASSGSWQL	IFGSGTQLTVMP	Traj22	8	Trbv29	YFCAS	SPGQGRERL	FFGHGTKLSVL	Trbj1-4	9	1
Trav16, 16D/DV11	YFCAM	RNNNNAP	RFGAGTKLSVKP	Traj43	7	Trbv5	YFCAS	SQDLTDQDTQ	YFGPGTRLLVL	Trbj2-5	10	1
												26

Table 5.24 The analysis of CD4 clones in the pancreas of original MUT2 donors (P_0, Plate CT23).

Trav	Va	N	Ja	Traj	Length, aa	Trbv	Vb	N	Jb	Trbj	Length, aa	Frequency
Trav4-3/Trav4D-3	YFCAA	EVTGNTGKL	IFGLGTTLQVQP	Traj37	9	Trbv13-2	YFCAS	GDRGQNTL	YFGAGTRLSVL	Trbj2-4	8	1
Trav5D-4	YFCAA	SNTGYQNF	YFGKGTSLTVIP	Traj49	8	Trbv15	YLCAS	SFGLYAEQ	FFGPGTRLTVL	Trbj2-1	8	1
Trav5D-4	YFCAA	NSNNRI	FFGDGTQLVVKP	Traj31	6	Trbv20	YLCGA	RDRGNQDTQ	YFGPGTRLLVL	Trbj2-5	9	1
Trav5D-4	YFCAA	SLTGNTGKL	IFGLGTTLQVQP	Traj37	9	Trbv5	YFCAS	SLLGGRYAEQ	FFGPGTRLTVL	Trbj2-1	10	1
Trav6-2	YYCVL	GYTGNYKY	VFGAGTRLKVIA	Traj40	8	Trbv2	YFCAS	SQDWGSQNTL	YFGAGTRLSVL	Trbj2-4	10	1
Trav6-4/Trav6D-4	YFCAL	VDQGGRAL	IFGTGTTVSVSP	Traj15	8	Trbv1	LYCTC	SADRVVSSYEQ	YFGPGTRLTVL	Trbj2-7	11	1
Trav6-4/Trav6D-4	YFCAL	VETGNTRKL	IFGLGTTLQVQP	Traj37	9	Trbv3	YFCAS	SLVGWEDTQ	YFGPGTRLLVL	Trbj2-5	9	1
Trav6-6/Trav6-7/DV9	YYCAL	GEGYAQGL	TFGLGTRVSVFP	Traj26	8	Trbv29	YFCAS	TGTGKDTQ	YFGPGTRLLVL	Trbj2-5	8	1
Trav6D-6	YYCAL	ASSTGGNNKL	TFGQGTVLSVIP	Traj56	10	Trbv14	YLCAS	SQVQAWNSPL	YFAAGTRLTVT	Trbj1-6	10	1
Trav6D-7	YYCAL	SDLRGSNAKL	TFGKGTKLSVKS	Traj42	10	Trbv29	YFCAS	SLSTGSQNTL	YFGAGTRLSVL	Trbj2-4	10	1
Trav7-1	YFCAV	GTNTGKL	TFGDGTVLTVKP	Traj27	7	Trbv13-1	YFCAS	SAWGLQDTQ	YFGPGTRLLVL	Trbj2-5	9	1
Trav7-4/7D-4	YFCAA	YNTNTGKL	TFGDGTVLTVKP	Traj27	8	Trbv13-1	YFCAS	SEGLGASQNTL	YFGAGTRLSVL	Trbj2-4	11	1
Trav8-1/Trav8D-1	YFCAT	DAGGSNAKL	TFGKGTKLSVKS	Traj42	9	Trbv14	YLCAS	SLSGGVNTL	YFGAGTRLSVL	Trbj2-4	9	1
Trav9-1/Trav9D-3	YFCAV	SLNNYAQGL	TFGLGTRVSVFP	Traj26	9	Trbv19	FLCAS	SIPGGYAEQ	FFGPGTRLTVL	Trbj2-1	9	1
Trav9D-4	YFCAL	SGNMGYKL	TFGTGTSLLVDP	Traj9	8	Trbv26	YLCAS	SLQGGEV	FFGKGTRLTVV	Trbj1-1	7	1
Trav11/Trav11-D	YICVV	GDRGSALGRL	HFGAGTQLIVIP	Traj18	10	Trbv1	LYCTC	SADWGANYAEQ	FFGPGTRLTVL	Trbj2-1	11	1
Trav12D-1	YYCAL	SEGTGGYKV	VFGSGTRLLVSP	Traj12	9	Trbv2	YFCAS	SQDRGQGYEQ	YFGPGTRLTVL	Trbj2-7	10	1
Trav12D-1/Trav12-2/Trav12D-2/Trav12-3/Trav12D-3	YYCAL	ALVISNTNKV	VFGTGTRLQVLP	Traj34	10	Trbv13-1	YFCAS	SAASNTEV	FFGKGTRLTVV	Trbj1-1	8	1
Trav13-2	YLCAI	SNTDKV	VFGTGTRLQVSP	Traj34	6	Trbv13-1	YFCAS	SAQGADQDTQ	YFGPGTRLLVL	Trbj2-5	10	1
Trav13-2	YLCAI	LNSGGSNAKL	TFGKGTKLSVKS	Traj42	10	Trbv3	YFCAS	SPDSNYAEQ	FFGPGTRLTVL	Trbj2-1	9	1
Trav13D-4	YLCAM	ANTGYQNF	YFGKGTSLTVIP	Traj49	8	Trbv14	YLCAS	SLGGNTGQL	YFGEGSKLTVL	Trbj2-2	9	1
Trav14-1	YFCAA	SLPGTGSNRL	TFGKGTKFSLIP	Traj28	10	Trbv13-2	YFCAS	GGGTGGSQNTL	YFGAGTRLSVL	Trbj2-4	11	1
Trav14-1	YFCAA	SRGQGGSAKL	IFGEGTKLTVSS	Traj57	10	Trbv2	YFCAS	SQVPNTGQL	YFGEGSKLTVL	Trbj2-2	9	1
Trav14-3	YFCAA	RDMQQGTGSK	SFGKGAKLTVSP	Traj58	11	Trbv13-1	YFCAS	SDGQSSYEQ	YFGPGTRLTVL	Trbj2-7	9	1
Trav14-3	YFCAA	SAGSGYNKL	TFGKGTVLLVSP	Traj11	9	Trbv20	YLCGA	RDSAETL	YFGSGTRLTVL	Trbj2-3	7	1
Trav14-3	YFCAA	KSAGNTRKL	IFGLGTTLQVQP	Traj37		Trbv29	YFCAS	SLYRGQDTQ	YFGPGTRLLVL	Trbj2-5	9	1
Trav14-3	YFCAA	SKPGYQNF	YFGKGTSLTVIP	Traj49	8	Trbv3	YFCAS	SLGQYAEQ	FFGPGTRLTVL	Trbj2-1	8	1
Trav19	YLCAA	SANTGANTGK	TFGHGTILRVHP	Traj52	12	Trbv5	YFCAS	SLDWGQNTL	YFGAGTRLSVL	Trbj2-4	9	1
Trav3-1	YFCAA	NTGANTGKL	TFGHGTILRVHP	Traj52	9	Trbv12-1	YFCAS	SPLQGRVQKRM	YFGSGTRLTVL	Trbj2-3	11	1

29

Table 5.25 The analysis of CD4 clones in the spleen of MUT2 secondary recipient mice (S_2<S_1, Plate CT44).

Trav	Va	N	Ja	Traj	Length, aa	Trbv	Vb	N	Jb	Trbj	Length, aa	Frequency
Trav4-3 or 4D-3	YFCAA	ENYAQGL	TFGLGTRVSVFP	Traj26	7	Trbv3	YFCAS	SLQGRAEQ	FFGPGTRLTVL	Trbj2-1	8	1
Trav4-3 or 4D-3	YFCAA	ENYAQGL	TFGLGTRVSVFP	Traj26	7	Trbv5	YFCAS	SQDRGQDTEV	FFGKGTRLTVV	Trbj1-1	10	1
Trav6D-7, 6-5	YFCAL	SKGHKCLP-HPEPRTCCA				Trbv5	YFCAS	SQDRGQDTEV	FFGKGTRLTVV	Trbj1-1	10	17
Trav9-1, Trav9D-3	YFCAV	SAHSNNRI	FFGDGTQLVVKP	Traj31	8	Trbv26	YLCAS	SPGTAEQ	YFGPGTRLTVL	Trbv2-7	7	1
												20

Table 5.26 The analysis of CD4 clones in the spleen of MUT2 secondary recipient mice (S_2<P_1, Plate CT46).

Trav	Va	N	Ja	Traj	Length, aa	Trbv	Vb	N	Jb	Trbj	Length, aa	Frequency
Trav4-3 or 4D-3	YFCAA	ENYAQGL	TFGLGTRVSVFP	Traj26(1)	7	Trbv5	YFCAS	SQDRGQDTDV	FFGKGTRLTVV	Trbj1-1	10	10
Trav6D-7, 6-5	YFCAL	SKGHKCLP-HPEPRTCCA				Trbv5	YFCAS	SQDRGQDTEV	FFGKGTRLTVV	Trbj1-1	10	13
												23

Table 5.27 The analysis of CD8 clones in the spleen of original WT1 donor mice (S_0, Plate CT33).

Trav	Va	N	Ja	Traj	Length, aa	Trbv	Vb	N	Jb	Trbj	Length, aa	Frequency
Trav5-1	YFCSA	TSGGNYKP	TFGKGTSLVVHP	Traj6	8	Trbv13-1	YFCAS	SDADWGQDTQ	YFGPGTRLLVL	Trbj2-5	10	1
Trav6-1	YFCAL	VDYANKM	IFGLGTILRVRP	Traj47	7	Trbv19	FLCAS	SRQGSNSDY	TFGSGTRLLVI	Trbj1-2	9	1
Trav6-5	YYCAL	SDLNYNQGKL	IFGQGTKLSIKP	Traj23	10	Trbv2	YFCAS	SQELWGQDTQ	YFGPGTRLLVL	Trbj2-5	10	1
Trav6-6	YYCAL	GDSVGDNSKL	IWGLGTSLVVNP	Traj38	10	Trbv20	YLCGA	RGTLNSPL	YFAAGTRLTVT	Trbj1-6	8	1
Trav6-7/DV9	YYCAL	GDTNAYKV	IFGKGTHLHVLP	Traj30	8	Trbv14	YLCAS	SYRGNTEV	FFGKGTRLTVV	Trbj1-1	8	1
Trav6D-5, 6,6-7/DV9	YYCAL	GDKDTNAYKV	IFGKGTHLHVLP	Traj30	10	Trbv1	YCTCS	GDRGNTQ	YFGPGTRLLVL	Trbj2-5	7	1
Trav6D-5, 6,6-7/DV9	YYCAL	GEPSGSWQL	IFGSGTQLTVMP	Traj22	9	Trbv5	YFCAS	SQEGGPGQNTL	YFGAGTRLSVL	Trbj2-4	11	1
Trav6D-7	YYCAL	SDRDYANKM	IFGLGTILRVRP	Traj47	9	Trbv19	FLCAS	SISSSGNTL	YFGEGSRLIVV	Trbj1-3	9	1
Trav7-3, 7D-3	YLCAV	SNGNAYKV	IFGKGTHLHVLP	Traj30	8	Trbv14	YLCAS	SPTEVV	FFGKGTRLTV	Trbj1-1	6	1
Trav7-3, 7D-3	YLCAV	NNAGAKL	TFGGGTRLTVRP	Traj39	7	Trbv29	YFCAS	SLQGNYAEQ	FFGPGTRLTVL	Trbj2-1	9	1
Trav7D-2	YLCAA	STGNTGKL	IFGLGTTLQVQP	Traj37	8	Trbv13-3	YFCAS	SQGFTEV	FFGKGTRLTVV	Trbj1-1	7	1
Trav9?	YFCVL	SASSGSWQL	IFGSGTQLTVMP	Traj22	9	Trbv29	YFCAS	RTGAQDTQ	YFGPGTRLLVL	Trbj2-5	8	1
Trav9-1	YFCAV	SVTSGSWQL	IFGSGTQLTVMP	Traj22	9	Trbv23	YLCSS	SQYSEWGGNYAE(	FFGPGTRLTVL	Trbj2-1	13	1
Trav9-1	YFCAV	SADMGYKL	**TFGTGTSLLVDP**	Traj9	8	Trbv13-2	YFCAS	GDGTEV	FFGKGTRLTVV	Trbj1-1	6	1
Trav9-1	YFCAV	SAASSGQKL	VFGQGTILKVYL	Traj16	9		YFCAS	RLRDWGGYAEQ	FFGPGTRLTVL	Trbj2-1	11	1
Trav9D-4	YFCVL	SANTGKL	TFGDGTVLTVKP	Traj27	7	Trbv13-2	YFCAS	GDRVEDTQ	YFGPGTRLLVL	Trbj2-5	8	1
TRAC12D-1, 2, D-2, 3, D-3	YYCAL	LSSGSWQL	IFGSGTQLTVMP	Traj22	8	Trbv19	FLCAS	SNWGNTL	YFGAGTRLSVL	Trbj2-4	7	1
Trav12D-1, 2, D-2, 3, D-3	YYCAL	DYANKM	IFGLGTILRVRP	Traj37	6	Trbv2	YFCAS	SQQGSGNTL	YFGEGSRLIVV	Trbj1-3	9	1
Trav12D-1, 2, D-2, 3, D-3	YYCAL	SDSNYQL	IWGSGTKLIIKP	Traj33	7	Trbv29	YFCAS	SLTDQAP	LFGEGTRLSVL	Trbj1-5	7	1
Trav13-1, D-4	YLCAM	DSGTYQ	RFGTGTKLQVVP	Traj13	6	Trbv3	YFCAS	SPNQDTQ	YFGPGTRLLVL	Trbj2-5	7	1
Trav13D-1	YLCAL	EGASSSFSKL	VFGQGTSLSVVP	Traj50	10	Trbv13-3	YFCAS	SGDNYEQ	YFGPGTRLTVL	Trbv2-7	7	1
Trav13D-1	YLCAL	EVPGYQNF	YFGKGTSLTVIP	Traj49	8	Trbv19	FLCAS	SMGGEQ	YFGPGTRLTVL	Trbv2-7	6	1
Trav13D-1, 13-2	YFCAT	YTNTGKL	TFGDGTVLTVKP	Traj27	7	Trbv29	YFCAS	SQGARDTQ	YFGPGTRLLVL	Trbj2-5	8	1
Trav14-1	YFCAA	SRAYQ	RFGTGTKLQVVP	Traj13	5	Trbv29	YFCAS	SSTTSAETL	YFGSGTRLTVL	Trbj2-3	9	1
Trav14-1	YFCAA	RPSSSFSKL	VFGQGTSLSVVP	Traj50	9	Trbv5	YFCAS	SQGVYEQ	YFGPGTRLTVL	Trbv2-7	7	1
Trav15D-1/DV6D-1	YFCAL	WELNSNNRI	FFGDGTQLVVKP	Traj31	9	Trbv31	YLCAW	SRLGGRGAETL	YFGSGTRLTVL	Trbj2-3	11	1
Trav16, 16D/DV11	YFCAN	NNNAP	RFGAGTKLSVKP	Traj43	5	Trbv17	YLCAS	SRVWGGYEQ	YFGPGTRLTVL	Trbv2-7	9	1
Trav16, 16D/DV11	YFCAM	REGTSGGNYKP	TFGKGTSLVV	Traj6	11	Trbv13-3	YFCAS	SGDNYEQ	YFGPGTRLTL	Trbj2-5	7	1
Trav17	YFCAL	EEQGTGSKL	SFGKGAKLTVSP	Traj58	9	Trbv14	YLCAS	SFRGAETL	YFGSGTRLTVL	Trbj2-3	8	1
												29

Table 5.28 The analysis of CD8 clones in the spleen of WT1 primary recipient mice (S_1, Plate CT43).

Trav	Va	N	Ja	Traj	Length, aa	Trbv	Vb	N	Jb	Trbj	Length, aa	Frequency
Trav9-3, Trav9-4, D-4 Trav12D-1, Trav12-2	YFCAV	DTNAYKV	IFGKGTHLHVLP	Traj30	7	Trbv3	YFCAS	SLVWGAHEQ	YFGPGTRLTVL	Trbv2-7	9	1
Trav12D-2, Trav12-3, Trav12D-3	YYCAL	SDFLLLQQAG	KHPEPRTCCVPV		10	Trbv17	YLCAS	GGYEQ	YFGPGTRLTVL	Trbv2-7	5	1
												2

Table 5.29 The analysis of CD8 clones in the spleen of WT1 secondary recipient mice (S_2, Plate CT61).

Trav	Va	N	Ja	Traj	Length, aa	Trbv	Vb	N	Jb	Trbj	Length, aa	Frequency
Trav3-1	YFCAV	GNSGGSNAKL	TFGKGTKLSVKS	Traj42	10	Trbv13-3	YFCAS	RDRDTQ	YFGPGTRLLVL	Trbj2-5	6	9
Trav3-1	YFCAV	GNSGGSNAKL	TFGKGTKLSVKS	Traj42	10	Trbv13-2	YFCAS	GEGGANTGQL	YFGEGSKLTVL	Trbj2-2	10	1
Trav7D-5	HLCAV	ETNAYKV	IFGKGTHLHVLP	Traj30	7	Trbv16	YLCAS	SSWGGNQDTQ	YFGPGTRLLVL	Trbj2-5	10	1
Trav10, 10D	YFCAA	SMSNNRI	FFGDGTQLVVKP	Traj31	7	Trbv31	DLCAW	SPQTNTDV	FFGKGTRLTTV	Trbj1-1	8	1
Trav10, 10D	YFCAA	SRGNNNAP	RFGAGTKLSVKP	Traj43	8	Trbv1	LYCTC	SAHRGQNTL	YFGAGTRLSVL	Trbj2-4	9	1
Trav10, 10D	YFCAA	SNMGYKL	TFGTGTSLLVDP	Traj9	7	Trbv3	YFCAS	SPQGQDTQ	YFGPGTRLLVL	Trbj2-5	8	2
Trav14D-3/DV8	YFCAA	SGSGSWQL	IFGSGTQLTVMP	Traj22	8	Trbv13-1	YFCAS	SDEQGD	YTFGSGTRLLVI	Trbj1-2	6	1
Trav14D-3/DV8	YFCAA	SGSGSWQL	IFGSGTQLTVMP	Traj22	8	Trbv13-1	YFCAS	SDEQGD	YTFGSGTRLLVI	Trbj1-2	6	1
Trav16, Trav16D/DV11	YFCAM	REGRTGNYKY	VFGAGTRLKVIA	Traj40	10	Trbv13-2	YFCAS	GGTGGAETL	YFGSGTRLTVL	Trbj2-3	9	1
												18

Table 5.30 The analysis of CD8 clones in the spleen of original MUT1 donor mice (S_0, Plate CT39).

Trav	Va	N	Ja	Traj	Length, aa	Trbv	Vb	N	Jb	Trbj	Length, aa	Frequency
Trav3-1	YFCAV	SHSNNRI	FFGDGTQLVVKP	Traj31	7	Trbv29	YFCAS	SSGTNYAEQ	FFGPGTRLTVL	Trbj2-1	9	1
Trav3-3, 3D-3	YFCAV	SVDSNYQL	IWGSGTKLIIKP	Traj33	8	Trbv13-3	YFCAS	SNRGPGAEQ	FFGPGTRLTVL	Trbj2-1	9	1
Trav3-3, 3D-3	YFCAV	SDTGGADRL	TFGKGTQLII		9	Trbv5	YFCAS	SQGTENTEV	FFGKGTRLTVV	Trbj1-1	9	1
Trav5D-4	YFCAA	SGANTGKL	TFGHGTILRVHP	Traj52	8	Trbv31	YLCAW	SLGGRQNTL	YFGAGTRLSVL	Trbj2-4	9	1
Trav6-4 6D-4	YFCAL	DNNNRI	FFGDGTQLVVKP	Traj31	6	Trbv14	YLCAS	SFSGVQNTL	YFGAGTRLSVL	Trbj2-4	9	1
Trav6-4 6D-4	YYCVL	GWDYSNNRL	TLGKGTQVVVLP	Traj7	9	Trbv29	YFCAS	SPGHNSD	YTFGSGTRLLV	Trbj1-2	7	1
Trav6-4, 6D-4	YFCAL	VANNYAQGL	TFGLGTRVSVFP	Traj26(1)	9	Trbv13-2, 13-	YFCAS	GDWDNSGNTL	YFGEGSRLIVV	Trbj1-3	10	1
Trav6-5, 6-6, 6D-7	YFCAL	SENSNNRI	FFGDGTQLVVKP	Traj31	8	Trbv1	LYCTC	SAAGGDAEQ	FFGPGTRLTVL	Trbj2-1	9	1
Trav6D-5, 6-6, 6-7/DV9	YYCAL	GFNYAQGL	TFGLGTRVSVFP	Traj26(1)	8	Trbv2	YFCAS	SQDYEQ	YFGPGTRLTVL	Trbv2-7	6	1
Trav7-3, D-3	YLCAA	NSGTYQ	RFGTGTKLQVVP	Traj13	6	Trbv1	LYCTC	SADSTGGYAEQ	FFGPGTRLTVL	Trbj2-1	11	1
Trav7-3,7D-3	YLCAK	ASSGSWQL	IFGSGTQLTVMP	Traj22	8	Trbv1	LYCTC	SAGGGVNQDTQ	YFGPGTRLLVL	Trbj2-5	11	1
Trav7-3,7D-3	YLCAV	SNYGNEKI	TFGAGTKLTIKP	Traj48	8	Trbv19	FLCAS	SIGDTNSGNTL	YFGEGSRLIVV	Trbj1-3	11	1
Trav7-4, D-4	YFCAA	RNYAQGL	TFGLGTRVSVFP	Traj26(1)	7	Trbv1	LYCTC	SADDRNSDY	TFGSGTRLLVI	Trbj1-2	9	1
Trav7-4, D-4	YFCAA	STEGADRL	TFGKGTQLIIQP	Traj45	8	Trbv13-2	YFCAS	GDDNERL	FFGHGTKLSVL	Trbj1-4	7	1
Trav7-4, D-4	YFCAA	SDEGYQNF	YFGKGTSLTVIP	Traj49	8	Trbv19	FLCAS	SIGQQAP	LFGEGTRLSVL	Trbj1-5	7	1
Trav7D-5	YLCAV	STASLGKL	QFGTGTQVVVTP	Traj24	8	Trbv13-2	YFCAS	GDWGDNQDTQ	YFGPGTRLLVL	Trbj2-5	10	1
Trav8D-2	YFCAT	EGSNAKL	TFGKGTKLSVKS	Traj42	7	Trbv31	YLCAW	TGPSAETL	YFGSGTRLTVL	Trbj2-3	8	1
Trav9D-4	YFCAL	SPHMGYKL	TFGTGTSLLVDP	Traj9	8	Trbv3	YFCAS	SLELGASQNTL	YFGAGTRLSVL	Trbj2-4	11	1
Trav10,10D	YFCAA	SEDNNRI	FFGDGTQLVVKP	Traj31	7	Trbv13-1	YFCAS	SDAGIEQ	YFGPGTRLTVL	Trbv2-7	7	1
Trav10,10D	YFCAA	SNTGYQNF	YFGKGTSLTVIP	Traj49	8	Trbv19	**FLCAS**	SIANQDTQ	YFGPGTRLLVL	Trbj2-5	8	1
Trav11, 11D	YICVV	GAAGNTGKL	IFGLGTTLQVQP	Traj37	9	Trbv13-2	YFCAS	DTGQL	YFGEGSKLTVL	Trbj2-2	5	1
Trav12D-1, 12-2, 12D-2, 12-3, 12D-3	YYCAL	SDSAYKV	IFGKGTHLHVLP	Traj30	7	Trbv5	YFCAS	SQGGSGNTL	YFGEGSRLIVV	Trbj1-3	9	2
Trav14-1	YFCAA	DYANKM	IFGLGTILRVRP	Traj47	6	Trbv12-2	YFCAS	SLGLGGRAAETL	YFGSGTRLTVL	Trbj2-3	12	1
Trav16,16D/DV11	YFCAM	RERDTGYQNF	YFGKGTSLTVIP	Traj49	10	Trbv13-1	YFCAS	SVRTGYEQ	YFGPGTRLTVL	Trbv2-7	8	1
Trav16,16D/DV11	YFCAM	RGPTASLGKL	QFGTGTQVVVTP	Traj24	10	Trbv13-3	YFCAS	SDPGISNERL	FFGHGTKLSVL	Trbj1-4	10	1
Trav17	YFCAL	EGNYAQGL	TFGLGTRVSVFP	Traj26(1)	8	Trbv31	YLCAW	SPGGSYEQ	YFGPGTRLTVL	Trbv2-7	8	1
Trav18	YFCAR	DTGANTGKL	TFGHGTILRVHP	Traj52	9	Trbv13-1	YFCAS	SDLGFNQDTQ	YFGPGTRLLVL	Trbj2-5	10	1
Trav19	YLCAA	GQGGSAKL	IFGEGTKLTVSS	Traj57	8	Trbv19	FLCAS	SIGGARERL	FFGHGTKLSVL	Trbj1-4	9	1
Trav21/DV12	YHCIL	RVGGSGGSNYKL	TFGKGTLLTVTP	Traj53	12	Trbv13-3	YFCAS	SERRKNTL	YFGAGTRLSVL	Trbj2-4	8	1
												30

Table 5.31 The analysis of CD8 clones in the pancreas of original MUT1 donor mice (P_0, Plate CT25).

Trav	Va	N	Ja	Traj	Length, aa	Trbv	Vb	N	Jb	Trbj	Length, aa	Frequency
Trav6-4, 6D-4	YFCAL	VDSNYQL	IWGSGTKLIIKP	Traj33	7	Trbv13-2	YFCAS	GGNSSYEQ	YFGPGTRLTVL	Trbv2-7	8	1
Trav6-6, 6D-6, 6D-7	YYCAL	GNTGYQNF	YFGKGTSLTVIP	Traj49	8	Trbv17	YLCAS	SHWGRSAETL	YFGSGTRLTVL	Trbj2-3	10	1
Trav7-3, 7D-3	YLCAV	RAMGYKL	TFGTGTSLLVDP	Traj9	7	Trbv1	LYCTC	SADNSGNTL	YFGEGSRLIVV	Trbj1-3	9	1
Trav7-6	YLCAV	RRNSNNRL	FFGDGTQLAVKP		8	Trbv1	LYCTC	RDISYEQ	YFGPGTRLTVL	Trbv2-7	7	1
Trav9-1, 9D-3	YFCAV	ISSGSWQL	IFGSGTQLTVMP	Traj22	8	Trbv13-1	YFCAS	SDASSGNTL	YFGEGSRLIVV	Trbj1-3	9	1
Trav9D-2, 9-4	YFCAV	SIEGTGSKL	SFGKGAKLTVSP	Traj58	9	Trbv13-3	YFCAS	SDLGGQNTL	YFGAGTRLSVL	Trbj2-4	9	1
Trav12D-1, 12-2, 12D-2, 12-3, 12D-3	YYCAL	MGNYQL	IWGSGTKLIIKP	Traj33	6	Trbv12-2	YFCAS	SPTGEDTQ	YFGPGTRLLVL	Trbj2-5	8	1
Trav12D-1, 12-2, 12D-2, 12-3, 12D-3	YYCAL	SDTEGADRL	TFGKGTQLIIQP	Traj45	9	Trbv15	YLCAS	RPGHANSDY	TFGSGTRLLVI	Trbj1-2	9	1
Trav12D-1, 12-2, 12D-2, 12-3, 12D-3	YYCAL	SDSAYKV	IFGKGTHLHVLP	Traj30	7	Trbv5	YFCAS	SQGGSGNTL	YFGEGSRLIVV	Trbj1-3	9	1
Trav13-1, 13-4/DV7, 13D-4	YLCAM	EQDRGSALGRL	HFGAGTQLIVIP	Traj18	11	Trbv29	YFCAS	SLGAGTGQL	YFGEGSKLTVL	Trbj2-2	9	1
Trav13-2	YFCAI	DTEGADRL	TFGKGTQLIIQP	Traj45	8	Trbv13-3	YFCAS	SQGFTEV	FFGKGTRLTVV	Trbj1-1	7	1
Trav14-1	YFCAA	S-YRKLQIR	LWSRYQTEGYST		9	Trbv19	FLCAS	SIGTPNERL	FFGHGTKLSVL	Trbj1-4	9	1
Trav14-1, 14-2, 14D-2	YFCAA	HNYAQGL	TFGVGTRVLVFP		7	Trbv19	FLCAS	SLTASGNTL	YFGEGSRLIVV	Trbj1-3	9	1
Trav16, 16D/DV11	YFCAM	RDTNAYKV	IFGKGTHLHVLP	Traj30	8	Trbv31	YLCAW	SRDRDNSPL	YFAAGTRLTVT	Trbj1-6	9	1
Trav21/DV12	YHCIL	RGRLCKCAD	IWIWHKSHSM		9	Trbv13-3	YFCAS	SLGRGGYAEQ	FFGPGTRLTVL	Trbj2-1	10	1
Trav21/DV12	YHCIP	PNYGNEKI	TFGAGTKLTIKP	Traj48	8	Trbv3	YFCAS	SLRTGNTGQL	YFGEGSKLTVL	Trbj2-2	10	1
Trav6-4, 6D-4	YFCAL	VDSNYQL	IWGSGTKLIIKP	Traj33	7	Trbv13-2	YFCAS	GGNSSYEQ	YFGPGTRLTVL	Trbv2-7	8	1
Trav6-6, 6D-6, 6D-7	YYCAL	GNTGYQNF	YFGKGTSLTVIP	Traj49	8	Trbv17	YLCAS	SHWGRSAETL	YFGSGTRLTVL	Trbj2-3	10	1
Trav7-3, 7D-3	YLCAV	RAMGYKL	TFGTGTSLLVDP	Traj9	7	Trbv1	LYCTC	SADNSGNTL	YFGEGSRLIVV	Trbj1-3	9	1
Trav7-6	YLCAV	RRNSNNRL	FFGDGTQLAVKP		8	Trbv1	LYCTC	RDISYEQ	YFGPGTRLTVL	Trbv2-7	7	1
Trav9-1, 9D-3	YFCAV	ISSGSWQL	IFGSGTQLTVMP	Traj22	8	Trbv13-1	YFCAS	SDASSGNTL	YFGEGSRLIVV	Trbj1-3	9	1
Trav9D-2, 9-4	YFCAV	SIEGTGSKL	SFGKGAKLTVSP	Traj58	9	Trbv13-3	YFCAS	SDLGGQNTL	YFGAGTRLSVL	Trbj2-4	9	1
												22

Table 5.32 The analysis of CD8 clones in the spleen of MUT1 secondary recipient mice (S_2<S_1, Plate CT49).

Trav	Va	N	Ja	Traj	Length, aa	Trbv	Vb	N	Jb	Trbj	Length, aa	Frequency
Trav3-4	YFCAV	SGPGYQNF	YFGKGTSLTVIP	Traj49	8	Trbv17	YLCAS	RTGGGTQ	YFGPGTRLLVL	Trbj2-5	7	1
Trav6-4, 6D-4	YFCAL	VDSNYQL	IWGSGTKLIIKP	Traj33	7	Trbv13-2	YFCAS	GGNSSYEQ	YFGPGTRLTVL	Trbv2-7	8	2
Trav7-1	YFCAV	SSSGSWQL	IFGSGTQLTVMP	Traj22	8	Trbv1	LYCTC	SADREGHEQ	YFGPGTRLTVL	Trbv2-7	9	1
Trav7-3, 7D-3	YLCAV	NTGANTGKL	TFGHGTILRVHP	Traj52	9	Trbv1	LYCTC	SADREGHEQ	YFGPGTRLTVL	Trbv2-7	9	14
Trav7-4., 7D-4	YFCAA	SDANKM	IFGLGTILRVRP	Traj47	6	Trbv19	FLCAS	RKLGNQDTQ	YFGPGTRLLVL	Trbj2-5	9	8
Trav8-1 or 8D-1	YFCAT	ANSGGSNAKL	TFGKGTKLSVKS	Traj42	10	Trbv14	YLCAS	SLGSGIQDTQ	YFGPGTRLLVL	Trbj2-5	10	2
Trav8-2	YFCAT	DNNYAQGL	TFGLGTRVSVFP	Traj26(1)	8	Trbv29	YFCAS	STGDAGQL	YFGEGSKLTVL	Trbj2-2	8	8
Trav8-2	YFCAT	DNNYAQGL	TFGLGTRV**C**VFP	Traj26	8	Trbv5	YFCAS	SQDRANTGQL	YFGEGSKLTVL	Trbj2-2	10	1
Trav14-1	YFCAA	SSNTDKV	VFGTGTRLQVSP	Traj34	7	Trbv19	FLCAS	CIAGGSGNTL	YFGEGSRLIVV	Trbj1-3	10	1
												38

Table 5.33 The analysis of CD8 clones in the pancreas of MUT1 secondary recipient mice (P_2<S_1, Plate CT51).

Trav	Va	N	Ja	Traj	Length, aa	Trbv	Vb	N	Jb	Trbj	Length, aa	Frequency
Trav2	YYCIV	TVNTEGADRL	TFGKGTQLIIQP	Traj45	10	Trbv13-1	YFCAS	SDPFSNERL	FFGHGTKRSVL		9	1
Trav7-1	YFCAV	RVGDNSKL	IWGLGTSLVVNP	Traj38	8	Trbv1	LYCTC	SADRGGNTL	YFGEGSRLIVV	Trbj1-3	9	4
Trav7-3, 7D-3	YLCAV	IDYANKM	IFGLGTILRVRP	Traj47	7	Trbv13-1	YFCAS	TGQNYAEQ	FFGPGTRLTVL	Trbj2-1	8	25
Trav7-3, 7D-3	YLCAV	NTGANTGKL	TFGHGTILRVHP	Traj52	9	Trbv1	LYCTC	SADREGHEQ	YFGPGTRLTVL	Trbv2-7	9	21
												51

Table 5.34 The analysis of CD8 clones in the spleen of MUT1 secondary recipient mice (S_2<P_1).

Trav	Va	N	Ja	Traj	Length, aa	Trbv	Vb	N	Jb	Trbj	Length, aa	Frequency
Trav6-4, 6D-4	YFCAL	VDSNYQL	IWGSGTKLIIKP	Traj33	7	Trbv13-2	YFCAS	GGNSSYEQ	YFGPGTRLTVL	Trbv2-7	8	1
Trav6D-6	YYCAL	SDSGGSNAKL	TFGKGTKLSVKS	Traj42	10	Trbv13-3	YFCAS	SDGNSDY	TFGSGTRLLVI	Trbj1-2	7	1
Trav7-3, 7D-3	YLCAV	NTGANTGKL	TFGHGTILRVHP	Traj52	9	Trbv1	LYCTC	SADREGHEQ	YFGPGTRLTVL	Trbv2-7	9	5
Trav7-3, 7D-3	YLCAV	NTGANTGKL	TFGHGTILRVHP	Traj52	9	Trbv13-2	YFCAS	GDNNERL	FFGHGTKLSVL	Trbj1-4	7	1
Trav8-2	YFCAT	DNNYAQGL	TFGLGTRVSVFP	Traj26(1)	8	Trbv29	YFCAS	STGDAGQL	YFGEGSKLTVL	Trbj2-2	8	6
Trav9-3,9-4, 9D-4	YFCVL	TINSAGNKL	TFGIGTRVLVRP	Traj17	9	Trbv13-2	YFCAS	GDNNERL	FFGHGTKLSVL	Trbj1-4	7	15
Trav9-3,9-4, 9D-4	YFCVL	TINSAGNKL	TFGIGTRVLVRP	Traj17	9	Trbv29	YFCAS	STGDAGQL	YFGEGSKLTVL	Trbj2-2	8	1
Trav12-1	YFCAL	SEDGSALGRL	HFGAGTQLIVIP	Traj18	10	Trbv13-2	YFCAS	GDRGGSAETL	YFGSGTRLTVL	Trbj2-3	10	1
												31

Table 5.35 The analysis of CD8 clones in the pancreas of MUT1 secondary recipient mice (P_2<P_1, Plate CT63, 64).

Trav	Va	N	Ja	Traj	Length, aa	Trbv	Vb	N	Jb	Trbj	Length, aa	Frequency
Trav6-4, 6D-4	YFCAL	VDSNYQL	IWGSGTKLIIKP	Traj33	7	Trbv13-2	YFCAS	GGNSSYEQ	YFGPGTRLTVL	Trbv2-7	8	30
Trav7-3, 7D-3	YLCAV	NTGANTGKL	TFGHGTILRVHP	Traj52	9	Trbv1	LYCTC	SADREGHEQ	YFGPGTRLTVL	Trbv2-7	8	42
Trav13-1	YLCAM	HQGGSAKL	IFGEGTKLTVSS	Traj57	8	Trbv13-2	YFCAS	GGPGQGANERL	FFGHGTKLSVL	Trbj1-4	11	1
												73

Table 5.36 The analysis of CD8 clones in the spleen of original donors of WT2 mice (S_0, Plate CT29).

Trav	Va	N	Ja	Traj	Length, aa	Trbv	Vb	N	Jb	Trbj	Length, aa	Frequency
Trav4-3, 4D-3	YFCAG	ASSGSWQL	IFGSGTQLTVMP	Traj22	8	Trbv13-2	YFCAS	GWGDYAEQ	FFGPGTRLTVL	Trbj2-1	8	1
Trav5D-4	YFCAA	RQGGRAL	IFGTGTTVSVSP	Traj15	7	Trbv13-2	YFCAS	GGGALYNSPL	YFAAGTRLTVT	Trbj1-6	10	1
Trav5D-4	YFCAA	SDTNAYKV	IFGKGTHLHVLP	Traj30	8	Trbv17	YLCAS	SSGNQDTQ	YFGPGTRLLVL	Trbj2-5	8	1
Trav5D-4	YFCAA	SATEGADRL	TFGKGTQLIIQP	Traj45	9	Trbv31	YLCAW	TGGTGQL	YFGEGSKLTVL	Trbj2-2	7	1
Trav6-3, 6D-3	YYCAM	RDTEGADRL	TFGKGTQLIIQP	Traj45	9	Trbv13-3	YFCAS	SDAGLQDTQ	YFGPGTRLLVL	Trbj2-5	9	1
Trav6-4, 6D-4	YFCAL	VATGGNNKL	TFGQGTVLSVIP	Traj56	9	Trbv26	YLCAS	SPDREDTQ	YFGPGTRLLVL	Trbj2-5	8	1
Trav6-5	YYCAL	SDTNAYKV	IFGKGTHLHVLP	Traj30	8	Trbv19	FLCAS	SIDRENTL	YFGAGTRLSVL	Trbj2-4	8	1
Trav6-5, 6D-6, 6D-7	YFCAL	SMTNSAGNKL	TFGIGTRVLVRP	Traj17	10	Trbv19	FLCAS	SIGWGEDTQ	YFGPGTRLLVL	Trbj2-5	9	1
Trav6D-7	YYCAL	SDGNEKI	TFGAGTKLTIKP	Traj48	8	Trbv5	YFCAS	SQEGGARDTL	YFGAGTRLSVL	Trbj2-4	10	1
Trav6D-7	YYCAL	SDQESSSFSKL	VFGQGTSLSVVP	Traj50	11	Trbv19	FLCAS	SIWGGYEQ	YFGPGTRLTVL	Trbv2-7	8	1
Trav7D-2	YLCAA	SNGSSGNKL	IFGIGTLLSVKP	Traj32	9	Trbv13-3	YFCAS	SDAGQVSNERL	FFGHGTKLSVL	Trbj1-4	11	1
Trav7D-5	YLCAV	TGGYKV	VFGSGTRLLVSP	Traj12	6	Trbv14	YLCAS	SFAGEGTETL	YFGSGTRLTVL	Trbj2-3	10	1
Trav12-1	YYCAL	TTASLGKL	QFGTGTQVVVTP	Traj24	8	Trbv16	YLCAS	RLDTGRAEQ	FFGPGTRLTVL	Trbj2-1	9	1
Trav12D-1, 12-2, 12D-2, 12-3, 12D-3	YYCAL	DYSNNRL	TLGKGTQVVVLP	Traj7	7	Trbv13-2	YFCAS	GDAGQAEV	FFGKGTRLTVV	Trbj1-1	8	1
Trav12D-1, 12-2, 12D-2, 12-3, 12D-3	YYCAL	DYSNNRL	TLGKGTQVVVLP	Traj7	7	Trbv19	FLCAS	SIQNTL	YFGEGSRLIVV	Trbj1-3	6	1
Trav12D-1, 12-2, 12D-2, 12-3, 12D-3	YYCAL	SDQDNMGYKL	TFGTGTSLLVDP	Traj9	10	Trbv1	LYCTC	SADQGGQDTQ	YFGPGTRLLVL	Trbj2-5	10	1
Trav13-1	YLCAM	VNQGGSAKL	IFGEGTKLTVSS	Traj57	9	Trbv14	YLCAS	RPGQNYAEQ	FFGPGTRLTVL	Trbj2-1	9	1
Trav13-2, 13D-2	YLCAI	DHQGGRAL	IFGTGTTVSVSP	Traj15	8	Trbv16	YLCAS	SPGTANTEV	FFGKGTRLTVV	Trbj1-1	9	1
Trav13-2, 13D-2	YLCAF	GQGGSAKL	IFGEGTKLTVSS	Traj57	8	Trbv30	YFCSS	IGTGGGEQ	YFGPGTRLTVL	Trbv2-7	8	1
Trav13-4/DV7	YLCAM	ERGNEKI	TFGAGTKLTIKP	Traj48	7	Trbv16	YLCAS	SFRLGVNQDTQ	YFGPGTRLLVL	Trbj2-5	11	1
Trav13D-4	YLCAM	ESPSGSWQL	IFGSGTQLTVMP	Traj22	9	Trbv4(2)	YLCAS	SYTANSDY	TFGSGTRLLVI	Trbj1-2	8	1
Trav14-1	YFCAA	SSDYGNEKI	TFGAGTKLTIKP	Traj48	9	Trbv1	LYCTC	TYRGERL	FFGHGTKLSVL	Trbj1-4	7	1
Trav14-3	YFCAA	SVTGSGGKL	TLGAGTRLQVNL	Traj44	9	Trbv13-3	YFCAS	SWTGGATEV	FFGKGTRLTVV	Trbj1-1	9	1
Trav14D-3/DV8	YFCAA	SDDSNNRI	FFGDGTQLVVKP	Traj31	8	Trbv3	YFCAS	SHRGLAEQ	FFGPGTRLTVL	Trbj2-1	8	1
Trav16, 16D/DV11	YFCAM	REGANNNAP	RFGAGTKLSVKP	Traj43	9	Trbv13-1	YFCAS	SDRQGLSNERL	FFGHGTKLSVL	Trbj1-4	11	1
Trav21/DV12	YHCIL	RVRETGANTGKL	TFGHGTILRVHP	Traj52	12	Trbv13-3	YFCAS	SHRGLSAETL	YFGSGTRLTVL	Trbj2-3	10	1
												26

Table 5.37 The analysis of CD8 clones in the spleen of WT2 primary recipient mice (S_1, Plate CT42).

Trav	Va	N	Ja	Traj	Length, aa	Trbv	Vb	N	Jb	Trbj	Length, aa	Frequency
Trav3-1	YFCAV	TGANTGKL	TFGHGTILRVHP	Traj52	8	Trbv14	YLCAS	SWAGNSDY	TFGSGTRLLVI	Trbj1-2	8	1
Trav7-4, &-4D	YFCAA	SEQSTGNYKY	VFGAGTRLKVIA	Traj40	10	Trbv3	YFCAS	SLAGEGDTQ	YFGPGTRLLVL	Trbj2-5	9	1
Trav7-5	YLCAM	TTASLGKL	QFGTGTQVVVTP	Traj24	8	Trbv2	YFCAS	SQETVNTEV	FFGKGTRLTVV	Trbj1-1	9	1
Trav7D-3	YLCAV	SLNNAGAKL	TFGGGTRLTVRP	Traj39	9	Trbv13-3	YFCAS	GGDWGGTYEQ	YFGPGTRLTVL	Trbv2-7	10	1
Trav9-3, 4, 4-D	YFCVF	MATGGNNKL	TFGQGTVLSVIP	Traj56	9	Trbv13-3	YFCAS	SETLSYEQ	YFGPGTRLTVL	Trbv2-7	8	1
Trav9D-3	YFCAV	SGNSNNRI	FFGDGTQLVVKP	Traj31	8	Trbv16	YLCAS	SSWGGNQDTQ	YFGPGTRLLVL	Trbj2-5	10	1
Trav12D-1, 2, D-2, 3, D-3	YYCAL	SGTNYAQGL	TFGLGTRVSVFP	Traj26	9	Trbv1	YCTCS	ADRGPYEQ	YFGPGTRLTVL	Trbv2-7	8	1
Trav13-2, 13D-2	YFCAI	DGANTGKL	TFGHGTILRVHP	Traj52	8	Trbv13-3	YFCAS	SWTGGQDTQ	YFGPGTRLLVL	Trbj2-5	9	1
Trav21/D12	YHCIL	NPSGGNYKP	TFGKGTSLVVHP	Traj6	9	Trbv3	YFCAS	SLAGEGDTQ	YFGPGTRLLVL	Trbj2-5	9	1
												9

Table 5.38 The analysis of CD8 clones in the spleen of WT2 secondary recipient mice (S_2, Plate CT59).

Trav	Va	N	Ja	Traj	Length, aa	Trbv	Vb	N	Jb	Trbj	Length, aa	Frequency
Trav6-6	YYCAL	GDYGNEKI	TFGAGTKLTIKP	Traj48	8	Trbv29	YFCAS	SRQGNTGQL	YFGEGSKLTVL	Trbj2-2	9	2
Trav6-6, 6D-6	YYCAL	AKRNNNNAP	RFGAGTKLSVKP	Traj43	9	Trbv4(2)	YLCAS	SQDWGANQDTQ	YFGPGTRLLVL	Trbj2-5	11	1
Trav13-2	YLCAL	ELDYANKM	IFGLGTILRVRP	Traj47	8	Trbv13-3	YFCAS	SDAGGANERL	FFGHGTKLSVL	Trbj1-4	10	2
Trav14-3	YFCAA	DSSSGSWQL	IFGSGTQLTVMP	Traj22	9	Trbv3	YFCAS	SLGARGERL	FFGHGTKLSVL	Trbj1-4	9	1
												6

Table 5.39 The analysis of CD8 clones in the spleen of original MUT2 donor mice (S_0, Plate CT35).

Trav	Va	N	Ja	Traj	Length, aa	Trbv	Vb	N	Jb	Trbj	Length, aa	Frequency
Trav1	YLCAE	NQGGRAL	IFGTGTTVSVSP	Traj15	7	Trbv29	YFCAS	SSTGQGAEQ	FFGPGTRLTVL	Trbj2-1	9	1
Trav3-1	YFCAV	SADSGSWQL	IFGSGTQLTVMP	Traj22	9	Trbv13-2	YFCAS	GGLGGRGAETL	YFGSGTRLTVL	Trbj2-3	11	1
Trav5D-4	YFCAA	SGGTGNYK	YVFGAGTRLKVIA	Traj40	8	Trbv13-3	YFCAS	REQGANSD	YTFGSGTRLLVI	Trbj1-2	8	1
Trav6-1, 2, 3, D-3, 4, D-4, 5, D-5, 6, D-6, 7, D-7	YYCVL	GEGTGGYKV	VFGSGTRLLVSP	Traj12	9	Trbv13-3	YFCAS	RDFSAETL	YFGSGTRLTVL	Trbj2-3	8	1
Trav6-1, 2, 3, D-3, 4, D-4, 5, D-5, 6, D-6, 7, D-7	YFCAV	SMNYNQGKL	IFGQGTKLSIKP	Traj23	9	Trbv26	YLCAS	SLSQGGDTQ	YFGPGTRLLVL	Trbj2-5	9	1
Trav6-1, 2, 3, D-3, 4, D-4, 5, D-5, 6, D-6, 7, D-7	YFCAV	NMGYKL	TFGTGTSLLVDP	Traj9	6	Trbv31	YLCAW	SPGHLNTEV	FFGKGTRLTVV	Trbj1-1	9	1
Trav6-2	YYCVL	GDTGGLSGKL	TFGEGTQVTVIS	Traj2	10	Trbv13-2	YFCAS	GDMGGYAEQ	FFGPGTRLTVL	Trbj2-1	9	1
Trav6-5, D-5	YYCAL	NNYAQGL	TFGLGTRVSVFP	Traj26(1)	7	Trbv31	YLCAW	SEEV	FFGKGTRLTVV	Trbj1-1	4	1
Trav6D-7	YYCAL	SEDNNAP	RFGAGTKLSVKP	Traj43	7	Trbv16	YLCASS	LWGSSYEQ	YFGPGTRLTVL	Trbv2-7	8	1
Trav7-4 or D-4	YFCAA	SDYGNEKI	TFGAGTKLTIKP	Traj48	8	Trbv29	YFCAS	SLSQSQNTL	YFGAGTRLSVL	Trbj2-4	9	1
Trav7D-5	YLCAV	SDTGN	YKYVFGA	Traj40	5	Trbv1	LYCTC	SADQDTEV	FFGKGTRLTVV	Trbj1-1	8	1
Trav7D-5	YLCAV	SSNNNAGAKL	TFGGGTRLTVRP	Traj39	10	Trbv5	YFCAS	SQYWGGYAEQ	FFGPGTRLTVL	Trbj2-1	10	1
Trav9-3, 4, D-4	YFCVL	SVDSNYQL	IWGSGTKLIIKP	Traj33	8	Trbv13-3	YFCAS	SDGGEDTQ	YFGPGTRLLVL	Trbj2-5	8	1
Trav9-3, 9-4	YFCVL	SASNYNVL	YFGSGTKLTVEP	Traj21	8	Trbv31	YLCAW	SHGNTEV	FFGKGTRLTVV	Trbj1-1	7	1
Trav9D-3, 4, D-4	YFCAV	SSNYNQGKL	IFGQGTKLSIKP	Traj23	9	Trbv5	YFCAS	SQDGGAQEQ	YFGPGTRLTVL	Trbv2-7	9	1
Trav10, 10D	YFCAA	SMDNNNAP	RFGAGTKLSVKP	Traj43	8	Trbv20	YLCGA	RDSWDQNTL	YFGAGTRLSVL	Trbj2-4	9	1
Trav12-1, D-1, 2, D-2, 3, D-3	YYCAL	SGTGGLSGKL	TFGEGTQVTVIS	Traj2	10	Trbv1	LYCTC	SAGREQDTQ	YFGPGTRLLVL	Trbj2-5	9	1
Trav12D-1, 2, D-2, 3, D-3	YYCAL	STNAYKV	IFGKGTHLHVLP	Traj30	7	Trbv13-2	YFCAS	GGQEDTQ	YFGPGTRLLVL	Trbj2-5	7	1
Trav13-1, D-1	YLCAL	EQTGFASAL	TFGSGTKVIPCLP	Traj35	9	Trbv13-3	YFCAS	SGDRTGNTL	YFGEGSRLIVV	Trbj1-3	9	1
Trav13-1, D-1	YLCAM	ASNTNKV	VFGTGTRLQVLP		7	Trbv26	YLCAS	SLYRGEDTQ	YFGPGTRLLVL	Trbj2-5	9	1
Trav13-2	YLCAI	RDSNYQL	IWGSGTKLIIKP	Traj33	7		YFCSS	RPGLGAEQ	YFGPGTRLTVL	Trbv2-7	8	1
Trav14-3	YFCAA	TSSGQKL	VFGQGTILKVYL	Traj16	7	Trbv13-2	YFCAS	GDKNYAEQ	FFGPGTRLTVL	Trbj2-1	8	1
Trav16, 16D/DV11	YFCAM	REGDGANTGKL	TFGHGTILRVHP	Traj52	11	Trbv13-3	YFCAS	SDSGISNERL	FFGHGTKLSVL	Trbj1-4	10	1
Trav16, 16D/DV11	YFCAM	REGNYGSSGNKL	IFGIGTLLSVKP	Traj32	12	Trbv19	FLCAS	SMGLGYEQ	YFGPGTRLTVL	Trbv2-7	8	1
Trav16, 16D/DV11	YFCAM	REGNYGNEKI	TFGAGTKLTIKP	Traj48	10	Trbv19	FLCAS	DSQNTL	YFGAGTRLSVL	Trbj2-4	6	1
Trav21/DV12	YHCIV	RVDTGYQKF	YFGKGTSLTVIP	Traj49	9	Trbv1	LYCTC	SAVLGTSAETL	YFGSGTRLTVL	Trbj2-3	11	1
Trav21/DV12	YHCIL	RVRQQGTGSKL	SFGKGAKLTVSP	Traj58	11	Trbv1	LYCTC	SARTGSSAETL	YFGSGTRLTVL	Trbj2-3	11	1
												27

Table 5.40 The analysis of CD8 clones in the pancreas of original MUT2 donor mice (P_0, Plate CT24).

Trav	Va	N	Ja	Traj	Length, aa	Trbv	Vb	N	Jb	Trbj	Length, aa	Frequency
Trav3-4	YFCAV	SADTNAYKV	IFGKGTHLHVLP	Traj30	9	Trbv16	YLCAS	LGPTGTANTGC	YFGEGSKLTVL	Trbj2-2	13	1
Trav3-4	YFCAV	GQMLTKSSLEKGH	IFMFSLTSRTQ		14	Trbv4	YLCAS	SSGTPSQNTL	YFGAGTRLSVL	Trbj2-4	10	1
Trav3-4	YFCAV	IDSNYQL	IWGSGTKLIIKP	Traj33	7	Trbv3	**YFCAS**	SLGSGDTQ	YFGPGTRLLVL	Trbj2-5	8	1
Trav5D-4	YFCAA	SEHYGNEKI	TFGAGTKLTIKP	Traj48	9	Trbv2	YFCAS	SQDSQNTL	YFGAGTRLSVL	Trbj2-4	8	1
Trav5D-4	YFCAA	SPNTNKV	VFGTGTRLQVLP		7	Trbv19	FLCAS	SIGNTEV	FFGKGTRLTVV	Trbj1-1	7	1
Trav6-3, 6D-3	YYCAM	RDPSGGSNYKL	TFGKGTLLTVTP	Traj53	11	Trbv29	YFCAS	SFQGSTGQL	YFGEGSKLTVL	Trbj2-2	9	1
Trav6-7/DV9	YYCAL	GDSGYNKL	TFGKGTVLLVSP	Traj11	8	Trbv1	LYCTC	SAATGGNAEQ	FFGPGTRLTVL	Trbj2-1	10	1
Trav6D-5, 6-6, 6-7/DV9	YYCAL	GTGGNNKL	TFGQGTVLSVIP	Traj56	8	Trbv13-3	YFCAS	SDAGSQNTL	YFGAGTRLSVL	Trbj2-4	9	1
Trav7-4 or 7D-4	YFCAA	SDVDYANKM	IFGLGTILRVRP	Traj47	9	Trbv13-2	YFCAS	GERGVSYEQ	YFGPGTRLTVL	Trbv2-7	9	1
Trav7-4 or Trav7D-4	YFCAA	SDVGDNSKL	IWGLGTSLVVNP	Traj38	9	Trbv26	YLCAS	SLDREDTQ	YFGPGTRLLVL	Trbj2-5	8	1
Trav7-4 or Trav7D-4	YFCAV	SELSNYNVL	YFGSGTKLTVEP	Traj21	9	Trbv2	YFCAS	SQEDRGYEQ	YFGPGTRLTVL	Trbv2-7	9	1
Trav7-4, Trav7D-4	YFCAA	SDVDYANKM	IFGLGTILRVRP	Traj47	9	Trbv13-2	YFCAS	GERGVSYEQ	YFGPGTRLTVL	Trbv2-7	9	1
Trav7D-2	YLCAA	SMDNMGYKL	TFGTGTSLLVDP	Traj9	9	Trbv19	FLCAS	STGGTYEQ	YFGPGTRLTVL	Trbv2-7	8	1
Trav7D-5	YLCAV	SMKYRQIN	AHSEAKHPEPRT		8	Trbv19	FLCAS	SIHTEV	FFGKGTRLTVV	Trbj1-1	6	1
Trav8-2	YFCAK	DGNYAQGL	TFGLGTRVSVFP	Traj26(1)	8	Trbv29	YFCAS	STGDAGQL	YFGEGSKLTVL	Trbj2-2	8	1
Trav9-1, D-1, 2, D-4	YFCAY	NYAQGL	TFGLGTRVSVFP	Traj26(1)	6	Trbv19	FLCAS	SIGGTNTGQL	YFGEGSKLTVL	Trbj2-2	10	1
Trav9-3 or 9-4	YFCAV	STNAYKV	IFGKGTHLHVLP	Traj30	7	Trbv1	LYCTC	SAEGTGGEYEC	YFGPGTRLTVL	Trbv2-7	11	1
Trav9D-2, 2, 4	YFCAV	ANYGNEKI	TFGAGTKLTIKP	Traj48	8	Trbv1	LYCTC	SAGGQDTQ	YFGPGTRLLVL	Trbj2-5	8	1
Trav9D-3	YFCAV	SANYNQGKL	IFGQGTKLSIKP	Traj23	9	Trbv5	YFCAS	SQDGGNQNTL	YFGAGTRLSVL	Trbj2-4	10	2
,Trav14D-1	YFCAA	SEDTGNYKY	VFGAGTRLKVIA	Traj40	9	Trbv31	YLCAW	PGLGGSNTGQ	YFGEGSKLTVL	Trbj2-2	12	1
Trav10 or 10D	YFCAA	SPQSNYKVL	YFGSGTKLTVE		9	Trbv2	YFCAS	SQEPNSGNTL	YFGEGSRLIVV	Trbj1-3	10	1
Trav12D-1, 2, D-2, 3, D-3	YYCAP	NSNNRI	FFGDGTQLVVKP	Traj31	6	Trbv13-2	YFCAS	GDWGSSQNTL	YFGAGTRLSVL	Trbj2-4	10	1
Trav12D-1, 2, D-2, 3, D-3	YYCAL	SDSAYKV	IFGKGTHLHVLP	Traj30	7	Trbv5	YFCAS	SQGGSGNTL	YFGEGSRLIVV	Trbj1-3	9	1
Trav12D-1, 2, D-2, 3, D-3	YYCAL	SVTGNTGKL	IFGLGTTLQVQP	Traj37	9	Trbv14	YLCAS	SSGGTQ	YFGPGTRLLVL	Trbj2-5	6	1
Trav12D-1, 2, D-2, 3, D-3	YYCAL	SDRGTGSKL	SFGKGAKLTVSP	Traj58	9	Trbv31	YLCAW	SRDWGYEQ	YFGPGTRLTVL	Trbv2-7	8	1
Trav12D-1, 2, D-2, 3, D-3	YYCAL	SVGGSNYKL	TFGKGTLLTVTP	Traj53	9	Trbv13-1	YFCAS	SEIGNEQ	YFGPGTRLTVL	Trbv2-7	7	1
Trav12D-1, 2, D-2, 3, D-3	YYCAL	SEWGTGGYKV	VFGSGTRLLVSP	Traj12	10	Trbv31	YLCAW	SELGGQNTL	YFGAGTRLSVL	Trbj2-4	9	1
Trav12D-1, 2, D-2, 3, D-3	YYCNY	NVL	YFGSGTKLTVEP	Traj21	3		YLCAS	SLGGGRAQNTL	YFGAGTRLSVL	Trbj2-4	11	1
Trav13-1 or ,Trav13D-4	YLCAM	QGTGSKL	SFGKGAKLTVSP	Traj58	7	Trbv2	YFCAS	SRDWGAAEQ	FFGPGTRLTVL	Trbj2-1	9	1
Trav13-1 or Trav13D-4	YLCAM	ENTGYQNF	YFGKGTSLTVIP	Traj49	8	Trbv4(2)	YLCAS	SLLGGLGTL	YFGAGTRLSVL	Trbj2-4	9	1
Trav13D-1	YLCAL	ERGDSNYQL	IWGSGTKLIIKP	Traj33	9	Trbv31	YLCAW	TGGTSAETL	YFGSGTRLTVL	Trbj2-3	9	1
Trav14-1	YFCAA	SGNEKI	TFGAGTKLTIKP	Traj48	6	Trbv31	YLCAW	SRGNQDTQ	YFGPGTRLLVL	Trbj2-5	8	1
Trav14-2	YFCAA	SATSGSWQL	IFGSGTQLTVMP	Traj22	9	Trbv19	FLCAS	SIPGAGNTL	YFGEGSRLIVV	Trbj1-3	9	1
Trav14-2	YFCAA	SAQVVGQL	TFGRGTRLQVYA	Traj5	8	Trbv1	LYCTC	LSADRHSNER	FFGHGT**ER**SVL	Trbj1-4	10	1
Trav16 or Trav16D/DV11	YFCAM	RENNNAGAKL	TFGGGTRLTVRP	Traj39	10	Trbv13-3	YFCAS	RQGAVNSPL	Y**S**AAGTRLTV	Trbj1-6	9	1
Trav16 or Trav16D/DV11	YFCAM	RERDTGYQNF	YFGKGTSLTVIP	Traj49	10	Trbv13-1	YFCAS	SVRTGYEQ	YFGPGTRLTVL	Trbv2-7	8	1
Trav19	YLCAA	GTGSKL	SFGKGAKLTVSP	Traj58	6	Trbv4(2)	YLCAS	SYLGGRQDTQ	YFGPGTRLLVL	Trbj2-5	10	1
												38

Table 5.41 The analysis of CD8 clones in the pancreas of MUT2 primary recipient mice (P_1, Plate CT40).

Trav	Va	N	Ja	Traj	Length, aa	Trbv	Vb	N	Jb	Trbj	Length, aa	
Trav6-4, 6D-4	YFCAL	VDSNYQL	IWGSGTKLIIKP	Traj33	7	Trbv13-2	YFCAS	GGNSSYEQ	YFGPGTRLTVL	Trbv2-7	8	8
												8

Table 5.42 The analysis of CD8 clones in the spleen of MUT2 secondary recipient mice (S_2<S_1, Plate CT45).

Trav	Va	N	Ja	Traj	Length, aa	Trbv	Vb	N	Jb	Trbj	Length, aa	Frequency
Trav6-4 or Trav6D-4	YFCAL	VDSNYQL	IWGSGTKLIIKP	Traj33	7	Trbv13-2	YFCAS	GGNSSYEQ	YFGPGTRLTVL	Trbv2-7	8	3
												3

Table 5.43 The analysis of CD8 clones in the spleen of MUT2 secondary recipient mice (S_2<P_1, Plate CT47).

Trav	Va	N	Ja	Traj	Length, aa	Trbv	Vb	N	Jb	Trbj	Length, aa	Frequency
Trav6-4 or Trav6D-4	YFCAL	VDSNYQL	IWGSGTKLIIKP	Traj33	7	Trbv13-2	YFCAS	GGNSSYEQ	YFGPGTRLTVL	Trbv2-7	9	1
Trav7-3 or 7D-3	YLCAV	NTGANTGKL	TFGHGTILRVHP	Traj52	9	Trbv1	LYCTC	SADREGHEQ	YFGPGTRLTVL	Trbv2-7	9	2
Trav7-3 or 7D-3	YLCAV	NTGANTGKL	TFGHGTILRVHP	Traj52	9	Trbv5	YFCAS	SQDRGQDTEV	FFGKGTRLTV	Trbj1-1	10	2
												5

Table 5.44 The analysis of CD4 clones in the spleen of WT3 secondary recipient mice (S_2<S_1, Plate CT22).

Trav	Va	CDR3a	Ja	Traj	Length, aa	Trbv	Vb	CDR3b	Jb	Trbj	Length, aa	Frequency
Trav3-1, 3-4	YFCAV	GTGNYKY	VFGAGTRLKVIA	Traj40	7	Trbv31	YLCAW	SLGTGGVKETL	YFGSGTRLTVL	Trbj2-3	11	1
Trav4-2	YFCAA	GTGGYKV	VFGSGTRLLVSP	Traj12	7	Trbv1	YCTCS	ADWEGQNTL	YFGAGTRLSVL	Trbj2-4	9	1
Trav4-2	YFCAA	GTGGYKV	VFGSGTRLLVSP	Traj12	7	Trbv1	YCTCS	ADWEGQNTL	YFGAGTRLSVL	Trbj2-4	9	1
Trav4-2	YFCAA	EASTNAYKV	IFGKGTHLHVLP	Traj30	9	Trbv19	FLCAS	SPGTGDEQ	YFGPGTRLTVL	Trbv2-7	8	1
Trav4D-2	YFFAA	ASSGSRQL	IFGSGTQLTVMP	Traj22	8	Trbv2	YFCAS	SHGTVNSDY	TFGSGTRLLVI	Trbj1-2	9	1
Trav4D-2	YFCAA	EASTNAYKV	IFGKGTHLHVLP	Traj30	9	Trbv5	YFCAS	SQGDRTNTGQL	YFGEGSKLTVL	Trbj2-2	11	1
Trav4D-2	YFCAA	DTNAYKV	IFGKGTHLHVLP	Traj30	7	Trbv31	YLCAW	SQLGGGYAEQ	FFGPGTRLTVL	Trbj2-1	10	1
Trav4D-2	YFCAA	EAPNTNKV	VFGTGTRLQVLP	Traj34	8	Trbv19	FLCAS	SPDWGQNTL	YFGAGTRLSVL	Trbj2-4	9	1
Trav5D-4	YFCAA	SPNAYKV	IFGKGTHLHVLP	Traj30	7	Trbv2	YFCAS	SQAGTGRDTQ	YFGPGTRLLVL	Trbj2-5	10	1
Trav5D-4	YFCAA	SPNAYKV	IFGKGTHLHVLP	Traj30	7	Trbv5	YFCAS	SQGDRTNTGQL	YFGEGSKLTVL	Trbj2-2	11	1
Trav5D-4	YFCAA	SGGDSNYKL	TFGKGTLLTVTP	Traj53	9	Trbv12-2	YFCAS	SLGGSQDTQ	YFGPGTRLLVL	Trbj2-5	9	1
Trav6-5	YYCAL	LGSNMGYKL	TFGTGTSLLVDP	Traj9	9	Trbv23	YLCSS	GTASAETL	YFGSGTRLTVL	Trbj2-3	8	1
Trav6-6	YYCAL	GMSXHNL	LYFGSGTKLT	Traj21	7	Trbv15	YLCAS	TGEGYAEQ	FFGPGTRLTVL	Trbj2-1	8	1
Trav6-6, 6D-6	YYCAL	GDQSSSFSKL	VFGQGTSLSVVP	Traj50	10	Trbv2	YFCAS	SQAGTGRDTQ	YFGPGTRLLVL	Trbj2-5	10	1
Trav6-7/DV9, Trav6D-7	YYCAL	RLTGSGGKL	TLGAGTRLQVNL	Traj44	9	Trbv20	YLCGA	RSGGAAETL	YFGSGTRLTVL	Trbj2-3	9	1
Trav6D-4, 6-5, 6D-5, 6-66D-6, 6-7/DV9, 6D-7	YCARG	SNMGYKL	TFGTGTSLLVDP	Traj9	7	Trbv23	YLCSS	GTASAETL	YFGSGTRLTVL	Trbj2-3	8	1
Trav6D-5	YYCAL	GSNMGYKL	TFGTGTSLLVDP	Traj9	8	Trbv23	YLCSS	GTASAETL	YFGSGTRLTVL	Trbj2-3	8	1
Trav6D-5, 6-6, 6-7/DV9	YYCAL	GMNTEGADRL	TFGKGTQLIIQP	Traj45	10	Trbv4	YLCAS	SYYNSPL	YFAAGTRLTVT	Trbj1-6		1
Trav10, 10D	YFCAA	SINNRI	FFGDGTQLVVKP	Traj31	6	Trbv26	YLCAS	SLTGGNTEV	FFGKGTRLTVV	Trbj1-1	9	1
Trav12-1	YYCAL	SVTNTGKL	TFGDGTVLTVKP	Traj27	8	Trbv13-2	YFCAS	GDAWGDGEQ	YFGPGTRLTVL	Trbv2-7	9	1
Trav12-1	YFCAF	SGGNYKP	TFGKGTSLVVHP	Traj6	7	Trbv1	YCTCS	ADWEGQNTL	YFGAGTRLSVL	Trbj2-4	9	1
Trav12-1	YFCAF	SGGNYKP	TFGKGTSLVVHP	Traj6	7	Trbv16	YLCAS	SLDWGNYAEQ	FFGPGTRLTVL	Trbj2-1	10	1
Trav12D-1, 12-2, 12D-2, 12-3, 12D-3	YYCAL	SGGGGGNNKL	TFGQGTVLSVIP	Traj56	10	Trbv31	YLCAR	SLSRGENSPL	YFAAGTRLTVT	Trbj1-6	10	1
Trav13-2	YLCAL	ERGGSGGKL	TLGAGTRLQVNL	Traj44	9	Trbv13-2	YFCAS	GDAQGQNTL	YFGAGTRLSVL	Trbj2-4	9	1
Trav13-4/DV7	YLCAM	DTGYQNF	YFGKGTSLTVIP	Traj48	7	Trbv20	YLCGA	QTGAYEQ	YFGPGTRLTVL	Trbv2-7	7	1
Trav14-1	YFCAA	SSTGNYKY	VFGAGTRLKVIA	Traj40	8	Trbv26	YLCAS	LSLQGTNER	FFGHGTKLSVL	Trbj1-4	9	1
Trav14-1	YFCAA	SRNNNAP	RFGAGTKLSVKP	Traj43	7	Trbv2	YFCAS	SQDSNTEV	FFGKGTRLTVV	Trbj1-1	8	1
Trav14-1	YFCAA	SGVSGGSNYKL	TFGKGTLLTVTP	Traj53	11	Trbv26	YLCAS	SQGSQNTL	YFGAGTRLSVL	Trbj2-4	8	2
Trav14-2	YFCAA	SESNNRI	FFGDGTQLVVKP	Traj31	7	Trbv31	YLWAW	SLPRGGGEQ	SFGPGTRLTVL	Trbj2-1/7	9	1
Trav14-2	YFCAA	SSTGNYKY	VFGAGTRLKVI	Traj40	8	Trbv26	YLCAS	SLQGTNERL	FFGHGTKLSV	Trbj1-4	9	2
Trav14-3	YFCAA	SGSNNRI	FFGDGTQLVVKP	Traj31	7	Trbv16	YLCAS	SLDFGGXRGQNTL	YFGAGTRLSVL	Trbj2-4	13	1
Trav14D-3/DV8	YFCAA	NYGNEKI	TFGAGTKLTIKP	Traj48	7	Trbv19	FLCAS	SRTHSGNT	YFGEGSRLIVV	Trbj1-3	8	1
Trav16, 16D/DV11	YFCAM	RGTSGRAL	IFGTGTTVSVSP	Traj15	8	Trbv19	FLCAS	SPDKYEQ	YFGPGTRLTVL	Trbv2-7	7	1
												35

Table 5.45 The analysis of CD4 clones in the spleen of MUT3 secondary recipients receiving pancreas-infiltrating lymphocytes (S_2<P_1, Plate CT20).

Trav	Va	CDR3a	Ja	Traj	Length, aa	Trbv	Vb	CDR3b	Jb	Trbj	Length, aa	Frequency
Trav1	YLCAV	RDPTNAYKV	IFGKXTHLHVLP	Traj30	9	Trbv5	YFCAS	SQDRTAYEQ	YFGPGTRLTVL	Trbj2-5	9	1
Trav3-3, Trav3D-3	YFCAV	SEGNNNRI	FFGDGTQLVVKP	Traj31	8	Trbv20	YLCGA	RYRDWGGFEQ	YFGPGTRLTVL	Trbv2-7	10	1
Trav4-3, 4D-3	YFCAA	EANYGNEKI	TFGAGTKLTIKP	Traj48	9	Trbv20	YLCGA	QGNYAEQ	FFGPGTRLTVL	Trbj2-1	7	1
Trav4-4/DV10	YFCAA	EGSSNTDKV	VFGTGTRLQVSP	Traj34	9	Trbv20	YLCGA	IQGYEQ	YFGPGTRLTVL	Trbv2-7	6	1
Trav4-4/DV10	YFCAA	VNNNNAP	RFGAGTKLTVKP	Traj43	7	Trbv13-2	YFCAS	GTGGYNSPL	YFAAATRLTVT	Trbj1-6	9	1
Trav4D-2, 4-3, 4D-3, 4/DV10	YFCAA	EANYGNEKI	TFGAGTKLTIKP	Traj48	9	Trbv20	YLCGA	QGNYAEQ	FFGPGTRLTVL	Trbj2-1	7	1
Trav7-5	YLCAM	SMRGGSALGRL	HFGAGTQLIVIP	Traj18	11	Trbv31	YLCAW	SLGLGGRYAEQ	FFGPGTRLTVL	Trbj2-1	11	1
Trav7D-5	YXCAV	SAHYGSSGNKL	IFGIGTLLSVKP	Traj32	11	Trbv13-2	YFCAS	GDPGLGNYAEQ	FFGPGTRLTVL	Trbj2-1	11	1
Trav8-1, 8D-1	YFCAT	GGSNAKL	TFGKGTKLSVKS	Traj42	7	Trbv5	YFCAS	SQEGQGQDTQ	YFGPGTRLLVL	Trbj2-5	10	1
Trav8-2	YFCAT	DKRNSNNRI	FFGDGTQLVVKP	Traj31	9	Trbv13-2	YFCAS	GPQGYAEQ	FFGPGTRLTVL	Trbj2-1	8	1
Trav13D-1	YLCAM	GDNNAGAKL	TFGGGTRLTVRP	Traj39	9	Trbv20	YLCGA	RDNYAEQ	FFGPGTRLTVL	Trbj2-1	7	3
Trav14-1	YXCAA	SAGXGGGGKL	TLGAGTRLQVNL	Traj44	10	Trbv20	YLCGA	SDWGYEQ	YFGPGTRLTVL	Trbv2-7	7	1
Trav14-2	YFCAA	SPNNNNAP	RFGAGTKLTVKP	Traj43	8	Trbv13-1	YFCAS	SAGTGGNSDY	TFGSGTRLLVI	Trbj1-2	10	1
Trav16, 16D/DV11	YFCAM	RAWTGGYKV	VFGSGTRLLVSP	Traj12	9	Trbv26	YLCAS	TPGQGANSDY	TFGSGXRLLVI	Trbj1-2	10	1
												16

Table 5.46 The analysis of CD4 clones in the pancreas of MUT3 secondary recipients receiving pancreas-infiltrating lymphocytes (P_2<P_1, Plate CT17).

Trav	Va	CDR3a	Ja	Traj	Length, aa	Trbv	Vb	CDR3b	Jb	Trbj	Length, aa	Frequency
Trav6-3, D-3	YYCAM	RENNAGAKL	TFGGGTRLTVRP	Traj39	9	Trbv13-3	YFCAS	SPDRDSDF	TFGSGTRLXVI	Trbj1-2	8	1
Trav6D-5	YYCAL	LGSNMGYK	TFGTGTSLLVDP	Traj9	8	Trbv23	YLCSS	GTASAETL	YFGSGTRLTVL	Trbj2-3	8	1
Trav7-3, D-3	YLCAV	SIFGGSNAKL	TFGKGTKLSVKS	Traj42	10	Trbv31	YLCAW	SLYSSAETL	YFGSGTRLTVL	Trbj2-3	11	1
Trav7-4, 7D-4	YFCAA	SEPNSGGSNAKL	TFGKGTKLSVKS	Traj42	12	Trbv5	YFCAS	SQTENTL	YFGAGTRLSVL	Trbj2-4	7	1
Trav7-5	YLCAG	SNTGANTGKL	TFGHGTILRVHP	Traj52	10	Trbv20	YLCGA	RQGSYEQ	YFGPGTRLTVL	Trbv2-7	7	1
Trav7D-5	YLCAG	SNTGANTGKL	TFGHGTILRVHP	Traj52	10	Trbv20	YLCGG	ARQGSYEQ	YFGPGTRLTVL	Trbv2-7	8	1
Trav8-1, 8D-1	YFCAT	GGNYAQGL	TFGLGTRVSVFP	Traj26	8	Trbv1	YCTCS	ADWEGQNTL	YFGAGTRLSVL	Trbj2-4	9	1
Trav13D-1	YLCAM	GDNNAGAKL	TFGGGTRLTVRP	Traj39	9	Trbv20	YLCGG	ARQGSYEQ	YFGPGTRLTVL	Trbv2-7	8	1
Trav14-1	YFCAA	SGVSGGSNYKL	TFGKGTLLTV	Traj53	11	Trbv26	YLCAS	SQGSQNTL	YFGAGTRLSVL	Trbj2-4	8	1
Trav14-3	YFCAA	TGANTGKL	TFGHGTILRVHP	Traj52	8	Trbv4	YLCAS	SPRQIYEQ	YFGPGTRLTVL	Trbv2-7	8	1
Trav14D-3/DV8	YFCAA	SANSGTYQ	RFGTGTKLQVVP	Traj13	8	Trbv5	YFCAS	SPGANSDY	TFGSGTRLLV	Trbj1-2	8	1
Trav16, 16D/DV11	YFCAM	RAWTGGYKV	VFGSGTRLLVSP	Traj12		Trbv26	YLCAS	SPGQGANSDV	YTFGSGTRLL	Trbj1-2	10	1
Trav21/DV12	YHCIL	RANSGGS	'KLTFGKGTLLTVTP	Traj53	7	Trbv31	YLCAW	SYNYAEQ	FFGPGTRLTVL	Trbj2-1	11	1
Trav21/DV12	YHCIL	RANSGGSNYKL	TFGKGTLLTVTP	Traj53	11	Trbv31	YLCAW	SYNYAEQ	FFGPGTRLTVL	Trbj2-1	7	2
												15

Table 5.47 The analysis of CD8 clones in the spleen of WT3 secondary recipients (S_2<S_1, Plate CT21).

Trav	Va	CDR3a	Ja	Traj	Length, aa	Trbv	Vb	CDR3b	Jb	Trbj	Length, aa	Frequency
Trav3-1	YFCAV	SAGRASNTNKV	VFGTGTRLQVLP	Traj34	11	Trbv13-3	YLCAS	SDEGAGTGQL	YFGEGSKL	Trbj2-2	10	1
Trav4-2 or Trav4D-2	YFCAA	ASGGSNYKL	TFGKGTLLTVTP	Traj53	9	Trbv17	YLCAS	SRKGGEQ	YFGPGTRLTVL	Trbv2-7	7	1
Trav4-3 or Trav4D-3	YFCAA		IFGEGTKLTVSS	Traj57	7	Trbv19	FLCAS		YFGPGTRLTV	Trbv2-7	8	5
Trav4-3	YFCAA	EGGSAKL	IFGEGTKLTVSS	Traj57	7	Trbv19	FLCAS	SMGLGYEQY	FGPGTRLTVL	Trbj2-1	8	1
Trav4-3	YFCAA	EGGSAKL	IFGEGTKLTVSS	Traj57	7	Trbv19	VFLCAS	SMGLGYEQ	YFGPGTRLTV	Trbv2-7	8	1
Trav6-2	YYCVL	GFTGSGGKLT	LGAGTRLQVNL	Traj44	10	Trbv13-2	YFCAS	GDAWGVSAETL	YFGSGTRL	Trbj2-3	11	1
Trav6-6	YYCAL	GDANSAGNKL	TFGIGTRVLVRP	Traj17	10	Trbv13-1	YFCAS	SGTGGYAEQ	FFGPGTRLTVL	Trbj2-1	9	1
Trav6-6	YCAL	GNSNNRI	FFGDGTQLVVKP	Traj31	7	Trbv17	YLCAS	KQGARDTQ	YFGPGTRLLV	Trbj2-5	8	1
Trav6D-6	YYCAL	GDANSAGNKL	TFGIGTRVLVRP	Traj17	10	Trbv13-1	YFCAS	SGTGGYAEQ	FFGPGTRLT	Trbj2-1	9	1
Trav7-1	YFCAV	SSSGSWQL	IFGSGTQLTV	Traj22	8	Trbv1	YCTCS	GDSSGNTL	YFGEGSRLIVV	Trbj1-3	8	1
Trav7D-5	YLCAV	GASSSFSKL	VFGQGTSLSVVP	Traj50	9	Trbv1	YCTCS	AHRGSYNSPL	YFAAGTRLTV	Trbj1-6	10	1
Trav8-1 or Trav8D-1	YFCAT	PSNTNKV	VFGTGTRLQVLP	Traj34	7	Trbv19	FLCAS	SDWGGYEQ	YFGPGTRLTV	Trbv2-7	8	1
Trav8-2	YFCAT	DFNTNKV	VFGTGTRLQV	Traj34	7	Trbv13-3	YFCAS	RTGGAYEQ	YFGPGTRLTV	Trbv2-7	8	1
Trav10 or Trav10D	YFCAA	SSTGGYKV	VFGSGTRLLVSP	Traj12	8	Trbv13-2	YFCAS	GDAGVQDTQ	YFGPGTXLLVL	Trbj2-5	9	1
Trav13-1	YLCAM	ESSSGSWQL	IFGSGTQLT	Traj22		Trbv13-2	YFCAS	GDGRGSYEQ	YFGPGTRLTV	Trbv2-7	9	1
Trav13-2	YLCAI	SGSFNKLT	FGAGTRLAVCP	Traj40	8	Trbv5	YFCAS	SQGETL	YFGSGTRLTV	Trbj2-3	6	1
Trav13-4/DV7	YLCAM	DQGGSAKL	IFGEGTKLTVSS	Traj57	8	Trbv14	YLCAS	RQVNQDTQ	YFGPGTRLLV	Trbj2-5	8	1
Trav16 or Trav16D	YFCAM	REGDQGGRAL	IFGTGTTV	Traj15	10	Trbv13-2	YFCAS	GDGRGSYEQ	YFGPGTRLTV	Trbv2-7	9	1
Trav16 or Trav16D	YFCAM	REGDQGGRAL	IFGTGTTVSV	Traj15		Trbv13-1	YFCAS	SDGGAREQ	YFGPGTRLTV	Trbv2-7	8	1
Trav19	YLCAA	GTGGNNKL	TFGQGTVLSVIP	Traj56	8	Trbv14	YLCAS	RQVNQDTQ	YFGPGTRLLV	Trbj2-5	8	1
												24

Table 5.48 The analysis of CD8 clones in the spleen of MUT3 secondary recipients receiving pancreas-infiltrating lymphocytes (S_2<P_1, Plate CT19).

Trav	Va	CDR3a	Ja	Traj	Length, aa	Trbv	Vb	CDR3b	Jb	Trbj	Length, aa	Frequency
Trav7-1	YFCAV	SSSGSWQL	IFGSGTQLTVMP	Traj22	8	Trbv1	YCTCS	GDSSGNTL	YFGEGSRLIVV	Trbj1-3	8	12
Trav7-1	YFCAV	SGGSNYQL	IWGSGTKLIIKP	Traj33	8	Trbv1	YCTCS	GDRGGNTL	YFGEGSRLIVV	Trbj1-3	8	8
Trav12D-1, 2, D-2, 3	YYCAL	SDTSSGQKL	VFGQGTILKVYL	Traj16	9	Trbv14	YLCAS	SFGTGAYAEQ	FFGPGTRLTVL	Trbj2-1	10	7
Trav1	YLCAV	RPNSGTYQ	RFGTGTKLQVVP	Traj13	8	Trbv13-3	YFCAS	SGTDRASQNTL	YFGAGTRLSVL	Trbj2-4	11	1
Trav4-3, 4D-3	YFCAA	EGYQNF	YFGKGTSLTVIP	Traj49	6	Trbv31	YLCAW	SLAYEQ	YFGPGTRLTVL	Trbv2-7	6	1
Trav7-1	YFCAV	SSSGSWQL	IFGSGTQLTVMP	Traj22	8	Trbv19	FLCAS	SIQNSYNSPL	YFAAGTRLTVT	Trbj1-6	10	1
Trav7-1	YLCAV	TSGGNYKP	TFGKGTSLVVHP	Traj6	8	Trbv13-1	YFCAS	SDERTGSYAEQ	FFGPGTRLTVL	Trbj2-1	11	1
Trav7-1	YFCAV	SSSGSWQL	IFGSGTQLTVMP	Traj22	8	Trbv13-1	YFCAS	SDERTGSYAEQ	FFGPGTRLTVL	Trbj2-4	11	1
Trav7D-2	YLCAA	SNYSNNRL	TLGKGTQVVVLP	Traj7	8	Trbv13-1	YFCAS	SEGQNTL	YFGAGTRLSVL	Trbj2-4	7	1
Trav8D-2	XFCAT	DYNQGKL	IFGQGTKLSIKP	Traj23	7	Trbv17	YLCAS	SRAGGEDTQ	YFGPGTRLLVL	Trbj2-5	9	1
Trav12-1	YFCAL	SEGGPGRQSSD	IWNRNHGISQP		11	Trbv1	YCTCS	GDRGGNTL	YFGEGSRLIVV	Trbj1-3	8	1
Trav12D-1, 2, D-2, 3	YYCAL	SGNTGYQNF	YFGKGTSLTVIP	Traj49	9	Trbv1	LYCTC	SGDRGGNTL	YFGEGSRLIVV	Trbj1-3	8	1
Trav14-3	YFCAA	SRGTQVVGQL	TFGRGTRLQVYA	Traj5	10	Trbv26	YLCAS	SLWDWSSYEQ	YFGPGTRLTVL	Trbv2-7	10	1
												37

Table 5.49 The analysis of CD8 clones in the pancreas of MUT3 secondary recipients receiving pancreas-infiltrating lymphocytes (P_2<P_1, Plate CT16).

Trav	Va	CDR3a	Ja	Traj	Length, aa	Trbv	Vb	CDR3b	Jb	Trbj	Length, aa	Frequency
Trav7-1	YFCAV	SSSGSWQL	IFGSGTQLT	Traj22	8	Trbv1	YCTCS	GDSSGNTL	YFGEGSRLIVV	Trbj1-3	8	29
Trav7-1	YFCAV	SGGSNYQL	IWGSGTKL	Traj33	8	Trbv1	YCTCS	GDSSGNTL	YFGEGSRLIVV	Trbj1-3	8	9
Trav1	YLCAV	RPNSGTYQ	RFGTGTKLQV	Traj13	8	Trbv13-3	YFCAS	SGTDRASQNTL	YFGAGTRLSVL	Trbj2-4	11	1
Trav6-6	YCAL	GLNNYAQGL	TFGLGTRVSV	Traj26	9	Trbv13-1	YFCAS	SADRNYAEQ	FFGPGTRLTVL	Trbj2-1	9	1
Trav12D-1, 2, D-2, 3	YYCAL	SGNTGYQNF	YFGKGTSLTV	Traj49	9	Trbv1	YCTCS	DRANSPL	YFAAGTRLTVT	Trbj1-6	7	1
Trav14D-1	YFCAA	SRDDSAGNKL	TFGIGTRV	Traj17	10	Trbv16	YLCAS	SLAGGRFAETL	YFGSGTRL	Trbj2-3	11	1
												42

Chapter 8

References

Aaltonen, J., Horelli-Kuitunen, N., Fan, J.B., Bjorses, P., Perheentupa, J., Myers, R., Palotie, A., and Peltonen, L. (1997). High-resolution physical and transcriptional mapping of the autoimmune polyendocrinopathy-candidiasis-ectodermal dystrophy locus on chromosome 21q22.3 by FISH. Genome research *7*, 820-829.

Abramson, J., Giraud, M., Benoist, C., and Mathis, D. (2010). Aire's partners in the molecular control of immunological tolerance. Cell *140*, 123-135.

Adamson, K.A., Pearce, S.H., Lamb, J.R., Seckl, J.R., and Howie, S.E. (2004). A comparative study of mRNA and protein expression of the autoimmune regulator gene (Aire) in embryonic and adult murine tissues. J Pathol *202*, 180-187.

Akkaraju, S., Canaan, K., and Goodnow, C.C. (1997a). Self-reactive B cells are not eliminated or inactivated by autoantigen expressed on thyroid epithelial cells. The Journal of experimental medicine *186*, 2005-2012.

Akkaraju, S., Ho, W.Y., Leong, D., Canaan, K., Davis, M.M., and Goodnow, C.C. (1997b). A range of CD4 T cell tolerance: partial inactivation to organ-specific antigen allows nondestructive thyroiditis or insulitis. Immunity *7*, 255-271.

Alam, C., Bittoun, E., Bhagwat, D., Valkonen, S., Saari, A., Jaakkola, U., Eerola, E., Huovinen, P., and Hanninen, A. (2011). Effects of a germ-free environment on gut immune regulation and diabetes progression in non-obese diabetic (NOD) mice. Diabetologia *54*, 1398-1406.

Alderson, M.R., Tough, T.W., Davis-Smith, T., Braddy, S., Falk, B., Schooley, K.A., Goodwin, R.G., Smith, C.A., Ramsdell, F., and Lynch, D.H. (1995). Fas ligand mediates activation-induced cell death in human T lymphocytes. The Journal of experimental medicine *181*, 71-77.

Aliahmad, P., and Kaye, J. (2008). Development of all CD4 T lineages requires nuclear factor TOX. The Journal of experimental medicine *205*, 245-256.

Allen, P.M., Matsueda, G.R., Evans, R.J., Dunbar, J.B., Jr., Marshall, G.R., and Unanue, E.R. (1987). Identification of the T-cell and Ia contact residues of a T-cell antigenic epitope. Nature *327*, 713-715.

Alleva, D.G., Maki, R.A., Putnam, A.L., Robinson, J.M., Kipnes, M.S., Dandona, P., Marks, J.B., Simmons, D.L., Greenbaum, C.J., Jimenez, R.G.*, et al.* (2006). Immunomodulation in type 1 diabetes by NBI-6024, an altered peptide ligand of the insulin B epitope. Scandinavian journal of immunology *63*, 59-69.

Altin, J.A., Tian, L., Liston, A., Bertram, E.M., Goodnow, C.C., and Cook, M.C. (2011). Decreased T-cell receptor signaling through CARD11 differentially

compromises forkhead box protein 3-positive regulatory versus T(H)2 effector cells to cause allergy. The Journal of allergy and clinical immunology *127*, 1277-1285 e1275.

Amrani, A., Serra, P., Yamanouchi, J., Han, B., Thiessen, S., Verdaguer, J., and Santamaria, P. (2002). CD154-dependent priming of diabetogenic CD4(+) T cells dissociated from activation of antigen-presenting cells. Immunity *16*, 719-732.

Amrani, A., Serra, P., Yamanouchi, J., Trudeau, J.D., Tan, R., Elliott, J.F., and Santamaria, P. (2001). Expansion of the antigenic repertoire of a single T cell receptor upon T cell activation. J Immunol *167*, 655-666.

Anandasabapathy, N., Ford, G.S., Bloom, D., Holness, C., Paragas, V., Seroogy, C., Skrenta, H., Hollenhorst, M., Fathman, C.G., and Soares, L. (2003). GRAIL: an E3 ubiquitin ligase that inhibits cytokine gene transcription is expressed in anergic CD4+ T cells. Immunity *18*, 535-547.

Anderson, A.C., Nicholson, L.B., Legge, K.L., Turchin, V., Zaghouani, H., and Kuchroo, V.K. (2000). High frequency of autoreactive myelin proteolipid protein-specific T cells in the periphery of naive mice: mechanisms of selection of the self-reactive repertoire. The Journal of experimental medicine *191*, 761-770.

Anderson, B., Park, B.J., Verdaguer, J., Amrani, A., and Santamaria, P. (1999). Prevalent CD8(+) T cell response against one peptide/MHC complex in autoimmune diabetes. Proceedings of the National Academy of Sciences of the United States of America *96*, 9311-9316.

Anderson, M.S., Venanzi, E.S., Chen, Z., Berzins, S.P., Benoist, C., and Mathis, D. (2005). The cellular mechanism of Aire control of T cell tolerance. Immunity *23*, 227-239.

Anderson, M.S., Venanzi, E.S., Klein, L., Chen, Z., Berzins, S.P., Turley, S.J., von Boehmer, H., Bronson, R., Dierich, A., Benoist, C*., et al.* (2002). Projection of an immunological self shadow within the thymus by the aire protein. Science (New York, NY *298*, 1395-1401.

Andrade, W., Johnston, M.G., and Hay, J.B. (1996). The exit of lymphocytes and RBCs from the peritoneal cavity of sheep. Immunobiology *195*, 77-90.

Aparisi, L., Farre, A., Gomez-Cambronero, L., Martinez, J., De Las Heras, G., Corts, J., Navarro, S., Mora, J., Lopez-Hoyos, M., Sabater, L*., et al.* (2005). Antibodies to carbonic anhydrase and IgG4 levels in idiopathic chronic pancreatitis: relevance for diagnosis of autoimmune pancreatitis. Gut *54*, 703-709.

Araten, D.J., Golde, D.W., Zhang, R.H., Thaler, H.T., Gargiulo, L., Notaro, R., and Luzzatto, L. (2005). A quantitative measurement of the human somatic mutation rate. Cancer research *65*, 8111-8117.

Arstila, T.P., Casrouge, A., Baron, V., Even, J., Kanellopoulos, J., and Kourilsky, P. (1999). A direct estimate of the human alphabeta T cell receptor diversity. Science (New York, NY *286*, 958-961.

Asada, M., Nishio, A., Uchida, K., Kido, M., Ueno, S., Uza, N., Kiriya, K., Inoue, S., Kitamura, H., Ohashi, S.*, et al.* (2006). Identification of a novel autoantibody against pancreatic secretory trypsin inhibitor in patients with autoimmune pancreatitis. Pancreas *33*, 20-26.

Asano, K., Matsushita, T., Umeno, J., Hosono, N., Takahashi, A., Kawaguchi, T., Matsumoto, T., Matsui, T., Kakuta, Y., Kinouchi, Y.*, et al.* (2009). A genome-wide association study identifies three new susceptibility loci for ulcerative colitis in the Japanese population. Nature genetics *41*, 1325-1329.

Bachmaier, K., Krawczyk, C., Kozieradzki, I., Kong, Y.Y., Sasaki, T., Oliveira-dos-Santos, A., Mariathasan, S., Bouchard, D., Wakeham, A., Itie, A.*, et al.* (2000). Negative regulation of lymphocyte activation and autoimmunity by the molecular adaptor Cbl-b. Nature *403*, 211-216.

Barrett, J.C., Clayton, D.G., Concannon, P., Akolkar, B., Cooper, J.D., Erlich, H.A., Julier, C., Morahan, G., Nerup, J., Nierras, C.*, et al.* (2009). Genome-wide association study and meta-analysis find that over 40 loci affect risk of type 1 diabetes. Nature genetics.

Barthlott, T., Kassiotis, G., and Stockinger, B. (2003). T cell regulation as a side effect of homeostasis and competition. The Journal of experimental medicine *197*, 451-460.

Bell, J.J., and Bhandoola, A. (2008). The earliest thymic progenitors for T cells possess myeloid lineage potential. Nature *452*, 764-767.

Bendelac, A., Carnaud, C., Boitard, C., and Bach, J.F. (1987). Syngeneic transfer of autoimmune diabetes from diabetic NOD mice to healthy neonates. Requirement for both L3T4+ and Lyt-2+ T cells. The Journal of experimental medicine *166*, 823-832.

Bennett, C.L., Christie, J., Ramsdell, F., Brunkow, M.E., Ferguson, P.J., Whitesell, L., Kelly, T.E., Saulsbury, F.T., Chance, P.F., and Ochs, H.D. (2001). The immune dysregulation, polyendocrinopathy, enteropathy, X-linked syndrome (IPEX) is caused by mutations of FOXP3. Nature genetics *27*, 20-21.

Berg, L.J., Pullen, A.M., Fazekas de St Groth, B., Mathis, D., Benoist, C., and Davis, M.M. (1989). Antigen/MHC-specific T cells are preferentially exported from the thymus in the presence of their MHC ligand. Cell *58*, 1035-1046.

Bernatsky, S., Boivin, J.F., Joseph, L., Rajan, R., Zoma, A., Manzi, S., Ginzler, E., Urowitz, M., Gladman, D., Fortin, P.R.*, et al.* (2005). An international cohort study of cancer in systemic lupus erythematosus. Arthritis and rheumatism *52*, 1481-1490.

Bertossi, A., Aichinger, M., Sansonetti, P., Lech, M., Neff, F., Pal, M., Wunderlich, F.T., Anders, H.J., Klein, L., and Schmidt-Supprian, M. (2011). Loss of Roquin induces early death and immune deregulation but not autoimmunity. The Journal of experimental medicine *208*, 1749-1756.

Betterle, C., Greggio, N.A., and Volpato, M. (1998). Clinical review 93: Autoimmune polyglandular syndrome type 1. The Journal of clinical endocrinology and metabolism *83*, 1049-1055.

Bielekova, B., Goodwin, B., Richert, N., Cortese, I., Kondo, T., Afshar, G., Gran, B., Eaton, J., Antel, J., Frank, J.A., *et al.* (2000). Encephalitogenic potential of the myelin basic protein peptide (amino acids 83-99) in multiple sclerosis: results of a phase II clinical trial with an altered peptide ligand. Nature medicine *6*, 1167-1175.

Billingham, R.E., Brent, L., and Medawar, P.B. (1953). Actively acquired tolerance of foreign cells. Nature *172*, 603-606.

Bjorses, P., Aaltonen, J., Horelli-Kuitunen, N., Yaspo, M.L., and Peltonen, L. (1998). Gene defect behind APECED: a new clue to autoimmunity. Human molecular genetics *7*, 1547-1553.

Blechschmidt, K., Schweiger, M., Wertz, K., Poulson, R., Christensen, H.M., Rosenthal, A., Lehrach, H., and Yaspo, M.L. (1999). The mouse Aire gene: comparative genomic sequencing, gene organization, and expression. Genome research *9*, 158-166.

Borgulya, P., Kishi, H., Uematsu, Y., and von Boehmer, H. (1992). Exclusion and inclusion of alpha and beta T cell receptor alleles. Cell *69*, 529-537.

Bouillet, P., Metcalf, D., Huang, D.C., Tarlinton, D.M., Kay, T.W., Kontgen, F., Adams, J.M., and Strasser, A. (1999). Proapoptotic Bcl-2 relative Bim required for certain apoptotic responses, leukocyte homeostasis, and to preclude autoimmunity. Science (New York, NY *286*, 1735-1738.

Bouillet, P., Purton, J.F., Godfrey, D.I., Zhang, L.C., Coultas, L., Puthalakath, H., Pellegrini, M., Cory, S., Adams, J.M., and Strasser, A. (2002). BH3-only Bcl-2 family member Bim is required for apoptosis of autoreactive thymocytes. Nature *415*, 922-926.

Bretscher, P., and Cohn, M. (1970). A theory of self-nonself discrimination. Science (New York, NY *169*, 1042-1049.

Brunkow, M.E., Jeffery, E.W., Hjerrild, K.A., Paeper, B., Clark, L.B., Yasayko, S.A., Wilkinson, J.E., Galas, D., Ziegler, S.F., and Ramsdell, F. (2001). Disruption of a new forkhead/winged-helix protein, scurfin, results in the fatal lymphoproliferative disorder of the scurfy mouse. Nature genetics *27*, 68-73.

Brunner, T., Mogil, R.J., LaFace, D., Yoo, N.J., Mahboubi, A., Echeverri, F., Martin, S.J., Force, W.R., Lynch, D.H., Ware, C.F., *et al.* (1995). Cell-autonomous Fas (CD95)/Fas-ligand interaction mediates activation-induced apoptosis in T-cell hybridomas. Nature *373*, 441-444.

Buckner, J.H., and Ziegler, S.F. (2008). Functional analysis of FOXP3. Annals of the New York Academy of Sciences *1143*, 151-169.

Burnet, F.M. (1959). The clonal selection theory of acquired immunity. (London, Cambridge University Press).

Burnet, F.M. (1976). A modification of Jerne's theory of antibody production using the concept of clonal selection. CA: a cancer journal for clinicians *26*, 119-121.

Burnet, F.M., and Fenner, F. (1948). Genetics and immunology. Heredity *2*, 289-324.

Burnett, F.M. (1972). Autoimmunity and autoimmune diseases (Lancaster,UK, Medical and Technical Publishing Co Ltd).

Campbell, I.L., Oxbrow, L., and Harrison, L.C. (1991). Reduction in insulitis following administration of IFN-gamma and TNF-alpha in the NOD mouse. Journal of autoimmunity *4*, 249-262.

Casanova, J.L., Romero, P., Widmann, C., Kourilsky, P., and Maryanski, J.L. (1991). T cell receptor genes in a series of class I major histocompatibility complex-restricted cytotoxic T lymphocyte clones specific for a Plasmodium berghei nonapeptide: implications for T cell allelic exclusion and antigen-specific repertoire. The Journal of experimental medicine *174*, 1371-1383.

Casrouge, A., Beaudoing, E., Dalle, S., Pannetier, C., Kanellopoulos, J., and Kourilsky, P. (2000). Size estimate of the alpha beta TCR repertoire of naive mouse splenocytes. J Immunol *164*, 5782-5787.

Catera, R., Silverman, G.J., Hatzi, K., Seiler, T., Didier, S., Zhang, L., Herve, M., Meffre, E., Oscier, D.G., Vlassara, H.*, et al.* (2008). Chronic lymphocytic leukemia cells recognize conserved epitopes associated with apoptosis and oxidation. Molecular medicine (Cambridge, Mass *14*, 665-674.

Cetani, F., Barbesino, G., Borsari, S., Pardi, E., Cianferotti, L., Pinchera, A., and Marcocci, C. (2001). A novel mutation of the autoimmune regulator gene in an Italian kindred with autoimmune polyendocrinopathy-candidiasis-ectodermal dystrophy, acting in a dominant fashion and strongly cosegregating with hypothyroid autoimmune thyroiditis. The Journal of clinical endocrinology and metabolism *86*, 4747-4752.

Chang, M., Jin, W., Chang, J.H., Xiao, Y., Brittain, G.C., Yu, J., Zhou, X., Wang, Y.H., Cheng, X., Li, P.*, et al.* (2011). The ubiquitin ligase Peli1 negatively regulates T cell activation and prevents autoimmunity. Nature immunology.

Chatila, T.A., Blaeser, F., Ho, N., Lederman, H.M., Voulgaropoulos, C., Helms, C., and Bowcock, A.M. (2000). JM2, encoding a fork head-related protein, is mutated in X-linked autoimmunity-allergic disregulation syndrome. The Journal of clinical investigation *106*, R75-81.

Chen, Z., Benoist, C., and Mathis, D. (2005). How defects in central tolerance impinge on a deficiency in regulatory T cells. Proceedings of the National Academy of Sciences of the United States of America *102*, 14735-14740.

Cheng, L.E., Chan, F.K., Cado, D., and Winoto, A. (1997). Functional redundancy of the Nur77 and Nor-1 orphan steroid receptors in T-cell apoptosis. The EMBO journal *16*, 1865-1875.

Chiang, Y.J., Kole, H.K., Brown, K., Naramura, M., Fukuhara, S., Hu, R.J., Jang, I.K., Gutkind, J.S., Shevach, E., and Gu, H. (2000). Cbl-b regulates the CD28 dependence of T-cell activation. Nature *403*, 216-220.

Choisy-Rossi, C.M., Holl, T.M., Pierce, M.A., Chapman, H.D., and Serreze, D.V. (2004). Enhanced pathogenicity of diabetogenic T cells escaping a non-MHC gene-controlled near death experience. J Immunol *173*, 3791-3800.

Christianson, S.W., Shultz, L.D., and Leiter, E.H. (1993). Adoptive transfer of diabetes into immunodeficient NOD-scid/scid mice. Relative contributions of CD4+ and CD8+ T-cells from diabetic versus prediabetic NOD.NON-Thy-1a donors. Diabetes *42*, 44-55.

Chu, C.C., Catera, R., Zhang, L., Didier, S., Agagnina, B.M., Damle, R.N., Kaufman, M.S., Kolitz, J.E., Allen, S.L., Rai, K.R., *et al.* (2010). Many chronic lymphocytic leukemia antibodies recognize apoptotic cells with exposed nonmuscle myosin heavy chain IIA: implications for patient outcome and cell of origin. Blood *115*, 3907-3915.

Chuang, W.Y., Strobel, P., Belharazem, D., Rieckmann, P., Toyka, K.V., Nix, W., Schalke, B., Gold, R., Kiefer, R., Klinker, E., *et al.* (2009). The PTPN22gain-of-function+1858T(+) genotypes correlate with low IL-2 expression in thymomas and predispose to myasthenia gravis. Genes and immunity *10*, 667-672.

Cohen, J.N., Guidi, C.J., Tewalt, E.F., Qiao, H., Rouhani, S.J., Ruddell, A., Farr, A.G., Tung, K.S., and Engelhard, V.H. (2010). Lymph node-resident lymphatic endothelial cells mediate peripheral tolerance via Aire-independent direct antigen presentation. The Journal of experimental medicine.

Cohen, P.L., and Eisenberg, R.A. (1991). Lpr and gld: single gene models of systemic autoimmunity and lymphoproliferative disease. Annual review of immunology *9*, 243-269.

Collins, A., Littman, D.R., and Taniuchi, I. (2009). RUNX proteins in transcription factor networks that regulate T-cell lineage choice. Nat Rev Immunol *9*, 106-115.

Comabella, M., Craig, D.W., Camina-Tato, M., Morcillo, C., Lopez, C., Navarro, A., Rio, J., Montalban, X., and Martin, R. (2008). Identification of a novel risk locus for multiple sclerosis at 13q31.3 by a pooled genome-wide scan of 500,000 single nucleotide polymorphisms. PloS one *3*, e3490.

Consortium, F.-G.A. (1997). An autoimmune disease, APECED, caused by mutations in a novel gene featuring two PHD-type zinc-finger domains. Nature genetics *17*, 399-403.

Consortium, W.T. (2007). Genome-wide association study of 14,000 cases of seven common diseases and 3,000 shared controls. Nature *447*, 661-678.

Coombes, J.L., Siddiqui, K.R., Arancibia-Carcamo, C.V., Hall, J., Sun, C.M., Belkaid, Y., and Powrie, F. (2007). A functionally specialized population of mucosal CD103+ DCs induces Foxp3+ regulatory T cells via a TGF-beta and retinoic acid-dependent mechanism. The Journal of experimental medicine *204*, 1757-1764.

Cooper, J.D., Smyth, D.J., Smiles, A.M., Plagnol, V., Walker, N.M., Allen, J.E., Downes, K., Barrett, J.C., Healy, B.C., Mychaleckyj, J.C., *et al.* (2008). Meta-analysis of genome-wide association study data identifies additional type 1 diabetes risk loci. Nature genetics *40*, 1399-1401.

Cornall, R.J., Cyster, J.G., Hibbs, M.L., Dunn, A.R., Otipoby, K.L., Clark, E.A., and Goodnow, C.C. (1998). Polygenic autoimmune traits: Lyn, CD22, and SHP-1 are limiting elements of a biochemical pathway regulating BCR signaling and selection. Immunity *8*, 497-508.

Corrado, L., Bergamaschi, L., Barizzone, N., Fasano, M.E., Guerini, F.R., Salvetti, M., Galimberti, D., Benedetti, M.D., Leone, M., and D'Alfonso, S. (2010). Association of the CBLB gene with multiple sclerosis: new evidence from a replication study in an Italian population. Journal of medical genetics *48*, 210-211.

Cosgrove, D., Gray, D., Dierich, A., Kaufman, J., Lemeur, M., Benoist, C., and Mathis, D. (1991). Mice lacking MHC class II molecules. Cell *66*, 1051-1066.

Culp, K.S., Fleming, C.R., Duffy, J., Baldus, W.P., and Dickson, E.R. (1982). Autoimmune associations in primary biliary cirrhosis. Mayo Clinic proceedings *57*, 365-370.

Daniel, D., and Wegmann, D.R. (1996). Protection of nonobese diabetic mice from diabetes by intranasal or subcutaneous administration of insulin peptide B-(9-23). Proceedings of the National Academy of Sciences of the United States of America *93*, 956-960.

Dash, P., McClaren, J.L., Oguin, T.H., 3rd, Rothwell, W., Todd, B., Morris, M.Y., Becksfort, J., Reynolds, C., Brown, S.A., Doherty, P.C.*, et al.* (2011). Paired analysis of TCRalpha and TCRbeta chains at the single-cell level in mice. The Journal of clinical investigation *121*, 288-295.

Davis, M.M., and Bjorkman, P.J. (1988). T-cell antigen receptor genes and T-cell recognition. Nature *334*, 395-402.

De Jager, P.L., Jia, X., Wang, J., de Bakker, P.I., Ottoboni, L., Aggarwal, N.T., Piccio, L., Raychaudhuri, S., Tran, D., Aubin, C.*, et al.* (2009). Meta-analysis of genome scans and replication identify CD6, IRF8 and TNFRSF1A as new multiple sclerosis susceptibility loci. Nature genetics *41*, 776-782.

Derbinski, J., Gabler, J., Brors, B., Tierling, S., Jonnakuty, S., Hergenhahn, M., Peltonen, L., Walter, J., and Kyewski, B. (2005). Promiscuous gene expression in thymic epithelial cells is regulated at multiple levels. The Journal of experimental medicine *202*, 33-45.

Derbinski, J., Pinto, S., Rosch, S., Hexel, K., and Kyewski, B. (2008). Promiscuous gene expression patterns in single medullary thymic epithelial cells argue for a stochastic mechanism. Proceedings of the National Academy of Sciences of the United States of America *105*, 657-662.

Derbinski, J., Schulte, A., Kyewski, B., and Klein, L. (2001). Promiscuous gene expression in medullary thymic epithelial cells mirrors the peripheral self. Nature immunology *2*, 1032-1039.

Desai-Mehta, A., Mao, C., Rajagopalan, S., Robinson, T., and Datta, S.K. (1995). Structure and specificity of T cell receptors expressed by potentially pathogenic anti-DNA autoantibody-inducing T cells in human lupus. The Journal of clinical investigation *95*, 531-541.

DeVoss, J., Hou, Y., Johannes, K., Lu, W., Liou, G.I., Rinn, J., Chang, H., Caspi, R.R., Fong, L., and Anderson, M.S. (2006). Spontaneous autoimmunity prevented by thymic

expression of a single self-antigen. The Journal of experimental medicine *203*, 2727-2735.

DeVoss, J.J., and Anderson, M.S. (2007). Lessons on immune tolerance from the monogenic disease APS1. Current opinion in genetics & development *17*, 193-200.

DeVoss, J.J., LeClair, N.P., Hou, Y., Grewal, N.K., Johannes, K.P., Lu, W., Yang, T., Meagher, C., Fong, L., Strauss, E.C.*, et al.* (2010). An autoimmune response to odorant binding protein 1a is associated with dry eye in the Aire-deficient mouse. J Immunol *184*, 4236-4246.

DiLorenzo, T.P., Graser, R.T., Ono, T., Christianson, G.J., Chapman, H.D., Roopenian, D.C., Nathenson, S.G., and Serreze, D.V. (1998). Major histocompatibility complex class I-restricted T cells are required for all but the end stages of diabetes development in nonobese diabetic mice and use a prevalent T cell receptor alpha chain gene rearrangement. Proceedings of the National Academy of Sciences of the United States of America *95*, 12538-12543.

DiLorenzo, T.P., and Serreze, D.V. (2005). The good turned ugly: immunopathogenic basis for diabetogenic CD8+ T cells in NOD mice. Immunological reviews *204*, 250-263.

Doniz-Padilla, L., Martinez-Jimenez, V., Nino-Moreno, P., Abud-Mendoza, C., Hernandez-Castro, B., Gonzalez-Amaro, R., Layseca-Espinosa, E., and Baranda-Candido, L. (2011). Expression and function of Cbl-b in T cells from patients with systemic lupus erythematosus, and detection of the 2126 A/G Cblb gene polymorphism in the Mexican mestizo population. Lupus *20*, 628-635.

Dubois, P.C., Trynka, G., Franke, L., Hunt, K.A., Romanos, J., Curtotti, A., Zhernakova, A., Heap, G.A., Adany, R., Aromaa, A.*, et al.* (2010). Multiple common variants for celiac disease influencing immune gene expression. Nature genetics *42*, 295-302.

Ebert, P.J., Li, Q.J., Huppa, J.B., and Davis, M.M. (2010). Functional development of the T cell receptor for antigen. Progress in molecular biology and translational science *92*, 65-100.

Ege, M., Ma, Y., Manfras, B., Kalwak, K., Lu, H., Lieber, M.R., Schwarz, K., and Pannicke, U. (2005). Omenn syndrome due to ARTEMIS mutations. Blood *105*, 4179-4186.

Erhrlich, P. (1901). Die Schutzstoffe des blutes. Dtsch Med Wochenschr *27*, 888–891.

Ernst, B., Lee, D.S., Chang, J.M., Sprent, J., and Surh, C.D. (1999). The peptide ligands mediating positive selection in the thymus control T cell survival and homeostatic proliferation in the periphery. Immunity *11*, 173-181.

Fang, D., and Liu, Y.C. (2001). Proteolysis-independent regulation of PI3K by Cbl-b-mediated ubiquitination in T cells. Nature immunology *2*, 870-875.

Fischer, A., Rieux-Laucat, F., and Le Deist, F. (2000). Autoimmune lymphoproliferative syndromes (ALPS): models for the study of peripheral tolerance. Reviews in immunogenetics *2*, 52-60.

Fisher, G.H., Rosenberg, F.J., Straus, S.E., Dale, J.K., Middleton, L.A., Lin, A.Y., Strober, W., Lenardo, M.J., and Puck, J.M. (1995). Dominant interfering Fas gene mutations impair apoptosis in a human autoimmune lymphoproliferative syndrome. Cell *81*, 935-946.

Fletcher, A.L., Seach, N., Reiseger, J.J., Lowen, T.E., Hammett, M.V., Scott, H.S., and Boyd, R.L. (2009). Reduced thymic Aire expression and abnormal NF-kappa B2 signaling in a model of systemic autoimmunity. J Immunol *182*, 2690-2699.

Fontenot, J.D., Gavin, M.A., and Rudensky, A.Y. (2003). Foxp3 programs the development and function of CD4+CD25+ regulatory T cells. Nature immunology *4*, 330-336.

Ford, M.S., Young, K.J., Zhang, Z., Ohashi, P.S., and Zhang, L. (2002). The immune regulatory function of lymphoproliferative double negative T cells in vitro and in vivo. The Journal of experimental medicine *196*, 261-267.

Fortner, K.A., Bouillet, P., Strasser, A., and Budd, R.C. (2010). Apoptosis regulators Fas and Bim synergistically control T-lymphocyte homeostatic proliferation. European journal of immunology.

Frank, J., Pignata, C., Panteleyev, A.A., Prowse, D.M., Baden, H., Weiner, L., Gaetaniello, L., Ahmad, W., Pozzi, N., Cserhalmi-Friedman, P.B.*, et al.* (1999). Exposing the human nude phenotype. Nature *398*, 473-474.

Franke, A., Balschun, T., Karlsen, T.H., Hedderich, J., May, S., Lu, T., Schuldt, D., Nikolaus, S., Rosenstiel, P., Krawczak, M.*, et al.* (2008). Replication of signals from recent studies of Crohn's disease identifies previously unknown disease loci for ulcerative colitis. Nature genetics *40*, 713-715.

Franke, A., Balschun, T., Sina, C., Ellinghaus, D., Hasler, R., Mayr, G., Albrecht, M., Wittig, M., Buchert, E., Nikolaus, S.*, et al.* (2010). Genome-wide association study for ulcerative colitis identifies risk loci at 7q22 and 22q13 (IL17REL). Nature genetics *42*, 292-294.

Frulloni, L., Lunardi, C., Simone, R., Dolcino, M., Scattolini, C., Falconi, M., Benini, L., Vantini, I., Corrocher, R., and Puccetti, A. (2009). Identification of a novel antibody associated with autoimmune pancreatitis. The New England journal of medicine *361*, 2135-2142.

Gambineri, E., Torgerson, T.R., and Ochs, H.D. (2003). Immune dysregulation, polyendocrinopathy, enteropathy, and X-linked inheritance (IPEX), a syndrome of systemic autoimmunity caused by mutations of FOXP3, a critical regulator of T-cell homeostasis. Current opinion in rheumatology *15*, 430-435.

Gao, J.X., Zhang, H., Bai, X.F., Wen, J., Zheng, X., Liu, J., Zheng, P., and Liu, Y. (2002). Perinatal blockade of b7-1 and b7-2 inhibits clonal deletion of highly pathogenic autoreactive T cells. The Journal of experimental medicine *195*, 959-971.

Gardner, J.M., Devoss, J.J., Friedman, R.S., Wong, D.J., Tan, Y.X., Zhou, X., Johannes, K.P., Su, M.A., Chang, H.Y., Krummel, M.F., *et al.* (2008). Deletional tolerance mediated by extrathymic Aire-expressing cells. Science (New York, NY *321*, 843-847.

Gascoigne, N.R., Chien, Y., Becker, D.M., Kavaler, J., and Davis, M.M. (1984). Genomic organization and sequence of T-cell receptor beta-chain constant- and joining-region genes. Nature *310*, 387-391.

Gavanescu, I., Benoist, C., and Mathis, D. (2008). B cells are required for Aire-deficient mice to develop multi-organ autoinflammation: A therapeutic approach for APECED patients. Proceedings of the National Academy of Sciences of the United States of America *105*, 13009-13014.

Gavanescu, I., Kessler, B., Ploegh, H., Benoist, C., and Mathis, D. (2007). Loss of Aire-dependent thymic expression of a peripheral tissue antigen renders it a target of autoimmunity. Proceedings of the National Academy of Sciences of the United States of America *104*, 4583-4587.

Genain, C.P., and Zamvil, S.S. (2000). Specific immunotherapy: one size does not fit all. Nature medicine *6*, 1098-1100.

Gennery, A.R., Hodges, E., Williams, A.P., Harris, S., Villa, A., Angus, B., Cant, A.J., and Smith, J.L. (2005). Omenn's syndrome occurring in patients without mutations in recombination activating genes. Clinical immunology (Orlando, Fla *116*, 246-256.

Giraud, M., Yoshida, H., Abramson, J., Rahl, P.B., Young, R.A., Mathis, D., and Benoist, C. (2012). Aire unleashes stalled RNA polymerase to induce ectopic gene expression in thymic epithelial cells. Proceedings of the National Academy of Sciences of the United States of America *109*, 535-540.

Giudicelli, V., Duroux, P., Ginestoux, C., Folch, G., Jabado-Michaloud, J., Chaume, D., and Lefranc, M.P. (2006). IMGT/LIGM-DB, the IMGT comprehensive database of immunoglobulin and T cell receptor nucleotide sequences. Nucleic acids research *34*, D781-784.

Godfrey, D.I., Kennedy, J., Suda, T., and Zlotnik, A. (1993). A developmental pathway involving four phenotypically and functionally distinct subsets of CD3-CD4-CD8-triple-negative adult mouse thymocytes defined by CD44 and CD25 expression. J Immunol *150*, 4244-4252.

Goldrath, A.W., and Bevan, M.J. (1999). Low-affinity ligands for the TCR drive proliferation of mature CD8+ T cells in lymphopenic hosts. Immunity *11*, 183-190.

Gong, Q., Cheng, A.M., Akk, A.M., Alberola-Ila, J., Gong, G., Pawson, T., and Chan, A.C. (2001). Disruption of T cell signaling networks and development by Grb2 haploid insufficiency. Nature immunology *2*, 29-36.

Goodnow, C.C. (2007). Multistep pathogenesis of autoimmune disease. Cell *130*, 25-35.

Goodnow, C.C., Crosbie, J., Adelstein, S., Lavoie, T.B., Smith-Gill, S.J., Brink, R.A., Pritchard-Briscoe, H., Wotherspoon, J.S., Loblay, R.H., Raphael, K., *et al.* (1988).

Altered immunoglobulin expression and functional silencing of self-reactive B lymphocytes in transgenic mice. Nature *334*, 676-682.

Goodnow, C.C., Sprent, J., Fazekas de St Groth, B., and Vinuesa, C.G. (2005). Cellular and genetic mechanisms of self tolerance and autoimmunity. Nature *435*, 590-597.

Goransson, L.G., Herigstad, A., Tjensvoll, A.B., Harboe, E., Mellgren, S.I., and Omdal, R. (2006). Peripheral neuropathy in primary sjogren syndrome: a population-based study. Archives of neurology *63*, 1612-1615.

Graham, R.R., Cotsapas, C., Davies, L., Hackett, R., Lessard, C.J., Leon, J.M., Burtt, N.P., Guiducci, C., Parkin, M., Gates, C.*, et al.* (2008). Genetic variants near TNFAIP3 on 6q23 are associated with systemic lupus erythematosus. Nature genetics *40*, 1059-1061.

Gray, D.H., Gavanescu, I., Benoist, C., and Mathis, D. (2007). Danger-free autoimmune disease in Aire-deficient mice. Proceedings of the National Academy of Sciences of the United States of America *104*, 18193-18198.

Gray, D.H., Seach, N., Ueno, T., Milton, M.K., Liston, A., Lew, A.M., Goodnow, C.C., and Boyd, R.L. (2006). Developmental kinetics, turnover, and stimulatory capacity of thymic epithelial cells. Blood *108*, 3777-3785.

Gronski, M.A., Boulter, J.M., Moskophidis, D., Nguyen, L.T., Holmberg, K., Elford, A.R., Deenick, E.K., Kim, H.O., Penninger, J.M., Odermatt, B.*, et al.* (2004). TCR affinity and negative regulation limit autoimmunity. Nature medicine *10*, 1234-1239.

Guarneri, F., Guarneri, C., and Benvenga, S. (2005). Helicobacter pylori and autoimmune pancreatitis: role of carbonic anhydrase via molecular mimicry? Journal of cellular and molecular medicine *9*, 741-744.

Haag-Liautard, C., Dorris, M., Maside, X., Macaskill, S., Halligan, D.L., Houle, D., Charlesworth, B., and Keightley, P.D. (2007). Direct estimation of per nucleotide and genomic deleterious mutation rates in Drosophila. Nature *445*, 82-85.

Hafler, D.A., Compston, A., Sawcer, S., Lander, E.S., Daly, M.J., De Jager, P.L., de Bakker, P.I., Gabriel, S.B., Mirel, D.B., Ivinson, A.J.*, et al.* (2007). Risk alleles for multiple sclerosis identified by a genomewide study. The New England journal of medicine *357*, 851-862.

Halonen, M., Eskelin, P., Myhre, A.G., Perheentupa, J., Husebye, E.S., Kampe, O., Rorsman, F., Peltonen, L., Ulmanen, I., and Partanen, J. (2002). AIRE mutations and human leukocyte antigen genotypes as determinants of the autoimmune polyendocrinopathy-candidiasis-ectodermal dystrophy phenotype. The Journal of clinical endocrinology and metabolism *87*, 2568-2574.

Halonen, M., Pelto-Huikko, M., Eskelin, P., Peltonen, L., Ulmanen, I., and Kolmer, M. (2001). Subcellular location and expression pattern of autoimmune regulator (Aire), the mouse orthologue for human gene defective in autoimmune polyendocrinopathy candidiasis ectodermal dystrophy (APECED). J Histochem Cytochem *49*, 197-208.

Han, B., Serra, P., Amrani, A., Yamanouchi, J., Maree, A.F., Edelstein-Keshet, L., and Santamaria, P. (2005a). Prevention of diabetes by manipulation of anti-IGRP autoimmunity: high efficiency of a low-affinity peptide. Nature medicine *11*, 645-652.

Han, B., Serra, P., Yamanouchi, J., Amrani, A., Elliott, J.F., Dickie, P., Dilorenzo, T.P., and Santamaria, P. (2005b). Developmental control of CD8 T cell-avidity maturation in autoimmune diabetes. The Journal of clinical investigation *115*, 1879-1887.

Han, J.W., Zheng, H.F., Cui, Y., Sun, L.D., Ye, D.Q., Hu, Z., Xu, J.H., Cai, Z.M., Huang, W., Zhao, G.P.*, et al.* (2009). Genome-wide association study in a Chinese Han population identifies nine new susceptibility loci for systemic lupus erythematosus. Nature genetics *41*, 1234-1237.

Hanahan, D. (1998). Peripheral-antigen-expressing cells in thymic medulla: factors in self-tolerance and autoimmunity. Current opinion in immunology *10*, 656-662.

Hanahan, D., and Weinberg, R.A. (2000). The hallmarks of cancer. Cell *100*, 57-70.

Hanahan, D., and Weinberg, R.A. (2011). Hallmarks of cancer: the next generation. Cell *144*, 646-674.

Hara, H., Wada, T., Bakal, C., Kozieradzki, I., Suzuki, S., Suzuki, N., Nghiem, M., Griffiths, E.K., Krawczyk, C., Bauer, B.*, et al.* (2003). The MAGUK family protein CARD11 is essential for lymphocyte activation. Immunity *18*, 763-775.

Harada, Y., Harada, Y., Elly, C., Ying, G., Paik, J.H., DePinho, R.A., and Liu, Y.C. (2010). Transcription factors Foxo3a and Foxo1 couple the E3 ligase Cbl-b to the induction of Foxp3 expression in induced regulatory T cells. The Journal of experimental medicine *207*, 1381-1391.

Havran, W.L., and Allison, J.P. (1988). Developmentally ordered appearance of thymocytes expressing different T-cell antigen receptors. Nature *335*, 443-445.

Hayday, A.C. (2009). Gammadelta T cells and the lymphoid stress-surveillance response. Immunity *31*, 184-196.

Hayes, S.M., and Love, P.E. (2007). A retrospective on the requirements for gammadelta T-cell development. Immunological reviews *215*, 8-14.

Heath, W.R., Carbone, F.R., Bertolino, P., Kelly, J., Cose, S., and Miller, J.F. (1995). Expression of two T cell receptor alpha chains on the surface of normal murine T cells. European journal of immunology *25*, 1617-1623.

Hein, W.R., and Mackay, C.R. (1991). Prominence of gamma delta T cells in the ruminant immune system. Immunology today *12*, 30-34.

Heino, M., Peterson, P., Kudoh, J., Nagamine, K., Lagerstedt, A., Ovod, V., Ranki, A., Rantala, I., Nieminen, M., Tuukkanen, J.*, et al.* (1999). Autoimmune regulator is expressed in the cells regulating immune tolerance in thymus medulla. Biochemical and biophysical research communications *257*, 821-825.

Heissmeyer, V., Macian, F., Im, S.H., Varma, R., Feske, S., Venuprasad, K., Gu, H., Liu, Y.C., Dustin, M.L., and Rao, A. (2004). Calcineurin imposes T cell unresponsiveness through targeted proteolysis of signaling proteins. Nature immunology *5*, 255-265.

Heissmeyer, V., and Rao, A. (2004). E3 ligases in T cell anergy--turning immune responses into tolerance. Sci STKE *2004*, pe29.

Helmick, C.G., Felson, D.T., Lawrence, R.C., Gabriel, S., Hirsch, R., Kwoh, C.K., Liang, M.H., Kremers, H.M., Mayes, M.D., Merkel, P.A*., et al.* (2008). Estimates of the prevalence of arthritis and other rheumatic conditions in the United States. Part I. Arthritis and rheumatism *58*, 15-25.

Hernandez, J., Aung, S., Marquardt, K., and Sherman, L.A. (2002). Uncoupling of proliferative potential and gain of effector function by CD8(+) T cells responding to self-antigens. The Journal of experimental medicine *196*, 323-333.

Hinterberger, M., Aichinger, M., da Costa, O.P., Voehringer, D., Hoffmann, R., and Klein, L. (2010). Autonomous role of medullary thymic epithelial cells in central CD4(+) T cell tolerance. Nature immunology *11*, 512-519.

Ho, W.Y., Cooke, M.P., Goodnow, C.C., and Davis, M.M. (1994). Resting and anergic B cells are defective in CD28-dependent costimulation of naive CD4+ T cells. The Journal of experimental medicine *179*, 1539-1549.

Hogquist, K.A., Jameson, S.C., Heath, W.R., Howard, J.L., Bevan, M.J., and Carbone, F.R. (1994). T cell receptor antagonist peptides induce positive selection. Cell *76*, 17-27.

Holler, P.D., Yamagata, T., Jiang, W., Feuerer, M., Benoist, C., and Mathis, D. (2007). The same genomic region conditions clonal deletion and clonal deviation to the CD8alphaalpha and regulatory T cell lineages in NOD versus C57BL/6 mice. Proceedings of the National Academy of Sciences of the United States of America *104*, 7187-7192.

Holst, J., Szymczak-Workman, A.L., Vignali, K.M., Burton, A.R., Workman, C.J., and Vignali, D.A. (2006a). Generation of T-cell receptor retrogenic mice. Nature protocols *1*, 406-417.

Holst, J., Vignali, K.M., Burton, A.R., and Vignali, D.A. (2006b). Rapid analysis of T-cell selection in vivo using T cell-receptor retrogenic mice. Nature methods *3*, 191-197.

Hong, J., Zang, Y.C., Tejada-Simon, M.V., Kozovska, M., Li, S., Singh, R.A., Yang, D., Rivera, V.M., Killian, J.K., and Zhang, J.Z. (1999). A common TCR V-D-J sequence in V beta 13.1 T cells recognizing an immunodominant peptide of myelin basic protein in multiple sclerosis. J Immunol *163*, 3530-3538.

Hori, S., Nomura, T., and Sakaguchi, S. (2003). Control of regulatory T cell development by the transcription factor Foxp3. Science (New York, NY *299*, 1057-1061.

Hou, Y., DeVoss, J., Dao, V., Kwek, S., Simko, J.P., McNeel, D.G., Anderson, M.S., and Fong, L. (2009). An aberrant prostate antigen-specific immune response causes prostatitis in mice and is associated with chronic prostatitis in humans. The Journal of clinical investigation *119*, 2031-2041.

Hoyne, G.F., Flening, E., Yabas, M., Teh, C., Altin, J.A., Randall, K., Thien, C.B., Langdon, W.Y., and Goodnow, C.C. (2011a). Visualizing the role of Cbl-b in control of islet-reactive CD4 T cells and susceptibility to type 1 diabetes. J Immunol *186*, 2024-2032.

Hoyne, G.F., Flening, E., Yabas, M., Teh, C., Altin, J.A., Randall, K., Thien, C.B., Langdon, W.Y., and Goodnow, C.C. (2011b). Visualizing the Role of Cbl-b in Control of Islet-Reactive CD4 T Cells and Susceptibility to Type 1 Diabetes. J Immunol.

Hu, Y., Shen, F., Crellin, N.K., and Ouyang, W. (2010). The IL-17 pathway as a major therapeutic target in autoimmune diseases. Annals of the New York Academy of Sciences *1217*, 60-76.

Hubert, F.X., Kinkel, S.A., Crewther, P.E., Cannon, P.Z., Webster, K.E., Link, M., Uibo, R., O'Bryan, M.K., Meager, A., Forehan, S.P.*, et al.* (2009). Aire-deficient C57BL/6 mice mimicking the common human 13-base pair deletion mutation present with only a mild autoimmune phenotype. J Immunol *182*, 3902-3918.

Husebye, E.S., Perheentupa, J., Rautemaa, R., and Kampe, O. (2009). Clinical manifestations and management of patients with autoimmune polyendocrine syndrome type I. Journal of internal medicine *265*, 514-529.

Hussain, R., Dawood, G., Abrar, N., Toossi, Z., Minai, A., Dojki, M., and Ellner, J.J. (1995). Selective increases in antibody isotypes and immunoglobulin G subclass responses to secreted antigens in tuberculosis patients and healthy household contacts of the patients. Clinical and diagnostic laboratory immunology *2*, 726-732.

Hyttinen, V., Kaprio, J., Kinnunen, L., Koskenvuo, M., and Tuomilehto, J. (2003). Genetic liability of type 1 diabetes and the onset age among 22,650 young Finnish twin pairs: a nationwide follow-up study. Diabetes *52*, 1052-1055.

Irie, J., Wu, Y., Wicker, L.S., Rainbow, D., Nalesnik, M.A., Hirsch, R., Peterson, L.B., Leung, P.S., Cheng, C., Mackay, I.R.*, et al.* (2006). NOD.c3c4 congenic mice develop autoimmune biliary disease that serologically and pathogenetically models human primary biliary cirrhosis. The Journal of experimental medicine *203*, 1209-1219.

Ise, W., Kohyama, M., Nutsch, K.M., Lee, H.M., Suri, A., Unanue, E.R., Murphy, T.L., and Murphy, K.M. (2010). CTLA-4 suppresses the pathogenicity of self antigen-specific T cells by cell-intrinsic and cell-extrinsic mechanisms. Nature immunology *11*, 129-135.

Ishii, T., Suzuki, Y., Ando, N., Matsuo, N., and Ogata, T. (2000). Novel mutations of the autoimmune regulator gene in two siblings with autoimmune polyendocrinopathy-candidiasis-ectodermal dystrophy. The Journal of clinical endocrinology and metabolism *85*, 2922-2926.

Jeon, M.S., Atfield, A., Venuprasad, K., Krawczyk, C., Sarao, R., Elly, C., Yang, C., Arya, S., Bachmaier, K., Su, L.*, et al.* (2004). Essential role of the E3 ubiquitin ligase Cbl-b in T cell anergy induction. Immunity *21*, 167-177.

Jiang, W., Anderson, M.S., Bronson, R., Mathis, D., and Benoist, C. (2005). Modifier loci condition autoimmunity provoked by Aire deficiency. The Journal of experimental medicine *202*, 805-815.

Jin, C.X., Hayakawa, T., Kitagawa, M., and Ishiguro, H. (2009). Lactoferrin in chronic pancreatitis. Jop *10*, 237-241.

Johnston, R.J., Poholek, A.C., DiToro, D., Yusuf, I., Eto, D., Barnett, B., Dent, A.L., Craft, J., and Crotty, S. (2009). Bcl6 and Blimp-1 are reciprocal and antagonistic regulators of T follicular helper cell differentiation. Science (New York, NY *325*, 1006-1010.

Jolicoeur, C., Hanahan, D., and Smith, K.M. (1994). T-cell tolerance toward a transgenic beta-cell antigen and transcription of endogenous pancreatic genes in thymus. Proceedings of the National Academy of Sciences of the United States of America *91*, 6707-6711.

Jordan, M.S., Boesteanu, A., Reed, A.J., Petrone, A.L., Holenbeck, A.E., Lerman, M.A., Naji, A., and Caton, A.J. (2001). Thymic selection of CD4+CD25+ regulatory T cells induced by an agonist self-peptide. Nature immunology *2*, 301-306.

Josefowicz, S.Z., and Rudensky, A. (2009). Control of regulatory T cell lineage commitment and maintenance. Immunity *30*, 616-625.

Jun, J.E., Wilson, L.E., Vinuesa, C.G., Lesage, S., Blery, M., Miosge, L.A., Cook, M.C., Kucharska, E.M., Hara, H., Penninger, J.M.*, et al.* (2003). Identifying the MAGUK protein Carma-1 as a central regulator of humoral immune responses and atopy by genome-wide mouse mutagenesis. Immunity *18*, 751-762.

Kappler, J.W., Roehm, N., and Marrack, P. (1987). T cell tolerance by clonal elimination in the thymus. Cell *49*, 273-280.

Kappos, L., Comi, G., Panitch, H., Oger, J., Antel, J., Conlon, P., and Steinman, L. (2000). Induction of a non-encephalitogenic type 2 T helper-cell autoimmune response in multiple sclerosis after administration of an altered peptide ligand in a placebo-controlled, randomized phase II trial. The Altered Peptide Ligand in Relapsing MS Study Group. Nature medicine *6*, 1176-1182.

Kawahata, K., Misaki, Y., Yamauchi, M., Tsunekawa, S., Setoguchi, K., Miyazaki, J., and Yamamoto, K. (2002). Generation of CD4(+)CD25(+) regulatory T cells from autoreactive T cells simultaneously with their negative selection in the thymus and from nonautoreactive T cells by endogenous TCR expression. J Immunol *168*, 4399-4405.

Keating, G.M. (2010). Rituximab: a review of its use in chronic lymphocytic leukaemia, low-grade or follicular lymphoma and diffuse large B-cell lymphoma. Drugs *70*, 1445-1476.

Kedzierska, K., Valkenburg, S.A., Guillonneau, C., Hubert, F.X., Cukalac, T., Curtis, J.M., Stambas, J., Scott, H.S., Kedzierski, L., Venturi, V.*, et al.* (2010). Diversity and clonotypic composition of influenza-specific CD8+ TCR repertoires remain unaltered in the absence of Aire. European journal of immunology *40*, 849-858.

Keir, M.E., Francisco, L.M., and Sharpe, A.H. (2007). PD-1 and its ligands in T-cell immunity. Current opinion in immunology *19*, 309-314.

Kekalainen, E., Miettinen, A., and Arstila, T.P. (2007a). Does the deficiency of Aire in mice really resemble human APECED? Nat Rev Immunol *7*, 1.

Kekalainen, E., Tuovinen, H., Joensuu, J., Gylling, M., Franssila, R., Pontynen, N., Talvensaari, K., Perheentupa, J., Miettinen, A., and Arstila, T.P. (2007b). A defect of regulatory T cells in patients with autoimmune polyendocrinopathy-candidiasis-ectodermal dystrophy. J Immunol *178*, 1208-1215.

Khader, S.A., Gaffen, S.L., and Kolls, J.K. (2009). Th17 cells at the crossroads of innate and adaptive immunity against infectious diseases at the mucosa. Mucosal immunology *2*, 403-411.

Khattri, R., Cox, T., Yasayko, S.A., and Ramsdell, F. (2003). An essential role for Scurfin in CD4+CD25+ T regulatory cells. Nature immunology *4*, 337-342.

Kieper, W.C., Troy, A., Burghardt, J.T., Ramsey, C., Lee, J.Y., Jiang, H.Q., Dummer, W., Shen, H., Cebra, J.J., and Surh, C.D. (2005). Recent immune status determines the source of antigens that drive homeostatic T cell expansion. J Immunol *174*, 3158-3163.

Kirkham, T.H. (1969). Scleroderma and Sjogren's syndrome. The British journal of ophthalmology *53*, 131-133.

Kisand, K., Boe Wolff, A.S., Podkrajsek, K.T., Tserel, L., Link, M., Kisand, K.V., Ersvaer, E., Perheentupa, J., Erichsen, M.M., Bratanic, N.*, et al.* (2010
). Chronic mucocutaneous candidiasis in APECED or thymoma patients correlates with autoimmunity to Th17-associated cytokines. The Journal of experimental medicine *207*, 299-308.

Kisand, K., Lilic, D., Casanova, J.L., Peterson, P., Meager, A., and Willcox, N. (2011). Mucocutaneous candidiasis and autoimmunity against cytokines in APECED and thymoma patients: clinical and pathogenetic implications. European journal of immunology *41*, 1517-1527.

Kishimoto, H., and Sprent, J. (1999a). Several different cell surface molecules control negative selection of medullary thymocytes. The Journal of experimental medicine *190*, 65-73.

Kishimoto, H., and Sprent, J. (1999b). Strong TCR ligation without costimulation causes rapid onset of Fas-dependent apoptosis of naive murine CD4+ T cells. J Immunol *163*, 1817-1826.

Kishimoto, H., and Sprent, J. (2001). A defect in central tolerance in NOD mice. Nature immunology *2*, 1025-1031.

Kishimoto, H., Surh, C.D., and Sprent, J. (1998). A role for Fas in negative selection of thymocytes in vivo. The Journal of experimental medicine *187*, 1427-1438.

Kisielow, P., Bluthmann, H., Staerz, U.D., Steinmetz, M., and von Boehmer, H. (1988). Tolerance in T-cell-receptor transgenic mice involves deletion of nonmature CD4+8+ thymocytes. Nature *333*, 742-746.

Klug, C.A., Cheshier, S., and Weissman, I.L. (2000). Inactivation of a GFP retrovirus occurs at multiple levels in long-term repopulating stem cells and their differentiated progeny. Blood *96*, 894-901.

Kojima, A., and Prehn, R.T. (1981). Genetic susceptibility to post-thymectomy autoimmune diseases in mice. Immunogenetics *14*, 15-27.

Krawczyk, C., Bachmaier, K., Sasaki, T., Jones, R.G., Snapper, S.B., Bouchard, D., Kozieradzki, I., Ohashi, P.S., Alt, F.W., and Penninger, J.M. (2000). Cbl-b is a negative regulator of receptor clustering and raft aggregation in T cells. Immunity *13*, 463-473.

Krueger, A., Fas, S.C., Baumann, S., and Krammer, P.H. (2003). The role of CD95 in the regulation of peripheral T-cell apoptosis. Immunological reviews *193*, 58-69.

Kugathasan, S., Baldassano, R.N., Bradfield, J.P., Sleiman, P.M., Imielinski, M., Guthery, S.L., Cucchiara, S., Kim, C.E., Frackelton, E.C., Annaiah, K.*, et al.* (2008). Loci on 20q13 and 21q22 are associated with pediatric-onset inflammatory bowel disease. Nature genetics *40*, 1211-1215.

Kundig, T.M., Shahinian, A., Kawai, K., Mittrucker, H.W., Sebzda, E., Bachmann, M.F., Mak, T.W., and Ohashi, P.S. (1996). Duration of TCR stimulation determines costimulatory requirement of T cells. Immunity *5*, 41-52.

Kuroda, N., Mitani, T., Takeda, N., Ishimaru, N., Arakaki, R., Hayashi, Y., Bando, Y., Izumi, K., Takahashi, T., Nomura, T.*, et al.* (2005). Development of autoimmunity against transcriptionally unrepressed target antigen in the thymus of Aire-deficient mice. J Immunol *174*, 1862-1870.

Kurts, C., Carbone, F.R., Barnden, M., Blanas, E., Allison, J., Heath, W.R., and Miller, J.F. (1997a). CD4+ T cell help impairs CD8+ T cell deletion induced by cross-presentation of self-antigens and favors autoimmunity. The Journal of experimental medicine *186*, 2057-2062.

Kurts, C., Heath, W.R., Carbone, F.R., Allison, J., Miller, J.F., and Kosaka, H. (1996). Constitutive class I-restricted exogenous presentation of self antigens in vivo. The Journal of experimental medicine *184*, 923-930.

Kurts, C., Kosaka, H., Carbone, F.R., Miller, J.F., and Heath, W.R. (1997b). Class I-restricted cross-presentation of exogenous self-antigens leads to deletion of autoreactive CD8(+) T cells. The Journal of experimental medicine *186*, 239-245.

Laakso, S.M., Kekalainen, E., Rossi, L.H., Laurinolli, T.T., Mannerstrom, H., Heikkila, N., Lehtoviita, A., Perheentupa, J., Jarva, H., and Arstila, T.P. (2011). IL-7 Dysregulation and Loss of CD8+ T Cell Homeostasis in the Monogenic Human Disease Autoimmune Polyendocrinopathy-Candidiasis-Ectodermal Dystrophy. J Immunol.

Laakso, S.M., Laurinolli, T.T., Rossi, L.H., Lehtoviita, A., Sairanen, H., Perheentupa, J., Kekalainen, E., and Arstila, T.P. (2010). Regulatory T cell defect in APECED patients is associated with loss of naive FOXP3(+) precursors and impaired activated population. Journal of autoimmunity *35*, 351-357.

Laan, M., Kisand, K., Kont, V., Moll, K., Tserel, L., Scott, H.S., and Peterson, P. (2009). Autoimmune regulator deficiency results in decreased expression of CCR4 and CCR7 ligands and in delayed migration of CD4+ thymocytes. J Immunol *183*, 7682-7691.

Lafferty, K.J., and Cunningham, A.J. (1975). A new analysis of allogeneic interactions. The Australian journal of experimental biology and medical science *53*, 27-42.

Lathrop, S.K., Bloom, S.M., Rao, S.M., Nutsch, K., Lio, C.W., Santacruz, N., Peterson, D.A., Stappenbeck, T.S., and Hsieh, C.S. (2011). Peripheral education of the immune system by colonic commensal microbiota. Nature.

Laufer, T.M., DeKoning, J., Markowitz, J.S., Lo, D., and Glimcher, L.H. (1996). Unopposed positive selection and autoreactivity in mice expressing class II MHC only on thymic cortex. Nature *383*, 81-85.

Laurie, K.L., La Gruta, N.L., Koch, N., van Driel, I.R., and Gleeson, P.A. (2004). Thymic expression of a gastritogenic epitope results in positive selection of self-reactive pathogenic T cells. J Immunol *172*, 5994-6002.

Lee, J.W., Epardaud, M., Sun, J., Becker, J.E., Cheng, A.C., Yonekura, A.R., Heath, J.K., and Turley, S.J. (2007). Peripheral antigen display by lymph node stroma promotes T cell tolerance to intestinal self. Nature immunology *8*, 181-190.

Leishman, A.J., Naidenko, O.V., Attinger, A., Koning, F., Lena, C.J., Xiong, Y., Chang, H.C., Reinherz, E., Kronenberg, M., and Cheroutre, H. (2001). T cell responses modulated through interaction between CD8alphaalpha and the nonclassical MHC class I molecule, TL. Science (New York, NY *294*, 1936-1939.

Lennon, G.P., Bettini, M., Burton, A.R., Vincent, E., Arnold, P.Y., Santamaria, P., and Vignali, D.A. (2009). T cell islet accumulation in type 1 diabetes is a tightly regulated, cell-autonomous event. Immunity *31*, 643-653.

Leonard, M.F. (1946). Chronic idiopathic hypoparathyroidism with superimposed Addison's disease in a child. The Journal of clinical endocrinology and metabolism *6*, 493-506.

Lerman, M.A., Larkin, J., 3rd, Cozzo, C., Jordan, M.S., and Caton, A.J. (2004). CD4+ CD25+ regulatory T cell repertoire formation in response to varying expression of a neo-self-antigen. J Immunol *173*, 236-244.

Lesage, S., Hartley, S.B., Akkaraju, S., Wilson, J., Townsend, M., and Goodnow, C.C. (2002). Failure to censor forbidden clones of CD4 T cells in autoimmune diabetes. The Journal of experimental medicine *196*, 1175-1188.

Li, L., Salido, E., Zhou, Y., Bhattacharyya, S., Yannone, S.M., Dunn, E., Meneses, J., Feeney, A.J., and Cowan, M.J. (2005). Targeted disruption of the Artemis murine

counterpart results in SCID and defective V(D)J recombination that is partially corrected with bone marrow transplantation. J Immunol *174*, 2420-2428.

Li, M.O., Wan, Y.Y., and Flavell, R.A. (2007). T cell-produced transforming growth factor-beta1 controls T cell tolerance and regulates Th1- and Th17-cell differentiation. Immunity *26*, 579-591.

Lieberman, S.M., Evans, A.M., Han, B., Takaki, T., Vinnitskaya, Y., Caldwell, J.A., Serreze, D.V., Shabanowitz, J., Hunt, D.F., Nathenson, S.G.*, et al.* (2003). Identification of the beta cell antigen targeted by a prevalent population of pathogenic CD8+ T cells in autoimmune diabetes. Proceedings of the National Academy of Sciences of the United States of America *100*, 8384-8388.

Lindh, E., Lind, S.M., Lindmark, E., Hassler, S., Perheentupa, J., Peltonen, L., Winqvist, O., and Karlsson, M.C. (2008). AIRE regulates T-cell-independent B-cell responses through BAFF. Proceedings of the National Academy of Sciences of the United States of America *105*, 18466-18471.

Linsley, P.S., and Nadler, S.G. (2009). The clinical utility of inhibiting CD28-mediated costimulation. Immunological reviews *229*, 307-321.

Linterman, M.A., Rigby, R.J., Wong, R.K., Yu, D., Brink, R., Cannons, J.L., Schwartzberg, P.L., Cook, M.C., Walters, G.D., and Vinuesa, C.G. (2009). Follicular helper T cells are required for systemic autoimmunity. The Journal of experimental medicine *206*, 561-576.

Liston, A., Gray, D.H., Lesage, S., Fletcher, A.L., Wilson, J., Webster, K.E., Scott, H.S., Boyd, R.L., Peltonen, L., and Goodnow, C.C. (2004a). Gene dosage--limiting role of Aire in thymic expression, clonal deletion, and organ-specific autoimmunity. The Journal of experimental medicine *200*, 1015-1026.

Liston, A., Lesage, S., Gray, D.H., O'Reilly, L.A., Strasser, A., Fahrer, A.M., Boyd, R.L., Wilson, J., Baxter, A.G., Gallo, E.M.*, et al.* (2004b). Generalized resistance to thymic deletion in the NOD mouse; a polygenic trait characterized by defective induction of Bim. Immunity *21*, 817-830.

Liston, A., Lesage, S., Wilson, J., Peltonen, L., and Goodnow, C.C. (2003). Aire regulates negative selection of organ-specific T cells. Nature immunology *4*, 350-354.

Liston, A., Siggs, O.M., and Goodnow, C.C. (2007). Tracing the action of IL-2 in tolerance to islet-specific antigen. Immunology and cell biology *85*, 338-342.

Liu, Y., Helms, C., Liao, W., Zaba, L.C., Duan, S., Gardner, J., Wise, C., Miner, A., Malloy, M.J., Pullinger, C.R.*, et al.* (2008). A genome-wide association study of psoriasis and psoriatic arthritis identifies new disease loci. PLoS genetics *4*, e1000041.

Liu, Y.C. (2004). Ubiquitin ligases and the immune response. Annual review of immunology *22*, 81-127.

Macian, F., Garcia-Cozar, F., Im, S.H., Horton, H.F., Byrne, M.C., and Rao, A. (2002). Transcriptional mechanisms underlying lymphocyte tolerance. Cell *109*, 719-731.

Maldonado, M.A., Kakkanaiah, V., MacDonald, G.C., Chen, F., Reap, E.A., Balish, E., Farkas, W.R., Jennette, J.C., Madaio, M.P., Kotzin, B.L.*, et al.* (1999). The role of environmental antigens in the spontaneous development of autoimmunity in MRL-lpr mice. J Immunol *162*, 6322-6330.

Manolio, T.A., Collins, F.S., Cox, N.J., Goldstein, D.B., Hindorff, L.A., Hunter, D.J., McCarthy, M.I., Ramos, E.M., Cardon, L.R., Chakravarti, A.*, et al.* (2009). Finding the missing heritability of complex diseases. Nature *461*, 747-753.

Mariathasan, S., Zakarian, A., Bouchard, D., Michie, A.M., Zuniga-Pflucker, J.C., and Ohashi, P.S. (2001). Duration and strength of extracellular signal-regulated kinase signals are altered during positive versus negative thymocyte selection. J Immunol *167*, 4966-4973.

Markowitz, D., Goff, S., and Bank, A. (1988). A safe packaging line for gene transfer: separating viral genes on two different plasmids. Journal of virology *62*, 1120-1124.

Marrack, P., and Kappler, J. (2004). Control of T cell viability. Annual review of immunology *22*, 765-787.

Marx, A., Hohenberger, P., Hoffmann, H., Pfannschmidt, J., Schnabel, P., Hofmann, H.S., Wiebe, K., Schalke, B., Nix, W., Gold, R.*, et al.* (2010). The autoimmune regulator AIRE in thymoma biology: autoimmunity and beyond. J Thorac Oncol *5*, S266-272.

Matsumoto, M. (2011). Contrasting models for the roles of Aire in the differentiation program of epithelial cells in the thymic medulla. European journal of immunology *41*, 12-17.

Mavragani, C.P., and Crow, M.K. (2010). Activation of the type I interferon pathway in primary Sjogren's syndrome. Journal of autoimmunity *35*, 225-231.

McCarty, N., Paust, S., Ikizawa, K., Dan, I., Li, X., and Cantor, H. (2005). Signaling by the kinase MINK is essential in the negative selection of autoreactive thymocytes. Nature immunology *6*, 65-72.

McDevitt, H.O. (1980). Regulation of the immune response by the major histocompatibility system. The New England journal of medicine *303*, 1514-1517.

McDevitt, H.O., and Chinitz, A. (2004). Genetic control of the antibody responses: relationship between immune response and histocompatibility (H-2) type. 1969. J Immunol *173*, 1500-1501.

McDevitt, H.O., and Sela, M. (1965). Genetic control of the antibody response. I. Demonstration of determinant-specific differences in response to synthetic polypeptide antigens in two strains of inbred mice. The Journal of experimental medicine *122*, 517-531.

McIntire, K.R., Sell, S., and Miller, J.F. (1964). Pathogenesis of the Post-Neonatal Thymectomy Wasting Syndrome. Nature *204*, 151-155.

Meager, A., Visvalingam, K., Peterson, P., Moll, K., Murumagi, A., Krohn, K., Eskelin, P., Perheentupa, J., Husebye, E., Kadota, Y., *et al.* (2006). Anti-interferon autoantibodies in autoimmune polyendocrinopathy syndrome type 1. PLoS medicine *3*, e289.

Meagher, C., Tang, Q., Fife, B.T., Bour-Jordan, H., Wu, J., Pardoux, C., Bi, M., Melli, K., and Bluestone, J.A. (2008). Spontaneous development of a pancreatic exocrine disease in CD28-deficient NOD mice. J Immunol *180*, 7793-7803.

Meloni, A., Furcas, M., Cetani, F., Marcocci, C., Falorni, A., Perniola, R., Pura, M., Boe Wolff, A.S., Husebye, E.S., Lilic, D., *et al.* (2008). Autoantibodies against type I interferons as an additional diagnostic criterion for autoimmune polyendocrine syndrome type I. The Journal of clinical endocrinology and metabolism *93*, 4389-4397.

Miles, J.J., Douek, D.C., and Price, D.A. (2011). Bias in the alphabeta T-cell repertoire: implications for disease pathogenesis and vaccination. Immunology and cell biology *89*, 375-387.

Miller, B.J., Appel, M.C., O'Neil, J.J., and Wicker, L.S. (1988). Both the Lyt-2+ and L3T4+ T cell subsets are required for the transfer of diabetes in nonobese diabetic mice. J Immunol *140*, 52-58.

Miller, J.F. (1959). Role of the thymus in murine leukaemia. Nature *183*, 1069.

Miller, J.F. (1961). Immunological function of the thymus. Lancet *2*, 748-749.

Miller, J.F. (2011). The golden anniversary of the thymus. Nat Rev Immunol *11*, 489-495.

Molinero, L.L., Yang, J., Gajewski, T., Abraham, C., Farrar, M.A., and Alegre, M.L. (2009). CARMA1 controls an early checkpoint in the thymic development of FoxP3+ regulatory T cells. J Immunol *182*, 6736-6743.

Mombaerts, P., Iacomini, J., Johnson, R.S., Herrup, K., Tonegawa, S., and Papaioannou, V.E. (1992). RAG-1-deficient mice have no mature B and T lymphocytes. Cell *68*, 869-877.

Montefusco, P.P., Geiss, A.C., Bronzo, R.L., Randall, S., Kahn, E., and McKinley, M.J. (1984). Sclerosing cholangitis, chronic pancreatitis, and Sjogren's syndrome: a syndrome complex. American journal of surgery *147*, 822-826.

Mora, C., Wong, F.S., Chang, C.H., and Flavell, R.A. (1999). Pancreatic infiltration but not diabetes occurs in the relative absence of MHC class II-restricted CD4 T cells: studies using NOD/CIITA-deficient mice. J Immunol *162*, 4576-4588.

Moses, C.T., Thorstenson, K.M., Jameson, S.C., and Khoruts, A. (2003). Competition for self ligands restrains homeostatic proliferation of naive CD4 T cells. Proceedings of the National Academy of Sciences of the United States of America *100*, 1185-1190.

Mosmann, T.R., Cherwinski, H., Bond, M.W., Giedlin, M.A., and Coffman, R.L. (1986). Two types of murine helper T cell clone. I. Definition according to profiles of lymphokine activities and secreted proteins. J Immunol *136*, 2348-2357.

Musone, S.L., Taylor, K.E., Lu, T.T., Nititham, J., Ferreira, R.C., Ortmann, W., Shifrin, N., Petri, M.A., Kamboh, M.I., Manzi, S.*, et al.* (2008). Multiple polymorphisms in the TNFAIP3 region are independently associated with systemic lupus erythematosus. Nature genetics *40*, 1062-1064.

Nagamine, K., Peterson, P., Scott, H.S., Kudoh, J., Minoshima, S., Heino, M., Krohn, K.J., Lalioti, M.D., Mullis, P.E., Antonarakis, S.E.*, et al.* (1997). Positional cloning of the APECED gene. Nature genetics *17*, 393-398.

Nagata, M., Santamaria, P., Kawamura, T., Utsugi, T., and Yoon, J.W. (1994). Evidence for the role of CD8+ cytotoxic T cells in the destruction of pancreatic beta-cells in nonobese diabetic mice. J Immunol *152*, 2042-2050.

Nair, R.P., Duffin, K.C., Helms, C., Ding, J., Stuart, P.E., Goldgar, D., Gudjonsson, J.E., Li, Y., Tejasvi, T., Feng, B.J.*, et al.* (2009). Genome-wide scan reveals association of psoriasis with IL-23 and NF-kappaB pathways. Nature genetics *41*, 199-204.

Nakayama, M., Abiru, N., Moriyama, H., Babaya, N., Liu, E., Miao, D., Yu, L., Wegmann, D.R., Hutton, J.C., Elliott, J.F.*, et al.* (2005). Prime role for an insulin epitope in the development of type 1 diabetes in NOD mice. Nature *435*, 220-223.

Naramura, M., Jang, I.K., Kole, H., Huang, F., Haines, D., and Gu, H. (2002). c-Cbl and Cbl-b regulate T cell responsiveness by promoting ligand-induced TCR down-modulation. Nature immunology *3*, 1192-1199.

Naramura, M., Kole, H.K., Hu, R.J., and Gu, H. (1998). Altered thymic positive selection and intracellular signals in Cbl-deficient mice. Proceedings of the National Academy of Sciences of the United States of America *95*, 15547-15552.

Neighbors, M., Hartley, S.B., Xu, X., Castro, A.G., Bouley, D.M., and O'Garra, A. (2006). Breakpoints in immunoregulation required for Th1 cells to induce diabetes. European journal of immunology *36*, 2315-2323.

Nichols, L.A., Chen, Y., Colella, T.A., Bennett, C.L., Clausen, B.E., and Engelhard, V.H. (2007). Deletional self-tolerance to a melanocyte/melanoma antigen derived from tyrosinase is mediated by a radio-resistant cell in peripheral and mesenteric lymph nodes. J Immunol *179*, 993-1003.

Nieves, D.S., Phipps, R.P., Pollock, S.J., Ochs, H.D., Zhu, Q., Scott, G.A., Ryan, C.K., Kobayashi, I., Rossi, T.M., and Goldsmith, L.A. (2004). Dermatologic and immunologic findings in the immune dysregulation, polyendocrinopathy, enteropathy, X-linked syndrome. Archives of dermatology *140*, 466-472.

Niki, S., Oshikawa, K., Mouri, Y., Hirota, F., Matsushima, A., Yano, M., Han, H., Bando, Y., Izumi, K., Matsumoto, M.*, et al.* (2006). Alteration of intra-pancreatic target-organ specificity by abrogation of Aire in NOD mice. The Journal of clinical investigation *116*, 1292-1301.

Nikolic-Zugic, J. (1991). Phenotypic and functional stages in the intrathymic development of alpha beta T cells. Immunology today *12*, 65-70.

Nishimori, I., Miyaji, E., Morimoto, K., Nagao, K., Kamada, M., and Onishi, S. (2005). Serum antibodies to carbonic anhydrase IV in patients with autoimmune pancreatitis. Gut *54*, 274-281.

Nishizuka, Y., and Sakakura, T. (1969). Thymus and reproduction: sex-linked dysgenesia of the gonad after neonatal thymectomy in mice. Science (New York, NY *166*, 753-755.

Nossal, G.J. (1983). Cellular mechanisms of immunologic tolerance. Annual review of immunology *1*, 33-62.

Nossal, G.J., and Lederberg, J. (1958). Antibody production by single cells. Nature *181*, 1419-1420.

Nurieva, R.I., Chung, Y., Martinez, G.J., Yang, X.O., Tanaka, S., Matskevitch, T.D., Wang, Y.H., and Dong, C. (2009). Bcl6 mediates the development of T follicular helper cells. Science (New York, NY *325*, 1001-1005.

Okajima, M., Wada, T., Nishida, M., Yokoyama, T., Nakayama, Y., Hashida, Y., Shibata, F., Tone, Y., Ishizaki, A., Shimizu, M.*, et al.* (2009). Analysis of T cell receptor Vbeta diversity in peripheral CD4 and CD8 T lymphocytes in patients with autoimmune thyroid diseases. Clinical and experimental immunology *155*, 166-172.

Okazaki, K., Uchida, K., and Chiba, T. (2001). Recent concept of autoimmune-related pancreatitis. Journal of gastroenterology *36*, 293-302.

Oksenberg, J.R., Panzara, M.A., Begovich, A.B., Mitchell, D., Erlich, H.A., Murray, R.S., Shimonkevitz, R., Sherritt, M., Rothbard, J., Bernard, C.C.*, et al.* (1993). Selection for T-cell receptor V beta-D beta-J beta gene rearrangements with specificity for a myelin basic protein peptide in brain lesions of multiple sclerosis. Nature *362*, 68-70.

Owen, R.D. (1945). Immunogenetic Consequences of Vascular Anastomoses between Bovine Twins. Science (New York, NY *102*, 400-401.

Owens, T., Fazekas de St Groth, B., and Miller, J.F. (1987). Coaggregation of the T-cell receptor with CD4 and other T-cell surface molecules enhances T-cell activation. Proceedings of the National Academy of Sciences of the United States of America *84*, 9209-9213.

Padovan, E., Casorati, G., Dellabona, P., Meyer, S., Brockhaus, M., and Lanzavecchia, A. (1993). Expression of two T cell receptor alpha chains: dual receptor T cells. Science (New York, NY *262*, 422-424.

Pai, S.Y., Truitt, M.L., Ting, C.N., Leiden, J.M., Glimcher, L.H., and Ho, I.C. (2003). Critical roles for transcription factor GATA-3 in thymocyte development. Immunity *19*, 863-875.

Paolino, M., and Penninger, J.M. (2009). E3 ubiquitin ligases in T-cell tolerance. European journal of immunology *39*, 2337-2344.

Parungo, C.P., Soybel, D.I., Colson, Y.L., Kim, S.W., Ohnishi, S., DeGrand, A.M., Laurence, R.G., Soltesz, E.G., Chen, F.Y., Cohn, L.H.*, et al.* (2007). Lymphatic

drainage of the peritoneal space: a pattern dependent on bowel lymphatics. Annals of surgical oncology *14*, 286-298.

Patel, M., and Fine, D.R. (2005). Fibrogenesis in the pancreas after acinar cell injury. Scand J Surg *94*, 108-111.

Pearse, M., Wu, L., Egerton, M., Wilson, A., Shortman, K., and Scollay, R. (1989). A murine early thymocyte developmental sequence is marked by transient expression of the interleukin 2 receptor. Proceedings of the National Academy of Sciences of the United States of America *86*, 1614-1618.

Pena-Rossi, C., Zuckerman, L.A., Strong, J., Kwan, J., Ferris, W., Chan, S., Tarakhovsky, A., Beyers, A.D., and Killeen, N. (1999). Negative regulation of CD4 lineage development and responses by CD5. J Immunol *163*, 6494-6501.

Pentcheva-Hoang, T., Corse, E., and Allison, J.P. (2009). Negative regulators of T-cell activation: potential targets for therapeutic intervention in cancer, autoimmune disease, and persistent infections. Immunological reviews *229*, 67-87.

Perez-Villar, J.J., Whitney, G.S., Bowen, M.A., Hewgill, D.H., Aruffo, A.A., and Kanner, S.B. (1999). CD5 negatively regulates the T-cell antigen receptor signal transduction pathway: involvement of SH2-containing phosphotyrosine phosphatase SHP-1. Molecular and cellular biology *19*, 2903-2912.

Perheentupa, J. (2006). Autoimmune polyendocrinopathy-candidiasis-ectodermal dystrophy. The Journal of clinical endocrinology and metabolism *91*, 2843-2850.

Peterson, J.D., and Haskins, K. (1996). Transfer of diabetes in the NOD-scid mouse by CD4 T-cell clones. Differential requirement for CD8 T-cells. Diabetes *45*, 328-336.

Peterson, P., and Peltonen, L. (2005). Autoimmune polyendocrinopathy syndrome type 1 (APS1) and AIRE gene: new views on molecular basis of autoimmunity. Journal of autoimmunity *25 Suppl*, 49-55.

Petrie, H.T., Livak, F., Schatz, D.G., Strasser, A., Crispe, I.N., and Shortman, K. (1993). Multiple rearrangements in T cell receptor alpha chain genes maximize the production of useful thymocytes. The Journal of experimental medicine *178*, 615-622.

Pircher, H., Burki, K., Lang, R., Hengartner, H., and Zinkernagel, R.M. (1989). Tolerance induction in double specific T-cell receptor transgenic mice varies with antigen. Nature *342*, 559-561.

Plenge, R.M., Cotsapas, C., Davies, L., Price, A.L., de Bakker, P.I., Maller, J., Pe'er, I., Burtt, N.P., Blumenstiel, B., DeFelice, M.*, et al.* (2007). Two independent alleles at 6q23 associated with risk of rheumatoid arthritis. Nature genetics *39*, 1477-1482.

Pociot, F., and McDermott, M.F. (2002). Genetics of type 1 diabetes mellitus. Genes and immunity *3*, 235-249.

Ponnuraj, E.M., and Hayward, A.R. (2001). Intact intestinal mRNAs and intestinal epithelial cell esterase, but not Cryptosporidium parvum, reach mesenteric lymph nodes of infected mice. J Immunol *167*, 5321-5328.

Porritt, H.E., Rumfelt, L.L., Tabrizifard, S., Schmitt, T.M., Zuniga-Pflucker, J.C., and Petrie, H.T. (2004). Heterogeneity among DN1 prothymocytes reveals multiple progenitors with different capacities to generate T cell and non-T cell lineages. Immunity *20*, 735-745.

Prabu, A., Marshall, T., Gordon, C., Plant, T., Bawendi, A., Heaton, S., Jobson, S., Briggs, D., and Bowman, S.J. (2003). Use of patient age and anti-Ro/La antibody status to determine the probability of patients with systemic lupus erythematosus and sicca symptoms fulfilling criteria for secondary Sjogren's syndrome. Rheumatology (Oxford, England) *42*, 189-191.

Priatel, J.J., Teh, S.J., Dower, N.A., Stone, J.C., and Teh, H.S. (2002). RasGRP1 transduces low-grade TCR signals which are critical for T cell development, homeostasis, and differentiation. Immunity *17*, 617-627.

Priatel, J.J., Utting, O., and Teh, H.S. (2001). TCR/self-antigen interactions drive double-negative T cell peripheral expansion and differentiation into suppressor cells. J Immunol *167*, 6188-6194.

Probert, C.S., Chott, A., Saubermann, L.J., Stevens, A.C., Balk, S.P., and Blumberg, R.S. (2001). Prevalence of an ulcerative colitis-associated CD8+ T cell receptor beta-chain CDR3-region motif and its association with disease activity. Journal of clinical immunology *21*, 126-134.

Puel, A., Cypowyj, S., Bustamante, J., Wright, J.F., Liu, L., Lim, H.K., Migaud, M., Israel, L., Chrabieh, M., Audry, M.*, et al.* (2011). Chronic mucocutaneous candidiasis in humans with inborn errors of interleukin-17 immunity. Science (New York, NY *332*, 65-68.

Puel, A., Doffinger, R., Natividad, A., Chrabieh, M., Barcenas-Morales, G., Picard, C., Cobat, A., Ouachee-Chardin, M., Toulon, A., Bustamante, J.*, et al.* (2010). Autoantibodies against IL-17A, IL-17F, and IL-22 in patients with chronic mucocutaneous candidiasis and autoimmune polyendocrine syndrome type I. The Journal of experimental medicine *207*, 291-297.

Pugliese, A., Zeller, M., Fernandez, A., Jr., Zalcberg, L.J., Bartlett, R.J., Ricordi, C., Pietropaolo, M., Eisenbarth, G.S., Bennett, S.T., and Patel, D.D. (1997). The insulin gene is transcribed in the human thymus and transcription levels correlated with allelic variation at the INS VNTR-IDDM2 susceptibility locus for type 1 diabetes. Nature genetics *15*, 293-297.

Punt, J.A., Osborne, B.A., Takahama, Y., Sharrow, S.O., and Singer, A. (1994). Negative selection of CD4+CD8+ thymocytes by T cell receptor-induced apoptosis requires a costimulatory signal that can be provided by CD28. The Journal of experimental medicine *179*, 709-713.

Qiao, G., Li, Z., Molinero, L., Alegre, M.L., Ying, H., Sun, Z., Penninger, J.M., and Zhang, J. (2008). T-cell receptor-induced NF-kappaB activation is negatively regulated by E3 ubiquitin ligase Cbl-b. Molecular and cellular biology *28*, 2470-2480.

Qureshi, O.S., Zheng, Y., Nakamura, K., Attridge, K., Manzotti, C., Schmidt, E.M., Baker, J., Jeffery, L.E., Kaur, S., Briggs, Z., *et al.* (2011). Trans-endocytosis of CD80 and CD86: a molecular basis for the cell-extrinsic function of CTLA-4. Science (New York, NY *332*, 600-603.

Rai, E., and Wakeland, E.K. (2011). Genetic predisposition to autoimmunity--what have we learned? Seminars in immunology *23*, 67-83.

Ramsey, C., Bukrinsky, A., and Peltonen, L. (2002a). Systematic mutagenesis of the functional domains of AIRE reveals their role in intracellular targeting. Human molecular genetics *11*, 3299-3308.

Ramsey, C., Hassler, S., Marits, P., Kampe, O., Surh, C.D., Peltonen, L., and Winqvist, O. (2006). Increased antigen presenting cell-mediated T cell activation in mice and patients without the autoimmune regulator. European journal of immunology *36*, 305-317.

Ramsey, C., Winqvist, O., Puhakka, L., Halonen, M., Moro, A., Kampe, O., Eskelin, P., Pelto-Huikko, M., and Peltonen, L. (2002b). Aire deficient mice develop multiple features of APECED phenotype and show altered immune response. Human molecular genetics *11*, 397-409.

Rathmell, J.C., Lindsten, T., Zong, W.X., Cinalli, R.M., and Thompson, C.B. (2002). Deficiency in Bak and Bax perturbs thymic selection and lymphoid homeostasis. Nature immunology *3*, 932-939.

Rathmell, J.C., and Thompson, C.B. (2002). Pathways of apoptosis in lymphocyte development, homeostasis, and disease. Cell *109 Suppl*, S97-107.

Ravetch, J.V., and Lanier, L.L. (2000). Immune inhibitory receptors. Science (New York, NY *290*, 84-89.

Reader, S.R., Whyte, H.M., and Elmes, P.C. (1951). Sjogren's disease and rheumatoid arthritis. Annals of the rheumatic diseases *10*, 288-297.

Richie, L.I., Ebert, P.J., Wu, L.C., Krummel, M.F., Owen, J.J., and Davis, M.M. (2002). Imaging synapse formation during thymocyte selection: inability of CD3zeta to form a stable central accumulation during negative selection. Immunity *16*, 595-606.

Rincon, M., Whitmarsh, A., Yang, D.D., Weiss, L., Derijard, B., Jayaraj, P., Davis, R.J., and Flavell, R.A. (1998). The JNK pathway regulates the In vivo deletion of immature CD4(+)CD8(+) thymocytes. The Journal of experimental medicine *188*, 1817-1830.

Rioux, J.D., and Abbas, A.K. (2005). Paths to understanding the genetic basis of autoimmune disease. Nature *435*, 584-589.

Roths, J.B., Murphy, E.D., and Eicher, E.M. (1984). A new mutation, gld, that produces lymphoproliferation and autoimmunity in C3H/HeJ mice. The Journal of experimental medicine *159*, 1-20.

Ruan, Q.G., and She, J.X. (2004). Autoimmune polyglandular syndrome type 1 and the autoimmune regulator. Clin Lab Med *24*, 305-317.

Rudolph, M.G., Stanfield, R.L., and Wilson, I.A. (2006). How TCRs bind MHCs, peptides, and coreceptors. Annual review of immunology *24*, 419-466.

Ryan, K.R., Lawson, C.A., Lorenzi, A.R., Arkwright, P.D., Isaacs, J.D., and Lilic, D. (2005). CD4+CD25+ T-regulatory cells are decreased in patients with autoimmune polyendocrinopathy candidiasis ectodermal dystrophy. The Journal of allergy and clinical immunology *116*, 1158-1159.

Saito, T., Sussman, J.L., Ashwell, J.D., and Germain, R.N. (1989). Marked differences in the efficiency of expression of distinct alpha beta T cell receptor heterodimers. J Immunol *143*, 3379-3384.

Sakaguchi, N., Takahashi, T., Hata, H., Nomura, T., Tagami, T., Yamazaki, S., Sakihama, T., Matsutani, T., Negishi, I., Nakatsuru, S.*, et al.* (2003). Altered thymic T-cell selection due to a mutation of the ZAP-70 gene causes autoimmune arthritis in mice. Nature *426*, 454-460.

Sakaguchi, S., Miyara, M., Costantino, C.M., and Hafler, D.A. (2010). FOXP3+ regulatory T cells in the human immune system. Nat Rev Immunol *10*, 490-500.

Sakaguchi, S., Sakaguchi, N., Asano, M., Itoh, M., and Toda, M. (1995). Immunologic self-tolerance maintained by activated T cells expressing IL-2 receptor alpha-chains (CD25). Breakdown of a single mechanism of self-tolerance causes various autoimmune diseases. J Immunol *155*, 1151-1164.

Sakaguchi, S., Takahashi, T., and Nishizuka, Y. (1982). Study on cellular events in postthymectomy autoimmune oophoritis in mice. I. Requirement of Lyt-1 effector cells for oocytes damage after adoptive transfer. The Journal of experimental medicine *156*, 1565-1576.

Sakaguchi, S., Wing, K., and Yamaguchi, T. (2009). Dynamics of peripheral tolerance and immune regulation mediated by Treg. European journal of immunology *39*, 2331-2336.

Salmena, L., Lemmers, B., Hakem, A., Matysiak-Zablocki, E., Murakami, K., Au, P.Y., Berry, D.M., Tamblyn, L., Shehabeldin, A., Migon, E.*, et al.* (2003). Essential role for caspase 8 in T-cell homeostasis and T-cell-mediated immunity. Genes & development *17*, 883-895.

Salomon, B., Lenschow, D.J., Rhee, L., Ashourian, N., Singh, B., Sharpe, A., and Bluestone, J.A. (2000). B7/CD28 costimulation is essential for the homeostasis of the CD4+CD25+ immunoregulatory T cells that control autoimmune diabetes. Immunity *12*, 431-440.

Salomon, B., Rhee, L., Bour-Jordan, H., Hsin, H., Montag, A., Soliven, B., Arcella, J., Girvin, A.M., Padilla, J., Miller, S.D.*, et al.* (2001). Development of spontaneous autoimmune peripheral polyneuropathy in B7-2-deficient NOD mice. The Journal of experimental medicine *194*, 677-684.

Sanna, S., Pitzalis, M., Zoledziewska, M., Zara, I., Sidore, C., Murru, R., Whalen, M.B., Busonero, F., Maschio, A., Costa, G.*, et al.* (2010). Variants within the

immunoregulatory CBLB gene are associated with multiple sclerosis. Nature genetics *42*, 495-497.

Santagata, S., Villa, A., Sobacchi, C., Cortes, P., and Vezzoni, P. (2000). The genetic and biochemical basis of Omenn syndrome. Immunological reviews *178*, 64-74.

Santamaria, P., Utsugi, T., Park, B.J., Averill, N., Kawazu, S., and Yoon, J.W. (1995). Beta-cell-cytotoxic CD8+ T cells from nonobese diabetic mice use highly homologous T cell receptor alpha-chain CDR3 sequences. J Immunol *154*, 2494-2503.

Sasaki, M., Nakamura, S., Ohyama, Y., Shinohara, M., Ezaki, I., Hara, H., Kadena, T., Kishihara, K., Yamamoto, K., Nomoto, K.*, et al.* (2000). Accumulation of common T cell clonotypes in the salivary glands of patients with human T lymphotropic virus type I-associated and idiopathic Sjogren's syndrome. J Immunol *164*, 2823-2831.

Saubermann, L.J., Probert, C.S., Christ, A.D., Chott, A., Turner, J.R., Stevens, A.C., Balk, S.P., and Blumberg, R.S. (1999). Evidence of T cell receptor beta-chain patterns in inflammatory and noninflammatory bowel disease states. The American journal of physiology *276*, G613-621.

Schmidt, E.M., Wang, C.J., Ryan, G.A., Clough, L.E., Qureshi, O.S., Goodall, M., Abbas, A.K., Sharpe, A.H., Sansom, D.M., and Walker, L.S. (2009). Ctla-4 controls regulatory T cell peripheral homeostasis and is required for suppression of pancreatic islet autoimmunity. J Immunol *182*, 274-282.

Schork, N.J., Murray, S.S., Frazer, K.A., and Topol, E.J. (2009). Common vs. rare allele hypotheses for complex diseases. Current opinion in genetics & development *19*, 212-219.

Schwartz, R.H. (1990). A cell culture model for T lymphocyte clonal anergy. Science (New York, NY *248*, 1349-1356.

Schwartz, R.H. (2003). T cell anergy. Annual review of immunology *21*, 305-334.

Seach, N., Ueno, T., Fletcher, A.L., Lowen, T., Mattesich, M., Engwerda, C.R., Scott, H.S., Ware, C.F., Chidgey, A.P., Gray, D.H.*, et al.* (2008). The lymphotoxin pathway regulates Aire-independent expression of ectopic genes and chemokines in thymic stromal cells. J Immunol *180*, 5384-5392.

Sedger, L.M., Katewa, A., Pettersen, A.K., Osvath, S.R., Farrell, G.C., Stewart, G.J., Bendall, L.J., and Alexander, S.I. (2010). Extreme lymphoproliferative disease and fatal autoimmune thrombocytopenia in FasL and TRAIL double-deficient mice. Blood *115*, 3258-3268.

Serra, P., Amrani, A., Han, B., Yamanouchi, J., Thiessen, S.J., and Santamaria, P. (2002). RAG-dependent peripheral T cell receptor diversification in CD8+ T lymphocytes. Proceedings of the National Academy of Sciences of the United States of America *99*, 15566-15571.

Serreze, D.V., Johnson, E.A., Chapman, H.D., Graser, R.T., Marron, M.P., DiLorenzo, T.P., Silveira, P., Yoshimura, Y., Nathenson, S.G., and Joyce, S. (2001). Autoreactive

diabetogenic T-cells in NOD mice can efficiently expand from a greatly reduced precursor pool. Diabetes *50*, 1992-2000.

Sha, W.C., Nelson, C.A., Newberry, R.D., Kranz, D.M., Russell, J.H., and Loh, D.Y. (1988). Positive and negative selection of an antigen receptor on T cells in transgenic mice. Nature *336*, 73-76.

Sharpe, A.H., and Freeman, G.J. (2002). The B7-CD28 superfamily. Nat Rev Immunol *2*, 116-126.

Sharpe, A.H., Wherry, E.J., Ahmed, R., and Freeman, G.J. (2007). The function of programmed cell death 1 and its ligands in regulating autoimmunity and infection. Nature immunology *8*, 239-245.

Shen, N., Fu, Q., Deng, Y., Qian, X., Zhao, J., Kaufman, K.M., Wu, Y.L., Yu, C.Y., Tang, Y., Chen, J.Y.*, et al.* (2010). Sex-specific association of X-linked Toll-like receptor 7 (TLR7) with male systemic lupus erythematosus. Proceedings of the National Academy of Sciences of the United States of America *107*, 15838-15843.

Shevach, E.M. (2009). Mechanisms of foxp3+ T regulatory cell-mediated suppression. Immunity *30*, 636-645.

Shinkai, Y., Rathbun, G., Lam, K.P., Oltz, E.M., Stewart, V., Mendelsohn, M., Charron, J., Datta, M., Young, F., Stall, A.M.*, et al.* (1992). RAG-2-deficient mice lack mature lymphocytes owing to inability to initiate V(D)J rearrangement. Cell *68*, 855-867.

Shull, M.M., Ormsby, I., Kier, A.B., Pawlowski, S., Diebold, R.J., Yin, M., Allen, R., Sidman, C., Proetzel, G., Calvin, D.*, et al.* (1992). Targeted disruption of the mouse transforming growth factor-beta 1 gene results in multifocal inflammatory disease. Nature *359*, 693-699.

Shum, A.K., DeVoss, J., Tan, C.L., Hou, Y., Johannes, K., O'Gorman, C.S., Jones, K.D., Sochett, E.B., Fong, L., and Anderson, M.S. (2009). Identification of an autoantigen demonstrates a link between interstitial lung disease and a defect in central tolerance. Science translational medicine *1*, 9ra20.

Sidman, C.L., Marshall, J.D., and Von Boehmer, H. (1992). Transgenic T cell receptor interactions in the lymphoproliferative and autoimmune syndromes of lpr and gld mutant mice. European journal of immunology *22*, 499-504.

Silva, D.G., Daley, S.R., Hogan, J., Lee, S.K., Teh, C.E., Hu, D.Y., Lam, K.P., Goodnow, C.C., and Vinuesa, C.G. (2011). Anti-islet autoantibodies trigger autoimmune diabetes in the presence of an increased frequency of islet-reactive CD4 T cells. Diabetes *60*, 2102-2111.

Singer, G.G., and Abbas, A.K. (1994). The fas antigen is involved in peripheral but not thymic deletion of T lymphocytes in T cell receptor transgenic mice. Immunity *1*, 365-371.

Sloan-Lancaster, J., Evavold, B.D., and Allen, P.M. (1993). Induction of T-cell anergy by altered T-cell-receptor ligand on live antigen-presenting cells. Nature *363*, 156-159.

Smedby, K.E., Hjalgrim, H., Askling, J., Chang, E.T., Gregersen, H., Porwit-MacDonald, A., Sundstrom, C., Akerman, M., Melbye, M., Glimelius, B.*, et al.* (2006). Autoimmune and chronic inflammatory disorders and risk of non-Hodgkin lymphoma by subtype. Journal of the National Cancer Institute *98*, 51-60.

Smith, K., Seddon, B., Purbhoo, M.A., Zamoyska, R., Fisher, A.G., and Merkenschlager, M. (2001). Sensory adaptation in naive peripheral CD4 T cells. The Journal of experimental medicine *194*, 1253-1261.

Stahl, E.A., Raychaudhuri, S., Remmers, E.F., Xie, G., Eyre, S., Thomson, B.P., Li, Y., Kurreeman, F.A., Zhernakova, A., Hinks, A.*, et al.* (2010). Genome-wide association study meta-analysis identifies seven new rheumatoid arthritis risk loci. Nature genetics *42*, 508-514.

Steinberg, A.D. (1994). MRL-lpr/lpr disease: theories meet Fas. Seminars in immunology *6*, 55-69.

Steinman, R.M., Hawiger, D., and Nussenzweig, M.C. (2003). Tolerogenic dendritic cells. Annual review of immunology *21*, 685-711.

Stockinger, B., and Veldhoen, M. (2007). Differentiation and function of Th17 T cells. Current opinion in immunology *19*, 281-286.

Strasser, A., and Bouillet, P. (2003). The control of apoptosis in lymphocyte selection. Immunological reviews *193*, 82-92.

Strasser, A., Harris, A.W., and Cory, S. (1991). bcl-2 transgene inhibits T cell death and perturbs thymic self-censorship. Cell *67*, 889-899.

Strasser, A., Harris, A.W., von Boehmer, H., and Cory, S. (1994). Positive and negative selection of T cells in T-cell receptor transgenic mice expressing a bcl-2 transgene. Proceedings of the National Academy of Sciences of the United States of America *91*, 1376-1380.

Su, M.A., Giang, K., Zumer, K., Jiang, H., Oven, I., Rinn, J.L., Devoss, J.J., Johannes, K.P., Lu, W., Gardner, J.*, et al.* (2008). Mechanisms of an autoimmunity syndrome in mice caused by a dominant mutation in Aire. The Journal of clinical investigation *118*, 1712-1726.

Sun, W., Nie, H., Li, N., Zang, Y.C., Zhang, D., Feng, G., Ni, L., Xu, R., Prasad, S., Robinson, R.R.*, et al.* (2005). Skewed T-cell receptor BV14 and BV16 expression and shared CDR3 sequence and common sequence motifs in synovial T cells of rheumatoid arthritis. Genes and immunity *6*, 248-261.

Sytwu, H.K., Liblau, R.S., and McDevitt, H.O. (1996). The roles of Fas/APO-1 (CD95) and TNF in antigen-induced programmed cell death in T cell receptor transgenic mice. Immunity *5*, 17-30.

Szymczak, A.L., Workman, C.J., Wang, Y., Vignali, K.M., Dilioglou, S., Vanin, E.F., and Vignali, D.A. (2004). Correction of multi-gene deficiency in vivo using a single 'self-cleaving' 2A peptide-based retroviral vector. Nature biotechnology *22*, 589-594.

Takahashi, H., Yamamoto, M., Suzuki, C., Naishiro, Y., Shinomura, Y., and Imai, K. (2011). The birthday of a new syndrome: IgG4-related diseases constitute a clinical entity. Autoimmunity reviews *9*, 591-594.

Takahashi, T., Tanaka, M., Brannan, C.I., Jenkins, N.A., Copeland, N.G., Suda, T., and Nagata, S. (1994). Generalized lymphoproliferative disease in mice, caused by a point mutation in the Fas ligand. Cell *76*, 969-976.

Takizawa, S., Endo, T., Wanjia, X., Tanaka, S., Takahashi, M., and Kobayashi, T. (2009). HSP 10 is a new autoantigen in both autoimmune pancreatitis and fulminant type 1 diabetes. Biochemical and biophysical research communications *386*, 192-196.

Talmage, D.W. (1957). Allergy and immunology. Annual review of medicine *8*, 239-256.

Teh, C.E., Daley, S.R., Enders, A., and Goodnow, C.C. (2010). T-cell regulation by casitas B-lineage lymphoma (Cblb) is a critical failsafe against autoimmune disease due to autoimmune regulator (Aire) deficiency. Proceedings of the National Academy of Sciences of the United States of America *107*, 14709-14714.

Teh, H.S., Kisielow, P., Scott, B., Kishi, H., Uematsu, Y., Bluthmann, H., and von Boehmer, H. (1988). Thymic major histocompatibility complex antigens and the alpha beta T-cell receptor determine the CD4/CD8 phenotype of T cells. Nature *335*, 229-233.

Teh, S.J., Dutz, J.P., Motyka, B., and Teh, H.S. (1996). Fas (CD95)-independent regulation of immune responses by antigen-specific CD4-CD8+ T cells. International immunology *8*, 675-681.

Thien, C.B., Bowtell, D.D., and Langdon, W.Y. (1999). Perturbed regulation of ZAP-70 and sustained tyrosine phosphorylation of LAT and SLP-76 in c-Cbl-deficient thymocytes. J Immunol *162*, 7133-7139.

Thien, C.B., and Langdon, W.Y. (2005). c-Cbl and Cbl-b ubiquitin ligases: substrate diversity and the negative regulation of signalling responses. The Biochemical journal *391*, 153-166.

Thomson, W., Barton, A., Ke, X., Eyre, S., Hinks, A., Bowes, J., Donn, R., Symmons, D., Hider, S., Bruce, I.N.*, et al.* (2007). Rheumatoid arthritis association at 6q23. Nature genetics *39*, 1431-1433.

Tivol, E.A., Borriello, F., Schweitzer, A.N., Lynch, W.P., Bluestone, J.A., and Sharpe, A.H. (1995). Loss of CTLA-4 leads to massive lymphoproliferation and fatal multiorgan tissue destruction, revealing a critical negative regulatory role of CTLA-4. Immunity *3*, 541-547.

Todd, J.A., Walker, N.M., Cooper, J.D., Smyth, D.J., Downes, K., Plagnol, V., Bailey, R., Nejentsev, S., Field, S.F., Payne, F.*, et al.* (2007). Robust associations of four new chromosome regions from genome-wide analyses of type 1 diabetes. Nature genetics *39*, 857-864.

Todd, J.A., and Wicker, L.S. (2001). Genetic protection from the inflammatory disease type 1 diabetes in humans and animal models. Immunity *15*, 387-395.

Tourne, S., Kouskoff, V., Ho, W., Davis, M., Benoist, C., and Mathis, D. (1999). Inhibition of thymocyte positive selection by natural MHC: peptide ligands. European journal of immunology *29*, 394-402.

Tran, D.Q., Ramsey, H., and Shevach, E.M. (2007). Induction of FOXP3 expression in naive human CD4+FOXP3 T cells by T-cell receptor stimulation is transforming growth factor-beta dependent but does not confer a regulatory phenotype. Blood *110*, 2983-2990.

Trynka, G., Zhernakova, A., Romanos, J., Franke, L., Hunt, K.A., Turner, G., Bruinenberg, M., Heap, G.A., Platteel, M., Ryan, A.W.*, et al.* (2009). Coeliac disease-associated risk variants in TNFAIP3 and REL implicate altered NF-kappaB signalling. Gut *58*, 1078-1083.

Tsai, S., Shameli, A., Yamanouchi, J., Clemente-Casares, X., Wang, J., Serra, P., Yang, Y., Medarova, Z., Moore, A., and Santamaria, P. (2010). Reversal of autoimmunity by boosting memory-like autoregulatory T cells. Immunity *32*, 568-580.

Tsubata, R., Tsubata, T., Hiai, H., Shinkura, R., Matsumura, R., Sumida, T., Miyawaki, S., Ishida, H., Kumagai, S., Nakao, K.*, et al.* (1996). Autoimmune disease of exocrine organs in immunodeficient alymphoplasia mice: a spontaneous model for Sjogren's syndrome. European journal of immunology *26*, 2742-2748.

Turley, S.J., Lee, J.W., Dutton-Swain, N., Mathis, D., and Benoist, C. (2005). Endocrine self and gut non-self intersect in the pancreatic lymph nodes. Proceedings of the National Academy of Sciences of the United States of America *102*, 17729-17733.

Tze, L.E., Horikawa, K., Domaschenz, H., Howard, D.R., Roots, C.M., Rigby, R.J., Way, D.A., Ohmura-Hoshino, M., Ishido, S., Andoniou, C.E.*, et al.* (2011). CD83 increases MHC II and CD86 on dendritic cells by opposing IL-10-driven MARCH1-mediated ubiquitination and degradation. The Journal of experimental medicine *208*, 149-165.

Uchida, K., Okazaki, K., Nishi, T., Uose, S., Nakase, H., Ohana, M., Matsushima, Y., Omori, K., and Chiba, T. (2002). Experimental immune-mediated pancreatitis in neonatally thymectomized mice immunized with carbonic anhydrase II and lactoferrin. Laboratory investigation; a journal of technical methods and pathology *82*, 411-424.

Ueda, H., Howson, J.M., Esposito, L., Heward, J., Snook, H., Chamberlain, G., Rainbow, D.B., Hunter, K.M., Smith, A.N., Di Genova, G.*, et al.* (2003). Association of the T-cell regulatory gene CTLA4 with susceptibility to autoimmune disease. Nature *423*, 506-511.

Vafiadis, P., Bennett, S.T., Todd, J.A., Nadeau, J., Grabs, R., Goodyer, C.G., Wickramasinghe, S., Colle, E., and Polychronakos, C. (1997). Insulin expression in human thymus is modulated by INS VNTR alleles at the IDDM2 locus. Nature genetics *15*, 289-292.

van Heel, D.A., Franke, L., Hunt, K.A., Gwilliam, R., Zhernakova, A., Inouye, M., Wapenaar, M.C., Barnardo, M.C., Bethel, G., Holmes, G.K.*, et al.* (2007). A genome-

wide association study for celiac disease identifies risk variants in the region harboring IL2 and IL21. Nature genetics *39*, 827-829.

Van Parijs, L., Peterson, D.A., and Abbas, A.K. (1998). The Fas/Fas ligand pathway and Bcl-2 regulate T cell responses to model self and foreign antigens. Immunity *8*, 265-274.

Venanzi, E.S., Benoist, C., and Mathis, D. (2004). Good riddance: Thymocyte clonal deletion prevents autoimmunity. Current opinion in immunology *16*, 197-202.

Venanzi, E.S., Gray, D.H., Benoist, C., and Mathis, D. (2007). Lymphotoxin pathway and Aire influences on thymic medullary epithelial cells are unconnected. J Immunol *179*, 5693-5700.

Verdaguer, J., Schmidt, D., Amrani, A., Anderson, B., Averill, N., and Santamaria, P. (1997). Spontaneous autoimmune diabetes in monoclonal T cell nonobese diabetic mice. The Journal of experimental medicine *186*, 1663-1676.

Verdaguer, J., Yoon, J.W., Anderson, B., Averill, N., Utsugi, T., Park, B.J., and Santamaria, P. (1996). Acceleration of spontaneous diabetes in TCR-beta-transgenic nonobese diabetic mice by beta-cell cytotoxic CD8+ T cells expressing identical endogenous TCR-alpha chains. J Immunol *157*, 4726-4735.

Vignali, D.A., Collison, L.W., and Workman, C.J. (2008). How regulatory T cells work. Nat Rev Immunol *8*, 523-532.

Villa, A., Notarangelo, L., Macchi, P., Mantuano, E., Cavagni, G., Brugnoni, D., Strina, D., Patrosso, M.C., Ramenghi, U., Sacco, M.G.*, et al.* (1995). X-linked thrombocytopenia and Wiskott-Aldrich syndrome are allelic diseases with mutations in the WASP gene. Nature genetics *9*, 414-417.

Villa, A., Santagata, S., Bozzi, F., Giliani, S., Frattini, A., Imberti, L., Gatta, L.B., Ochs, H.D., Schwarz, K., Notarangelo, L.D.*, et al.* (1998). Partial V(D)J recombination activity leads to Omenn syndrome. Cell *93*, 885-896.

Villunger, A., Scott, C., Bouillet, P., and Strasser, A. (2003). Essential role for the BH3-only protein Bim but redundant roles for Bax, Bcl-2, and Bcl-w in the control of granulocyte survival. Blood *101*, 2393-2400.

Vinuesa, C.G., Cook, M.C., Angelucci, C., Athanasopoulos, V., Rui, L., Hill, K.M., Yu, D., Domaschenz, H., Whittle, B., Lambe, T.*, et al.* (2005a). A RING-type ubiquitin ligase family member required to repress follicular helper T cells and autoimmunity. Nature *435*, 452-458.

Vinuesa, C.G., Tangye, S.G., Moser, B., and Mackay, C.R. (2005b). Follicular B helper T cells in antibody responses and autoimmunity. Nat Rev Immunol *5*, 853-865.

Vitali, C. (2003). Classification criteria for Sjogren's syndrome. Annals of the rheumatic diseases *62*, 94-95; author reply 95.

von Boehmer, H. (2005). Unique features of the pre-T-cell receptor alpha-chain: not just a surrogate. Nat Rev Immunol *5*, 571-577.

Waldmann, T.A. (2007). Anti-Tac (daclizumab, Zenapax) in the treatment of leukemia, autoimmune diseases, and in the prevention of allograft rejection: a 25-year personal odyssey. Journal of clinical immunology *27*, 1-18.

Walker, L.S., and Abbas, A.K. (2002). The enemy within: keeping self-reactive T cells at bay in the periphery. Nat Rev Immunol *2*, 11-19.

Walker, L.S., Gulbranson-Judge, A., Flynn, S., Brocker, T., and Lane, P.J. (2000). Co-stimulation and selection for T-cell help for germinal centres: the role of CD28 and OX40. Immunology today *21*, 333-337.

Walker, M.R., Carson, B.D., Nepom, G.T., Ziegler, S.F., and Buckner, J.H. (2005). De novo generation of antigen-specific CD4+CD25+ regulatory T cells from human CD4+CD25- cells. Proceedings of the National Academy of Sciences of the United States of America *102*, 4103-4108.

Walter, M., Philotheou, A., Bonnici, F., Ziegler, A.G., and Jimenez, R. (2009). No effect of the altered peptide ligand NBI-6024 on beta-cell residual function and insulin needs in new-onset type 1 diabetes. Diabetes care *32*, 2036-2040.

Wandstrat, A., and Wakeland, E. (2001). The genetics of complex autoimmune diseases: non-MHC susceptibility genes. Nature immunology *2*, 802-809.

Wang, B., Gonzalez, A., Benoist, C., and Mathis, D. (1996). The role of CD8+ T cells in the initiation of insulin-dependent diabetes mellitus. European journal of immunology *26*, 1762-1769.

Wang, L., and Bosselut, R. (2009). CD4-CD8 lineage differentiation: Thpok-ing into the nucleus. J Immunol *183*, 2903-2910.

Watanabe, N., Ikuta, K., Fagarasan, S., Yazumi, S., Chiba, T., and Honjo, T. (2000). Migration and differentiation of autoreactive B-1 cells induced by activated gamma/delta T cells in antierythrocyte immunoglobulin transgenic mice. The Journal of experimental medicine *192*, 1577-1586.

Watanabe, S., Suzuki, K., Kawauchi, Y., Yamagiwa, S., Yoneyama, H., Kawachi, H., Okada, Y., Shimizu, F., Asakura, H., and Aoyagi, Y. (2003). Kinetic analysis of the development of pancreatic lesions in mice infected with a murine retrovirus. Clinical immunology (Orlando, Fla *109*, 212-223.

Watanabe-Fukunaga, R., Brannan, C.I., Copeland, N.G., Jenkins, N.A., and Nagata, S. (1992). Lymphoproliferation disorder in mice explained by defects in Fas antigen that mediates apoptosis. Nature *356*, 314-317.

Waterhouse, P., Penninger, J.M., Timms, E., Wakeham, A., Shahinian, A., Lee, K.P., Thompson, C.B., Griesser, H., and Mak, T.W. (1995). Lymphoproliferative disorders with early lethality in mice deficient in Ctla-4. Science (New York, NY *270*, 985-988.

Weinreich, M.A., Takada, K., Skon, C., Reiner, S.L., Jameson, S.C., and Hogquist, K.A. (2009). KLF2 transcription-factor deficiency in T cells results in unrestrained cytokine production and upregulation of bystander chemokine receptors. Immunity *31*, 122-130.

Wiberg, M.E., Saari, S.A., Westermarck, E., and Meri, S. (2000). Cellular and humoral immune responses in atrophic lymphocytic pancreatitis in German shepherd dogs and rough-coated collies. Veterinary immunology and immunopathology *76*, 103-115.

Wildin, R.S., Ramsdell, F., Peake, J., Faravelli, F., Casanova, J.L., Buist, N., Levy-Lahad, E., Mazzella, M., Goulet, O., Perroni, L.*, et al.* (2001). X-linked neonatal diabetes mellitus, enteropathy and endocrinopathy syndrome is the human equivalent of mouse scurfy. Nature genetics *27*, 18-20.

Wildin, R.S., Smyk-Pearson, S., and Filipovich, A.H. (2002). Clinical and molecular features of the immunodysregulation, polyendocrinopathy, enteropathy, X linked (IPEX) syndrome. Journal of medical genetics *39*, 537-545.

Wing, K., Onishi, Y., Prieto-Martin, P., Yamaguchi, T., Miyara, M., Fehervari, Z., Nomura, T., and Sakaguchi, S. (2008). CTLA-4 control over Foxp3+ regulatory T cell function. Science (New York, NY *322*, 271-275.

Wing, K., and Sakaguchi, S. (2010). Regulatory T cells exert checks and balances on self tolerance and autoimmunity. Nature immunology *11*, 7-13.

Wohlfert, E.A., Callahan, M.K., and Clark, R.B. (2004). Resistance to CD4+CD25+ regulatory T cells and TGF-beta in Cbl-b-/- mice. J Immunol *173*, 1059-1065.

Wohlfert, E.A., Gorelik, L., Mittler, R., Flavell, R.A., and Clark, R.B. (2006). Cutting edge: deficiency in the E3 ubiquitin ligase Cbl-b results in a multifunctional defect in T cell TGF-beta sensitivity in vitro and in vivo. J Immunol *176*, 1316-1320.

Wolff, A.S., Oftedal, B.E., Kisand, K., Ersvaer, E., Lima, K., and Husebye, E.S. (2010). Flow cytometry study of blood cell subtypes reflects autoimmune and inflammatory processes in autoimmune polyendocrine syndrome type I. Scandinavian journal of immunology *71*, 459-467.

Wong, F.S., Karttunen, J., Dumont, C., Wen, L., Visintin, I., Pilip, I.M., Shastri, N., Pamer, E.G., and Janeway, C.A., Jr. (1999). Identification of an MHC class I-restricted autoantigen in type 1 diabetes by screening an organ-specific cDNA library. Nature medicine *5*, 1026-1031.

Wong, F.S., Visintin, I., Wen, L., Flavell, R.A., and Janeway, C.A., Jr. (1996). CD8 T cell clones from young nonobese diabetic (NOD) islets can transfer rapid onset of diabetes in NOD mice in the absence of CD4 cells. The Journal of experimental medicine *183*, 67-76.

Wong, F.S., Visintin, I., Wen, L., Granata, J., Flavell, R., and Janeway, C.A. (1998). The role of lymphocyte subsets in accelerated diabetes in nonobese diabetic-rat insulin promoter-B7-1 (NOD-RIP-B7-1) mice. The Journal of experimental medicine *187*, 1985-1993.

Wong, P., Barton, G.M., Forbush, K.A., and Rudensky, A.Y. (2001). Dynamic tuning of T cell reactivity by self-peptide-major histocompatibility complex ligands. The Journal of experimental medicine *193*, 1179-1187.

Woodland, D., Happ, M.P., Bill, J., and Palmer, E. (1990). Requirement for cotolerogenic gene products in the clonal deletion of I-E reactive T cells. Science (New York, NY *247*, 964-967.

Woodland, D.L., Happ, M.P., Gollob, K.J., and Palmer, E. (1991a). An endogenous retrovirus mediating deletion of alpha beta T cells? Nature *349*, 529-530.

Woodland, D.L., Lund, F.E., Happ, M.P., Blackman, M.A., Palmer, E., and Corley, R.B. (1991b). Endogenous superantigen expression is controlled by mouse mammary tumor proviral loci. The Journal of experimental medicine *174*, 1255-1258.

Woronicz, J.D., Calnan, B., Ngo, V., and Winoto, A. (1994). Requirement for the orphan steroid receptor Nur77 in apoptosis of T-cell hybridomas. Nature *367*, 277-281.

Wu, L., Antica, M., Johnson, G.R., Scollay, R., and Shortman, K. (1991). Developmental potential of the earliest precursor cells from the adult mouse thymus. The Journal of experimental medicine *174*, 1617-1627.

Wucherpfennig, K.W., Ota, K., Endo, N., Seidman, J.G., Rosenzweig, A., Weiner, H.L., and Hafler, D.A. (1990). Shared human T cell receptor V beta usage to immunodominant regions of myelin basic protein. Science (New York, NY *248*, 1016-1019.

Xue, Y., Chomez, P., Castanos-Velez, E., Biberfeld, P., Perlmann, T., and Jondal, M. (1997). Positive and negative thymic selection in T cell receptor-transgenic mice correlate with Nur77 mRNA expression. European journal of immunology *27*, 2048-2056.

Yagi, H., Matsumoto, M., Kunimoto, K., Kawaguchi, J., Makino, S., and Harada, M. (1992). Analysis of the roles of CD4+ and CD8+ T cells in autoimmune diabetes of NOD mice using transfer to NOD athymic nude mice. European journal of immunology *22*, 2387-2393.

Yamagata, T., Mathis, D., and Benoist, C. (2004). Self-reactivity in thymic double-positive cells commits cells to a CD8 alpha alpha lineage with characteristics of innate immune cells. Nature immunology *5*, 597-605.

Yamamichi, M., Matsuoka, N., Tomioka, T., Eguchi, K., Nagataki, S., and Kanematsu, T. (1997). Shared TCR Vbeta gene expression by the pancreas and salivary gland in immunodeficient alymphoplasic mice. J Immunol *159*, 427-432.

Yamamoto, M., Harada, S., Ohara, M., Suzuki, C., Naishiro, Y., Yamamoto, H., Takahashi, H., and Imai, K. (2005). Clinical and pathological differences between Mikulicz's disease and Sjogren's syndrome. Rheumatology (Oxford, England) *44*, 227-234.

Yang, J.M., Nagasaka, S., Yatagai, T., Nakamura, T., Kusaka, I., Ishikawa, S.E., Saito, T., and Ishibashi, S. (2006). Interleukin-12p40 gene (IL-12B) polymorphism and Type 1 diabetes mellitus in Japanese: possible role in subjects without having high-risk HLA haplotypes. Diabetes research and clinical practice *71*, 164-169.

Yang, W., Shen, N., Ye, D.Q., Liu, Q., Zhang, Y., Qian, X.X., Hirankarn, N., Ying, D., Pan, H.F., Mok, C.C., *et al.* (2010). Genome-wide association study in Asian populations identifies variants in ETS1 and WDFY4 associated with systemic lupus erythematosus. PLoS genetics *6*, e1000841.

Yip, L., Su, L., Sheng, D., Chang, P., Atkinson, M., Czesak, M., Albert, P.R., Collier, A.R., Turley, S.J., Fathman, C.G., *et al.* (2009). Deaf1 isoforms control the expression of genes encoding peripheral tissue antigens in the pancreatic lymph nodes during type 1 diabetes. Nature immunology *10*, 1026-1033.

Yokoi, N., Hayashi, C., Fujiwara, Y., Wang, H.Y., and Seino, S. (2007). Genetic reconstitution of autoimmune type 1 diabetes with two major susceptibility genes in the rat. Diabetes *56*, 506-512.

Yokoi, N., Komeda, K., Wang, H.Y., Yano, H., Kitada, K., Saitoh, Y., Seino, Y., Yasuda, K., Serikawa, T., and Seino, S. (2002). Cblb is a major susceptibility gene for rat type 1 diabetes mellitus. Nature genetics *31*, 391-394.

Yoshida, K., Toki, F., Takeuchi, T., Watanabe, S., Shiratori, K., and Hayashi, N. (1995). Chronic pancreatitis caused by an autoimmune abnormality. Proposal of the concept of autoimmune pancreatitis. Digestive diseases and sciences *40*, 1561-1568.

Yu, D., Rao, S., Tsai, L.M., Lee, S.K., He, Y., Sutcliffe, E.L., Srivastava, M., Linterman, M., Zheng, L., Simpson, N., *et al.* (2009). The transcriptional repressor Bcl-6 directs T follicular helper cell lineage commitment. Immunity *31*, 457-468.

Zal, T., Weiss, S., Mellor, A., and Stockinger, B. (1996). Expression of a second receptor rescues self-specific T cells from thymic deletion and allows activation of autoreactive effector function. Proceedings of the National Academy of Sciences of the United States of America *93*, 9102-9107.

Zhang, Z.X., Yang, L., Young, K.J., DuTemple, B., and Zhang, L. (2000). Identification of a previously unknown antigen-specific regulatory T cell and its mechanism of suppression. Nature medicine *6*, 782-789.

Zijlstra, M., Bix, M., Simister, N.E., Loring, J.M., Raulet, D.H., and Jaenisch, R. (1990). Beta 2-microglobulin deficient mice lack CD4-8+ cytolytic T cells. Nature *344*, 742-746.

Zinkernagel, R.M., and Doherty, P.C. (1974a). Immunological surveillance against altered self components by sensitised T lymphocytes in lymphocytic choriomeningitis. Nature *251*, 547-548.

Zinkernagel, R.M., and Doherty, P.C. (1974b). Restriction of in vitro T cell-mediated cytotoxicity in lymphocytic choriomeningitis within a syngeneic or semiallogeneic system. Nature *248*, 701-702.

Zintzaras, E., Voulgarelis, M., and Moutsopoulos, H.M. (2005). The risk of lymphoma development in autoimmune diseases: a meta-analysis. Archives of internal medicine *165*, 2337-2344.